

DRAFT TECHNICAL REPORT

BLM LIBRARY



88009805

AIR QUALITY

RECEIVED

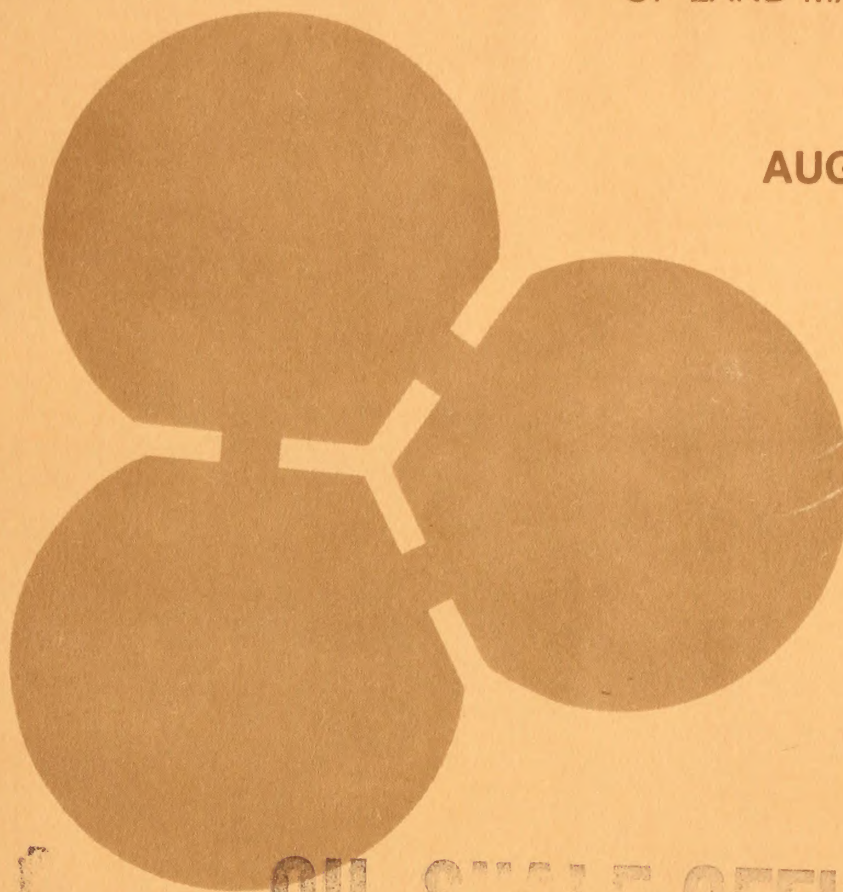
SEP 9 1982

OIL SHALE

SYSTEMS APPLICATIONS INC.

PREPARED FOR BUREAU
OF LAND MANGEMENT

AUGUST 1982



OIL SHALE OFFICE

CENTRAL LIBRARY

UINTAH BASIN SYNFUELS DEVELOPMENT

88004805

BLM Library
D-553A, Building 50
Denver Federal Center
P. O. Box 25047
Denver, CO 80225-0047

7D
195
-595
u35
1982
Suppl. 4

DRAFT
AIR QUALITY
TECHNICAL REPORT

for the

UINTAH BASIN SYNFUELS DEVELOPMENT
ENVIRONMENTAL IMPACT STATEMENT

OIL SHALE OFFICE
CENTRAL LIBRARY

Prepared by Systems Applications, Incorporated for
U.S. Department of the Interior, Bureau of Land Management

This study report was prepared by the following technical
personnel at Systems Applications, Inc.:

Principal Investigators

Douglas A. Latimer
William R. Oliver
Mark A. Yocke

Contributing Technical Staff

Jody Ames
Don H. Hern
Henry Hogo
Clark D. Johnson
John E. Langstaff
Ralph E. Morris
Thomas C. Myers
Pradeep Saxena
David R. Souten

ACKNOWLEDGMENTS

We express our gratitude to Bill Wagner of the Bureau of Land Management, whose guidance, encouragement, and helpful comments were of great benefit to us and our work.

We also thank Mary Ann Grasser of the National Park Service for coordinating and managing the PEDCo work, which provided valuable input to us and for assisting us with the secondary emissions work for Utah. Her significant contribution to this effort is deeply appreciated.

Helpful comments on the draft report were received from Bill Wagner, Mark Green, and Dick Traylor of BLM, Rich Fisher and Dave Joseph of EPA Region VIII, Dennis Haddow of the U.S. Forest Service, Dave Shaver of the National Park Service, Charles Cameron of the Ute Indian Tribe, and George Lauderdale of the Colorado Department of Health.

Finally, we thank Sandra Golding, Judy Rodich, and other members of the Systems Applications, Inc. Publication Center for editing, typing, and producing this report.

EXECUTIVE SUMMARY

This report documents an analysis of air quality impacts that was performed by Systems Applications, Inc. for the Bureau of Land Management (BLM) of synthetic fuel developments in the Uinta Basin of Utah. This analysis is to support the Environmental Impact Statement (EIS) that BLM is preparing for each of five specific synthetic fuel developments and cumulative regional impacts.

The primary objective of the study was to evaluate the air quality impacts of five synthetic fuel (oil shale and tar sands) facilities proposed to be developed in the Uinta Basin: Enercor-Mono Power (Rainbow site), Magic Circle, Paraho, Syntana-Utah, and Tosco. Three additional facilities that are at a conceptual design phase--Enercor-Mono Power (PR Springs site), Geokinetics, and Sohio--were also studied in regional scenarios. The impacts associated with two levels of oil production in the Uinta Basin of 121,400 and 320,500 barrels per day were studied.

Since cumulative regional impacts were considered to be important in this study, impacts of other industrial facilities were also examined. In the Uinta Basin these included the Moon Lake power plant (units 1 and 2), White River oil shale project (100,000 barrel per day capacity), Plateau refinery, and five other small projects. In the Piceance Basin in Colorado the air quality impacts of oil shale facilities having capacities totaling 271,000 and 639,000 barrels per day were included in regional assessments. The total synthetic fuel production capacity in the Uinta and Piceance basins studied in the low- and high-oil-production scenarios was 492,000 and 1,059,500 barrels per day, respectively.

Air quality impacts in the region were previously studied by both Systems Applications and Los Alamos Scientific Laboratory. The current study provides a more detailed analysis than did the previous policy and screening analyses. The current report is based on detailed emission inventories developed by synthetic fuel developers, Systems Applications, and PEDCo Environmental; measured meteorological conditions in the region; and additional regional data such as ambient air quality, topography, and visibility.

ANALYSIS METHODOLOGY

The methodology used in this study consisted of the following major tasks:

- > Collection of Data. Emission data for the Uinta Basin synfuel facilities were collected from the developers. Information concerning Colorado point and area source emissions and Utah population projections were obtained from a study performed for the National Park Service by PEDCo. Meteorological and topographical data were collected for the region.
- > Emission Inventory Development. Emission data were reviewed, checked, revised, and converted to input files for air quality modeling. Utah population data and projections were used to generate secondary area source emission files for the portion of Utah in the study region for the year 1980 baseline and for future low- and high-oil-production scenarios.
- > Air Quality Modeling. With the emissions, meteorological, and topographical data as input, several air quality simulation models were applied to address specific concerns. The most extensive modeling was performed by means of the Gaussian Puff Model (GPM), which was applied to 110-km x 110-km and 180-km x 268-km, regions encompassing the Uinta Basin and the combined Uinta and Piceance basins, respectively. Impacts were computed for every 3-hour period in a year to determine maximum 3-hour, 24-hour, and annual averages for every receptor in these regions. This model, which is believed to be conservative as applied in this study, was used to identify upper-bound estimates of worst-case impacts. Additional calculations using the Regional Transport Model (RTM) were made for a worst-case regional transport day identified by GPM. The EPA Gaussian, sector-average COMPLEX I Model was applied to evaluate the impact of multiple point ground-level TSP emissions within a given facility on near-source (< 5 km downwind) TSP concentrations for which the GPM calculations are inappropriate. Worst-case photochemical smog and visibility impairment scenarios were evaluated by means of EKMA and PLUVUE, respectively. Acid deposition was evaluated from GPM results.

ANALYSIS RESULTS

Although there is uncertainty in the regional modeling results of this study, this uncertainty was explicitly identified and quantified by providing lower and upper bounds on estimated ground-level concentrations. Even with this uncertainty,* the following major conclusions were made on the basis of this study:

- > Uinta Basin Site-Specifics. The air quality impacts resulting from direct emissions from the five proposed site-specific facilities in the Uinta Basin--Enercor-Mono Power, Magic Circle, Paraho, Syntana-Utah, and Tosco--when evaluated separately or together with other planned projects in the Uinta Basin, will be less than all applicable air quality standards and PSD increments. Near-source, maximum 24-hour average TSP concentrations are close to the Class II PSD increment, however.
- > Uinta Basin Conceptuals. The air quality impacts resulting from direct emissions from the proposed projects in the Uinta Basin that are at a conceptual design stage--Enercor-Mono Power, Geokinetics, and the Sohio tar sands facility--will be within all applicable air quality standards and PSD increments (when emissions are treated separately or together with the site-specifics and other interrelated projects in the Uinta Basin). One exception to this general statement is the possibility that near the Sohio facility the PSD Class II increment for the maximum 24-hour average TSP concentration may be exceeded. This potential violation could be mitigated provided that better TSP emission controls can be implemented in the detailed design phase of this project.
- > Piceance Basin Oil Shale Facilities. All of the proposed oil shale facilities in Colorado can be sited without exceedance of applicable air quality standards and PSD increments, except the Cathedral Bluffs facility which could violate the 24-hour average SO₂ PSD Class II

* Cases in which the use of an upper-bound estimate would result in a conclusion different from that of a lower-bound estimate are identified. Most of the conclusions in this summary are unequivocal even within the estimated range of uncertainty which is as large as an order of magnitude.

increment and possibly the Class I increment in the Flat Tops Wilderness Area (see additional discussion of Flat Tops impacts below). These violations could be avoided if, as recently announced, the Cathedral Bluffs facility is not built or if better emission control technology than that assumed in this analysis could be employed. Maximum 24-hour average TSP concentrations at the site boundaries of a number of these Piceance Basin oil shale facilities will approach the Class II increment.

- > Secondary Emissions. The impacts of associated regional population growth and residential and commercial development (so-called secondary impacts) will be within all applicable standards, except that total suspended particulate (TSP) concentrations, which are currently in excess of standards throughout much of the region, will be exacerbated. Most of this impact is due to windblown dust and dust raised from unpaved and gravel roads. These large particles are not respirable and do not affect regional visibility. In addition, if this fugitive dust from secondary sources is included in the consumption of the PSD increments for TSP, and mitigation measures, such as paving roadways, are not employed, it is quite likely that PSD Class II increments for TSP will be exceeded in much of the region and that PSD Class I increments for TSP in Flat Tops and Mt. Zirkel will be exceeded.*
- > Flat Tops Wilderness. The existing mandatory Class I area with maximum impacts from the proposed synfuel industry in the Uinta and Piceance basins is the Flat Tops Wilderness. If secondary TSP emissions in the Piceance Basin are not mitigated and are counted in the Class I increment consumption, without question there will be a violation of the Class I TSP increment. If not, then the Class I SO₂ increment could be constraining if all the Uinta and Piceance sources are considered and upper-bound estimates of maximum 3- and 24-hour average SO₂ concentrations in

* This possibility raises an interesting policy question. Since in many areas of the study region, ambient air quality standards for TSP are currently exceeded, it is not clear that these areas should remain designated as attainment areas subject to PSD regulations. If these areas are redesignated as nonattainment for TSP, presumably existing TSP emissions would have to be mitigated to provide necessary offsets to accommodate proposed development and population growth.

Flat Tops are utilized. However, even if upper-bound estimates are used and secondary TSP emissions are included in the increment, the Uinta Basin synfuel facilities (both the site-specific and conceptual proposals) could be operated without violations of Class I increments in Flat Tops if some of the Piceance Basin sources are not built. Indeed, the substantial emissions from the proposed Cathedral Bluffs facility dominate impacts in Flat Tops. If this project is shelved indefinitely, as recently announced, the Class I increment is not likely to be consumed in Flat Tops.

- > Dinosaur and Colorado National Monuments. The Dinosaur and Colorado national monuments are currently Federal Class II areas that are under consideration for redesignation to Class I. These areas are also Colorado Category I for SO₂. It is possible, depending on what set of Uinta and Piceance basin emission sources are considered and on whether upper-bound estimates of impacts are utilized, that PSD Class I and Colorado Category I increments would be exceeded in these two areas.
- > Visibility Impairment. Even for the maximum synthetic fuel development scenario studied, regional visual range (visibility) will largely be unaffected by the industrial, commercial, and residential developments. Significant, local reductions in visual range could be observed in stagnant haze layers principally in the winter. These hazes would be caused by TSP emissions from industrial facilities, windblown dust, dust from roadways, and smoke from residential wood stoves and fireplaces. These hazes would be infrequent and localized and would not affect regional visibility and views in wilderness areas. Worst-case reductions in regional visual range are anticipated to occur in the summer when sulfate formation rates are highest. Worst visual range reduction is projected to be less than 10 percent and would be principally due to sulfate aerosol formed in the atmosphere from regional SO₂ emissions from synthetic fuel facilities and power plants. The predicted high TSP concentrations from secondary emissions are not expected to greatly reduce regional visibility. They would only cause local dust clouds. Yellow-brown atmospheric plume discoloration may be visible on fewer than 50 days, primarily on mornings with clear, light-wind, stable conditions in the vicinity of synthetic fuel facilities, on the Uintah/Ouray Indian Reservation, and at Dinosaur National Monument.

- > Acid Deposition. Wet and dry acid deposition in the middle of the developed areas in the Uinta and Piceance basins and in the Grand Junction area is expected to be at rates as great as those experienced currently in large areas of the eastern United States and in Europe. However, at distances beyond about 50 km from development areas, in wilderness areas, and throughout most of the region, deposition rates are expected to be typical of worldwide background conditions.

- > Perspective on Air Quality Impacts. The regional air quality impacts of the proposed synthetic fuel industry can be put in perspective by comparing projected emissions to the atmosphere with other emission sources with which we have more experience. For example, the largest of the synfuel facilities in the Uinta Basin have SO₂ and NO_x emissions rates equivalent to a very well-controlled, 300-Mwe coal-fired power plant. All the projected regional emissions of SO₂ and NO_x from all sources in both the Uinta and Piceance basins for the high-oil-production scenario, which are spread throughout a 15,000 square kilometer region, are the equivalent of the well-controlled emissions from 5000 Mwe of low-sulfur-coal-fired power plant capacity.

CONTENTS

ACKNOWLEDGMENTS.....	ii
EXECUTIVE SUMMARY.....	iii
LIST OF ILLUSTRATIONS.....	xii
LIST OF TABLES.....	xviii
1 INTRODUCTION.....	1-1
1.1 SCOPE OF THE STUDY.....	1-2
1.2 REPORT CONTENTS.....	1-2
2 THE AFFECTED ENVIRONMENT.....	2-1
2.1 TOPOGRAPHY.....	2-1
2.2 METEOROLOGY AND CLIMATOLOGY.....	2-1
2.2.1 Wind Direction.....	2-7
2.2.2 Wind Speeds.....	2-10
2.2.3 Stability.....	2-10
2.2.4 Effect of Terrain on Wind Fields.....	2-15
2.3 EXISTING AIR QUALITY.....	2-15
3 AIR QUALITY IMPACT SIGNIFICANCE CRITERIA.....	3-1
3.1 AMBIENT AIR QUALITY STANDARDS.....	3-1
3.2 PREVENTION OF SIGNIFICANT DETERIORATION.....	3-3
3.3 DETERMINATION OF SIGNIFICANT VISIBILITY IMPAIRMENT.....	3-5
3.4 PROTECTION OF AIR-QUALITY-RELATED VALUES.....	3-6
4 ANALYSIS METHODOLOGY.....	4-1
4.1 DEVELOPMENT OF EMISSION INVENTORIES.....	4-3
4.1.1 Utah Synfuel Projects.....	4-7
4.1.2 Other Planned Projects (Utah).....	4-8
4.1.3 Utah Baseline Point Sources.....	4-11

4.1.4	Colorado Oil Shale, Point, and Area Sources.....	4-13
4.1.5	Utah Baseline Area Sources.....	4-13
4.1.6	Utah Area Sources: Regional High-Oil- Production Scenario.....	4-30
4.1.7	Utah Area Sources: Regional Low-Oil- Production Scenario.....	4-43
4.1.8	Utah Area Source Summary.....	4-46
4.1.9	Socioeconomic Data Comparison for Utah.....	4-46
4.1.10	Concluding Remarks Pertaining to Inventory Activities.....	4-50
4.2	DESCRIPTION OF MODELING APPROACHES.....	4-53
4.2.1	Modeling Methodology.....	4-53
5	REGIONAL AIR QUALITY IMPACTS.....	5-1
5.1	CONCENTRATION ESTIMATION APPROACH.....	5-2
5.2	IMPACTS OF INDUSTRIAL GROWTH.....	5-6
5.2.1	Low-Oil-Production Scenario.....	5-8
5.2.2	High-Oil-Production Scenario.....	5-34
5.3	IMPACTS OF POPULATION AND ASSOCIATED GROWTH.....	5-70
5.3.1	Low-Production Scenario.....	5-70
5.3.2	High-Production Scenario.....	5-87
5.4	CUMULATIVE AIR QUALITY IMPACTS OF ALL REGIONAL EMISSIONS.....	5-87
5.4.1	SO ₂ Impacts.....	5-87
5.4.2	TSP Impacts.....	5-105
5.5	PHOTOCHEMICAL SMOG.....	5-112
5.6	VISIBILITY IMPAIRMENT.....	5-115
5.6.1	Plume Discoloration.....	5-119
5.6.2	Regional Haze.....	5-122
5.7	ACID DEPOSITION.....	5-128
5.8	AIR QUALITY IMPACTS ASSOCIATED WITH CONSTRUCTION ACTIVITIES.....	5-134
6	AIR QUALITY IMPACTS OF SPECIFIC PROPOSED ACTIONS.....	6-1
6.1	ENERCOR-MONO POWER.....	6-2
6.2	MAGIC CIRCLE.....	6-2
6.3	PARAHO	6-22
6.4	SYNTANA-UTAH.....	6-22

6.5	TOSCO.....	6-22
6.6	SUMMARY AND COMPARISON WITH OTHER ANALYSES.....	6-44
APPENDIX A	UPPER LEVEL WIND ROSE STRATIFIED BY SEASON AND TIME OF DAY FOR STUDY REGION IN 1978.....	A-1
APPENDIX B	SURFACE (10 m) WIND ROSE STRATIFIED BY SEASON AND TIME OF DAY AT U-A, U-B SITE IN 1978.....	B-1
APPENDIX C	TECHNICAL DISCUSSION OF MODELS USED IN STUDY.....	C-1
APPENDIX D	LEVEL-1 VISIBILITY SCREENING RESULTS FOR EMISSIONS FROM ALL SYNTHETIC FUEL FACILITIES IN THE REGION AT THE HIGH OIL PRODUCTION RATES.....	D-1
REFERENCES.....		R-1

LIST OF ILLUSTRATIONS

1-1	Locations of Sources, Towns, Counties, and Mandatory and Potential Class I Areas in Study Region.....	1-5
2-1	Terrain Elevation Contours (ft MSL) in Study Region.....	2-2
2-2	Perspective of Terrain in Study Region.....	2-3
2-3	Average Upper Air Wind Rose for Study Region.....	2-5
2-4	Wind Direction Frequency Distributions for All Morning Soundings.....	2-8
2-5	Vertical Wind Direction Distribution Profiles for All Afternoon Soundings.....	2-9
2-6	Wind Speed Frequency Distributions for All Morning Soundings.....	2-11
2-7	Wind Speed Frequency Distributions for All Afternoon Soundings.....	2-12
2-8	Computed Wind Fields for Eight Synoptic Wind Directions for the Study Region (Lowest Modeled Layer from 4300 ft MSL or Terrain Elevation, to 6800 ft MSL).....	2-17
2-9	Computed Wind Fields for Down-Slope and Up-Slope Flow Conditions and Zero Upper-Air Winds (Lowest Modeled Layer from 4300 ft MSL or Terrain Elevation, to 6800 ft MSL).....	2-25
2-10	Existing Annual Average SO ₂ Concentrations (µg/m ³).....	2-28
2-11	Correlations between TSP Emissions and Ambient Concentrations.....	2-31
2-12	Model Estimates of Existing Total Suspended Particulate (TSP) Concentrations in Study Region.....	2-32

2-13	Frequency Distribution of Visual Range at Dinosaur National Monument in Summer 1979.....	2-34
4-1	Overall Flow Diagram of Analysis Methodology.....	4-2
4-2	Schematic Diagram of Activities for the Emission Inventory Development Process.....	4-4
4-3	Area Emission Source Inventory for the Study Region in the Baseline Year 1980 (tons/yr/100 km ²).....	4-33
4-4	Total Cumulative Population in the Uinta Basin with High-Level Synfuel Development.....	4-52
4-5	Schematic Diagram of Modeling Methodology.....	4-55
4-6	3-D Perspective of Terrain in Regional Modeling Area.....	4-62
4-7	Temporal Variation of First Grid Layer Depth.....	4-68
4-8	Schematic Diagram of Methodology for Applying the Complex-Terrain Wind Model (CTWM) in the "Composite" Mode.....	4-73
4-9	Spatial Distribution of Land Use Categories.....	4-78
5-1	24-Hour SO ₂ Concentration Estimates for 27 July 1978 from Direct Source SO ₂ Emissions and for the High Oil Production Scenario.....	5-4
5-2	Schematic Representation of Estimated Ranges in the Regional Air Quality Impacts Assessment.....	5-7
5-3	Impact of Direct Source Emissions from Moon Lake Unit 2 on Ground-Level SO ₂ Concentrations (µg/m ³).....	5-9
5-4	Impact of Direct Source Emissions from Moon Lake Unit 2 on Ground-Level TSP Concentrations (µg/m ³).....	5-12
5-5	Impact of Direct Source Emissions from White River Shale Project on Ground-Level SO ₂ Concentrations (µg/m ³).....	5-14

5-6	Impact of Direct Source Emissions from White River Shale Project on Ground-Level TSP Concentrations ($\mu\text{g}/\text{m}^3$)	5-17
5-7	Impact of Direct Source Emissions from Uinta Basin Site-Specifics on Ground-Level SO_2 Concentrations ($\mu\text{g}/\text{m}^3$) for Low Oil Production Scenario.....	5-19
5-8	Impact of Direct Source Emissions from Uinta Basin Site-Specifics on Ground-Level TSP Concentrations ($\mu\text{g}/\text{m}^3$) for Low Oil Production Scenario.....	5-22
5-9	Impact of Direct Source Emissions from Uinta Basin Site-Specifics and Conceptuals on Ground-Level SO_2 Concentrations ($\mu\text{g}/\text{m}^3$) for Low Oil Production Scenario.....	5-24
5-10	Impact of Direct Source Emissions from Uinta Basin Site-Specifics on Ground-Level TSP Concentrations ($\mu\text{g}/\text{m}^3$) for Low Oil Production Scenario.....	5-27
5-11	Impact of Direct Source Emissions from Colorado Emission Sources on Ground-Level SO_2 Concentrations ($\mu\text{g}/\text{m}^3$) for the Low Oil Production Scenario.....	5-29
5-12	Impact of Direct Source Emissions from Colorado Point Sources on Ground-Level TSP Concentrations ($\mu\text{g}/\text{m}^3$) for Low Oil Production Scenario.....	5-32
5-13	Impact of Direct Source Emissions on Ground-Level SO_2 Concentrations ($\mu\text{g}/\text{m}^3$) for the Low Oil Production Scenario.....	5-35
5-14	Impact of Direct Source Emissions on Ground-Level TSP Concentrations ($\mu\text{g}/\text{m}^3$) for the Low Oil Production Scenario.....	5-38
5-15	Impact of Direct Source Emissions from Uinta Basin Site-Specifics on Ground-Level SO_2 Concentrations ($\mu\text{g}/\text{m}^3$) for the High Oil Production Scenario.....	5-40
5-16	Impact of Direct Source Emissions from Uinta Basin Site-Specifics on Ground-Level TSP Concentrations ($\mu\text{g}/\text{m}^3$) for the High Oil Production Scenario.....	5-43

5-17	Impact of Direct Source Emissions from Uinta Basin Site-Specifics and Conceptuals on Ground-Level SO ₂ Concentrations (µg/m ³) for the High Oil Production Scenario.....	5-45
5-18	Impact of Direct Source Emissions from Uinta Basin Site-Specifics and Conceptuals on Ground-Level TSP Concentrations (µg/m ³) for the High Oil Production Scenario.....	5-48
5-19	Maximum 24-Hour Average, Near-Source TSP Concentrations (µg/m ³) Resulting from Direct Source Emissions from the Sohio Conceptual Tar Sands Facility on the Basis of COMPLEX-I Calculations.....	5-51
5-20	Impact of Direct Source Emissions from Colorado Point Sources on Ground-Level SO ₂ Concentrations (µg/m ³) for the High Oil Production Scenario.....	5-52
5-21	Impact of Direct Source Emissions from Colorado Point Sources on Ground-Level TSP Concentrations (µg/m ³) for the High Oil Production Scenario.....	5-55
5-22	Maximum 24-Hour Average Near Source TSP Concentrations Resulting from Direct Source Emissions from Oil Shale Facilities in the Piceance Basin of Colorado Based on COMPLEX-I.....	5-57
5-23	Maximum Near-Source SO ₂ Concentrations Resulting from Direct Source Emissions from Cathedral Bluffs on the Basis of COMPLEX-I Calculations.....	5-68
5-24	Impact of Direct Source Emissions on Ground-Level SO ₂ Concentrations (µg/m ³) for the High Oil Production Scenario.....	5-71
5-25	Impact of Direct Source Emissions on Ground-Level TSP Concentrations (µg/m ³) for the High Oil Production Scenario.....	5-74
5-26	Impact of Area Source Emissions on Ground-Level SO ₂ Concentrations (µg/m ³) for the Low Oil Production Scenario.....	5-76

5-27	Impact of Area Source Emissions on Ground-Level TSP Concentrations ($\mu\text{g}/\text{m}^3$) for the Low Oil Production Scenario.....	5-79
5-28	Area Source Emission Densities for Low Oil Production Scenario ($\text{tons}/\text{yr}/100 \text{ km}^2$).....	5-81
5-29	Impact of Area Source Emissions on Ground-Level SO_2 Concentrations ($\mu\text{g}/\text{m}^3$) for the High Oil Production Scenario.....	5-88
5-30	Impact of Area Source Emissions on Ground-Level TSP Concentrations ($\mu\text{g}/\text{m}^3$) for the High Oil Production Scenario.....	5-91
5-31	Area Source Emission Densities for High Oil Production Scenario ($\text{tons}/\text{yr}/100 \text{ km}^2$).....	5-93
5-32	Summary of SO_2 Concentration Estimates for Various Averaging Times Compared to Air Quality Standards and PSD Increments.....	5-106
5-33	Summary of TSP Concentration Estimates for Various Averaging Times Compared to Ambient Air Quality Standards and PSD Increments for Both the Low and High Oil Production Scenarios.....	5-113
5-34	Two Trajectories Modeled for Worst-Case Photochemical Oxidant (Ozone) Impact.....	5-114
5-35	Cumulative Frequency of Perceptible Plume Discoloration Resulting from Emissions from Various Uinta Basin Sources at Dinosaur National Monument.....	5-123
5-36	Cumulative Frequency of Perceptible Plume Discoloration Resulting from Emissions from Various Uinta Basin Sources at Uintah and Ouray Indian Reservation.....	5-125
5-37	Annual Sulfur Anion Dry Deposition ($\text{G}/\text{M}^2/\text{yr}$) for the High Oil Production Scenario.....	5-132
5-38	Annual Nitrogen Anion Dry Deposition ($\text{G}/\text{M}^2/\text{yr}$) for the High Oil Production Scenario.....	5-133

6-1	Ground-Level SO ₂ Concentrations (μg/m ³) due to Enercor-Mono Power Emissions.....	6-5
6-2	Ground-Level TSP Concentrations (μg/m ³) due to Enercor-Mono Power Emissions.....	6-8
6-3	Ground-Level SO ₂ Concentrations (μg/m ³) due to Magic Circle Emissions.....	6-14
6-4	Ground-Level TSP Concentrations (μg/m ³) due to Magic Circle Emissions.....	6-17
6-5	Ground-Level SO ₂ Concentrations (μg/m ³) due to Paraho Emissions.....	6-26
6-6	Ground-Level TSP Concentrations (μg/m ³) due to Paraho Emissions.....	6-29
6-7	Ground-Level SO ₂ Concentrations (μg/m ³) due to Syntana-Utah Emissions.....	6-37
6-8	Ground-Level TSP Concentrations (μg/m ³) due to Syntana-Utah Emissions.....	6-40
6-9	Ground-Level SO ₂ Concentrations (μg/m ³) due to Tosco Emissions.....	6-48
6-10	Ground-Level TSP Concentrations (μg/m ³) due to Tosco Emissions.....	6-51

LIST OF TABLES

1-1	Uinta Basin Synthetic Fuel Facilities.....	1-3
1-2	Piceance Basin Oil Shale Facilities.....	1-4
1-3	Industrial Facilities in Study Region.....	1-6
2-1	Frequency of Occurrence of Atmospheric Stability at the 500-m Level (AGL).....	2-13
2-2	Seasonal and Annual-Average Morning and Afternoon Mixed-Layer Heights and Wind Speeds for Grand Junction, Colorado.....	2-16
2-3	Measured Ambient Concentrations of Total Suspended Particulates (TSP) in Study Region.....	2-29
3-1	Applicable State and Federal Ambient Air Quality Standards.....	3-2
3-2	Prevention of Significant Deterioration Increments.....	3-3
3-3	EPA Significant (de minimis) Emission Rates.....	3-4
3-4	Categories of Potential Air Quality Impacts on Air-Quality-Related Values of Class I Areas.....	3-7
4-1	Production and Emission Rates for Utah Synfuel Projects-- High-Oil-Production Scenario.....	4-9
4-2	Production and Emission Rates for Utah Synfuel Projects-- Low-Oil-Production Scenario.....	4-10
4-3	Emission Totals for Other Planned Projects in Utah.....	4-12
4-4	Emission Totals for Baseline Point Sources in Utah.....	4-14
4-5	Emission Totals for Colorado Oil Shale Projects.....	4-15

4-6	Emission Totals for Non-Oil Shale Sources in Colorado.....	4-17
4-7	Area Source Categorization Scheme.....	4-18
4-8	Emission Factors for 1980 Baseline.....	4-21
4-9	Area Source Spatial Allocation Parameters.....	4-29
4-10	1980 Baseline Area Source Emission Inventory for Uintah County.....	4-31
4-11	1980 Baseline Area Source Emission Inventory for Grand County.....	4-32
4-12	Emission Factors for On-Road Motor Vehicles (Exhaust) for 1990.....	4-40
4-13	Area Source Projection Parameters.....	4-41
4-14	Regional High Oil Production Scenario Area Source Emission Inventory for Uintah County.....	4-44
4-15	Regional High Oil Production Scenario Area Source Emission Inventory for Grand County.....	4-45
4-16	Regional Low Oil Production Scenario Area Source Emission Inventory for Uintah County.....	4-47
4-17	Regional Low Oil Production Scenario Area Source Emission Inventory for Grand County.....	4-48
4-18	Emission Totals for Area Sources in Utah.....	4-49
4-19	Total Population for 1990 Regional Scenarios (NPS).....	4-51
4-20	Summary of the Relative Capabilities of the Models Used in This Study.....	4-59
4-21	Morning Stable Layer Depths from the Four Upper-Air Stations, and the Average Used by RTM.....	4-66
4-22	USGS Land Use Categories.....	4-76
4-23	Land Use Categories, Surface Roughness Lengths, and Deposition Velocities for the Study Area.....	4-79

5-1	Summary of Ambient Air Quality Impacts Associated with the Low Oil Production Scenario.....	5-99
5-2	Summary of Ambient Air Quality Impacts Associated with the High Oil Production Scenario.....	5-102
5-3	Summary of Ambient Air Quality Impacts Associated with the Low Oil Production Scenario.....	5-108
5-4	Summary of Ambient Air Quality Impacts Associated with the High Oil Production Scenario.....	5-110
5-5	Summary of EKMA Results for Trajectory 1.....	5-116
5-6	Summary of EKMA Results for Trajectory 2.....	5-117
5-7	Magnitude [$\Delta(L*a*b^*)$] of Plume Discoloration.....	5-120
5-8	Particle Size Distributions and Deposition Velocities Assumed in Visibility Model Simulations.....	5-129
5-9	Worst-Case Reduction of Visual Range for a View from Flat Tops Wilderness Area Looking Toward the Northwest.....	5-130
5-10	Summary of World-Wide Wet and Dry, Sulfuric and Nitric Acid Deposition Measurements.....	5-135
6-1	Summary of PSD Increment Consumption by Enercor-Mono Power.....	6-3
6-2	Summary of Maximum Ambient Air Quality Impacts of Enercor-Mono Power Compared with Applicable Standards.....	6-4
6-3	Level-1 Screening Analysis Results for Visibility Impacts of Enercor-Mono Power.....	6-10
6-4	Summary of PSD Increment Consumption by Magic Circle.....	6-11
6-5	Summary of Maximum Ambient Air Quality Impacts of Magic Circle Compared with Applicable Standards.....	6-13
6-6	Level-1 Screening Analysis Results for Visibility Impacts of Magic Circle.....	6-21

6-7	Summary of PSD Increment Consumption by Paraho.....	6-23
6-8	Summary of Maximum Ambient Air Quality Impacts of Paraho Compared with Applicable Standards.....	6-25
6-9	Level-1 Screening Analysis Results for Visibility Impacts of Paraho.....	6-33
6-10	Summary of PSD Increment Consumption by Syntana.....	6-34
6-11	Summary of Maximum Ambient Air Quality Impacts of Syntana Compared with Applicable Standards.....	6-36
6-12	Level-1 Screening Analysis Results for Visibility Impacts of Syntana.....	6-43
6-13	Summary of PSD Increment Consumption by Tosco.....	6-45
6-14	Summary of Maximum Ambient Air Quality Impacts of Tosco Compared with Applicable Standards.....	6-47
6-15	Level-1 Screening Analysis Results for Visibility Impacts of Tosco.....	6-55
6-16	Summary of Model Approaches Used by Applicants.....	6-56
6-17	Comparison of Worst-Case Calculations of 24-Hour Concentrations near Specific Proposed Synthetic Fuel Facilities.....	6-57

1 INTRODUCTION

Plans are being made to produce synthetic fuels from oil shale and tar sand deposits in the Piceance Basin of Colorado and the Uinta Basin of Utah. The air quality impact of this development is an important environmental concern to government, industry, and many citizens. This concern arises because of the substantial industrial development and population growth that is projected in a region that currently has nearly pristine air quality, surrounded by several national parks, national monuments, and wilderness areas. Concerns related to air quality impacts range from such regulatory issues as consumption of Prevention of Significant Deterioration (PSD) increments and ground-level concentrations compared with federal and state ambient air quality standards to air quality impacts that are not regulated by specific numerical limits, such as visibility impairment and acid deposition. Air quality impacts of individual industrial facilities, cumulative regional industrial development (primarily energy-related) and cumulative regional development associated with population growth are concerns that were analyzed in this study.

This report documents an analysis of air quality impacts that was performed by Systems Applications, Inc. for the Bureau of Land Management (BLM) of synthetic fuel development in the Uinta Basin of Utah. This analysis is to support the Environmental Impact Statement (EIS) that BLM is preparing for each of five specific synthetic fuel developments and cumulative regional impacts. The cumulative impacts of regional emissions to the atmosphere from these five projects, from other planned energy developments in the Uinta and Piceance basins, and from additional development and activities associated with regional population growth were studied.

The current study is more detailed than the previous policy and screening analyses of air quality impacts in the region performed by both Systems Applications (Anderson et al., 1980 and 1981; Latimer and Doyle, 1981) and Los Alamos Scientific Laboratory (Williams et al., 1981). The current report is based on (1) detailed emission inventories developed by synthetic fuel developers, Systems Applications, and PEDCo Environmental, Inc. (1981); (2) measured meteorological conditions in the region; and (3) additional regional data such as ambient air quality, topography, and visibility.

1.1 SCOPE OF THE STUDY

The primary objective of the study was to evaluate the air quality impacts of five synthetic fuel facilities proposed to be developed in the Uinta Basin: Enercor-Mono Power (Rainbow site), Magic Circle, Paraho, Syntana-Utah, and Tosco. Three additional facilities that are in a conceptual-design phase--Enercor-Mono Power (PR Springs site), Geo-kinetics, and Sohio--were also studied in regional scenarios. The impacts associated with two levels of production from each of these facilities was studied. Table 1-1 summarizes the production levels.

Since cumulative regional impacts were considered to be important in this study, other industrial facilities were also examined. In the Uinta Basin these included the Moon Lake power plant (units 1 and 2), White River oil shale project (100,000 barrel per day capacity), Plateau refinery, and five other small projects. In the Piceance Basin in Colorado, the air quality impacts of the oil shale facilities listed in table 1-2 were included in regional assessments. The total synthetic fuel production in the Uinta and Piceance basins studied in the high- and low-oil-production scenarios was 1,059,500 and 492,000 barrels per day, respectively.

Figure 1-1 shows the 180 x 268-km region studied in this analysis and the locations of the major industrial facilities, towns, and state and county boundaries. Also shown are Flat Tops Wilderness Area, the only federal PSD Class I area in the study region, and Dinosaur and Colorado national monuments, which are currently federal Class II and Colorado category I areas but may potentially be redesignated federal Class I. Outside, but adjacent to the study region, are the Mt. Zirkel and Maroon Bells/Snowmass wilderness areas, which are currently Federal Class I areas, and the Uinta Primitive Area, which may be redesignated Class I. Table 1-3 provides a legend for the industrial facilities (shown in figure 1-1) that were studied in the regional air quality analysis.

1.2 REPORT CONTENTS

This report is divided into six sections. Section 2 discusses the topography, climatology, meteorology, and existing air quality of the study region shown in figure 1-1. The criteria for judging the significance of air quality impacts, such as federal and state ambient air quality standards and Prevention of Significant Deterioration (PSD)

TABLE 1-1. UINTA BASIN SYNTHETIC FUEL FACILITIES

Project	Oil-Production Capacity (bpd)	
	Low Production	High Production
Enercor-Mono Power		
Rainbow ^a (tar sand)	5,000	5,000
P.R. Springs ^b (tar sand)	15,000	50,000
Magic Circle ^a (oil shale)	16,400	31,500
Paraho ^a (oil shale)	10,500	42,000
Syntana-Utah ^a (oil shale)	16,500	57,000
Tosco ^a (oil shale)	22,000	45,000
Geokinetics (oil shale)		
Lofreco (in-situ) ^b	20,000	50,000
Agency Draw ^b	11,000	20,000
Sohio Shale Oil ^b (tar sand)	5,000	20,000
Total	121,400	320,500

Note: bpd = barrels per calendar day.

^a Site-specific project.

^b Conceptual project.

TABLE 1-2. PICEANCE BASIN OIL SHALE FACILITIES*

Project	Oil-Production Capacity (bpd)	
	Low Production	High Production
Cathedral Bluffs	94,000	94,000
Chevron	15,000	100,000
Colony	47,000	47,000
Exxon	0	47,000
Getty	0	15,000
Mobil	0	50,000
Multimineral	0	50,000
Naval Oil Shale Reserve	0	50,000
Rio Blanco	50,000	86,000
Superior	15,000	15,000
Union	50,000	50,000
Total	271,000	639,000

* Development plans in Colorado are uncertain as suggested by several recent project modifications, delays, and cancellations. Therefore, the low- and high-production scenarios assumed for Colorado are quite speculative and indicative of general development plans at the time this study was started.

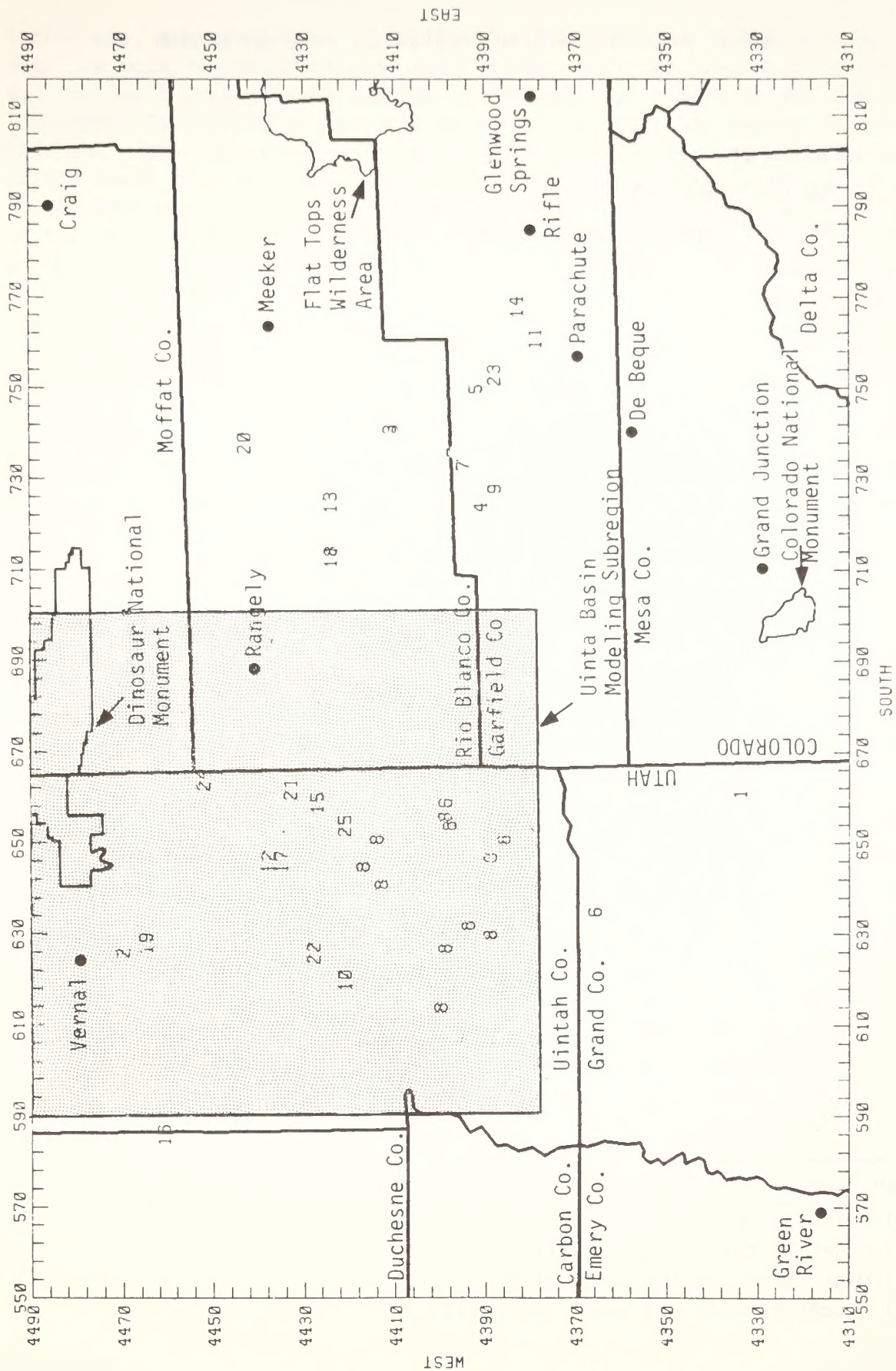


FIGURE 1-1. LOCATIONS OF SOURCES, TOWNS, COUNTIES, AND MANDATORY AND POTENTIAL CLASS I AREAS IN STUDY REGION

TABLE 1-3. INDUSTRIAL FACILITIES IN STUDY REGION

1. Baker (O)
2. C&A Tar Sands (O)
3. Cathedral Bluffs, C-b site (P)
4. Chevron (P)
5. Colony (P)
6. Enercor-Mono Power (U)
7. Exxon (P)
8. Geokinetics (U)
9. Getty (P)
10. Magic Circle (U)
11. Mobil (P)
12. Moon Lake Power Plant (E, O)
13. Multimineral (P)
14. Naval Oil Shale (P)
15. Paraho (U)
16. Plateau Refinery (E, O)
17. Ramex (O)
18. Rio Blanco, C-a site (P)
19. Sohio (U)
20. Superior (P)
21. Syntana (U)
22. Tosco (U)
23. Union (P)
24. Western Tar Sands (O)
25. White River, U-a, U-b site (O)

Legend:

- (E) Existing source in 1980
- (O) Other planned sources (Uinta Basin)
- (U) Uinta Basin synfuel facilities
- (P) Piceance Basin oil shale facilities

increments, are summarized in section 3. The emission inventory development and modeling methodologies used in the study are presented in section 4. Section 5 presents the cumulative air quality impacts of all the industrial facilities and associated growth in the study region for the low- and high-synthetic-fuel-production scenarios. Impacts are segregated on the basis of direct source (primary) emissions and associated area (secondary) emissions. In this section the cumulative impacts of regional emissions on photochemical smog, visibility, and acid deposition are also presented. Section 6 presents the air quality impacts calculated for each of the five specific Uinta Basin synthetic fuel facilities--Enercor-Mono Power, Magic Circle, Paraho, Syntana-Utah, and Tosco. These air quality impacts are projected for the high-production scenarios. Impacts are presented separately for each of the facilities and together with the impacts of other sources (i.e., planned projects and existing sources).

2 THE AFFECTED ENVIRONMENT*

In this section we discuss the topography, climatology (including wind direction, wind speed, and atmospheric stability), and existing air quality of the study region.

2.1 TOPOGRAPHY

The 180 x 268-km study region (see figure 1-1) in which oil shale and tar sands development is planned is on the western slope of the Rockies in eastern Utah and northwestern Colorado. It is characterized by complex terrain (i.e., mountains and valleys), but large portions of the region are relatively flat plateaus. Figures 2-1 and 2-2 show terrain elevation contours and a perspective plot of the study region. Note the Colorado River cutting through the southern portion of the region near Grand Junction. The Uinta Basin is in relatively flat, high plateau country in the northwestern portion of the study region. The region becomes progressively more elevated, rugged, and mountainous to the east, where parts of the Flat Tops Wilderness Area lie above 10,000 ft MSL.

2.2 METEOROLOGY AND CLIMATOLOGY

The climate of the region is arid. Because of the typically dry atmosphere, there is a high frequency of occurrence of bright, sunny days and clear nights. The clear atmosphere, in turn, allows rapid heating of the ground surface during daylight hours and rapid cooling in the dark. Since heated air rises and cooled air falls, winds tend to blow up-slope during daytime and down-slope at night.

The up- and down-slope cycle occurs at all geographic scales; that is, the tendency can be noted on canyon walls, river courses, mountains, and mountain range slopes. The larger the horizontal scale of the geographic feature, the greater is the volume of air that moves, and the

* Portions of this section were excerpted from appendix H, entitled "Meteorological Characterization," by Anderson et al. (1981).



FIGURE 2-1. TERRAIN ELEVATION CONTOURS (FT MSL) IN STUDY REGION

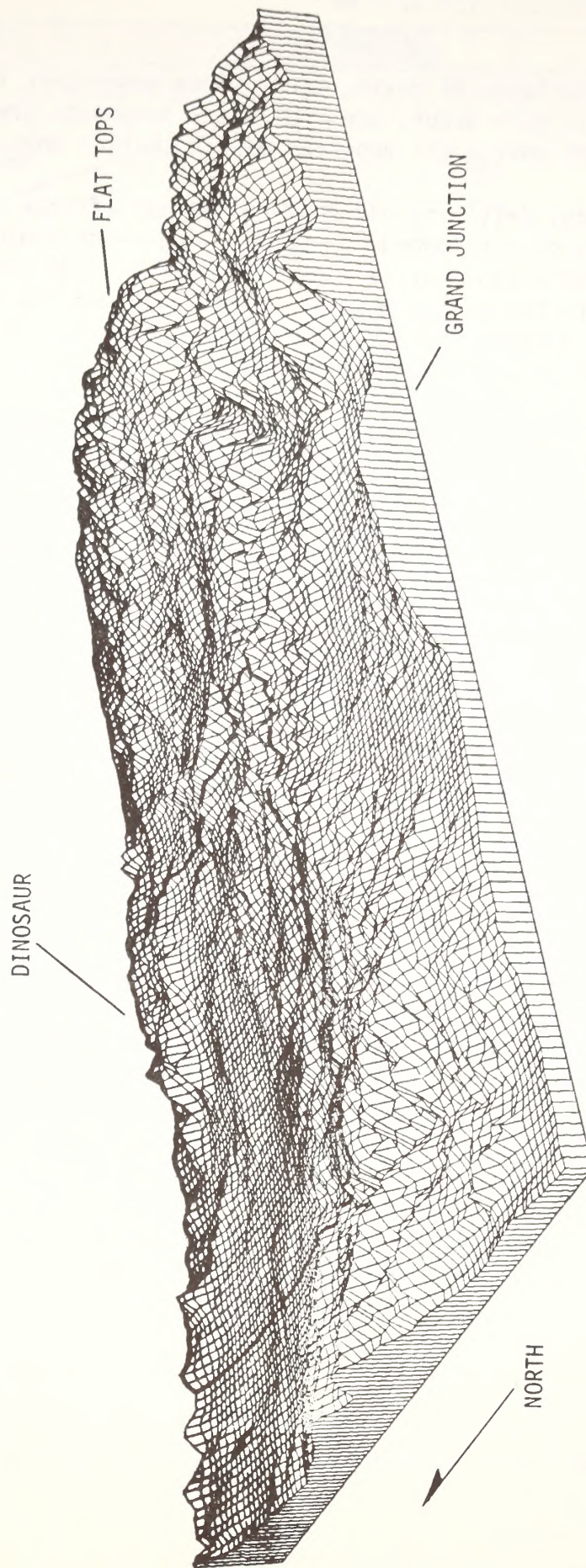


FIGURE 2-2. PERSPECTIVE OF TERRAIN IN STUDY REGION

Note: Dark internal boundaries delineate the Uinta Basin subregion.

thicker is the layer of moving air. Since geographic features of many scales overlies each other, the cyclic air movements are also complex, with thin layers of moving air embedded within thicker ones.

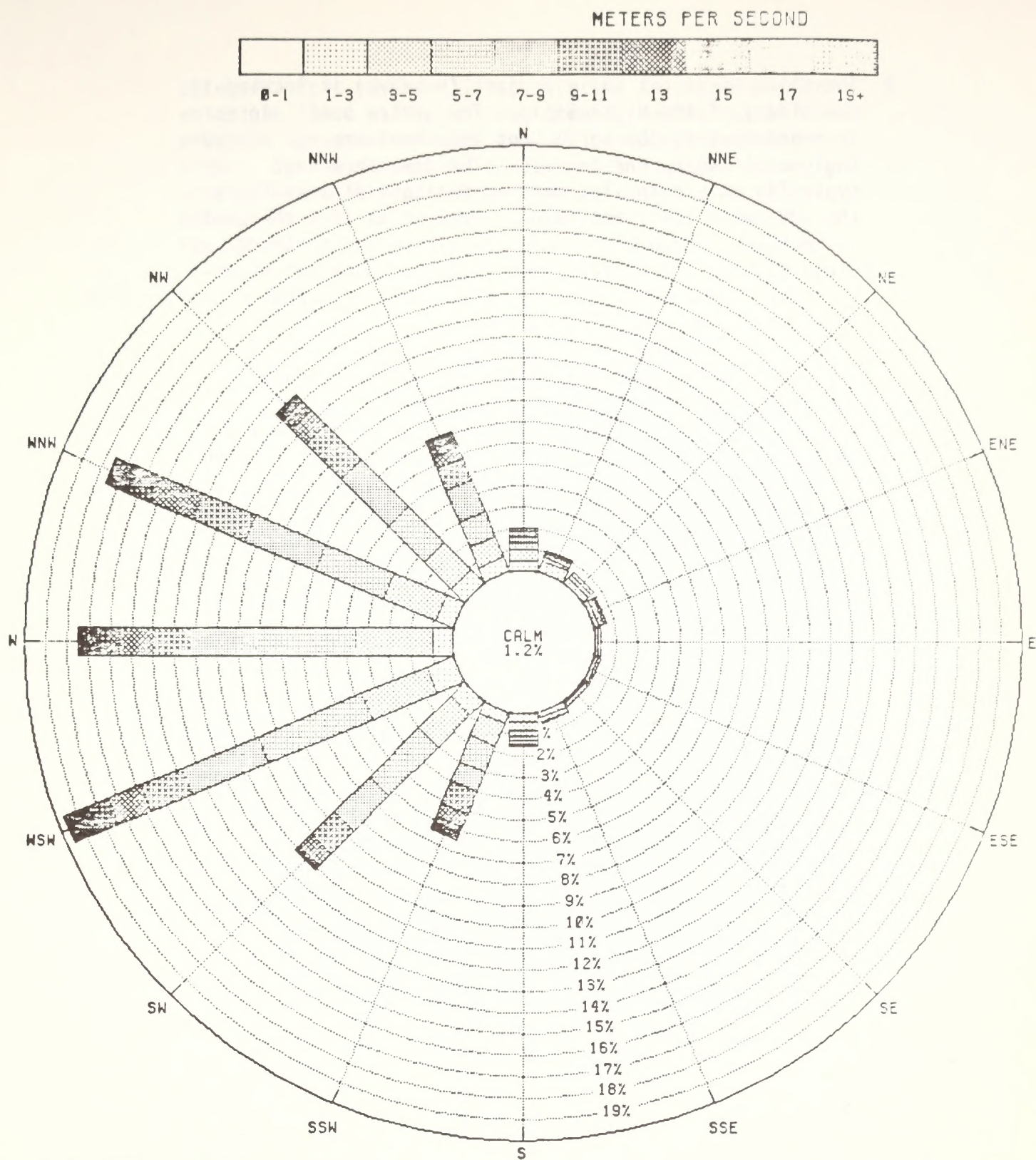
The winds, driven by alternating thermal effects are, in turn, perturbations of, and embedded within, larger-scale wind systems called "synoptic," or weather-scale winds. Synoptic winds are predominantly west to east, characterized by weather variations from day to day and significant guiding (channeling) by regional and local topography; that is, winds blow around hills and through valleys.

In this study, upper-level winds measured by the National Weather Service in 1978 and 1979 in Denver and Grand Junction, Colorado; Lander, Wyoming; and Salt Lake City, Utah, were averaged to characterize the upper-air synoptic flow. Winds at 6000 feet above ground level from each of these four NWS stations were used to derive figure 2-3, which shows a wind rose for the study region. See Appendix A for a more detailed breakdown of this gross wind rose. Note that flow is almost always from the western sectors, the west-southwesterly winds being most frequent. Although upper-air winds are largely unaffected by the complex terrain in the study region, the lower-level winds are influenced by such terrain.

To characterize local low-level flows, we used measurements at the following four sites in the study region:

- > Uinta Basin: the White River oil shale project site, tracts U-a, U-b (see site 25 in figure 1-1; see Appendix B for wind rose).
- > Piceance Basin: the Cathedral Bluffs oil shale project site, tract C-b (see site 3 in figure 1-1).
- > Grand Junction, Colorado.
- > Craig, Colorado.

These areas, which are of particular interest because each will be intensively developed, have the following characteristics:



Note: Based on the average of winds measured at NWS sites 6000 feet above ground level.

FIGURE 2-3. AVERAGE UPPER AIR WIND ROSE FOR STUDY REGION

- > The White River oil shale project (U-a/U-b) is located in the middle of the Uinta Basin. The entire basin slopes downward towards the north, but the winds are not exceedingly confined by the terrain. The data show that typically only a shallow morning drainage flow exists at the 300-meter level and below. Weak winds from the south to southwest predominate. In the afternoon, northwest up-slope flow at the surface, and south to southwest synoptic-scale* winds above the first 150 meters of the atmosphere are frequent.
- > The Cathedral Bluffs (C-b) site typically has shallow drainage flows in the morning. Above the first 150 meters, morning and afternoon winds are most often from the south to southwest. There is a tendency for up-slope northwesterly winds to occur in the summer and fall. Wind speeds are stronger than at the U-a/U-b site, particularly in the morning.
- > The Grand Junction, Colorado, site is located in the wide, deep Grand Valley of the Colorado river, and wind flow is highly confined. An up-slope/down-slope diurnal drainage cycle at least 500 meters in depth prevails all through the year. In the winter, the drainage flow that is only a nighttime phenomenon in other seasons persists through the afternoon on approximately 15 percent of the days.
- > The Craig, Colorado, site also experiences up-slope and down-slope flow conditions and channeling of winds, with northeasterly morning drainage winds and southwesterly afternoon winds.
- > At all sites, winter is the season in which the most stable atmosphere[†] occurs; Pasquill-Gifford E stability

* Synoptic-scale motions are those typically thought of as "weather," with high or low pressure systems of a few hundred to a few thousands of kilometers in extent.

[†] A stable atmosphere is one in which turbulent air motions tend to die out. In the Pasquill-Gifford classification system, the most unstable, turbulent air is classed "A," the most stable, smooth air "G". D represents a neutrally stable condition.

category often exists all day. Spring is the season in which the least stable morning occurs; neutral conditions are just as common or more common than unstable conditions. In the summer and fall, conditions tend to be stable in the morning and neutral or unstable in the afternoon.

2.2.1 Wind Direction

In figure 2-4, we compare the annual morning wind-direction frequency distribution at the 150-meter, 300-meter, 500-meter, and 1000-meter levels for all sites. In the morning, at all sites, there is a great deal of vertical wind shear, that is, the wind speed or direction varies with height above the ground. The shape of each site's wind-direction distribution curves is unique at the lower levels, but each resolves toward the west-southwesterly upper-air flow shown in figure 2-5. This occurrence demonstrates the importance of the complex terrain on lower-level wind directions.

The vertical wind-direction distribution profiles for the afternoon (figure 2-5) differ from the morning wind patterns. In general, in the afternoon, the vertical wind shear is much less at all sites, and the winds at the lower levels tend to be more westerly as are the 1000-meter winds (which change little from the morning). This phenomenon occurs because the atmosphere is well mixed in the afternoon, and the surface winds become coupled with the steady, persistent upper-level winds.

The Grand Junction site is in the Grand Valley, a wide and deep valley along the Colorado River. Here, as a result of the confining terrain, winds at the 500-meter level are nearly exclusively down-slope in the morning and up-slope in the afternoon. The Grand Junction drainage cycle occurs at least up to the 1000-meter level.

Because of its relatively high elevation, the Cathedral Bluffs (C-b) site does not have a well-defined drainage flow. High terrain rings the site from southwest to southeast, and at the 150-meter level the winds are well distributed from east to west. Above 150 meters the winds are predominantly southerly to southwesterly. In the afternoon, southerly to southwesterly flow predominates at the 500-meter level and below. The winds become more westerly at the 1000-meter level.

A diurnal wind cycle is evident at Craig and at the White River project (U-a/U-b) as well. At Craig, a morning east-drainage wind dominates up to the the 300-meter level. In the afternoon, the up-slope

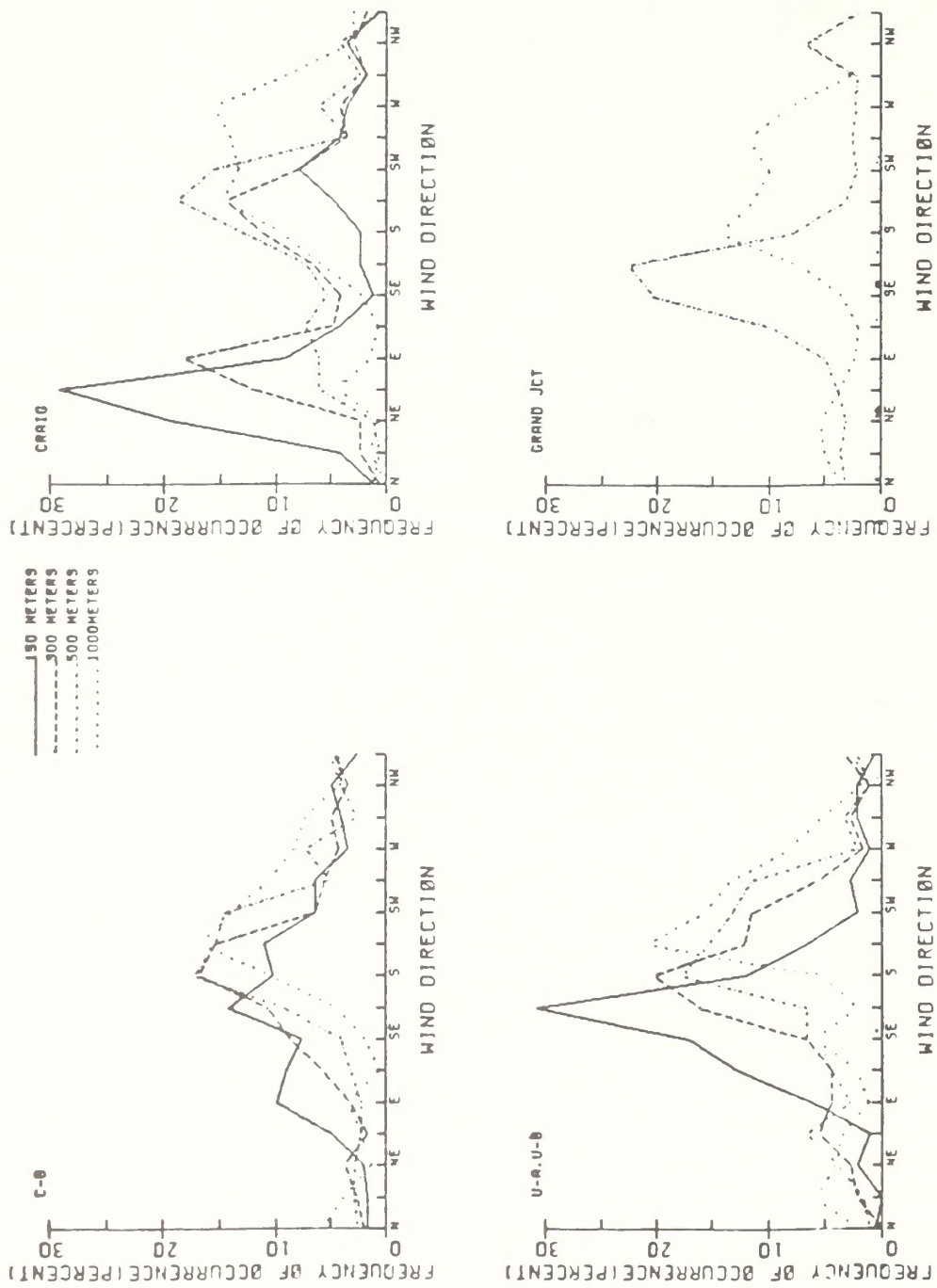


FIGURE 2-4. WIND DIRECTION FREQUENCY DISTRIBUTIONS FOR ALL MORNING SOUNDINGS

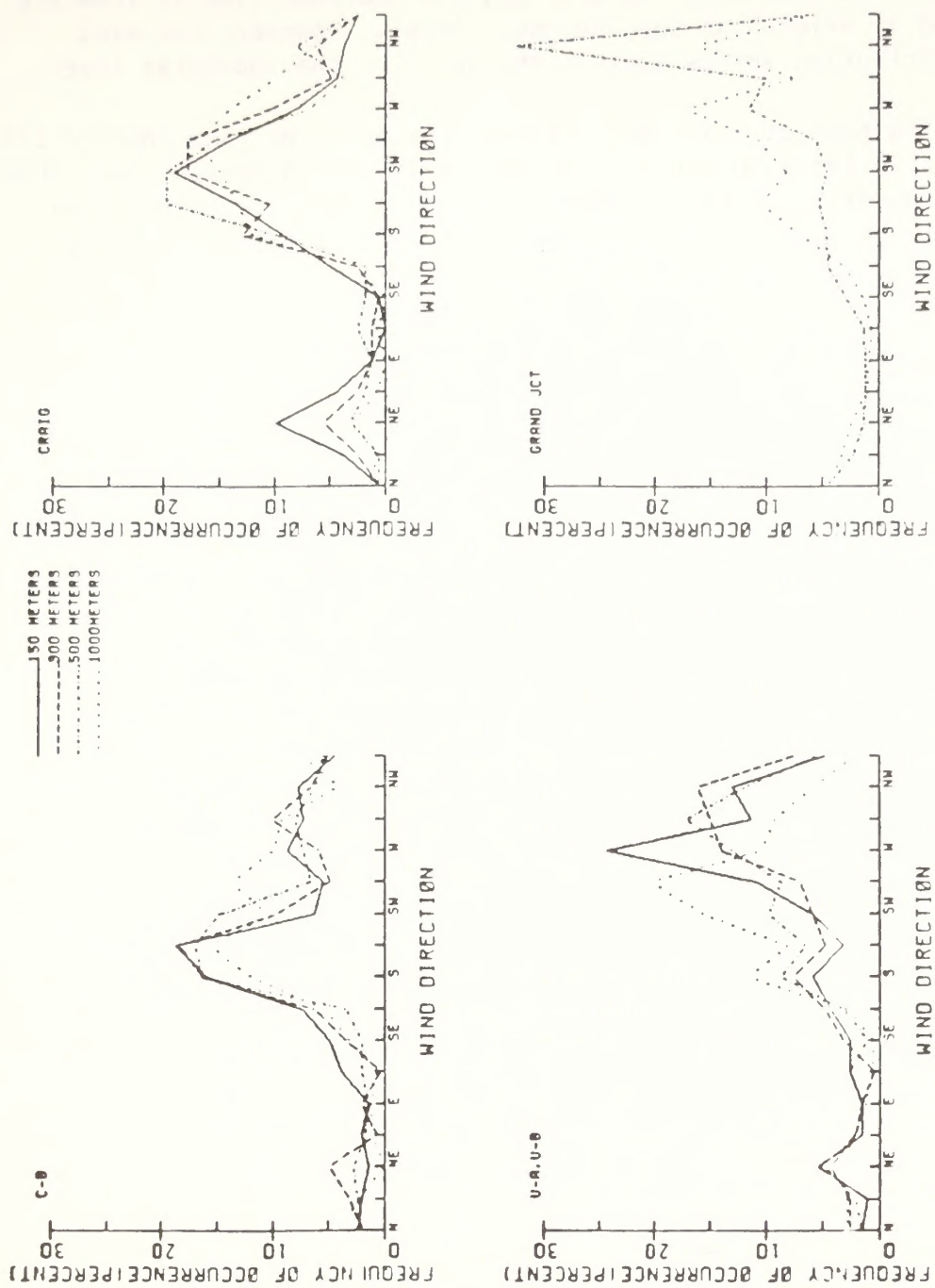


FIGURE 2-5. VERTICAL WIND DIRECTION DISTRIBUTION PROFILES FOR ALL AFTERNOON SOUNDINGS

and synoptic-scale winds reinforce each other, and the winds are predominantly westerly. The morning drainage flow on the U-a/U-b tract is shallower than that at Craig. At U-a/U-b, the drainage flow is from the southeast, and is evident at the 150-meter level. However, the wind direction distribution shifts towards the south by the 300-meter level.

In the afternoon at U-a/U-b, northwesterly up-slope flow (penetrating up to 500 meters) tends to occur more frequently over a deeper layer than does the morning drainage flow. Low-level wind speeds increase in the afternoon, but they still do not approach the wind speeds at Cathedral Bluffs (C-b).

2.2.2 Wind Speeds

The wind-speed distributions in the morning and afternoon for the 150-meter, 300-meter, 500-meter and 1000-meter levels are compared for the four upper-air sites in figures 2-6 and 2-7. As expected, the wind speed typically increases with height. The winds are weaker in the morning than in the afternoon, particularly at low levels. The 1000-meter-level wind-speed distributions do not change much from morning to afternoon.

The wind-direction distributions indicate that the Cathedral Bluffs (C-b) tract is the least influenced by drainage flows. As a result, the winds are not as weak in the morning as they are at the other sites, and there is less increase in wind speed with elevation, particularly in the afternoon. At Craig and at the White River (U-a/U-b,) tract, the 150-meter and 300-meter-level winds are very weak in the morning, when drainage conditions prevail.

There are no low-level data at Grand Junction. The 500-meter- and 1000-meter-level wind speeds in the morning and afternoon are similar. Weak winds at the 500-meter level occur more frequently in the afternoon than in the morning.

2.2.3 Stability

The frequency of occurrence of morning and afternoon stability categories at the 500-meter level at the four sites is shown in table 2-1. The morning (easterly) winds at Craig, Grand Junction, and the White River project (U-a/U-b) sites tend to be stable, as would be expected for these drainage flows. At the C-b site, where drainage flows are not as organized, neutral conditions predominate in the morning. The atmosphere is neutral most of the time at the 500-meter level in the afternoon at all sites.

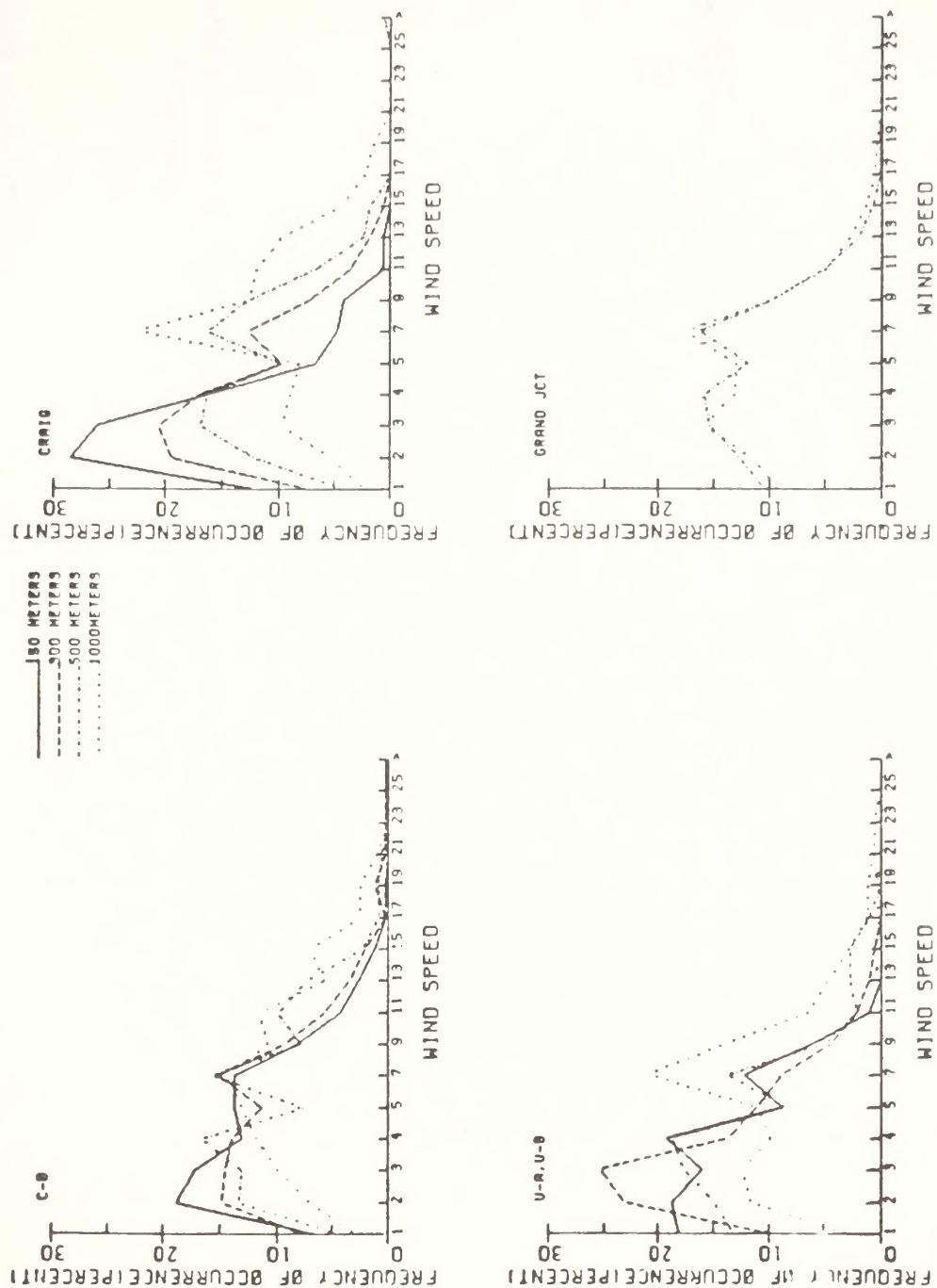


FIGURE 2-6. WIND SPEED FREQUENCY DISTRIBUTIONS FOR ALL MORNING SOUNDINGS

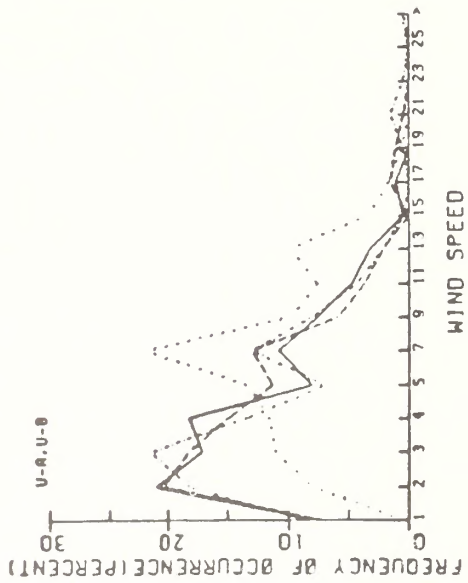
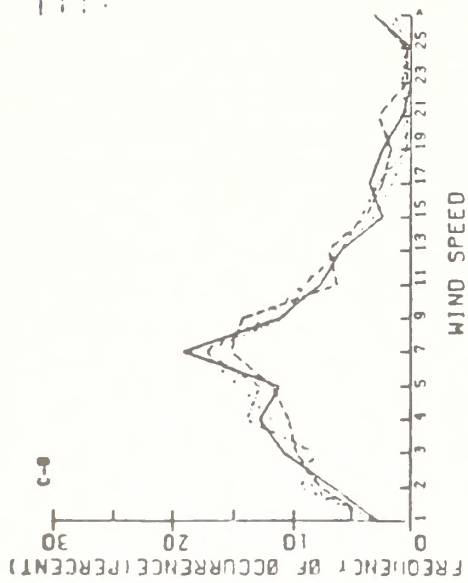
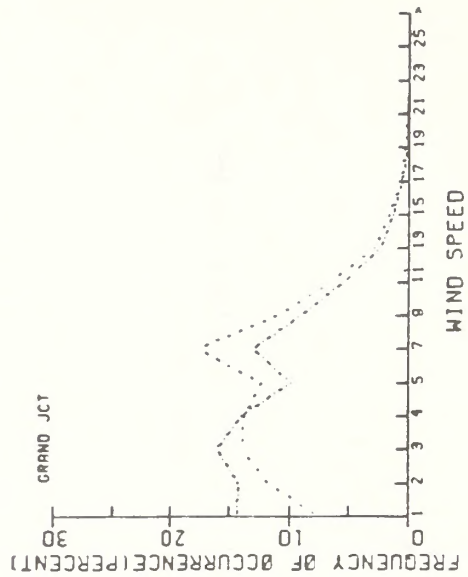
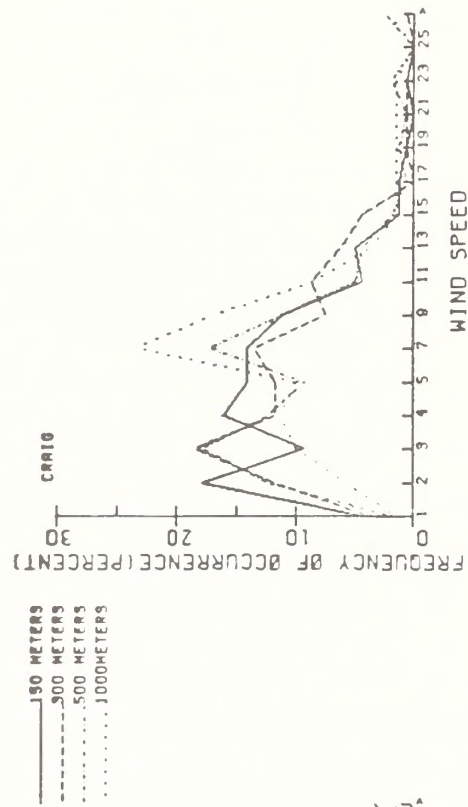


FIGURE 2-7. WIND SPEED FREQUENCY DISTRIBUTIONS FOR ALL AFTERNOON SOUNDINGS

TABLE 2-1. FREQUENCY OF OCCURRENCE OF ATMOSPHERIC STABILITY
AT THE 500-m LEVEL (AGL)

(percent)

(a) Cathedral Bluffs (C-b)

	Morning				Afternoon			
	Unstable (A,B,C)	Neutral (D)	Stable (E)	Very Stable (F)	Unstable (A,B,C)	Neutral (D)	Stable (E)	Very Stable (F)
Annual	10	55	34	0	19	55	27	0
Winter	2	48	50	0	6	69	25	0
Spring	11	61	28	0	34	54	12	0
Summer	13	51	36	0	45	32	23	0
Fall	10	61	27	2	17	63	21	0

(b) Craig, Colorado

	Morning				Afternoon			
	Unstable (A,B,C)	Neutral (D)	Stable (E)	Very Stable (F)	Unstable (A,B,C)	Neutral (D)	Stable (E)	Very Stable (F)
Annual	2	39	59	1	16	64	20	0
Winter	0	43	57	0	6	65	29	0
Spring	5	56	39	0	31	54	14	0
Summer	0	21	80	0	14	66	20	0
Fall	2	37	59	2	13	69	18	0

TABLE 2-1 (Concluded)

(c) White River (U-a, U-b)

	Morning				Afternoon			
	Unstable (A,B,C)	Neutral (D)	Stable (E)	Very Stable (F)	Unstable (A,B,C)	Neutral (D)	Stable (E)	Very Stable (F)
Annual	1	25	74	0	16	52	31	2
Winter	0	33	65	2	6	40	50	4
Spring	0	29	71	0	26	64	10	0
Summer	0	14	87	0	29	54	17	0
Fall	2	24	74	0	10	53	36	2

(d) Grand Junction, Colorado

	Morning				Afternoon			
	Unstable (A,B,C)	Neutral (D)	Stable (E)	Very Stable (F)	Unstable (A,B,C)	Neutral (D)	Stable (E)	Very Stable (F)
Annual	2	52	44	2	1	84	13	2
Winter	6	33	56	6	3	51	40	7
Spring	1	68	31	0	0	96	3	0
Summer	0	57	43	0	0	98	2	0
Fall	1	49	49	1	0	91	9	90

The morning and afternoon mixing depths for Grand Junction have been determined by Holzworth and are listed in table 2-2. Because of increased surface heating, the summer afternoon mixing depths are more than three times the average winter value.

2.2.4 Effect of Terrain on Wind Fields

The descriptions in this section of the effect of the complex terrain (hills, mountains, and valleys) in the study region are substantiated by the wind field modeling work performed as part of this analysis (see section 4). Figure 2-8 displays the computed wind fields for the lowest of the three atmospheric layers modeled, which is about 2500 feet (780 meters) thick and extends from the terrain or 4300 feet above mean sea level (MSL), whichever is highest, to 6800 feet MSL. Note in the figures that winds are channeled through valleys (the White, Green, and Colorado river basins), and winds are both accelerated and decelerated by the effects of complex terrain. Nominal synoptic winds of 10 m/s from indicated directions were assumed for these model calculations. (Clear plastic overlays showing various geographical features and terrain elevations are provided inside the back cover of this report.) The reader is encouraged to use these over the figures throughout this report so that the locations of important geographical features and sources can be identified.

Figure 2-9 shows similar plots for a zero upper air (synoptic) wind and two conditions of strong down- and up-slope flow induced by nocturnal terrain cooling and daytime heating, respectively. The nominal wind speed of 10 m/s was chosen for illustration purposes only; actual down- and up-slope flows would generally be expected to have much lower speeds. See Section 4.2 for discussion of techniques by which these nominal wind fields were scaled on the basis of measured winds.

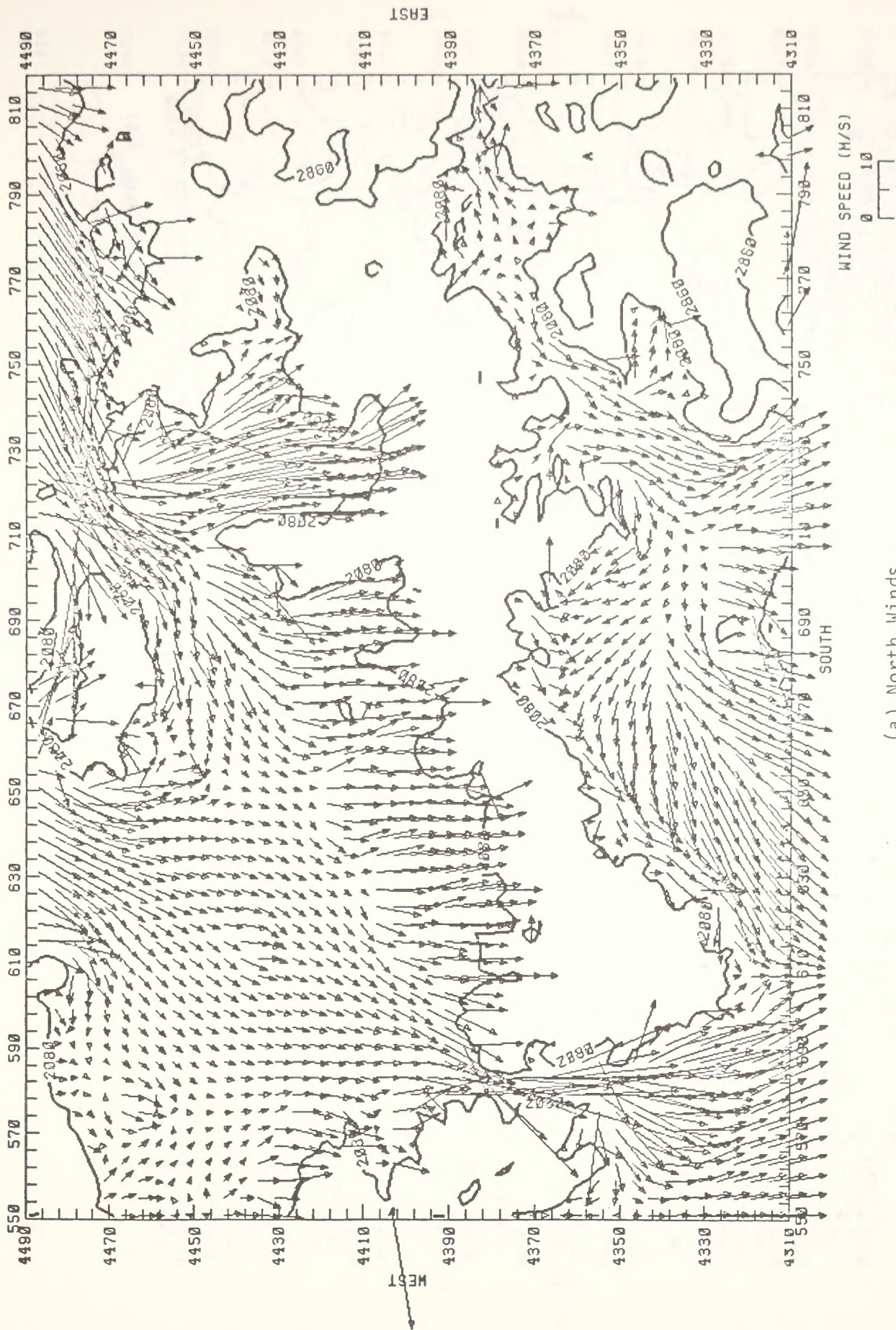
2.3 EXISTING AIR QUALITY

The existing air quality of the study region is typical of a largely undeveloped region in the western United States. The measured long-term average concentrations of the criteria pollutants in the Uinta Basin are well within ambient air quality standards except in populated areas where windblown dust and emissions from dirt and general roads cause routine exceedances of standards. Three-year averages of pollutant concentrations measured at the proposed site for the Paraho facility in the Uinta Basin are as follows:

TABLE 2-2. SEASONAL AND ANNUAL-AVERAGE MORNING AND AFTERNOON
MIXED-LAYER HEIGHTS AND WIND SPEEDS FOR
GRAND JUNCTION, COLORADO

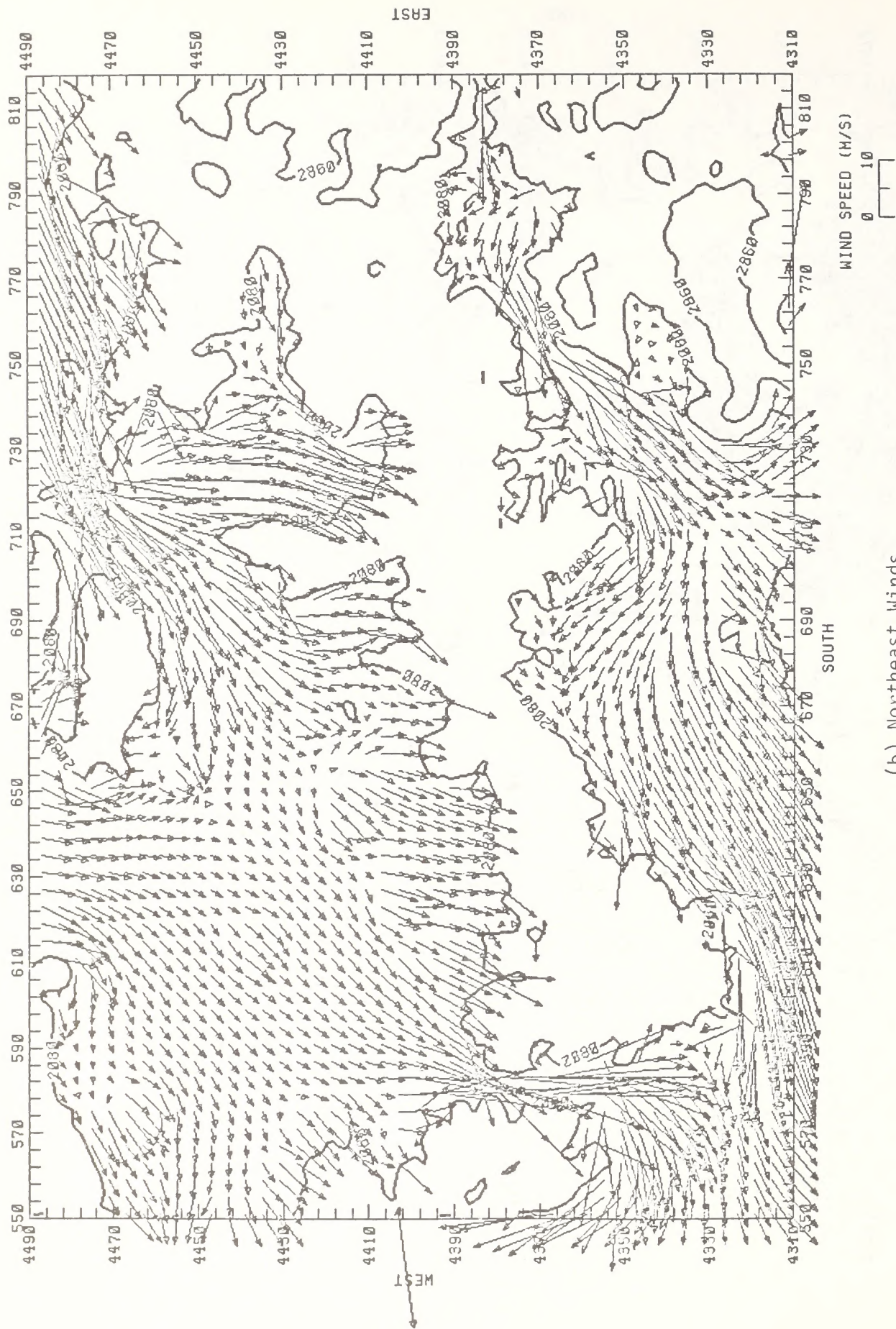
Season	Morning		Afternoon	
	Height (m)	Wind Speed (m/s)	Height (m)	Wind Speed (m/s)
Winter	329	3.4	1160	3.4
Spring	628	5.4	3166	6.6
Summer	307	4.7	3940	6.1
Autumn	273	3.9	2133	4.6
Annual	384	4.3	2600	5.2

Source: Holzworth (1972)



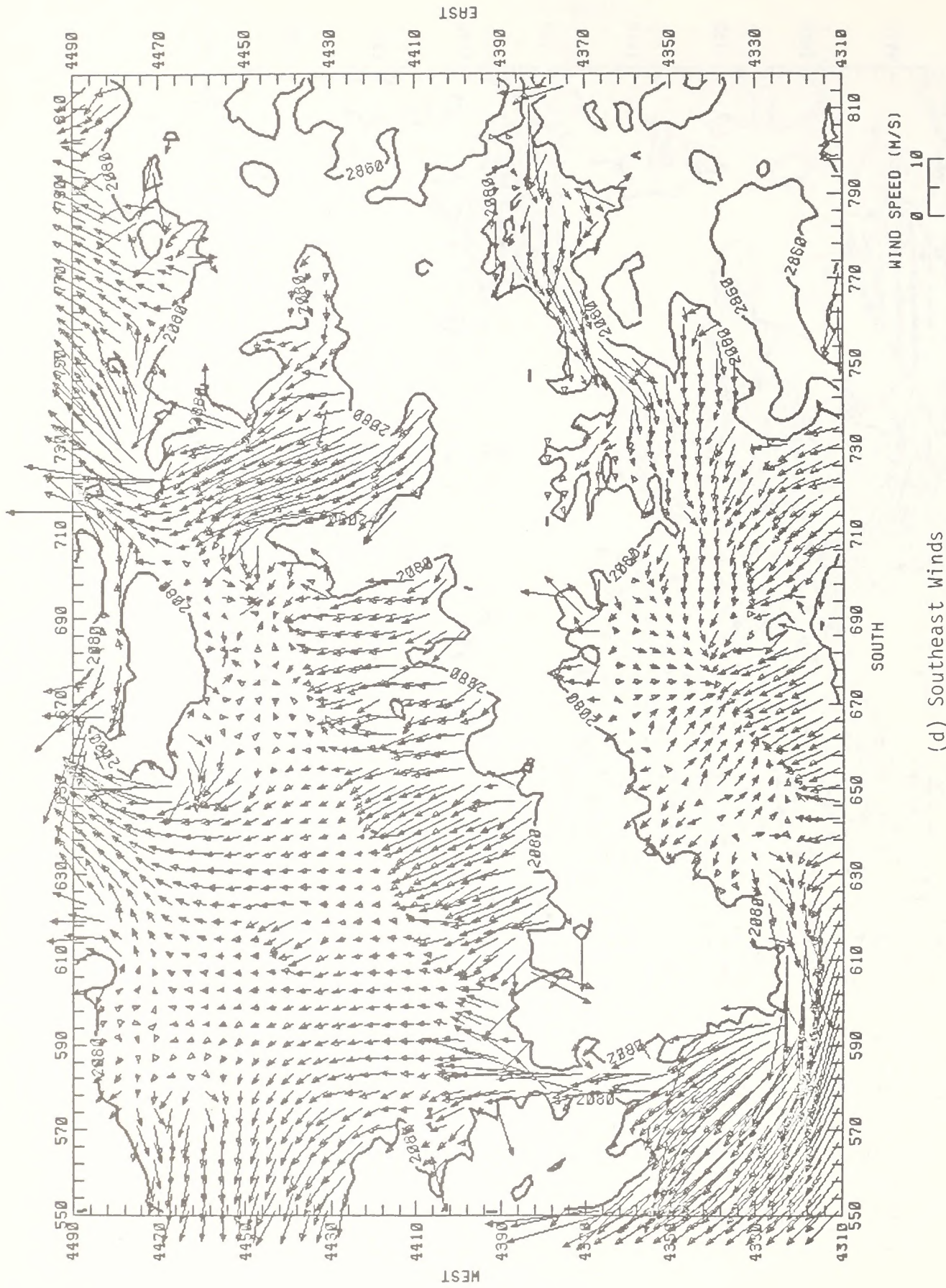
(a) North Winds

FIGURE 2-8. COMPUTED WIND FIELDS FOR EIGHT SYNOPTIC WIND DIRECTIONS FOR THE STUDY REGION (LOWEST MODELED LAYER FROM 4300 FT MSL OR TERRAIN ELEVATION, TO 6800 FT MSL)



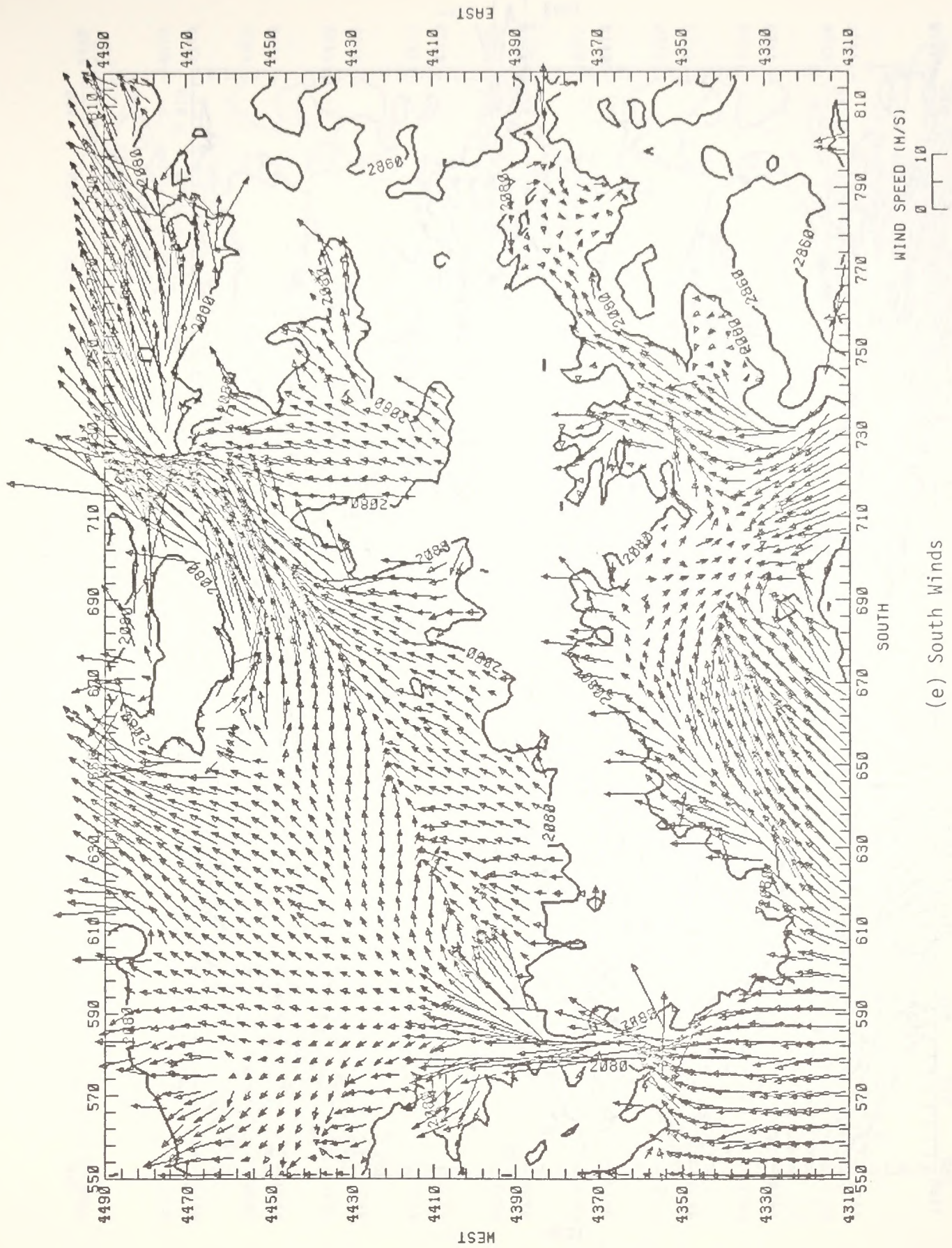
(b) Northeast Winds

FIGURE 2-8 (Continued)



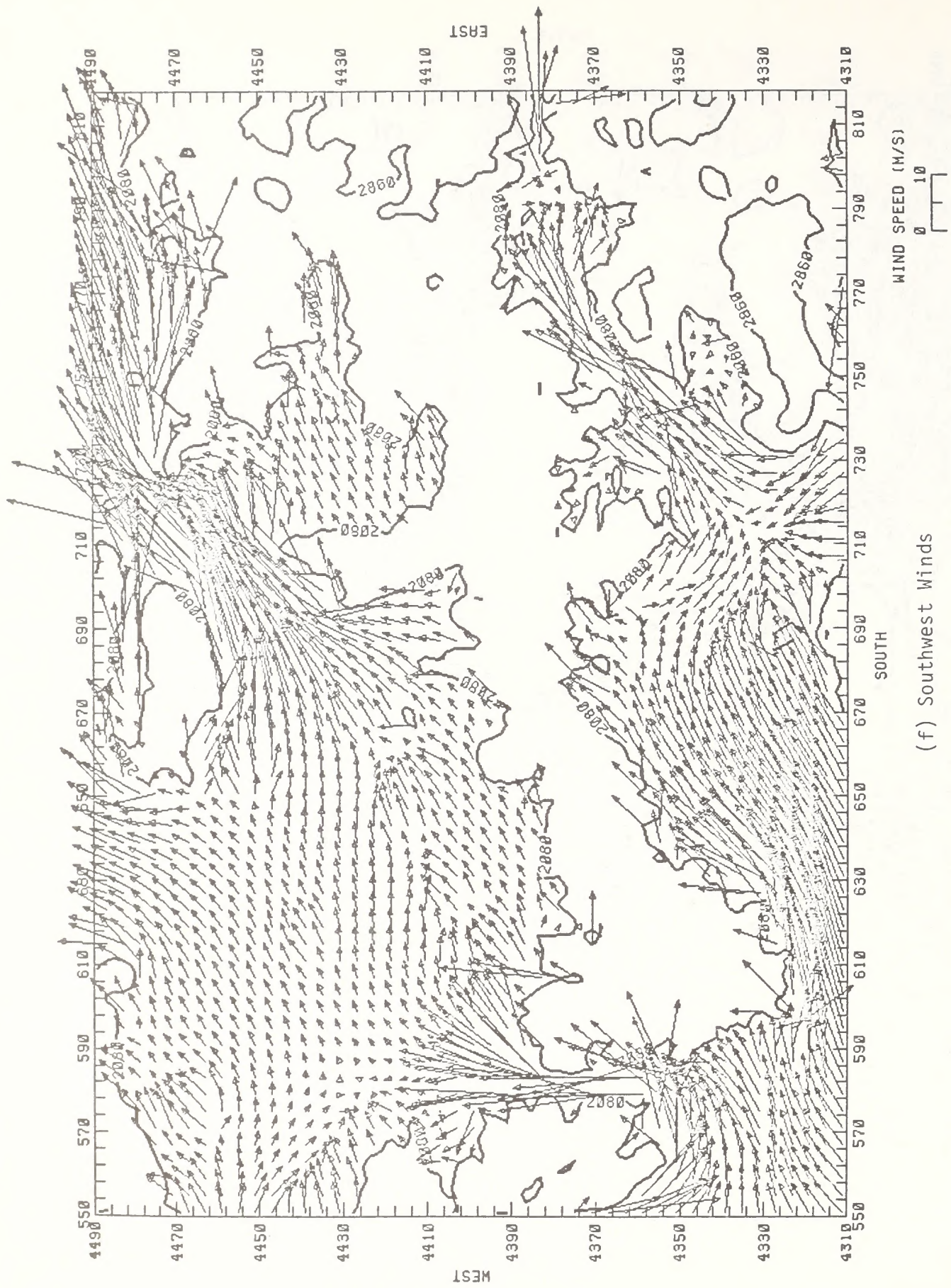
(d) Southeast Winds

FIGURE 2-8 (Continued)



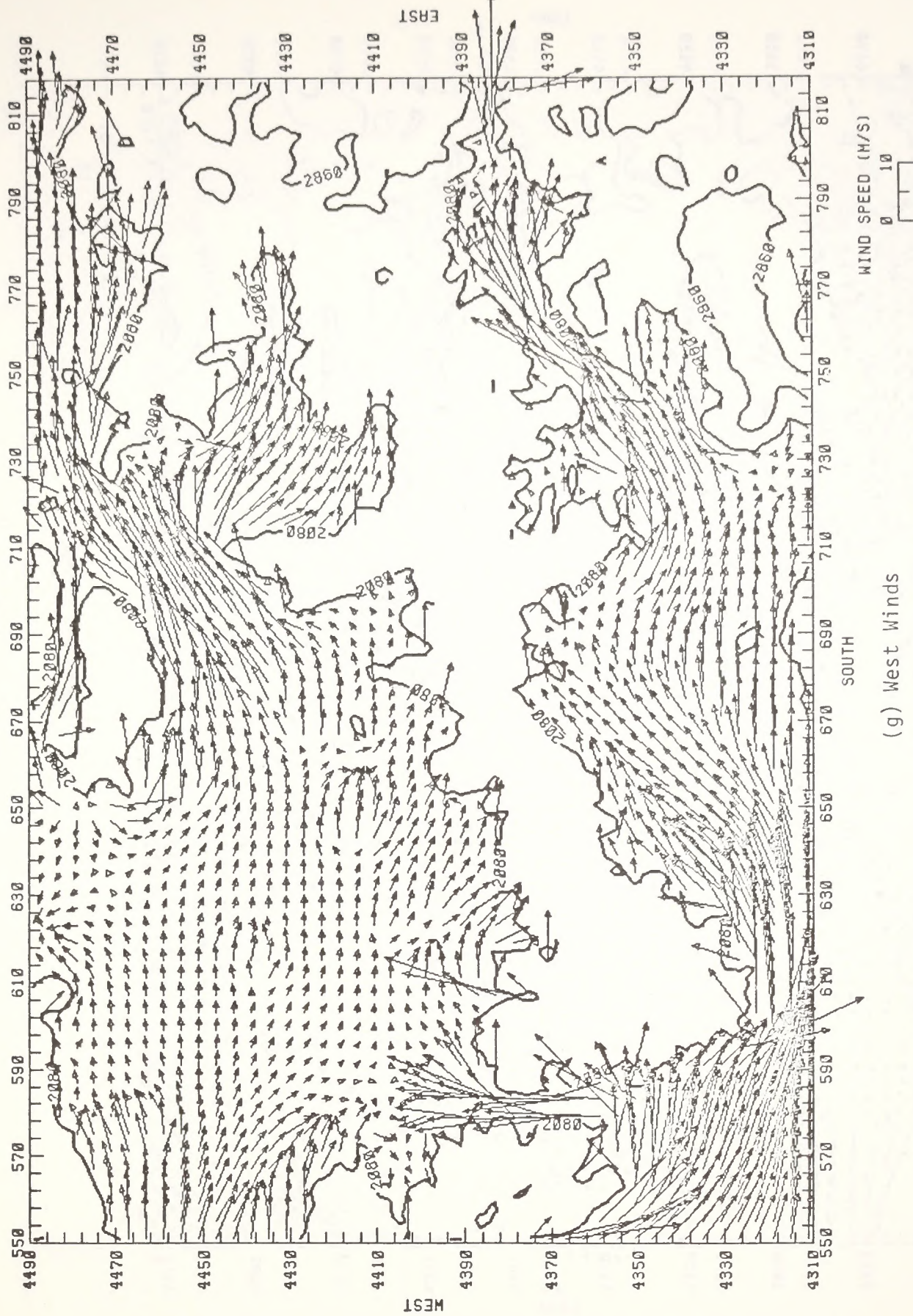
(e) South Winds

FIGURE 2-8 (Continued)



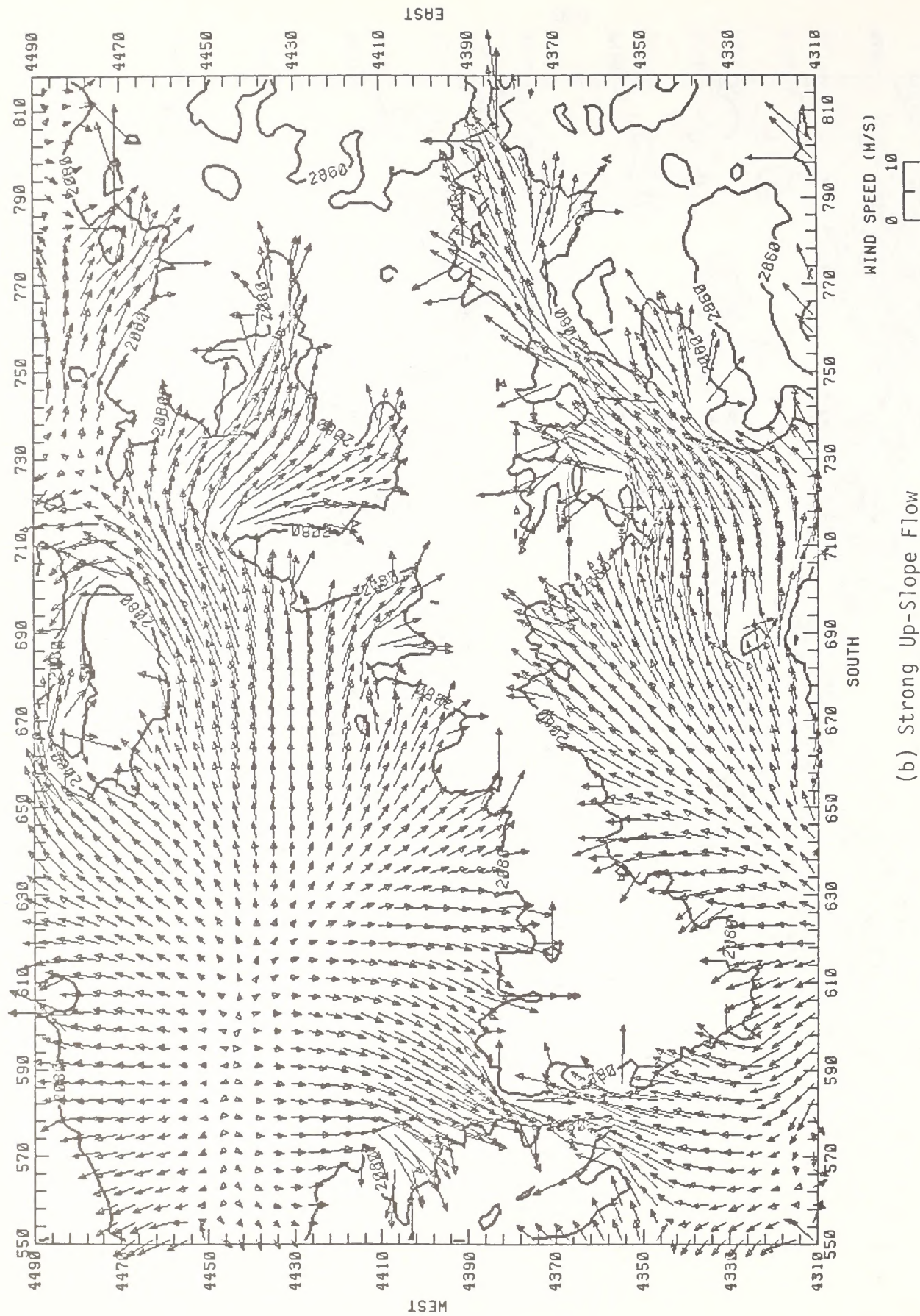
(f) Southwest Winds

FIGURE 2-8 (Continued)



(g) West Winds

FIGURE 2-8 (Continued)



(b) Strong Up-Slope Flow

FIGURE 2-9 (Concluded)

Pollutant	3-Year Average Measured Concentrations in Uinta Basin ($\mu\text{g}/\text{m}^3$)	Annual Average Federal Ambient Air Quality Standard ($\mu\text{g}/\text{m}^3$)
Sulfur dioxide (SO_2)	1.3	80
Total suspended particulates (TSP)	15.7	60

Pollutant	3-Year Average Measured Concentrations in Uinta Basin ($\mu\text{g}/\text{m}^3$)	Annual Average Federal Ambient Air Quality Standard ($\mu\text{g}/\text{m}^3$)
Carbon monoxide (CO)	200	10,000*
Ozone (O_3)	71	240†
Nitrogen Dioxide	1.3	100

* 8-hour standard.

† 1-hour standard.

Ambient measurements of SO_2 and NO_2 were also made by the state of Utah in Green River and Vernal, Utah, during the years 1977 to 1980. SO_2 concentrations were essentially zero, and the NO_2 annual concentrations ranged from zero to $20 \mu\text{g}/\text{m}^3$.

On the basis of an emission inventory developed for the region for the 1980 baseline year, as discussed in Section 4.1, the annual-average SO_2 concentration was modeled. The results are shown in figure 2-10. Note that concentrations are essentially zero except in the Grand Junction, Colorado, area, where SO_2 concentrations are higher than $6 \mu\text{g}/\text{m}^3$.

More ambient data were available for TSP than for other criteria pollutants for the study region. Table 2-3 summarizes measurements made by the states of Utah and Colorado in the study region. For most of the sites in the study area, TSP ambient air quality standards are exceeded. The primary cause of these exceedances is most likely windblown dust and dust from unpaved and gravel roads.

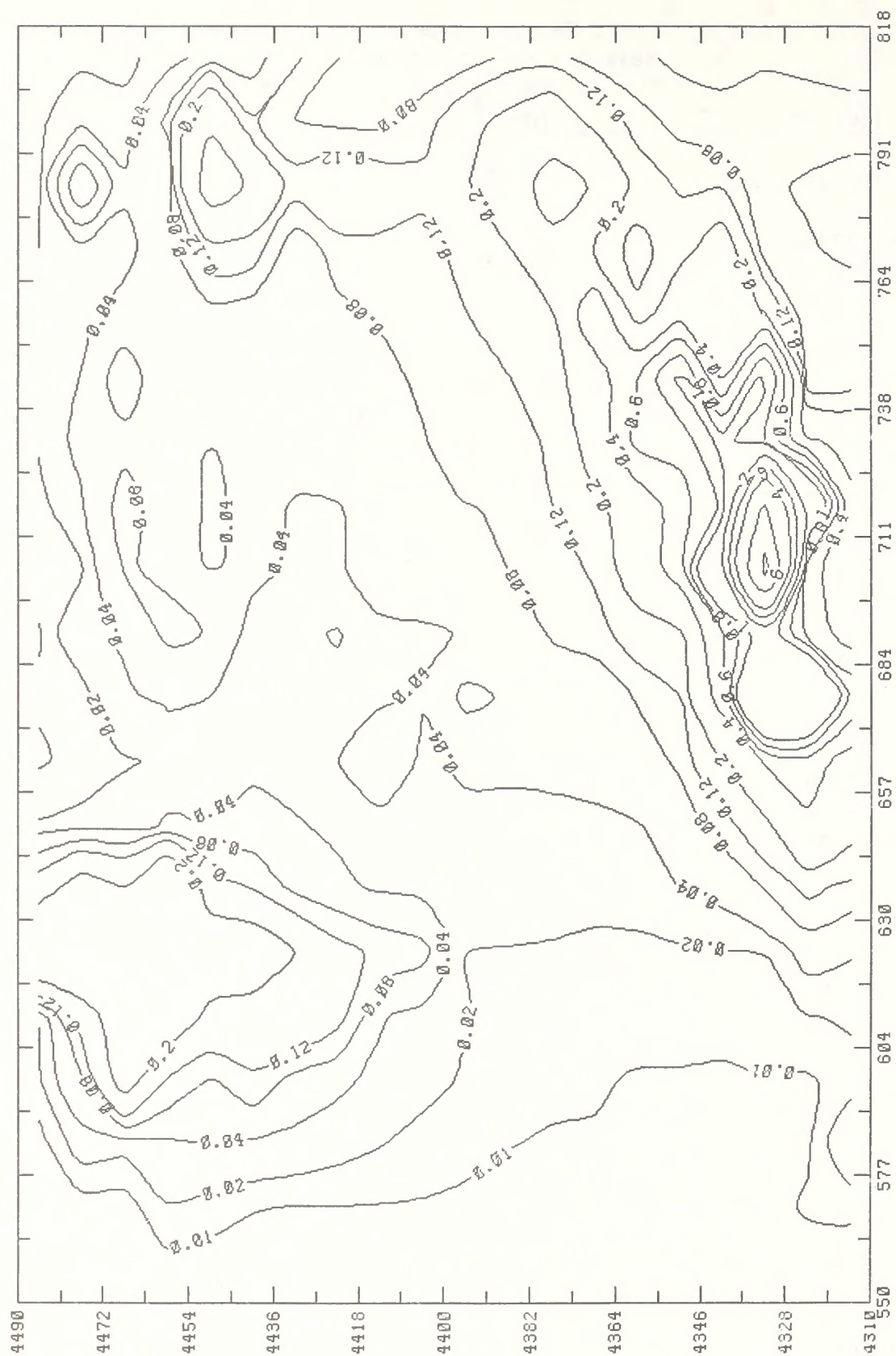


FIGURE 2-10. EXISTING ANNUAL AVERAGE SO_2 CONCENTRATIONS ($\mu\text{g}/\text{m}^3$)

TABLE 2-3. MEASURED AMBIENT CONCENTRATIONS OF TOTAL
SUSPENDED PARTICULATES (TSP) IN STUDY REGION

Site	Year	Maximum 24-hr	Annual Geometric Mean
<u>Colorado</u>			
Fruita	1979	173*	76†
	1980	166*	69*
Palisade	1979	130	43
	1980	163*	47
Rifle	1979	694†	128†
	1980	510†	156†
Glenwood Springs	1979	188*	57
	1980	203*	68*
Meeker	1980	212*	66*
Rangeley	1980	273†	70*
Craig	1980	382†	86†
<u>Utah</u>			
Green River	1979	196*	64*
	1980	163*	53
Vernal	1978	105	31
	1979	106	35
	1980	80	32
U-a, U-b	1978	63	15
	1979	53	13
<u>Federal and State Ambient Air Quality Standards</u>			
Primary		260	75
Secondary		150	60

* Exceedance of secondary standard.

† Exceedance of primary and secondary standards.

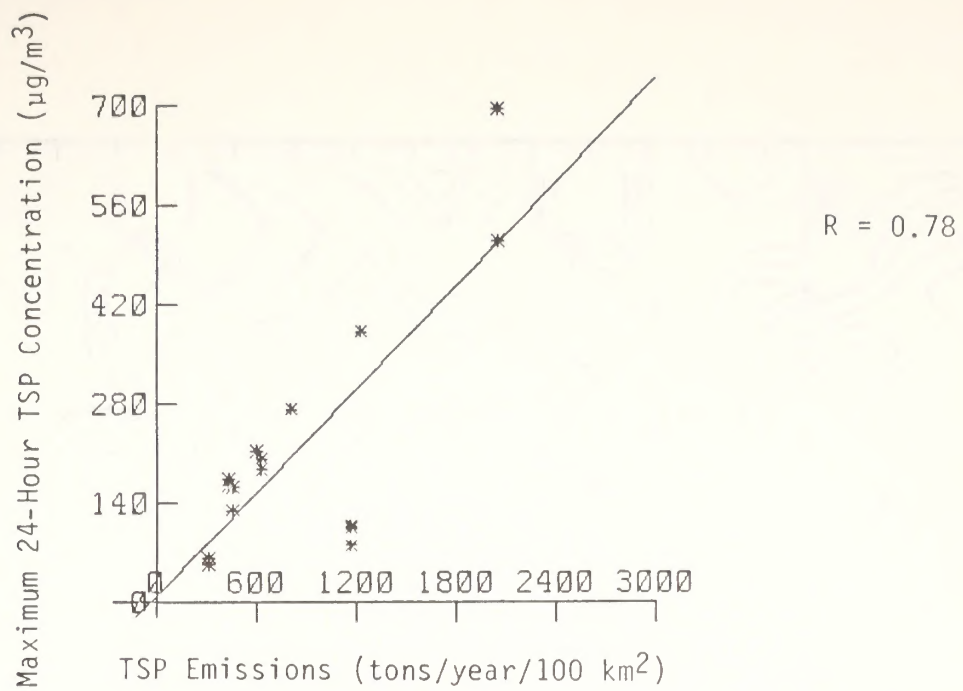
Utilizing the TSP emission inventory developed for the study region, we looked specifically at the emissions in locations for which we had TSP ambient data. We found a high correlation between local TSP emissions and ambient concentrations, as shown in figure 2-11. On the basis of these correlations, we developed the following empirical models:

$$\begin{aligned}\chi &= 55 + 0.267 d && \text{for maximum 24-hour average} \\ \chi &= 17 + 0.061 d && \text{for geometric mean}\end{aligned}$$

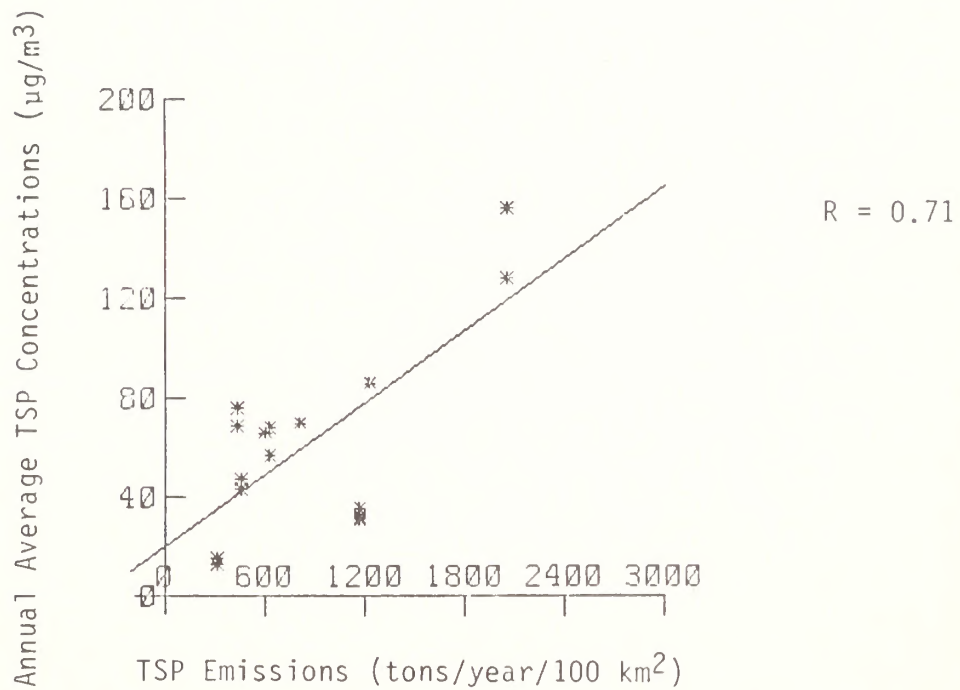
where χ is the ambient maximum 24-hour average or annual geometric mean TSP concentration in $\mu\text{g}/\text{m}^3$ and d is the particle emission density in tons per year per 100 km^2 .

These models were used to calculate impacts of secondary TSP emissions for the low and high oil production scenarios (see Section 5). The existing baseline ambient TSP concentrations for the study region are displayed in figure 2-12. Ambient annual-average TSP concentrations in excess of the air quality standards are predicted to exist in the Colorado River basin (near Grand Junction and Rifle) in the southeastern portion of the study region, and near Craig, Colorado, and Vernal, Utah. We estimate that annual-average TSP concentrations in most other sites in the study area are currently in the range of 20 to $40 \mu\text{g}/\text{m}^3$.

Visual-range (visibility) measurements were made by the National Park Service during the period 1978 to 1979 at Dinosaur National Monument at the northern edge of the study region. Visibility in the region is usually quite good--the mean visual range is 178 to 192 km in the summer, when most measurements were made. Figure 2-13 shows a frequency distribution of visual range in the summer of 1979. The mean visual range is 178 km, but visual range varied from 100 to over 300 km during this period. The good visibility conditions attest to the fact that both regional SO_2 emissions (and resultant sulfate ambient concentrations) and ambient TSP concentrations are currently low.



(a) Maximum 24-Hour Average



(b) Annual Average

FIGURE 2-11. CORRELATIONS BETWEEN TSP EMISSIONS AND AMBIENT CONCENTRATIONS

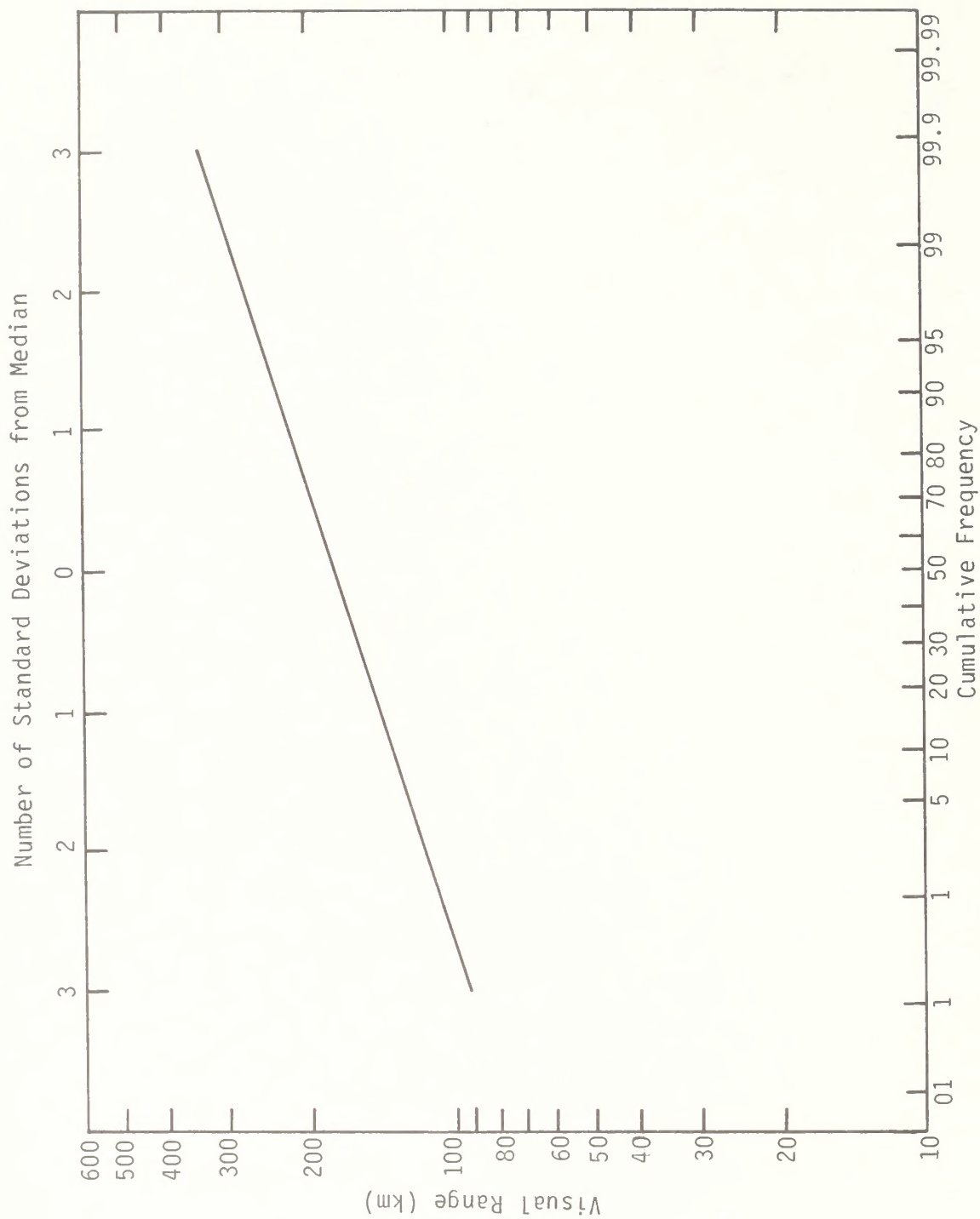


(a) Maximum 24-Hour Average

FIGURE 2-12. MODEL ESTIMATES OF EXISTING TOTAL SUSPENDED PARTICULATE (TSP) CONCENTRATIONS IN STUDY REGION



(b) Annual Average
FIGURE 2-12 (Concluded)



Source: Walther and Newburn (1980)

FIGURE 2-13. FREQUENCY DISTRIBUTION OF VISUAL RANGE AT DINOSAUR NATIONAL MONUMENT IN SUMMER 1979

3 AIR QUALITY IMPACT SIGNIFICANCE CRITERIA

In this section we identify the relevant criteria for determining whether air quality impacts would be considered to be significant. Most of these criteria are part of established state and federal air quality program requirements for

- > Maintenance of ambient air quality standards
- > Prevention of significant deterioration
- > Determination of significant visibility impairment
- > Protection of air-quality-related values.

These criteria are based on current air quality regulations. We have not attempted to address the possible revisions or additions to existing statutory and regulatory requirements that might be expected during the periods of proposed oil shale and tar sands facility development.

3.1 AMBIENT AIR QUALITY STANDARDS

In table 3-1, the applicable state and federal ambient air quality standards are listed. The Utah and Colorado standards are the same as the National Ambient Air Quality Standards. Wyoming has established tighter standards than the federal limits for sulfur dioxide (annual and 24-hour), total suspended particulates (annual and 24-hour), and ozone (1-hour). In addition, Wyoming has established ambient standards for fluorides and hydrogen sulfide. The federal hydrocarbon standard (0600 to 0900 average) has been established as a guide in evaluating attainment of the ozone standard, whereas the Wyoming hydrocarbon standard is not so interpreted.

All ambient air quality standards are of potential concern; however, for the region and sources of interest, SO₂, TSP, NO₂, CO, and O₃ are the pollutants of principal concern.

TABLE 3-1. APPLICABLE STATE AND FEDERAL AMBIENT AIR QUALITY STANDARDS
($\mu\text{g}/\text{m}^3$)

<u>Pollutant</u>	<u>Federal</u>	<u>Utah</u>	<u>Colorado</u>	<u>Wyoming</u>
SO_2				
(annual)	80	80	80	60
(24-hour)	365	365	365	260
(3-hour secondary)	1300	1300	1300	1300
TSP				
Primary				
(annual)	75	75	75	60
(24-hour)	260	260	260	150
Secondary				
(annual)	60	60	60	
(24-hour)	150	150	150	
CO				
(8-hour)	10,000	10,000	10,000	10,000
(1-hour)	40,000	40,000	40,000	40,000
O_3				
(1-hour)	240	240	240	160
NO_2				
(annual)	100	100	100	100
Hydrocarbons				
(3-hour)	160			160
Flourides as HF				
(24-hour)				0.8
Lead				
(1/4 year)	1.5			
H_2S				
(30-minute average)				70

3.2 PREVENTION OF SIGNIFICANT DETERIORATION

The U.S. EPA and state (Utah and Wyoming) prevention of significant deterioration requirements allow only a limited increase in the second-highest short-term TSP and SO₂ concentrations and annual-average TSP and SO₂ concentrations associated with emissions from a new source. These SO₂ and TSP increments are listed in table 3-2 for each area classification (I, II, and III).

TABLE 3-2. PREVENTION OF SIGNIFICANT DETERIORATION INCREMENTS

Pollutant	Averaging Time	Maximum Allowable Concentrations ($\mu\text{g}/\text{m}^3$)		
		Class I	Class II	Class III
SO ₂	Annual	2	20	40
	24-hr	5	91	182
	3-hr	25	512	700
TSP	Annual	5	19	37
	24-hr	10	37	75

Currently, no areas within Utah, Colorado, or Wyoming are designated Class III. Existing Class I areas that are likely to be most affected by development (see Latimer and Doyle, 1981) in the study area include

- > Flat Tops Wilderness
- > Mt. Zirkel Wilderness
- > Maroon Bells/Snowmass Wilderness.

These wilderness areas are all at distances of 50 km or more from the oil shale and tar sands development regions. Since all other areas within the study area are designated Class II, near-source impacts are evaluated against the PSD Class II increments.

Several requirements of PSD review apply only to pollutants emitted in significant amounts; these significant, or de minimis, levels are presented in table 3-3. These values provide criteria for determining whether specific pollutant emissions for a source are significant, thus requiring ambient air quality modeling.

TABLE 3-3. EPA SIGNIFICANT (DE MINIMIS) EMISSION RATES

Pollutant	Emission Rate (tons/year)
Carbon monoxide	100
Nitrogen oxides	40
Sulfur dioxide	40
Total suspended particulates	25
Ozone (volatile organic compounds)	40
Lead	0.6
Asbestos	0.007
Beryllium	0.0004
Mercury	0.1
Vinyl chloride	1.0
Fluorides	3
Sulfuric acid mist	7
Total reduced sulfur (including H ₂ S)	10
Reduced sulfur (including H ₂ S)	10
Hydrogen sulfide	10

In addition to the federal PSD requirements, the state of Colorado has adopted standards for sulfur dioxide (SO_2) expressed as allowable amounts of increase in ambient concentrations over an established baseline. Like PSD, these standards have been adopted for three categories (I, II, and III) of land areas or regions. The increment limits for these state categories are the same as the PSD Class I, II, and III increments for SO_2 . Colorado has included national monuments in category I, and two national monuments, Colorado and Dinosaur, are located within the study area. These two national monuments may also be redesignated federal Class I PSD areas. Also, to the northwest of the study region is the Uinta Primitive Area, an area of special concern that may also at some future date be redesignated Class I.

3.3 DETERMINATION OF SIGNIFICANT VISIBILITY IMPAIRMENT

Currently there are no clear objective criteria for judging adverse visibility impairment in Class I areas. However, the EPA visibility regulations, promulgated on 2 December 1980 (Federal Register, pp. 80084-80095) state that adverse visibility impairment will be determined on a ". . . case-by-case basis taking into account the geographic extent, intensity, duration, frequency and time of visibility impairments, and how these factors correlate with (1) times of visitor use of the federal class I area and (2) the frequency and timing of natural conditions."

More objective criteria for determining adverse visibility impairment are outlined in the EPA document entitled "Workbook for Estimating Visibility Impairment" (Latimer and Ireson, 1980). That document suggests the following criteria: if a plume contrast or sky/terrain contrast change greater than ± 0.10 , or a plume discoloration corresponding to a ΔE ($*L*a*b$) of 4, or a blue-red ratio of 0.9 is predicted to occur on the worst day, the probability of adverse visibility impairment cannot be ruled out.

The existing mandatory Class I areas in the study area that are currently afforded visibility protection are administered by the U.S. Forest Service (USFS). The USFS has not yet established specific criteria for judging the significance of visibility impairment, except to state that visibility effects, such as changes in contrast, coloration, and visual range, should be considered. The USFS has not identified any "integral vistas," which are views from within a Class I area of landscape features located outside an area, that are afforded visibility protection.

3.4 PROTECTION OF AIR-QUALITY-RELATED VALUES

The U.S. Forest Service has started to address the air-quality-related values of its Class I areas and has identified categories of effects that air quality impacts could have on air-quality-related values. These effects are listed in table 3-4.

The National Park Service (NPS) administers both the Dinosaur and Colorado national monuments, which are protected under the 1916 Organic Act. Although these areas are not Class I, their air-quality-related values are a major concern to the NPS.

TABLE 3-4. CATEGORIES OF POTENTIAL AIR QUALITY IMPACTS ON
AIR-QUALITY-RELATED VALUES OF CLASS I AREAS

Flora and fauna effects

- Growth
- Mortality
- Reproduction
- Diversity
- Visible injury
- Succession
- Productivity

Soil effects

- Cation exchange capacity
- Base saturation
- pH
- Structure
- Metals concentration

Water effects

- pH
- Metals concentration
- Total alkalinity

Visibility effects

- Contrast
- Coloration
- Visual range

Odor effects

Cultural, archaeological, and geological effects

- Deposition
- Decomposition

4 ANALYSIS METHODOLOGY

The methodology used in this study is indicated schematically in figure 4-1 and consisted of the following major tasks:

- > Collection of Data. Emission data for the Uinta Basin synfuel facilities were collected from the developers. Information concerning Colorado point and area source emissions and Utah population projections were obtained from a study performed for the National Park Service by PEDCo. Meteorological and topographical data were collected from the National Weather Service, various oil-shale tracts (U-a, U-b, C-a, C-b), and the U.S. Geological Survey.
- > Emission Inventory Development. Emission data were reviewed, developed, checked, and converted to input files for air quality modeling. Utah population projections were used to generate secondary growth area source emission files for the portion of Utah in the study region.
- > Air Quality Modeling. With the emissions, meteorological, and topographical data as input, several air quality simulation models were applied to address specific concerns. The most extensive modeling was performed by means of the Gaussian Puff Model (GPM), which was applied to both the 110-km x 110-km and 180-km x 268-km regions shown in figure 1-1 for every 3-hour period in a year to compute maximum 3-hour, 24-hour, and annual averages for every receptor in these regions. This conservative model was used to identify periods of worst-case impacts that were modeled with the more realistic finite-difference grid model--Regional Transport Model (RTM), which, because of its cost to run, was applied to only one worst-case regional transport day. For near-source (< 5 km downwind) TSP impacts the EPA Gaussian, sector-average COMPLEX I model was applied to take into account multiple TSP emission points within a given facility (GPM was not used

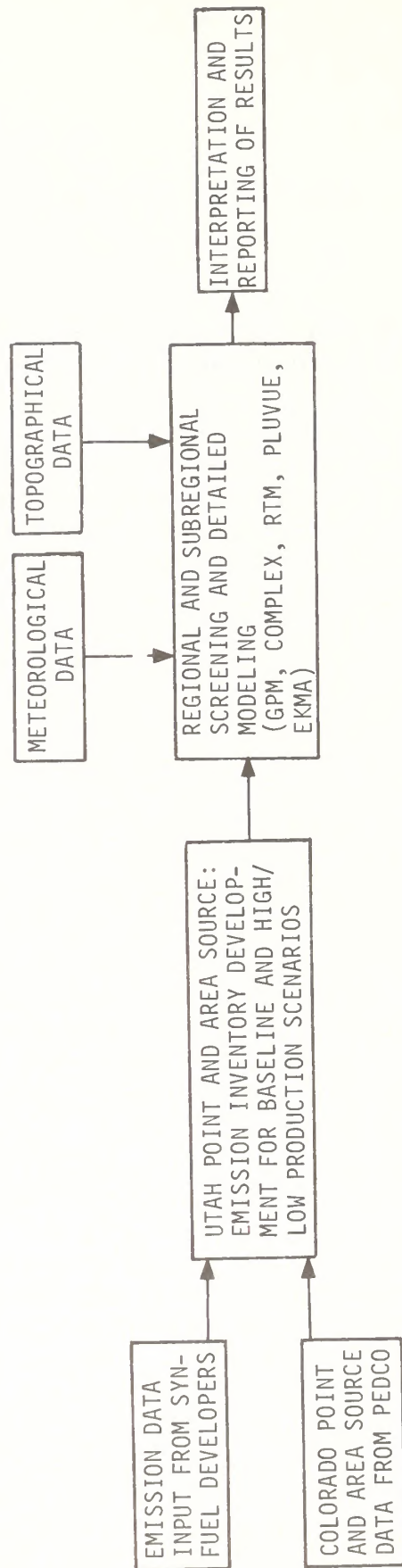


FIGURE 4-1. OVERALL FLOW DIAGRAM OF ANALYSIS METHODOLOGY

because of its cost). Worst-case photochemical smog and visibility impairment scenarios were evaluated by means of EKMA and PLUVUE, respectively. Acid deposition was evaluated from GPM results.

This chapter is divided into two major sections. Section 4.1 discusses the development of emission inventories and section 4.2 discusses the modeling methodology.

4.1 DEVELOPMENT OF EMISSION INVENTORIES

This section discusses the array of procedures used by Systems Applications to develop detailed emission inventories for the broad area encompassing the study region. Several of the characteristics of this study contributed to the large effort that was needed to complete the inventories. Principal among these was the large number of different groups of source types including proposed synfuel projects, existing point sources, other sources planned for future operation, and secondary growth sources, for which emission inventories had to be developed.

This work has resulted in the first comprehensive set of inventories for this region of the country. Figure 4-2 depicts the flow of activities for the inventory development process.

We began the inventory process by assigning the existing and proposed emission sources to specific groupings having common characteristics. Considerations of geographic location, general source type, and operational parameters were used to identify specific groups of source categories for baseline conditions and alternative scenarios of future operating conditions. Emission estimates were developed for the following source categories:

> Point sources

- Proposed Utah oil shale and tar sands projects
- Other planned projects in Utah
- 1980 baseline (existing) point sources in Utah

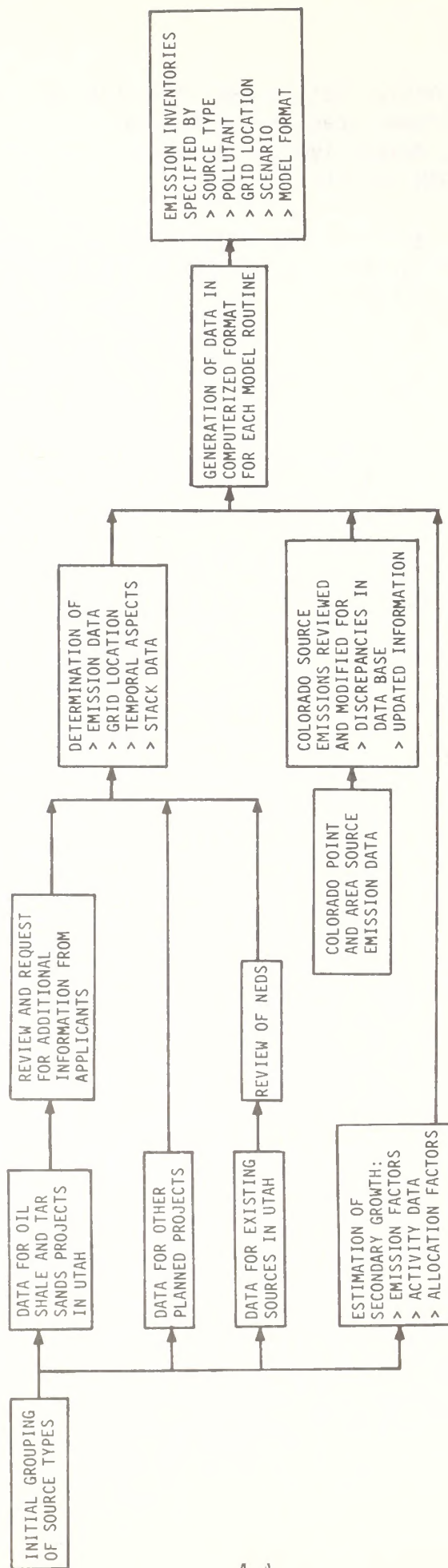


FIGURE 4-2. SCHEMATIC DIAGRAM OF ACTIVITIES FOR THE EMISSION INVENTORY DEVELOPMENT PROCESS

- Proposed Colorado oil shale facilities*
 - 1980 baseline point sources in Colorado
 - Future Colorado point sources for the low- and high-oil production scenarios, respectively.
- > Area sources
- 1980 baseline area sources in Utah
 - Future (including secondary growth) Utah area sources for the low- and high-oil-production scenarios.
 - 1980 baseline area sources in Colorado
 - Future Colorado area sources for the low- and high-oil-production scenarios, respectively.

Emission estimates in each case were derived for the five criteria pollutants:

- > Sulfur dioxide
- > Particulate matter
- > Nitrogen oxides
- > Hydrocarbons
- > Carbon monoxide.

Some speciation of these pollutants into sulfate, nitrogen dioxide, and reactive hydrocarbon categories was also performed. Insufficient data are available to evaluate the emissions and resultant air quality impacts of other species of potential concern such as trace metals and organic materials. Also, the potential long-term climatic effects of carbon dioxide emissions to the atmosphere were not evaluated.

As previously shown in figure 1-1, the study region consisted primarily of six counties in two states.

* Plans for developing oil shale resources in Colorado are currently in a state of uncertainty. This study was based on assumptions concerning these development plans.

> Utah (eastern)

- Uintah
- Grand

> Colorado (western)

- Moffat
- Rio Blanco
- Garfield
- Mesa.

Another effort conducted by PEDCo Environmental, Inc. and coordinated by the National Park Service and the Bureau of Land Management had resulted in estimates of emissions for sources located in the Colorado portion of the study region. Due to project scheduling constraints, Systems Applications developed inventories for sources located in Utah only and employed the PEDCo inventories for Colorado sources in the study region. During the course of the study, additional data were received from the State of Utah. These data were compared with the PEDCo data and found to be in reasonably close agreement. Because the derivation of the PEDCo estimates has been reported elsewhere (PEDCo, 1981), the majority of section 4.1 focuses on the development of the Utah point and area source inventories.

All emission data were developed on a gridded basis. Stack data were also derived for modeling the plume rise of individual emission points at each point source.

Baseline emission data were initially derived for all existing point and area sources in operation in 1980. Future emissions representative of various years were then estimated for the individual synfuel projects in Utah at peak operation and for the other planned projects in Utah. In a similar manner, area source emissions were projected to future years that corresponded to the specification of particular scenarios. All emission data were developed on an average basis of operating conditions without regard to considerations such as seasonal characteristics or differences in weekday/weekend operation.

The remainder of section 4.1 discusses the methods used to develop each of the point and area source emission files identified above.

4.1.1 Utah Synfuel Projects

Seven synthetic fuel (oil shale and tar sands) projects proposed for the Uinta Basin represented the principal focus for our study.

- > Enercor-Mono Power (tar sands)
- > Geokinetics (oil shale)
- > Magic Circle (oil shale)
- > Paraho (oil shale)
- > Sohio (tar sands)
- > Syntana-Utah (oil shale)
- > Tosco (oil shale).

Distinguishing features among these projects, in addition to their operating processes, are their site locations and project plans. Each of these projects, except Enercor-Mono Power and Geokinetics, would be a single facility developed at one site. Enercor-Mono Power plans to operate facilities at two sites (Rainbow and PR Springs), and Geokinetics intends to develop facilities at 11 locations (Agency Draw and ten other sites identified as LOFRECO). Furthermore, the plans for each proposed project are currently considered to be either "conceptual" in nature or more defined and certain ("site-specific"). The site-specific projects are the Rainbow site for Enercor-Mono Power, Magic Circle, Paraho, Syntana-Utah, and Tosco. The conceptual projects include the PR Springs site for Enercor-Mono Power, Geokinetics (all sites), and Sohio.

Information was submitted by all seven project applicants for use in estimating the direct emissions* from each facility. We reviewed the materials submitted by the applicants to ensure that the estimates were reasonable, thorough, and accurate; in some cases, we requested additional information. Our review focused primarily on the following emission-related areas:

* All "secondary growth" emissions are considered to be area sources and are discussed later.

- > Process description
- > Emission factors
- > Activity data
- > Anticipated control technology
- > Stack parameters.

The data from each applicant formed the initial basis of each project's emission estimates. Inventories for each project were constructed for both high and low levels of production. In certain instances, engineering judgment was used to complete the inventories for the synfuel projects. In addition, because of the large number of emission points at some projects, we consolidated the smaller emission rates into fewer emission points for the regional modeling cases in which this activity was technically justified; this effort reduced the complexity and cost of the regional modeling activities. In the case of near-source modeling, each emission point at a project was located by means of UTM coordinates, and stack data were developed for each point.

Tables 4-1 and 4-2 provide the production rates and direct emission totals for each of the Utah synfuel projects at the high and low levels of oil shale and tar sands production. As shown in these two tables, emission rates vary considerably from one project to another. This variation is due to several aspects of the proposed projects including process design, production rate, and emission control technology design. For example, Geokinetics proposes to employ an in-situ oil shale extraction process, unlike the other Utah projects which are above ground processes. Furthermore, Geokinetics is in an early stage of design; future designs may alter emission rates considerably from those presented in the tables. Similarly, emission levels for Sohio are quite different between the high and low oil production scenarios. This variation results from different assumed fuels and levels of control for steam generation at the Sohio tar sands facility. The reader is referred to the project descriptions and numerous supporting documentation for further elaboration on the derivation of the basic emission estimates.

4.1.2 Other Planned Projects (Utah)

Future point sources other than the seven Utah synfuel facilities were included in the emission estimates for Uintah and Grand counties in Utah. Eight other planned projects had significant emission rates; of these, three were estimated to account for the majority of total emissions from other planned projects in Utah:

TABLE 4-1. PRODUCTION AND EMISSION RATES FOR UTAH SYN FUEL
PROJECTS--HIGH-OIL-PRODUCTION SCENARIO

Project	Oil Production (barrels/day)	Emissions (kilograms per hour)*				
		Sulfur Dioxide	Particulate Matter	Nitrogen Oxides†	Total Hydrocarbon	Carbon Monoxide
Enercor-Mono Power	55,000	111	233	123	38	33
Geokinetics	70,000	1799	159	744	40	22
Magic Circle	31,500	147	107	823	4	53
Paraho	42,000	182	97	482	14	72
Sohio	20,000	373	644	327	88	29
Syntana-Utah	57,000	128	129	746	81	64
Tosco	45,000	94	127	786	183	9
Total	320,500	2834	1496	4031	448	282

* 1 kg/hr = 9.66 tons/year.

† NO_x emissions expressed as NO₂.

TABLE 4-2. PRODUCTION AND EMISSION RATES FOR UTAH SYN FUEL
PROJECTS--LOW-OIL-PRODUCTION SCENARIO

Project	Oil Production (barrels/day)	Emissions (kilograms per hour)*				
		Sulfur Dioxide	Particulate Matter	Nitrogen Oxides†	Total Hydrocarbon	Carbon Monoxide
Enercor-Mono Power	20,000	40	79	45	13	12
Geokinetics	31,000	764	71	331	18	12
Magic Circle	16,400	73	51	420	2	33
Paraho	10,500	45	54	105	3	21
Sohio	5,000	1	136	25	22	16
Syntana-Utah	16,500	40	38	230	18	19
Tosco	22,000	46	62	385	90	4
Total	121,400	1009	491	1541	166	117

* 1 kg/hr = 9.66 tons/year.

† NO_x emissions expressed as NO₂.

- > Moon Lake power plant unit 2
- > Plateau refinery expansion
- > White River oil shale project.

Emissions and stack parameters for the eight other planned projects were developed from information regarding each facility's source type, operating process, activity data, and proposed controls. In some cases, the conceptual nature of a particular project required considerable judgment to estimate the emission rates. Emission totals for the larger facilities and for the other planned projects are listed in table 4-3.

4.1.3 Utah Baseline Point Sources

Emissions for existing point sources with significant emission rates were developed from available data. We first reviewed the state of Utah emission files for Utah counties within the grid region (primarily Uintah and Grand counties). Although several sources were identified by the state, only one was considered to be significant for this study; the others were assumed to be covered adequately by the procedures used to derive the area source files.* In addition, we reviewed the National Emission Data System files, which listed only one or two point sources in the two primary Utah counties.

As a result of these reviews, two point sources were identified for the Utah baseline point source file:

- > Moon Lake power plant unit 1
- > Plateau refinery.

The first power plant unit for the Moon Lake facility was placed in the existing point source file because construction of this facility has begun. The existing Plateau refinery located in Duchesne County was also included because of its relatively significant emissions. Emission and stack data for the Moon Lake power plant were taken from the EPA Prevention of Significant Deterioration permit, whereas comparable data for the existing Plateau facility were derived from the 1980 state of Utah data.

* Also, computerized versions of Utah point source emissions were not readily available.

TABLE 4-3. EMISSION TOTALS FOR OTHER PLANNED PROJECTS IN UTAH

(kilograms per hour)

<u>Project</u>	<u>Sulfur Dioxide</u>	<u>Particulate Matter</u>	<u>Nitrogen Oxides*</u>	<u>Total Hydrocarbon</u>	<u>Carbon Monoxide</u>
Moon Lake unit 2	95	55	1012	0	0
Plateau expansion	29	44	58	245	67
White River	136	197	827	165	381
5 additional projects	<u>195</u>	<u>80</u>	<u>99</u>	<u>93</u>	<u>6</u>
Total	455	376	1996	503	454

* NO_x emissions expressed as NO₂.

Table 4-4 lists the emission data for these two facilities. Note that total future emission rates for each of these sources can be estimated by summing the emission rates provided in tables 4-3 and 4-4 for the Moon Lake and Plateau facilities.

4.1.4 Colorado Oil Shale, Point, and Area Sources

In another effort conducted by PEDCo Environmental, Inc. for the National Park Service (PEDCo, 1981), emission estimates were developed for existing and future point and area sources located in northwestern Colorado. The region included the Colorado counties of Moffat, Rio Blanco, Garfield, and Mesa. These Colorado emission estimates were used in the modeling portion of this Systems Applications study.

Colorado oil shale project emissions were developed by PEDCo for specific production rates in 1990 and 2000. These production rates correspond to the low- and high-oil-production regional scenarios developed for this study. This approach resulted in the estimation of emissions, including secondary growth, for five scenarios:

- > 1980 baseline
- > 1990 without oil shale
- > 1990 with oil shale
- > 2000 without oil shale
- > 2000 with oil shale.

Tables 4-5 and 4-6 provide the emission totals estimated by PEDCo for point and area sources in the four Colorado counties in the study region.

4.1.5 Utah Baseline Area Sources

Available emission inventory data for existing area sources in eastern Utah were very limited. Consequently, it was necessary to develop this information from the available data concerning area source activities. The inventory was first divided into 47 area source categories shown in table 4-7. Appropriate activity data such as fuel use and traffic counts were then obtained from several information sources. These data were combined with most of the same emission factors used by PEDCo for Colorado area sources. Allocation factors were finally used to assign emissions from each category to specific 10-km x 10-km (100 km²) grid

TABLE 4-4. EMISSION TOTALS FOR BASELINE POINT SOURCES IN UTAH

(kilograms per hour)

<u>Source</u>	<u>Sulfur Dioxide</u>	<u>Particulate Matter</u>	<u>Nitrogen Oxides*</u>	<u>Total Hydrocarbon</u>	<u>Carbon Monoxide</u>
Moon Lake unit 1	95	55	1012	0	0
Plateau refinery	<u>4</u>	<u>6</u>	<u>432</u>	<u>291</u>	<u>62</u>
Total	99	61	1444	291	62

* NO_x emissions expressed as NO₂.

TABLE 4-5. EMISSION TOTALS FOR COLORADO OIL SHALE PROJECTS*

(a) Low-Oil-Production Scenario

Project	Oil Production (barrels/day)	Emissions (kilograms per hour)				
		Sulfur Dioxide	Particulate Matter	Nitrogen Oxides	Total Hydrocarbon	Carbon Monoxide
Colony	47,000	128	240	878	158	28
Union	50,000	75	29	114	41	35
Cathedral Bluffs	94,000	852	363	3487	23	1400
Chevron	15,000	22	9	34	12	10
Rio Blanco	50,000	51	141	420	19	190
Superior	15,000	157	36	78	32	17
Total	271,000	1285	818	5011	285	1680

TABLE 4-5 (Concluded)

(b) High-Oil-Production Scenario

Project	Oil Production (barrels/day)	Emissions (kilograms per hour)			
		Sulfur Dioxide	Particulate Matter	Nitrogen Oxides	Total Hydrocarbon
Colony	47,000	128	240	878	158
Union	50,000	75	29	114	41
Cathedral Bluffs	94,000	852	363	3487	23
Chevron	100,000	150	57	229	81
Rio Blanco	86,000	88	243	723	33
Mobil	50,000	75	29	114	41
Exxon	47,000	128	240	878	158
Superior	15,000	157	36	78	32
Getty	50,000	75	29	114	41
Multimineral	50,000	75	29	114	41
Naval Oil Shale	50,000	50	208	511	10
Total	639,000	1853	1503	7240	659
					2065

* Direct project emissions only.

TABLE 4-6. EMISSION TOTALS FOR NON-OIL SHALE SOURCES IN COLORADO

(kilograms per hour)

<u>Scenario</u>	<u>Sulfur Dioxide</u>	<u>Particulate Matter</u>	<u>Nitrogen Oxides</u>	<u>Total Hydrocarbon</u>	<u>Carbon Monoxide</u>
1--1980 baseline	947	14,130	2328	1194	9354
2--1990 without oil shale	1988	16,268	4448	932	5649
3--1990 with oil shale*	2036	20,877	4851	1223	7915
4--2000 without oil shale	2002	17,118	4410	918	5146
5--2000 with oil shale*	2061	22,314	4808	1197	7198

* These emission totals exclude direct oil shale project emissions (table 4-5), but include secondary growth associated with oil shale development.

TABLE 4-7. AREA SOURCE CATEGORIZATION SCHEME

Petroleum marketing and transport

Truck unloading

Underground storage

Auto tank filling

Organic solvent usage

Surface coating

Petroleum drycleaning

Perchloroethylene drycleaning

Degreasing

1,1,1-trichloroethane

Trichloroethane

Graphic arts

Miscellaneous solvent usage

Pesticide usage

Fuel combustion

Industrial

Distillate oil

Residual oil

LPG

Natural gas

Commercial and institutional

Coal

Distillate oil

Residual oil

LPG

Natural gas

Residential

Coal

Distillate oil

LPG

Wood

Natural gas

TABLE 4-7 (Concluded)

Agricultural waste burning

Wildfires

Construction

Residential

Commercial

Public and institutional

Roads

Agricultural wind erosion

Tilling

Off-road mobile sources

Gasoline farm tractors

Diesel farm tractors

Construction equipment (diesel)

Other gasoline usage

Other diesel usage

Piston aircraft

Jet aircraft

Railroads

On-road motor vehicles (exhaust)

State highways

County roads

Class "D" roads

On-road motor vehicles (fugitive dust)

State highways (paved)

County roads (paved)

Class "D" roads (unpaved)

cells. The result was a set of emission inventories by source category for each of the two primary Utah counties in the study region--Uintah and Grand. The inventories are generally representative of baseline conditions for the year 1980.

4.1.5.1 Emission Factors

In order to make the Utah area source emission inventory consistent with the Colorado inventory, it was decided to use the majority of emission factors that PEDCo (1981) used to derive the 1980 baseline inventory for four Colorado counties. Our review of these emission factors led us to conclude that they were generally in agreement with those reported in the most recent revisions of the "AP-42" data base (EPA, 1981). In some cases these factors were derived from standard methods prescribed by the EPA (1980). Table 4-8 presents the emission factors used to develop the Utah area source inventories for the following primary pollutants:

- > Reactive hydrocabons (RHC)
- > Unreactive hydrocarbons (URHC)
- > Oxides of nitrogen (NO_x)
- > Sulfur dioxide (SO_2)
- > Particulate matter (TSP)
- > Carbon monoxide (CO).

Major differences from the PEDCo emission factors include the following:

- > The approach prescribed in AP-42 was used to compute the emission factors for wildfires. These factors were different from those for Colorado due to different field loading factors, that is, tons of combustible material per unit land.
- > An emission factor of 1.20 tons per acre per month was used for TSP from construction activity.
- > The wind erosion emissions are crop-specific. The emission factor for corn, as given in AP-42, was used because for eastern Utah, corn is the major crop for which there are wind erosion emissions.

TABLE 4-8. EMISSION FACTORS FOR 1980 BASELINE

Source Category	Hydrocarbons		NO _x	SO ₂	Particulate Matter	CO	Unit
	Reactive	Nonreactive					
Petroleum marketing and transport							
Truck unloading	7.3						lb/10 ³ gal
Underground storage	1.0						lb/10 ³ gal
Auto tank filling	9.7						lb/10 ³ gal
Organic solvent usage							
Surface coating	6.5						lb/capita
Petroleum drycleaning	0.36						lb/capita
Perchloroethylene drycleaning	1.14						lb/capita
Degreasing							
1,1,1-trichloroethane		1.0					lb/capita
Trichloroethane	3.0						lb/capita
Graphic arts	0.8						lb/capita
Miscellaneous solvent usage	6.3						lb/capita
Pesticide usage	2.0						lb/acre
Fuel combustion							
Industrial							
Distillate oil		1.0	22.0	36.0	2.0	.5.0	lb/10 ³ gal
Residual oil		1.0	60.0	143.1	11.6	5.0	lb/10 ³ gal
LPG		0.3	11.2	0.014	1.7	1.5	lb/10 ³ gal
Natural gas		3.0	175.0	0.6	10.0	17.0	lb/10 ⁶ ft ³
Commercial and institutional							
Coal	0.005	3.0	6.0	22.8	16.0	10.0	lb/ton
Distillate oil		1.0	22.0	36.0	2.0	5.0	lb/10 ³ gal
Residual oil		1.0	60.0	143.1	11.6	5.0	lb/10 ³ gal
LPG		0.7	11.0	0.014	1.8	1.9	lb/10 ³ gal
Natural gas		8.0	120.0	0.6	10.0	20.0	lb/10 ⁶ ft ³

TABLE 4-8 (Continued)

Source Category	Hydrocarbons		NO _x	SO ₂	Particulate Matter	CO	Unit
	Reactive	Nonreactive					
Residential							
Coal	0.005	20.0	3.0	22.8	20.0	90.0	1b/ton
Distillate oil		1.0	18.0	36.0	2.5	5.0	1b/10 ³ gal
LPG		0.7	7.0	0.014	1.8	1.9	1b/10 ³ gal
Wood	5.0		1.0		20.0	120.0	1b/ton
Natural gas		8.0	80.0	0.6	10.0	20.0	1b/10 ⁶ ft ³
Agricultural waste burning	10.52				9.1	53.82	10 ⁻⁴ tons/(acre-year)
Wildfires		11.90	1.98		8.43	69.44	Tons/(acre-year)
Construction							
Residential					1.2		Tons/(acre-month)
Commercial					1.2		Tons/(acre-month)
Public and institutional					1.2		Tons/(acre-month)
Roads					1.2		Tons/(acre-month)
Agricultural wind erosion					0.12		Tons/(acre-year)
Tilling (Grand/Uintah)					0.28/0.21		Tons/(acre-year)
Off-road mobile sources							
Gasoline farm tractors	6.84	184.5	151.0	5.31	8.0	32.60	1b/10 ³ gal
Diesel farm tractors	12.1	60.7	335.0	31.2	45.7	119.0	1b/10 ³ gal
Construction equipment (diesel)	6.77	29.08	407.1	31.15	26.14	95.24	1b/10 ³ gal
Other gasoline usage	6.5	210.5	68.8	5.4	6.11	34.63	1b/10 ³ gal
Other diesel usage	7.04	37.5	469.0	31.2	33.5	102.0	1b/10 ³ gal
Piston aircraft	0.85		0.05			38.01	1b/LT0
Jet aircraft	7.38		11.99	1.36	6.20	37.08	1b/LT0
Railroads	12.5	94.0	370.0	57.0	25.0	130.0	1b/10 ³ gal

TABLE 4-8 (Concluded)

Source Category	Hydrocarbons		NO _x	SO ₂	Particulate Matter	CO	Unit
	Reactive	Nonreactive					
On-road motor vehicles (exhaust)							
State highways	3.18		3.73	0.23	0.44	37.22	gm/km
County roads	4.07		2.85	0.21	0.43	49.47	gm/km
Class "D" roads	5.73		1.29	0.11	0.34	64.82	gm/km
On-road motor vehicles (fugitive dust)							
State highways (paved)					3.2		gm/km
County roads (paved)					3.2		gm/km
Class "D" roads (unpaved)					453.6		gm/km

- > For tilling operations, the emission factors were calculated by using appropriate soil silt content values in AP-42. These factors were different for Uintah and Grand counties.
- > For some source categories [notably agricultural waste burning, on-road motor vehicles (exhaust), and aircraft], the activity data available to us were not finely divided into subcategories; therefore, some aggregation of emission factors was warranted to make them compatible with the activity data.
- > The hydrocarbon emissions from on-road motor vehicles were further delineated into reactive and unreactive classes by assuming that the former constituted 90 percent of the total hydrocarbons, and the latter, the remaining 10 percent.

The fugitive dust emission factors for state highways and county roads were directly derived from AP-42 emission factors. Note that these factors do not include any tire wear, which has already been accounted for in the exhaust emission factors. The fugitive dust emission factors for class "D" roads were not directly available, however. Because of the condition of these unpaved roads, identified as class "D" by the state of Utah, their average vehicle speed is low. These roads are unimproved and are often simply tracks with sagebrush covering the middle of the path. They are best described as "primitive or less" (UDOT, 1982). For these reasons, after consulting with the Utah Department of Transportation, we assumed that the average travel speed on these roads ranges between 15 to 25 miles per hour. It was not possible to use the approach recommended in supplement 8 of AP-42 because its application is restricted to speeds above 30 miles per hour. Likewise, the county-specific emission factors provided in PEDCo (1981) for three types of unpaved roads could not be used because the speeds associated with these road types were outside the range appropriate for class "D" roads. Large variabilities in the Colorado emission factors ruled out a simple averaging process. In the absence of any better information, we assumed a particulate matter emission factor of 1 lb/km. This factor is slightly higher than that for gravel urban roads and significantly lower than that for gravel rural roads as provided in PEDCo (1981). The average speed that we have assumed for class "D" roads is in general agreement with the assumed fugitive dust emission factor.

4.1.5.2 Activity Data

For the purpose of this discussion, area sources are divided into the following classes:

- > Stationary sources
- > Off-road mobile sources
- > On-road motor vehicles.

4.1.5.2.1 Stationary sources

Gasoline consumption figures for the base year were available in thousands of gallons for Uintah and Grand counties (NPS, 1982). These were employed to estimate the emissions from petroleum marketing and transport-related categories.

Emissions due to organic solvent usage were derived from the total population of each county. The population data were available from the NPS (1982).

The number of acres that underwent pesticide applications was available from the Census of Agriculture (DOC, 1981). These acres were exposed to pesticide applications of sprays, dusts, granules, and fumigants. Hydrocarbon emissions are primarily due to the application of liquid pesticides, but no information was available to identify the acres that experienced the application of liquid pesticides only; thus, our emission estimates may be somewhat conservative.

The state totals of fuel oil, liquid petroleum gas (LPG), and natural gas consumed by industrial sources were available from the Energy Data Reports (DOE, 1981). Use of these fuels was apportioned to each county on the basis of the population of employees involved in manufacturing. Similar fuel consumption figures were available for coal, fuel oil, and natural gas for commercial and residential sources. The population and the number of dwelling units were used to apportion the state totals to each county for commercial and institutional, and residential sources, respectively. The total gallons of LPG consumed by residential and commercial sources were not further disaggregated into each category in the Energy Data Reports. Thus, we assumed that the ratio of LPG consumed by residential sources to LPG consumed by commercial sources was equal to the similar ratio for distillate fuel oil for each county. On the basis of the PEDCo report, residential wood consumption was estimated by assuming that 48 percent of the dwelling units had fireplaces, each burning 2.8 tons of wood every year.

The agricultural waste burning emissions were based on total cropland acres available from ORNL (1982).

The ratios of the area of forested land burned in wildfires nationwide to the total forested area were averaged over five years (1975-1979). This average was then multiplied by the total forested area to obtain the area of wildfires for each county. The total forested areas were estimated from Geological Survey topographic maps.

The construction-related TSP emissions were estimated by assuming that

- > Each residential construction project disturbed 0.20 acres of land for 3 months.
- > Each commercial, public, and institutional project disturbed the land for six months.
- > The average road width was 20 feet and the construction duration was eight months.

The NPS (1982) provided us with the number of housing units constructed, acres of commercial construction, acres of public and institutional construction, and miles of new roads constructed for each county.

The total number of agricultural acres (DOC, 1981) was employed to estimate the emissions caused by wind erosion and tilling. This included agricultural land used for the production of corn, sorghum, hay, wheat, oats, barley, and seed crops.

4.1.5.2.2 Off-road mobile sources

The sources included in this category are

- > Gasoline and diesel farm tractors
- > Construction equipment (diesel)
- > Other gasoline and diesel usage
- > Aircraft
- > Railroads.

The total number of wheel tractors and self-propelled grain and bean combines was obtained from published data on agricultural activity in the state of Utah (DOC, 1981). It was assumed that 60 percent of this equipment was gasoline-powered and 35 percent was diesel-powered and that each tractor consumed 1000 gallons of fuel every year. Emissions were scaled up to account for the remaining 5 percent of the population.

The employment figures for non-building construction employees (DOC, 1980) were used as an index of diesel construction equipment activity. It was assumed that 5000 gallons of diesel were consumed per employee per year.

Other gasoline and diesel usage was based on the assumption that 13 gallons of gasoline and 7.4 gallons of diesel were consumed annually per person. County population counts were available for this purpose from the NPS (1982).

Our review showed that there are only two airports of significance in eastern Utah. Both of these airports, Vernal and Roosevelt, are relatively small. We were unable to obtain any landing and takeoff figures from airport authorities and airlines operating at the Vernal airport. However, these estimates were available in a Uinta Basin transportation study performed for the Utah Department of Transportation (VanWagoner, 1980). All local flights were assumed to be general aviation and were attributed to piston engine planes. Similarly, all itinerant flights were assumed to be commercial and were ascribed to jet planes.

No information was available to compute the emissions due to railroad operations in Grand County (no major railroads exist in Uintah County). Emission rates for Grand County were obtained by scaling railroad emission estimates for the adjoining Mesa County using the ratio of the approximate lengths of rail in each of these counties.

4.1.5.2.3 On-road motor vehicles

Link-specific annual-average daily traffic (AADT) volumes were available from the Utah Department of Transportation (UDOT, 1979) for state highways. With the help of road and topographic maps, these data were used to generate total vehicle kilometers travelled (VKMT). However, no specific traffic counts were available for county roads or class "D" roads. At the recommendation of the Utah Department of Transportation (UDOT, 1982), we used an AADT of 150 for county roads and 50 for class "D" roads. Road lengths were then estimated from general highway maps with the class "D" road system. Total VKMT were computed from these AADT volumes and road length data. Urban VKMT totals, exclusive of state

highways, county roads, and class "D" roads, were also available for the cities of Vernal and Moab. These were added to VKMT for county roads.

4.1.5.3 Spatial Allocation Parameters

The emission totals by source category were spatially distributed to obtain gridded area source inventories for each county. This was accomplished by assigning an allocation parameter to each source category. Sufficient information was available to distribute these parameters over 10 x 10-km grid cells. Thus, the emission rate from a particular source category in a particular cell was obtained from

$$e = \frac{Ep}{P} ,$$

where e is the emission rate for a grid cell, E is the emission rate for the entire county, p is the value of the allocation parameter in that grid cell, and P, its value over the entire county. Table 4-9 presents the source category to allocation parameter relationships.

Population distributions were derived from the 1980 census data provided to us by the state of Utah. The population totals were allocated into appropriate grid cells by using the U.S. Bureau of Census population mappings that identify detailed population locations derived from the 1980 census.

The spatial distribution of land receiving pesticide applications was assumed to be the same as the distribution of cropland and pastures. For Uintah County, available land cover and land use maps were utilized to estimate the distribution of cropland and pastures. No such maps were available for Grand County; however, it was therefore assumed that the land not managed by any of the following agencies was potential farmland:

- > Bureau of Land Management
- > National Park Service
- > U.S. Forest Service
- > Fish and Wildlife Service.

Wilderness status maps from the state of Utah were used to determine the spatial distribution of potential farm land in Grand County. This distribution, in turn, was assumed to be an acceptable representation of the distribution of land that experienced pesticide applications. Also, this methodology was employed to spatially distribute tilled acres.

TABLE 4-9. AREA SOURCE SPATIAL ALLOCATION PARAMETERS

Source Category	Allocation Parameter
Petroleum marketing and transport	Population
Organic solvent usage	Population
Pesticide usage	Acres with pesticide application
Fuel combustion	
Industrial	Population
Commercial and institutional	Population
Residential	Population
Agricultural waste burning	Tilled acres
Wildfires	Forested acres
Construction	Population
Agricultural wind erosion	Tilled acres
Tilling	Tilled acres
Off-road mobile sources	
Gasoline farm tractors	Tilled acres
Diesel farm tractors	Tilled acres
Construction equipment (diesel)	Population
Other gasoline usage	Population
Other diesel usage	Population
Piston aircraft	Airport locations
Jet aircraft	Airport locations
Railroads	Rail locations
On-road motor vehicles (exhaust)	Vehicle kilometers travelled (by road type)
On-road motor vehicles (fugitive dust)	Vehicle kilometers travelled (by road type)

Ashley National Forest in Uintah County and Manti La Sal National Forest in Grand County were identified as the major U.S. Forest Service-administered forested areas. The Geological Survey topographic maps were used to allocate the Forest Service-administered areas, as well as other forested areas, to appropriate grid cells.

The exact locations of airports were used to grid aircraft emissions. Railroad emissions were gridded by the approximate railroad length in each grid cell.

Because gridded motor vehicle emissions were unavailable, a major effort in this study was the determination of spatially resolved exhaust and fugitive dust emissions from on-road motor vehicles. U.S. Geological Survey topographic maps and the Utah Department of Transportation general highway maps were employed to measure the road lengths in each grid cell. Such measurements were made for all three types of roads. For the major highways, these road lengths were multiplied by the appropriate link-specific AADT (UDOT, 1979) to obtain the total VKMT in each grid cell. The AADT estimates discussed in section 4.1.5.2.3 were used for county and class "D" roads. Thus, the spatial allocation of emissions from on-road motor vehicles was an integral part of the determination of total motor vehicle emissions.

4.1.5.4 Results

Tables 4-10 and 4-11 show emissions by source category for Uintah and Grand counties for all six pollutants. These inventories are generally representative of 1980 conditions. Gridded emission totals for the entire study region are presented in figure 4-3 for grid cells with significant emission rates. Clear plastic overlays showing geographical features are provided inside the cover of this report so that the reader can find the locations of area source emissions.

4.1.6 Utah Area Sources: Regional High-Oil-Production Scenario

Gridded emission inventories were prepared for the year 1990 assuming a high level of oil production in the Uinta Basin. These emission rates were obtained by projecting 1980 baseline emissions for all 47 area source categories. Emission factors were reviewed and revised where necessary. As described below, growth factors were derived from projected socioeconomic data for the future scenario. Pollutants were then spatially distributed on the basis of future-year socioeconomic data.

TABLE 4-10. 1980 BASELINE AREA SOURCE EMISSION INVENTORY FOR UTAH COUNTY

SOURCE CATEGORY	RHC	URHC	(tons per year)			TSP	CO
			NOx	SO ₂			
10 Petroleum -- Truck unloading	21.66	0.00	0.00	0.00	0.00	0.00	0.00
20 Petroleum -- Underground storage	17.77	0.00	0.00	0.00	0.00	0.00	0.00
30 Petroleum -- Auto tank filling	28.75	0.00	0.00	0.00	0.00	0.00	0.00
40 Surface coating	66.57	0.00	0.00	0.00	0.00	0.00	0.00
50 Petroleum drycleaning	3.70	0.00	0.00	0.00	0.00	0.00	0.00
60 Perchloroethylene drycleaning	11.67	0.00	0.00	0.00	0.00	0.00	0.00
70 1,1,1-trichloroethane degreasing	0.00	10.22	0.00	0.00	0.00	0.00	0.00
80 Trichloroethane degreasing	30.74	0.00	0.00	0.00	0.00	0.00	0.00
90 Graphic arts	8.20	0.00	0.00	0.00	0.00	0.00	0.00
100 Miscellaneous solvent usage	64.65	0.00	0.00	0.00	0.00	0.00	0.00
110 Pesticide usage	22.33	0.00	0.00	0.00	0.00	0.00	0.00
120 Ind. distillate oil combustion	0.00	0.07	1.96	3.18	0.12	0.40	0.00
130 Ind. residual oil combustion	0.00	0.07	6.90	16.43	1.32	0.56	0.00
140 Ind. LPG combustion	0.00	0.00	0.09	0.00	0.00	0.00	0.00
150 Ind. natural gas combustion	0.00	0.20	15.18	0.02	0.85	1.48	0.00
160 Comm. & Inst. coal combustion	0.02	17.73	35.51	134.89	94.60	59.15	0.00
170 Comm. & Inst. distillate oil combustion	0.00	0.20	5.43	8.87	0.46	1.20	0.00
180 Comm. & Inst. residual oil combustion	0.00	0.12	11.37	27.08	2.17	0.94	0.00
190 Comm. & Inst. LPG combustion	0.00	0.02	0.67	0.00	0.07	0.07	0.00
200 Comm. & Inst. natural gas combustion	0.00	1.10	16.34	0.06	1.30	2.74	0.00
210 Res. coal combustion	0.00	19.57	2.92	22.32	19.57	88.08	0.00
220 Res. distillate oil combustion	0.00	0.03	1.17	2.35	0.11	0.30	0.00
230 Res. LPG combustion	0.00	0.02	0.31	0.00	0.07	0.07	0.00
240 Res. wood combustion	18.76	0.00	3.72	0.00	74.91	449.93	0.00
250 Res. natural gas combustion	0.00	3.27	32.63	0.19	4.08	8.18	0.00
260 Agricultural waste burning	27.80	0.00	0.00	0.00	24.00	142.30	0.00
270 Wildfires	0.00	91.14	13.95	0.00	63.86	530.10	0.00
280 Res. construction	0.00	0.00	0.00	0.00	483.11	0.00	0.00
290 Comm. construction	0.00	0.00	0.00	0.00	57.54	0.00	0.00
300 Public & Inst. construction	0.00	0.00	0.00	0.00	107.98	0.00	0.00
310 Road construction	0.00	0.00	0.00	0.00	139.56	0.00	0.00
320 Agricultural wind erosion	0.00	0.00	0.00	0.00	488.00	0.00	0.00
330 Tilling	0.00	0.00	0.00	0.00	566.40	0.00	0.00
340 Gasoline farm tractors	1.90	51.05	41.80	1.45	2.20	9.00	0.00
350 Diesel farm tractors	1.95	9.80	54.15	5.05	7.40	19.25	0.00
360 Construction equipment (diesel)	3.29	14.31	200.55	15.31	12.87	46.93	0.00
370 Other gasoline usage	0.85	28.05	9.15	0.70	0.82	4.63	0.00
380 Other diesel usage	0.54	2.88	35.58	2.36	2.52	7.78	0.00
390 Piston aircraft	3.25	0.00	0.19	0.00	0.00	145.39	0.00
400 Jet aircraft	26.57	0.00	43.16	4.90	22.32	133.49	0.00
410 Railroads	0.00	0.00	0.00	0.00	0.00	0.00	0.00
420 Motor vehicle -- State highways	840.34	93.37	1095.20	67.54	129.19	10928.43	0.00
430 Motor vehicle -- County roads	450.16	50.02	350.21	25.84	52.83	6078.77	0.00
440 Motor vehicle -- Class "D" roads	540.74	60.08	135.29	11.51	35.60	6796.36	0.00
450 Motor vehicle -- State highways (fug. dust)	0.00	0.00	0.00	0.00	939.57	0.00	0.00
460 Motor vehicle -- County roads (fug. dust)	0.00	0.00	0.00	0.00	393.12	0.00	0.00
470 Motor vehicle -- Class "D" roads (fug. dust)	0.00	0.00	0.00	0.00	47549.62	0.00	0.00
--- TOTAL	2192.18	453.31	2113.40	350.04	51277.16	25455.34	0.00

TABLE 4-11. 1980 BASELINE AREA SOURCE EMISSION INVENTORY FOR GRAND COUNTY

SOURCE CATEGORY	(tons per year)					
	RHC	URHC	NOX	SO ₂	TSP	CO
10 Petroleum - Truck unloading	43.97	0.00	0.00	0.00	0.00	0.00
20 Petroleum - Underground storage	6.01	0.00	0.00	0.00	0.00	0.00
30 Petroleum - Auto tank filling	59.66	0.00	0.00	0.00	0.00	0.00
40 Surface coating	26.77	0.00	0.00	0.00	0.00	0.00
50 Petroleum drycleaning	1.47	0.00	0.00	0.00	0.00	0.00
60 Perchloroethylene drycleaning	4.71	0.00	0.00	0.00	0.00	0.00
70 1,1,1-trichloroethane degreasing	0.00	4.09	0.00	0.00	0.00	0.00
80 Trichloroethane degreasing	12.32	0.00	0.00	0.00	0.00	0.00
90 Graphic arts	3.20	0.00	0.00	0.00	0.00	0.00
100 Miscellaneous solvent usage	25.96	0.00	0.00	0.00	0.00	0.00
110 Pesticide usage	0.84	0.00	0.00	0.00	0.00	0.00
120 Ind. distillate oil combustion	0.00	0.02	0.44	0.73	0.03	0.09
130 Ind. residual oil combustion	0.00	0.02	1.54	3.70	0.30	0.13
140 Ind. LPG combustion	0.00	0.00	0.02	0.00	0.00	0.00
150 Ind. natural gas combustion	0.00	0.05	3.42	0.00	0.18	0.32
160 Comm. & Inst. coal combustion	0.01	7.10	14.22	53.93	37.86	23.16
170 Comm. & Inst. distillate oil combustion	0.00	0.09	2.14	3.52	0.18	0.49
180 Comm. & Inst. residual oil combustion	0.00	0.08	4.56	10.83	0.86	0.38
190 Comm. & Inst. LPG combustion	0.00	0.01	0.20	0.00	0.03	0.03
200 Comm. & Inst. natural gas combustion	0.00	0.43	6.52	0.02	0.51	0.98
210 Res. coal combustion	0.00	8.78	1.24	10.24	8.97	40.45
220 Res. distillate oil combustion	0.00	0.02	0.52	1.06	0.07	0.14
230 Res. LPG combustion	0.00	0.01	0.13	0.00	0.02	0.02
240 Res. wood combustion	7.53	0.00	1.48	0.00	30.82	180.70
250 Res. natural gas combustion	0.00	1.48	14.98	0.10	1.85	3.70
260 Agricultural waste burning	17.43	0.00	0.00	0.00	14.98	89.11
270 Wildfires	0.00	109.82	17.86	0.00	77.90	650.18
280 Res. construction	0.00	0.00	0.00	0.00	193.71	0.00
290 Comm. construction	0.00	0.00	0.00	0.00	21.62	0.00
300 Public & Inst. construction	0.00	0.00	0.00	0.00	43.18	0.00
310 Road construction	0.00	0.00	0.00	0.00	69.78	0.00
320 Agricultural wind erosion	0.00	0.00	0.00	0.00	35.49	0.00
330 Tilling	0.00	0.00	0.00	0.00	748.93	0.00
340 Gasoline farm tractors	0.21	5.53	4.55	0.14	0.21	0.98
350 Diesel farm tractors	0.21	1.05	6.02	0.56	0.84	2.10
360 Construction equipment (diesel)	0.67	2.87	40.70	3.11	2.59	9.53
370 Other gasoline usage	0.34	11.26	3.66	0.29	0.32	1.84
380 Other diesel usage	0.20	1.14	14.33	0.94	1.00	3.10
390 Piston aircraft	0.00	0.00	0.00	0.00	0.00	0.00
400 Jet aircraft	0.00	0.00	0.00	0.00	0.00	0.00
410 Railroads	38.96	290.72	1144.86	175.83	0.00	0.00
420 Motor vehicle - State highways	575.67	63.96	750.29	46.25	76.92	401.61
430 Motor vehicle - County roads	313.61	34.85	244.05	17.96	88.51	7486.57
440 Motor vehicle - Class "D" roads	136.64	15.18	34.22	2.96	36.80	4235.21
450 Motor vehicle - State highways (fug. dust)	0.00	0.00	0.00	0.00	9.04	1717.37
460 Motor vehicle - County roads (fug. dust)	0.00	0.00	0.00	0.00	643.65	0.00
470 Motor vehicle - Class "D" roads (fug. dust)	0.00	0.00	0.00	0.00	273.89	0.00
---	1275.45	558.75	2311.92	332.16	14435.99	14848.08
TOTAL						

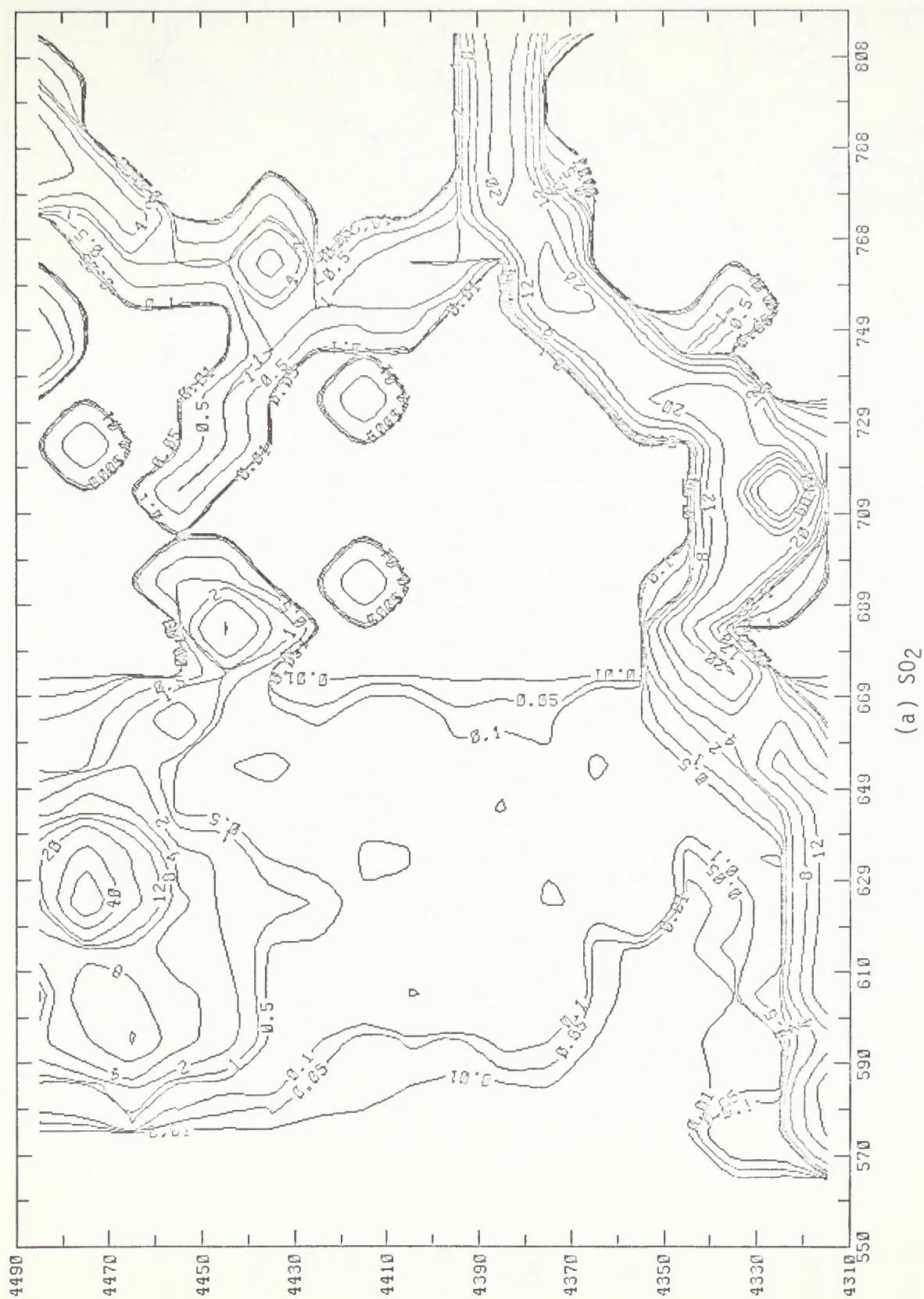
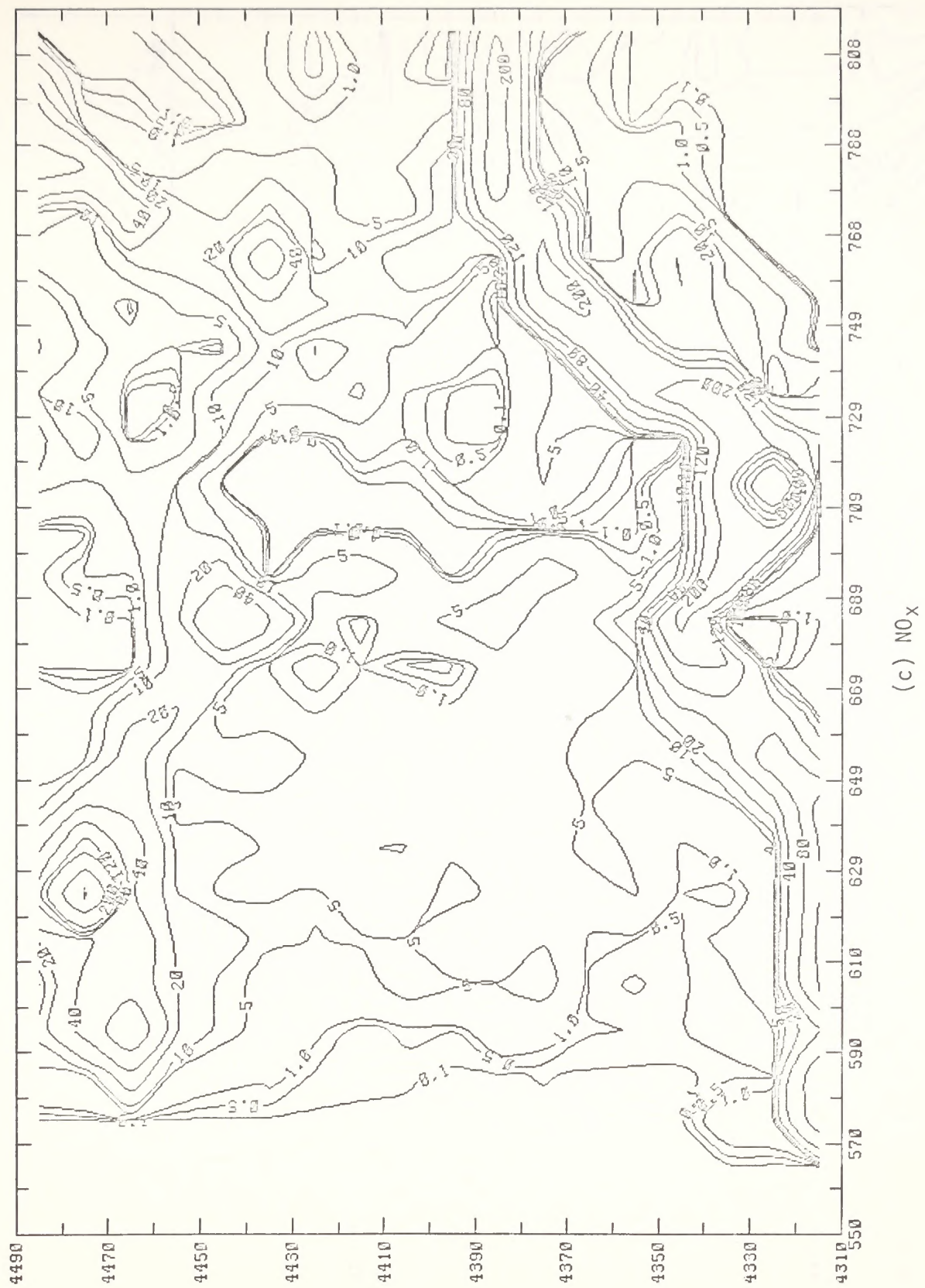


FIGURE 4-3. AREA EMISSION SOURCE INVENTORY FOR THE STUDY REGION IN THE BASELINE YEAR 1980 (tons/yr/100 km²)



(b) TSP

FIGURE 4-3 (Continued)



(c) NO_x

FIGURE 4-3 (Continued)



(d) C0

FIGURE 4-3 (Continued)



(e) Reactive Hydrocarbons

FIGURE 4-3 (Continued)



(f) Unreactive Hydrocarbons

4.1.6.1 Emission Factors

Emission factors given in Table 4-8 were used for all source categories except on-road motor vehicles (exhaust). The emission factors for these categories were available for 1990 from PEDCo (1981) and are given in table 4-12. As in the baseline case, 90 percent of the total hydrocarbons were assumed to be reactive.

4.1.6.2 Activity Projections

Each emission source category was related to an activity parameter based on socioeconomic information (illustrated in table 4-13). Such socioeconomic data were available from the NPS (1982) for the high-oil-production scenario as well as for the 1980 baseline. Some of the source categories for which information was sparse are discussed below.

No future projections of air traffic volume were available. We used the population of the city of Vernal as an index of commercial and general aviation growth in Uintah County. Both the airports included in the baseline inventory, Vernal and Roosevelt, are in the vicinity of Vernal.

It was assumed that railroads are employed mainly to haul mineral products, and thus mining employment was used as the activity parameter to project railroad emissions. There is no indication that the synfuel industry will utilize railroads significantly, and thus the mining employment related to the synfuel industry was not included.

The unavailability of pertinent data to project the emissions from class "D" roads posed a difficult situation. For the 1980 baseline, this category constitutes over 90 percent of total particulate emissions for Uintah County and over 80 percent for Grand County. Moreover, the baseline AADT estimate of 50 is an approximation, and we were cautioned (UDOT, 1982) about projecting this number. We estimate that there will be an increase in the class "D" road activity (vehicle kilometers travelled) and that this increase might range between 25 percent and 100 percent of the population increase. We would not expect an increase in VKMT for class "D" roads equivalent to the projected population growth because of the magnitude of this population increase. For example, many roads currently unimproved may be paved in the future, reflecting their increased use. This would significantly reduce particulate matter emissions from roadway travel. Furthermore, the rural nature of Uintah and Grand counties, which is directly related to class "D" road activity, will be altered dramatically by the projected population growth in the region. Fewer opportunities will be available for activities related to present class "D" road use as the area becomes more urbanized. In light

TABLE 4-12. EMISSION FACTORS FOR ON-ROAD MOTOR VEHICLES
(EXHAUST) FOR 1990

<u>Source Category</u>	<u>Hydrocarbons</u>	<u>NO_x</u>	<u>SO₂</u>	<u>Particulate Matter</u>	<u>CO</u>	<u>Unit</u>
State highways	0.93	2.27	0.25	0.48	12.22	gm/km
County roads	1.37	1.77	0.22	0.48	17.21	gm/km
Class "D" roads	1.90	0.83	0.13	0.36	22.49	gm/km

TABLE 4-13. AREA SOURCE PROJECTION PARAMETERS

Source Category	Projection Parameter
Petroleum marketing and transport	Gasoline consumption
Organic solvent usage	Population
Pesticide usage	Acres in farms
Fuel combustion	
Industrial	Assumed constant
Commercial and institutional	
Coal	Population
Distillate oil	Population
Residual oil	Assumed constant
LPG	Assumed constant
Natural gas	Population
Residential	Housing units by fuel use
Agricultural waste burning	Acres in farms
Wildfires	Assumed constant
Construction	
Residential	Housing units constructed
Commercial	Acres of commercial construction
Public and institutional	Acres of public and institutional construction
Roads	Miles of new roads
Agricultural wind erosion	Acres in farms
Tilling	Acres in farms
Off-road mobile sources	
Gasoline farm tractors	Acres in farms
Diesel farm tractors	Acres in farms
Construction equipment (diesel)	Nonbuilding construction employment
Other gasoline usage	Population
Other diesel usage	Population
Piston aircraft	Population of the city in which located
Jet aircraft	Population of the city in which located
Railroads	Mining employment (excluding synfuel)

TABLE 4-13 (Concluded)

Source Category	Projection Parameter
On-road motor vehicles (exhaust)	
State highways	Population
County roads	Population
Class "D" roads	A parameter based on population (refer to text)
On-road motor vehicles (fugitive dust)	
State highways (paved)	Population
County roads (paved)	Population
Class "D" roads (unpaved)	A parameter based on population (refer to text)

of these considerations, we assumed the future VKMT increase to be 50 percent of the total county population increase; e.g., if the population doubled, then the class "D" road activity would increase by a factor of 1.5 (i.e., $0.5 + 1$). It should be emphasized that a large degree of uncertainty is inherent in this estimate. The lack of relevant projections prevented a more accurate treatment.

4.1.6.3 Spatial Allocation

The source category/allocation parameter relationship presented in table 4-9 was used for the future scenarios; the revised gridded information accounted for changes in the spatial distribution of emissions with respect to the 1980 baseline. Careful examination of projected population data shows that within each county, certain areas will experience larger growth than others. In general, it was found that the urban areas were projected to undergo relatively larger population increases (NPS, 1982). This uneven growth in population was accounted for during the preparation of the gridded population files for the future-year scenario. Furthermore, a new town in Grand County and a construction camp in Uintah County were explicitly included by allocating population to the appropriate grid cells.

Although total emissions associated with agricultural activities were reduced from the 1980 baseline because of increased population, we assumed a uniform reduction in these emissions for the appropriate grid cells in each county. For the other allocation parameters, no information was available to redistribute the emissions with respect to the 1980 baseline inventory.

4.1.6.4 Results

Emission totals for Uintah and Grand counties are presented in tables 4-14 and 4-15, respectively. Emission density maps for this high-oil-production scenario are presented in section 5.

4.1.7 Utah Area Sources: Regional Low-Oil-Production Scenario

Area source emission inventories were prepared for Uintah and Grand counties for 1990 with the assumption of a low level of oil production on a regional scale. Procedures used to develop this inventory are similar to those for the estimation of the high-oil-shale scenario.

TABLE 4-14. REGIONAL HIGH OIL PRODUCTION SCENARIO AREA SOURCE EMISSION INVENTORY FOR UINTAH COUNTY

SOURCE CATEGORY	RHC	URHC	NDX	SO2	TSP	CO
(tons per year)						
10 Petroleum - Truck unloading	68.10	0.00	0.00	0.00	0.00	0.00
20 Petroleum - Underground storage	55.91	0.00	0.00	0.00	0.00	0.00
30 Petroleum - Auto tank filling	90.69	0.00	0.00	0.00	0.00	0.00
40 Surface coating	209.79	0.00	0.00	0.00	0.00	0.00
50 Petroleum drycleaning	11.53	0.00	0.00	0.00	0.00	0.00
60 Perchloroethylene drycleaning	36.79	0.00	0.00	0.00	0.00	0.00
70 1,1,1-trichloroethane degreasing	0.00	32.35	0.00	0.00	0.00	0.00
80 Trichloroethane degreasing	96.86	0.00	0.00	0.00	0.00	0.00
90 Graphic arts	25.74	0.00	0.00	0.00	0.00	0.00
100 Miscellaneous solvent usage	203.43	0.00	0.00	0.00	0.00	0.00
110 Pesticide usage	20.34	0.00	0.00	0.00	0.00	0.00
120 Ind distillate oil combustion	0.00	0.07	1.96	3.17	0.12	0.43
130 Ind residual oil combustion	0.00	0.09	6.87	16.49	1.32	0.56
140 Ind LPG combustion	0.00	0.00	0.09	0.00	0.00	0.00
150 Ind natural gas combustion	0.00	0.22	15.14	0.03	0.88	1.45
160 Comm. & Inst coal combustion	0.06	55.82	111.76	424.71	298.08	186.32
170 Comm & Inst distillate oil combustion	0.00	0.69	17.01	27.81	1.45	3.91
180 Comm & Inst residual oil combustion	0.00	0.13	11.38	27.10	2.18	0.93
190 Comm & Inst LPG combustion	0.00	0.02	0.55	0.00	0.07	0.07
200 Comm & Inst natural gas combustion	0.00	3.37	51.34	0.22	4.03	8.54
210 Res. coal combustion	0.00	61.74	9.21	70.36	61.74	277.96
220 Res distillate oil combustion	0.00	0.09	3.31	6.56	0.31	0.83
230 Res LPG combustion	0.00	0.06	0.79	0.00	0.22	0.22
240 Res. wood combustion	63.88	0.00	12.72	0.00	255.23	1533.64
250 Res. natural gas combustion	0.00	10.22	102.92	0.69	12.97	25.74
260 Agricultural waste burning	25.33	0.00	0.00	0.00	21.86	129.64
270 Wildfires	0.00	91.14	13.95	0.00	63.86	530.10
280 Res. construction	0.00	0.00	0.00	0.00	1520.02	0.00
290 Comm. construction	0.00	0.00	0.00	0.00	179.94	0.00
300 Public & Inst construction	0.00	0.00	0.00	0.00	338.30	0.00
310 Road construction	0.00	0.00	0.00	0.00	442.18	0.00
320 Agricultural wind erosion	0.00	0.00	0.00	0.00	444.57	0.00
330 Tilling	0.00	0.00	0.00	0.00	515.99	0.00
340 Gasoline farm tractors	1.73	46.51	38.08	1.32	2.00	8.20
350 Diesel farm tractors	1.78	8.93	49.33	4.60	6.74	17.54
360 Construction equipment (diesel)	8.22	35.47	497.62	38.07	31.92	116.48
370 Other gasoline usage	2.77	88.39	28.95	2.27	2.55	14.46
380 Other diesel usage	1.57	8.88	111.98	7.50	8.00	24.29
390 Piston aircraft	11.03	0.00	0.64	0.00	0.00	493.45
400 Jet aircraft	90.18	0.00	146.48	16.63	75.75	453.06
410 Railroads	0.00	0.00	0.00	0.00	0.00	0.00
420 Motor vehicle - State highways	773.95	85.99	2099.50	231.26	443.90	11299.99
430 Motor vehicle - County roads	477.17	53.02	685.01	85.27	185.75	6662.33
440 Motor vehicle - Class "D" roads	370.41	41.16	179.66	28.19	78.32	4934.16
450 Motor vehicle - State highways (fug. dust)	0.00	0.00	0.00	0.00	2959.64	0.00
460 Motor vehicle - County roads (fug. dust)	0.00	0.00	0.00	0.00	1238.32	0.00
470 Motor vehicle - Class "D" roads (fug. dust)	0.00	0.00	0.00	0.00	9865.48*	0.00
--- TOTAL	2647.21	624.34	4196.19	992.22	107861.84	26724.00

*See section 4.1.6.2 for an explanation of the uncertainty in this estimate.

TABLE 4-15. REGIONAL HIGH OIL PRODUCTION SCENARIO AREA SOURCE EMISSION INVENTORY FOR-GRAND COUNTY

SOURCE CATEGORY	RHC	URHC	NOX	SO2	TSP	CO
10 Petroleum - Truck unloading	84.63	0.00	0.00	0.00	0.00	0.00
20 Petroleum - Underground storage	11.46	0.00	0.00	0.00	0.00	0.00
30 Petroleum - Auto tank filling	112.80	0.00	0.00	0.00	0.00	0.00
40 Surface coating	51.43	0.00	0.00	0.00	0.00	0.00
50 Petroleum drycleaning	2.81	0.00	0.00	0.00	0.00	0.00
60 Perchloroethylene drycleaning	8.98	0.00	0.00	0.00	0.00	0.00
70 1,1,1-trichloroethane degreasing	0.00	7.84	0.00	0.00	0.00	0.00
80 Trichloroethane degreasing	23.76	0.00	0.00	0.00	0.00	0.00
90 Graphic arts	6.30	0.00	0.00	0.00	0.00	0.00
100 Miscellaneous solvent usage	49.88	0.00	0.00	0.00	0.00	0.00
110 Pesticide usage	0.82	0.00	0.00	0.00	0.00	0.00
120 Ind. distillate oil combustion	0.00	0.02	0.44	0.71	0.03	0.10
130 Ind. residual oil combustion	0.00	0.03	1.55	3.72	0.28	0.12
140 Ind. LPG combustion	0.00	0.00	0.02	0.00	0.00	0.00
150 Ind. natural gas combustion	0.00	0.05	3.41	0.00	0.19	0.32
160 Comm. & Inst. coal combustion	0.02	13.70	27.29	103.56	72.75	44.49
170 Comm. & Inst. distillate oil combustion	0.00	0.19	4.13	6.73	0.37	0.92
180 Comm. & Inst. residual oil combustion	0.00	0.09	4.54	10.77	0.85	0.38
190 Comm. & Inst. LPG combustion	0.00	0.01	0.21	0.00	0.03	0.03
200 Comm. & Inst. natural gas combustion	0.00	0.82	12.44	0.06	0.98	1.90
210 Res. coal combustion	0.00	17.29	2.37	19.73	17.31	77.75
220 Res. distillate oil combustion	0.00	0.06	1.01	2.06	0.14	0.29
230 Res. LPG combustion	0.00	0.02	0.23	0.00	0.05	0.06
240 Res. wood combustion	14.50	0.00	2.85	0.00	59.29	347.51
250 Res. natural gas combustion	0.00	2.84	28.71	0.19	3.57	7.15
260 Agricultural waste burning	17.10	0.00	0.00	0.00	14.70	87.42
270 Wildfires	0.00	109.82	17.86	0.00	77.90	650.18
280 Res. construction	0.00	0.00	0.00	0.00	373.05	0.00
290 Comm. construction	0.00	0.00	0.00	0.00	43.22	0.00
300 Public & Inst. construction	0.00	0.00	0.00	0.00	100.79	0.00
310 Road construction	0.00	0.00	0.00	0.00	116.42	0.00
320 Agricultural wind erosion	0.00	0.00	0.00	0.00	34.82	0.00
330 Tilling	0.00	0.00	0.00	0.00	734.70	0.00
340 Gasoline farm tractors	0.21	5.42	4.46	0.14	0.21	0.96
350 Diesel farm tractors	0.21	1.03	5.91	0.55	0.82	2.06
360 Construction equipment (diesel)	1.58	6.70	94.60	7.18	6.02	22.13
370 Other gasoline usage	0.67	21.55	7.05	0.52	0.62	3.56
380 Other diesel usage	0.40	2.17	27.45	1.81	1.94	5.94
390 Piston aircraft	0.00	0.00	0.00	0.00	0.00	0.00
400 Jet aircraft	0.00	0.00	0.00	0.00	0.00	0.00
410 Railroads	100.48	749.77	2952.59	453.47	198.38	1035.75
420 Motor vehicle - State highways	323.52	35.95	877.84	96.62	185.61	4724.03
430 Motor vehicle - County roads	202.91	22.55	291.39	36.17	78.97	2833.35
440 Motor vehicle - Class "D" roads	65.86	7.32	32.00	5.10	14.00	877.58
450 Motor vehicle - State highways (fug. dust)	0.00	0.00	0.00	0.00	1237.09	0.00
460 Motor vehicle - County roads (fug. dust)	0.00	0.00	0.00	0.00	526.41	0.00
470 Motor vehicle - Class "D" roads (fug. dust)	0.00	0.00	0.00	0.00	17554.10*	0.00
--- TOTAL	1080.30	1005.23	4400.28	749.06	21455.28	10723.86

*See section 4.1.6.2 for an explanation of the uncertainty in this estimate.

4.1.7.1 Emission Factors

For all emission source categories, except on-road motor vehicles (exhaust), the emission factors given in table 4-8 were employed. Emission factors given in table 4-12 were used for on-road motor vehicles (exhaust).

4.1.7.2 Activity Projections

The activity parameters were derived from socioeconomic data pertaining to the low-oil-shale-development scenario for 1990 (NPS, 1982). Source category-projection parameter relationships shown in table 4-13 were used.

4.1.7.3 Allocation Parameters

The procedures described for the development of the regional high scenario were used. Spatially nonuniform growth of population and a decline of agricultural activities were treated appropriately.

4.1.7.4 Results

Tables 4-16 and 4-17 show the emission totals for Uintah and Grand counties, respectively, for area sources. Spatial distributions of area source emissions are discussed in section 5.

4.1.8 Utah Area Source Summary

Table 4-18 summarizes the area source emission totals in kilograms per hour for each county and scenario. Note that approximately 80 to 90 percent of total particulate emissions from area sources are emitted as fugitive dust from unpaved roads.

4.1.9 Socioeconomic Data Comparison for Utah

The socioeconomic data used to project the Utah area source emissions to future years were developed by the NPS (1982). Because of the required schedule for completing the inventories, socioeconomic data developed by the Utah State Planning Coordinator's Office (1982) could not be employed for the air quality analysis, even though these data were used in other portions of the Uinta Basin Synfuels EIS. We have compared the Utah data

TABLE 4-16. REGIONAL LOW OIL PRODUCTION SCENARIO AREA SOURCE EMISSION INVENTORY FOR UTAH COUNTY

SOURCE CATEGORY	PM10	PM2.5	NOX	SO2	TSP	CO
10 Petroleum - Truck unloading	14.88	0.00	0.00	0.00	0.00	0.00
20 Petroleum - Underground storage	36.89	0.00	0.00	0.00	0.00	0.00
30 Petroleum - Auto tank filling	59.64	0.00	0.00	0.00	0.00	0.00
40 Surface coating	128.24	0.00	0.00	0.00	0.00	0.00
50 Petroleum truckcleaning	2.58	0.00	0.00	0.00	0.00	0.00
60 Perchloroethylene drycleaning	34.25	0.00	0.00	0.00	0.00	0.00
70 1,1,1-trichloroethane degreasing	0.60	21.00	0.00	0.00	0.00	0.00
80 Trichloroethane degreasing	62.82	0.00	0.00	0.00	0.00	0.00
90 Graphic arts	17.00	0.00	0.00	0.00	0.00	0.00
100 Miscellaneous solvent usage	134.01	0.00	0.00	0.00	0.00	0.00
110 Pesticide usage	21.33	0.00	0.00	0.00	0.00	0.00
120 Ind. distillate oil combustion	0.00	0.07	1.96	3.14	0.12	0.41
130 Ind. residual oil combustion	0.00	0.07	6.88	16.45	1.28	0.54
140 Ind. LPG combustion	0.00	0.22	15.13	0.03	0.86	1.49
150 Ind. natural gas combustion	0.04	36.79	73.66	279.91	196.35	122.82
160 Comm. & Inst. coal combustion	0.00	0.46	11.25	18.39	0.98	2.47
170 Comm. & Inst. distillate oil combustion	0.00	0.13	11.36	27.08	2.18	0.93
180 Comm. & Inst. residual oil combustion	0.00	0.02	0.58	0.00	0.07	0.07
190 Comm. & Inst. LPG combustion	0.00	2.24	33.82	0.12	2.62	5.67
200 Comm. & Inst. natural gas combustion	0.00	40.61	6.00	46.27	40.61	182.74
210 Res. coal combustion	0.00	0.06	2.20	4.29	0.21	0.49
220 Res. distillate oil combustion	0.00	0.04	0.48	0.00	0.15	0.15
230 Res. LPG combustion	41.87	0.00	8.41	0.00	167.76	1006.90
240 Res. wood combustion	0.00	6.74	67.56	0.37	8.47	16.97
250 Res. natural gas combustion	26.55	0.00	0.00	0.00	22.92	135.90
260 Agricultural waste burning	0.00	91.14	13.95	0.00	63.86	530.10
270 Wildfires	0.00	0.00	0.00	0.00	1004.45	0.00
280 Res. construction	0.00	0.00	0.00	0.00	115.20	0.00
290 Comm. construction	0.00	0.00	0.00	0.00	230.32	0.00
300 Public & Inst. construction	0.00	0.00	0.00	0.00	325.66	0.00
310 Road construction	0.00	0.00	0.00	0.00	466.04	0.00
320 Agricultural wind erosion	0.00	0.00	0.00	0.00	540.91	0.00
330 Tilling	1.81	48.75	39.92	1.38	2.10	8.59
340 Gasoline farm tractors	1.86	9.36	51.71	4.82	7.07	18.38
350 Diesel farm tractors	4.81	21.07	294.09	22.52	18.92	68.83
360 Construction equipment (diesel)	1.83	58.27	19.08	1.47	1.65	9.59
370 Other gasoline usage	1.06	3.92	73.91	4.90	5.23	16.15
380 Other diesel usage	7.06	0.00	0.41	0.00	0.00	315.93
390 Piston aircraft	57.74	0.00	93.79	10.65	48.50	290.07
400 Jet aircraft	0.00	0.00	0.00	0.00	0.00	0.00
410 Railroads	510.09	56.68	1384.33	152.44	292.62	7453.19
420 Motor vehicle - State highways	314.66	34.56	451.42	56.20	122.41	4388.87
430 Motor vehicle - County roads	274.70	30.52	133.12	20.89	58.03	3656.44
440 Motor vehicle - Class "D" roads	0.00	0.00	0.00	0.00	1950.55	0.00
450 Motor vehicle - State highways (fug. dust)	0.00	0.00	0.00	0.00	816.11	0.00
460 Motor vehicle - County roads (fug. dust)	0.00	0.00	0.00	0.00	73131.31*	0.00
470 Motor vehicle - Class "D" roads (fug. dust)	0.00	0.00	0.00	0.00	79643.77	18233.45
TOTAL	1791.68	465.40	2795.04	671.32	79643.77	18233.45

* See section 4.1.6.2 for an explanation of the uncertainty in the estimate.

TABLE 4-17. REGIONAL LOW OIL PRODUCTION SCENARIO AREA SOURCE EMISSION INVENTORY FOR GRAND COUNTY

(tons per year)

SOURCE CATEGORY	RHC	URHC	NOX	SO2	TSP	CO
10 Petroleum - Truck unloading	69 97	0.00	0.00	0.00	0.00	0.00
20 Petroleum - Underground storage	9 45	0.00	0.00	0.00	0.00	0.00
30 Petroleum - Auto tank filling	93 36	0.00	0.00	0.00	0.00	0.00
40 Surface coating	42 65	0.00	0.00	0.00	0.00	0.00
50 Petroleum drucleaning	2 34	0.00	0.00	0.00	0.00	0.00
60 Perchloroethylene drycleaning	7 43	0.00	0.00	0.00	0.00	0.00
70 1,1,1-trichloroethane degreasing	0 00	6.51	0.00	0.00	0.00	0.00
80 Trichloroethane degreasing	19 63	0.00	0.00	0.00	0.00	0.00
90 Graphic arts	5 20	0.00	0.00	0.00	0.00	0.00
100 Miscellaneous solvent usage	41 35	0.00	0.00	0.00	0.00	0.00
110 Pesticide usage	0 83	0.00	0.00	0.00	0.00	0.00
120 Ind. distillate oil combustion	0 00	0.01	0.43	0.71	0.04	0.10
130 Ind. residual oil combustion	0 00	0.03	1.55	3.72	0.30	0.12
140 Ind. LPG combustion	0 00	0.00	0.02	0.00	0.00	0.00
150 Ind. natural gas combustion	0 00	0.05	3.39	0.00	0.18	0.33
160 Comm. & Inst. coal combustion	0 02	11 31	22 58	85 72	60 20	36 80
170 Comm. & Inst. distillate oil combustion	0 00	0.16	3.40	5.57	0.27	0.76
180 Comm. & Inst. residual oil combustion	0 00	0.07	4.51	10 82	0.87	0.38
190 Comm. & Inst. LPG combustion	0 00	0.01	0.20	0.00	0.04	0.04
200 Comm. & Inst. natural gas combustion	0 00	0.67	10 28	0.09	0.81	1.98
210 Res. coal combustion	0 00	14 52	2 02	16 59	14 52	65 29
220 Res. distillate oil combustion	0 00	0.05	0.83	1.68	0.11	0.24
230 Res. LPG combustion	0 00	0.02	0.19	0.00	0.05	0.05
240 Res. wood combustion	11 87	0.00	2.35	0.00	48 57	285 00
250 Res. natural gas combustion	0 00	2 37	23 74	0.18	2 95	5 94
260 Agricultural waste burning	17 22	0.00	0.00	0.00	14 80	88 04
270 Wildfires	0 00	109 82	17 86	0.00	77 90	650 18
280 Res. construction	0 00	0.00	0.00	0.00	308 89	0.00
290 Comm. construction	0 00	0.00	0.00	0.00	35 99	0.00
300 Public & Inst. construction	0 00	0.00	0.00	0.00	79 17	0.00
310 Road construction	0 00	0.00	0.00	0.00	93 07	0.00
320 Agricultural wind erosion	0 00	0.00	0.00	0.00	39 06	0.00
330 Lilling	0 00	0.00	0.00	0.00	739 94	0.00
340 Gasoline farm tractors	0 21	5 46	4 50	0.14	0.21	0.97
350 Diesel farm tractors	0 21	1 04	5 95	0.55	0.83	2 07
360 Construction equipment (diesel)	1 58	6 70	94 63	7 18	6 02	22 16
370 Other gasoline usage	0 56	17 93	5 84	0 46	0 53	2 94
380 Other diesel usage	0 32	1 78	22 69	1 50	1 61	4 92
390 Piston aircraft	0 00	0.00	0.00	0.00	0.00	0.00
400 Jet aircraft	0 00	0.00	0.00	0.00	0.00	0.00
410 Railroads	100 48	749 77	2952 59	453 47	198 38	1035 75
420 Motor vehicle - State highways	267 68	29 74	726 28	79 97	153 65	3907 99
430 Motor vehicle - County roads	168 10	18 68	241 12	29 94	65 36	2346 30
440 Motor vehicle - Class "D" roads	58 48	6 50	28 37	4 53	12 42	779 69
450 Motor vehicle - State highways (fug. dust)	0 00	0.00	0.00	0.00	1024 05	0.00
460 Motor vehicle - County roads (fug. dust)	0 00	0.00	0.00	0.00	435 76	0.00
470 Motor vehicle - Class "D" roads (fug. dust)	0 00	0.00	0.00	0.00	15571 60*	0.00
TOTAL	918 93	983 17	4175 25	702 74	18983.89	9237 54

*See section 4.1.6.2 for an explanation of the uncertainty in this estimate.

TABLE 4-18. EMISSION TOTALS FOR AREA SOURCES IN UTAH

(kilograms per hour)

(a) Baseline

<u>County</u>	<u>Sulfur Dioxide</u>	<u>Particulate Matter</u>	<u>Nitrogen Oxides</u>	<u>Total Hydrocarbon</u>	<u>Carbon Monoxide</u>
Uintah	36	5310	219	274	2636
Grand	34	1495	239	190	1538

(b) Regional High Scenario

<u>County</u>	<u>Sulfur Dioxide</u>	<u>Particulate Matter</u>	<u>Nitrogen Oxides</u>	<u>Total Hydrocarbon</u>	<u>Carbon Monoxide</u>
Uintah	103	11,170	435	339	2768
Grand	78	2,222	456	216	1111

(c) Regional Low Scenario

<u>County</u>	<u>Sulfur Dioxide</u>	<u>Particulate Matter</u>	<u>Nitrogen Oxides</u>	<u>Total Hydrocarbon</u>	<u>Carbon Monoxide</u>
Uintah	70	8248	289	234	1888
Grand	73	1966	432	197	957

to the information we used to develop the future area source inventories and conclude that although there are differences, the magnitude of the difference is within the uncertainty of the projected values. For example, the Utah 1990 baseline population data are 8.4 percent greater and 2.6 percent less than the NPS data for Uintah and Grand counties, respectively. In the case of the regional high scenario for 1990, the Utah population data are 0.9 and 8.5 percent less than the comparable total population data we used for Uintah and Grand counties (see table 4-19 and figure 4-4). For the regional low scenario in 1990, however, the projections differ because of changes in assumed locations of new population. For this scenario, the Utah population data are 26.8 percent greater for Uintah County and 17.3 percent less for Grand County when compared to the NPS data we employed. Overall for both counties combined, the Utah population data are 16.4 percent greater for the regional low scenario. One of the primary differences between the two sets of projections is that the data we used included the new town of Westwater in Grand County whereas the state of Utah data for the low scenario did not.

4.1.10 Concluding Remarks Pertaining to Inventory Activities

Previous emission inventory work, particularly in the Utah portion of the study region, has been limited primarily because of the low level of activities in this sparsely populated area. Much of our inventory development process has resulted in the first comprehensive set of emission estimates for this part of the country. Elements of the inventory process that contribute to the unique and embryonic nature of this work include the following:

- > Synfuel projects. Oil shale and tar sands facilities are generally in the pilot plant stage at present. Emission factors for the several processes being proposed are uncertain, and the effectiveness of specific control technologies throughout portions of the processes remains unproven.
- > Other planned projects in Utah. Little information was available relative to facility size, process description, and proposed controls for most of these future point sources.
- > Area source activities and emission factors. Because of the sparse population in the region, area source activity data (e.g., commercial natural gas use, aircraft operations, and petroleum marketing) were limited in scope.

TABLE 4-19. TOTAL POPULATION FOR 1990 REGIONAL SCENARIOS (NPS)

<u>Location</u>	<u>Scenario</u>	
	<u>Low</u>	<u>High</u>
Uintah County		
Vernal	35,128	54,881
Bonanza construction camp	880	1,104
Rural area	<u>6,556</u>	<u>8,606</u>
County total	42,564	64,591
Grand County		
New town: Westwater	2,260	4,988
Moab	10,506	10,506
Rural area	<u>347</u>	<u>347</u>
County total	13,113	15,841

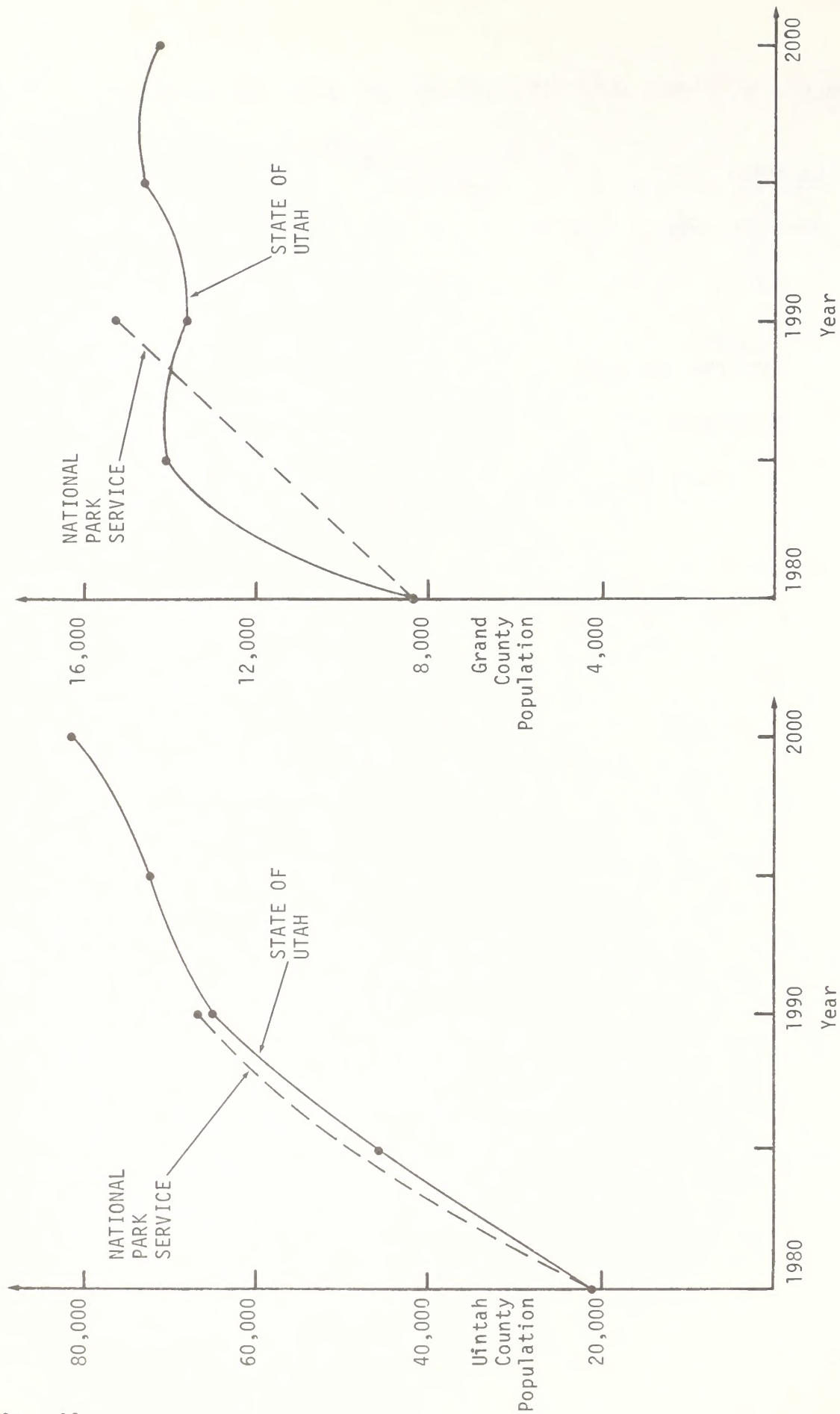


FIGURE 4-4. TOTAL CUMULATIVE POPULATION IN THE UINTA BASIN WITH HIGH-LEVEL SYNFUEL DEVELOPMENT

Often, activity data were not available even on a county-wide basis. Furthermore, emission factors have never been adapted to conditions in eastern Utah.

- > Area source gridding. This study represents the first set of gridded emission inventories for eastern Utah. Information that we normally use to grid area sources was either sparse or unavailable.
- > Projection techniques. Projecting emissions is always uncertain; when combined with the indeterminate and fluid nature of future energy development proposals for this region, emission projections should only be used with an understanding of their limitations.

Taking into consideration the aforementioned points as well as the large size of the study region, the cautious reviewer will understand that a large degree of uncertainty prevails in each of the inventories.

4.2 DESCRIPTION OF MODELING APPROACHES

In this section we describe the approach adopted for the analysis of regional-scale air quality and visibility impacts resulting from oil shale development in the Uinta Basin and in Colorado, and from other existing and anticipated emission sources.

4.2.1 Modeling Methodology

In this effort our aim was to apply the most sophisticated and realistic modeling methodology currently available. The complex dispersion processes that occur in the rugged terrain of the study region, the large size of the modeling region, and diverse temporal scales (3 hour, 24 hour, and annual averages) strain the capabilities of almost all routinely applied air quality models. The simple models (e.g., VALLEY, CRSTER, and COMPLEX), which have been previously applied to some of the proposed facilities studied here, are recognized as having serious shortcomings on a regional scale in this setting; among the most serious are

- > Inability to treat spatially and temporally varying wind fields.
- > Inability to treat spatially and temporally varying dispersion rates.

- > Inability to properly treat the effects of topography, slope winds and other physical processes in complex terrain (assuming instantaneous and straight-line plume transport).
- > Limited ability to treat chemical transformations and removal mechanisms.

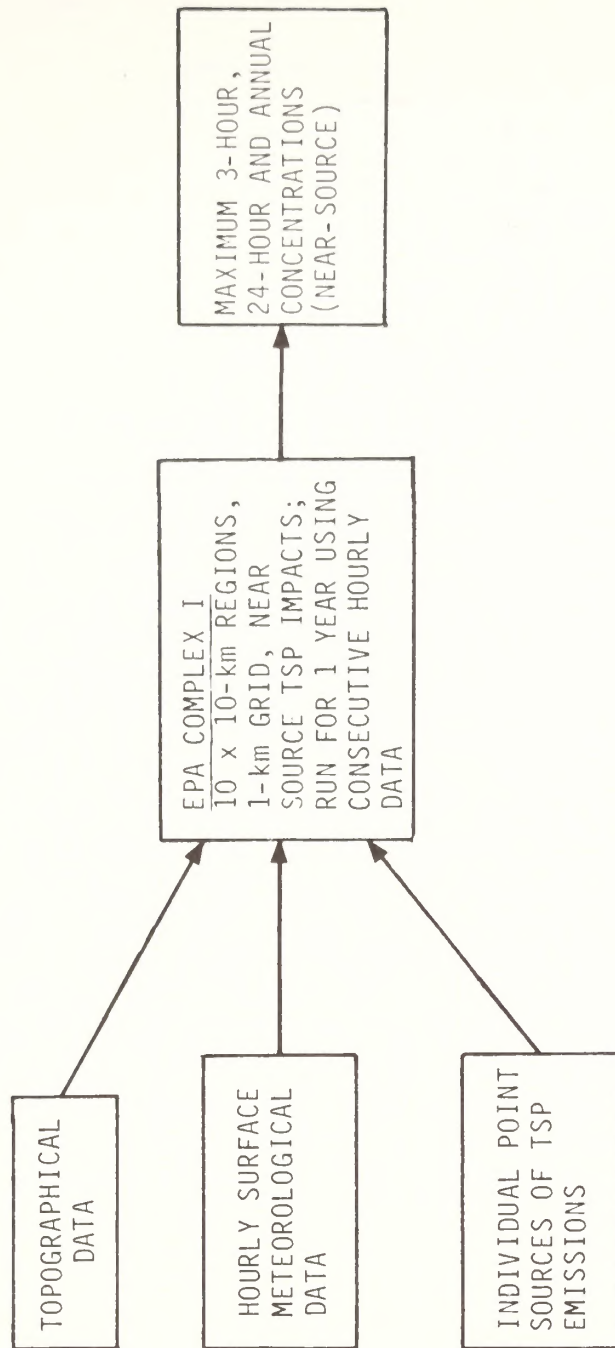
Furthermore, the model applications carried out thus far have not been extensive (i.e., allowing the assessment of cumulative impacts from all proposed developments) or consistent enough to contribute to a comprehensive impact assessment.

To achieve the study objectives, we selected a modeling methodology to assess cumulative impacts of future oil shale and other associated and nonassociated development on a regional scale, resolved to averaging periods of 3 hours, 24 hours, and 1 year, within the states of Colorado and Utah. The methodology selected is based on the utilization of several sophisticated component models: the Systems Applications Complex-Terrain Wind Model, the Systems Applications Gaussian Puff Model, the Systems Applications Regional Transport Model, the EKMA Model, and the Systems Applications/EPA PLUVUE Model. In addition, we applied EPA's COMPLEX-I Model for calculation of concentrations very near emission sources. Even though these models have previously been used, the demanding spatial and temporal scales involved in their application required an innovative and unique approach to configuring and coupling of models so that their inputs and outputs would be complementary and meet the objectives of this study.

Figure 4-5 presents a schematic diagram of the modeling methodology used in this study showing how the various model components were coupled. Each model component was intended to serve a purpose that is specific to the strengths of its particular formulation and that complements the strengths of the other components. A summary of the strengths and weaknesses of each model as applied in this study is given in Table 4-20. Descriptions of the rationale behind the use of each model and the way each is used are given below. All models were applied in a systematic fashion allowing the impacts of individual facilities or any combination of facilities to be determined with a minimum of model runs by combining the output from separate runs.

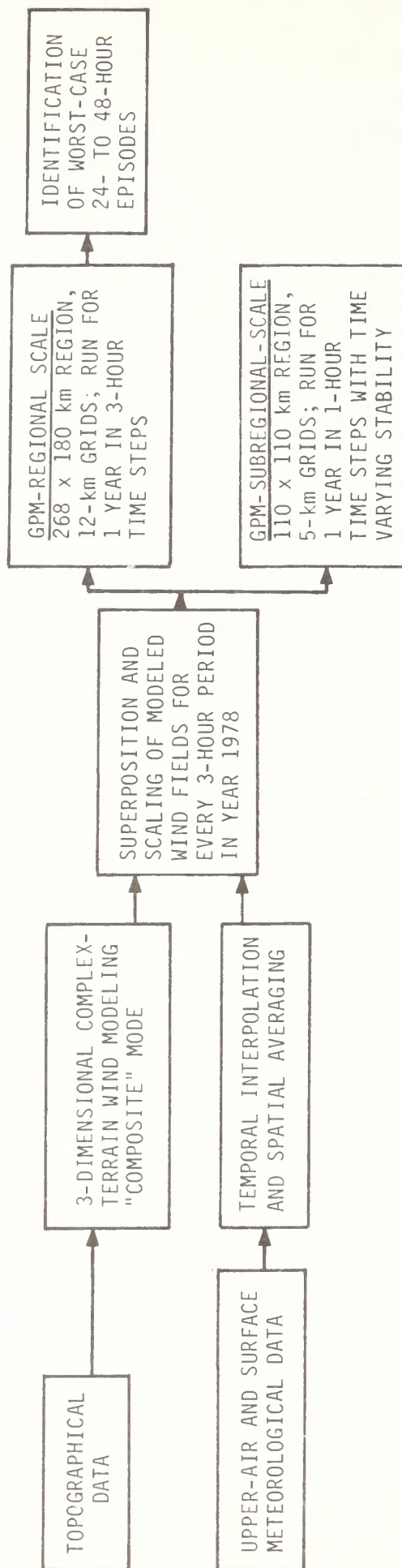
4.2.1.1 The Use of COMPLEX-I

The first part of our approach involves the application of COMPLEX-I, which was developed by the EPA specifically for complex terrain situations (COMPLEX-I is not currently an EPA-approved model). COMPLEX-I is applied



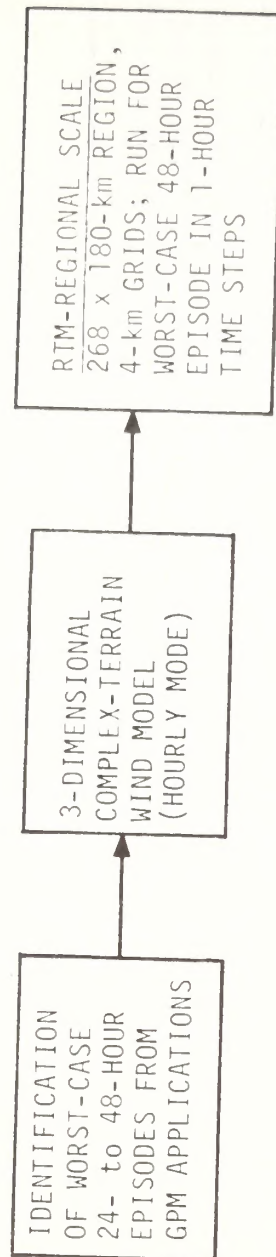
(a) Detailed, Near-Source Modeling Using EPA's COMPLEX I Model

FIGURE 4-5. SCHEMATIC DIAGRAM OF MODELING METHODOLOGY



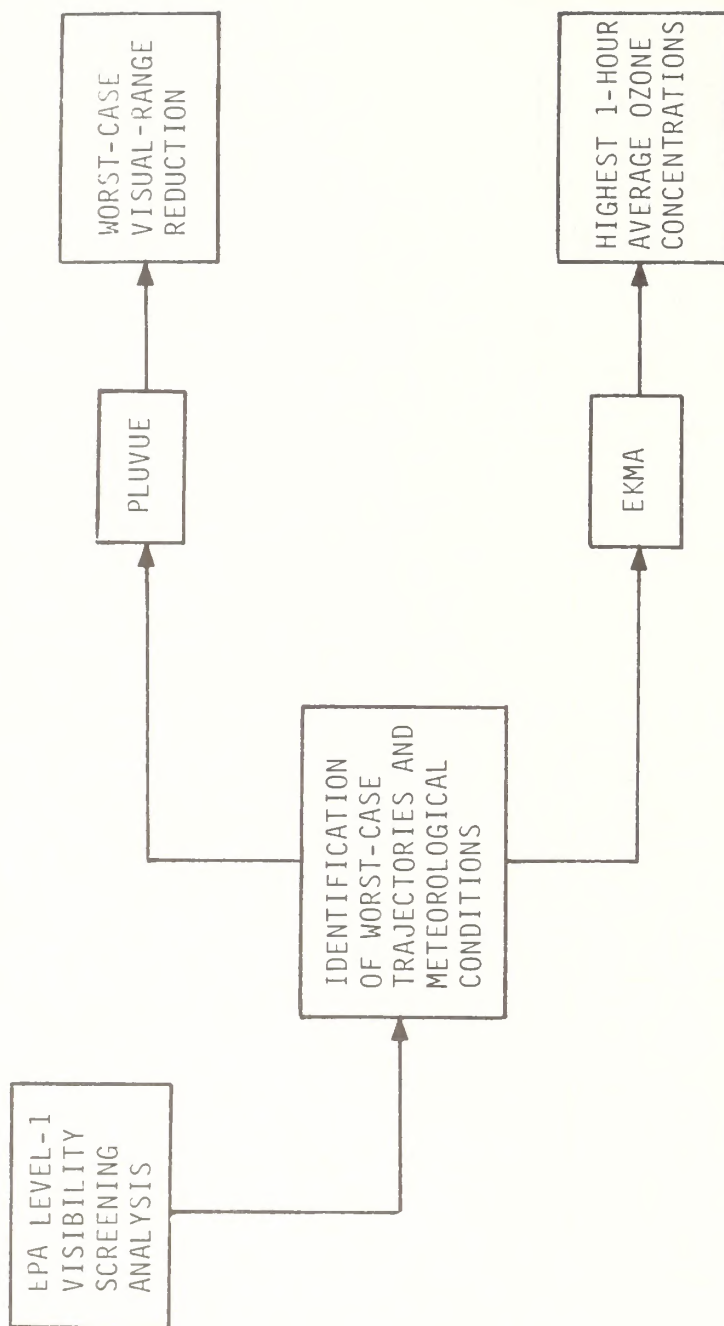
(h) Regional Impact Screening Using Gaussian Puff Model (GPM)

FIGURE 4-5 (Continued)



(c) Detailed Worst-Case Regional Modeling Using the Regional Transport Model (RTM)

FIGURE 4-5 (Continued)



(d) Visibility and Photochemical Oxidant Modeling

FIGURE 4-5 (Concluded)

TABLE 4-20. SUMMARY OF THE RELATIVE CAPABILITIES OF THE MODELS USED IN THIS STUDY[†]

Model	Capabilities							
	Photochemistry	Visibility	Short Range			Medium and Long Range		
			3 hr	24 hr	Annual	3 hr	24 hr	Annual
GPM*	X	X	-	-	-	-	-	-
RTM	X	X	-	-	X	+	+	X
COMPLEX-I	X	X	+	+	+	-	-	-
PLUVUE	X	+	+	+	X	+	+	X
EKMA	+	X	+	+	X	+	+	X

[†] Capabilities of a given model in a given category that are weaker than another model in the same category are indicated by -. The model with the strongest capabilities in a category is indicated by +. Lack of capability in a category is indicated by X.

* As configured and applied in this study to 8760 consecutive hours (1 year).

to the calculation of both SO_2 and TSP and provides impact calculations for one year with 1 hour, 3 hour, 24 hour, and annual averaging periods. COMPLEX-I is used in this study to provide near-source (within 5 to 10 km of the emissions facility) impact estimates. It was selected for the purpose because

- > It is a model developed by the EPA, and it is currently being evaluated by the EPA.
- > It is relatively inexpensive and simple to apply.
- > A meteorological data base was available for its application.
- > Near the source, its formulation is nearly equivalent to those of more sophisticated and expensive models.

Further, from the source (beyond 5 to 10 km), some well-known deficiencies of COMPLEX-I and other Gaussian plume models become limiting, especially in rugged terrain such as the terrain in our study area. Among the more serious of these deficiencies are

- > Assumption of spatially invariant winds and dispersion
- > Assumption of instantaneous transport.

More sophisticated models are required to overcome those deficiencies at moderate to long transport distances. Typically, COMPLEX-I has been used for point sources only. We have modified the code to treat area sources as well by increasing the initial dimension of the plume from an area source to those of the area source itself. A technical description of COMPLEX-I can be found in Appendix C.

For Utah sources, COMPLEX-I was applied using 1978 Ua, Ub 10-meter tower wind and ΔT data. The seasonal and diurnal variations in mixing depths suggested by Holzworth (1972) were used to construct an hourly mixing depth input for both Utah and Colorado sources. For Colorado sources, either the 1975 C-a or 1975 C-b 10 meter tower data (wind and ΔT) were used, depending on the location of each emitting facility in relation to the measurement sites. For both Colorado and Utah facilities, the data collected at the site closest to the facility were used. However, if the closest monitoring site was in a significantly different terrain setting, the sites whose terrain settings were most representative of that of the facilities were used.

4.2.1.2 Use of the Gaussian Puff Model

The Systems Applications Gaussian Puff Model (GPM) was used in conjunction with the Systems Applications Complex Terrain Wind Model (CTWM) to overcome some of the major shortcomings of the COMPLEX-I model for medium- to long-range transport distances. This strategy capitalizes on the capability of GPM to accommodate spatially and temporally varying wind fields and dispersion rates and CTWM's capability to provide realistic winds in complex terrain. Detailed discussion of the technical aspects of GPM and CTWM formulations can be found in Appendix C.

GPM was adapted to provide estimates of 3-hour, 24-hour, and annual average SO_2 and TSP concentration averages within the large study region. This adaptation was accomplished by running GPM for 8760 consecutive hours (one year). During this study the GPM code was extensively "streamlined" to permit its application to an entire year without incurring exorbitant computation costs. Complex-terrain wind fields for the puff model were provided by the CTWM following a "composite" approach developed in this study (described in section 4.2.1.4), which greatly reduces the cost of preparing 8760 hourly wind fields. GPM was applied to two grids contained in the Uinta Basin--the regional-scale grid (268 km by 180 km) and a sub-regional scale grid (110 km by 110 km). Both grid regions are shown in Figure 4-6. Two grid regions were employed largely because of cost. To cover the entire region of interest with sufficient receptor density would be prohibitively expensive. However, a loose receptor mesh is likely to miss the peaks in the concentration distributions, especially close to the emissions source where steep concentration gradients are more likely. The regional-scale grid is therefore intended mainly to provide concentration predictions at the larger downwind distances (e.g., greater than about 60 km downwind), whereas the sub-regional grid focuses on the shorter distances. Both grid region applications employ the CTWM in the "composite" mode to supply gridded hourly wind fields, and both utilize an aggregation of emissions sources (to reduce computational costs). The aggregation of emission sources probably results in GPM's overestimation of results very near the sources on either grid because an aggregated source plume is much more compact and concentrated than the composite of many individual plumes from a facility. However, in our application of the COMPLEX-I we do not aggregate sources; the results of COMPLEX-I thus do not suffer this shortcoming and are more appropriate for near-source impacts resulting from multiple point source releases.

In addition to the differences in the grid region sizes and receptor spacing between the regional and subregional applications, there are other differences between the two applications. One-hour time steps are used in the subregional applications, whereas three-hour time steps are used in

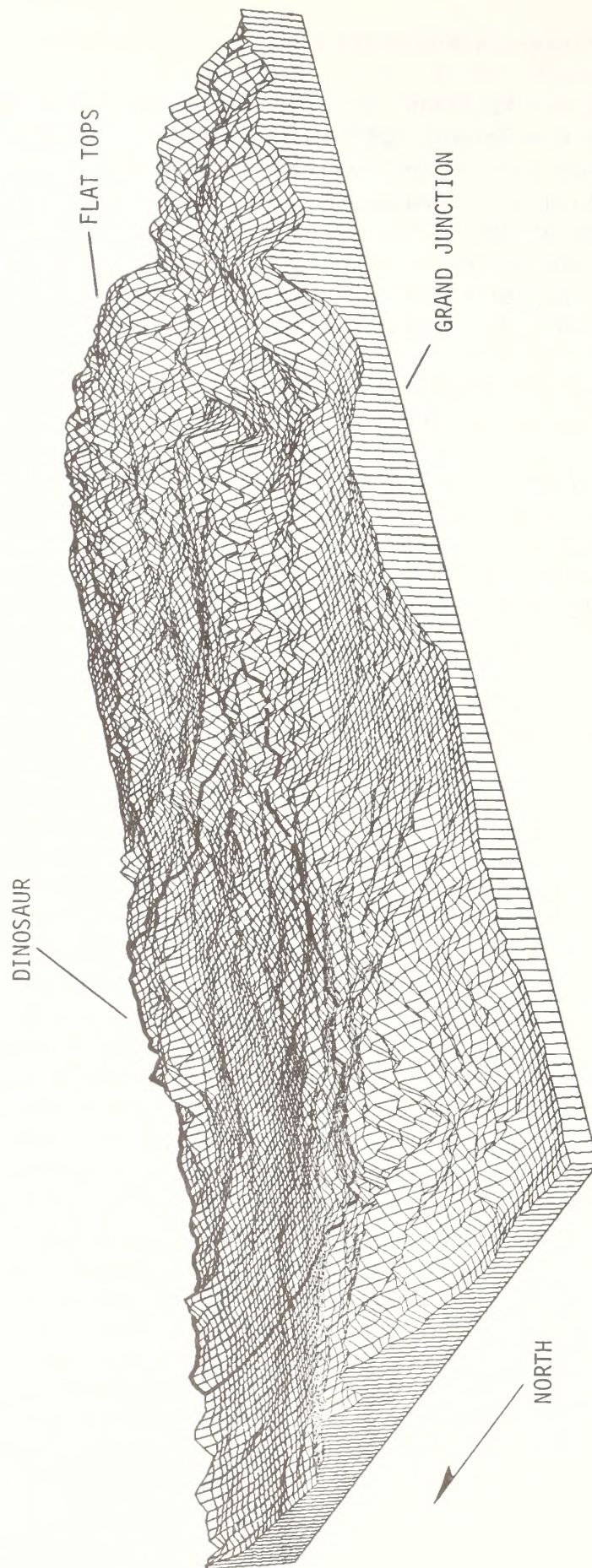


FIGURE 4-6. 3-D PERSPECTIVE OF TERRAIN IN REGIONAL MODELING AREA
(Viewed from the southwest)

Note: Dark internal boundaries delineate the sub-regional grid region.

the regional application. Furthermore, in the regional application, puffs are diffused assuming a Pasquill D stability class, whereas the stability class varies hourly between A and F stability in the subregional application. The assumption of D stability is made to improve computational efficiency in the regional GPM application, and is probably conservative because long-range impacts are more likely to be associated with neutral conditions at plume height. When stable conditions occur, they usually occur close to the ground, and plumes embedded in stable flow situations near the ground are unlikely to be transported large distances in concentrated form through complex terrain.

Another difference between the regional and subregional applications is the plume-terrain interaction treatment. In neutral or unstable conditions, a plume is allowed to approach to within one-half of its effective stack height (an EPA-recommended procedure) for both regional and subregional GPM applications. However, in the subregional applications, an additional algorithm is employed for stable conditions based upon a two-dimensional solution to the equations of motion (Queney, 1947). This algorithm is preferable to that used in EPA models because, unlike EPA's algorithm, it is applicable downwind of a plume's first encounter with terrain.

The deficiencies of the puff model approach are most severe at distances from the source where the size of the puffs becomes large enough so that the treatment of puff advection using the winds at the puff's center of mass is unrealistic. This deficiency is especially important in complex terrain. For example, the pollutant mass conceptually contained within a large puff will likely be advected in several directions by a divergent wind field; yet, GPM's formulation requires that puffs remain intact and be advected by the wind velocities at their centroids, and it does not account for the effective enhancement in dispersion. However, these deficiencies are probably not as limiting for long-term concentration averages or in flat terrain settings where wind fields are fairly uniform. In a recent study, RTM and a Gaussian puff model (MESOPUFF) similar to GPM were shown to yield similar results when applied to the relatively flat North Dakota terrain. The input winds were homogeneous for that comparison, and in some cases RTM predicted higher concentrations than did the puff model (Schock, 1981). However, in this complex terrain application, where the winds vary considerably in space, GPM can be expected to overpredict relative to RTM, and indeed this behavior can be observed in the results presented in Chapter 5.

In summary, it appears that GPM will be overly conservative in some situations:

- > Near-Source--because of source aggregation.
- > Short-Term (3 hour and 24 hours) at moderate to large distances in complex terrain--because of the assumption of puff advection by winds at the puff centroid. In complex terrain, the puff may be deformed or broken apart by non-homogeneous or divergent winds. The result may be that when a puff impacts a receptor, the predicted maximum short-term concentration is higher because the puff is more compact. However, compact puffs will impact receptors less often so that the long-term average concentration predictions are not severely affected. Furthermore, in complex terrain settings, GPM should generally be conservative because it does not account for the effects of complex terrain on dispersion. Complex terrain considerably enhances plume dilution. Also, additional dilution is expected to result from daytime heating and convective mixing throughout the mixed layer.

As mentioned above, the application of COMPLEX-I for near-source concentration impact calculations compensates for GPM's deficiencies near source. To compensate for GPM's deficiencies at moderate to large distances, we applied the Regional Transport Model (RTM) for short periods (24 to 48 hours). If it had been required that we use only GPM to provide "best estimate" concentration impacts, we would have made modifications to GPM's formulation (e.g., decomposition of puffs into subpuffs when required) to remedy the deficiencies at moderate to large distances. However, such modifications would increase the computation time required by GPM to such an extent that it would be prohibitively expensive even for short-term (24 to 28 hours) applications. RTM does not share GPM's deficiencies at moderate to long ranges. Furthermore, RTM is a more cost-effective alternative than modification of GPM because it is currently operational and cheaper to execute than an enhanced version of GPM would be. The use of RTM is described in the following subsection.

4.2.1.3 Use of the Regional Transport Model

For calculations of short-term regional-scale concentration averages, we applied the Systems Applications Regional Transport Model (RTM), which is better suited than GPM for treating the dispersion of pollutants from many sources over large transport times and distances. As mentioned earlier, this is true because RTM allows for variations in wind and

diffusivity across a puff whereas GPM cannot. This distinction between the model's capabilities is most pronounced after large transport times. Also, this distinction suggests that RTM will predict lower short-term peak concentrations than does GPM. As discussed earlier, GPM will tend to overpredict peak short-term concentrations because its puffs will remain compact even with nonhomogeneous and divergent wind fields present in complex terrain. Indeed, comparison of GPM and RTM results (see Chapter 5) confirms that RTM predictions are lower. However, there are other differences between the models' formulations and in the input data supplied to the two models (greater accuracy and resolution is provided in RTM's input data) that also account for differences in predictions. RTM is too costly to execute for an entire year, so its purpose is only to provide estimates of short-term (3-hour and 24-hour) concentration averages for the worst-case episode identified by GPM when run for an entire year. RTM is run with complex-terrain wind fields generated by the wind model, run in an hourly mode rather than in the composite mode (as was done for the GPM runs) to improve accuracy. For impacts closer to the source, the regional-scale application of RTM is not acceptable because of its coarse receptor spacing and lack of treatment of some important micrometeorological effects. While most previous applications of RTM have been in flat terrain settings, its ability to accept spatially and temporally varying wind, mixing depth, and diffusivity input permit its application to complex terrain. Proper specification of these inputs is the key to RTM's application in complex-terrain settings. Detailed discussions of RTM's formulation can be found in Appendix C.

4.2.1.3.1 Preparation of mixing layer depths for RTM

Mixing layer depths used with the RTM were calculated from four National Weather Service upper-air stations that lie in and around the area of study. These stations are Grand Junction, Colorado, which lies in the southern part of the study region, Denver, Colorado, which is approximately 200 km east of the region, Salt Lake City, Utah, which is approximately 100 km west of the region, and Lander, Wyoming, which is just north of the region.

The mixing layer depths were calculated for the worst-case modeling scenario identified by the Gaussian Puff Model for the year 1978, days 207 and 208. The four upper-air stations provided temperature profiles at 5:00 a.m. and 5:00 p.m. MST. The morning temperature profiles almost always revealed a surface-based inversion. The stable mixing layer depths estimated from the morning soundings were averaged to obtain a uniform depth over the entire study area for the nighttime stable periods. Table 4-21 lists the stable layer depths at the four stations and the average value used for the two modeling scenarios.

TABLE 4-21. MORNING STABLE LAYER DEPTHS FROM THE FOUR UPPER-AIR STATIONS,
AND THE AVERAGE USED BY RTM (in meters)

<u>Day</u>	<u>Time</u>	<u>Grand Junction</u>	<u>Denver</u>	<u>Salt Lake City</u>	<u>Lander, Wyoming</u>	<u>Average</u>
179	0500	94	286	428	143	238
180	0500	47	541	338	--	309
181	0500	97	272	271	106	187
182	0500	160	389	386	179	279
207	0500	260	134	244	229	217
208	0500	143	123	478	339	271

The afternoon temperature profiles on these two days from the four upper-air stations revealed that no temperature inversions were present within 20,000 feet of the surface. Thus, the maximum afternoon mixing height was conservatively assumed to be about 3500 meters above sea level. Therefore, daytime mixing height grow to this maximum height above sea level. The depth of the lowest grid layer is the difference between this time varying height and local terrain height. Since RTM is a terrain-following model, the influence of the terrain is then incorporated not only through the wind provided by the Complex-Terrain Wind Model, but also through the mixing layer (the lowest grid layer) depths that vary with terrain. It is assumed that the stable layer depth is constant from 10:00 p.m. MST until two hours after sunrise, or until 8:00 a.m. MST. Then the mixing depth is allowed to rise linearly, starting at the stable layer depth, until it reaches the maximum afternoon mixing depth at 5:00 p.m. MST. The mixing height is then held constant at this height until two hours after sunset (10:00 p.m. MST), when the first layer heights drop to the morning stable layer height. Figure 4-7 illustrates the temporal variations in mixing layer depth.

The current version of the Systems Applications Regional Transport Model contains a second layer that interacts with the mixing (bottom) layer of the model whenever spatial or temporal variations occur at the mixing height field. The top of this second layer is constant over the modeling region. The region top value used in this study is 2300 meters AGL, which minimizes the dilution caused by too deep a second layer, yet retains a second-layer thickness of at least 100 meters over the entire region.

The wind fields used by the Regional Transport Model were supplied hourly by the Complex-Terrain Wind Model (CTWM). Since RTM is a terrain-following model and CTWM is a sea-level-based model in which the terrain features are contained within the computational grid, an average of the wind fields at different vertical levels from the CTWM is used as input to RTM. For this application, a mixing height average of the two CTWM vertical levels of wind fields is used. Thus, when there is a low mixing layer depth, the wind field is represented mostly by the lowest CTWM layer that best represents the drainage flow associated with stable nighttime conditions. In the afternoon, a more geostrophic-like wind field develops because it has a much larger wind component from the second layer of the CTWM.

The surface wind speeds are needed for the surface layer of RTM. The surface wind speeds are taken from the lowest CTWM layer except when the terrain blocks this layer, in which case the second layer of the CTWM wind field is used.

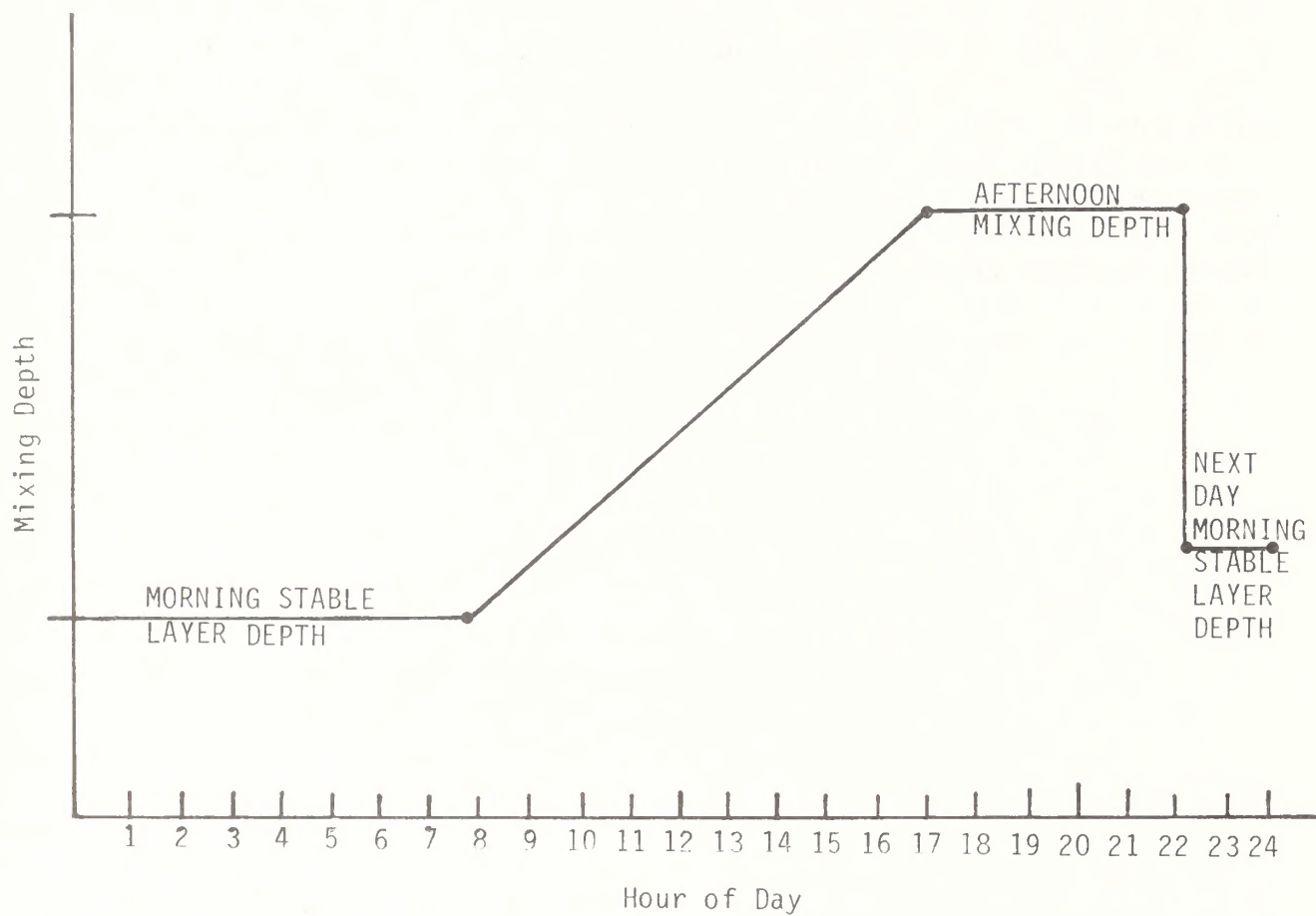


FIGURE 4-7. TEMPORAL VARIATION OF FIRST GRID LAYER DEPTH

4.2.1.3.2 Preparation of exposure class input to RTM

Exposure class, which is a measure of near ground-level atmospheric stability due to surface heating or cooling, is required RTM input data. For the morning hours from 0000 to 0800 and evening hours 2200 and 2300, an exposure class value of -2 is used, which corresponds to a stable Pasquill-Gifford classification. For the hours from 0900 to 2100, an exposure class value of 0 is used, which corresponds to a neutral Pasquill-Gifford classification.

4.2.1.3.3 Preparation of diffusivity input to RTM

On the regional scale, pollutant dispersal is strongly dependent on a length-scale characteristic of the effective turbulent eddies. Pertinent field observations indicate that the regional-scale horizontal diffusivity ranges in value from 10^3 to 10^5 m^2/s (Baur, 1973). In a study of the numerical simulation of the atmospheric circulation, Smagorinsky (1963) showed that nonlinear lateral diffusion can be formulated on the basis of similarity theory for turbulence in the equilibrium range (Heissenberg, 1948). Thus, the horizontal diffusivity coefficient can be derived as

$$K_H = 5/4 (\alpha \Delta) |\text{Def}| \quad ,$$

where Δ is the grid spacing, $\alpha \approx 0.28$, and $|\text{Def}|$ is the magnitude of the velocity deformation

$$|\text{Def}| = \left(\frac{\partial v}{\partial x} + \frac{\partial u}{\partial y} \right)^2 + \left(\frac{\partial u}{\partial x} - \frac{\partial v}{\partial y} \right)^2 \quad ^{1/2} .$$

The temporally and spatially varying fields of horizontal diffusivities used by RTM were calculated from the wind fields using the expressions above. The calculated values ranged from a minimum of 10^3 m^2/s to a maximum of 10^5 m^2/s .

4.2.1.3.4 Preparation of chemical reaction rate input to RTM

The homogeneous oxidation of SO_2 to SO_4^- is a function of the intensity of solar radiation. The Regional Transport Model allows this oxidation to vary spatially and temporally over the modeling region. The model treats the oxidation rate as a function of the solar zenith angle, or the solar intensity in the absence of cloud cover. RTM calculates the

oxidation rate for each grid cell and time on the basis of user-prescribed maximum noontime oxidation rate at the southernmost latitude, and the minimum nighttime oxidation rate for the region. The maximum oxidation rate used for this application is 1.32 percent per hour reported by Altshuller (1979). Less is known about the minimum nighttime oxidation rate of SO_2 , but the minimum nighttime oxidation rate used here is 0.01 percent per hour.

4.2.1.4 Use of the Complex-Terrain Wind Model

The Systems Applications Complex-Terrain Wind Model (CTWM) is a three-dimensional diagnostic model that solves the equation of mass continuity including parameterizations of the physical processes occurring in complex terrain. The model assumes steady-state conditions, and given boundary conditions and information about the stability, terrain, surface roughness, and temperature distributions within the modeling region, the model calculates a three-dimensional gridded wind field. A complete description of the formulation of CTWM can be found in Appendix C.

In the past, CTWM has been applied to many different complex terrain settings, and has usually been applied for one-hour periods. To model a 24-hour episode, for example, 24 one-hour runs would be made. This same method of CTWM application was used to generate wind fields for the RTM simulations of 24- to 48-hour episodes.

The upper-air wind data from each of the four National Weather Service monitoring sites at Salt Lake City, Utah; Lander, Colorado; Grand Junction, Colorado; and Denver, Colorado, provided wind information along the edges of the region at 12-hour intervals. The flow vectors for the intervening hours were obtained by means of linear interpolation. An examination of these data and the surface wind measurements collected at four U-a and U-b sites allowed the determination of wind model boundary conditions for the modeling region for each hour of each day modeled. The wind model was exercised on a 67 x 45 grid of 4-km cells. The origin was at 550. E, 4310. N, UTM zone 12. The grid extended 268 km to the east and 180 km to the north. The bottom of the modeling region was chosen to be 4260 feet above MSL, and the top, 11,940 feet above MSL. The region was divided into two layers of equal thickness, approximately 3840 feet each. Up-slope and down-slope flow parameters were determined as described in Appendix C.

However, for the GPM simulation of an entire year, the hourly mode of CTWM application would be too costly. Instead, a novel method of application was devised for this study, which is considerably less costly than the hourly approach. The new method is called the "composite" mode and involves the following steps:

- (1) Temporally interpolate between 0000Z and 1200Z upper-level soundings of wind at Salt Lake, Lander, Grand Junction, and Denver to yield hourly values at each site for the entire year.
- (2) Vector average the hourly upper level winds measured at the four sites and interpolated in step 1.
- (3) Determine the characteristics of up- and down-slope flow regimes. This is accomplished by comparing the surface-level wind direction at the U-a, U-b site in the Uinta Basin with the average upper-level wind directions from step (2) at the same hour and with the terrain slope at each surface monitoring station. Generalize several slope wind regimes.
- (4) Apply a methodology for automatic (by computer) identification of 8760 hourly wind regimes (for an entire year) and creation of an hourly data input file to be used later. Regimes are identified using average upper-level flow direction and speed in the region and the intensity of up-slope and down-slope winds. The methodology includes the following elements for each hour of the year:
 - Check several stations for measured surface wind direction to the slope wind input parameter.
 - Check average upper-level wind speed and direction from step (2).
 - Determine what component of average upper-level flow is aiding or retarding slope flow. Then determine the prevailing slope flow regime using the measured slope winds (minus the component of the upper-level flow).
- (5) Run wind model for 16 cardinal upper-level wind directions and an arbitrary wind speed of 10 m/sec and store the resulting wind field output files.
- (6) Run wind model for six slope wind regimes with zero upper-level wind velocity and store the resulting wind field output files. The six slope regimes are identified in step (3).

- (7) Calculate composite wind field for each hour of the year (8760 hours/year). The steps for calculating a composite wind field for each hour are
- Scale the wind field output file (i.e., multiplication of all wind speeds by a scalar) whose assumed upper-level wind direction is closest to the mean upper-level flow direction occurring during the hour. The scaling factor is computed by dividing the mean upper-level wind velocity for the hour by the arbitrary velocity assumed in the wind model runs. Scaling of wind fields is allowable because the CTWM is based upon the solution of an elliptical partial differential equation. Hence, the result of multiplying a predicted wind field by a factor is identical to the wind field predicted by the model after multiplying the driving wind (boundary condition) input by the same factor. The former, however, is considerably less costly.
 - Superimpose (vector addition) the wind field output file for the slope wind category appropriate for the hour upon the wind field file scaled by upper-level wind conditions for the hour. Superpositioning of model output is also a mathematically valid operation given the form of the model equations.

An illustration of the methodology applied to a hypothetical situation is provided in Figure 4-8. The main disadvantage of the "composite" mode of application is the requirement that the upper-level flow (boundary condition) be represented by an average wind speed and direction. The hourly mode allows both horizontal and vertical variations of this boundary condition and hence is capable of more realistic results. However, the "composite" mode was tested by comparison of surface winds measured at several sites in the modeling region during 25 randomly selected hours during 1978 with the corresponding winds predicted by the model. The comparison showed that the predicted surface wind directions were within 45° of the measured wind directions on all but two occasions. Predicted wind speeds were within 30 percent of the measured wind speeds in all but four instances where they were within 60 percent of the measured speeds.

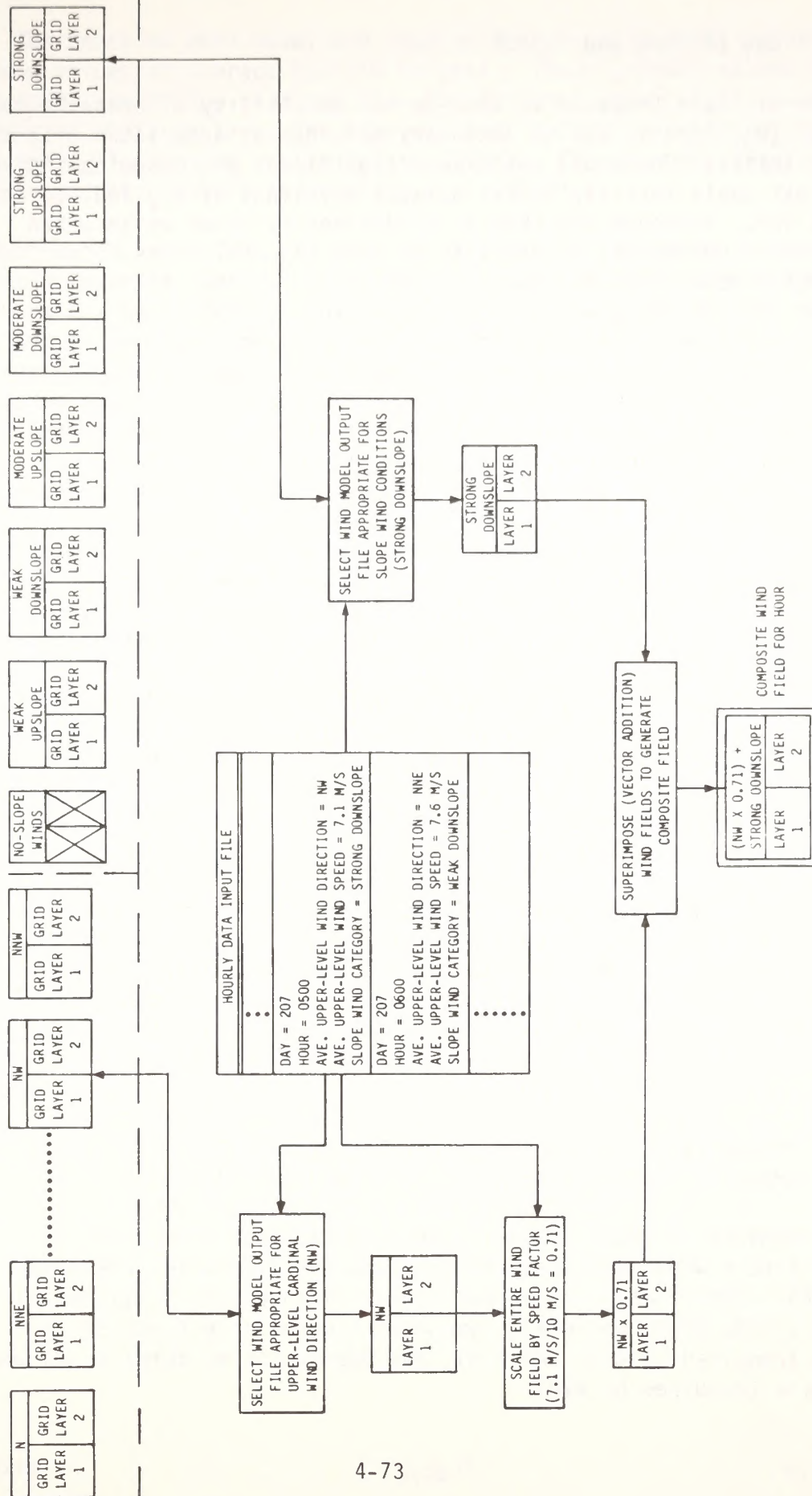


FIGURE 4-8. SCHEMATIC DIAGRAM OF METHODOLOGY FOR APPLYING THE COMPLEX-TERRAIN WIND MODEL (CTWM) IN THE "COMPOSITE" MODE (HYPOTHETICAL HOURLY INPUT DATA ARE USED IN THIS EXAMPLE)

4.2.1.5 Use of EKMA and PLUVUE

EKMA has been proposed to address the possibility of photochemical pollutant (O_3) impacts due to secondary development associated with the proposed leases. One would not expect significant photochemical impacts from an oil shale facility itself because emissions of NO_x and hydrocarbons are low. Although the EKMA is traditionally known as an urban photochemical box model, it can also be used in rural areas. The EKMA is a Lagrangian model that follows a parcel of air assumed to vary through space and time on the basis of some assumption of wind speed and wind direction. The parcel of air contains initial concentrations of hydrocarbon and NO_x that react according to a chemical mechanism. During the course of the transport of the puff along the trajectory, fresh emissions are introduced and the parcel is allowed to diffuse within a layer aloft. Pollutant concentrations are assumed to be spatially constant; therefore, there is no horizontal exchange of reactant concentrations.

The "trajectory" mode of the EKMA computer code is used to consider impacts due to specific sources in rural areas if the horizontal area (or size) of the parcel is small in relation to the size of the source. In this situation the horizontal exchange of reactants is not important.

For the present study, a slightly modified version of the EKMA computer code was used (Whitten and Hogo, 1978). A different chemical mechanism was used in the application of EKMA to account for the fact that chemical reactions in rural areas are those involving methane, CO, and trace organics such as naturally emitted terpenes. A technical discussion of EKMA's formulation is provided in Appendix C.

The potential for visibility impacts due to primary particulate emission and secondary particulate formation was addressed using PLUVUE. PLUVUE has most often been used to address the visibility impacts of isolated, elevated point sources. However, the model is capable of treating multiple ground level sources, including both point and area sources. A discussion of PLUVUE's formulation can be found in Appendix C.

4.2.1.6 Preparation of Time-Invariant Terrain and Surface Cover Model Input Data for RTM, GPM, CTWM, and COMPLEX-I

The Regional Transport Model, the Gaussian Puff Model, and the Complex-Terrain Wind Model require some spatially varying, time-invariant input data. These data include average terrain heights (required by COMPLEX-I, RTM, CTWM, and GPM), roughness lengths as a function of location (required by CTWM and RTM), and deposition velocity as a function of location (required by RTM).

The Gaussian Puff Model and Complex-Terrain Wind Model require gridded values of average terrain heights. These gridded values were extracted from a tape acquired from the National Geophysical and Solar-Terrestrial Data Center. The tape provides gridded terrain heights on a 30-second grid for the entire United States. The data are also used to prepare receptor height information for COMPLEX-I.

RTM, GPM, and CTWM also require aerodynamic roughness characteristics of the underlying terrain. The interaction of the atmospheric boundary layer with the underlying surface will modify the wind in lower-level flows. Indirectly, through the modification of wind profiles and turbulent diffusivities, the terrain surface can affect the ultimate concentration distribution at the ground. Surface roughness, then, is a key parameter of these wind and air quality models.

In general, the surface roughness length, z_0 , for a given surface cover may vary as a function of wind speed, wind direction, and season. In extensive studies of z_0 performed in the Sacramento, California (Myrup and Morgan, 1972) and Philadelphia, Pennsylvania (Slade, 1968) areas, it was found that the surface roughness length z_0 varied greatly as a function of season and wind direction. The variation of z_0 as a function of wind speed is especially important over water (Garratt, 1977) or tall deformable plants (Geiger, 1971). However, as a first approximation an average roughness length for a given surface type can be assigned.

The determination of roughness lengths for this study area is made from United States Geological Survey maps. Land-use categories defined by the USGS maps are given in table 4-22. The study area was divided into 2-km grids, and each grid cell was assigned a USGS land-use category (see figure 4-9). These land-use categories define the most prominent vegetation type for this area from which the average surface roughness length can be estimated. The deposition velocities for SO_2 , SO_4 , and TSP are also functions of vegetation type. Table 4-23 contains the USGS land-use categories used in this study and the roughness lengths and deposition velocities defined for each category. The deposition velocities used in this study were reported by McMahon and Denison (1978) in their survey of empirical atmospheric deposition parameters. It should be noted that the particulate deposition velocity is sometimes intended to represent both the deposition of fine particulates and the settling of larger particulates. The values used here are more representative of deposition velocities than of settling velocities because settling of larger particulates usually occurs close to the source, whereas deposition processes are more important on the regional scale. The Gaussian Puff Model uses spatially constant deposition velocities of 1 and 0.5 centimeter per second for SO_2 and TSP, respectively.

TABLE 4-22. USGS LAND USE CATEGORIES

Category No.	Description
Urban	
11	Residential
12	Commercial and services
13	Industrial
14	Transportation, communications, utilities
15	Industrial and commercial complexes
16	Mixed urban or built-up land
17	Other urban or built-up land
Agricultural	
21	Cropland and pasture
22	Orchards, groves, vineyards, nurseries, horticultural areas
23	Confined feeding operations
24	Other
Rangeland	
31	Herbaceous
32	Shrub and brush
33	Mixed
Forest land	
41	Deciduous
42	Evergreen
43	Mixed
Water	
51	Streams and canals
52	Lakes
53	Reservoirs
54	Bays and estuaries
Wetland	
61	Forested
62	Nonforested

TABLE 4-22 (Concluded)

Category No.	Description
	Barren land
71	Dry salt flats
72	Beaches
73	Sandy areas other than beaches
74	Base-exposed rock
75	Strip mines, quarries, gravel pits
76	Transitional areas
77	Mixed
	Tundra
81	Shrub and brush
82	Herbaceous
83	Bare ground
84	Wet
85	Mixed
	Perennial snow or ice
91	Perennial snowfields
92	Glaciers

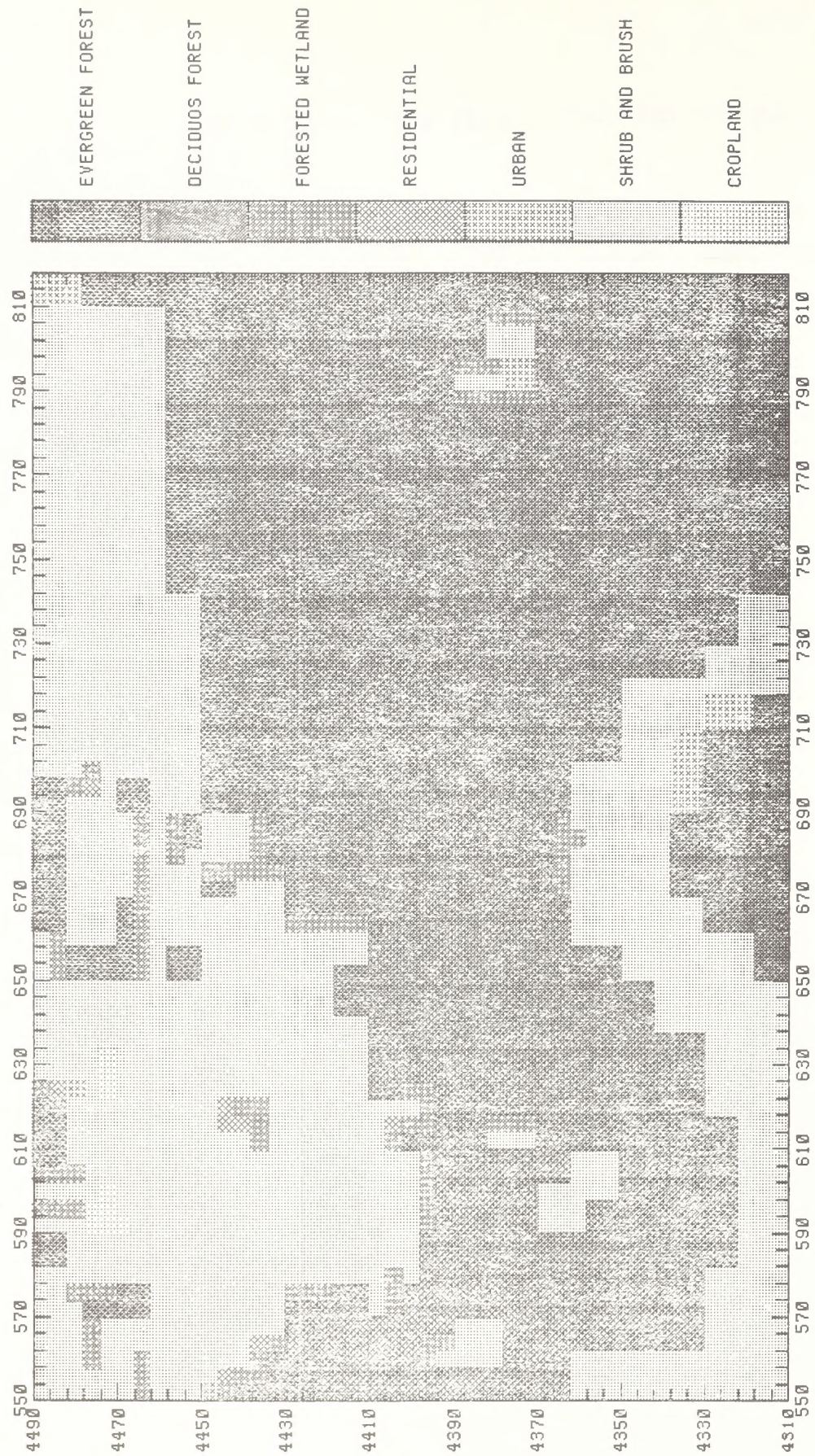


FIGURE 4-9. SPATIAL DISTRIBUTION OF LAND USE CATEGORIES

TABLE 4-23. LAND USE CATEGORIES, SURFACE ROUGHNESS LENGTHS, AND DEPOSITION VELOCITIES FOR THE STUDY AREA

Category Number	Description	Percent of Area	Roughness Length Z_0 (cm)	Deposition SO_2	Velocity SO_4	(cm/s)* TSP
10	Urban	1.22	40 [†]	1.5	0.3	0.5
11	Residential	0.08	60 [†]	1.5	0.3	0.5
21	Cropland	0.45	25 [§]	1.0	0.2	0.4
32	Shrub and brush	34.03	35 [§]	0.9	0.2	0.4
41	Deciduous forest land	0.12	270 ^{**}	1.5	0.5	0.7
42	Evergreen forest land	62.60	280 ^{††}	1.5	0.5	0.7
61	Forested wet lands	1.48	150 ^{§§}	1.1	0.4	0.6

* McMahon and Denison (1978)

† Myrup and Morgan (1972)

§ Ranzieri (1975)

** Szeicz (1969)

†† Sellers (1965)

§§ Assumed 50 percent forest land, 50 percent wet lands.

5 REGIONAL AIR QUALITY IMPACTS

In this section we examine the cumulative impacts of the following categories of emission sources:

- > Five site-specific Uinta Basin synthetic fuel facilities (Enercor-Mono Power, Magic Circle, Paraho, Syntana, and Tosco).
- > Five site-specific and four conceptual Uinta Basin synthetic fuel facilities (including the multiple-site Geokinetics oil shale development and the Sohio tar sands development, both at a conceptual stage of development).
- > Colorado oil shale development in the Piceance Basin at several sites (all development plans are very uncertain at this time for this category of sources).
- > All the above sources together plus other existing or planned projects such as the Moon Lake Power Plant and White River Shale Project.

Impacts of these different subsets of emission sources were evaluated for both the low- and high-oil-production scenarios discussed in sections 1 and 4. (The impact of each of the five site-specific facilities was evaluated separately and is discussed in section 6.) Impacts of the low- and high-oil-production scenarios were also broken out as to whether impacts are due to direct source emissions from industrial facilities (see subsection 5.2) or from so-called secondary emissions resulting from population growth and other regional developments associated with the synthetic fuel industry (see subsection 5.3). All categories of impacts are combined in summary tables (see subsection 5.4). Finally, other types of air quality impacts such as cumulative regional impacts on photo-chemical oxidant (ozone), visibility, acid deposition, and construction impacts are discussed.

Inside the back cover of this report we provide clear plastic overlays that can be used to identify the locations of the point sources, geographical features, and terrain elevations in the study region. The

graphic scale of the plots is indicated by the UTM coordinates (in kilometers).

5.1 CONCENTRATION ESTIMATION APPROACH

As discussed in Section 4, a variety of modeling approaches were used in the analysis of regional air quality impacts. For ground-level concentration estimates, the Gaussian Puff Model (GPM) was exercised for every three-hour period in an entire year based on measured meteorological conditions in the region. These GPM results were used to identify for each gridded receptor in the region the maximum 3-hour and 24-hour concentrations (occurring at different times at different receptors) and the annual average concentration. The maximum concentrations thus identified are expected to be upper-bound estimates of the future maximum concentrations in the region for a number of reasons. These reasons were discussed in Section 4.2, but are further amplified here.

The expected conservatism of the Gaussian Puff Model is due to several factors.

Puffs are diffused assuming Pasquill D dispersion coefficients; this is conservative at long range (> 25-50 km). Complex terrain considerably enhances plume dilution as a result of enhanced turbulence and spatially and temporally varying wind fields around terrain obstacles to air flow. Also, additional dilution is expected to result from daytime heating and resulting convective mixing throughout the mixed layer. These processes rapidly result in uniform vertical mixing throughout the mixed layer (the convective boundary layer) which is typically 1000 meters to over 4000 meters thick. By comparison, the vertical dispersion coefficient for Pasquill D stability at 50 km is 320 meters. Dispersion conditions during the daytime are typically Pasquill A, B, or C. The difference of just one stability class (say from Pasquill D to C) is a reduction in short-term concentrations by a factor of more than 5 and in annual averages by a factor of more than 2.

Puffs are assumed to be transported by the portions of the wind field that are at the centroid of puff mass. This assumption is conservative at long distances where puffs are large because a complex wind field will tend to transport different portions of the puffs in different directions. This effect is much larger than the dilution resulting from the small-scale turbulence that is accounted for in the Pasquill scheme.

The GPM model results are also conservative for near-source impacts (< 25 km) where there are multiple, ground-level releases of emissions (e.g., TSP) at a given facility. In this analysis, because of cost

considerations multiple emissions (there are as many as 30 TSP emission sources at oil shale facilities) are treated as emissions from a single point in the center of the emission source. To more rigorously model the near-source impacts of multiple ground-level emissions, we used COMPLEX-I (see Section 6).

Furthermore, wind field definition in GPM is based upon upper-level wind characterization, which is appropriate for long-range transport. For short-range, near-source calculations, lower-level or surface winds are more appropriate, and these exhibit greater temporal variability than upper level winds and hence would result in lower concentration averages. An even greater degree of conservatism is added to GPM by allowing puff centroids to approach high terrain features to within one-half their effective release heights, even under the assumed neutral stability conditions. One would expect this to occur in reality only under stable conditions, while in neutral and unstable conditions puffs should remain near their effective release heights.

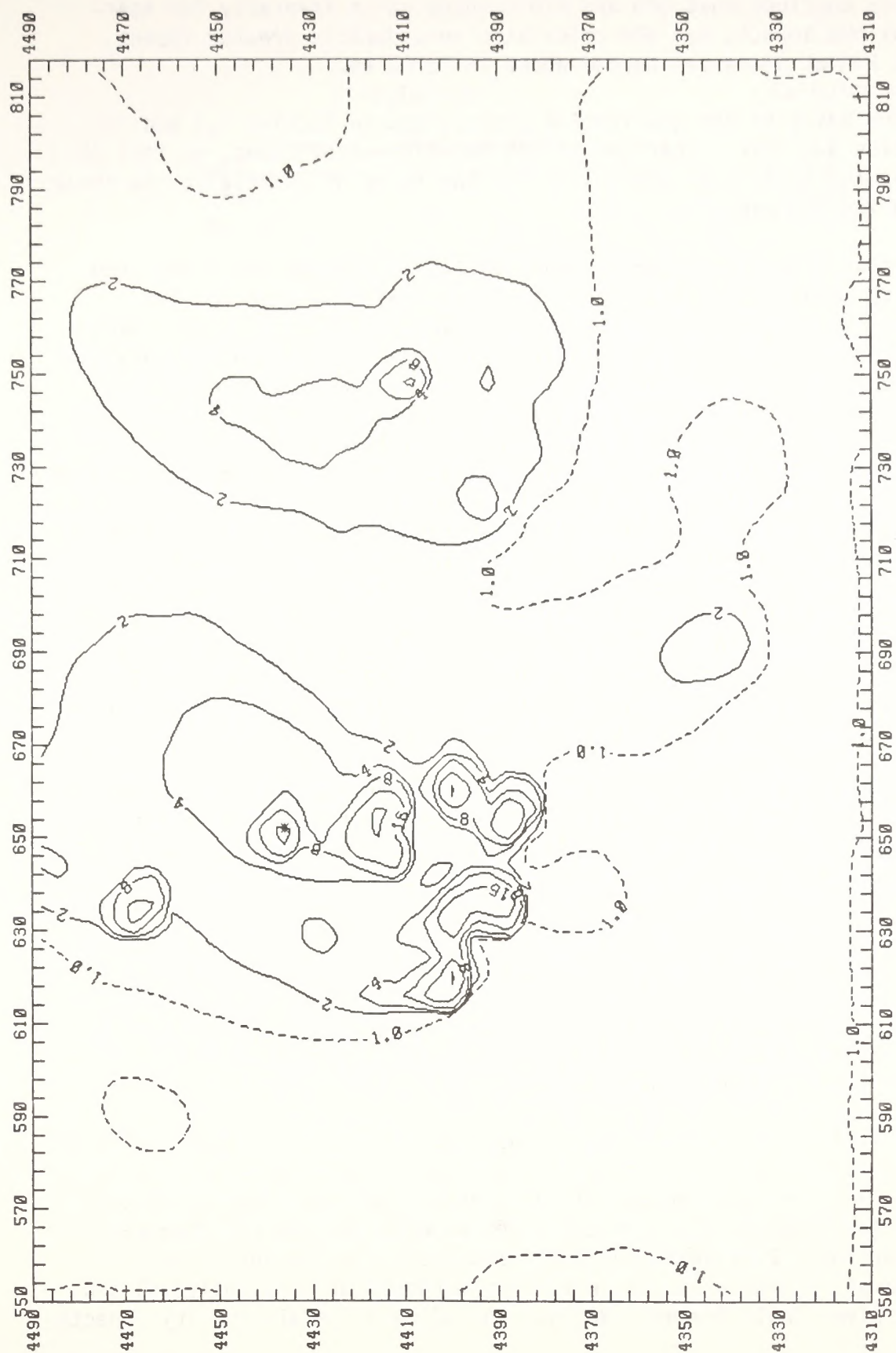
Another way to evaluate the potential conservatism of GPM is to compare GPM results with those of other regional models that are expected to be more realistic, such as RTM (see Section 4.2). One such comparison was performed for a day (27 July 1978) in the year modeled with GPM that resulted in the highest 24-hour average SO_2 concentration in the vicinity of the Flat Tops Wilderness. This 24-hour SO_2 concentration was predicted by GPM to be $19 \mu\text{g}/\text{m}^3$ and to occur to the west of Flat Tops. (The highest modeled 24-hour concentration within Flat Tops occurred on 20 October 1978 and was $12 \mu\text{g}/\text{m}^3$.) The Regional Transport Model, RTM (see discussion of this model in Section 4.2, and Appendix C), was exercised for the meteorological conditions on this 27 July 1978 day. Figure 5-1 compares the 24-hour average SO_2 concentrations using these two models for this one day.

GPM calculated a maximum concentration in Flat Tops greater than $6 \mu\text{g}/\text{m}^3$ on this day, while RTM calculated an impact of about $1 \mu\text{g}/\text{m}^3$. For the receptor in the vicinity of Flat Tops for which a $19 \mu\text{g}/\text{m}^3$ impact was calculated by GPM, RTM calculated an impact between 1 and $2 \mu\text{g}/\text{m}^3$. The maximum, near-source concentration in the entire region calculated by GPM was $51 \mu\text{g}/\text{m}^3$, which occurred near the White River Shale Project (U-a, U-b) in Utah. RTM calculated a maximum concentration at this location and 20 km to the north of $41 \mu\text{g}/\text{m}^3$. (These calculated impacts near the White River Shale Project may be unrealistically high because in both the GPM and RTM models, multiple ground-level SO_2 emission sources throughout the facility were combined into a single point source.) Maximum near-source concentrations calculated by both models in the Piceance Basin are near Cathedral Bluffs; GPM calculated a maximum concentration of $20 \mu\text{g}/\text{m}^3$, and RTM calculated $16 \mu\text{g}/\text{m}^3$. Although one should be careful in generalizing from the results of a model comparison for just one worst-case day, we can



(a) On the basis of GPM calculations

FIGURE 5-1. 24-HOUR SO₂ CONCENTRATION ESTIMATES FOR 27 JULY 1978 FROM DIRECT SOURCE SO₂ EMISSIONS AND FOR THE HIGH OIL PRODUCTION SCENARIO



(b) On the basis of RTM calculations

FIGURE 5-1 (Concluded)

tentatively conclude that GPM and RTM compare quite favorably for near-source maximum impact, but GPM calculates considerably greater impact, than does RTM at distances beyond about 25 to 50 km.

On the basis of the qualitative discussions in Section 4.2 and in this section and this comparison of GPM and RTM calculations, we feel it is appropriate to account explicitly for the range of uncertainty in these concentration estimates.

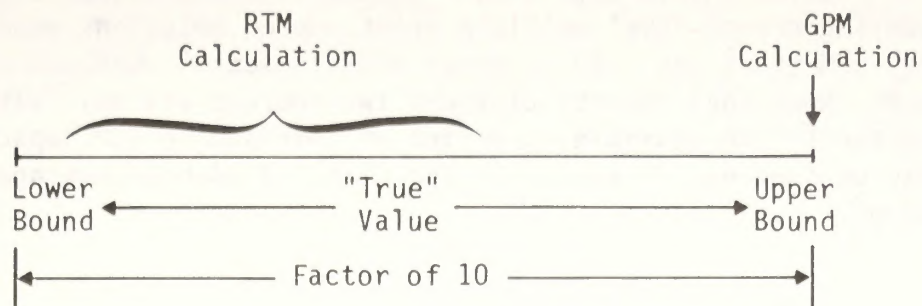
To account for the expected conservatism of GPM, we have projected air quality impacts by using ranges of concentrations, with the GPM predictions being the upper bound of that range. The size of this range is estimated to be an order of magnitude (a factor of 10) for the maximum 3-hour and 24-hour concentrations. This range is based on our professional judgment as to the uncertainty of concentration estimates and our belief that GPM calculations are certainly conservative (i.e., that concentration estimates predicted on the basis of GPM will be greater than actual concentrations). The GPM model is expected to be less conservative for annual averages than for short-term averages because underestimates of horizontal dispersion are cancelled out in the process of averaging concentrations over an entire year. GPM is still expected, however, to be somewhat conservative because it underestimates vertical dispersion. The empirical model used to calculate TSP concentrations from area source emission densities (described in Section 2) is expected to be unbiased since it is a least-squares fit, but it could underestimate or overestimate actual concentrations by an estimated factor of 2.

Concentration estimate ranges are thus constructed as shown schematically in Figure 5-2. Any conclusions about the magnitude and significance of air quality impact should be made recognizing that model estimates of regional impact are uncertain to this degree at this time.

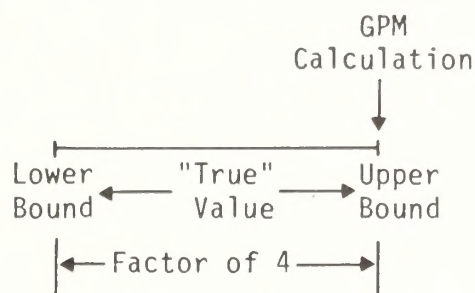
5.2 IMPACTS OF INDUSTRIAL GROWTH

In this subsection the calculated impacts of various subsets of the Uinta and Piceance basin emission sources are described for both the low- and high-oil-production scenarios.

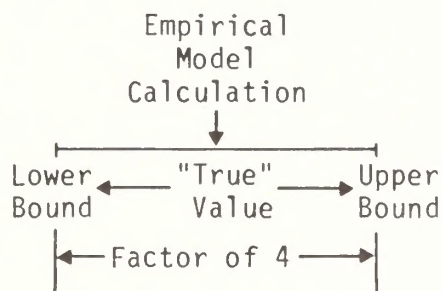
Common to these scenarios is the assumption that other (interrelated) projects in the Uinta Basin would be developed. Thus, regional impact scenarios including the impacts of these other sources. Dominating the emissions (and impacts) in this other source category are the Moon Lake Power Plant (Unit 1 is included in the 1980 baseline and Unit 2 is considered an interrelated source for the purposes of this analysis) and the White River Shale Project (WRSP). The SO₂ and TSP air quality impacts



(a) Estimates for maximum 3-hour and 24-hour average concentrations.



(b) Estimates for annual average concentrations.



(c) Estimates for area source TSP concentrations using empirical model.

FIGURE 5-2. SCHEMATIC REPRESENTATION OF ESTIMATED RANGES IN THE REGIONAL AIR QUALITY IMPACTS ASSESSMENT

associated with direct source emissions from these facilities are displayed in Figures 5-3 through 5-6. Because of the problems associated with modeling ground-level multiple point source emissions economically with GPM, COMPLEX-I was used to model WRSP impacts.* GPM was used for Moon Lake. Note that impacts of these two sources are well within PSD increments with the possible exception of near-source TSP impacts of WRSP, which may be somewhat in excess of the Class II 24-hour average increment of $37 \mu\text{g}/\text{m}^3$.

5.2.1 Low-Oil-Production Scenario

5.2.1.1 Incremental Impacts of Site-Specifics Alone

Figures 5-7 and 5-8 display the SO_2 and TSP impacts associated with the incremental impact of the five site-specific Uinta Basin synfuel facilities. All ground-level impacts associated with the cumulative emissions from these facilities are within all increments.

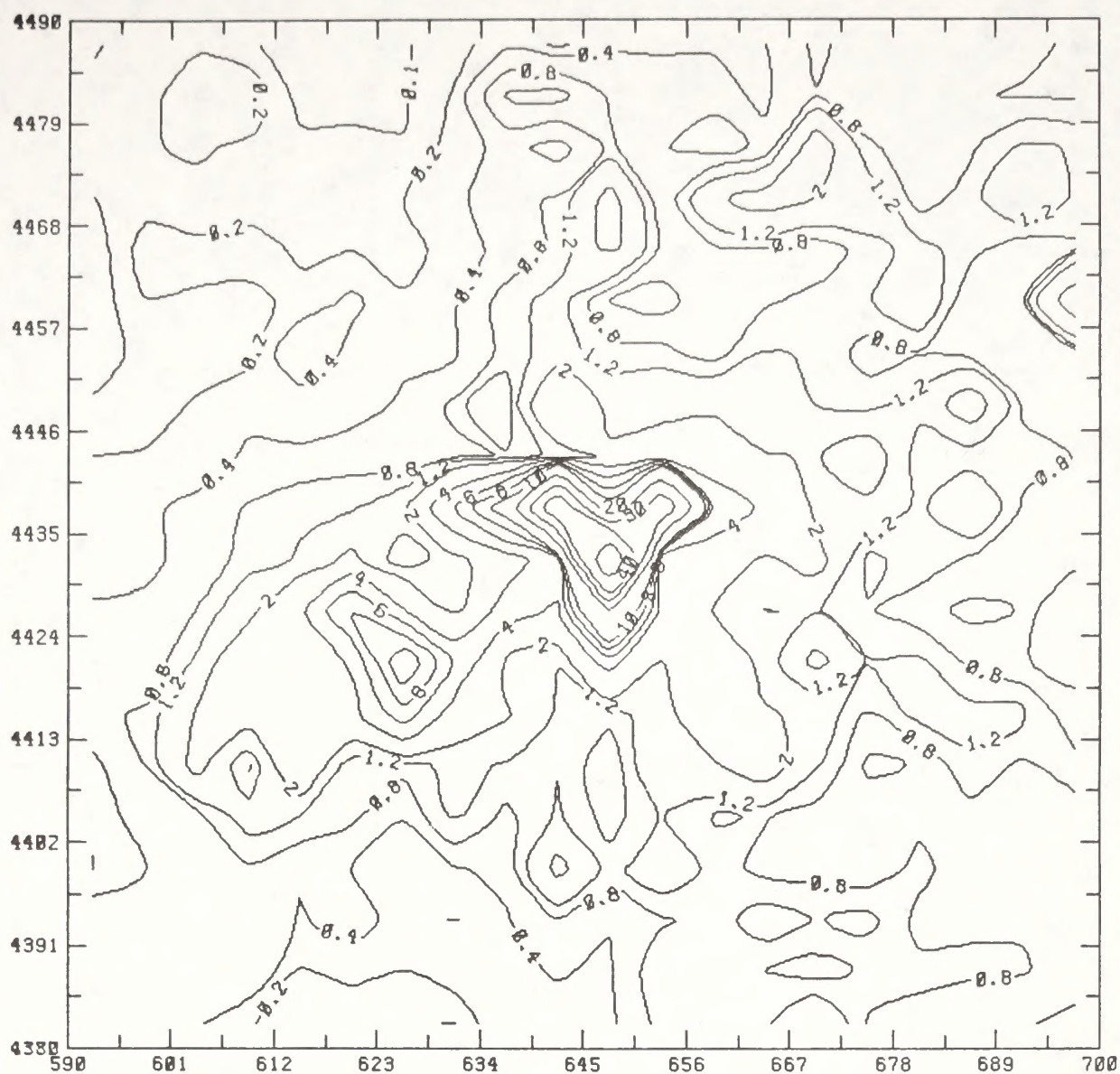
5.2.1.2 Incremental Impacts of Site-Specifics and Conceptuals

Figures 5-9 and 5-10 display SO_2 and TSP impacts associated with the incremental impacts of the Uinta Basin site-specifics together with the conceptual facilities. The Geokinetics facilities contribute significantly to the ambient SO_2 concentrations, and the conceptual proposal for the Sohio facility adds to the TSP impacts. It is possible that TSP concentrations near the Sohio facility could cause violations of the Class II 24-hour average increment, but because of the conceptual nature of the existing design information, this conclusion is quite speculative at this time.

5.2.1.3 Incremental Impact of Colorado Point Sources

Figures 5-11 and 5-12 display the incremental impacts of Piceance Basin oil shale facilities and other (existing) point sources near Grand Junction. The impacts of the Colorado sources are based on a development

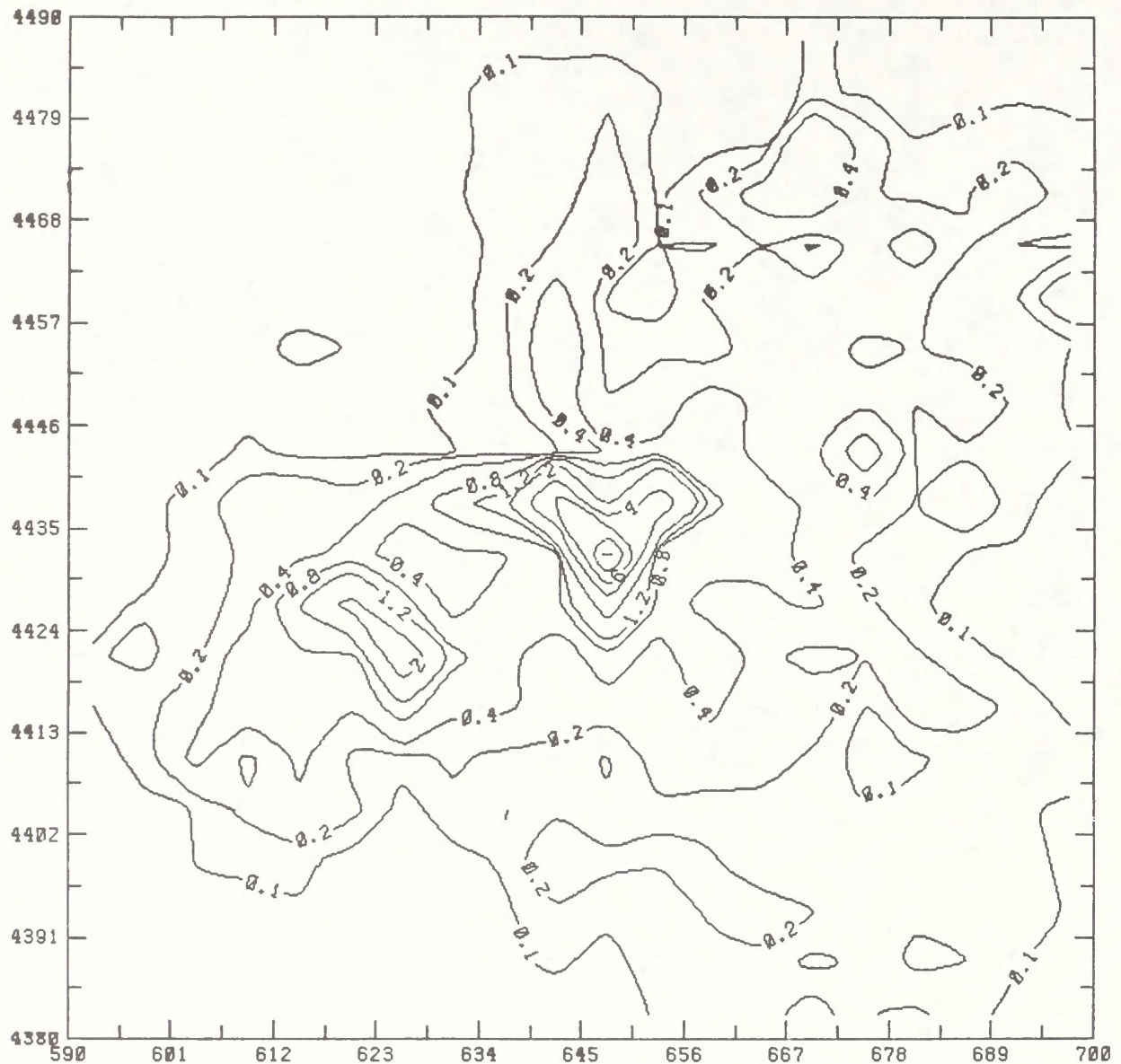
* Inappropriate isopleths in GPM regional plots near WRSP and near other facilities for TSP impacts have been replaced with corrected values based on COMPLEX-I. GPM calculations are overly conservative near sources with multiple ground-level release points because in GPM multiple emissions are treated as one (see section 4.2).



Note: These are upper-bound estimates of actual impacts and are non-simultaneous maxima calculated on the basis of one year's meteorological data.

(a) Maximum 3-hour average

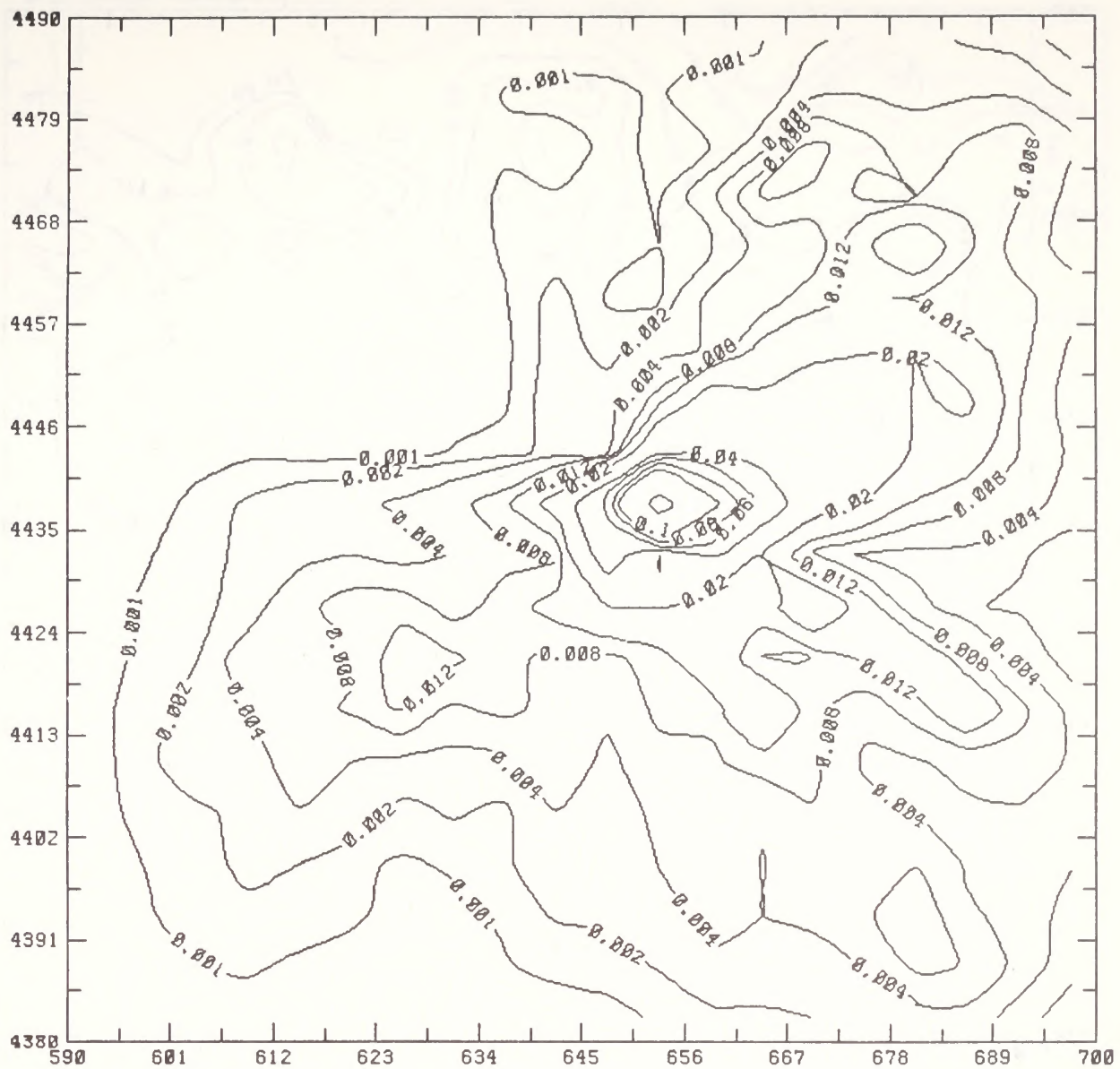
FIGURE 5-3. IMPACT OF DIRECT SOURCE EMISSIONS FROM MOON LAKE UNIT 2 ON GROUND-LEVEL SO_2 CONCENTRATIONS ($\mu\text{g}/\text{m}^3$)



Note: These are upper-bound estimates of actual impacts and are non-simultaneous maxima calculated on the basis of one year's meteorological data.

(b) Maximum 24-hour average

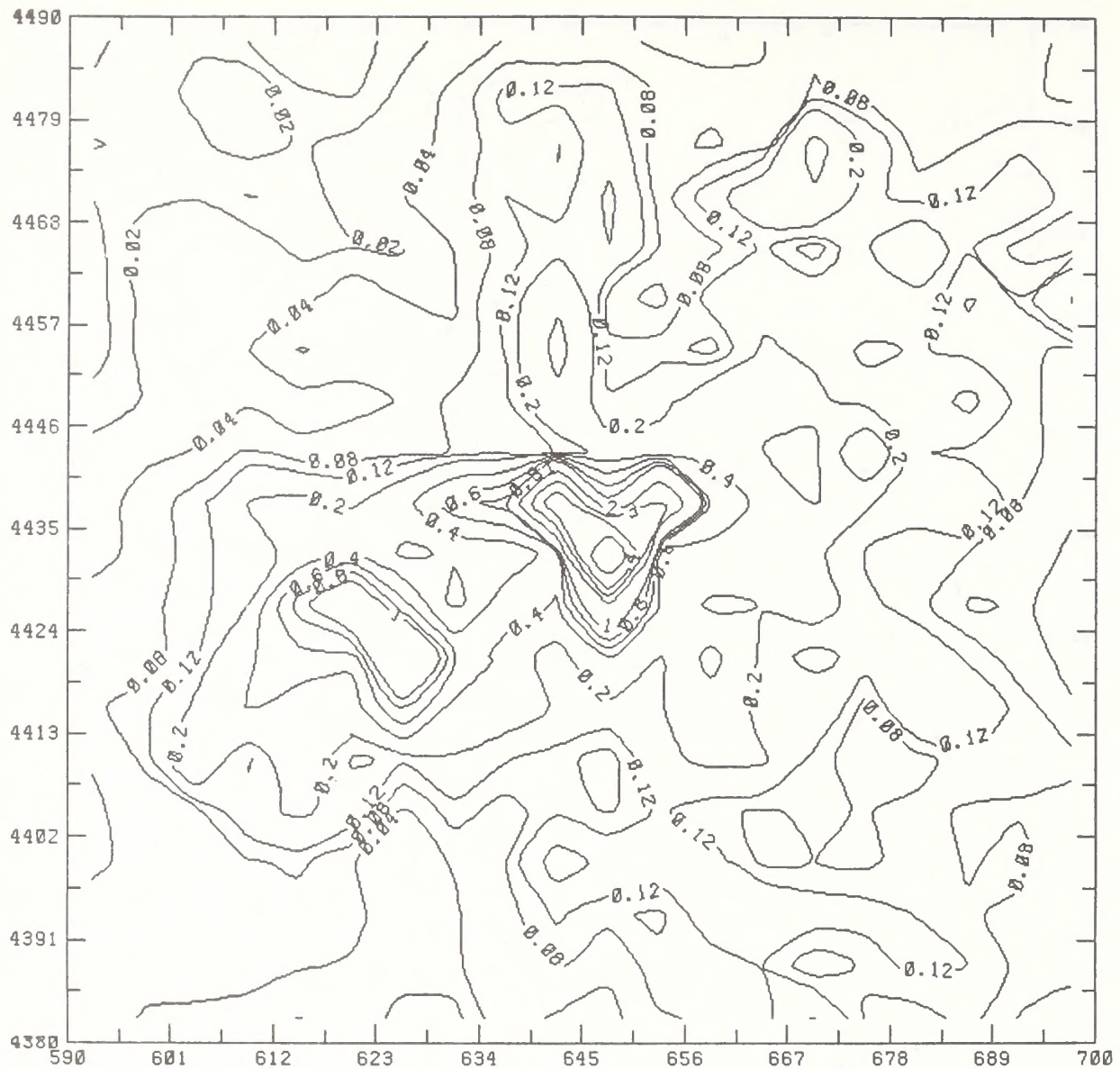
FIGURE 5-3 (Continued)



Note: These are upper-bound estimates
of actual impacts.

(c) Annual Average

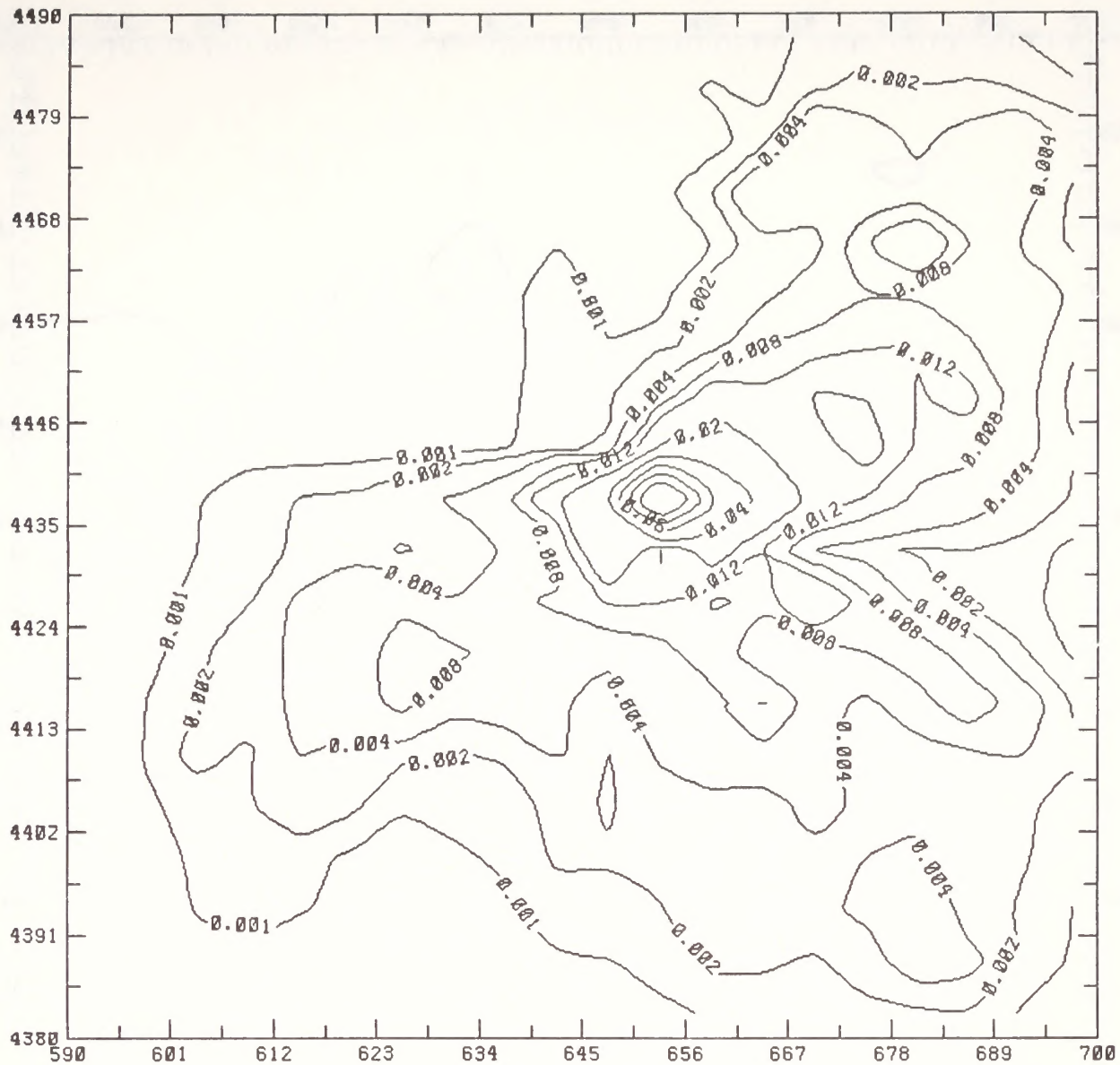
FIGURE 5-3 (Concluded)



Note: These are upper-bound estimates of actual impacts and are non-simultaneous maxima calculated on the basis of one year's meteorological data.

(a) Maximum 24-hour average

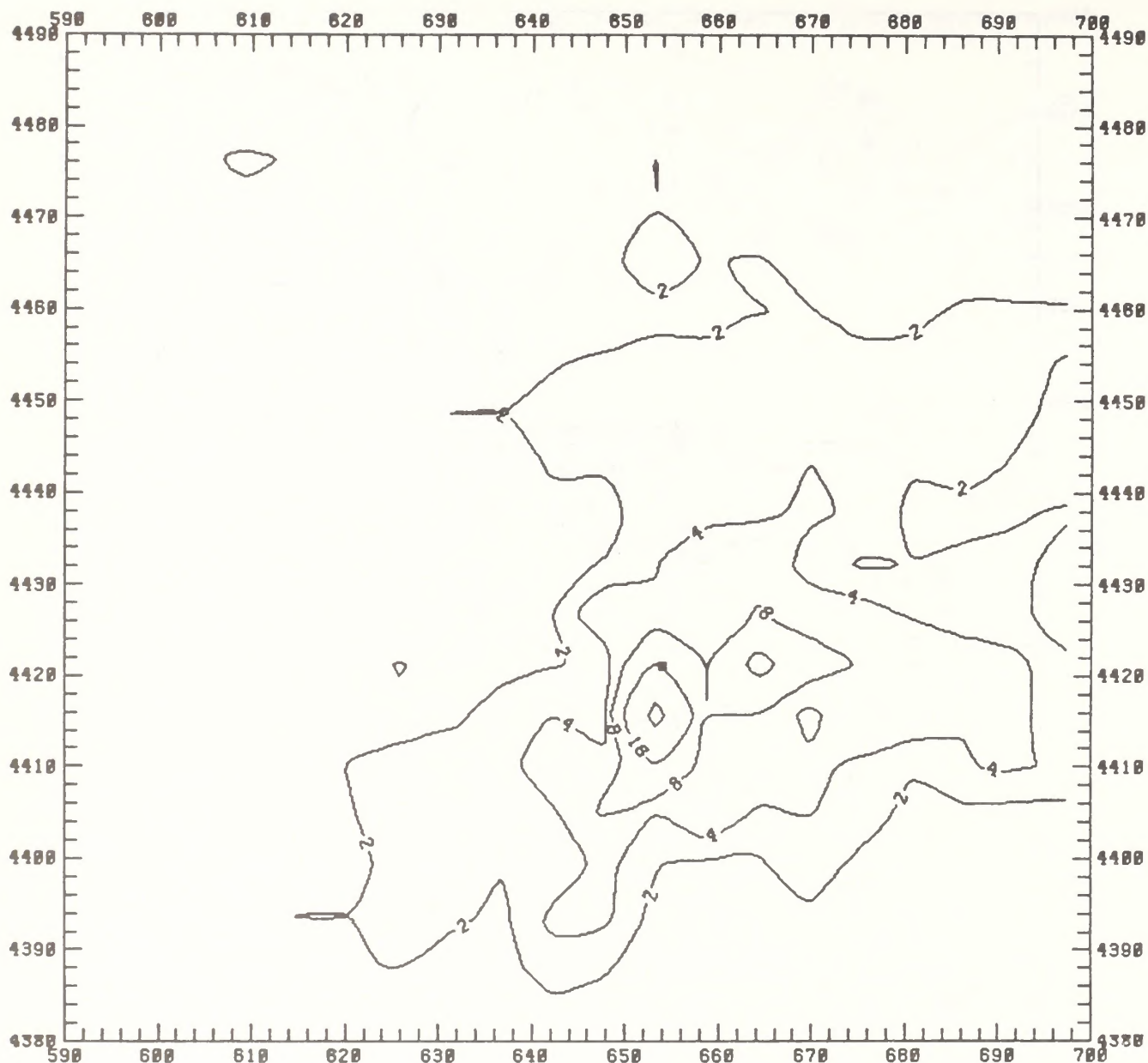
FIGURE 5-4. IMPACT OF DIRECT SOURCE EMISSIONS FROM MOON LAKE UNIT 2 ON GROUND-LEVEL TSP CONCENTRATIONS ($\mu\text{g}/\text{m}^3$)



Note: These are upper-bound estimates of actual impacts.

(b) Annual average

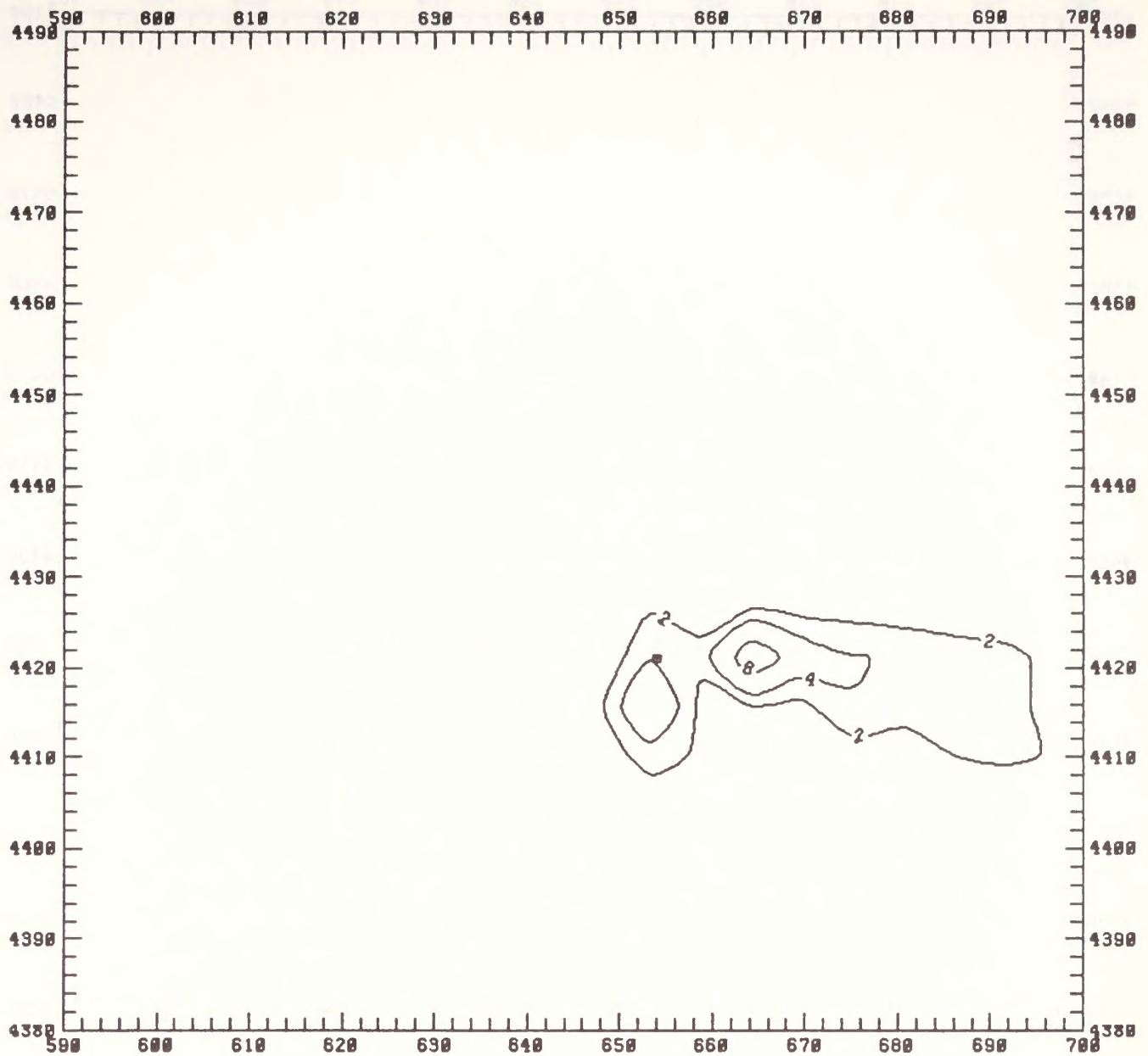
FIGURE 5-4 (Concluded)



Note: These are upper-bound estimates of actual impacts and are non-simultaneous maxima calculated on the basis of one year's meteorological data.

(a) Maximum 3-hour average

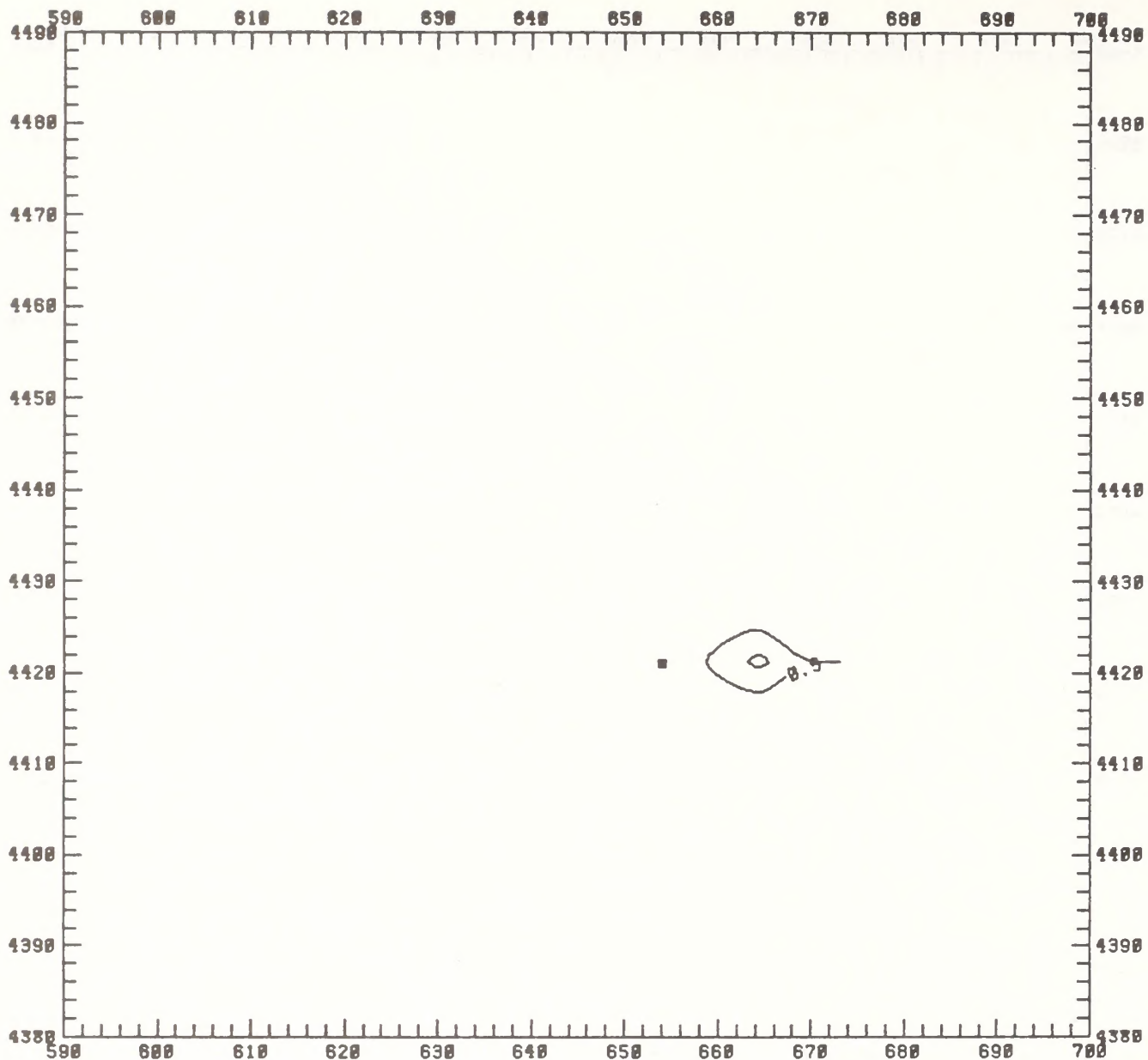
FIGURE 5-5. IMPACT OF DIRECT SOURCE EMISSIONS FROM WHITE RIVER SHALE PROJECT ON GROUND-LEVEL SO_2 CONCENTRATIONS ($\mu\text{g}/\text{m}^3$)



Note: These are upper-bound estimates of actual impacts and are non-simultaneous maxima calculated on the basis of one year's meteorological data.

(b) Maximum 24-hour average

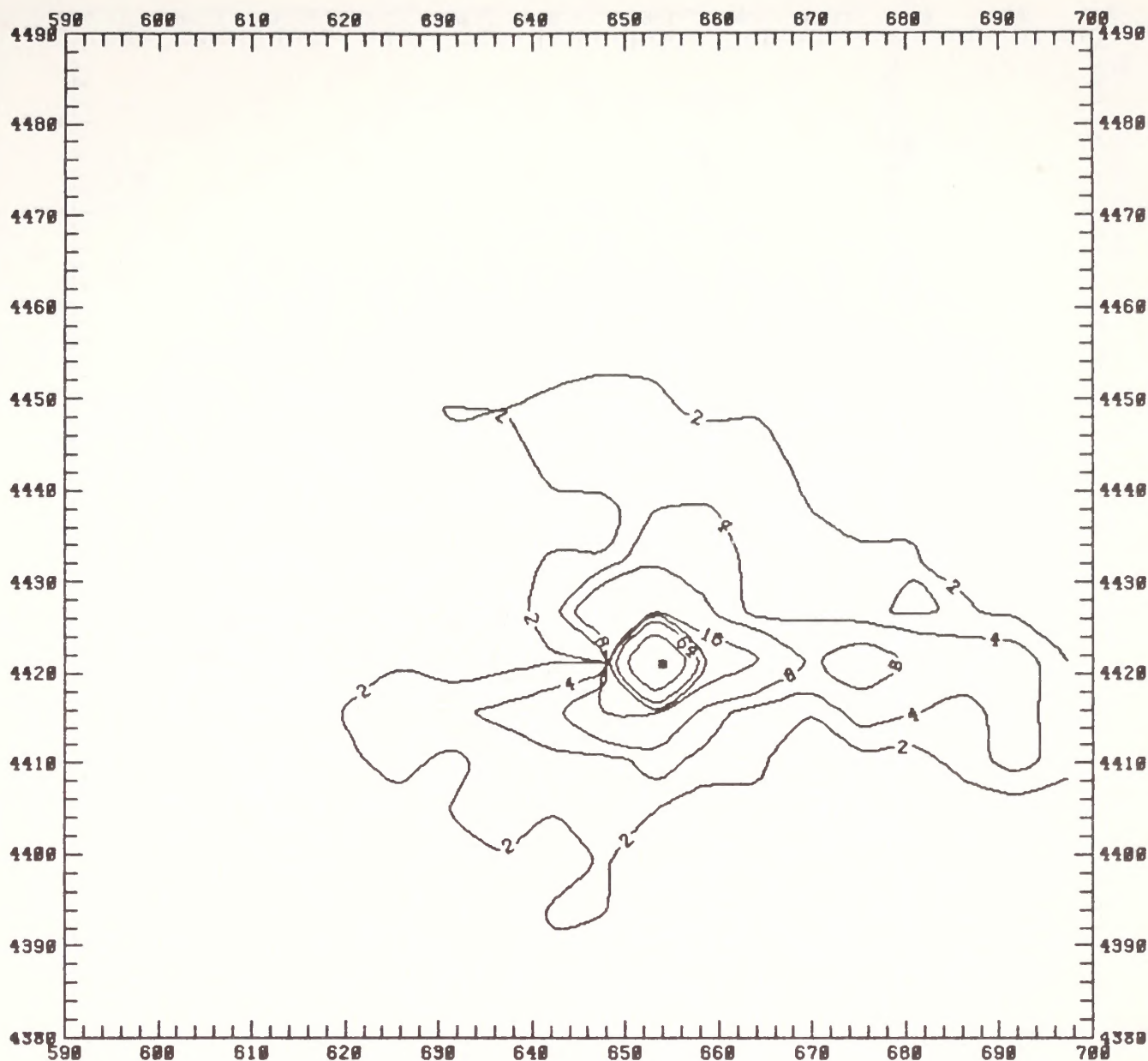
FIGURE 5-5 (Continued)



Note: These are upper-bound estimates
of actual impacts.

(c) Annual average

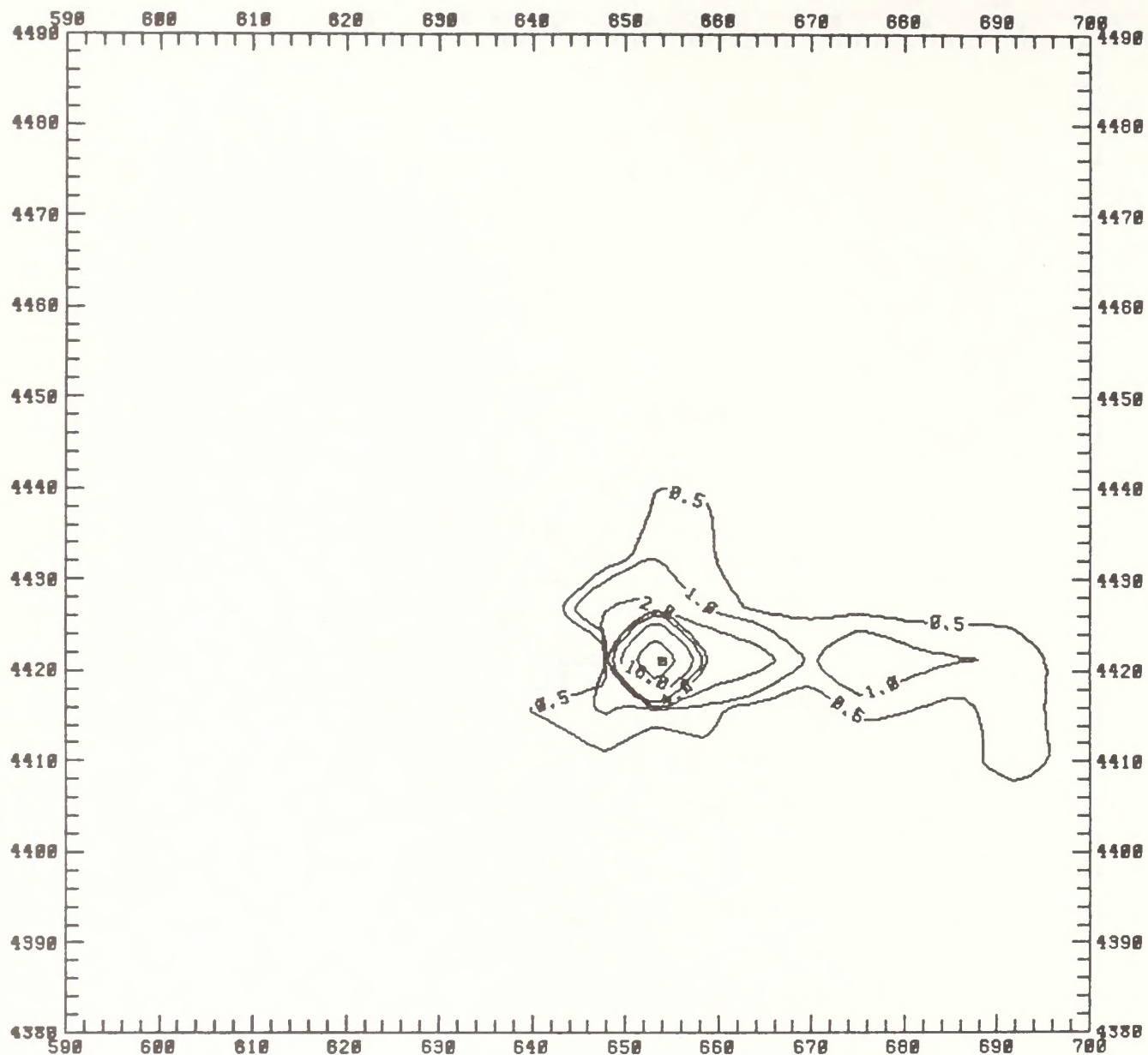
FIGURE 5-5 (Concluded)



Note: These are upper-bound estimates of actual impacts and are non-simultaneous maxima calculated on the basis of one year's meteorological data.

(a) Maximum 24-hour average

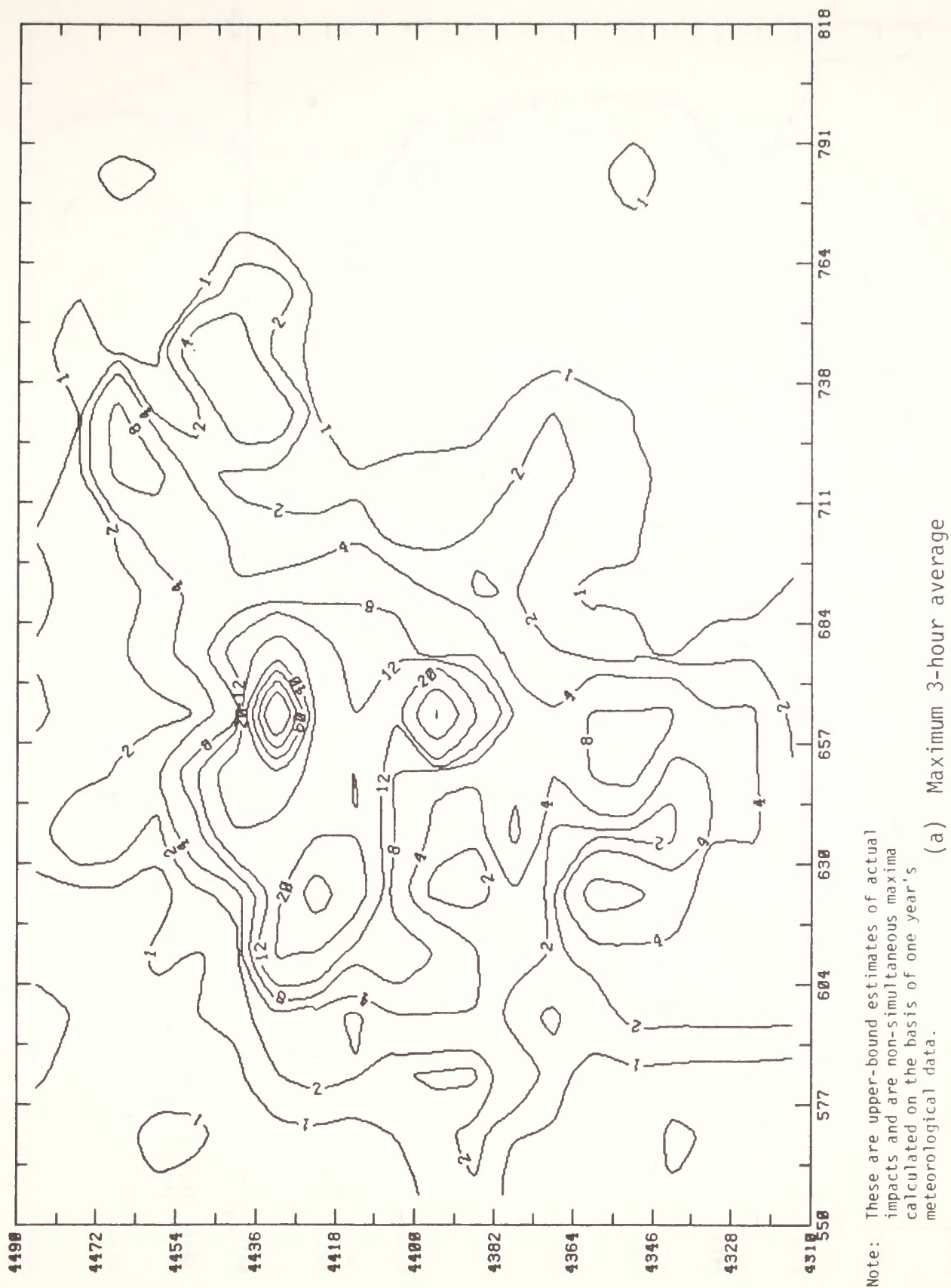
FIGURE 5-6. IMPACT OF DIRECT SOURCE EMISSIONS FROM WHITE RIVER SHALE PROJECT ON GROUND-LEVEL TSP CONCENTRATIONS ($\mu\text{g}/\text{m}^3$)



Note: These are upper-bound estimates
of actual impacts.

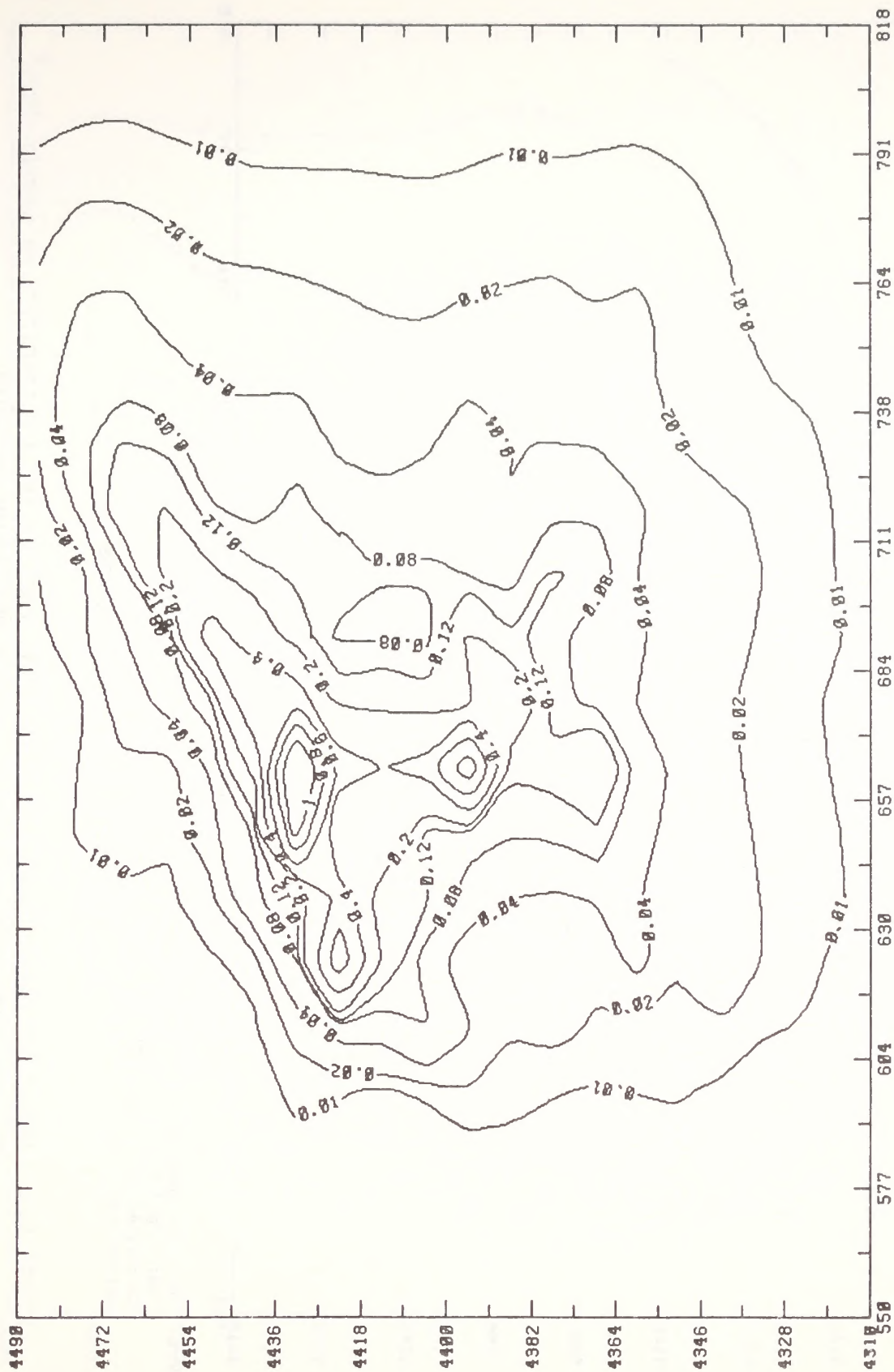
(b) Annual Average

FIGURE 5-6 (Concluded)



Note: These are upper-bound estimates of actual impacts and are non-simultaneous maxima calculated on the basis of one year's meteorological data.

FIGURE 5-7. IMPACT OF DIRECT SOURCE EMISSIONS FROM UINTA BASIN SITE-SPECIFICS ON GROUND-LEVEL SO_2 CONCENTRATIONS ($\mu\text{g}/\text{m}^3$) FOR LOW OIL PRODUCTION SCENARIO



Note: These are upper-bound estimates of actual impacts.

(c) Annual average

FIGURE 5-7 (Concluded)

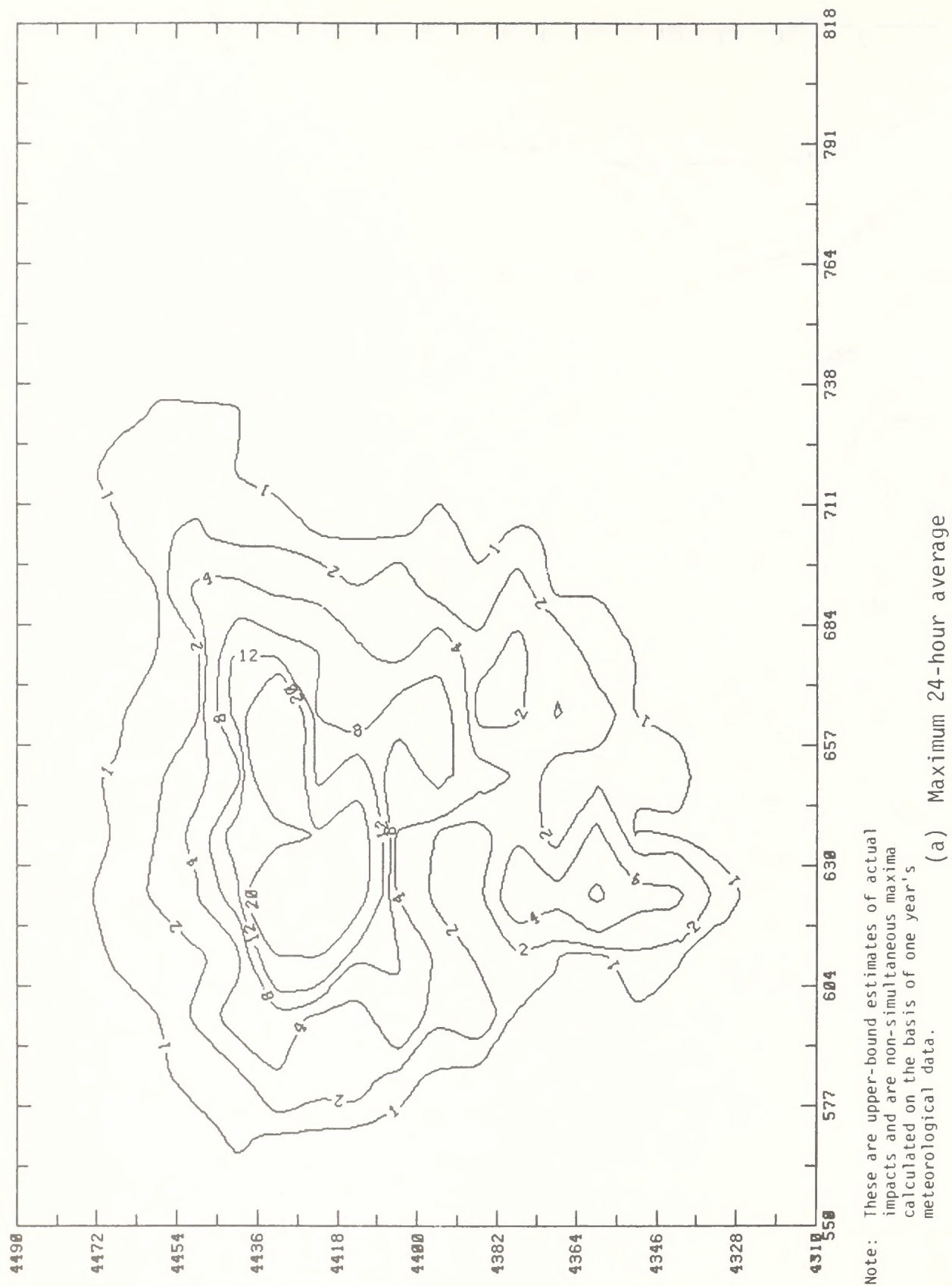
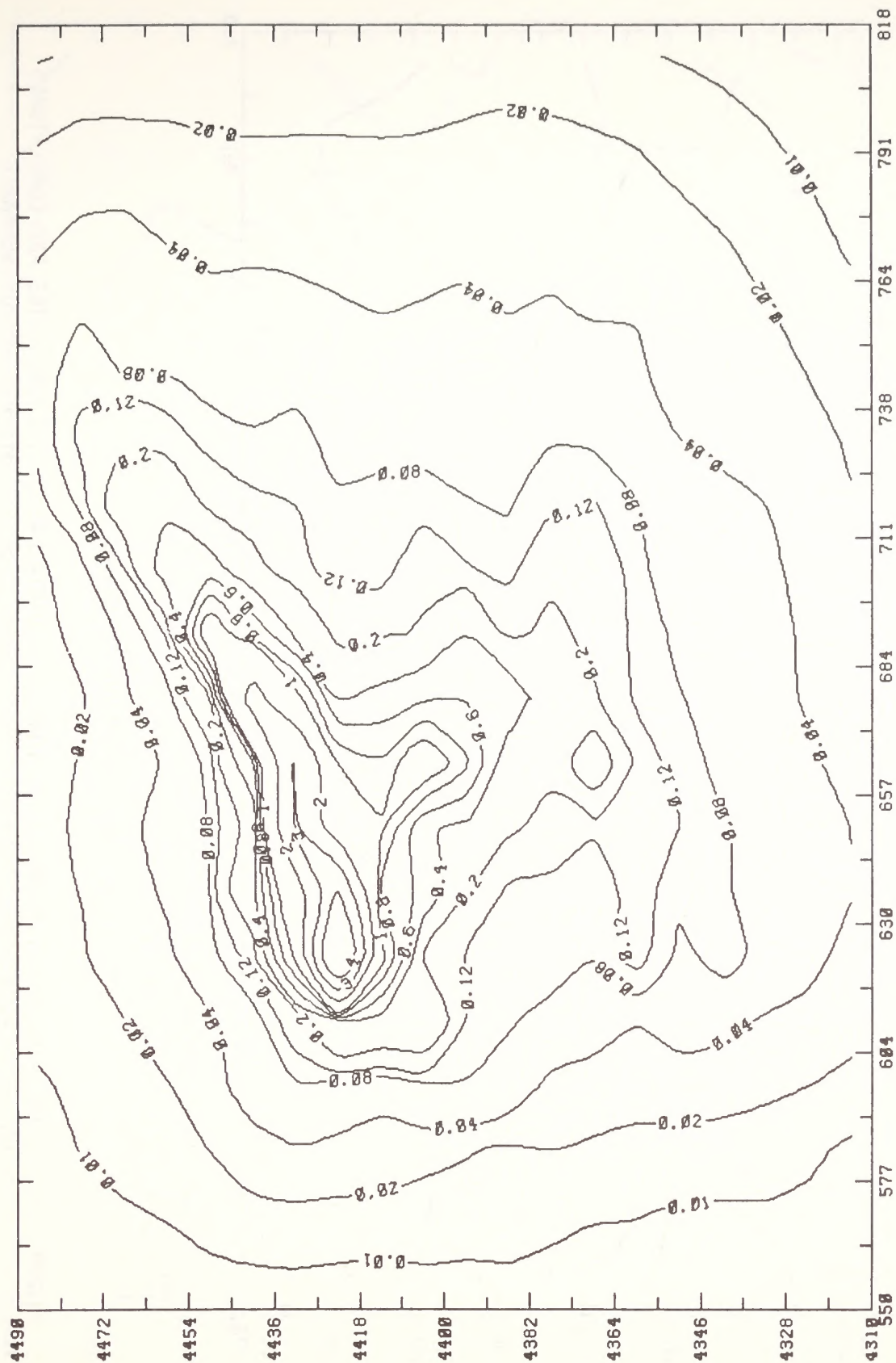


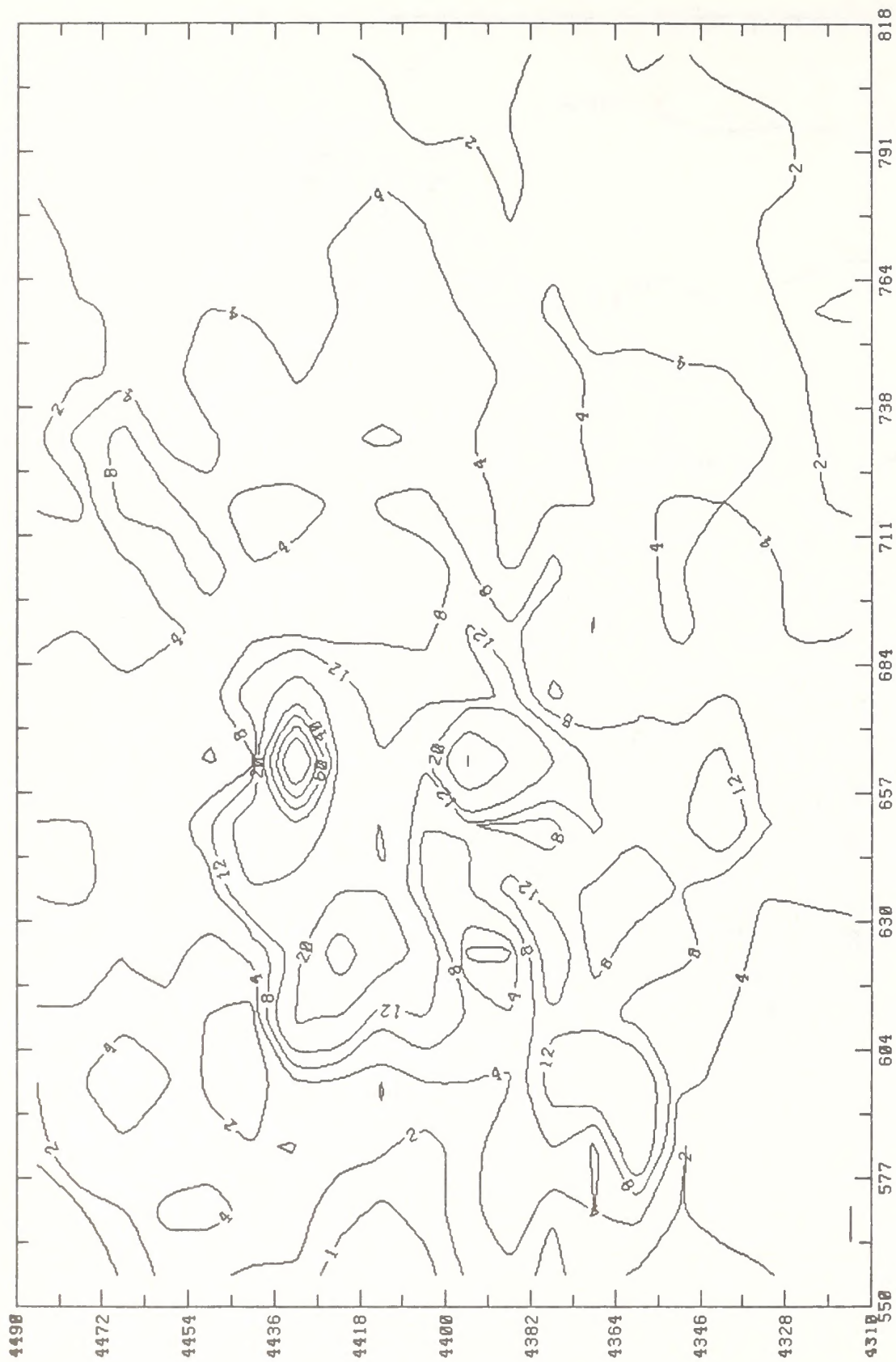
FIGURE 5-8. IMPACT OF DIRECT SOURCE EMISSIONS FROM UINTA BASIN SITE-SPECIFICS ON GROUND-LEVEL TSP CONCENTRATIONS ($\mu\text{g}/\text{m}^3$) FOR LOW OIL PRODUCTION SCENARIO



Note: These are upper-bound estimates of actual impacts.

(b) Annual average

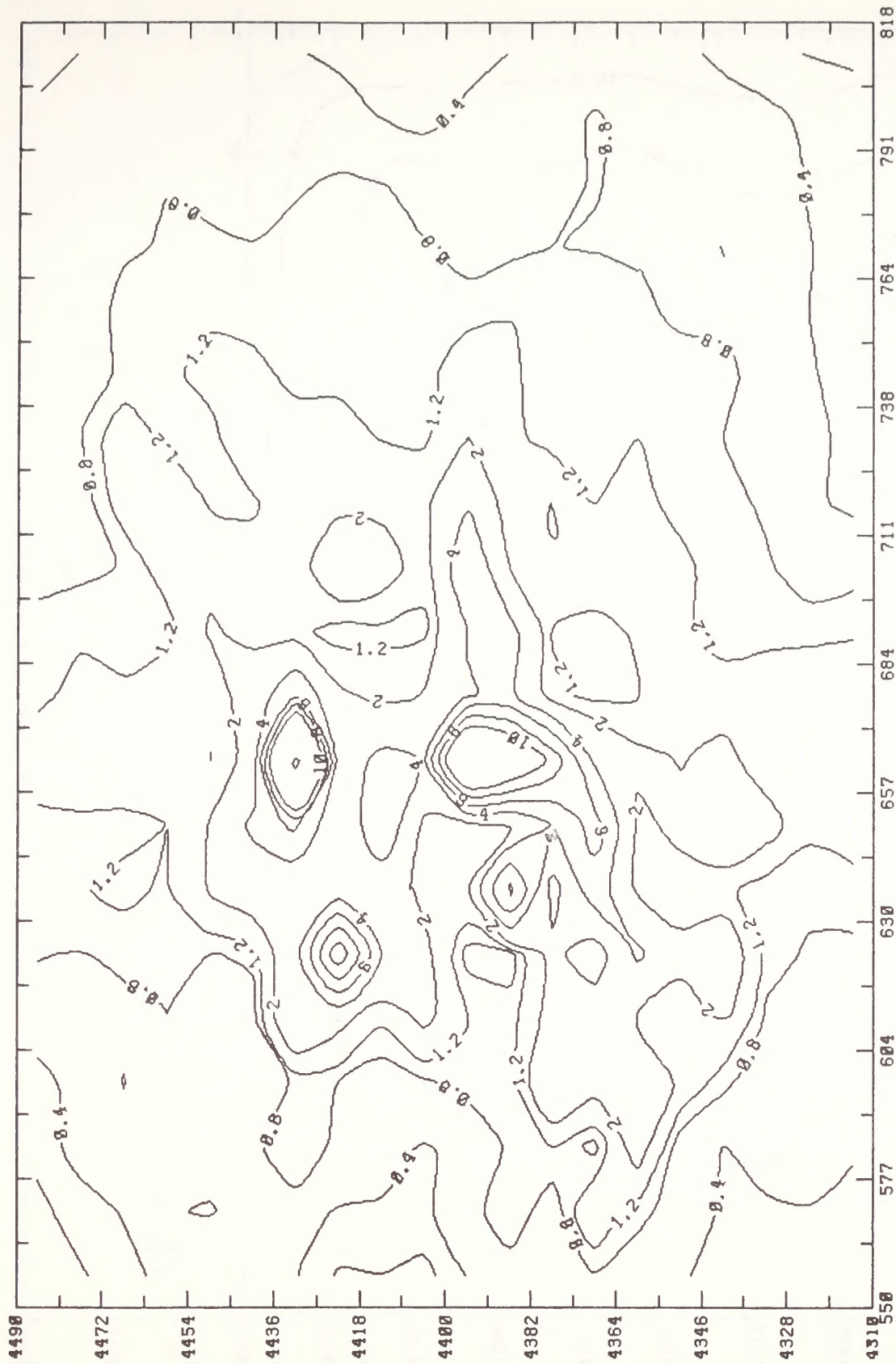
FIGURE 5-8 (Concluded)



Note: These are upper-bound estimates of actual impacts and are non-simultaneous maxima calculated on the basis of one year's meteorological data.

(a) Maximum 3-hour average

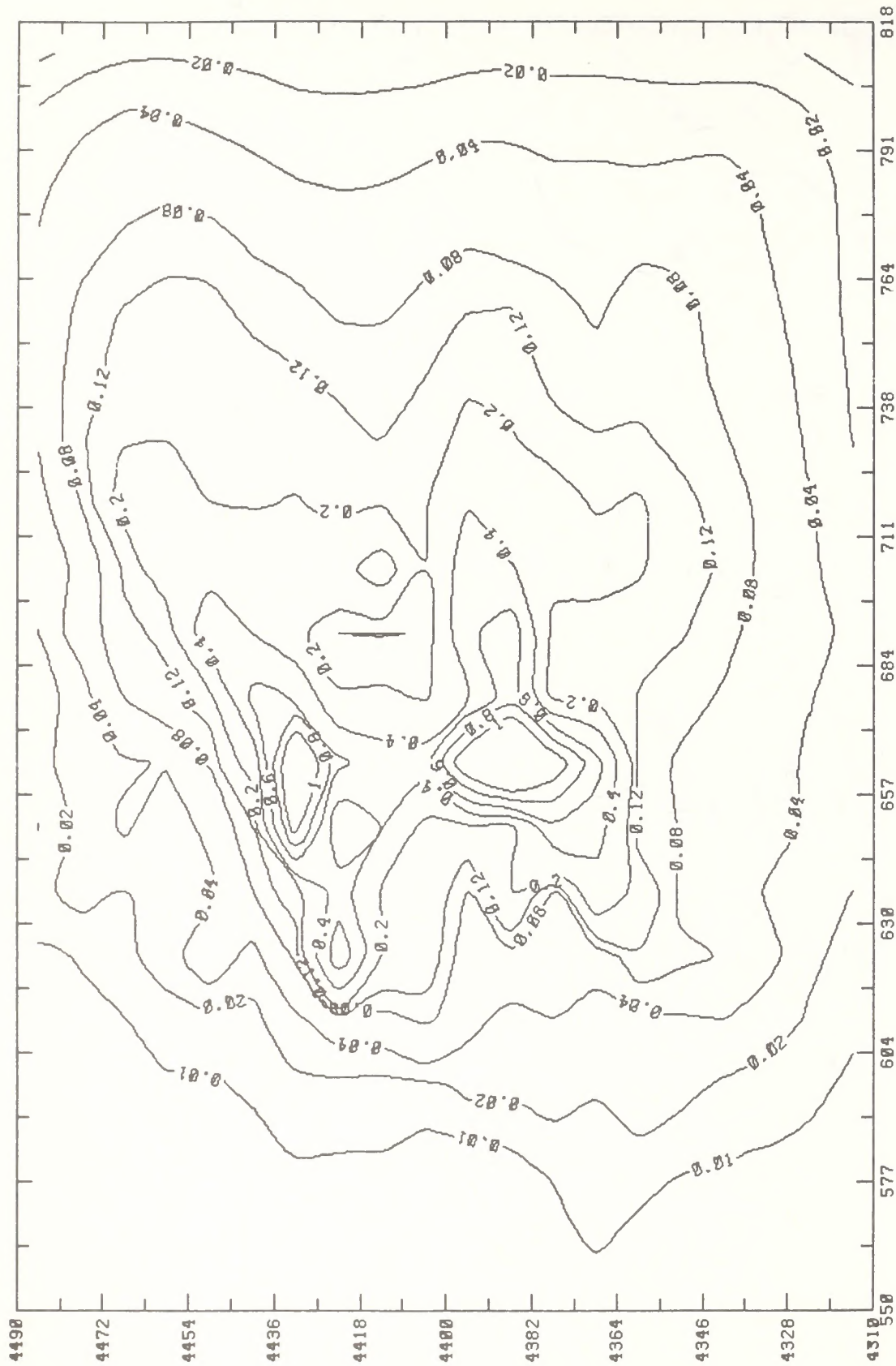
FIGURE 5-9. IMPACT OF DIRECT SOURCE EMISSIONS FROM UINTA BASIN SITE-SPECIFICS AND CONCEPTUALS ON GROUND-LEVEL SO₂ CONCENTRATIONS (µg/m³) FOR LOW OIL PRODUCTION SCENARIO



Note: These are upper-bound estimates of actual impacts and are non-simultaneous maxima calculated on the basis of one year's meteorological data.

(b) Maximum 24-hour average

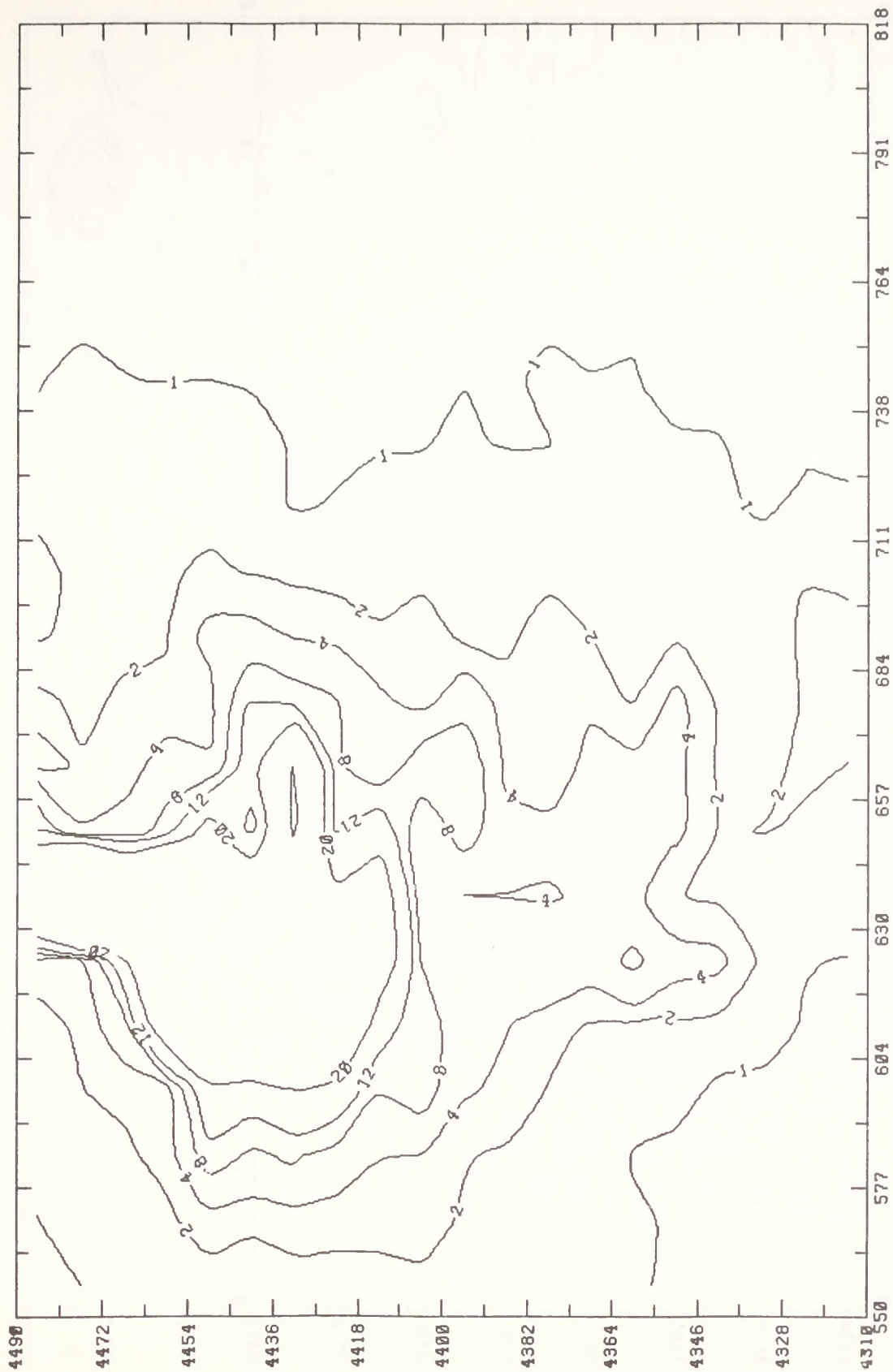
FIGURE 5-9 (Continued)



Note: These are upper-bound estimates of actual impacts.

(c) Annual average

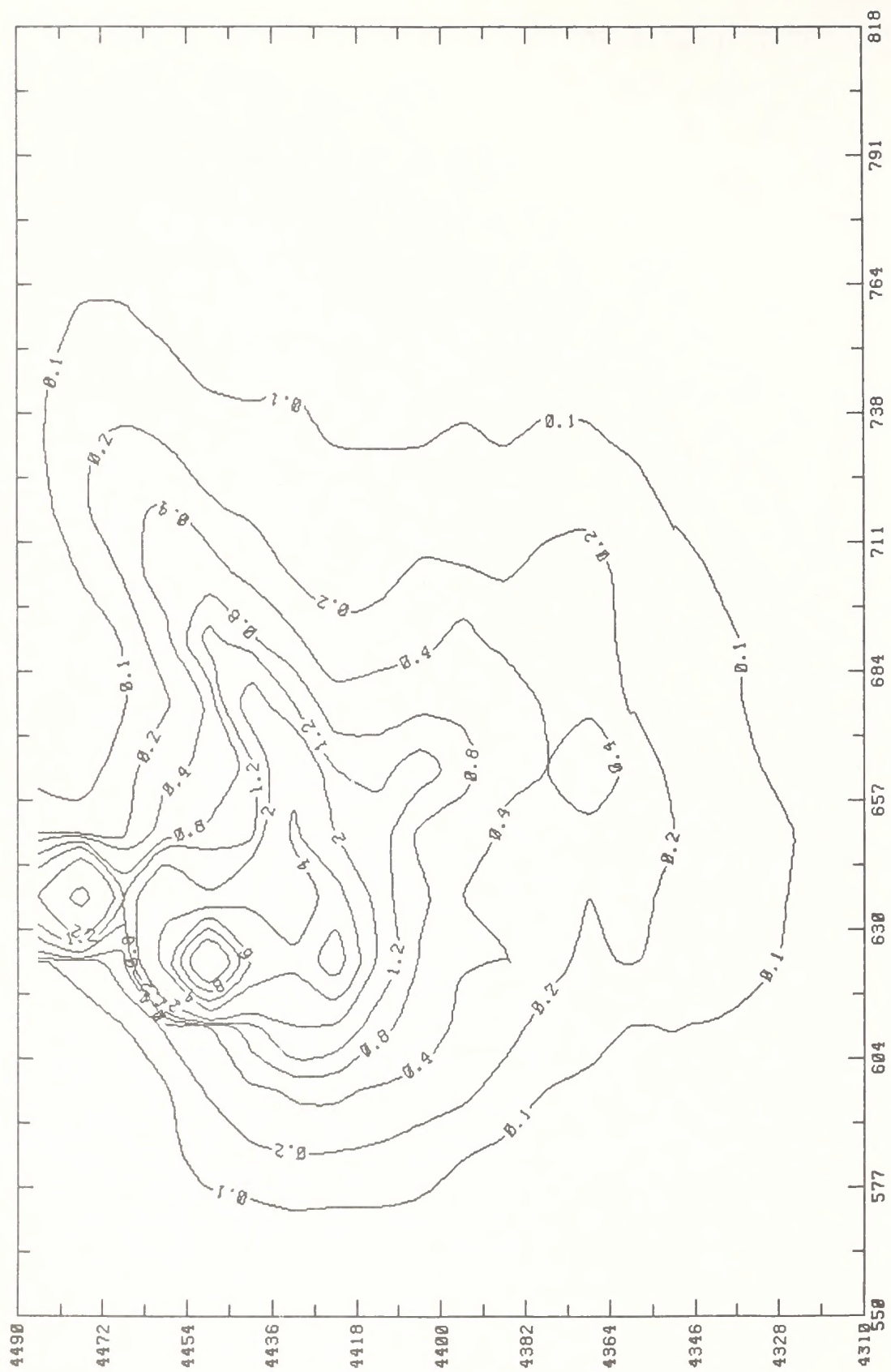
FIGURE 5-9 (Concluded)



Note: These are upper-bound estimates of actual impacts and are non-simultaneous maxima calculated on the basis of one year's meteorological data.

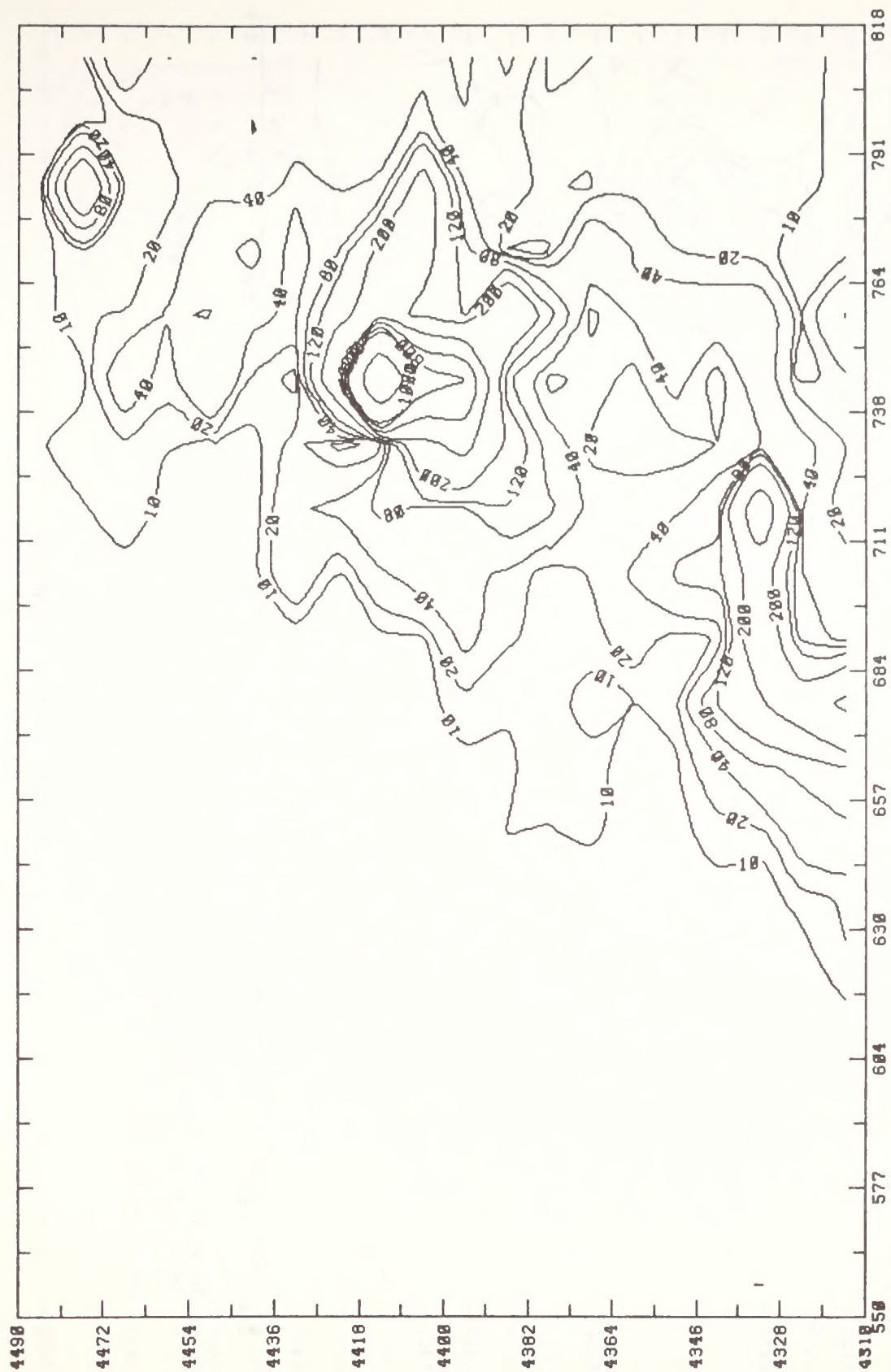
(a) Maximum 24-hour average

FIGURE 5-10. IMPACT OF DIRECT SOURCE EMISSIONS FROM UINTA BASIN SITE SPECIFICS ON GROUND-LEVEL TSP CONCENTRATIONS ($\mu\text{g}/\text{m}^3$) FOR LOW OIL PRODUCTION SCENARIO



(b) Annual Average

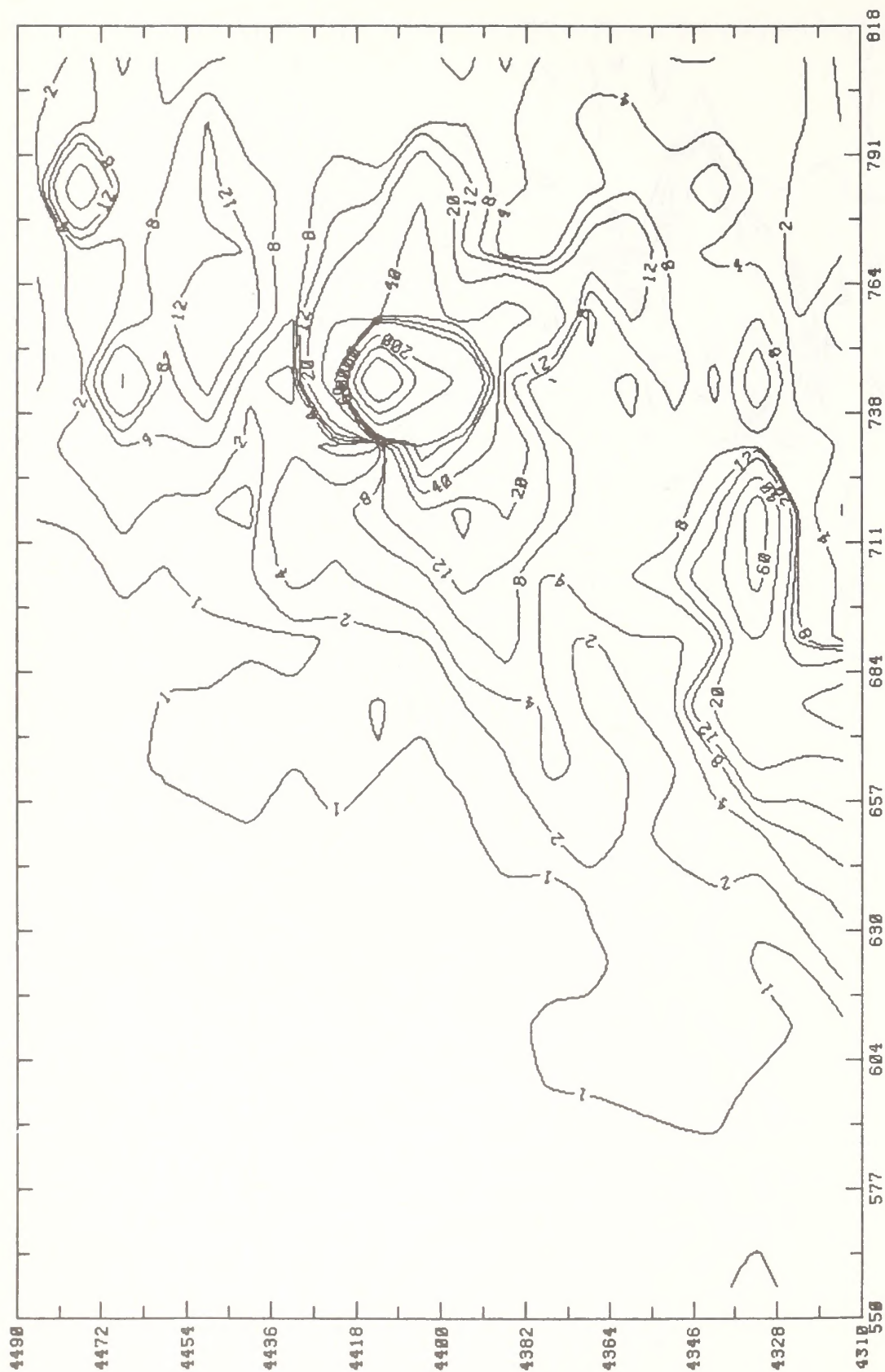
FIGURE 5-10 (Concluded)



Note: These are upper-bound estimates of actual impacts and are non-simultaneous maxima calculated on the basis of one year's meteorological data.

(a) Maximum 3-hour average

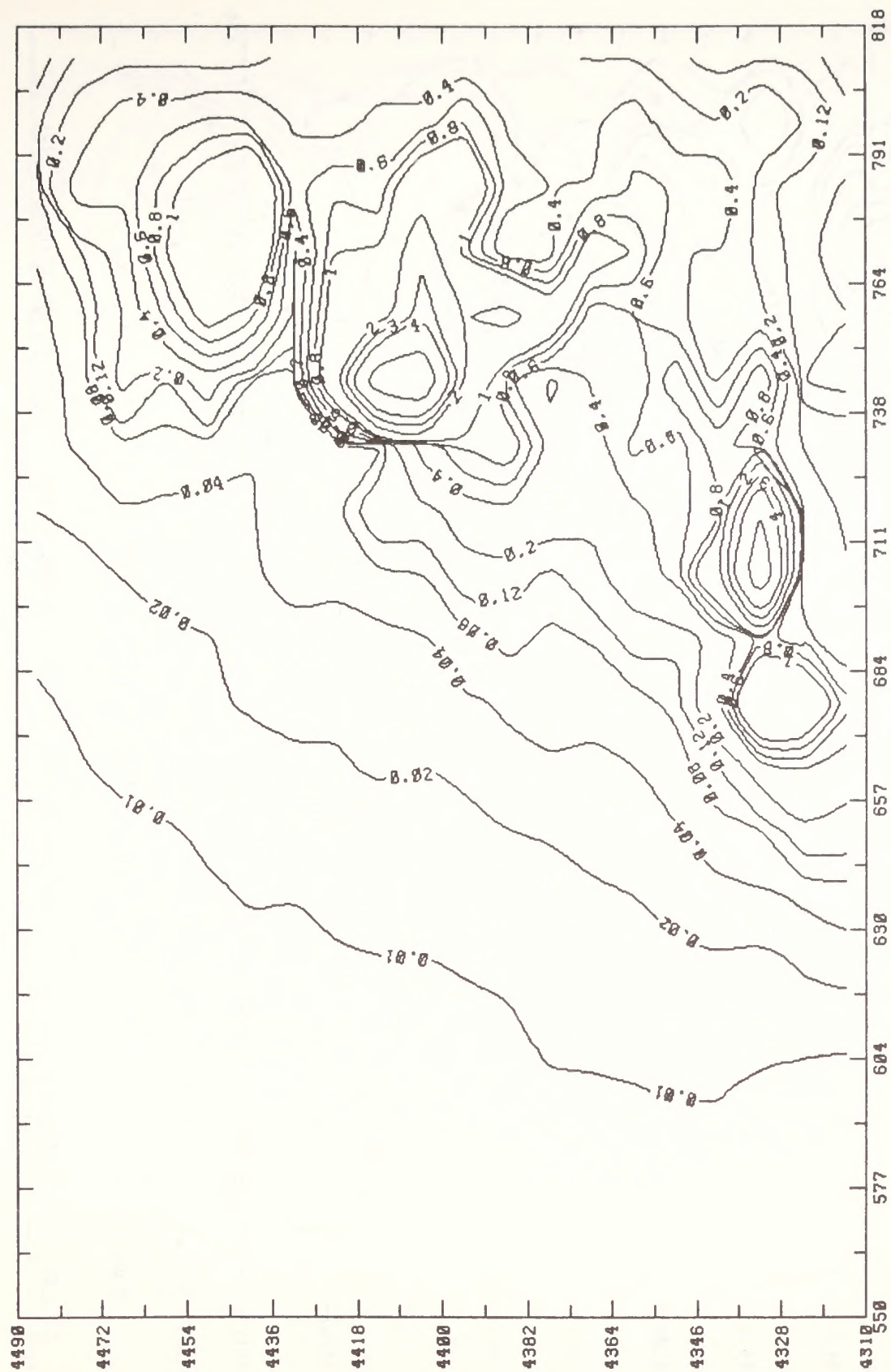
FIGURE 5-11. IMPACT OF DIRECT SOURCE EMISSIONS FROM COLORADO EMISSION SOURCES ON GROUND-LEVEL SO_2 CONCENTRATIONS ($\mu\text{g}/\text{m}^3$) FOR THE LOW OIL PRODUCTION SCENARIO



Note: These are upper-bound estimates of actual impacts and are non-simultaneous maxima calculated on the basis of one year's meteorological data.

(b) Maximum 24-hour average

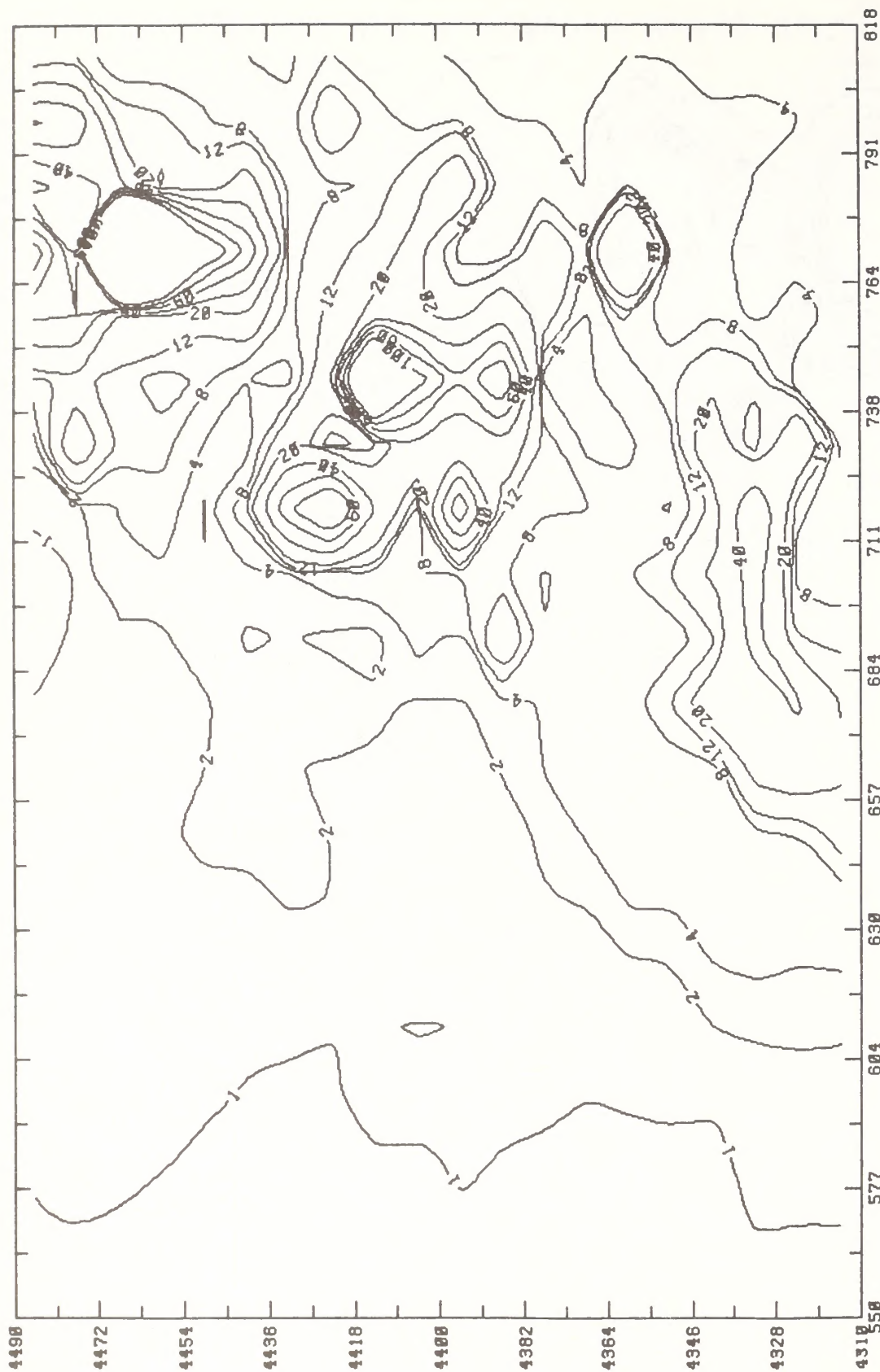
FIGURE 5-11 (Continued)



Note: These are upper-bound estimates of actual impacts.

(c) Annual average

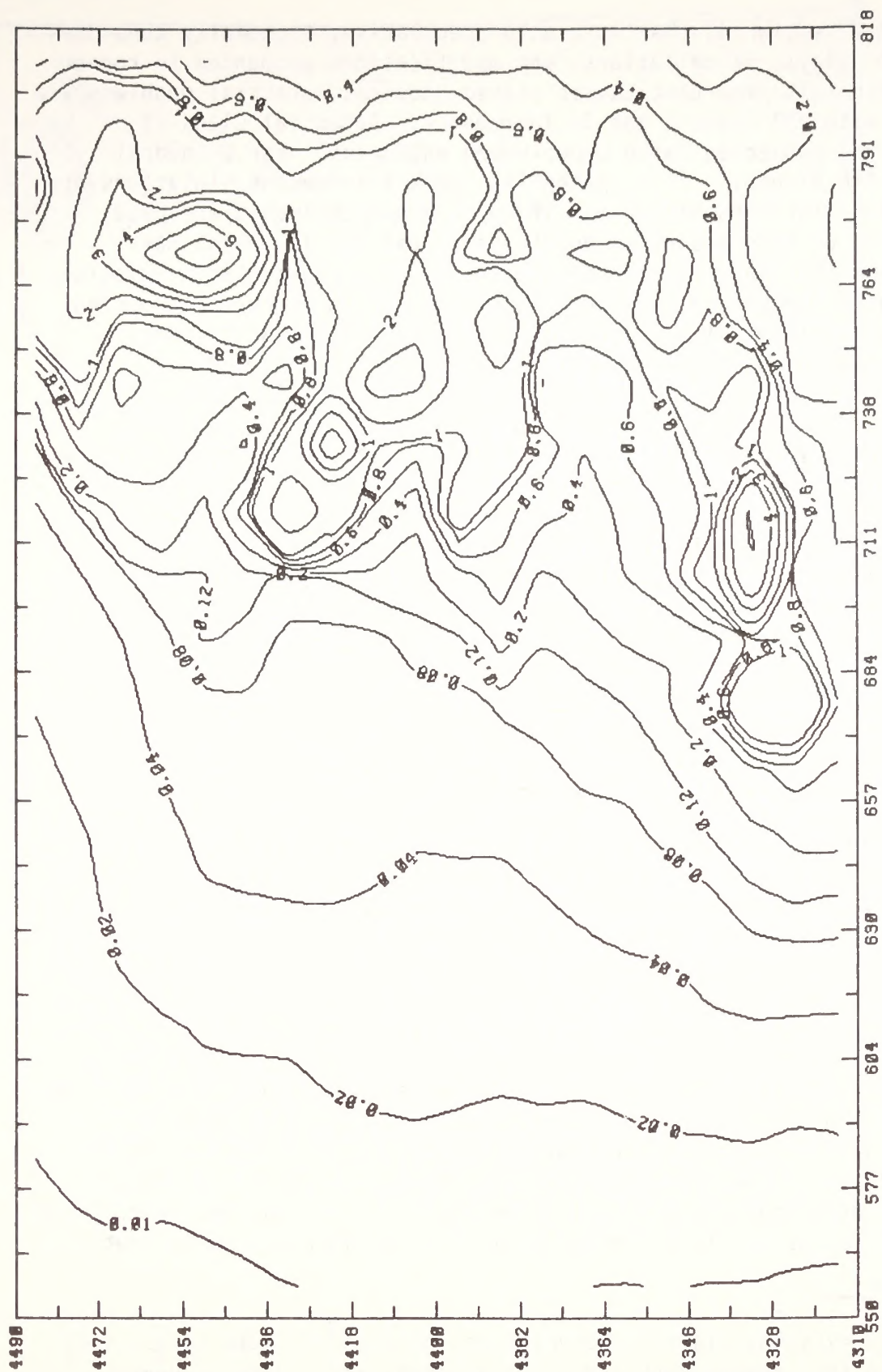
FIGURE 5-11 (Concluded)



Note: These are upper-bound estimates of actual impacts and are non-simultaneous maxima calculated on the basis of one year's meteorological data.

(a) Maximum 24-hour average

FIGURE 5-12. IMPACT OF DIRECT SOURCE EMISSIONS FROM COLORADO POINT SOURCES ON GROUND-LEVEL TSP CONCENTRATIONS ($\mu\text{g}/\text{m}^3$) FOR LOW OIL PRODUCTION SCENARIO



Note: These are upper-bound estimates of actual impacts.

(b) Annual Average

FIGURE 5-12 (Concluded)

scenario (see section 4) that is highly speculative, especially considering project delays, cancellations, and modifications announced in recent months. With this important caveat stated, several potential problems are identified with PSD Class I and II increments. Potential Class II violations are projected (with upper-bound estimates) near Cathedral Bluffs and Rio Blanco.* Also, potential Class I increment violations are projected for Flat Tops Wilderness if upper-bound estimates are used; however, most of this impact is due to Cathedral Bluffs, which has recently been shelved. (Cathedral Bluffs is the Piceance Basin emission source located closest to Flat Tops within 60 km, in a generally upwind location, west of the Class I area.) See Section 5.2.2.3 for more realistic modeling of these impacts.

5.2.1.4 Total Incremental Impact of Regional Industrial Growth for Low-Oil-Production Scenario

Figures 5-13 and 5-14 combine all the emissions from the previously displayed emission source subsets with the baseline and other (inter-related) sources in the Uinta Basin.

5.2.2 High Oil Production Scenario

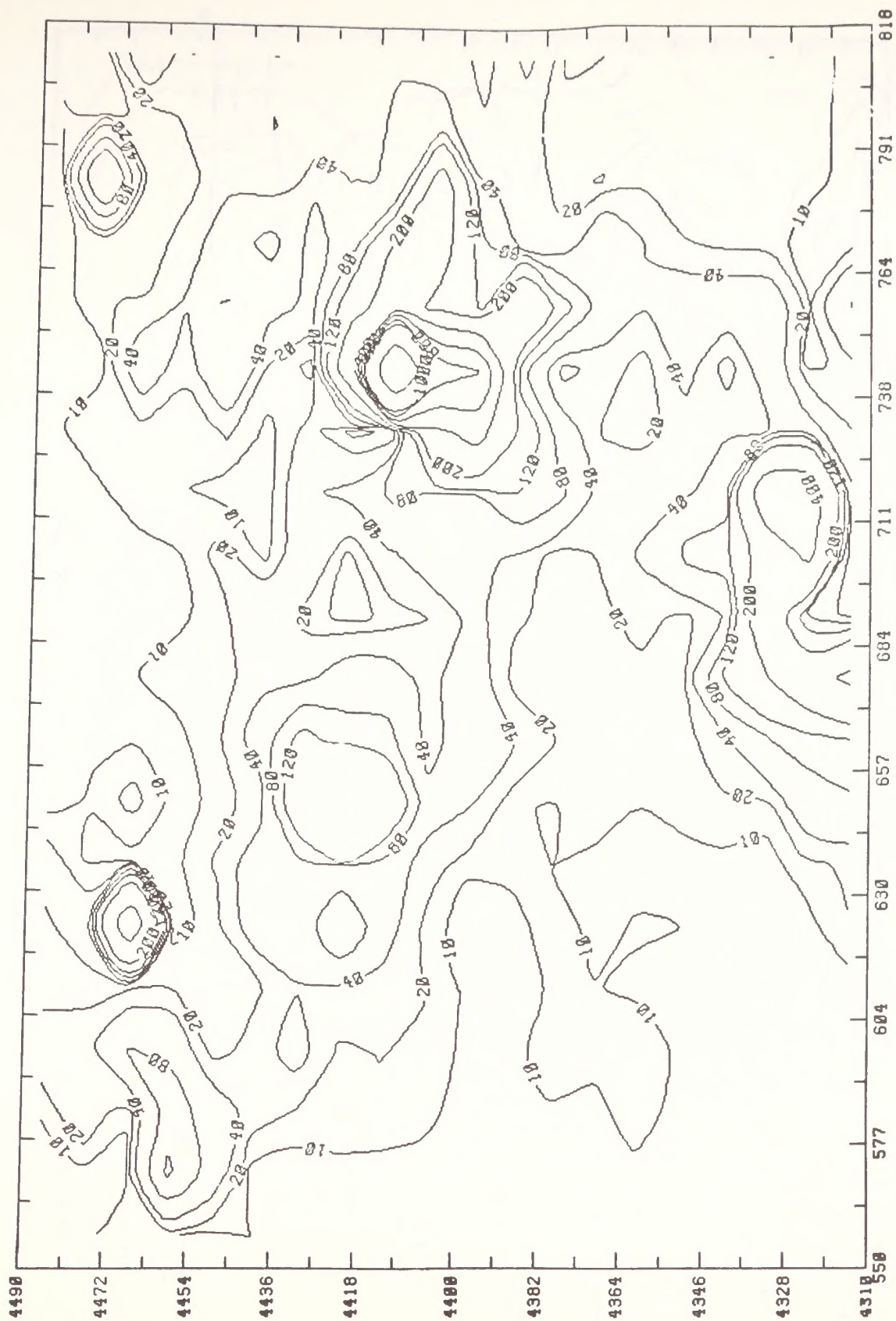
5.2.2.1 Incremental Impacts of Site-Specifics Alone

Figures 5-15 and 5-16 display the GPM model calculations of air quality impacts associated with the five site-specific Uinta Basin facilities at maximum oil production. Impacts are calculated to be within all applicable PSD increments.

5.2.2.2 Incremental Impacts of Site-Specifics and Conceptuals

Figures 5-17 and 5-18 illustrate the incremental impacts of the five site-specific proposals plus the four conceptual proposals on SO₂ and TSP concentrations. Except for TSP concentrations that are elevated in the vicinity of the conceptual Sohio tar sands facility, these conservative, upper-bound estimates are within increments. Since it was recognized that the aggregation of multiple ground-level releases into a single point

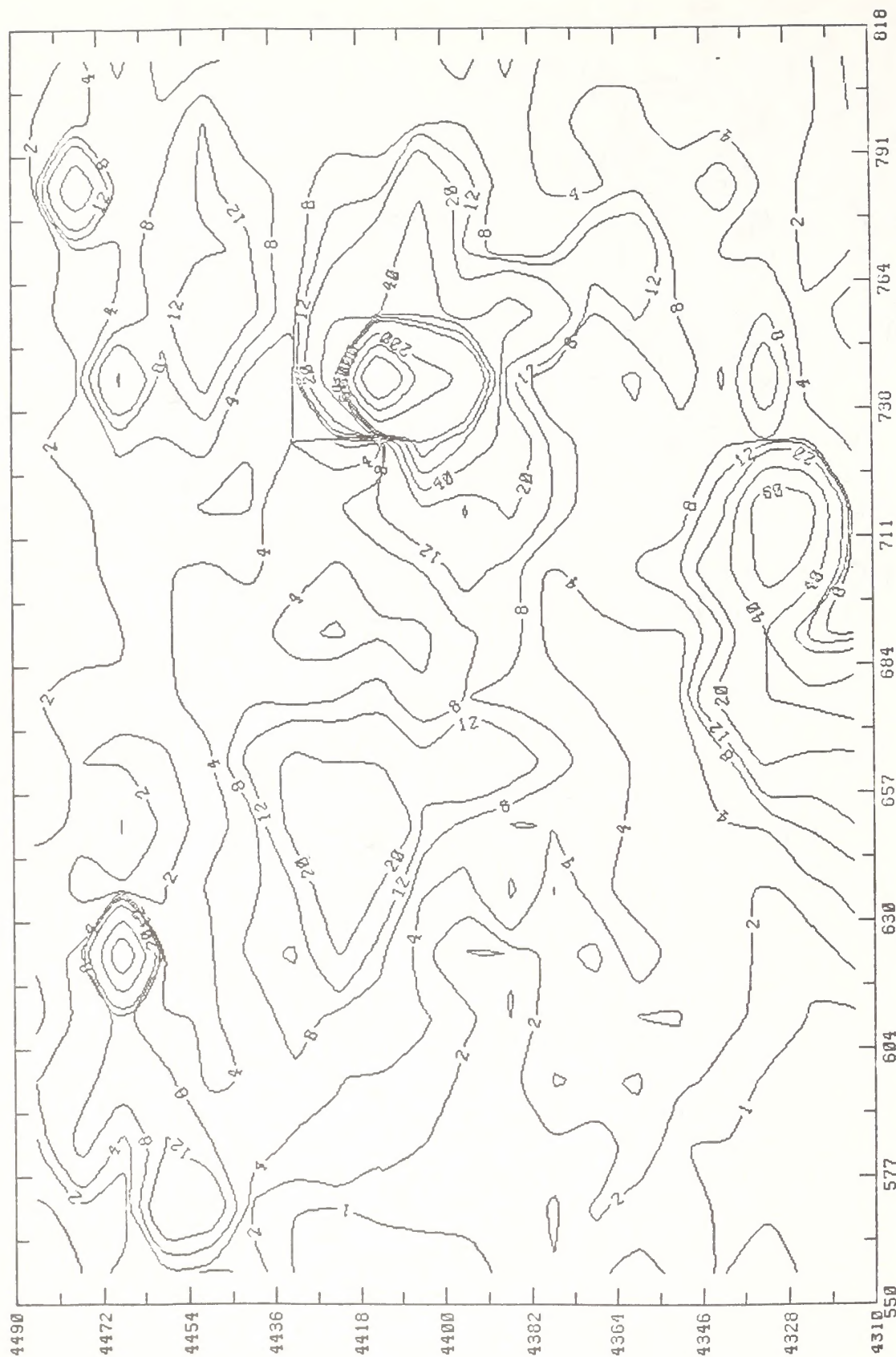
* Previously existing plans for development of both of these facilities, upon which this development scenario is based, are currently under evaluation for modification, delay, or cancellation.



Note: These are upper-bound estimates of actual impacts and are non-simultaneous maxima calculated on the basis of one year's meteorological data.

(a) Maximum 3-Hour Average

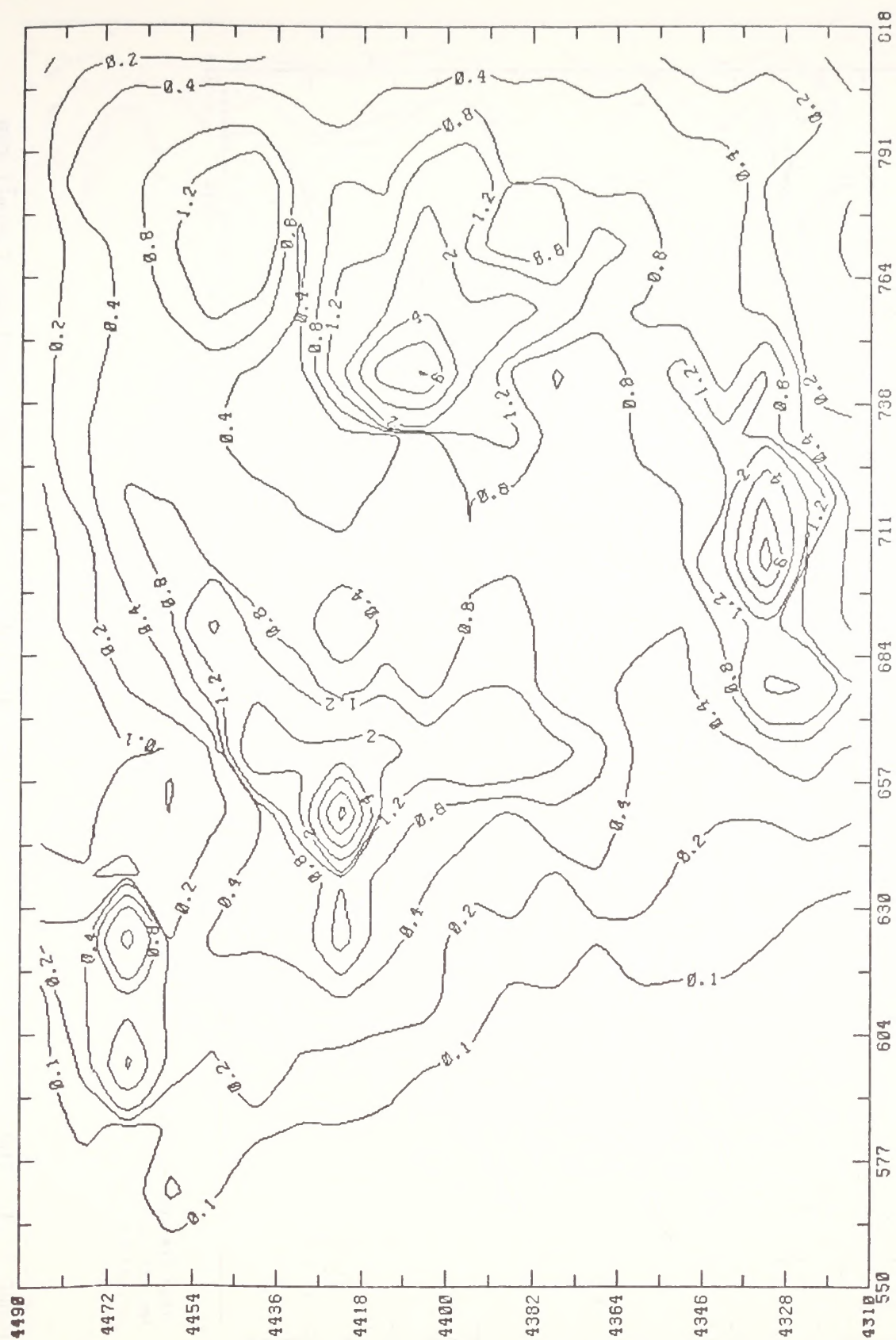
FIGURE 5-13. IMPACT OF DIRECT SOURCE EMISSIONS ON GROUND-LEVEL SO₂ CONCENTRATIONS (µg/m³) FOR THE LOW OIL PRODUCTION SCENARIO



Note: These are upper-bound estimates of actual impacts and are non-simultaneous maxima calculated on the basis of one year's meteorological data.

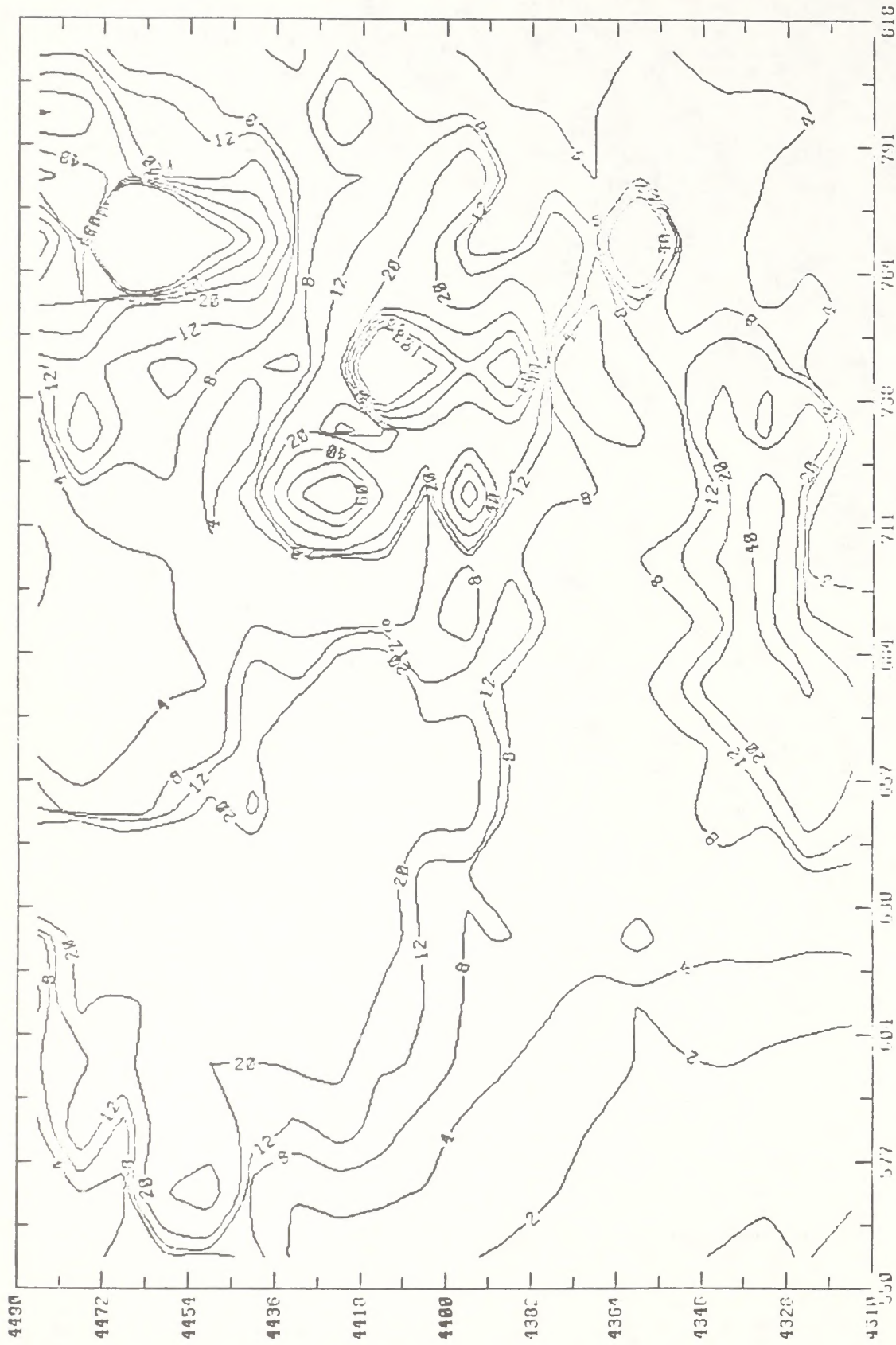
(b) Maximum 24-Hour Averages

FIGURE 5-13 (Continued)



(c) Annual Average

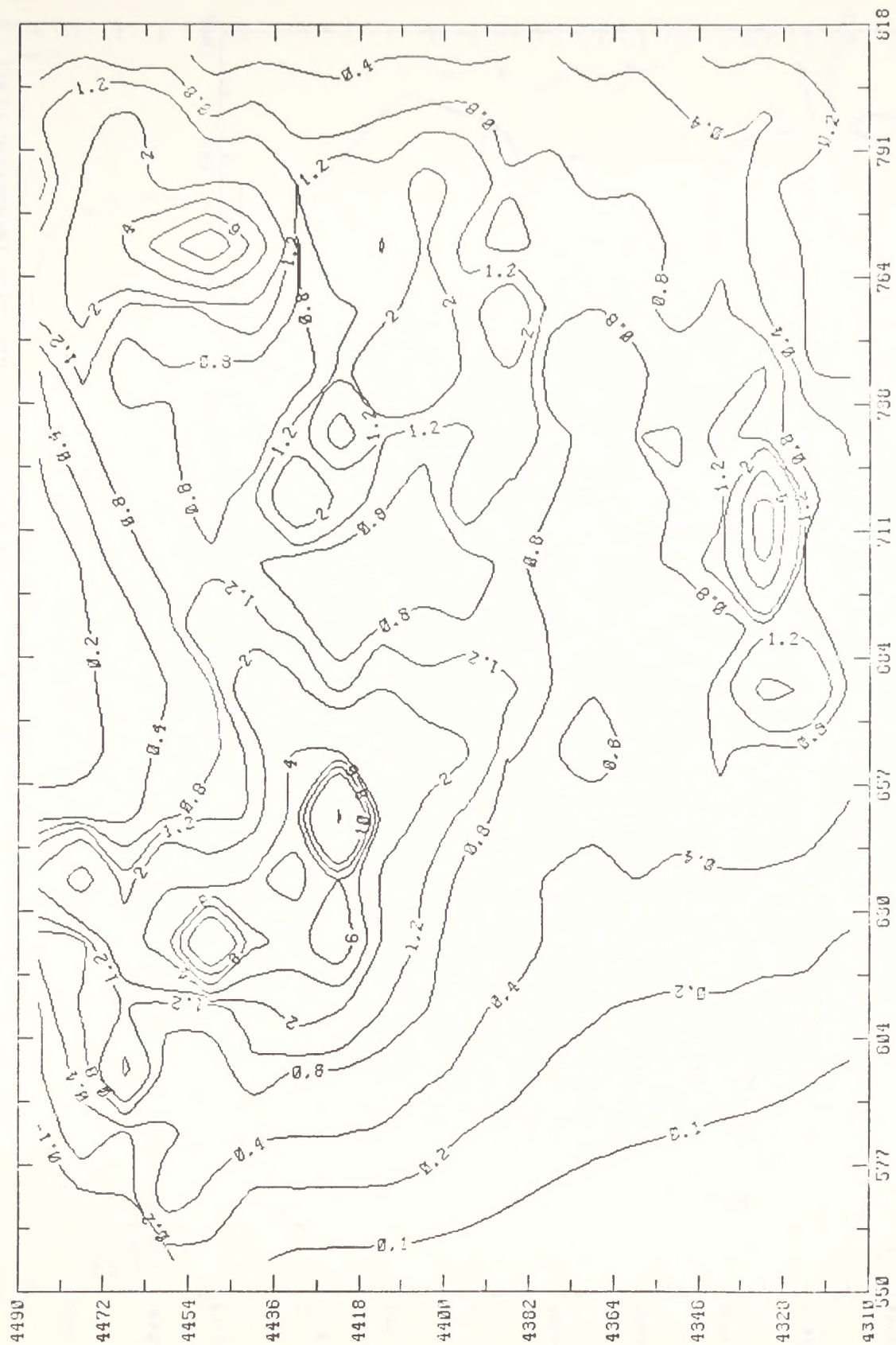
FIGURE 5-13 (Concluded)



Note: These are upper-bound estimates of actual impacts and are non-simultaneous maxima calculated on the basis of one year's meteorological data.

(a) Maximum 24-hour average

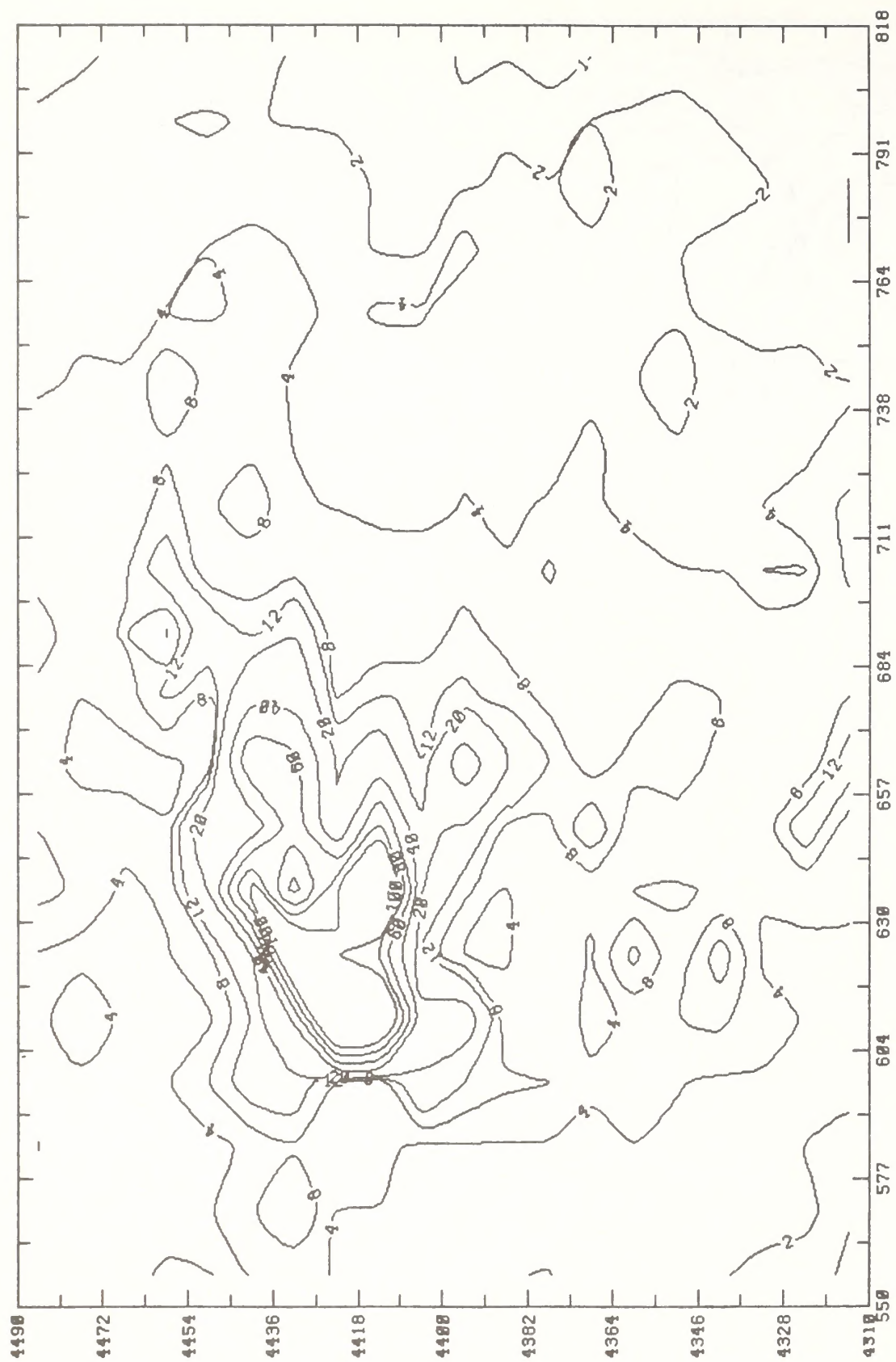
FIGURE 5-14. IMPACT OF DIRECT SOURCE EMISSIONS ON GROUND-LEVEL TSP CONCENTRATIONS ($\mu\text{g}/\text{m}^3$) FOR THE LOW OIL PRODUCTION SCENARIO



Note: These are upper-bound estimates of actual impacts.

(b) Annual average

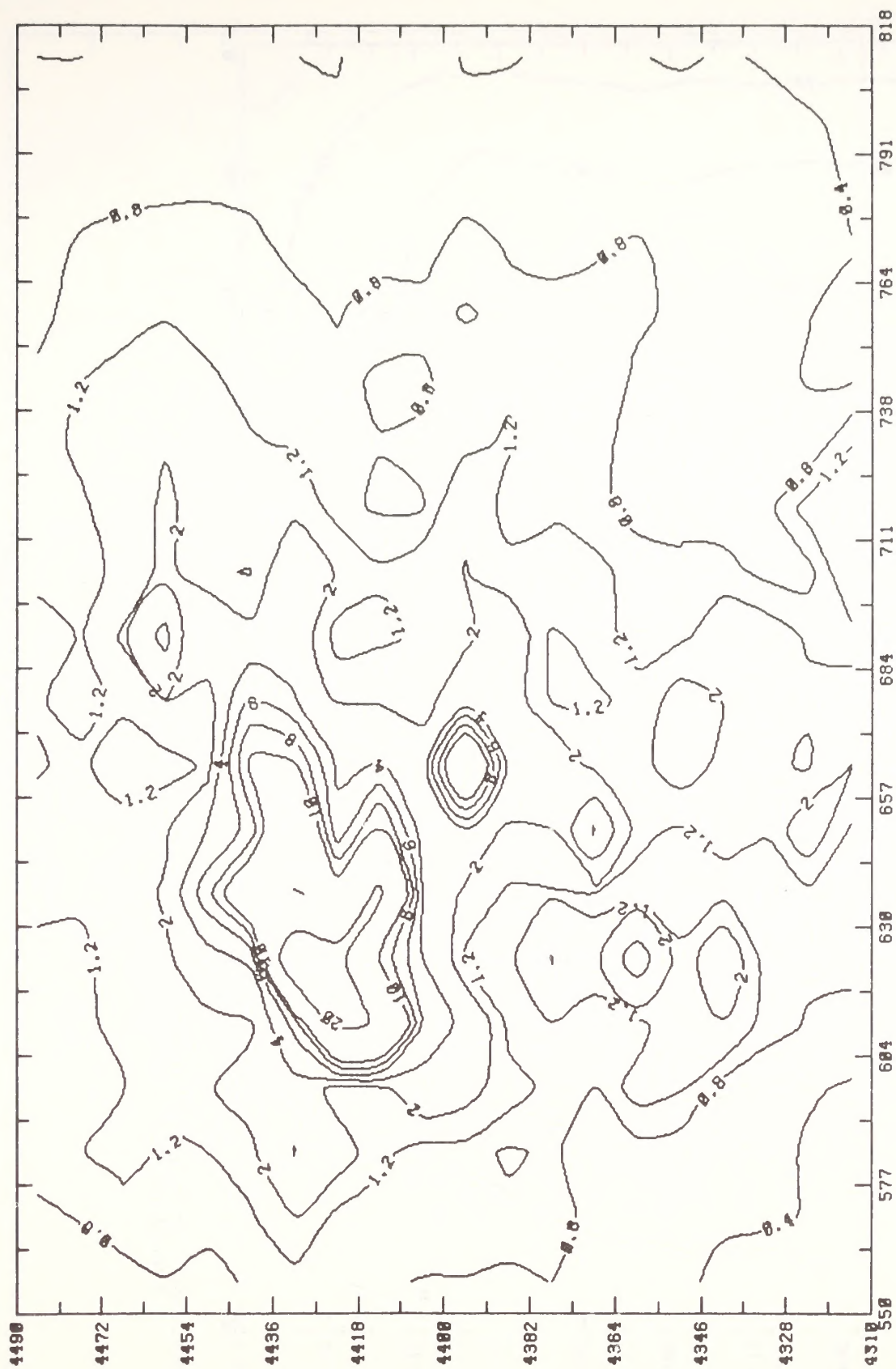
FIGURE 5-14 (Concluded)



Note: These are upper-bound estimates of actual impacts and are non-simultaneous maxima calculated on the basis of one year's meteorological data.

(a) Maximum 3-hour average

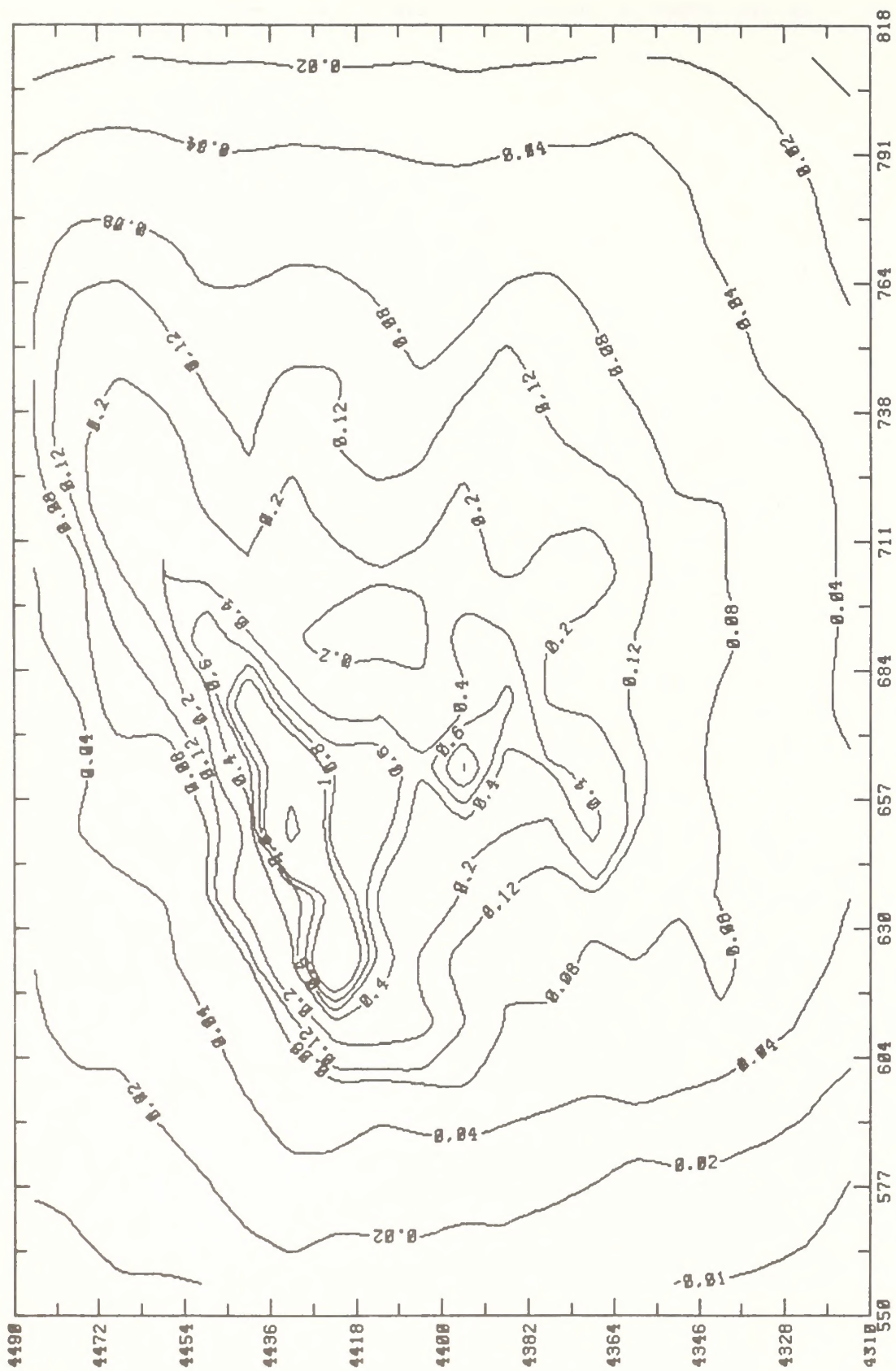
FIGURE 5-15. IMPACT OF DIRECT SOURCE EMISSIONS FROM UINTA BASIN SITE-SPECIFICS ON GROUND-LEVEL SO₂ CONCENTRATIONS (µg/m³) FOR THE HIGH OIL PRODUCTION SCENARIO



Note: These are upper-bound estimates of actual impacts and are non-simultaneous maxima calculated on the basis of one year's meteorological data.

(b) Maximum 24-hour average

FIGURE 5-15 (Continued)



Note: These are upper-bound estimates of actual impacts.

(c) Annual average

FIGURE 5-15 (Concluded)

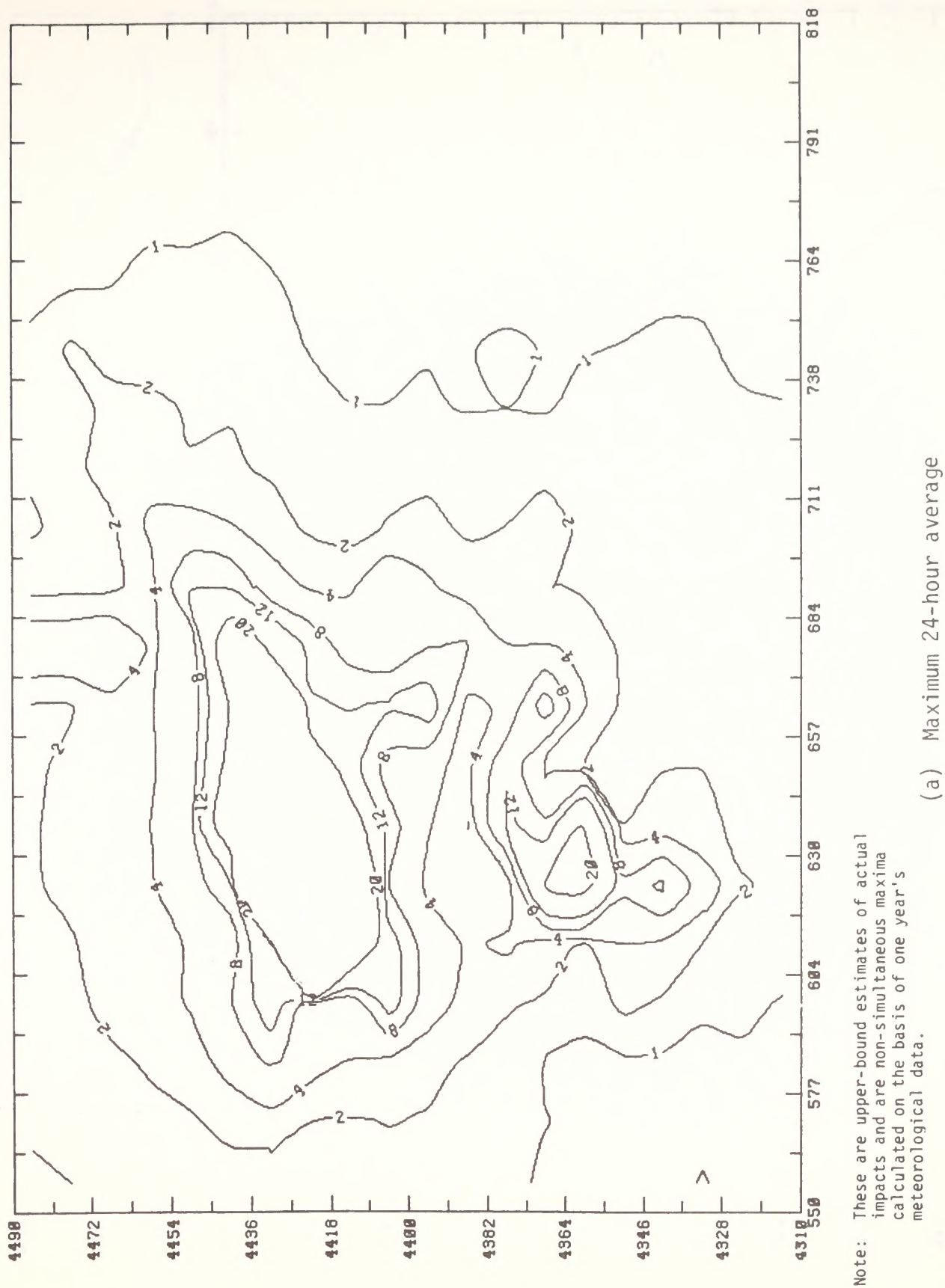
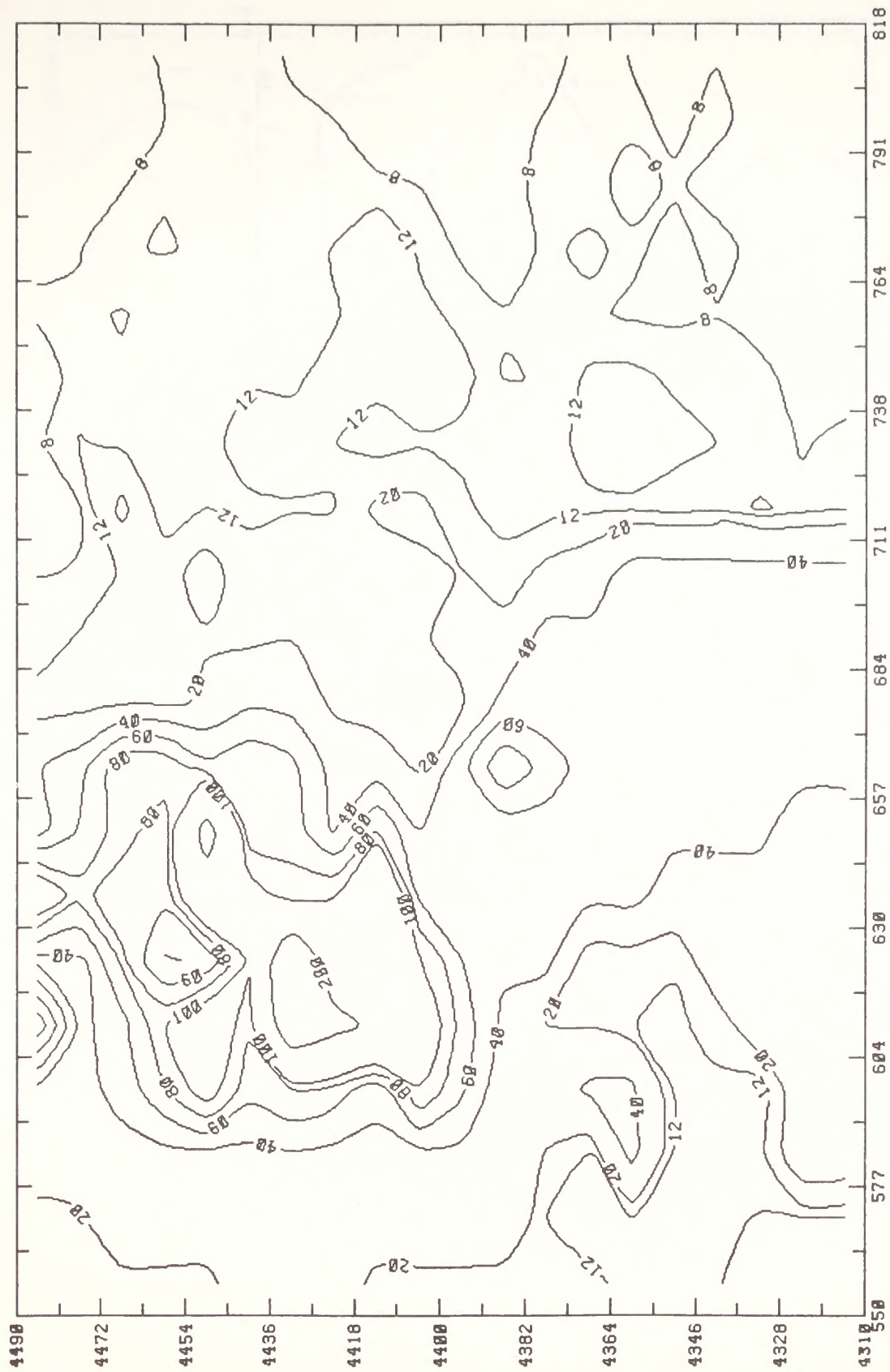


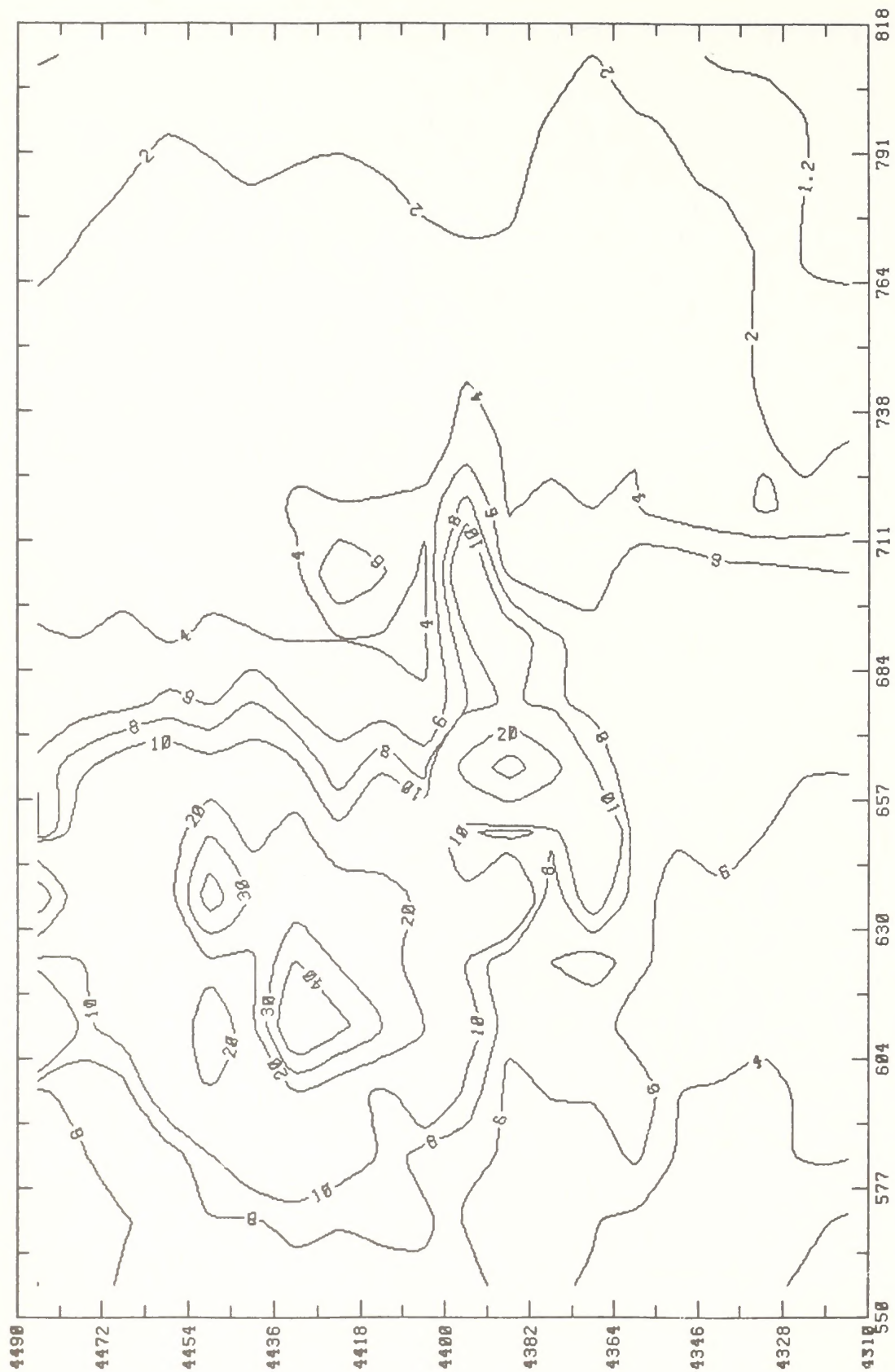
FIGURE 5-16. IMPACT OF DIRECT SOURCE EMISSIONS FROM UINTA BASIN SITE-SPECIFICS ON GROUND-LEVEL TSP CONCENTRATIONS ($\mu\text{g}/\text{m}^3$) FOR THE HIGH OIL PRODUCTION SCENARIO



Note: These are upper-bound estimates of actual impacts and are non-simultaneous maxima calculated on the basis of one year's meteorological data.

(a) Maximum 3-hour average

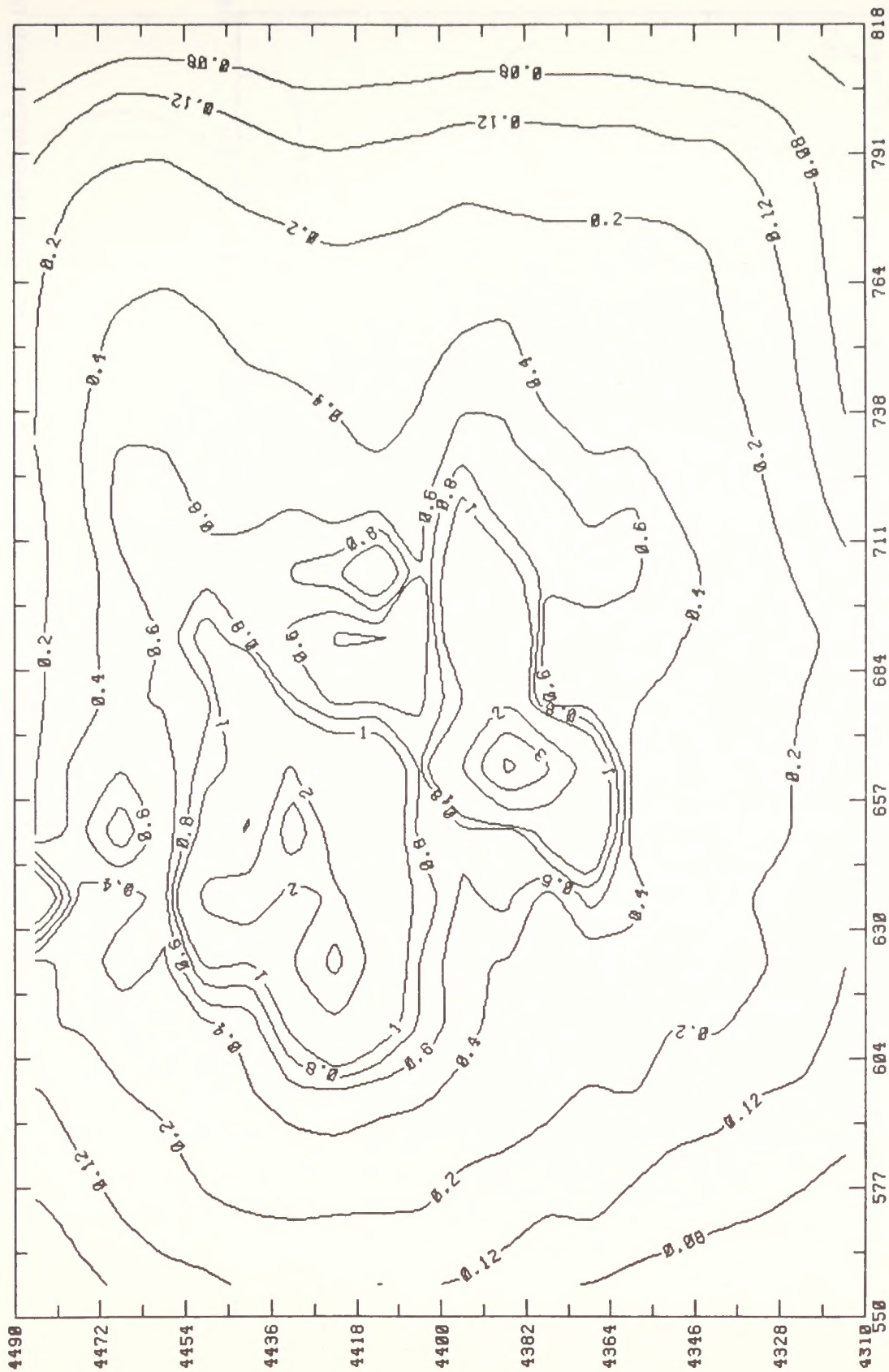
FIGURE 5-17. IMPACT OF DIRECT SOURCE EMISSIONS FROM UINTA BASIN SITE-SPECIFICS AND CONCEPTUALS ON GROUND-LEVEL SO_2 CONCENTRATIONS ($\mu\text{g}/\text{m}^3$) FOR THE HIGH OIL PRODUCTION SCENARIO



Note: These are upper-bound estimates of actual impacts and are non-simultaneous maxima calculated on the basis of one year's meteorological data.

(b) Maximum 24-hour average

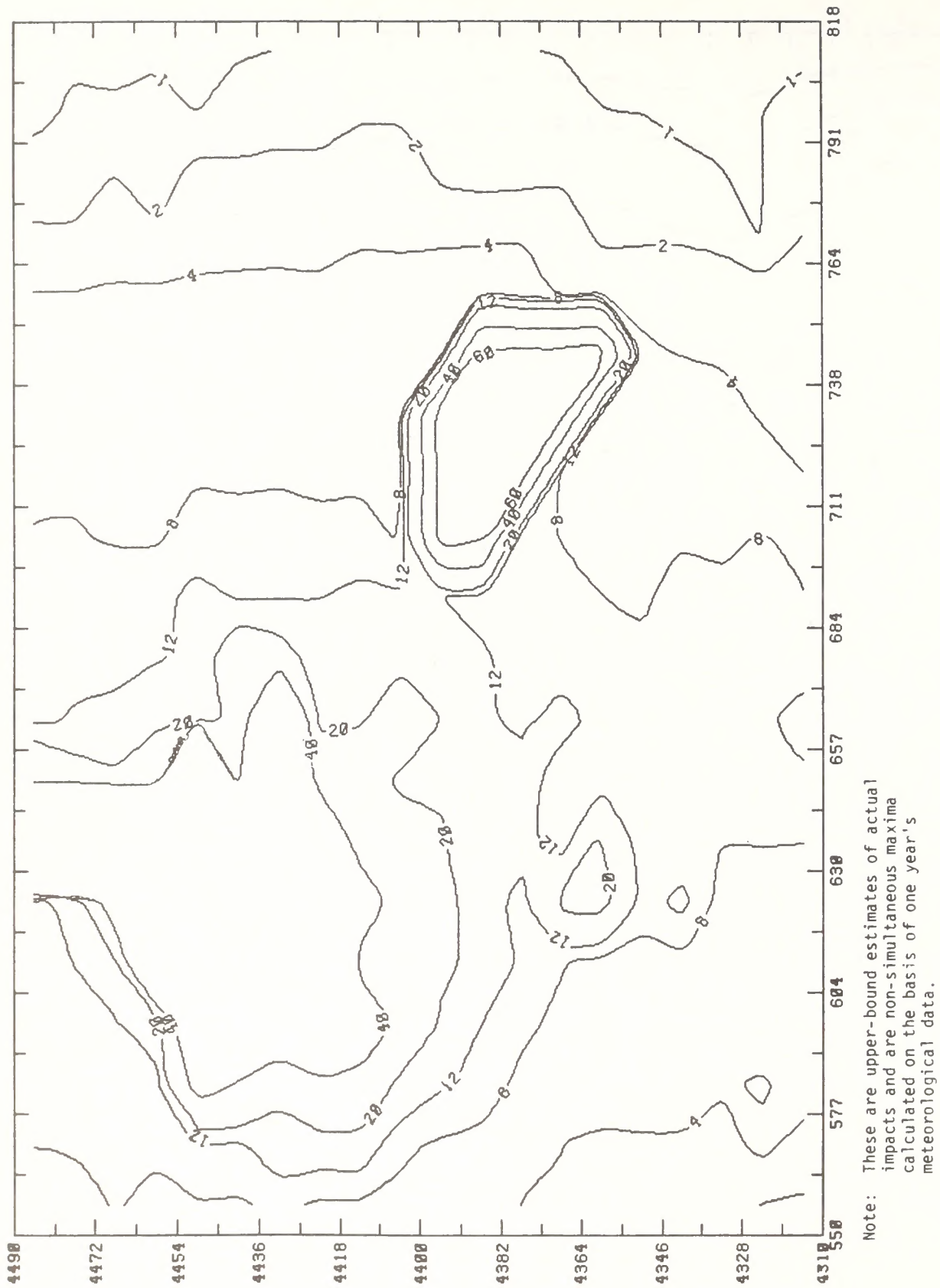
FIGURE 5-17 (Continued)



Note: These are upper-bound estimates of actual impacts.

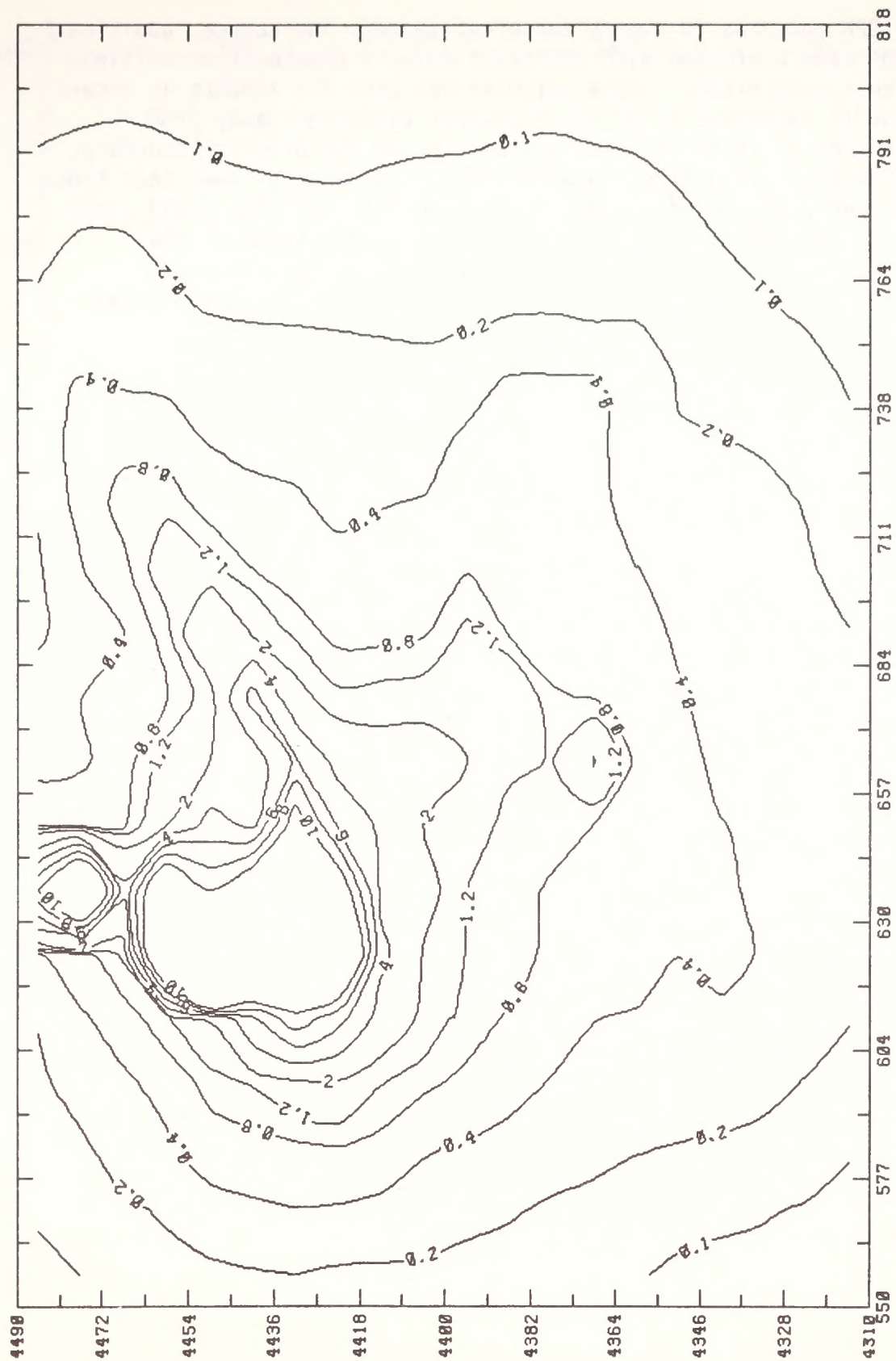
(c) Annual average

FIGURE 5-17 (Concluded)



(a) Maximum 24-hour average

FIGURE 5-18. IMPACT OF DIRECT SOURCE EMISSIONS FROM UINTA BASIN SITE-SPECIFICS AND CONCEPTUALS ON GROUND-LEVEL TSP CONCENTRATIONS ($\mu\text{g}/\text{m}^3$) FOR THE HIGH OIL PRODUCTION SCENARIO



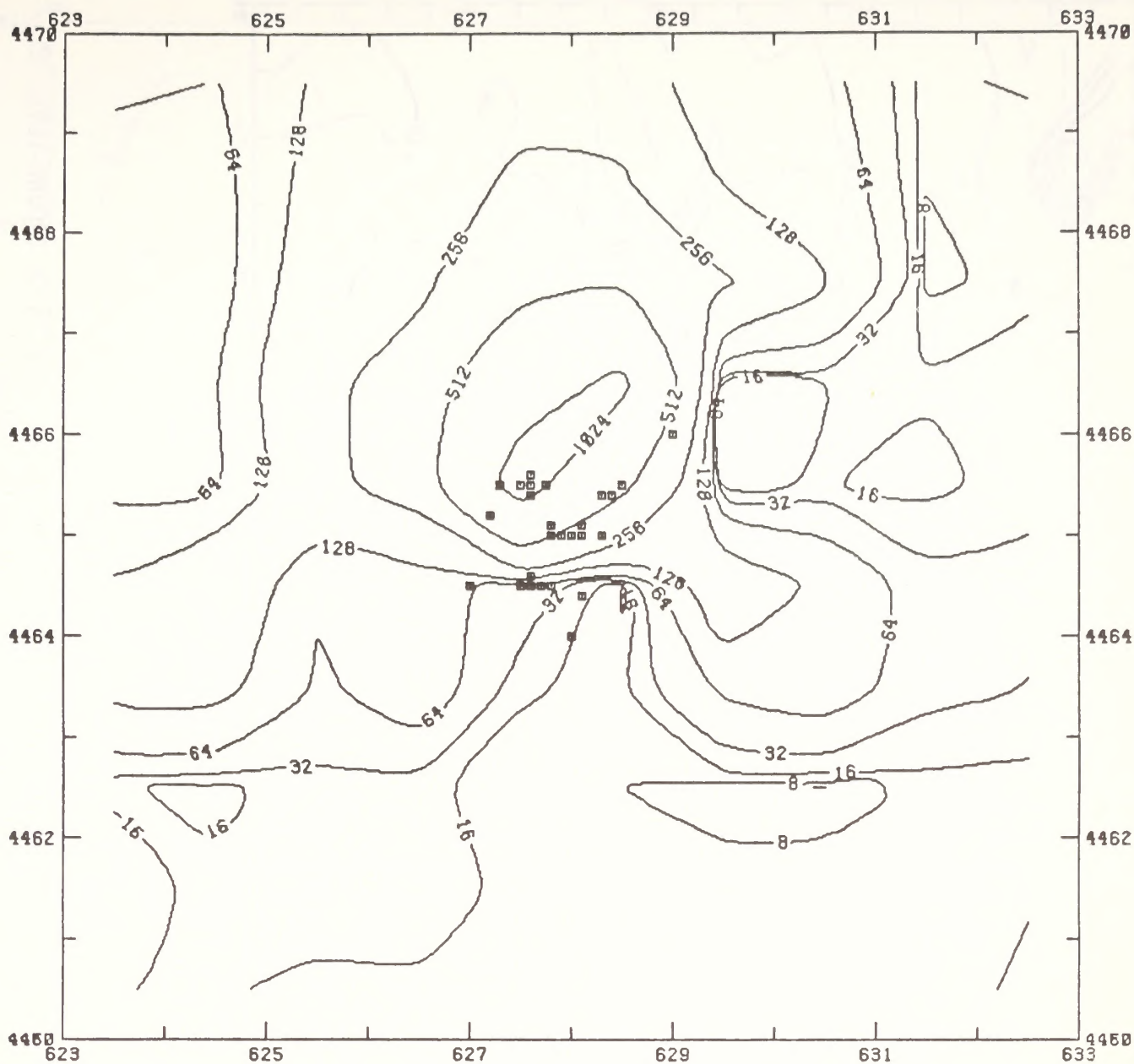
(b) Annual average
FIGURE 5-18 (Concluded)

source for GPM modeling is overly conservative near the source, additional calculations were performed with COMPLEX-I using a treatment of multiple sources (see Figure 5-19). These calculations show TSP impacts in excess of the Class II increment of $37 \mu\text{g}/\text{m}^3$ several kilometers away from emission sources at locations that may be outside the property boundary. Although COMPLEX-I calculates concentrations considerably lower than those of GPM, currently projected TSP emissions from this facility could cause violations of the TSP increment. It should be noted, however, that emission inventories for projects in a conceptual design phase are tentative and uncertain, thereby making impact projections speculative.

5.2.2.3 Incremental Impacts of Colorado Point Sources

Figures 5-20 and 5-21 show the incremental impacts due to direct source emissions from Colorado industrial impacts associated with the high-oil-production facilities.

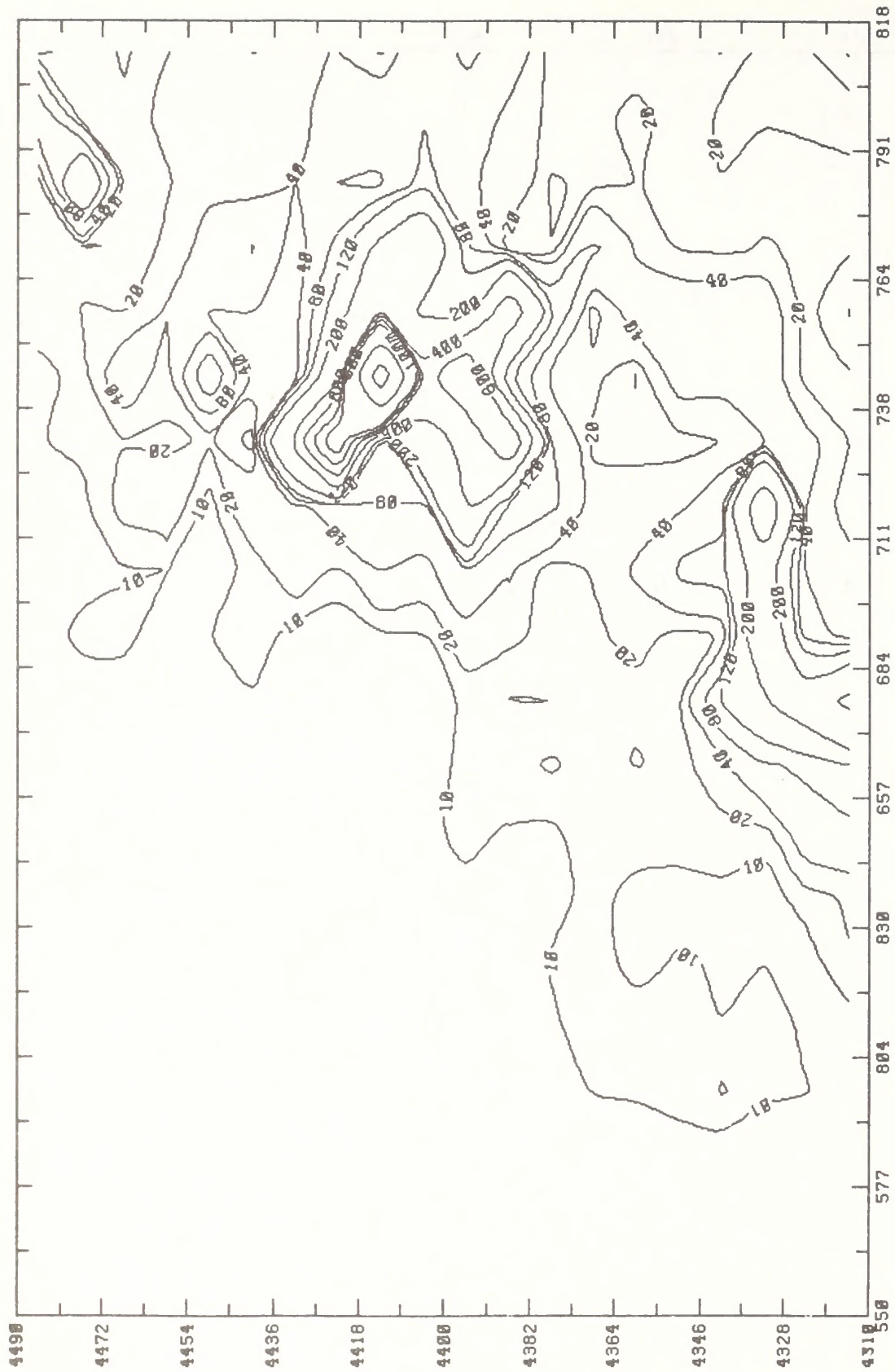
Both existing sources near Grand Junction and proposed oil shale facilities in the Piceance Basin are included. As noted previously, the emission inventory for these Colorado oil shale facilities is very uncertain because of the recently announced project modifications, delays, and even cancellations. Indeed, the one Colorado oil shale facility (Cathedral Bluffs) with maximum impacts, for which GPM calculates impacts above the PSD Class II increments, has recently been shelved. Except for Cathedral Bluffs, other Colorado oil shale facilities are not projected to have problems with PSD Class I and Class II increments for SO_2 , based on the conservative GPM calculations. Near-source violations of the PSD Class II increment for maximum 24-hour average TSP concentrations are projected on the basis of conservative GPM calculations for several facilities. However, when COMPLEX-I with appropriate gridding of multiple ground-level release points (TSP emissions were aggregated by treating multiple releases as one in the regional GPM calculations) was applied, TSP impacts are projected to be within the PSD Class II increments at all locations (see Figure 5-22) although impacts within the property boundaries may be in excess of the Class II increment of $37 \mu\text{g}/\text{m}^3$. On the basis of COMPLEX-I calculations of the near source SO_2 impacts of Cathedral Bluffs (see Figure 5-23), it is possible that the GPM projections of SO_2 Class II increment violations may also be inaccurate and that impacts would be within the 3- and 24-hour average SO_2 increments of 512 and $91 \mu\text{g}/\text{m}^3$, respectively.



Note: These are upper-bound estimates of actual impacts and are non-simultaneous maxima calculated on the basis of one year's meteorological data.

□ Point Sources

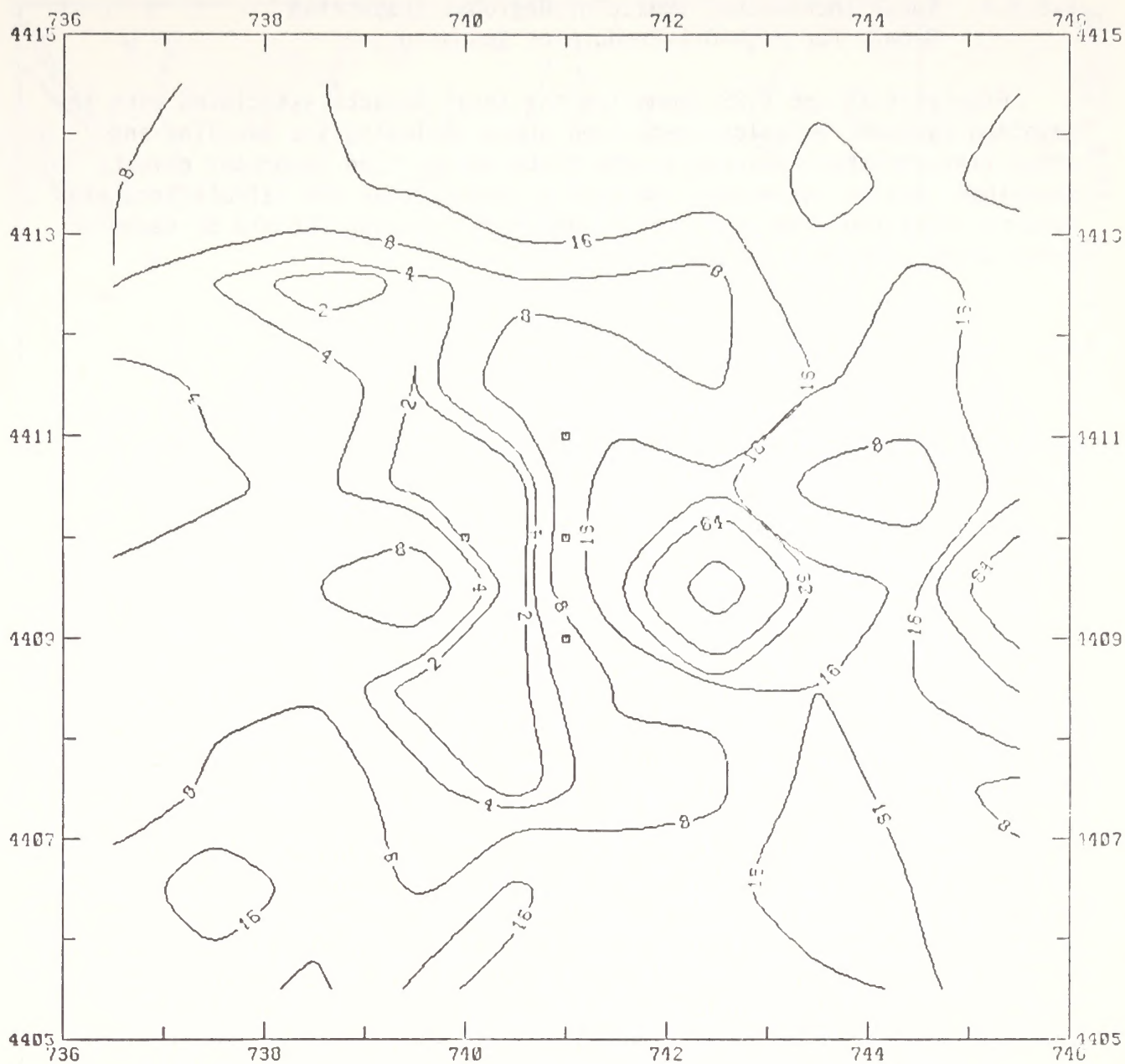
FIGURE 5-19. MAXIMUM 24-HOUR AVERAGE, NEAR-SOURCE TSP CONCENTRATIONS ($\mu\text{g}/\text{m}^3$) RESULTING FROM DIRECT SOURCE EMISSIONS FROM THE SOHIO CONCEPTUAL TAR SANDS FACILITY ON THE BASIS OF COMPLEX-I CALCULATIONS



Note: These are upper-bound estimates of actual impacts and are non-simultaneous maxima calculated on the basis of one year's meteorological data.

(a) Maximum 3-hour average

FIGURE 5-20. IMPACT OF DIRECT SOURCE EMISSIONS FROM COLORADO POINT SOURCES ON GROUND-LEVEL SO₂ CONCENTRATIONS (µg/m³) FOR THE HIGH OIL PRODUCTION SCENARIO



Note: These are upper-bound estimates of actual impacts and are non-simultaneous maxima calculated on the basis of one year's meteorological data.

□ Point Sources

(b) Maximum 24-hour average

FIGURE 5-23 (Concluded)

5.2.2.4 Total Incremental Impact of Regional Industrial Growth for High-Oil-Production Scenario

Figures 5-24 and 5-25 summarize the total impacts associated with the combined regional emissions described above including the baseline and other (interrelated) sources in the Uinta Basin. The important caveats described earlier concerning the overly conservative GPM calculations of impacts resulting from multiple, ground-level releases should be remembered when interpreting these plots.

5.3 IMPACTS OF POPULATION AND ASSOCIATED GROWTH

The impacts of area sources were modeled separately from those of the industrial sources since area source emissions are largely in different areas of the study region (in which the population is located).

5.3.1 Low-Production Scenario

Figure 5-26 displays the modeled ambient SO_2 impacts from area sources in the study region. Note that concentrations are much lower than the maximum ground-level impacts because of the oil shale facilities discussed in the previous section. The highest impacts are in the Grand Junction area because of existing sources, but throughout most of the study region impacts are extremely low.

Figure 5-27 displays the modeled TSP concentrations. The 24-hour ambient air quality standard of $150 \mu\text{g}/\text{m}^3$ is likely to be exceeded almost everywhere in the region. The annual-average TSP ambient air quality standard of $60 \mu\text{g}/\text{m}^3$ will also be exceeded in much of the area, especially in the Colorado River basin and in the vicinity of Meeker, Vernal, and Rangely. It should be noted, as discussed in Section 2, that TSP standards are currently being exceeded in these areas. Impacts are predicted to be somewhat higher than the existing baseline in the low-production scenario because of anticipated growth.

The projected emission densities of several pollutant species in the study region are presented in figure 5-28; these species include SO_2 , TSP, NO_x , CO, and hydrocarbons, both reactive and unreactive. Ground-level concentrations of various gaseous species can be assessed by scaling the SO_2 plots shown in figure 5-26 by the ratio in emission density of the given species and SO_2 . Using this procedure, for example, one can see that NO_2 concentrations will be approximately an order of magnitude higher than SO_2 concentrations, but annual-average maximum impacts (near Grand Junction) are less than $10 \mu\text{g}/\text{m}^3$, an order of magnitude lower than the



Note: These are upper-bound estimates of actual impacts and are non-simultaneous maxima calculated on the basis of one year's meteorological data.

(a) Maximum 3-Hour Average

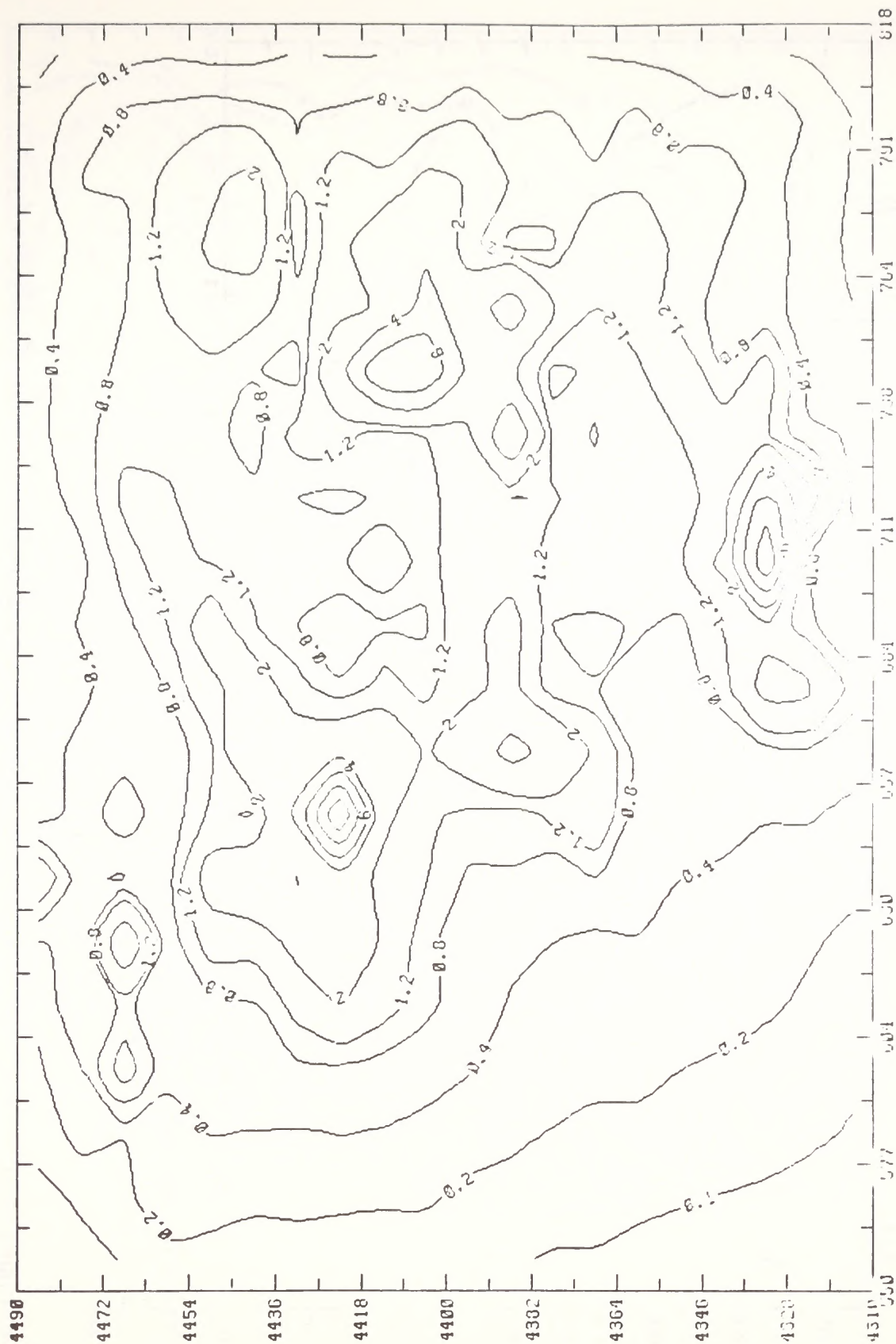
FIGURE 5-24. IMPACT OF DIRECT SOURCE EMISSIONS ON GROUND-LEVEL SO₂ CONCENTRATIONS (µg/m³) FOR THE HIGH OIL PRODUCTION SCENARIO



Note: These are upper-bound estimates of actual impacts and are non-simultaneous maxima calculated on the basis of one year's meteorological data.

(b) Maximum 24-Hour Average

FIGURE 5-24 (Continued)



Note: These are upper-bound estimates of actual impacts.

(c) Annual Average

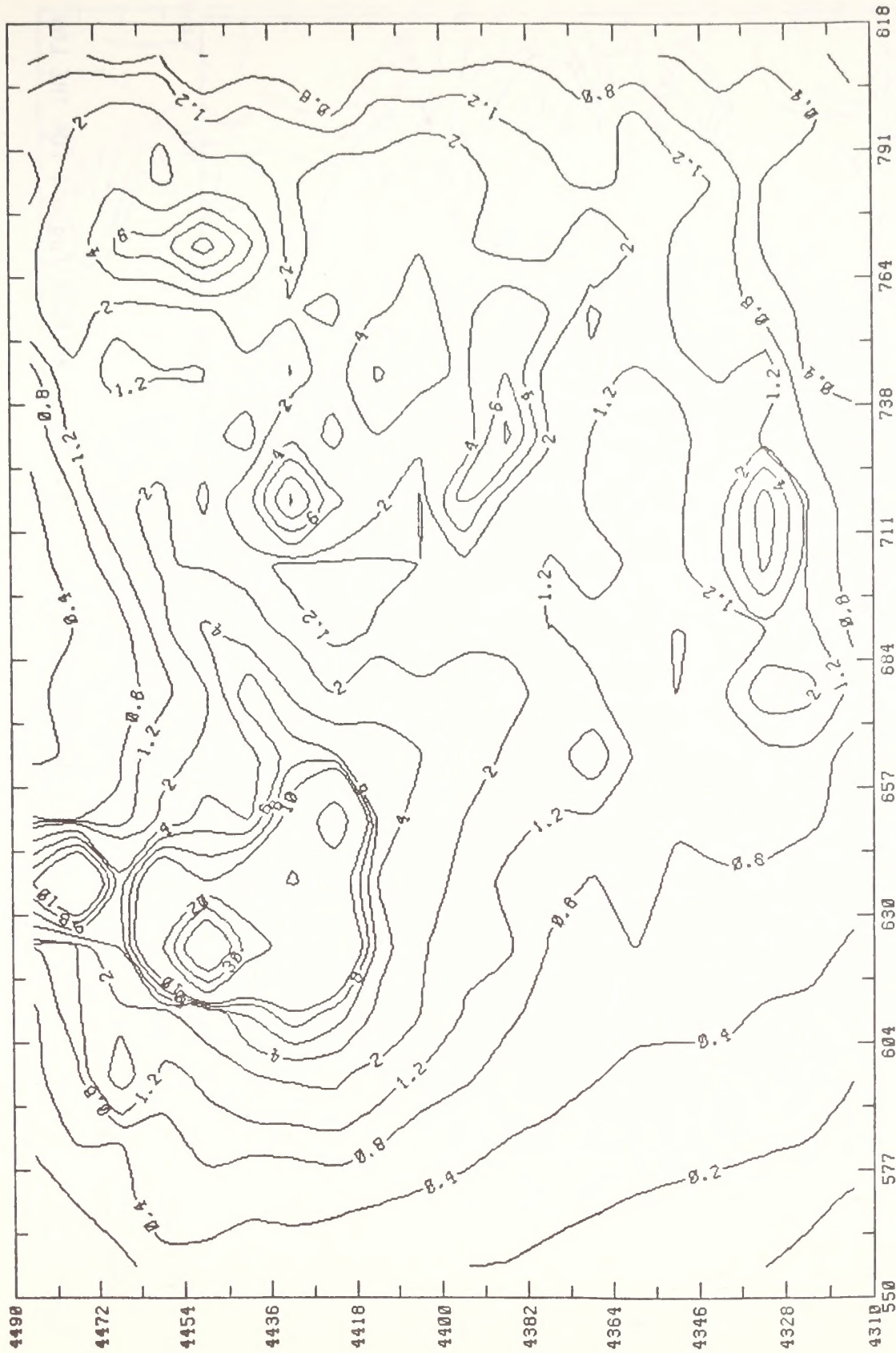
FIGURE 5-24 (Concluded)



Note: These are upper-bound estimates of actual impacts and are non-simultaneous maxima calculated on the basis of one year's meteorological data.

(a) Maximum 24-hour average

FIGURE 5-25. IMPACT OF DIRECT SOURCE EMISSIONS ON GROUND-LEVEL TSP CONCENTRATIONS ($\mu\text{g}/\text{m}^3$) FOR THE HIGH OIL PRODUCTION SCENARIO



Note: These are upper-bound estimates of actual impacts.

(b) Annual average

FIGURE 5-25 (Concluded)

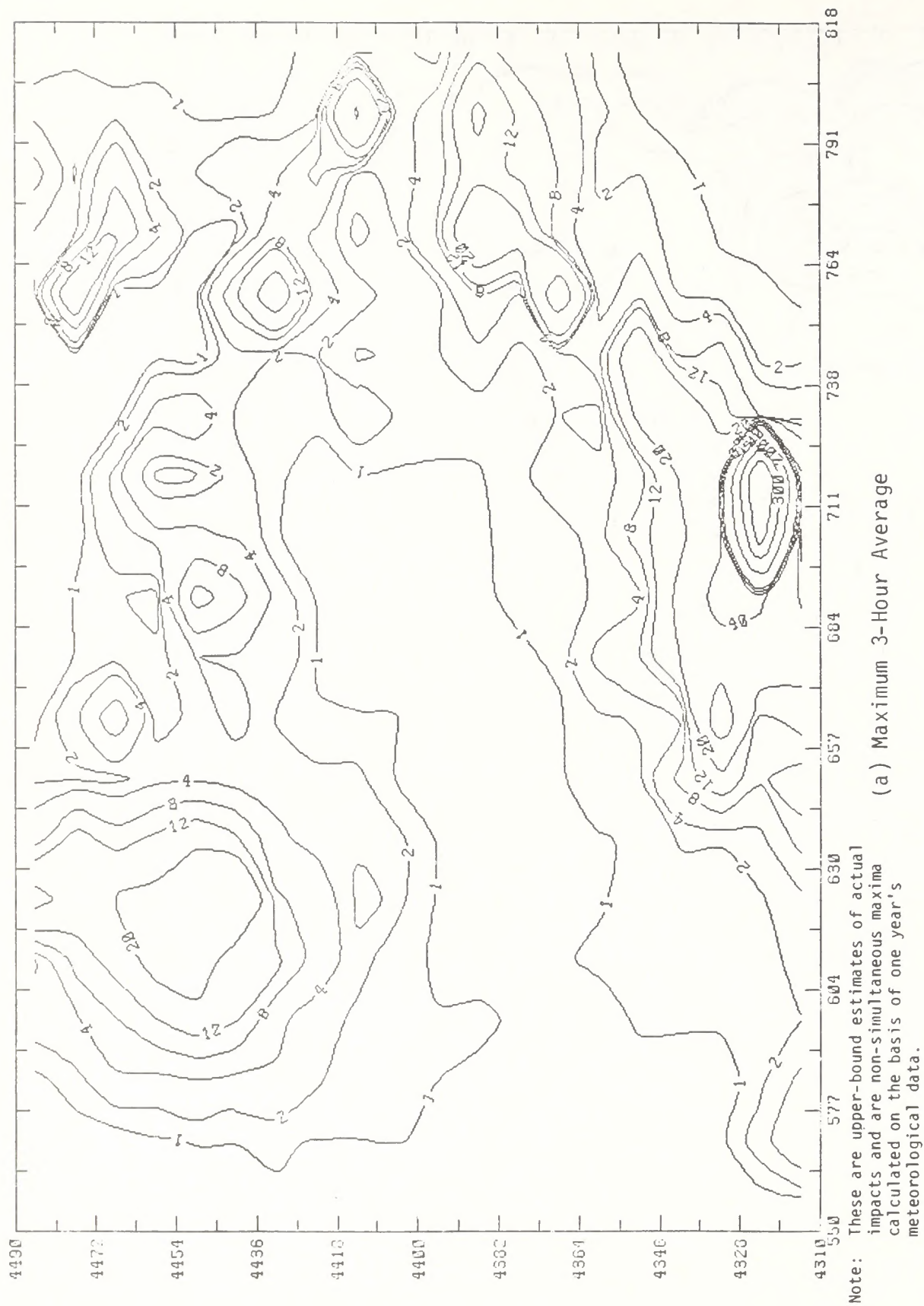
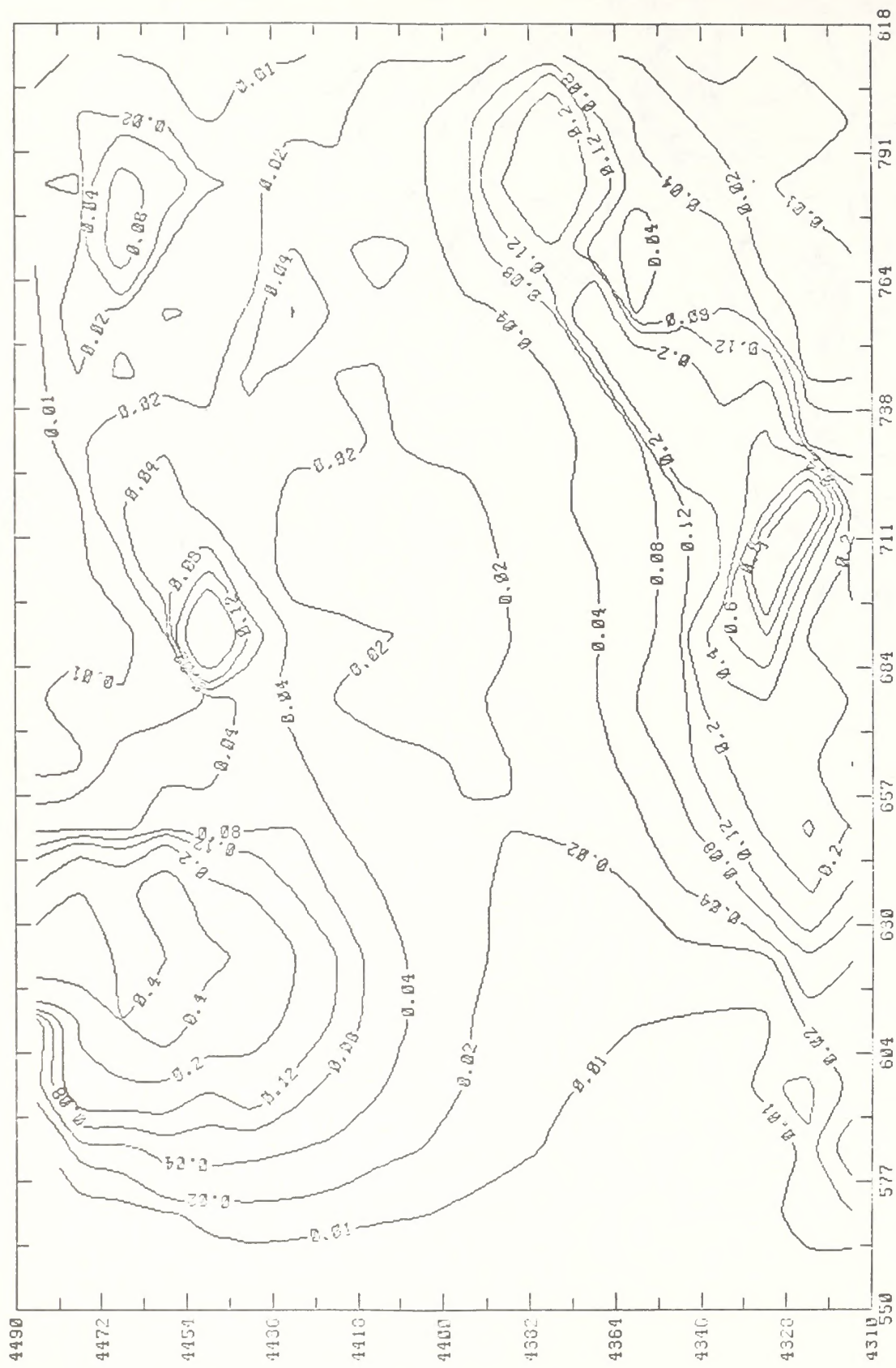


FIGURE 5-26. IMPACT OF AREA SOURCE EMISSIONS ON GROUND-LEVEL SO_2 CONCENTRATIONS ($\mu\text{g}/\text{m}^3$) FOR THE LOW OIL PRODUCTION SCENARIO



Note: These are upper-bound estimates of actual impacts.

(c) Annual Average

FIGURE 5-26 (Concluded)

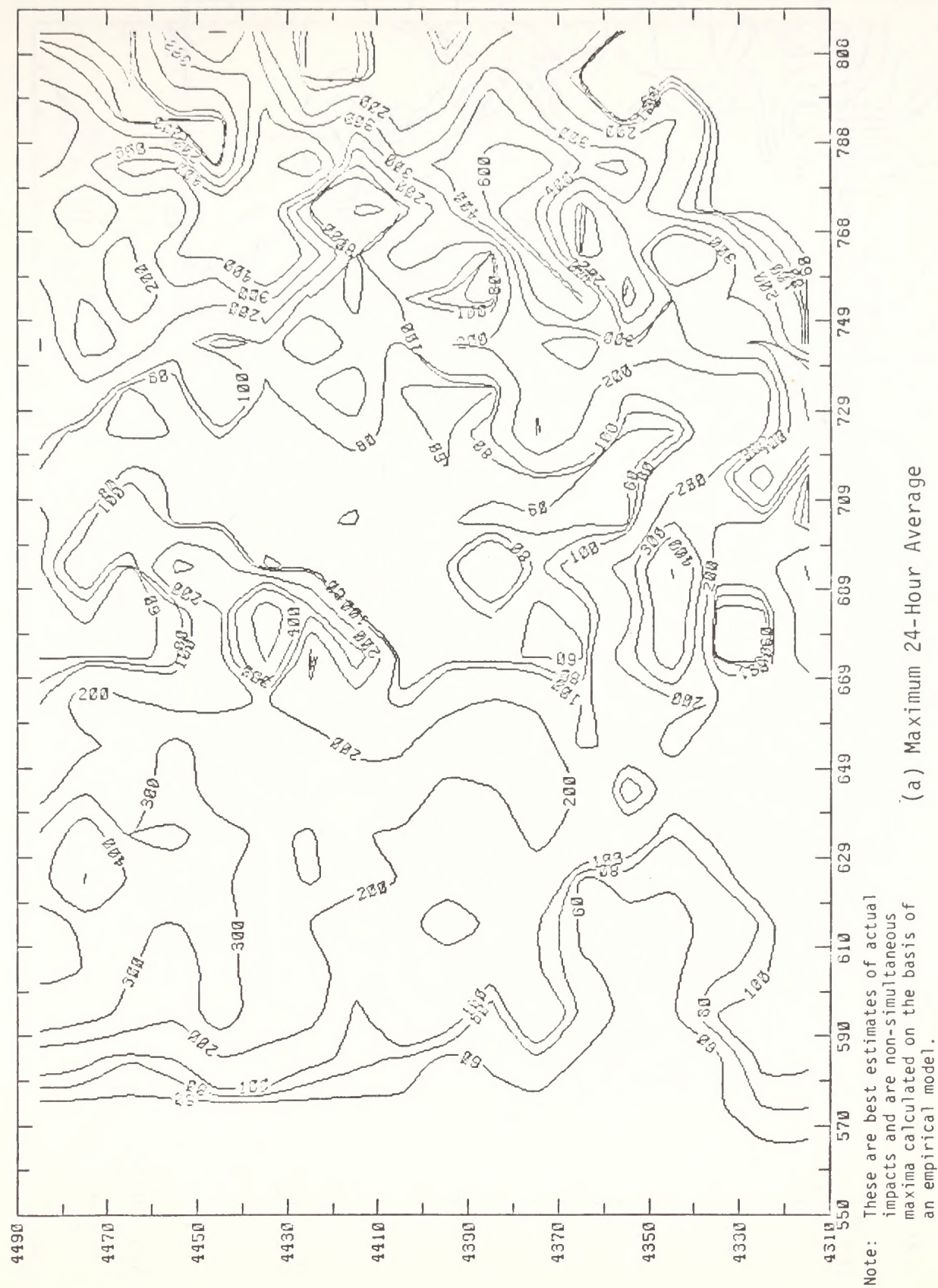
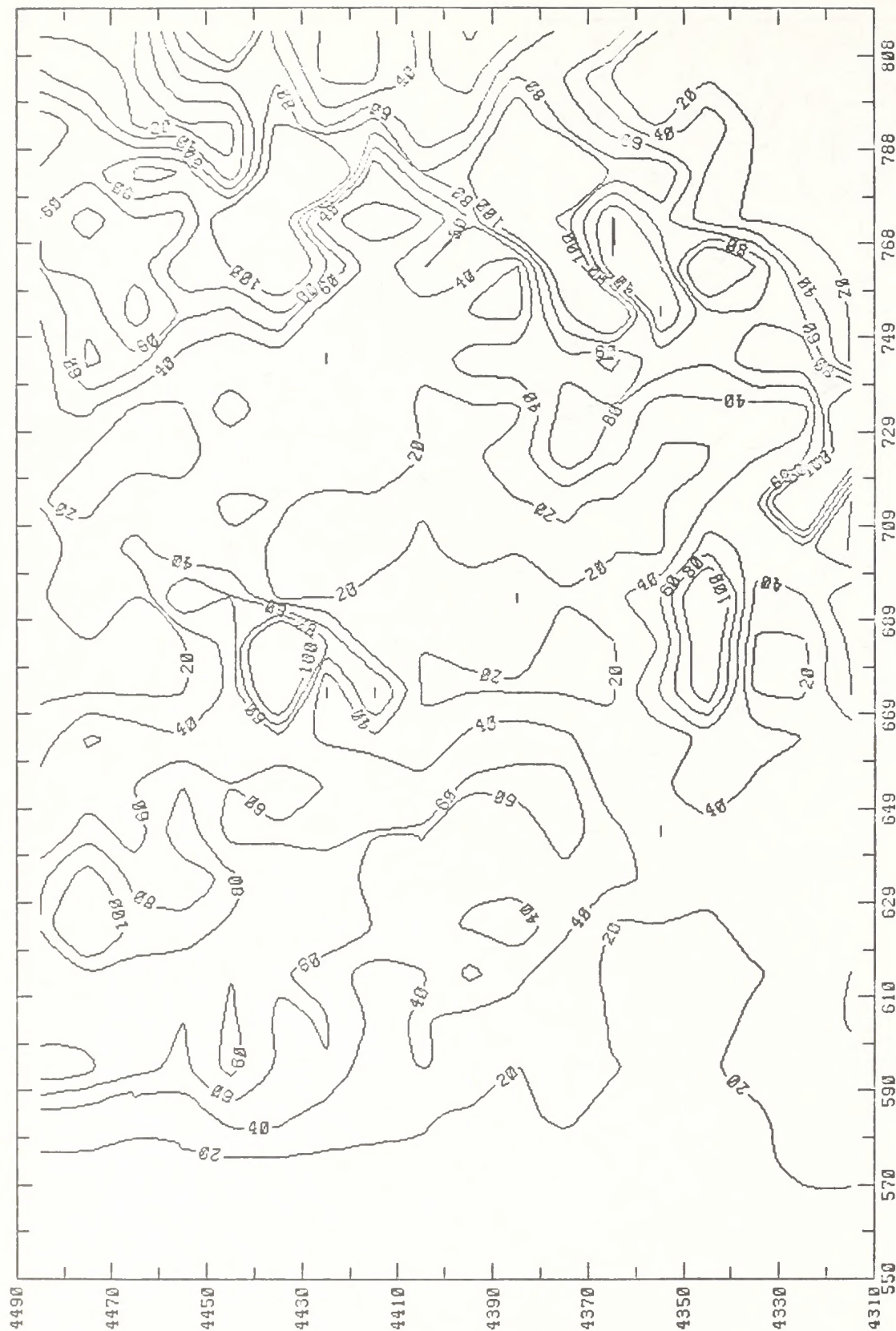


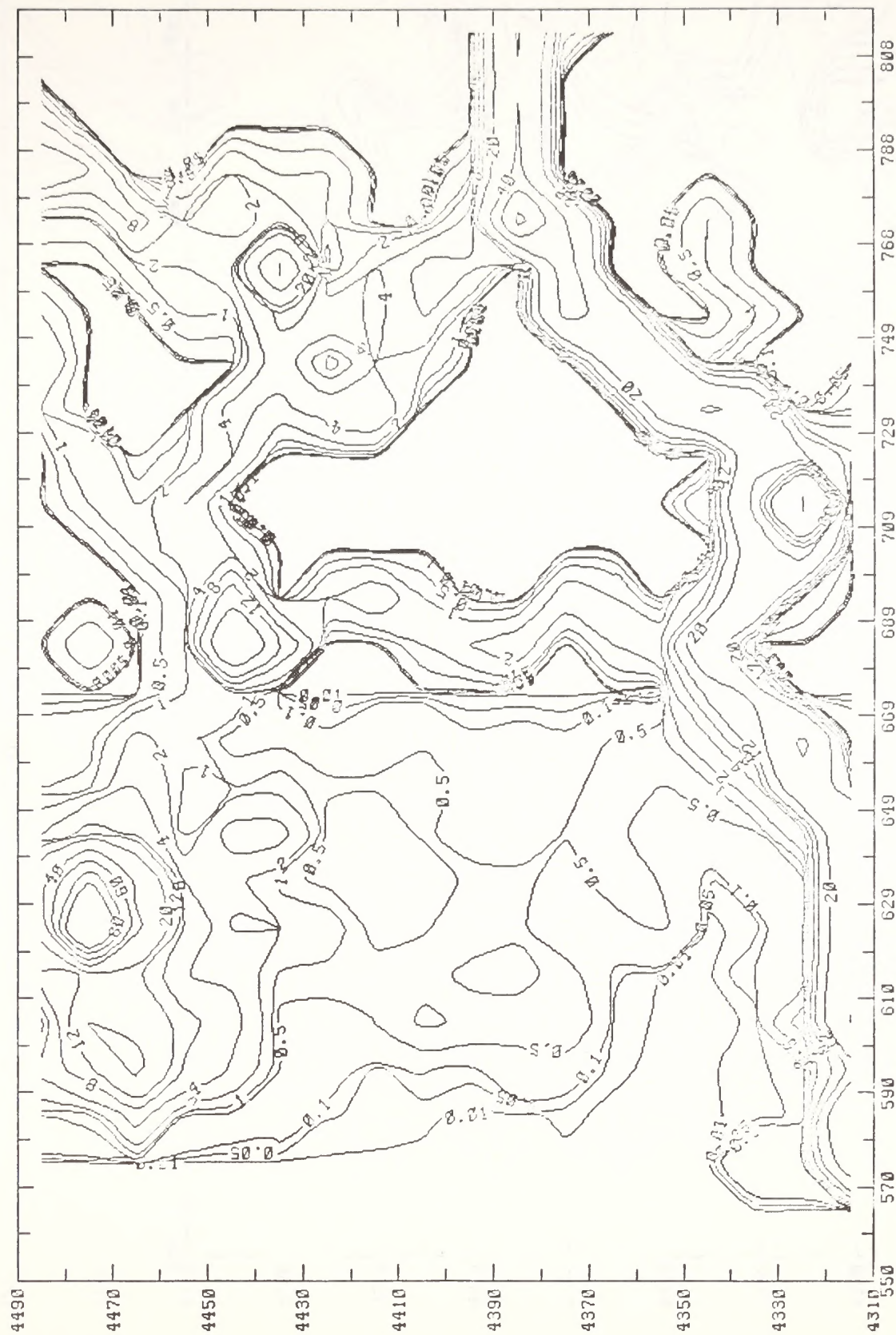
FIGURE 5-27. IMPACT OF AREA SOURCE EMISSIONS ON GROUND-LEVEL TSP CONCENTRATIONS ($\mu\text{g}/\text{m}^3$) FOR THE LOW OIL PRODUCTION SCENARIO



Note: These are best estimates of actual impacts calculated on the basis of an empirical model.

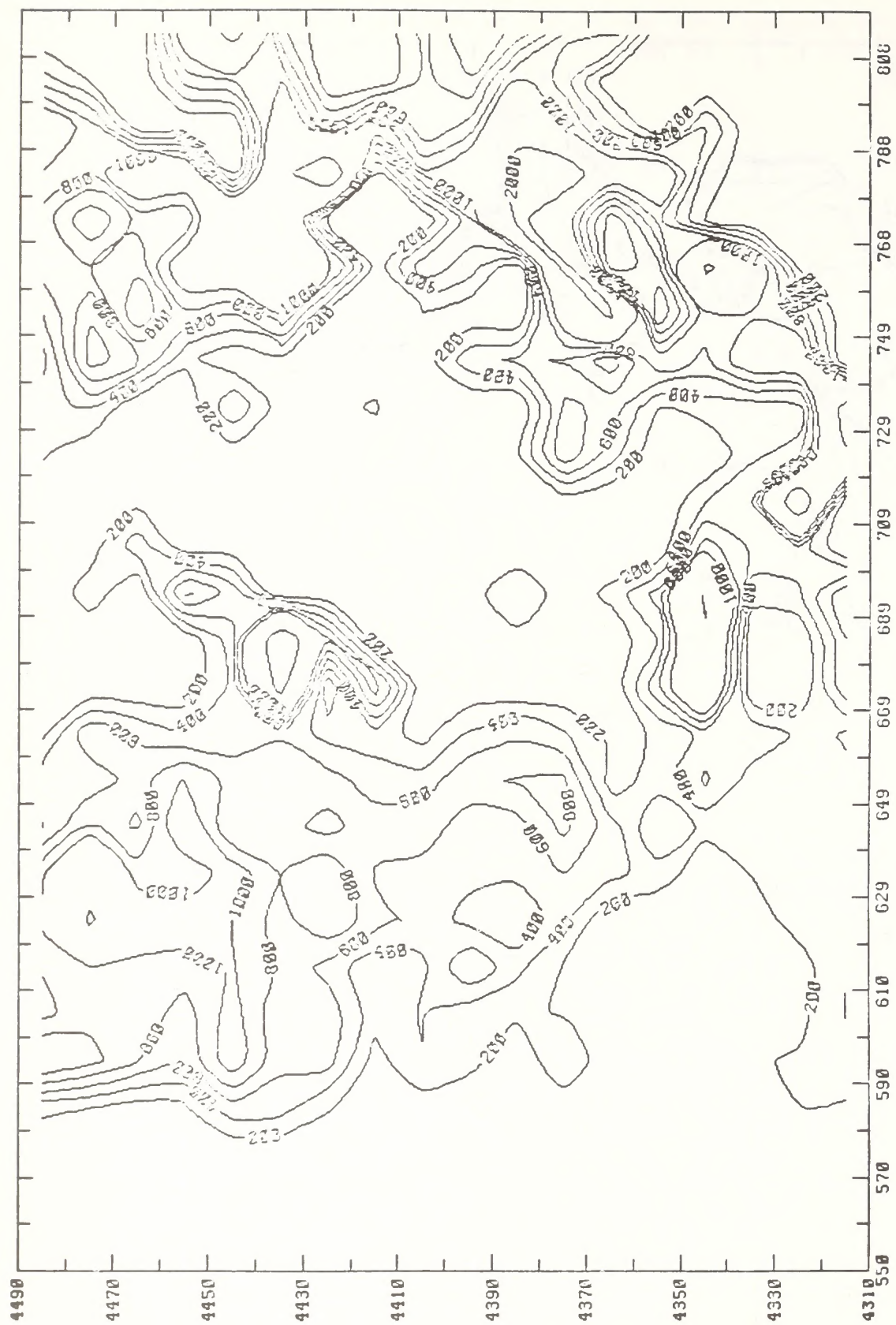
(b) Annual Average

FIGURE 5-27 (Concluded)



(a) SO₂

FIGURE 5-28. AREA SOURCE EMISSION DENSITIES FOR LOW OIL PRODUCTION SCENARIO (tons/yr/100 km²)



(b) TSP

FIGURE 5-28 (Continued)

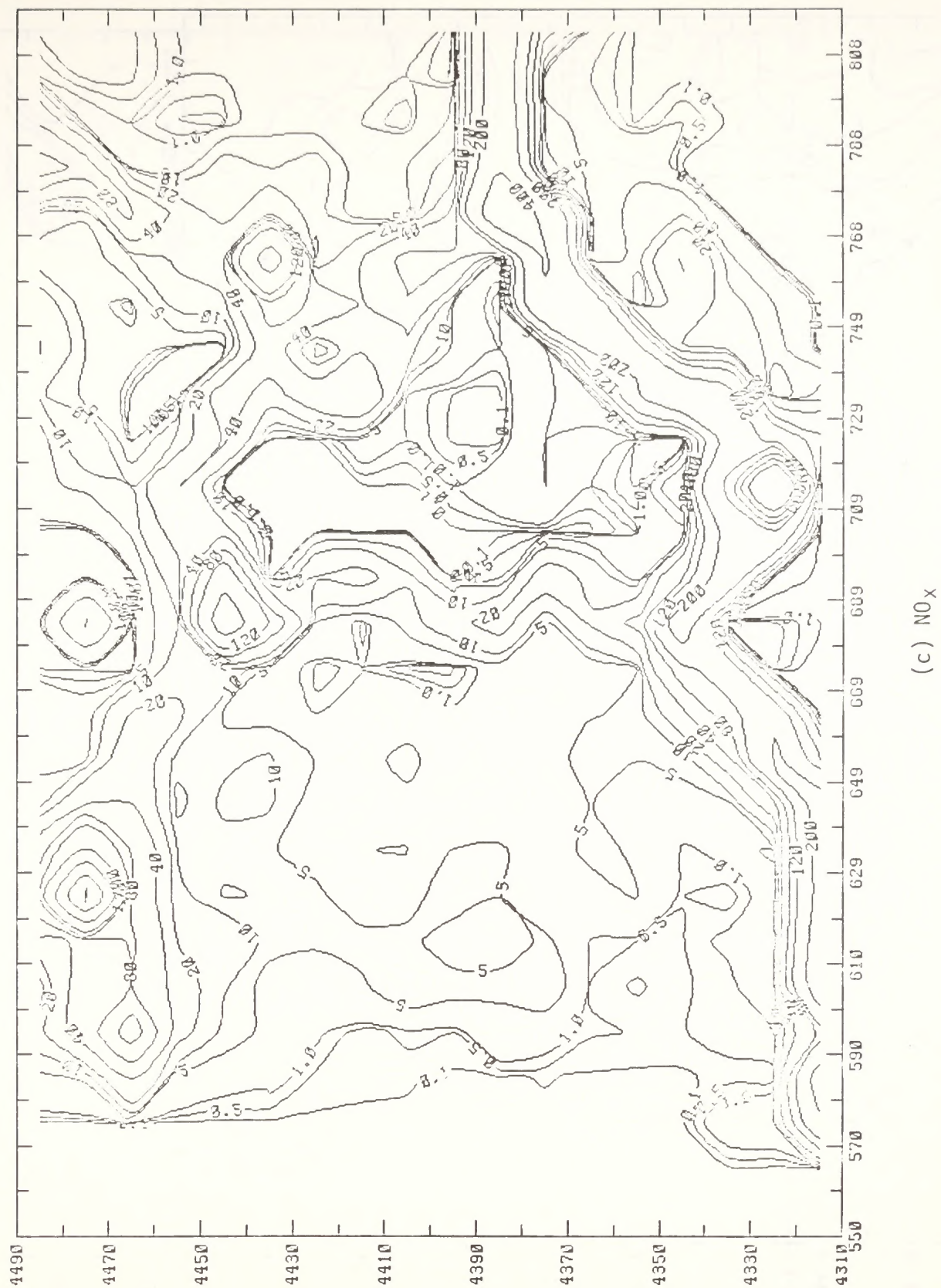
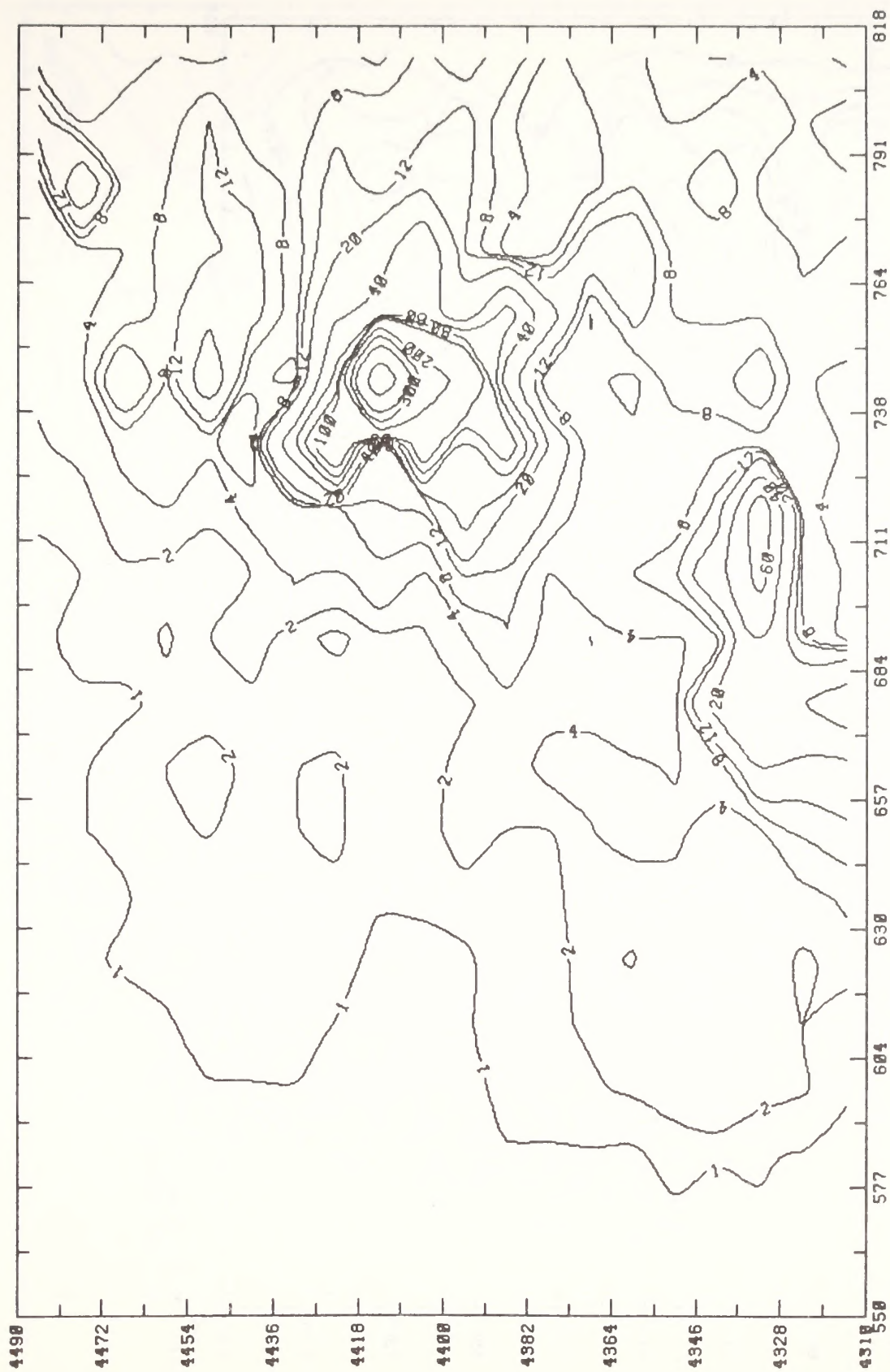


FIGURE 5-28 (Continued)



(d) C0

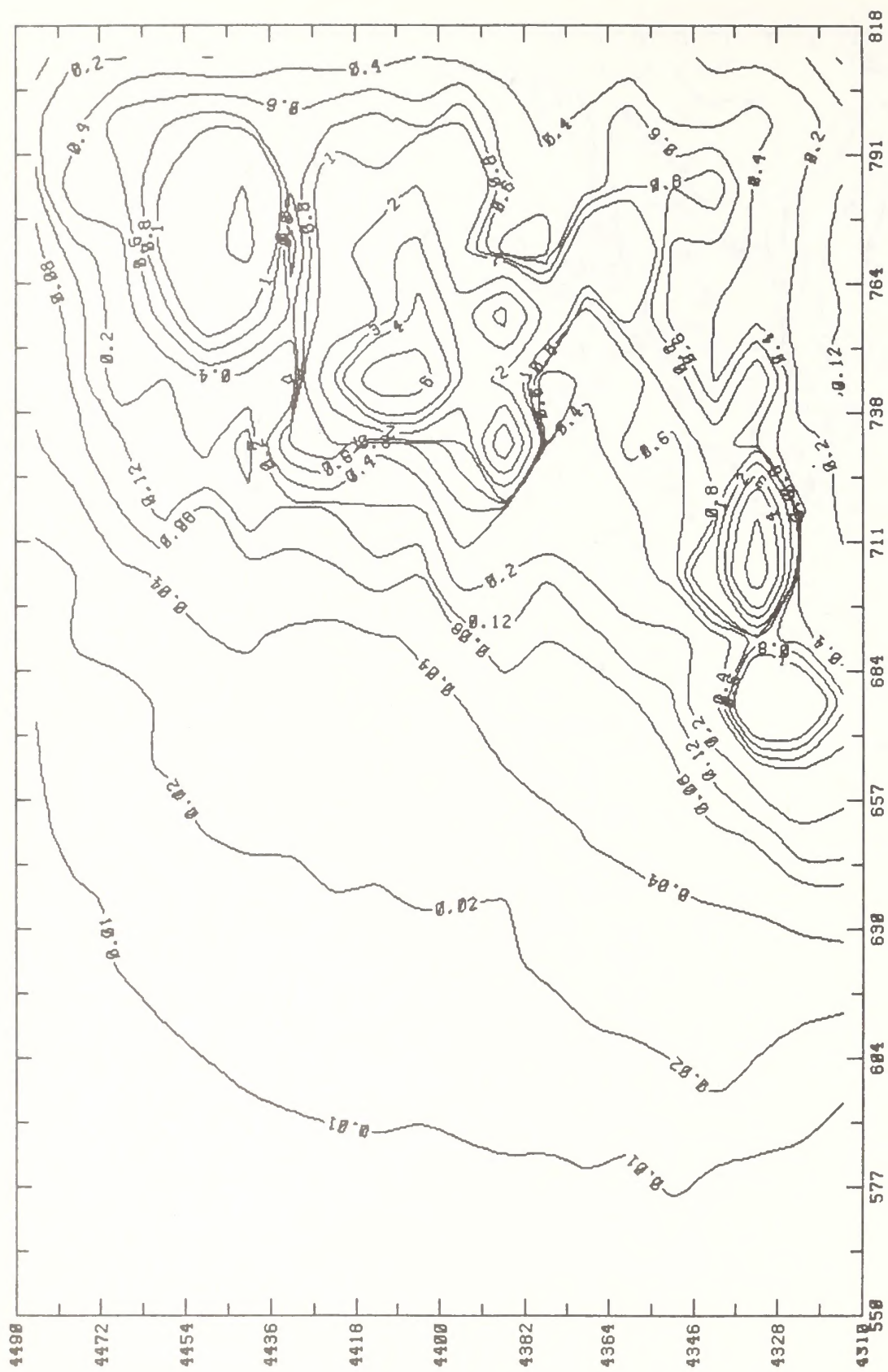
FIGURE 5-28 (Continued)



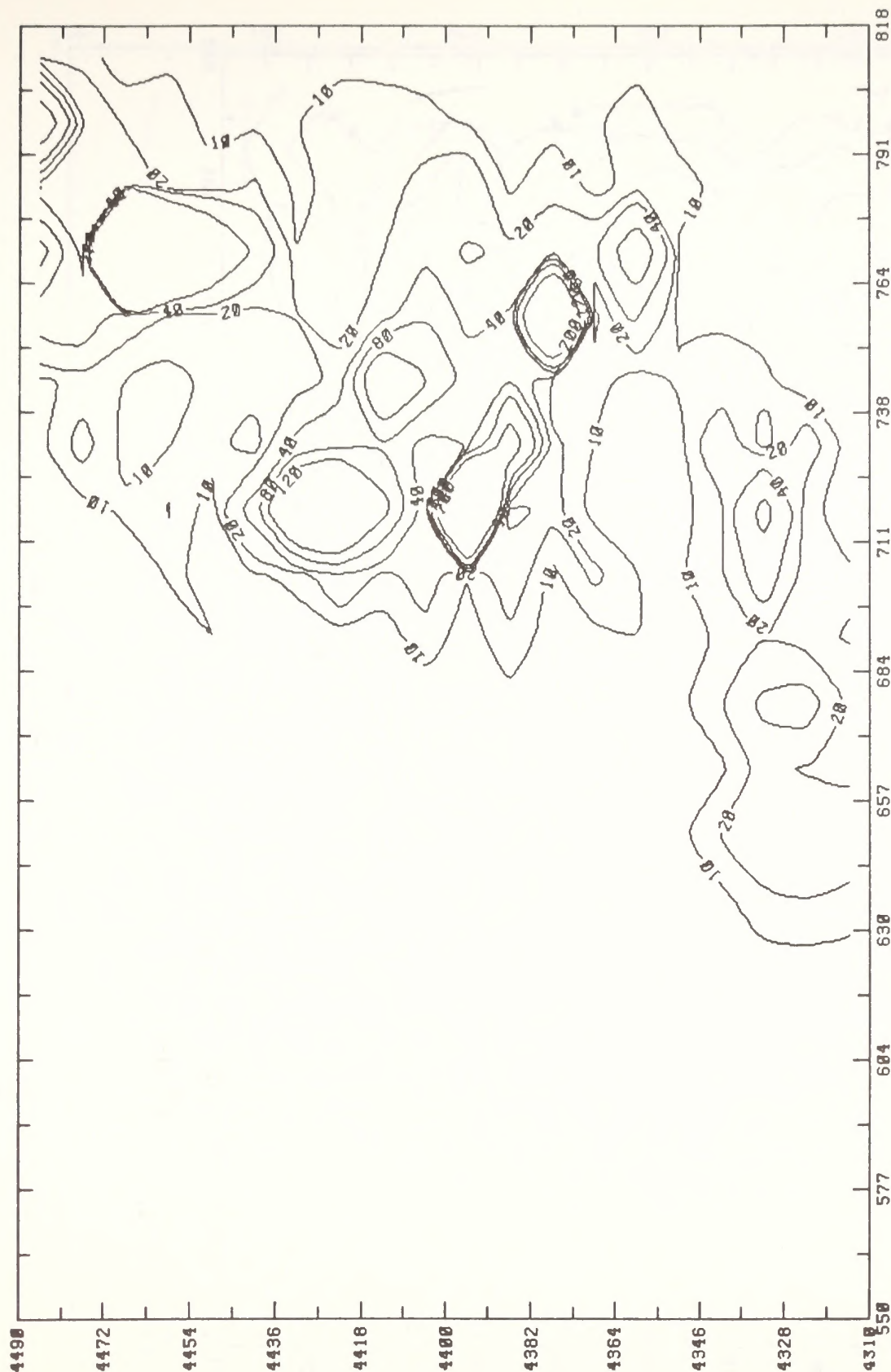
Note: These are upper-bound estimates of actual impacts and are non-simultaneous maxima calculated on the basis of one year's meteorological data.

(b) Maximum 24-hour average

FIGURE 5-20 (Continued)



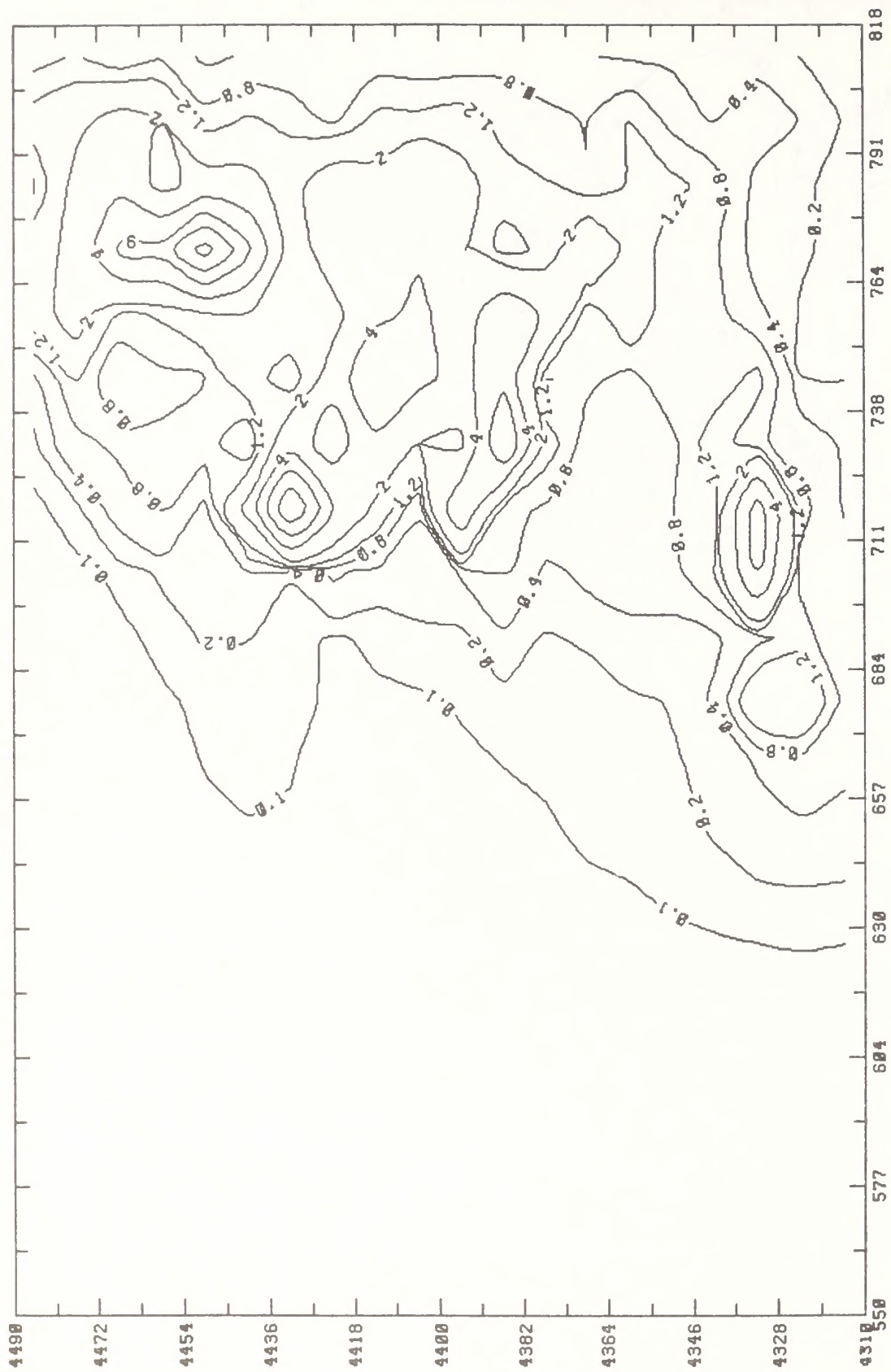
(c) Annual average



Note: These are upper-bound estimates of actual impacts and are non-simultaneous maxima calculated on the basis of one year's meteorological data.

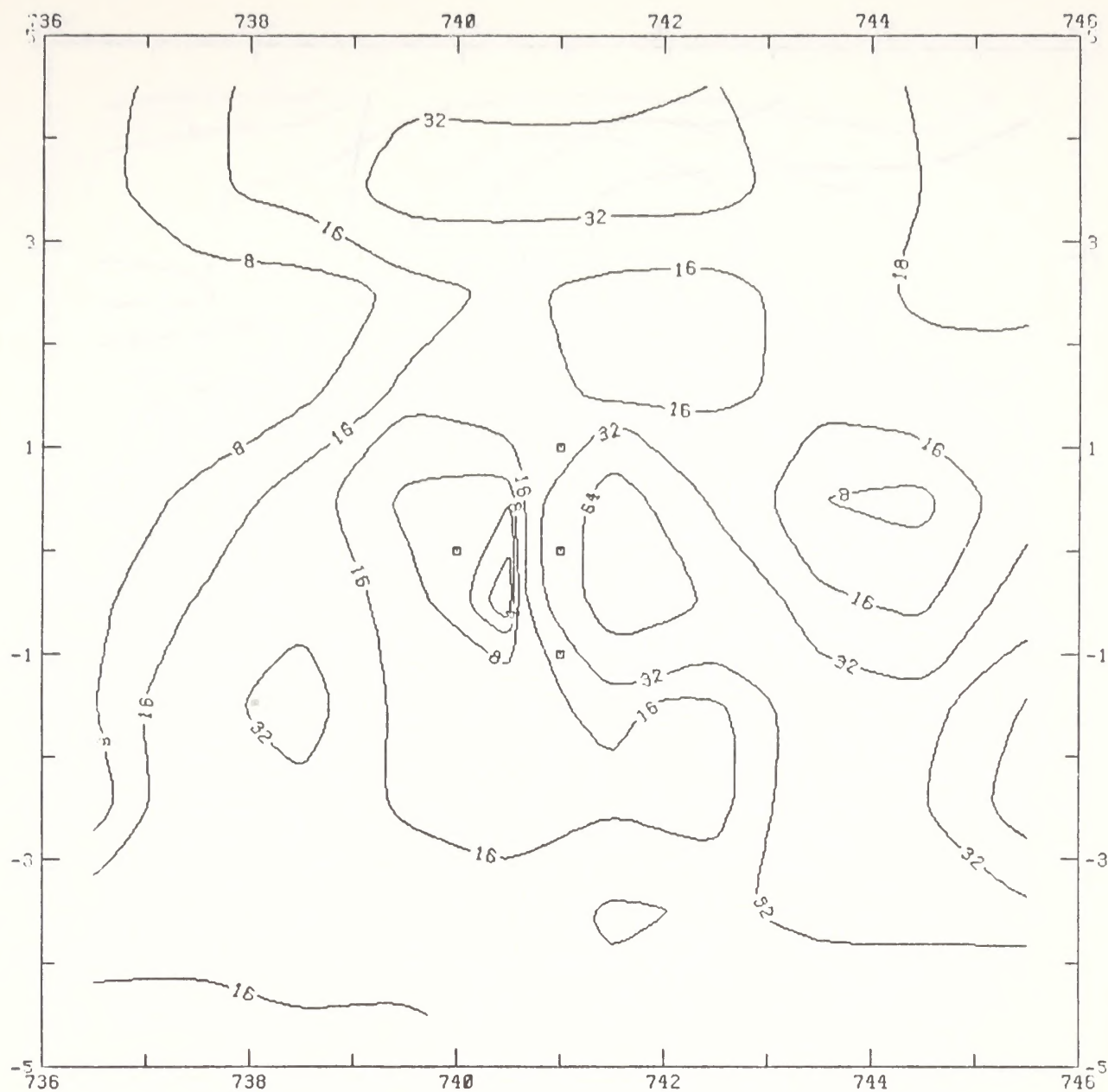
(a) Maximum 24-hour average

FIGURE 5-21. IMPACT OF DIRECT SOURCE EMISSIONS FROM COLORADO POINT SOURCES ON GROUND-LEVEL TSP CONCENTRATIONS ($\mu\text{g}/\text{m}^3$) FOR THE HIGH OIL PRODUCTION SCENARIO



Note: These are upper-bound estimates of actual impacts.

(b) Annual average
FIGURE 5-21 (Concluded)

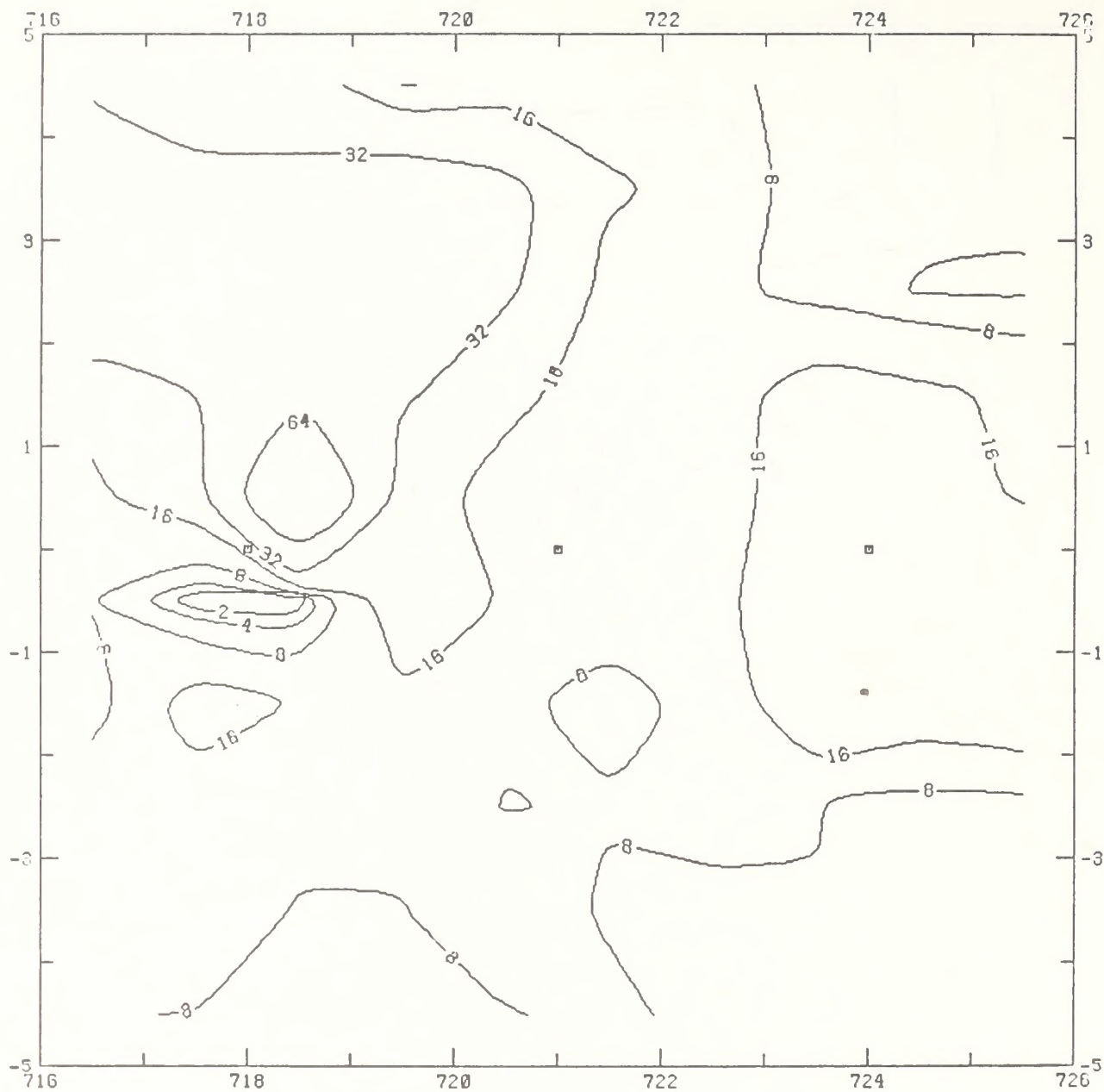


Note: These are upper-bound estimates of actual impacts and are non-simultaneous maxima calculated on the basis of one year's meteorological data.

□ Point Sources

(a) Cathedral Bluffs

FIGURE 5-22. MAXIMUM 24-HOUR AVERAGE NEAR SOURCE TSP CONCENTRATIONS RESULTING FROM DIRECT SOURCE EMISSIONS FROM OIL SHALE FACILITIES IN THE PICEANCE BASIN OF COLORADO BASED ON COMPLEX-I.

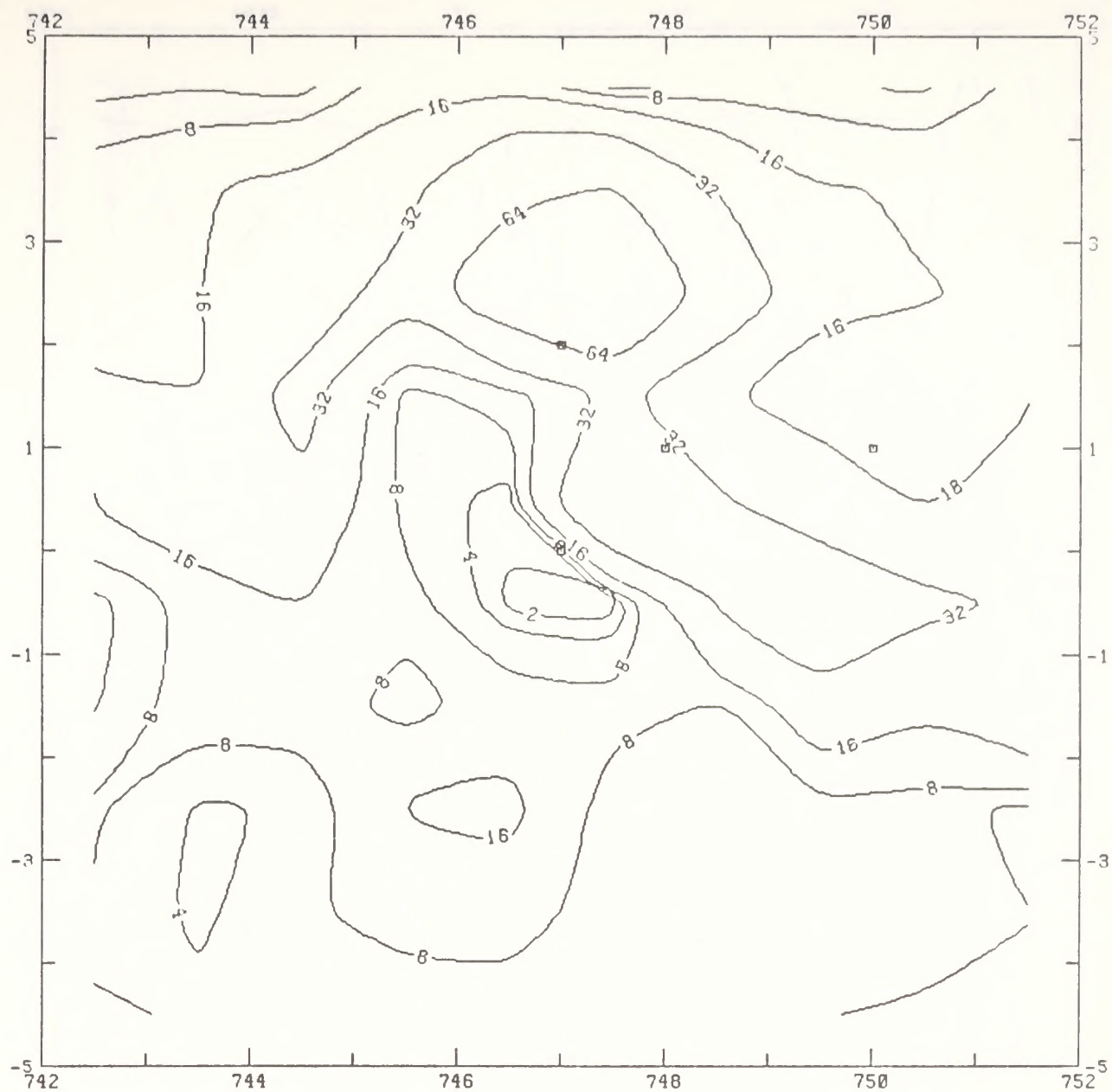


Note: These are upper-bound estimates of actual impacts and are non-simultaneous maxima calculated on the basis of one year's meteorological data.

□ Point Sources

(b) Chevron

FIGURE 5-22 (Continued)

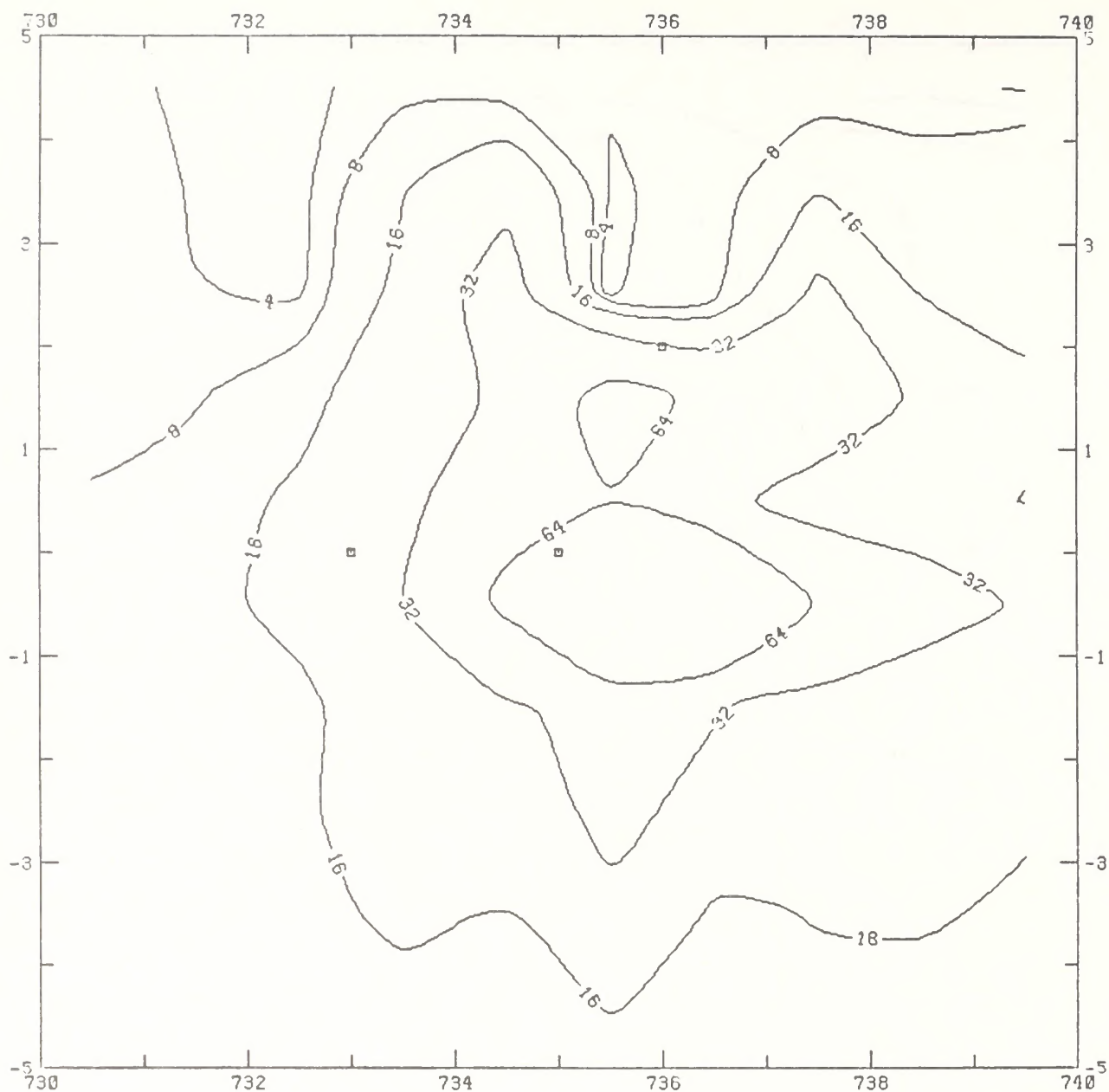


Note: These are upper-bound estimates of actual impacts and are non-simultaneous maxima calculated on the basis of one year's meteorological data.

□ Point Sources

(c) Colony

FIGURE 5-22 (Continued)

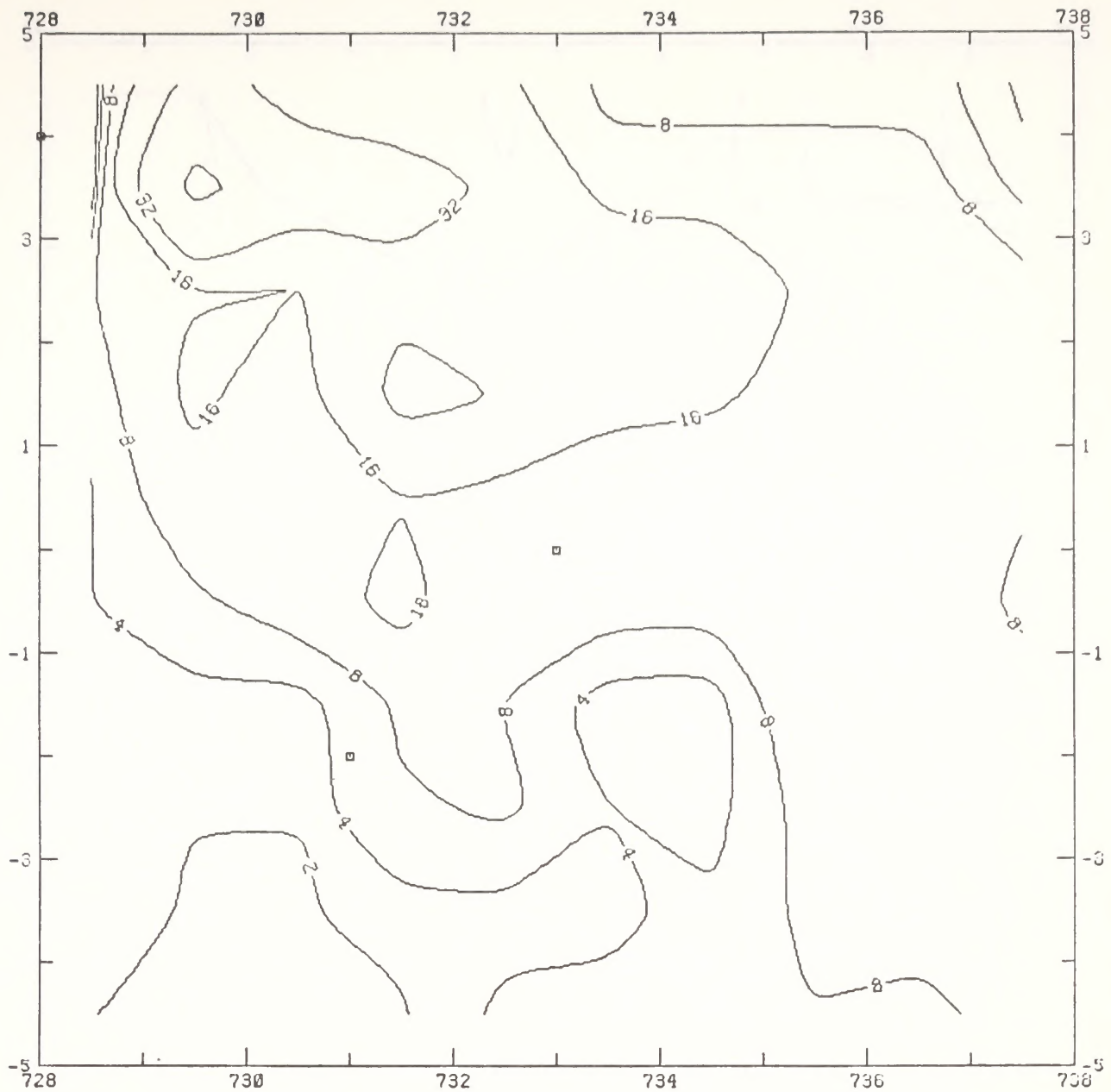


Note: These are upper-bound estimates of actual impacts and are non-simultaneous maxima calculated on the basis of one year's meteorological data.

□ Point Sources

(d) Exxon

FIGURE 5-22 (Continued)

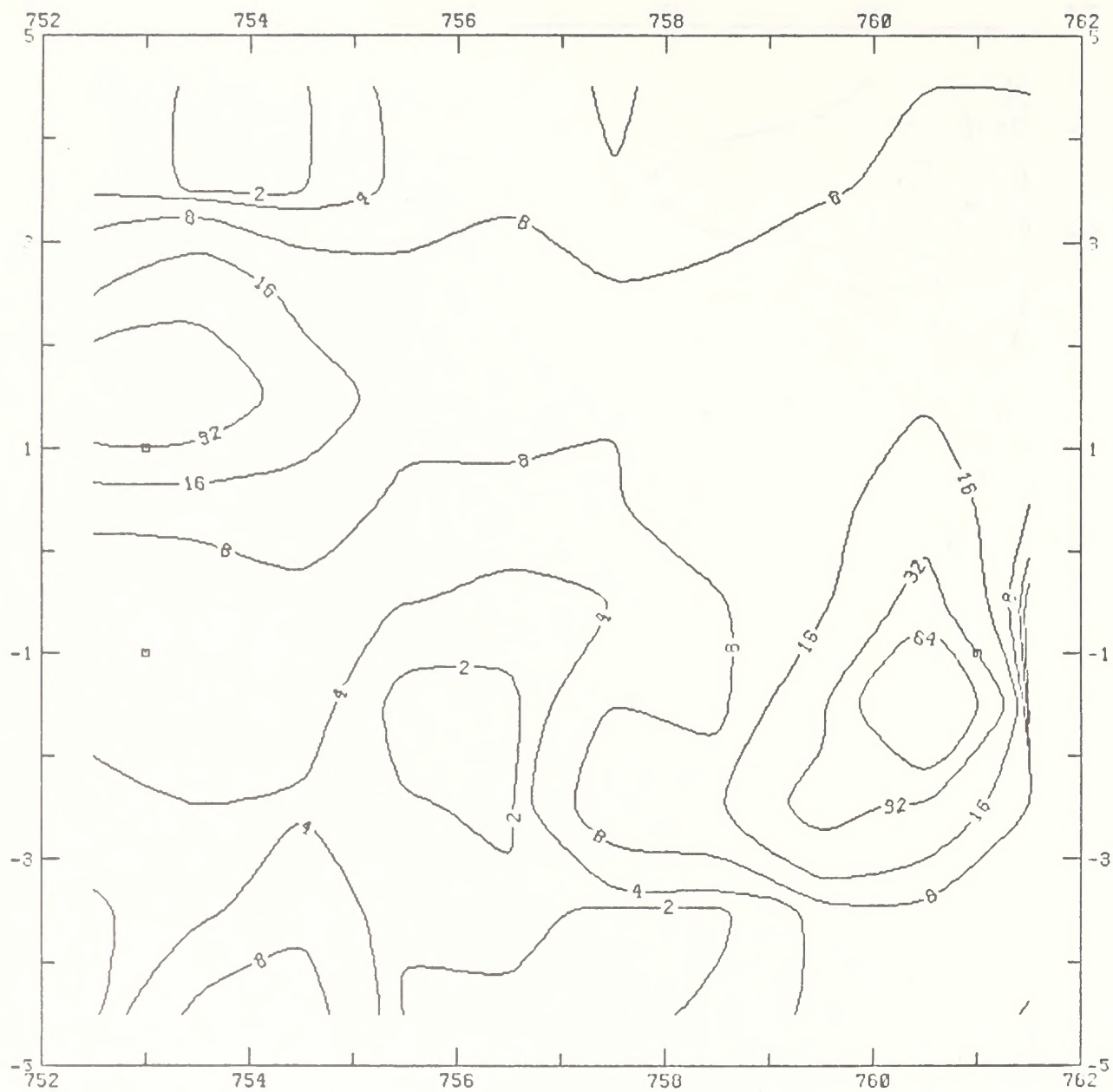


Note: These are upper-bound estimates of actual impacts and are non-simultaneous maxima calculated on the basis of one year's meteorological data.

□ Point Sources

(e) Getty

FIGURE 5-22 (Continued)

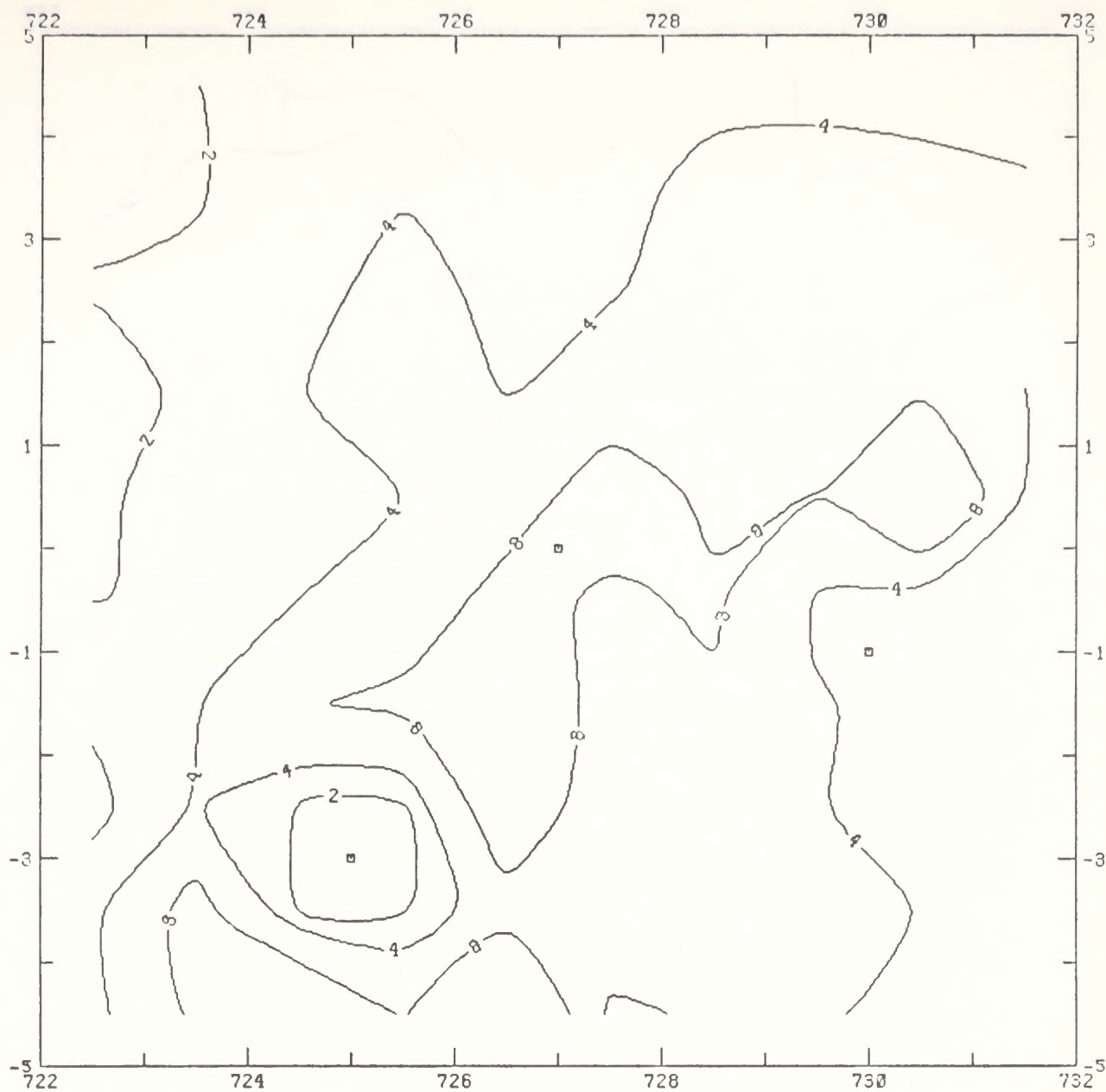


Note: These are upper-bound estimates of actual impacts and are non-simultaneous maxima calculated on the basis of one year's meteorological data.

□ Point Sources

(f) Mobil

FIGURE 5-22 (Continued)

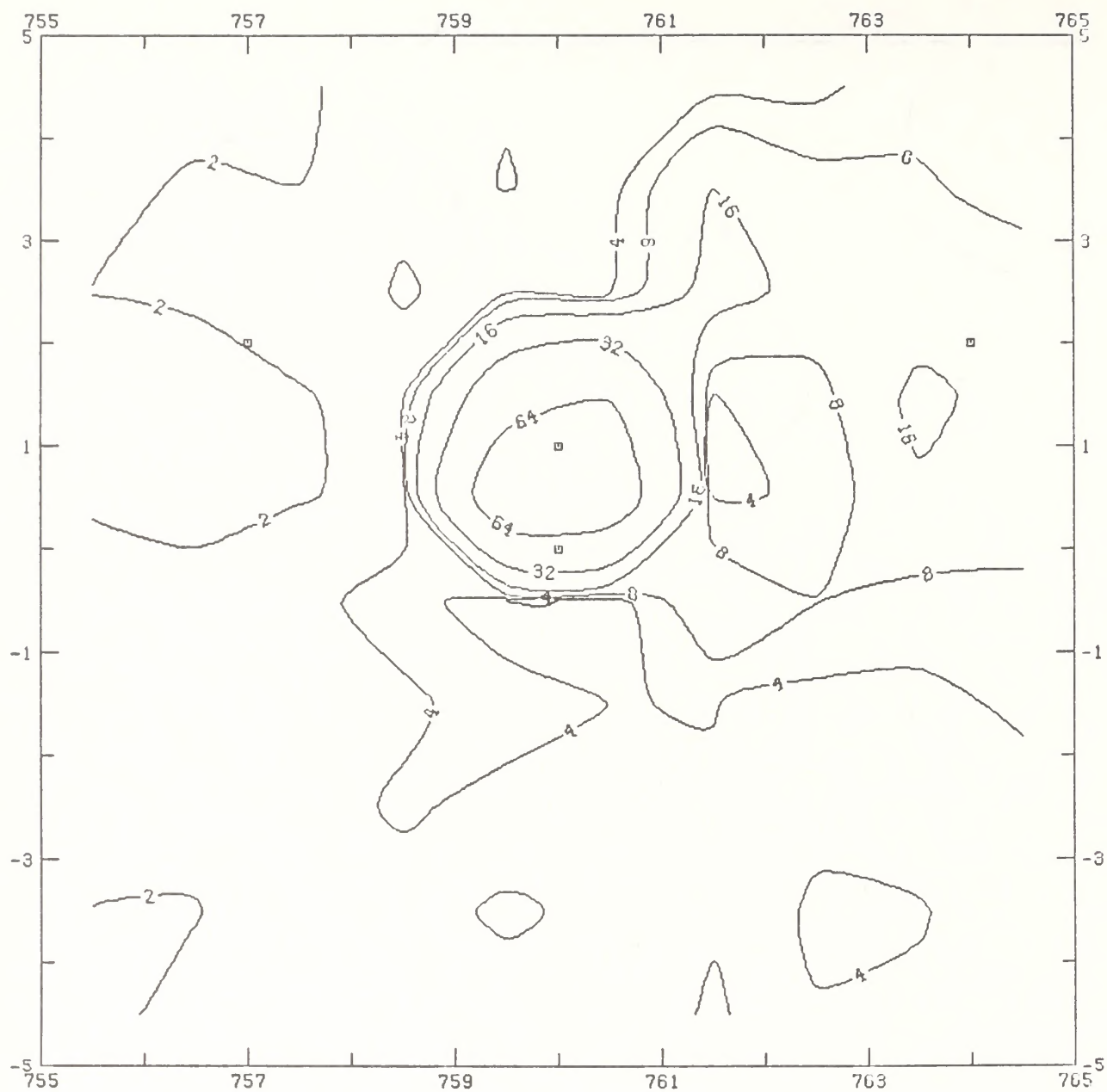


Note: These are upper-bound estimates of actual impacts and are non-simultaneous maxima calculated on the basis of one year's meteorological data.

□ Point Sources

(g) Multi Mineral

FIGURE 5-22 (Continued)

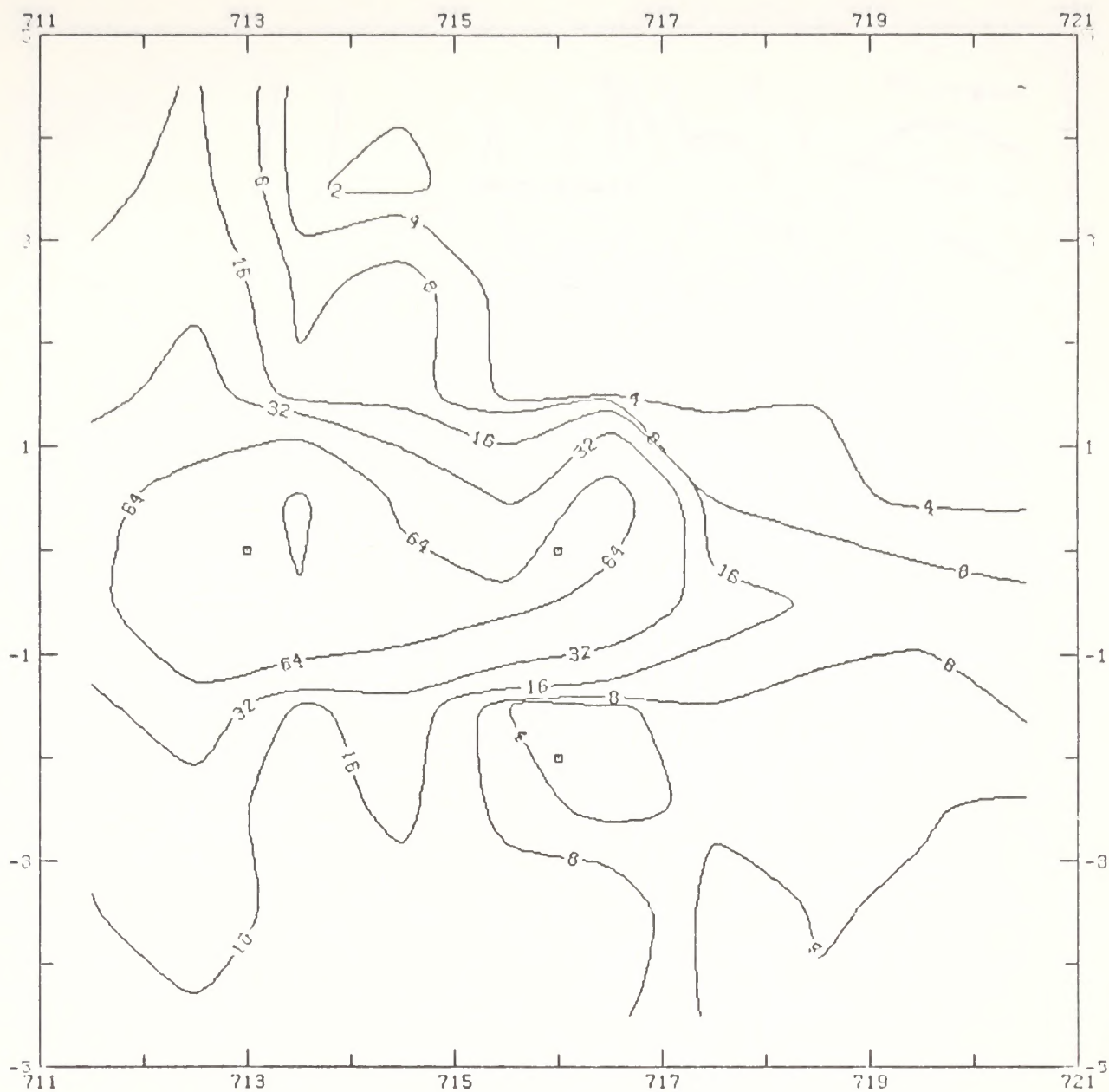


Note: These are upper-bound estimates of actual impacts and are non-simultaneous maxima calculated on the basis of one year's meteorological data.

□ Point Sources

(h) Naval Oil Shale Reserve

FIGURE 5-22 (Continued)



Note: These are upper-bound estimates of actual impacts and are non-simultaneous maxima calculated on the basis of one year's meteorological data.

□ Point Sources

(i) Rio Blanco

FIGURE 5-22 (Continued)

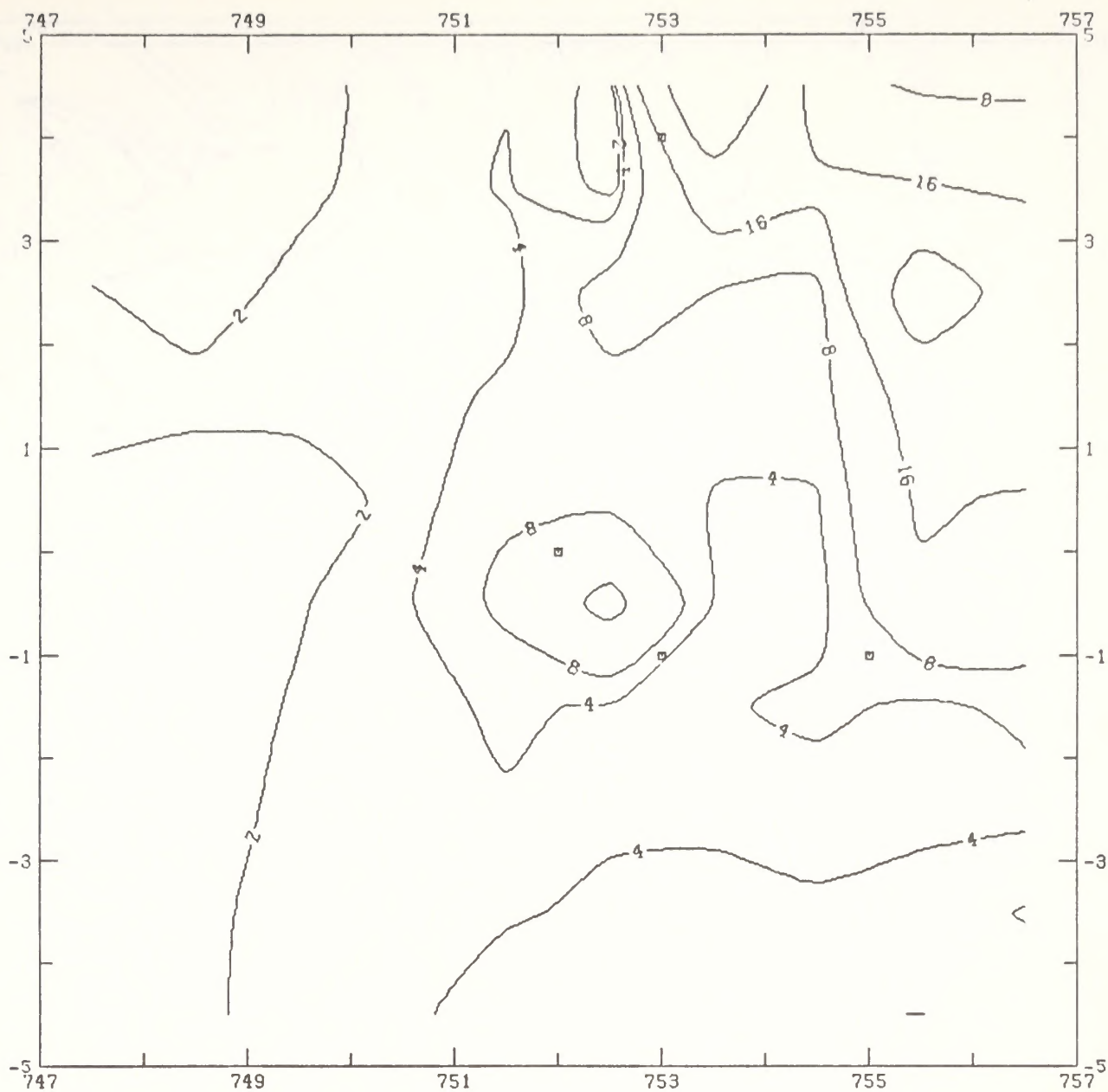


Note: These are upper-bound estimates of actual impacts and are non-simultaneous maxima calculated on the basis of one year's meteorological data.

□ Point Sources

(j) Superior

FIGURE 5-22 (Continued)

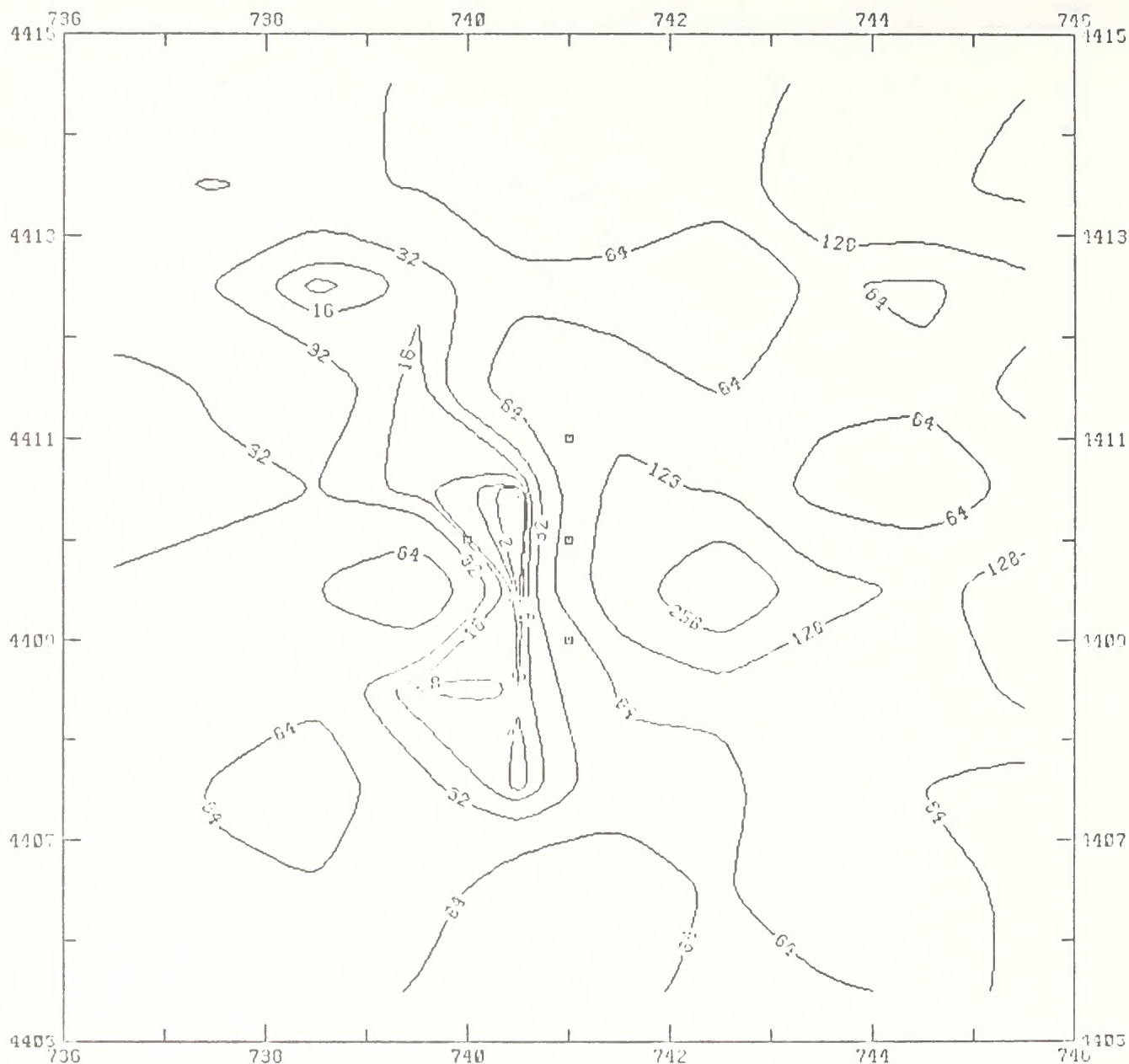


Note: These are upper-bound estimates of actual impacts and are non-simultaneous maxima calculated on the basis of one year's meteorological data.

□ Point Sources

(k) Union

FIGURE 5-22 (Concluded)



Note: These are upper-bound estimates of actual impacts and are non-simultaneous maxima calculated on the basis of one year's meteorological data.

□ Point Sources

(a) Maximum 3-hour average

FIGURE 5-23. MAXIMUM NEAR-SOURCE SO_2 CONCENTRATIONS RESULTING FROM DIRECT SOURCE EMISSIONS FROM CATHEDRAL BLUFFS ON THE BASIS OF COMPLEX-I CALCULATIONS

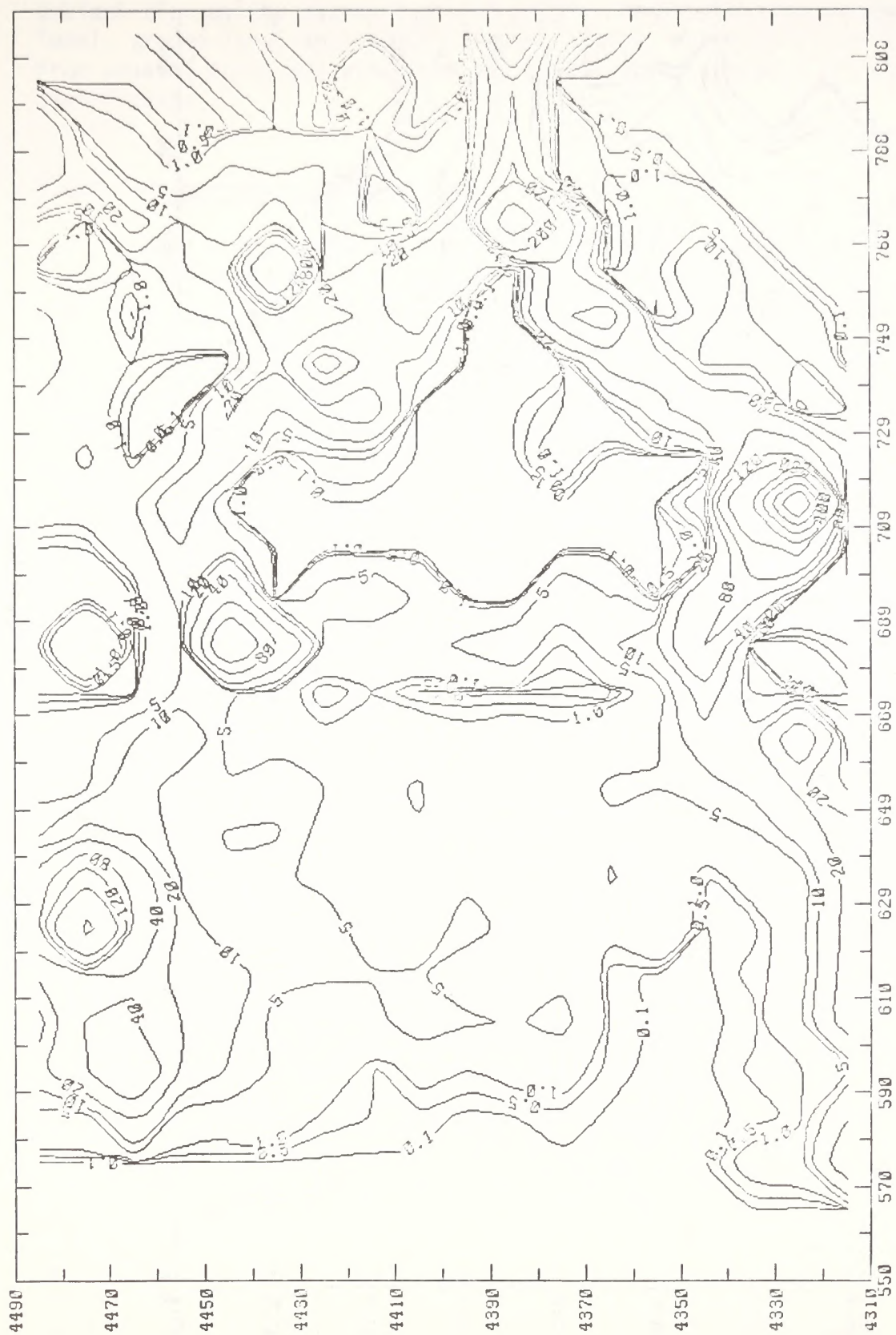


FIGURE 5-28 (Continued)



(f) Unreactive Hydrocarbons

FIGURE 5-28 (Concluded)

ambient air quality standard of $100 \mu\text{g}/\text{m}^3$. Except for the impacts on local, ground-level ambient TSP concentrations, which result primarily from unpaved roads and windblown dust, area source impacts are not significant.

5.3.2 High-Production Scenario

Figures 5-29, 5-30, and 5-31 show the corresponding area source plots (SO_2 and TSP concentrations and emission densities) for the high-production scenario. Concentrations and emissions are somewhat higher than those for the low-production scenario. Area source TSP impacts are significant, with concentrations above standards. Other air quality impacts-- SO_2 , NO_2 , and CO--are small. For example, annual SO_2 and NO_2 concentrations are less than 1 and $10 \mu\text{g}/\text{m}^3$, respectively.

5.4 CUMULATIVE AIR QUALITY IMPACTS OF ALL REGIONAL EMISSIONS

In the previous two subsections we displayed estimates of impacts resulting separately from emissions from industrial facilities (point sources) and area sources associated with population and related growth. In this subsection we investigate the total regional air quality impacts resulting from both point and area source emissions. In addition, we explicitly consider the estimated uncertainty in our impact calculations (see section 5.1) to evaluate the significance of air quality impacts compared to the air quality significance criteria discussed in section 3, namely, the ambient air quality standards and the Prevention of Significant Deterioration (PSD) increments for Class I and Class II areas.

5.4.1 SO_2 Impacts

Tables 5-1 and 5-2 summarize the total SO_2 impacts of regional emission sources for a variety of receptors of interest for the low- and high-oil-production scenarios, respectively. Maximum 3-hour and 24-hour SO_2 concentrations (maximum concentrations in a year) as well as annual average concentrations are provided. Ranges of maximum concentrations are given for each receptor, taking into account the conservatism of the GPM calculations as discussed in Section 4 and in subsection 5.1. From this table it is clear that impacts will be well within ambient air quality standards everywhere in the region; this conclusion is unambiguous within the estimated range of uncertainty since even the upper-bound estimates are within standards. The maximum SO_2 impacts are predicted in the Grand Junction area (including Colorado National Monument) with maximum 3-hour concentrations estimated to be in the range 66 to $664 \mu\text{g}/\text{m}^3$. Most of this

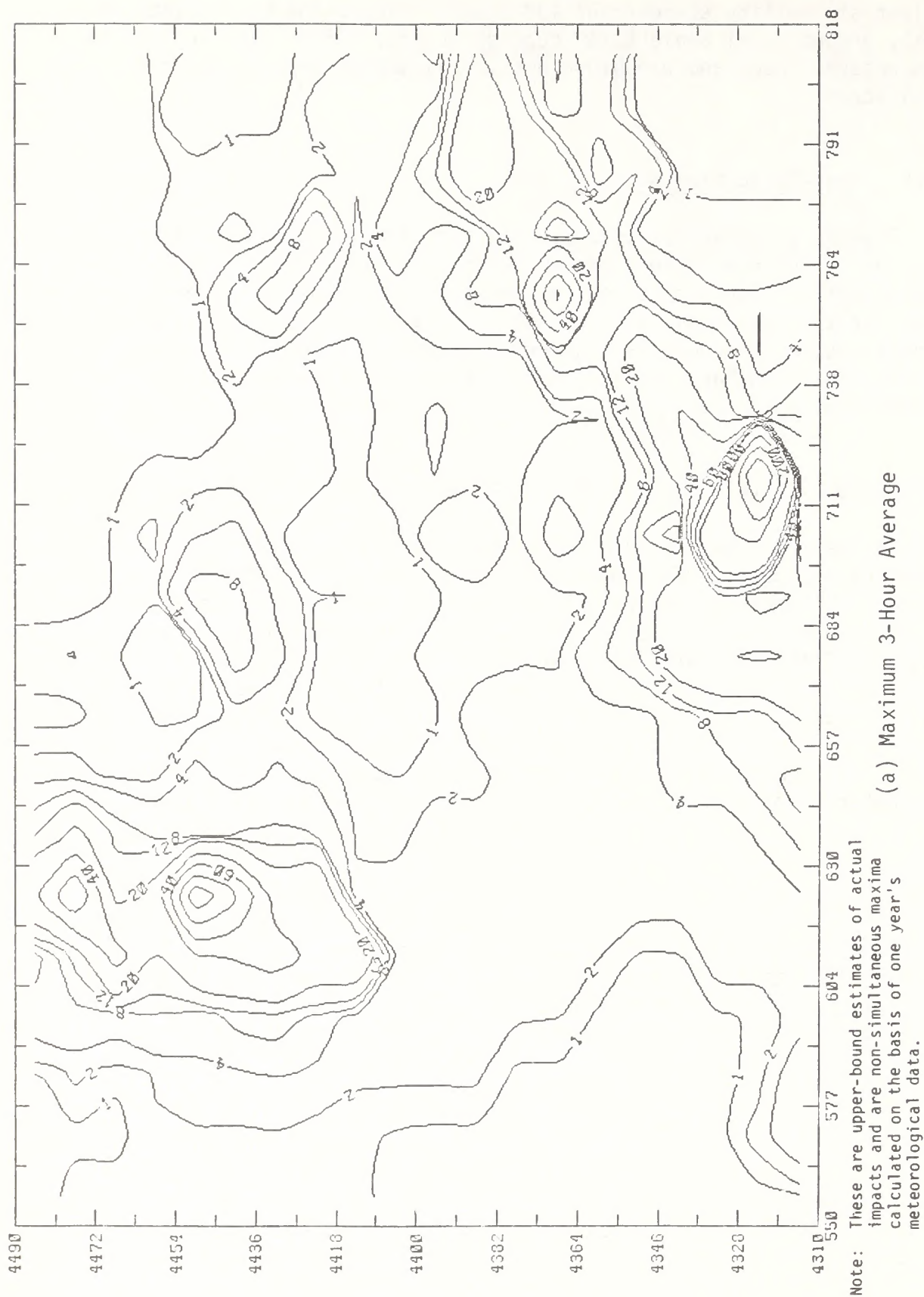
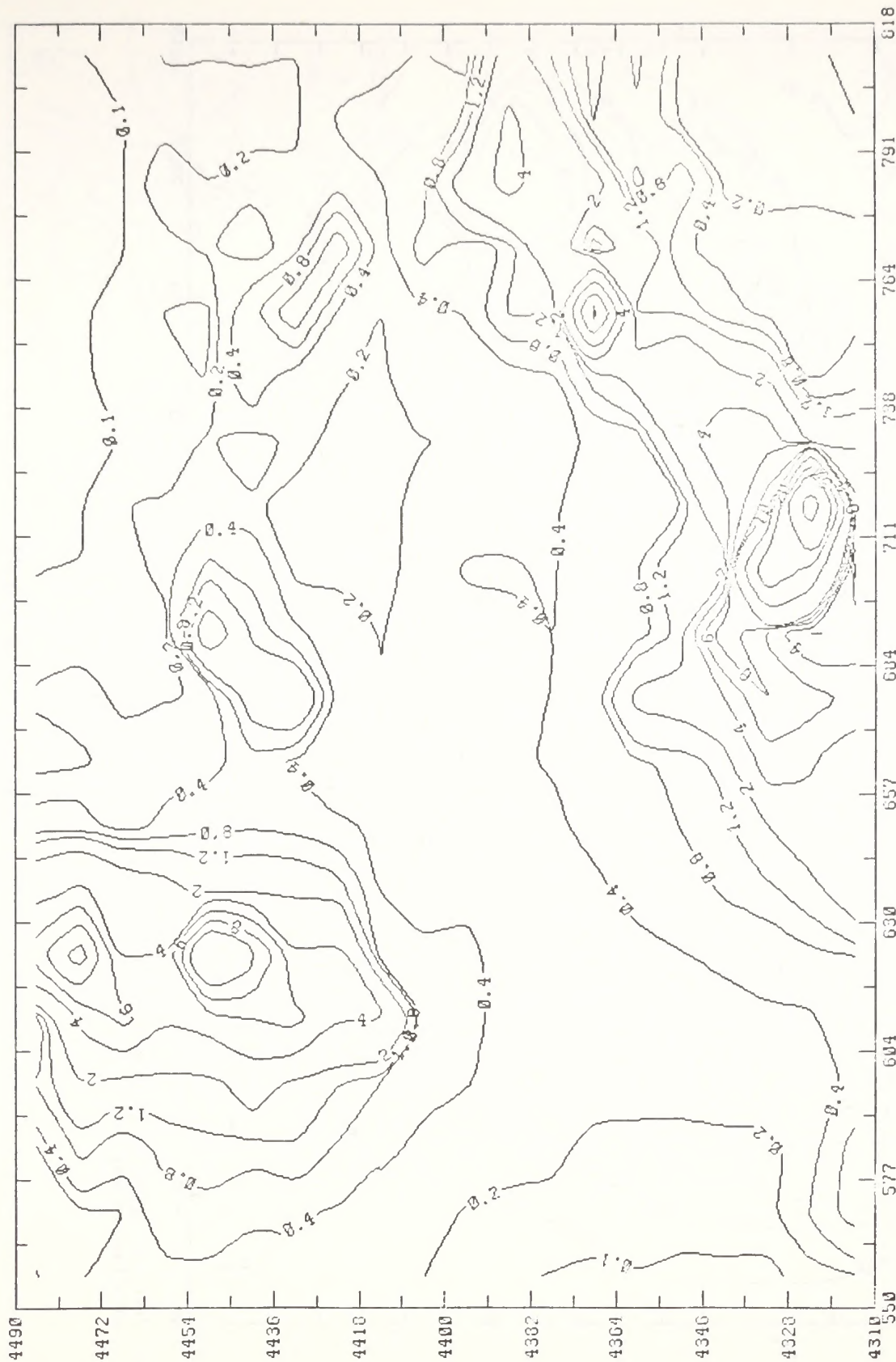


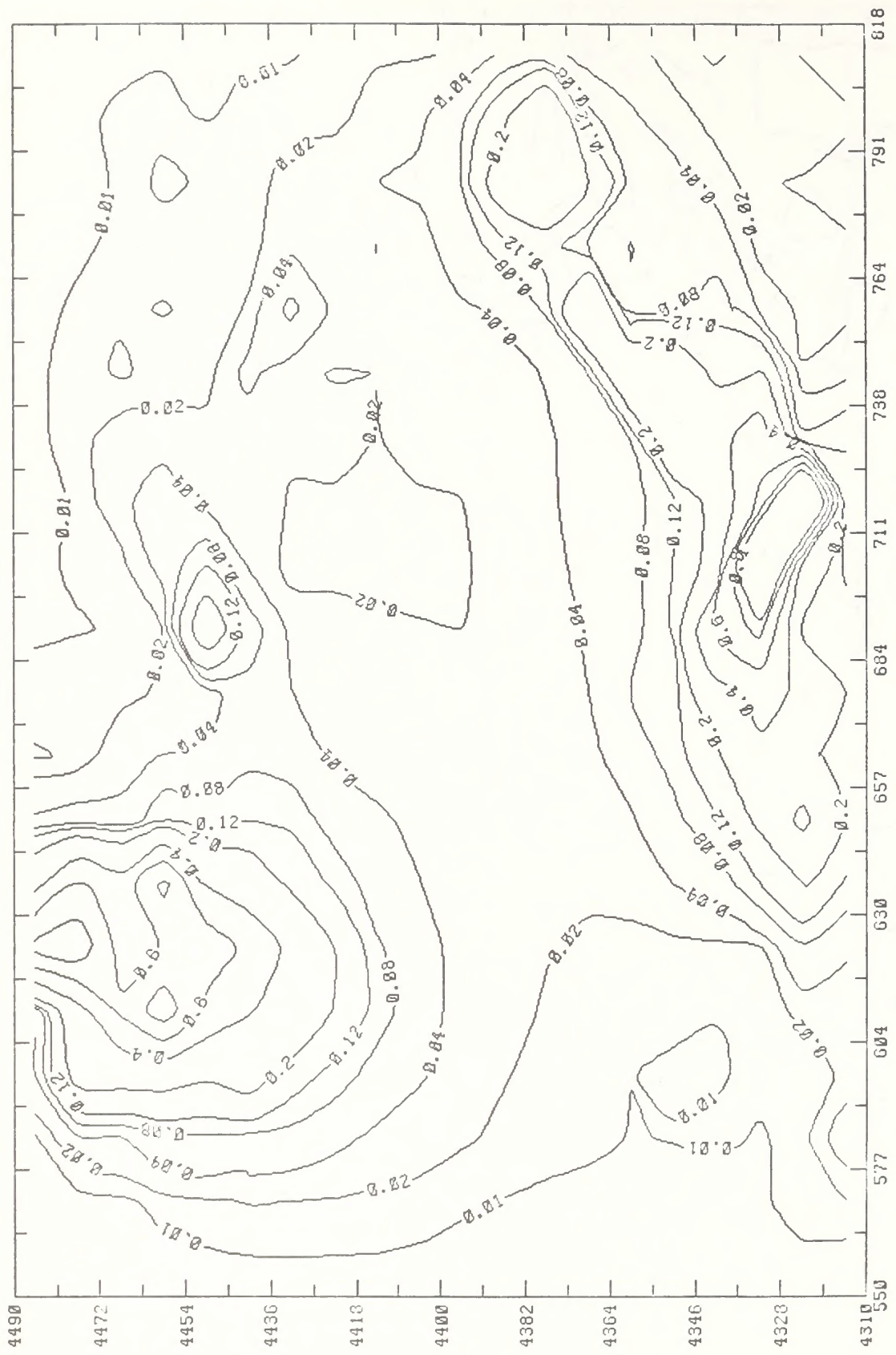
FIGURE 5-29. IMPACT OF AREA SOURCE EMISSIONS ON GROUND-LEVEL SO₂ CONCENTRATIONS ($\mu\text{g}/\text{m}^3$) FOR THE HIGH OIL PRODUCTION SCENARIO



Note: These are upper-bound estimates of actual impacts and are non-simultaneous maxima calculated on the basis of one year's meteorological data.

(b) Maximum 24-Hour Average

FIGURE 5-29 (Continued)



Note: These are upper-bound estimates of actual impacts.

(c) Annual Average

FIGURE 5-29 (Concluded)

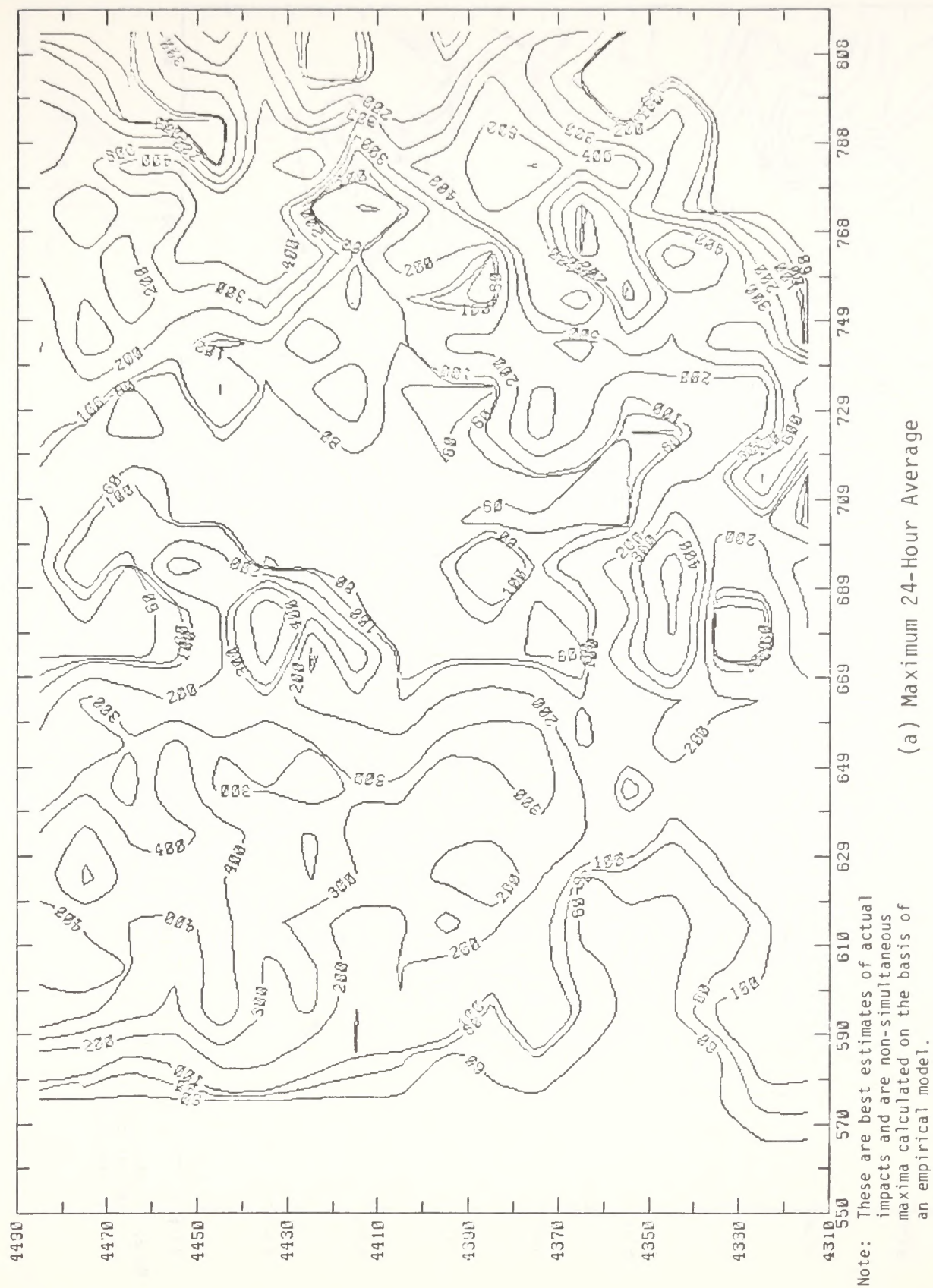


FIGURE 5-30. IMPACT OF AREA SOURCE EMISSIONS ON GROUND-LEVEL TSP CONCENTRATIONS ($\mu\text{g}/\text{m}^3$) FOR THE HIGH OIL PRODUCTION SCENARIO



Note: These are best estimates of actual impacts calculated on the basis of an empirical model.

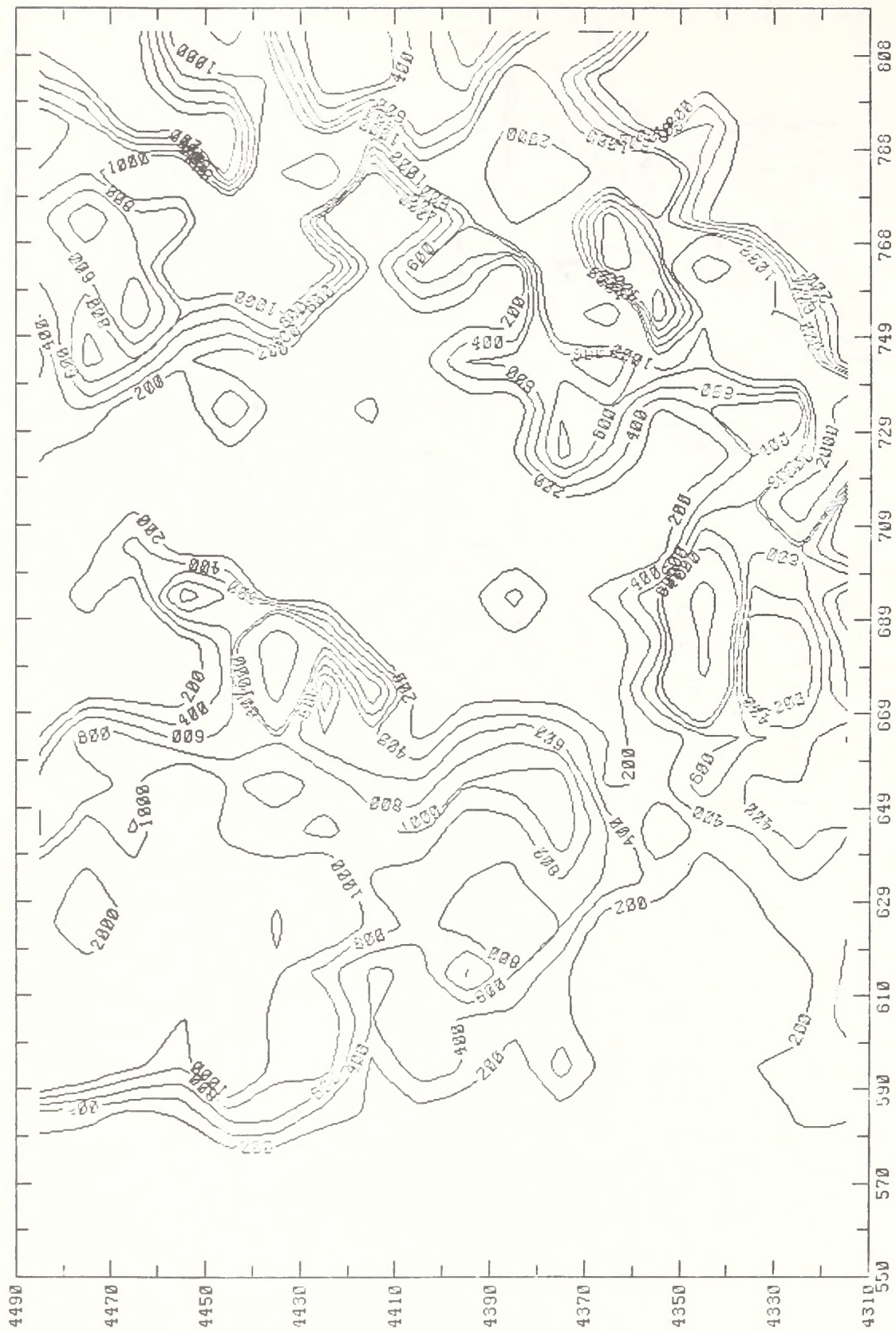
(b) Annual Average

FIGURE 5-30 (Concluded)



(a) SO_2

FIGURE 5-31. AREA SOURCE EMISSION DENSITIES FOR HIGH OIL PRODUCTION SCENARIO (tons/yr/100 km²)



(b) TSP

FIGURE 5-31 (Continued)



(c) NO_x

FIGURE 5-31 (Continued)



(d) C0

FIGURE 5-31 (Continued)



(f) Unreactive Hydrocarbons

FIGURE 5-31 (Concluded)

TABLE 5-1. SUMMARY OF AMBIENT AIR QUALITY IMPACTS ASSOCIATED WITH THE LOW OIL PRODUCTION SCENARIO

(a) Maximum 3-hour Average SO_2 Concentrations*

Receptor	Maximum 3-hour Average SO ₂ Concentrations (µg/m ³)														
	(1) Uinta Basin		(2) Uinta Basin		(3) Other Uinta		(4) Piceance Basin		(5) 1980	Increment Consumption			Total Ambient Concentration Including 1980 Baseline		
	Site-Specific		Conceptuals		Basin Sources		(Colorado Sources)			Above Baseline					
	Direct	Secondary	Direct	Secondary	Direct	Secondary	Direct	Secondary		Baseline	(1+2)	(1+2+3)		(1+2+3+4)	
Population Centers															
Vernal	0-1	1-6	1-5	0-3	0	0	0	0	5-45	2-15	2-19	2-19	7-60	7-64	7-64
Green River	0	0	0-3	0	0	0	0	0	0-4	0-3	0-3	0-7	0-7	0-7	0-11
Rangely	1-5	0-3	0-2	0-1	0-3	0-1	0	0-3	0	1-1	1-15	1-12	1-12	1-16	1-23
Meeker	1-3	0	0-1	0	0-2	0	5-50	0	2-16	1-4	1-6	6-56	3-20	3-22	8-72
Craig	0-1	0	0-1	0	0-1	0	1-10	0	20-196	0-2	0-3	1-13	20-198	20-199	21-209
Glenwood Springs	0	0	0-2	0	0	0	1-10	0	1-9	0-2	0-2	1-12	1-11	1-11	2-21
Rifle	0	0	0-3	0	0	0	1-10	0	2-19	0-3	0-3	1-13	2-22	2-22	3-32
Parachute	0-1	0	0-2	0	0	0	1-10	2-20	2-21	0-3	0-3	3-33	2-24	2-24	5-54
De Beque	0-1	0	0-4	0	0	0	1-10	0	5-52	0-5	0-5	1-15	5-57	5-57	6-67
Grand Junction	0-1	0	0-4	0	0	0	1-10	0	60-607	0-5	0-5	1-15	60-612	60-612	61-622
Existing or Potential Class I Areas and Other Areas of Special Concern															
Flet Topa Wilderness	0	0	0-4	0	0-1	0	4-40 [†]	0	4-39	0-4	0-5	4-45 [†]	4-43	4-44	8-84
Mt. Zirkel Wilderness	0	0	0-2	0	0	0	1-10	0	0-3	0-2	0-2	1-12	0-5	0-5	1-15
Dinosaur National Monument	0-3	0-2	0-3	0-1	0-4	0-1	1-10	0	1-5	0-9	0-14	1-24	1-14	1-19	2-29
Colorado National Monument	0-1	0	0-2	0	0	0	1-10	0	32-318	0-3	0-3	1-13	32-321	32-321	33-331
Utah and Ouray Indian Reservation	2-21	0	0	0	0-8	0	1-10	0	19-185	2-21	2-29	3-39	21-206	21-214	22-224
Uinte Primitive Area	0-1	0	0	0	0	0	0	0	0-1	0-1	0-1	0-1	0-2	0-2	0-2
Class II Area Receptors with Maximum Impacts from Direct Source Emissions in Uinta Basin															
14-140	0	0	0	0	0-5	0	0-10	0	1-10	14-140	14-145	15-155	15-150	15-155	16-165

* Note that concentration ranges, not point estimates, are provided; lower and upper bounds of predicted maximum concentration are provided.

A Standard or increment is applicable.

TABLE 5-1 (Continued)
(b) Maximum 24-hour Average SO₂ Concentrations*

Receptor	Maximum 24-hour Average SO ₂ Concentrations (µg/m ³)											
	(1) Uinta Basin		(2) Uinta Basin		(3) Other Units		(4) Picesance Basin		(5) 1980		Increment Consumption	
	Site-Specifics		Conceptuals		Basin Sources		Colorado Sources		Baseline		Above Baseline	
	Direct	Secondary	Direct	Secondary	Direct	Secondary	Direct	Secondary	Baseline	(1+2)	(1+2+3+4)	Total Ambient Concentration Including 1980 Baseline (1+2+3+5) (1+2+3+4+5)
Population Centers												
Vernal	0	0-1	0-1	0	0	0	0	0	1-6	0-2	0-2	1-8
Green River	0	0	0	0	0	0	0-1	0	0-1	0	0-1	1-8
Rangely	0-2	0	0	0	0	0	0-1	0	0-1	0-2	0-3	0-1
Meeker	0	0	0-1	0	0	0	1-14	0-1	1-5	0-1	1-16	0-3
Craig	0	0	0	0	0	0	0-2	0	3-28	0	0-2	1-6
Glenwood Springs	0	0	0	0	0	0	0-3	0	0-2	0	0-2	2-21
Rifle	0	0	0-1	0	0	0	0-3	0	0-3	0-1	0-4	3-30
Parachute	0	0	0-1	0	0	0	0-3	0-3	0-3	0-1	0-4	0-5
De Beque	0	0	0-1	0	0	0	0-3	0	1-11	0-1	0-4	0-7
Grand Junction	0	0	0-1	0	0	0	0-3	0	8-82	0-1	0-4	0-10
Existing or Potential Class I Areas and Other Areas of Special Concern												
Flat Tops Wilderness	0	0	0	0	0	0	1-6 [†]	0	1-5	0	0	1-5
Mt. Zirkel Wilderness	0	0	0	0	0	0	0-2	0	0-1	0	0-2	1-5
Dinosaur National Monument	0-1	0	0	0	0	0	0-1	0	1-5	0-1	0-2	0-3
Colorado National Monument	0	0	0-1	0	0	0	0-3	0	4-40	0-1	0-4	1-6
Utah and Ouray Indian Reservation	0-3	0	0	0	0-2	0	0-2	0	2-23	0-3	0-7	1-7
Uinta Primitive Area	0	0	0	0	0	0	0	0	0-1	0	0	4-41
Class II Area Receptors with Maximum Impacts from Direct Source Emissions in Uinta Basin												
2-22	0	0	0	0	0-1	0	0-1	0	0-1	2-22	2-23	2-24
Ambient Air Quality Standard or Prevention of Significant Deterioration Increment												
PSD Class I Increment	A	A	A	A	A	A	A	A	NA	A	A	NA
PSD Class II Increment	A	A	A	A	A	A	A	A	NA	A	A	NA
AAQS	NA	NA	NA	NA	NA	NA	NA	NA	A	NA	NA	A

* Note that concentration ranges, not point estimates, are provided; lower and upper bounds of predicted maximum concentration are provided.
[†] Indicates violation of applicable standard or increment.
 A Standard or increment is applicable.
 NA Standard or increment is not applicable.

TABLE 5-1 (Concluded)

(c) Annual Average SO₂ Concentrations*

Receptor	Annual Average SO ₂ Concentrations (µg/m ³)											
	(1) Uinta Basin		(2) Uinta Basin		(3) Other Uinta		(4) Piceance Basin		(5) 1980		Total Ambient Concentration Including 1980 Baseline (1+2+3+4+5)	
	Site-Specifics		Conceptuals		Basin Sources		Colorado Sources		Baseline			
	Direct	Secondary	Direct	Secondary	Direct	Secondary	Direct	Secondary	(1+2)	(1+2+3)		(1+2+3+4)
Population Centers												
Vernal	0	0	0	0	0	0	0	0	0	0	0	0
Green River	0	0	0	0	0	0	0	0	0	0	0	0
Rangely	0	0	0	0	0	0	0	0	0	0	0	0
Meeker	0	0	0	0	0	0	0-1	0	0	0	0	0-1
Craig	0	0	0	0	0	0	0	0	0	0	0	0
Glenwood Springs	0	0	0	0	0	0	0	0	0	0	0	0
Rifle	0	0	0	0	0	0	0	0-1	0	0	0-1	0-1
Parachute	0	0	0	0	0	0	0	0-1	0	0	0-1	0-1
De Beque	0	0	0	0	0	0	0	0-1	0	0	0-1	0-1
Grand Junction	0	0	0	0	0	0	0	0-9	0	0	0-9	0-9
Existing or Potential Class I Areas and Other Areas of Special Concern												
Flat Top Wilderness	0	0	0	0	0	0	0	0	0	0	0	0
Mt. Zirkel Wilderness	0	0	0	0	0	0	0	0	0	0	0	0
Dinosaur National Monument	0	0	0	0	0	0	0	0	0	0	0	0
Colorado National Monument	0	0	0	0	0	0	0	0-1	0	0-1	0-1	0-1
Utah and Ouray Indian Reservation	0	0	0	0	0	0	0	0	0	0	0	0
Uinta Primitive Area	0	0	0	0	0	0	0	0	0	0	0	0
Class II Area Receptors with Maximum Impacts from Direct Source Emissions in Uinta Basin												
	0	0	0-2	0	0	0	0	0	0-1	0-2	0-3	0-3
Ambient Air Quality Standard or Prevention of Significant Deterioration Increment												
PSD Class I Increment	A	A	A	A	A	A	A	A	NA	A	NA	NA
PSD Class II Increment	A	A	A	A	A	A	A	A	NA	A	NA	NA
AAQS	NA	NA	NA	NA	NA	NA	NA	NA	A	NA	A	A

* Note that concentration ranges, not point estimates, are provided; lower and upper bounds of predicted maximum concentration are provided.

† Indicates violation of applicable standard or increment.

A Standard or increment is applicable.

NA Standard or increment is not applicable.

TABLE 5-2 (Continued)

(b) Maximum 24-hour Average SO₂ Concentrations*

Receptor	Maximum 24-hour Average SO ₂ Concentrations (µg/m ³)															
	(1) Uinta Basin Site-Specifics		(2) Uinta Basin Conceptuals		(3) Other Uinta Basin Sources		(4) Piceance Basin (Colorado Sources)		(5) 1980 Baseline		Increment Consumption		Total Ambient Concentration Including 1980 Baseline (1+2+5) (1+2+3+5) (1+2+3+4+5)			
	Direct	Secondary	Direct	Secondary	Direct	Secondary	Direct	Secondary	(1+2)	(1+2+3)	(1+2+3+4)					
Population Centers																
Vernal	0-1	0-2	1-9	0-1	0	0-1	0	0-1	0	1-6	1-13	1-14	1-15	2-19	2-20	2-21
Green River	0	0	0-2	0	0	0	0	0-1	0	0-1	0-2	0-2	0-3	0-3	0-3	0-4
Rangely	0-2	0	0-2	0	0	0	0	0-3	0	0-1	0-4	0-4	0-7	0-5	0-5	0-8
Meeker	0-1	0	0-2	0	0	0	0	1-14	0-1	1-5	0-3	0-3	1-18	1-8	1-8	2-23
Craig	0-1	0	0-1	0	0	0	0	2-15	0	3-28	0-2	0-2	2-17	3-30	3-30	5-45
Glenwood Springs	0	0	0-2	0	0	0	0	1-12	0	0-2	0-2	0-2	2-14	0-4	0-4	2-16
Rifle	0-1	0	0-1	0	0	0	0	1-6	0	0-3	0-2	0-2	1-8	0-5	0-5	1-11
Parachute	0-1	0	0-2	0	0	0	0	3-25	0-5	0-3	0-3	0-3	3-33	0-6	0-6	3-36
De Beque	0-1	0	0-2	0	0	0	0	0-3	0	1-11	0-3	0-3	0-6	1-14	1-14	1-17
Grand Junction	0-1	0	1-6	0	0	0	0	0-1	0	8-82	1-7	1-7	1-8	9-89	9-89	9-90
Existing or Potential Class I Areas and Other Areas of Special Concern																
Flat Tops Wilderness	0-1	0	0-1	0	0	0	0	1-10 [†]	0	1-5	0-2	0-2	1-12 [†]	1-7	1-7	2-17
Mt. Zirkel Wilderness	0	0	0-1	0	0	0	0	0-2	0	0-1	0-1	0-1	0-3	0-2	0-2	0-4
Dinosaur National Monument	0-2	0-1	1-10	0	0	0	0	0-1	0	1-5	1-13 [§]	1-13 [§]	1-14 [§]	2-18	2-18	2-19
Colorado National Monument	0-2	0	0-4	0	0	0	0	0-1	0	4-40	0-6 [§]	0-6 [§]	0-7 [§]	4-46	4-46	4-47
Utah and Ouray Indian Reservation	2-21	0	3-34	0	0-2	0	0-3	0	0	2-23	5-55	5-57	5-60	7-78	7-80	7-83
Uinta Primitive Area	D-1	0	0-3	0	0	0	0	0	0	0-1	0-4	0-4	0-4	0-5	0-5	0-5
Class II Area Receptors with Maximum Impacts from Direct Source Emissions in Uinta Basin																
	1-7	0	4-39	0	0-1	0	0-3	0	0	0-1	5-46	5-47	5-50	5-47	5-48	5-51
Ambient Air Quality Standard or Prevention of Significant Deterioration Increment																
PSD Class I Increment	5	A	A	A	A	A	A	A	A	NA	A	A	A	NA	NA	NA
PSD Class II Increment	91	A	A	A	A	A	A	A	A	NA	A	A	A	NA	NA	NA
AQS	365	NA	NA	NA	NA	NA	NA	NA	NA	A	NA	NA	NA	A	A	A

* Note that concentration ranges, not point estimates, are provided; lower and upper bounds of predicted maximum concentration are provided.

† Indicates violation of applicable standard or increment.

A Standard or increment is applicable.

NA Standard or increment is not applicable.

§ Indicates violation of increment if monument is redesignated Class I.

TABLE 5-2 (Concluded)

(c) Annual Average SO₂ Concentrations*

Receptor	Annual Average SO ₂ Concentrations (µg/m ³)											
	(1) Uinta Basin		(2) Uinta Basin		(3) Other Uinta		(4) Piceance Basin		(5) 1980		Total Ambient Concentration Including 1980 Baseline (1+2+3+4+5)	
	Site-Specifics		Conceptuals		Basin Sources		(Colorado Sources)		(5) 1980			
	Direct	Secondary	Direct	Secondary	Direct	Secondary	Direct	Secondary	Baseline			
Population Centers												
Vernal	0	0-1	0	0	0	0	0	0	0	0-1	0-1	0-1
Green River	0	0	0	0	0	0	0	0	0	0	0	0
Rangely	0	0	0-1	0	0	0	0	0	0	0-1	0-1	0-1
Meeker	0	0	0	0	0	0	0-1	0	0	0	0	0-1
Craig	0	0	0	0	0	0	0	0	0	0	0	0
Glenwood Springs	0	0	0	0	0	0	0	0	0	0	0	0
Rifle	0	0	0	0	0	0	0-1	0	0-1	0-1	0-1	0-2
Parachute	0	0	0	0	0	0	0-1	0	0	0-1	0-1	0-2
De Beque	0	0	0	0	0	0	0-1	0	0	0-1	0-1	0-2
Grand Junction	0	0	0	0	0	0	0-1	0	0	0-1	0-9	0-10
Existing or Potential Class I Areas and Other Areas of Special Concern												
Flat Topa Wilderness	0	0	0	0	0	0	0-1	0	0	0	0	0-1
Mt. Zirkel Wilderness	0	0	0	0	0	0	0	0	0	0	0	0
Dinosaur National Monument	0	0	0-1	0	0	0	0	0	0	0-1	0-1	0-1
Colorado National Monument	0	0	0	0	0	0	0	0	0-1	0	0-1	0-1
Utah and Ouray Indian Reservation	0	0	0-2	0	0	0	0	0	0	0-2	0-2	0-2
Uinta Primitive Area	0	0	0	0	0	0	0	0	0	0	0	0
Class II Area Receptors with Maximum Impacts from Direct Source Emissions												
In Uinta Basin	0-1	0	1-3	0	0	0	0	0	0	1-4	1-4	1-4
Ambient Air Quality Standard or Prevention of Significant Deterioration Increment												
PSD Class I Increment	A	A	A	A	A	A	A	A	NA	A	NA	NA
PSD Class II Increment	A	A	A	A	A	A	A	A	NA	A	NA	NA
AAQS	NA	NA	NA	NA	NA	NA	NA	NA	A	NA	A	A

* Note that concentration ranges, not point estimates, are provided; lower and upper bounds of predicted maximum concentration are provided.

† Indicates violation of applicable standard or increment.

A Standard or increment is applicable.

NA Standard or increment is not applicable.

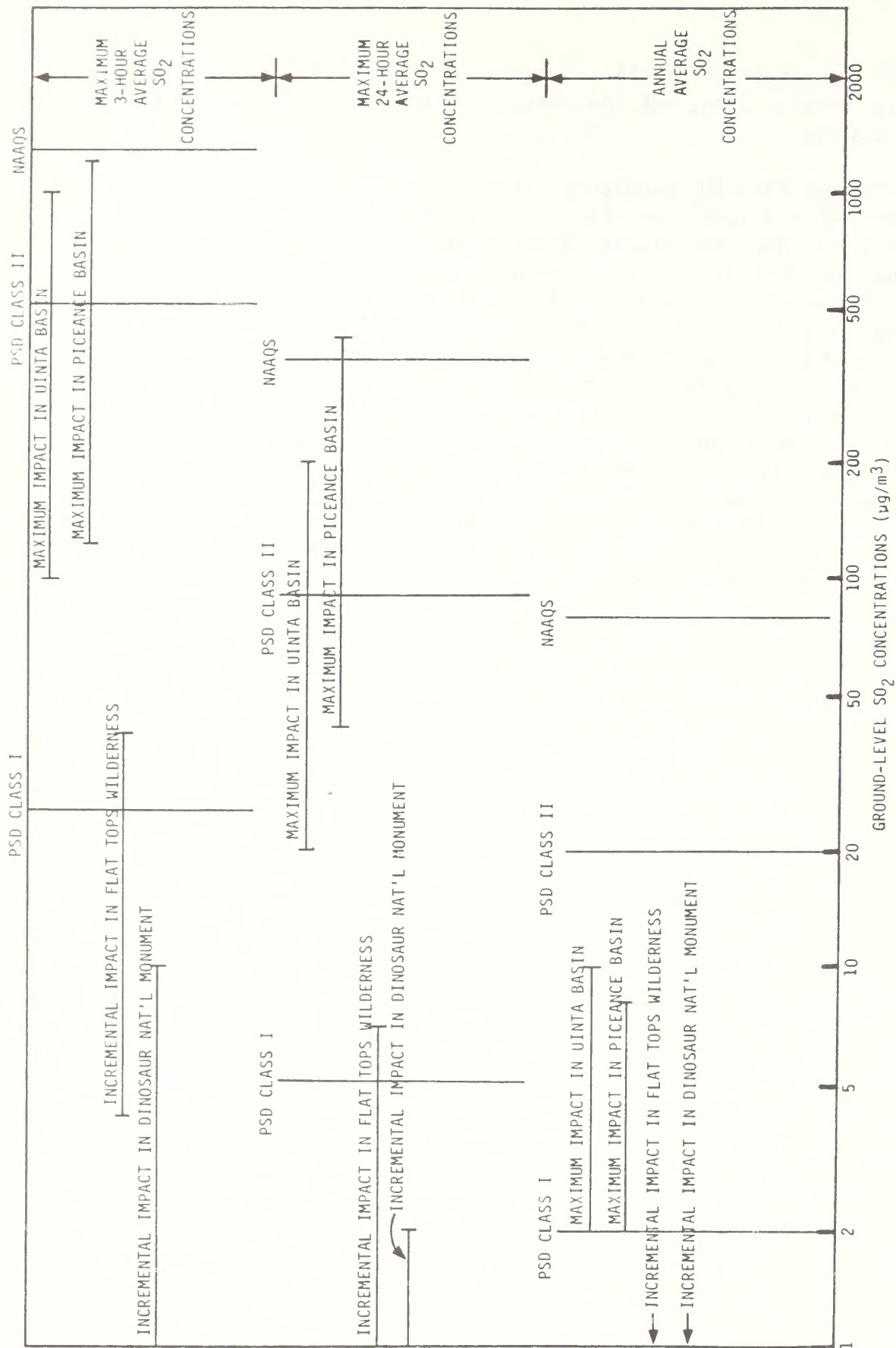
impact is the result of existing industrial or area source emissions on the Grand Junction area, not the projected emissions from the synthetic fuels industry.

In the existing SO₂ mandatory Class I area most adversely affected by the projected emissions, the Flat Tops Wilderness Area, conclusions are more ambiguous since the projected ranges of SO₂ concentrations overlap the 3-hour and 24-hour SO₂ Class I PSD increments for the high-oil-production scenario. In other words, if the upper-bound estimate were used, the Class I increments would be exceeded; if the lower-bound estimate were used, the increments would not be exceeded. Although it is our professional judgment that the conservative upper-bound estimates based on GPM calculations are considerably in excess of what the actual magnitude of impacts would be in the area, it is impossible to rigorously quantify this judgment. Given the error bounds measuring the range of uncertainty, it is our judgment that there is a small, but nonzero probability that PSD Class I increments in Flat Tops and Mt. Zirkel would be exceeded as a result of cumulative regional emissions. However, it should be pointed out that the upper-bound estimate of the impact of the Uinta Basin sources by themselves is well within the Class I increment. Piceance Basin sources, development plans for which are currently uncertain, cause most of the projected impact in Flat Tops. Indeed, the Cathedral Bluffs facility that has been recently shelved accounts for half of the increment consumption in Flat Tops.

In addition, for the high-oil-production scenario there is a similar probability that the Colorado Category I (PSD Class I) increments will be exceeded in Dinosaur National Monument. Although total impacts in Colorado National Monument are large, almost all the impact is due to existing point and area sources in the Grand Junction area that do not consume the increment. Figure 5-32 summarizes these impacts in a graphical representation.

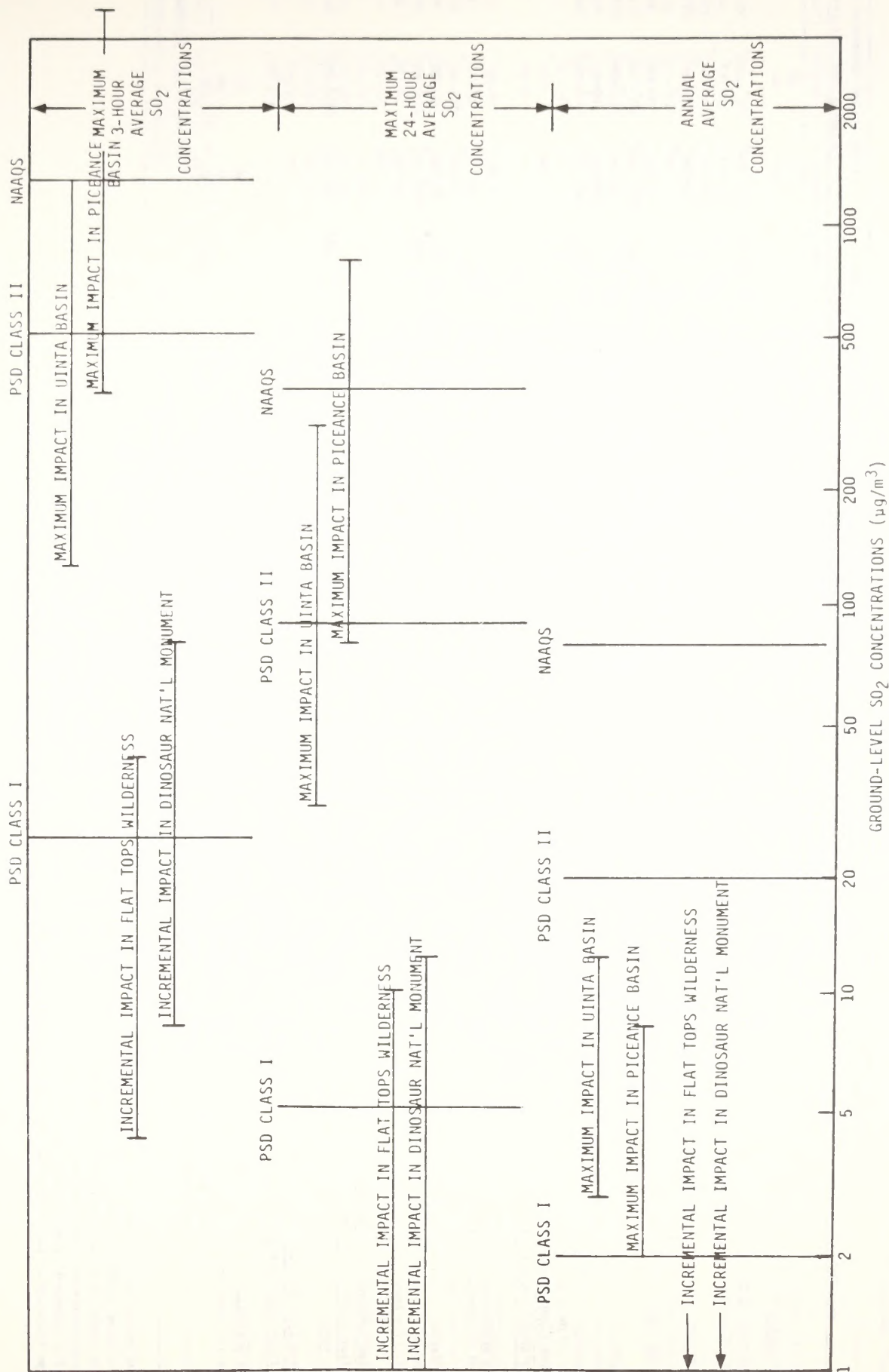
5.4.2 TSP Impacts

Tables 5-3 and 5-4 summarize the total TSP impacts of regional emission sources for several important receptor areas for the low- and high-oil-production scenarios, respectively. It is clear from these tables that secondary TSP area emission sources (principally emissions from dirt and gravel roads) dominate the total impact and that impacts in many areas will be greater than ambient air quality standards. If secondary emissions from additional vehicles on dirt roads associated with development-induced population growth are included in the PSD increment consumption, there is little doubt that PSD Class II increments for TSP will be exceeded in many areas throughout the study area. (These impacts



(a) FOR LOW-OIL-PRODUCTION SCENARIO

FIGURE 5-32. SUMMARY OF SO_2 CONCENTRATION ESTIMATES FOR VARIOUS AVERAGING TIMES COMPARED TO AIR QUALITY STANDARDS AND PSD INCREMENTS



(b) FOR HIGH-OIL-PRODUCTION SCENARIO

FIGURE 5-32 (Concluded)

TABLE 5-3. SUMMARY OF AMBIENT AIR QUALITY IMPACTS ASSOCIATED WITH THE LOW OIL PRODUCTION SCENARIO

(a) Maximum 24-hour Average TSP Concentrations*

Receptor	Maximum 24-hour Average TSP Concentrations (µg/m ³)													
	(1) Uinta Basin		(2) Uinta Basin		(3) Other Uinta Basin Sources		(4) Piceance Basin (Colorado Sources)		(5) 1980		Increment Consumption		Total Ambient Concentration	
	Site-Specifics		Conceptuals		Basin Sources		Colorado Sources		Base line		Above Baseline		Including 1980 Baseline	
	Direct	Secondary	Direct	Secondary	Direct	Secondary	Direct	Secondary	Base line	(1+2)	(1+2+3)	(1+2+3+4)	(1+2+5)	(1+2+3+4+5)
Population Centers														
Vernal	0-1	40 [†] -160 [†]	0-3	20-80 [†]	0-1	60 [†] -240 [†]	0	0	185 [†] -740 [†]	60 [†] -244 [†]	120 [†] -485 [†]	245 [†] -984 [†]	305 [†] -1225 [†]	305 [†] -1225 [†]
Green River	0	2-8	0-1	1-4	0	1-4	0	0	38-150 [†]	3-13	4-17	41-163 [†]	42-167 [†]	42-167 [†]
Rangely	1-5	60 [†] -240 [†]	0	30-120 [†]	0-2	30-120 [†]	0-3	120 [†] -480 [†]	135-540 [†]	91 [†] -365 [†]	121 [†] -487 [†]	226 [†] -905 [†]	256 [†] -1027 [†]	376 [†] -1510 [†]
Meeker	0-1	0	0	0	0-1	0	2-17	140 [†] -560 [†]	110-440 [†]	0-1	0-2	110-441 [†]	110-442 [†]	252 [†] -1019 [†]
Craig	0	0	0-1	0	0	0	1-13	10-40 [†]	190 [†] -760 [†]	0-1	0-1	190 [†] -761 [†]	190 [†] -761 [†]	201 [†] -814 [†]
Glenwood Springs	0	0	0	0	0	0	0-3	30-120 [†]	110-450 [†]	0	0	110-450 [†]	110-450 [†]	140-573 [†]
Rifla	0-1	0	0	0	0	0	1-6	60 [†] -240 [†]	300 [†] -1200 [†]	0-1	0-1	300 [†] -1201 [†]	300 [†] -1201 [†]	361 [†] -1447 [†]
Parachuta	0	0	0	0	0	0	0-4	80 [†] -320 [†]	235 [†] -940 [†]	0	0	235 [†] -940 [†]	235 [†] -940 [†]	315 [†] -1264 [†]
De Beque	0-1	0	0	0	0	0	0-4	40 [†] -160 [†]	120 [†] -480 [†]	0-1	0-1	120-481 [†]	120-481 [†]	160 [†] -645 [†]
Grand Junction	0-1	0	0-1	0	0	0	0-4	70 [†] -280 [†]	310 [†] -1200 [†]	0-2	0-2	310 [†] -1202 [†]	310 [†] -1202 [†]	380 [†] -1486 [†]
Existing or Potential Class I Areas and Other Areas of Special Concern														
Flat Tops Wilderness	0	0	0-1	0	0	0	2-17 [†]	13 [†] -52 [†]	75-300 [†]	0-1	0-1	75-301 [†]	75-301 [†]	90-370 [†]
Mt. Zirkel Wildmaas	0	0	0	0	0	0	0-4	6-24 [†]	30-110 [†]	0	0	30-110	30-110	36-138
Dinosaur National Monument	0-1	15 [†] -60 [†]	0-3	5-20 [†]	0-1	20 [†] -80 [†]	0-2	0	100-400 [†]	21-84 [†]	41 [†] -165 [†]	121-484 [†]	141-565 [†]	141-567 [†]
Colorado National Monument	0-1	0	0-1	0	0	0	0-4	15 [†] -60 [†]	80-320 [†]	0-2	0-2	80-322 [†]	80-322 [†]	95-386 [†]
Utah and Ouray Indian Reservation	2-21	30-120 [†]	13-131 [†]	10-40 [†]	0-2	35-140 [†]	0-2	0	125-500 [†]	55 [†] -312 [†]	90 [†] -454 [†]	180 [†] -812 [†]	215 [†] -954 [†]	215 [†] -956 [†]
Uinta Primitive Area	0-1	0	0	0	0	0	0	0	25-110	0-1	0-1	25-111	25-111	25-111
Class II Area Receptors with Maximum														
Impacts from Direct Source Emissions in Uinta Basin														
2-21	30-120 [†]	13-131 [†]	10-40	35-140 [†]	0-2	0	0-2	55 [†] -312 [†]	125-500 [†]	90 [†] -454 [†]	180 [†] -812 [†]	215 [†] -953 [†]	215 [†] -956 [†]	215 [†] -956 [†]

* Note that concentration ranges, not point estimates, are provided; lower and upper bounds of predicted maximum concentration are provided.

† Indicates violation of applicable standard or increment.

A Standard or increment is applicable.

NA Standard or increment is not applicable.

§ Indicates violation of increment if monument is redesignated Class I.

TABLE 5-3 (Concluded)

(b) Annual Average TSP Concentrations*

Receptor	Annual Average TSP Concentrations ($\mu\text{g}/\text{m}^3$)									
	(1) Uinta Basin		(2) Uinta Basin		(3) Other Uinta		(4) Piceance Basin		(5) 1980	
	Site-Specifics		Conceptuals		Basin Sources		(Colorado Sources)		Baseline	
	Direct	Secondary	Direct	Secondary	Direct	Secondary	Direct	Secondary	Baseline	Secondary
Population Centers										
Vernal	0	10-40†	0	3-12	0	15-60†	0	0	45-180†	13-52†
Green River	0	0-1	0	0	0	1-2	0	0	10-40	0-1
Rangely	0-1	10-40†	0	5-20†	0	10-40†	0	30†-120†	30-120†	15-61†
Meeker	0	0	0	0	0	0	1-5	30†-120†	30-120†	0
Craig	0	0	0	0	0	0	0-1	3-12	45-180†	0
Glenwood Springs	0	0	0	0	0	0	0	4-16	30-120†	0
Rifle	0	0	0	0	0	0	0-1	15-60†	70†-280†	0
Parachute	0	0	0	0	0	0	0-1	20†-80†	55-220†	0
De Beque	0	0	0	0	0	0	0-1	8-32†	30-120†	0
Grand Junction	0	0	0	0	0	0	0-1	20†-80†	70†-280†	0
Existing or Potential Class I Areas and Other Areas of Special Concern										
Flat Tops Wilderness	0	0	0	0	0	0	0-1	3-10†	20-80†	0
Mt. Zirkel Wilderness	0	0	0	0	0	0	0	1-4	10-40	0
Dinosaur National Monument	0	4-16§	0	2-8§	0	5§-20†	0	0	25-100†	6§-24†
Colorado National Monument	0	0	0	0	0	0	0-1	4-16§	20-80†	0
Utah and Durray Indian Reservation	0-1	5-20†	1-6	2-8	0	6-24†	0	0	35-140†	8-35†
Uinta Primitive Area	0	0	0	0	0	0	0	0	10-40	0
Class II Area Receptors with Maximum Impacts from Direct Source Emissions in Uinta Basin										
PSD Class I Increment	5	A	A	A	A	A	A	A	NA	A
PSD Class II Increment	19	A	A	A	A	A	A	A	NA	A
AAQS	60, 75	NA	NA	NA	NA	NA	NA	NA	A	A
Ambient Air Quality Standard or Prevention of Significant Deterioration Increment										
PSD Class I Increment	5	A	A	A	A	A	A	A	NA	A
PSD Class II Increment	19	A	A	A	A	A	A	A	NA	A
AAQS	60, 75	NA	NA	NA	NA	NA	NA	NA	A	A

* Note that concentration ranges, not point estimates, are provided; lower and upper bounds of predicted maximum concentration are provided.

† Indicates violation of applicable standard or increment.

A Standard or increment is applicable.

NA Standard or increment is not applicable.

§ Indicates violation of increment if monument is redesignated Class I.

TABLE 5-4. SUMMARY OF AMBIENT AIR QUALITY IMPACTS ASSOCIATED WITH THE HIGH OIL PRODUCTION SCENARIO

(a) Maximum 24-hour Average TSP Concentrations*

Maximum 24-hour Average TSP Concentrations (µg/m ³)													
Receptor	(1) Uinta Basin		(2) Uinta Basin		(3) Other Uinta		(4) Piceance Basin		(5) 1980		Total Ambient Concentration		
	Sita-Specifics		Conceptuals		Basin Sources		(Colorado Sources)		Baseline		Including 1980 Baseline		
	Direct	Secondary	Direct	Secondary	Direct	Secondary	Direct	Secondary	Baseline	Above Baseline	(1+2+5)	(1+2+3+4+5)	
Population Centers													
Vernal	0-2	125 [†] -500 [†]	1-14	60 [†] -240 [†]	0-1	60 [†] -240 [†]	0	0	185 [†] -740 [†]	186 [†] -756 [†]	246 [†] -997 [†]	371 [†] -1496 [†]	431 [†] -1737 [†]
Green River	0-1	3-12	0-4	2-8	0	1-4	0	0	38-150	5-25	6-29	43-175 [†]	44-179 [†]
Rangely	1-12	60 [†] -240 [†]	2-17	30-120 [†]	0-2	30-120 [†]	1-10	130 [†] -520 [†]	135-540 [†]	93 [†] -389 [†]	123 [†] -509 [†]	228 [†] -929 [†]	389 [†] -1579 [†]
Meeker	0-2	0	0-3	0	0-1	0	7-70 [†]	140 [†] -560 [†]	110-440 [†]	0-5	0-6	110-445 [†]	257 [†] -1076 [†]
Craig	0-1	0	0	0	0	0	2-20	10-40 [†]	190 [†] -760 [†]	0-1	0-1	190 [†] -761 [†]	202 [†] -821 [†]
Glenwood Springs	0-1	0	0	0	0	0	1-10	40 [†] -160 [†]	110-450 [†]	0-1	0-1	110-451 [†]	151 [†] -621 [†]
Rifle	0-1	0	0	0	0	0	2-20	100 [†] -400 [†]	300 [†] -1200 [†]	0-1	0-1	300 [†] -1201 [†]	402 [†] -1621 [†]
Parachute	0-1	0	0-3	0	0	0	1-10	135 [†] -540 [†]	235 [†] -940 [†]	0-4	0-4	235 [†] -944 [†]	371 [†] -1494 [†]
De Beque	0-1	0	1-6	0	0	0	1-10	60 [†] -240 [†]	120-480 [†]	1-7	1-7	121-487 [†]	182 [†] -737 [†]
Grand Junction	0-1	0	1-6	0	0	0	1-10	120 [†] -480 [†]	310 [†] -1200 [†]	1-7	1-7	311 [†] -1207 [†]	432 [†] -1697 [†]
Existing or Potential Class I Areas and Other Areas of Special Concern													
Flat Tops Wilderness	0-1	0	0-1	0	0	0	2-17 [†]	22 [†] -88 [†]	75-300 [†]	0-2	0-2	75-302 [†]	99-407 [†]
Mt. Zirkel Wilderness	0-1	0	0-1	0	0	0	0-4	10 [†] -40 [†]	30-110	0-2	0-2	30-112	40-156 [†]
Dinosaur National Monument	1-6	40 [†] -60 [†]	3-30 [§]	20 [§] -80 [†]	0-1	20 [§] -80 [†]	0	0	100-400 [†]	64 [†] -276 [†]	84 [†] -357 [†]	164 [†] -676 [†]	184 [†] -757 [†]
Colorado National Monument	0-2	0	1-7	0	0	0	1-10 [§]	30 [§] -120 [†]	80-320 [†]	1-9	1-9	81-329 [†]	112-459 [†]
Utah and Ouray Indian Reservation	17-171 [†]	70 [†] -280 [†]	45 [†] -453 [†]	36-140 [†]	0-2	35-140 [†]	1-10	0	125-500 [†]	167 [†] -1044 [†]	202 [†] -1186 [†]	292 [†] -1544 [†]	328 [†] -1696 [†]
Uinta Primitive Area	0-1	0	0-4	0	0	0	0	0	25-110	0-5	0-5	25-115	25-115
Class II Area Receptors with Maximum Impacts from Direct Source Emissions in Uinta Basin													
	1-11	70 [†] -280 [†]	61-613 [†]	35-140 [†]	0-1	35-140 [†]	1-10	0	90-360 [†]	167 [†] -1044 [†]	203 [†] -1185 [†]	257 [†] -1404 [†]	293 [†] -1545 [†]
Ambient Air Quality Standard or Prevention of Significant Deterioration Increment													
PSD Class I Increment	A	A	A	A	A	A	A	A	NA	A	A	NA	NA
PSD Class II Increment	A	A	A	A	A	A	A	A	NA	A	A	NA	NA
AAQS	NA	NA	NA	NA	NA	NA	NA	NA	A	NA	NA	A	A

* Note that concentration ranges, not point estimates, are provided;
† lower and upper bounds of predicted maximum concentration are provided.
‡ Indicates violation of applicable standard or increment.
§ Standard or increment is not applicable.
NA Standard or increment is not applicable.
§ Indicates violation of increment if monument is redesignated Class I.

(b)(6) Annual Average TSP Concentrations*

[illegible]

6 Indicates violation of increment if monument is redesignated Class I.
Increases of increments are not applicable.

could possibly be mitigated by paving these roads.) If just the direct TSP emissions from the synthetic fuel facilities are considered to consume the PSD increment, and secondary emissions are excluded, it is quite likely that PSD Class I and II increments for TSP will not be consumed or exceeded in the region except for the potential problems near Sohio's conceptual tar sands facility noted in Section 5.2. Figure 5-33 summarizes these impacts.

5.5 PHOTOCHEMICAL SMOG

The photochemical conversion of emissions of hydrocarbons and nitrogen oxides is a potential air quality concern because elevated concentrations of ozone (O_3) and other reactive species might exceed the one-hour ambient air quality standard of $240 \mu\text{g}/\text{m}^3$ (0.12 ppm). The impact of direct and secondary emissions from oil shale development and associated population growth was evaluated by means of the Empirical Kinetics Modeling Approach (EKMA) for the two trajectories shown in figure 5-15. These trajectories pass through the areas of maximum oil shale development.

Meteorological conditions were selected to represent a hypothetical, worst-case event associated with a shallow mixed layer (250 m in the morning to 1500 m in the afternoon) on a summer day (27 July). Because of the relatively limited sample of background concentration data for the study region, we decided to analyze two background air quality conditions recommended by Killus and Whitten (1981). The high-concentration background condition is more representative of urban areas, and the low-concentration background condition is representative of rural areas. The Rio Blanco and Garfield county areas and existing point source emissions were assumed to be concentrated along the trajectory paths shown in figure 5-34, while the Uintah County area and existing point source emissions were assumed to be spread out over the entire county. Thus, the land areas used to determine emission densities are as follows:

Uintah	--	$1.16 \times 10^{10} \text{ m}^2$	(county area)
Rio Blanco	--	$2.88 \times 10^9 \text{ m}^2$	(20-km x 144-km strip)
Garfield	--	$2.8 \times 10^9 \text{ m}^2$	(20-km x 140-km strip)

Emissions from oil shale developments were distributed over smaller regions:

Uintah (trajectory 1)	--	$1.12 \times 10^9 \text{ m}^2$	(20-km x 56-km strip)
Uintah (trajectory 2)	--	$1.2 \times 10^9 \text{ m}^2$	(20-km x 60-km strip)
Rio Blanco	--	$8 \times 10^8 \text{ m}^2$	(20-km x 40-km strip)
Garfield	--	$1.04 \times 10^9 \text{ m}^2$	(20-km x 52-km strip)

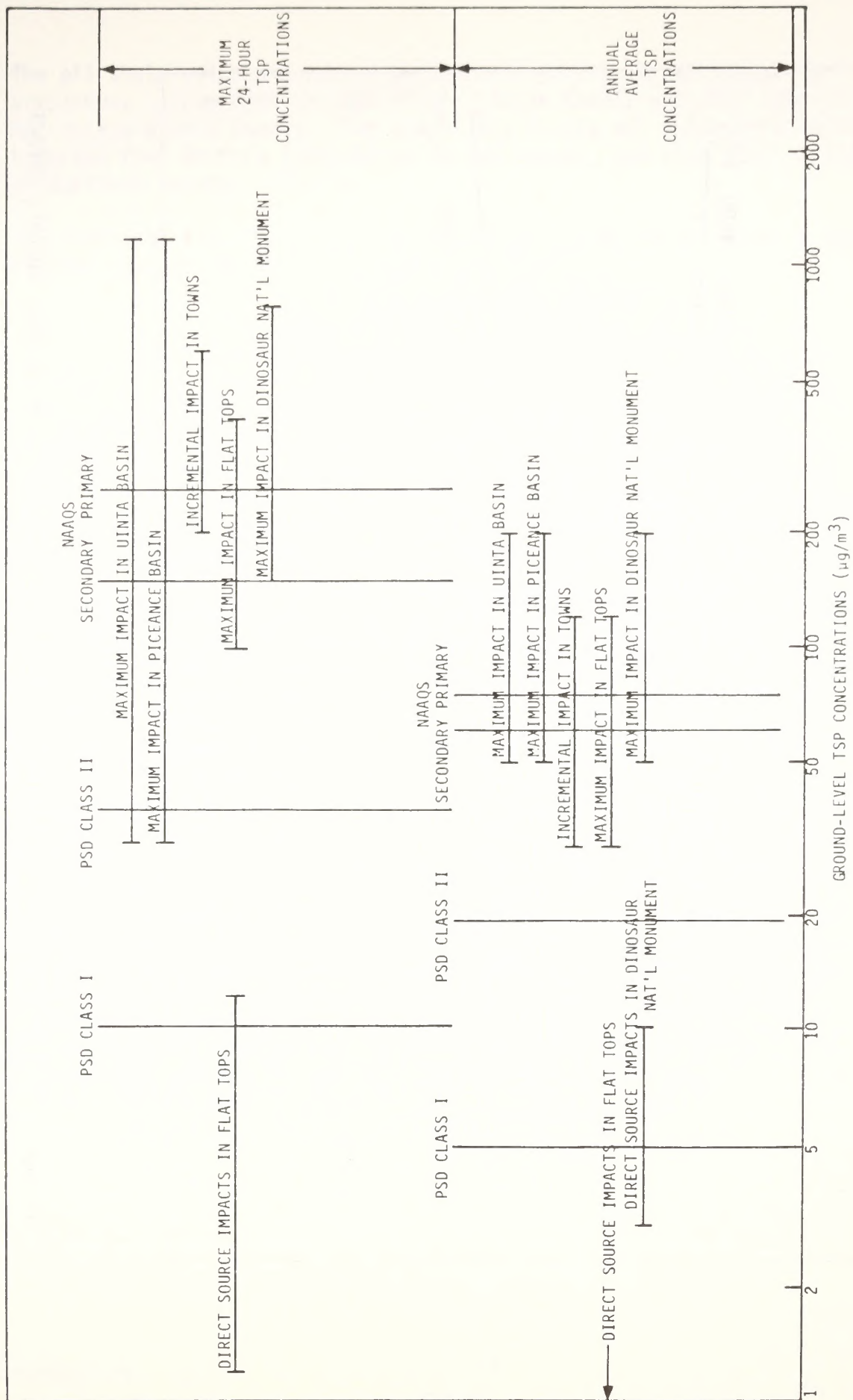


FIGURE 5-33. SUMMARY OF TSP CONCENTRATION ESTIMATES FOR VARIOUS AVERAGING TIMES COMPARED TO AMBIENT AIR QUALITY STANDARDS AND PSD INCREMENTS FOR BOTH THE LOW AND HIGH OIL PRODUCTION SCENARIOS

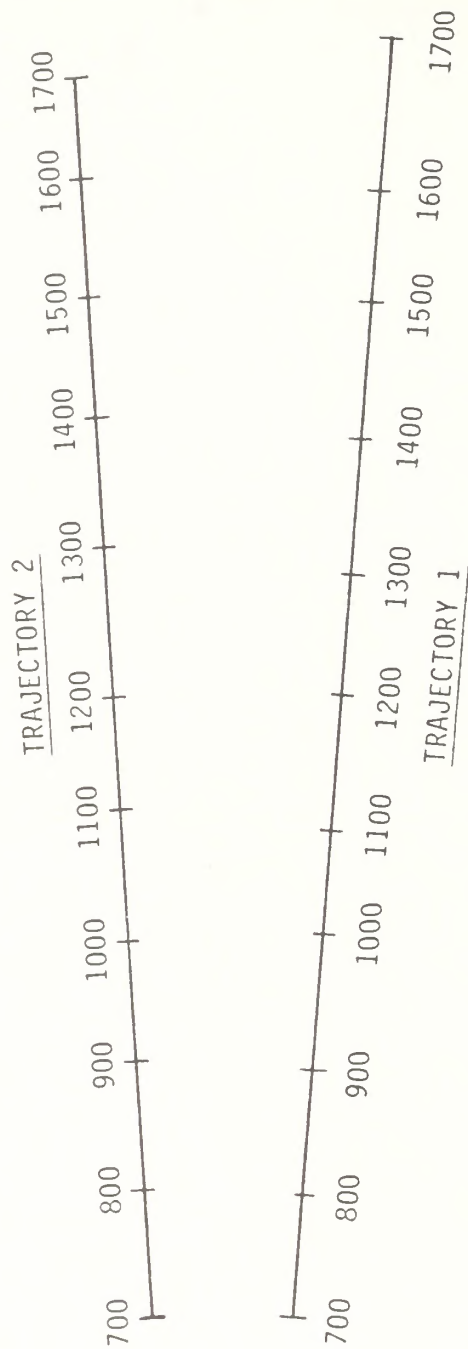


FIGURE 5-34. TWO TRAJECTORIES MODELED FOR WORST-CASE PHOTOCHEMICAL OXIDANT (OZONE) IMPACT

Note: Reader can use clear plastic overlay (see back cover) to indicate locations of sources and counties.

The oil shale emissions were injected into an air parcel following trajectory 1 from 0800 to 1000 MST in Uintah County and from 1200 to 1400 MST in Rio Blanco County. For trajectory 2, the oil shale emissions were injected from 0800 to 1000 MST in Uintah County, and from 1300 to 1500 MST in Garfield County.

The EKMA trajectory model was used to examine three emission scenarios for each of the two trajectories:

- (1) 1980 baseline
- (2) Low-oil-production scenario
- (3) High-oil-production scenario.

For each emission scenario, we used each of the two background air quality conditions discussed previously.

Tables 5-5 and 5-6 show the results obtained exercising the EKMA trajectory model for the three emission scenarios described. Table 5-5 shows the results for trajectory 1, and table 5-6 shows the results for trajectory 2; both trajectories give similar results for ozone and NO₂.

For both the high- and low-background air quality conditions, results indicate that oil shale development does not lead to exceedance of the ozone standard of 0.12 ppm. Because the oil shale emission rates are low, background air quality conditions tend to dominate these simulations.

5.6 VISIBILITY IMPAIRMENT

Some visibility impairment will occur as a result of emissions from oil shale facilities of particulate matter, sulfur dioxide (which is converted in the atmosphere to sulfate aerosol), and nitric oxide (which is converted to nitrogen dioxide). Particulate matter (both primary emissions and secondary aerosol) scatters light and thereby causes white or gray plumes, reduces the contrast of terrain features, and reduces visual range. Nitrogen dioxide discolors the sky, causing yellow or brown hazes. As noted in Section 3, the judgment as to whether projected emissions are adverse is subjective since there are no specific criteria for such adversity judgments, which are made by the federal land managers and the states.

TABLE 5-5. SUMMARY OF EKMA RESULTS FOR TRAJECTORY 1

(a) High Concentration Background

<u>Species</u>	<u>1980 Baseline Scenario</u>	<u>Low Oil- Production Scenario</u>	<u>High Oil- Production Scenario</u>
O ₃ (ppm)	0.066	0.078	0.077
NO ₂ (ppm)	0.0024	0.0038	0.0055
Sulfur aerosol (μg/m ³)	0.323	1.07	1.34
Organic nitrate (μg/m ³)	1.55	2.22	2.21

(b) Low Concentration Background

<u>Species</u>	<u>1980 Baseline Scenario</u>	<u>Low Oil- Production Scenario</u>	<u>High Oil- Production Scenario</u>
O ₃ (ppm)	0.042	0.048	0.042
NO ₂ (ppm)	0.00054	0.0034	0.0053
Sulfur aerosol (μg/m ³)	0.213	0.748	0.700
Organic nitrate (μg/m ³)	0.518	0.974	0.703

TABLE 5-6. SUMMARY OF EKMA RESULTS FOR TRAJECTORY 2

(a) High Concentration Background

<u>Species</u>	<u>1980 Baseline Scenario</u>	<u>Low Oil- Production Scenario</u>	<u>High Oil- Production Scenario</u>
O ₃ (ppm)	0.067	0.074	0.079
NO ₂ (ppm)	0.0024	0.0025	0.0046
Sulfur aerosol (μg/m ³)	0.333	0.813	1.58
Organic nitrate (μg/m ³)	1.60	2.01	2.29

(b) Low Concentration Background

<u>Species</u>	<u>1980 Baseline Scenario</u>	<u>Low Oil- Production Scenario</u>	<u>High Oil- Production Scenario</u>
O ₃ (ppm)	0.043	0.051	0.049
NO ₂ (ppm)	0.00054	0.0014	0.0042
Sulfur aerosol (μg/m ³)	0.235	0.759	1.16
Organic nitrate (μg/m ³)	0.585	1.07	1.03

We performed an EPA Level-1 visibility screening analysis (Latimer and Ireson, 1980) for each of the synthetic fuel facilities in the study region. Screening was done for maximum emissions from each facility associated with the high oil production scenario. Screening was performed for the only existing mandatory Class I area in the study region, the Flat Tops Wilderness Area; for two potential Class I areas, the Dinosaur and Colorado National monuments; and two other areas of special concern, the Uintah/Ouray Indian Reservation and the Uinta Primitive Area.

The Level-1 analysis allows one to determine the likelihood that visibility impairment will be considered to be adverse. This analysis functions as a screening test in that it overestimates (by design) impacts to the extent that if the test is passed, there is little possibility that significant visibility impairment will take place.

Level-1 screening contrast parameters (C_1 , C_2 , C_3) were calculated to indicate potential problems for three scenarios: a dark (NO_2) plume visible against the sky, a light (particulate) plume visible against terrain, and regional reductions in terrain/sky contrast and visual range. Appendix D summarizes the results. If any of these contrast parameters is greater or less than -0.1, a potentially adverse problem cannot be ruled out.

This screening analysis suggests that the possibility of adverse visibility impairment due to the Uinta Basin sources on Flat Tops can be ruled out, although the screening identifies several proposed oil shale facilities in Colorado that could cause potentially adverse visibility impairment in this existing mandatory Class I area. The screening identified, however, that adverse impacts in Dinosaur National Monument, a potential Class I area, cannot be ruled out as a result of emissions from Moon Lake and White River, both existing or other (interrelated) projects in the Uinta Basin; Syntana, a site-specific Uinta Basin project; and Sohio, a Uinta Basin conceptual. Similar, potential problems were also indicated by screening to occur in the Uintah/Ouray Indian Reservation, an area of special concern which is very close to several of the proposed Uinta Basin facilities. Potential visual impacts identified by the screening are associated with the perceptibility of nitrogen dioxide or particulate plumes during worst-case, stable, light-wind meteorological conditions. In addition to these potential plume discoloration (so-called plume blight) concerns in these areas close to the Uinta Basin sources, Level-1 screening identified that, although Uinta Basin sources, both separately and together would not cause potentially adverse regional reduction in visual range, all regional emissions, including Colorado sources, could do so. (The third screening test gave C_3 values of 0.09, 0.06, and 0.14, respectively, for the cumulative Uinta Basin, Piceance Basin, and combined emissions for the high-oil-production scenario.)

To investigate these potential local plume discoloration and regional haze (visual range reduction) problems, we performed more detailed (and less conservative) Level-2 and Level-3 analyses for

- > Worst-case plume discoloration due primarily to nitrogen oxide emissions.
- > Worst-case incremental contributions to regional haze.

5.6.1 Plume Discoloration

An analysis of the magnitude and frequency of occurrence of plume visual impact (a Level-3 analysis) was performed. It was reasoned that although the Level-1 screening test identified potential problems with both nitrogen oxide (C_1) and particulate (C_2) plumes, the principal plume visual impact will be associated with the former. Particle emissions from scattered, ground-level fugitive dust sources within a synfuel facility are expected to be in a size range having large settling velocities and low light-scattering efficiencies. Therefore, ground-level particulates from fugitive dust sources will probably not be a significant visual impact in the region, although the possibility of local dust clouds being perceptible at the development sites cannot be ruled out. The most likely visual impact associated with individual plumes from facilities is yellow or brown discoloration resulting from atmospheric conversion of emissions of nitric oxide to nitrogen dioxide, a dark brown gas. Near-source, quite perceptible visual impacts caused by this colored gas are probable. Nitrogen oxide is emitted in hot flue gas emissions from stacks at synfuel facilities, along with some particulate and SO_2 emissions. The stack emission rates of the largest of the Uinta Basin synfuel facilities are similar to those of a modern, well-controlled 300 Mwe coal-fired power plant. Experience with existing power plants of this size suggests that yellow or brown plume discoloration will be perceptible during stable, light-wind conditions that occur most frequently in the morning.

The magnitude of plume discoloration for each of the Uinta Basin sources was evaluated using PLUVUE (see Appendix C) for three worst-case meteorological scenarios. These scenarios assume that a plume is transported within a 22.5° sector centered on the observer with a 2.5 meter per second wind and D, E, and F stability conditions. Table 5-7 provides values of the plume perceptibility parameter, $\Delta E(L \cdot a \cdot b^*)$, calculated for observers located in Dinosaur National Monument and on the Uintah/Ouray Indian Reservation. Various studies suggest that plume discoloration will be perceptible when ΔE is greater than 1 to 4.

TABLE 5-7. MAGNITUDE $[\Delta E(L^*a^*b^*)]$ OF PLUME DISCOLORATION

(a) Observed in Dinosaur National Monument

Emission Source	Distance (km)	Dispersion Condition*		
		F, 2.5 m/s	E, 2.5 m/s	D, 2.5 m/s
Enercor-Mono Power	80	0.6	0.3	0.2
Geokinetics				
Agency Draw	80	1.0	0.6	0.3
LOFRECO	60	0.3	0.2	0.1
Magic Circle	60	4.2	3.1	1.7
Moon Lake 1 & 2	40	10.5	8.3	4.9
Paraho	50	2.4	1.8	1.0
Sohio	20	1.6	1.4	1.1
Syntana	40	3.9	3.1	1.8
Tosco	50	4.0	2.9	1.6
White River	50	4.2	3.1	1.7

TABLE 5-7 (Concluded)

(b) Observed in the Uintah/Ouray Indian
Reservation

Emission Source	Distance (km)	Dispersion Condition*		
		F, 2.5 m/s	E, 2.5 m/s	D, 2.5 m/s
Enercor-Mono Power	40	0.6	0.5	0.3
Geokinetics				
Agency Draw	40	1.1	0.9	0.5
LOFRECO	20	0.3	0.2	0.1
Magic Circle	10	4.2	3.3	2.7
Moon Lake 1 & 2	10	8.9	8.0	6.7
Paraho	30	2.5	2.1	1.4
Sohio	30	1.7	1.4	0.9
Syntana	30	3.9	3.3	2.1
Tosco	10	3.1	2.8	2.5
White River	30	4.3	3.6	2.4

* Worst-case dispersion scenario with low wind speed and transport within 22.5° sector directly toward the observer.

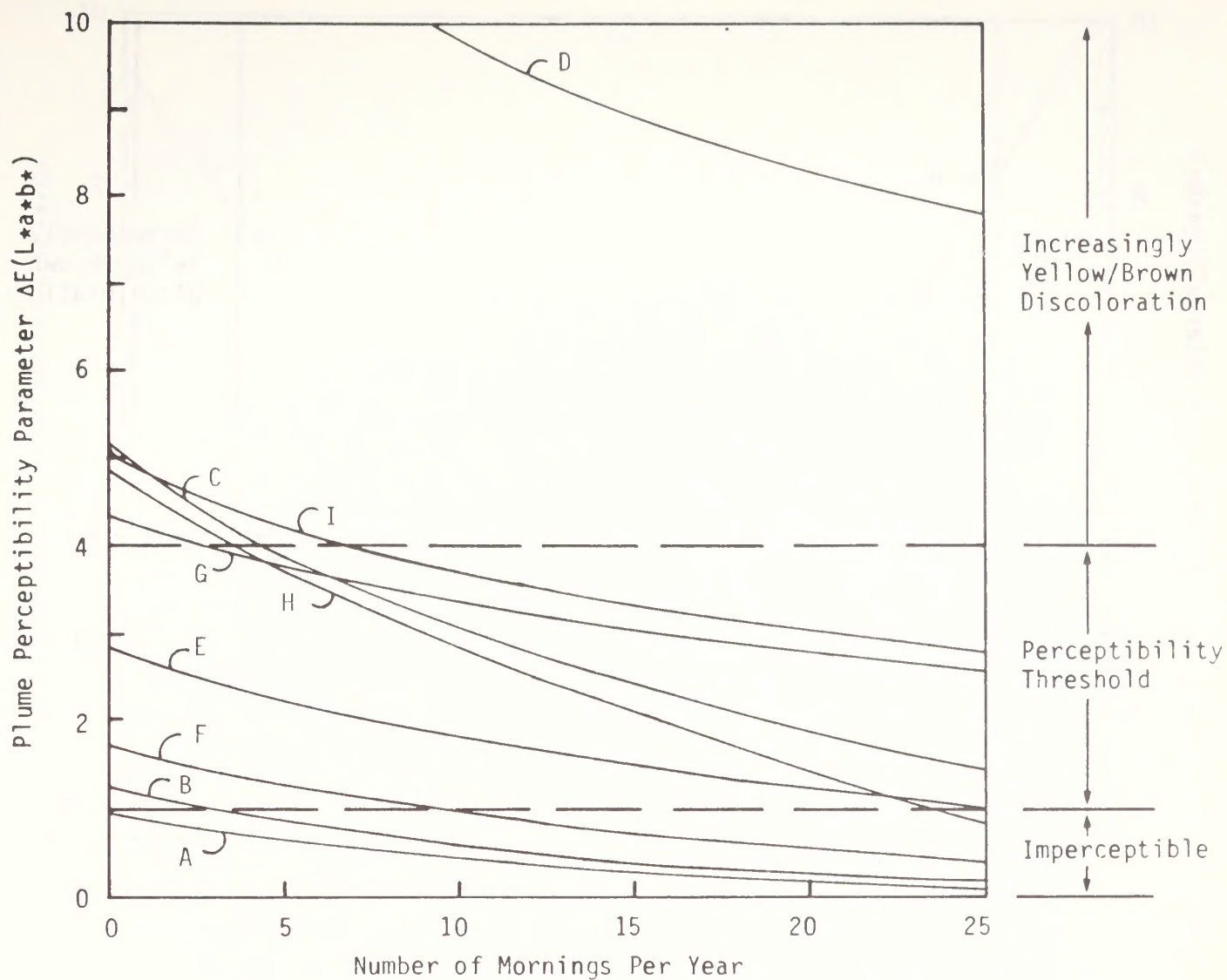
The frequency with which these worst-case meteorological conditions would occur and the resulting visual impacts would be perceived was estimated using upper-air meteorological data collected at effective stack height near the Moon Lake Power Plant (Burns & McDonnell, 1980). These pibal and radiosonde measurements were made twice daily, one-half hour after sunrise and at 2:00 p.m. LST, every other day for the period October 1976 through January 1978. Although the year 1977 may be atypical because of drought conditions, it is believed that this data base is most representative of stability conditions at plume height for the Uinta Basin synfuel facilities. Figures 5-35 and 5-36 show cumulative frequencies of ΔE at Dinosaur and the reservation. Depending on whether one selects a ΔE of 1 or 4 as the perceptibility threshold, plumes are predicted to be visible from one or more synfuel facilities at Dinosaur or the reservation from about 5 to 50 mornings per year. Impacts in the afternoon are much less frequent. It should be noted that the magnitude and frequency of occurrence of plume discoloration from the Moon Lake Power Plant will be much greater than that resulting from a single synfuel facility. However, because there may be a number of discolored plumes visible at any one time from the Uinta Basin synfuel facilities, it is difficult to judge whether the adversity of perceived plume visual impact of the many synfuel facilities will be greater or less than the single plume from the Moon Lake Power Plant.

One final caveat is in order with regard to these estimates. A recent intensive field measurement program in the vicinity of a large coal-fired power plant suggests that the PLUVUE model reasonably accurately predicts observed plume discoloration. However, there is considerable uncertainty in individual model calculations and the model tends to overpredict, on the average, by a factor of two (Bergstrom et al., 1981).

5.6.2 Regional Haze

Worst-case impacts of regional emissions on visual range would be seen with the simultaneous occurrence of

- > Low wind speeds (stagnant conditions).
- > Low mixing heights.
- > High insolation (to maximize sulfate aerosol formation rates).
- > Wind directions that permit an air parcel to pick up emissions from many sources.

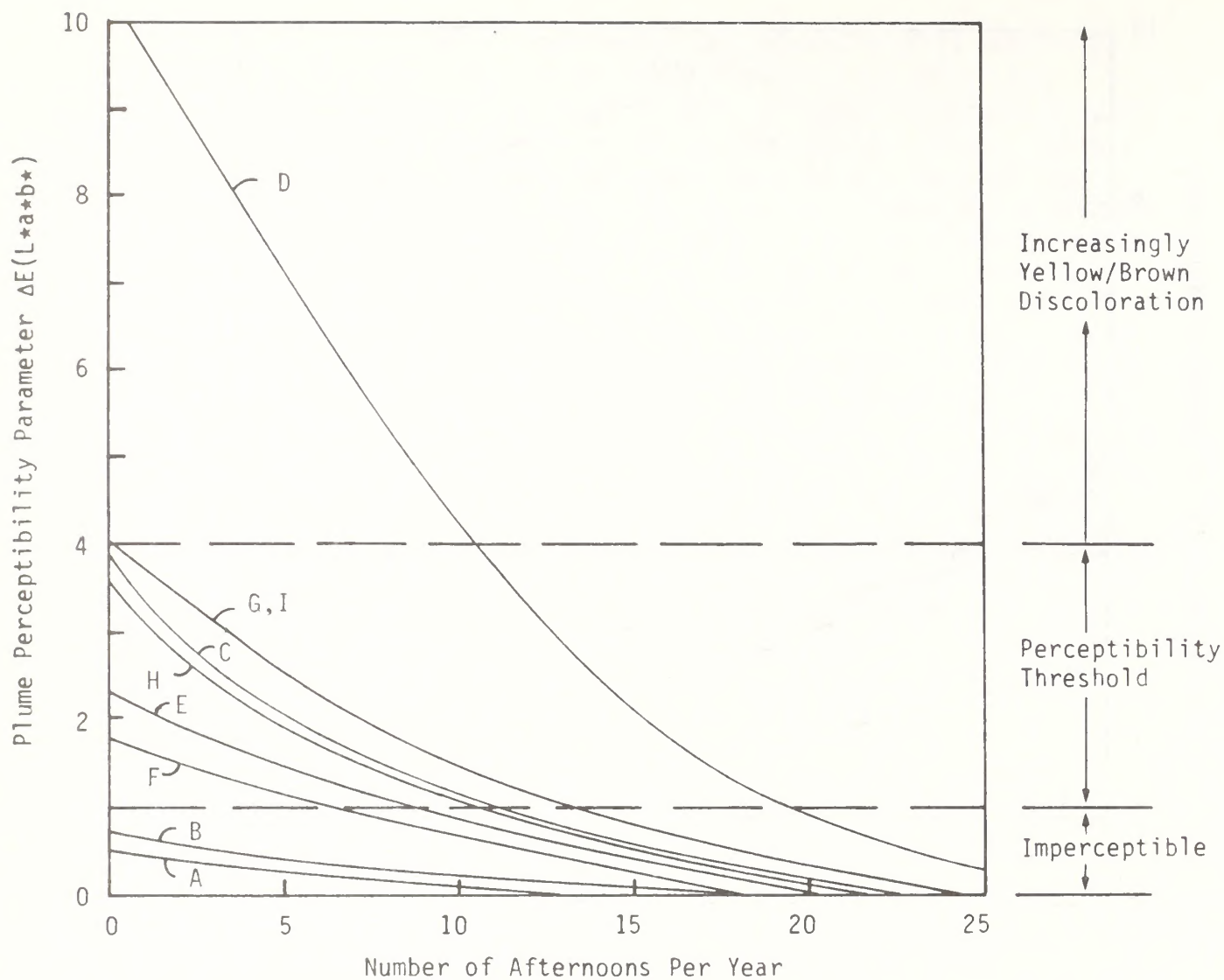


Key to Emission Sources:

- A - Enercor-Mono Power
- B - Geokinetics
- C - Magic Circle
- D - Moon Lake Power Plant Units 1 and 2
- E - Paraho
- F - Sohio
- G - Syntana
- H - Tosco
- I - White River

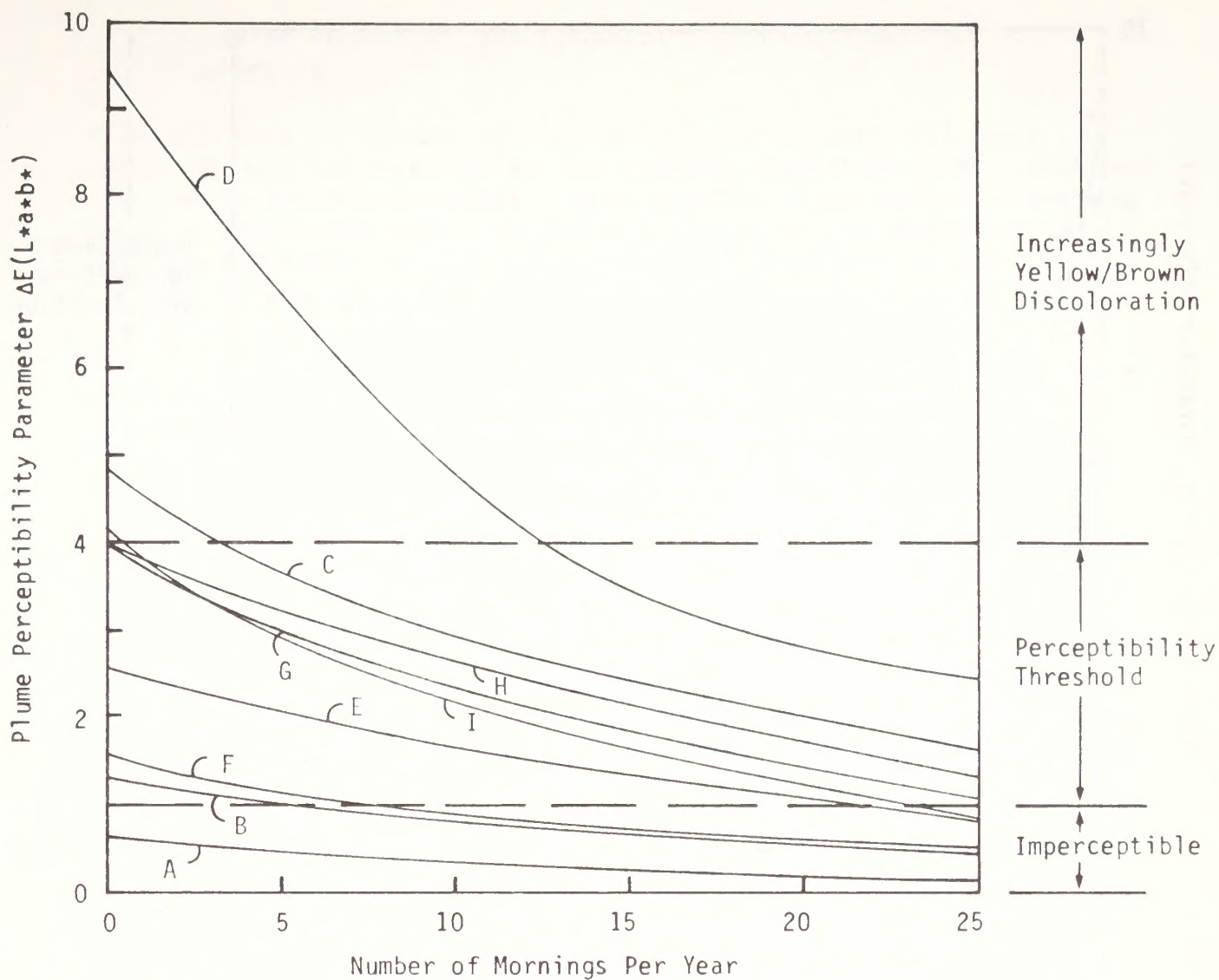
(a) Morning impacts

FIGURE 5-35. CUMULATIVE FREQUENCY OF PERCEPTIBLE PLUME DISCOLORATION RESULTING FROM EMISSIONS FROM VARIOUS UINTA BASIN SOURCES AT DINOSAUR NATIONAL MONUMENT



(b) Afternoon impacts

FIGURE 5-35 (Concluded)

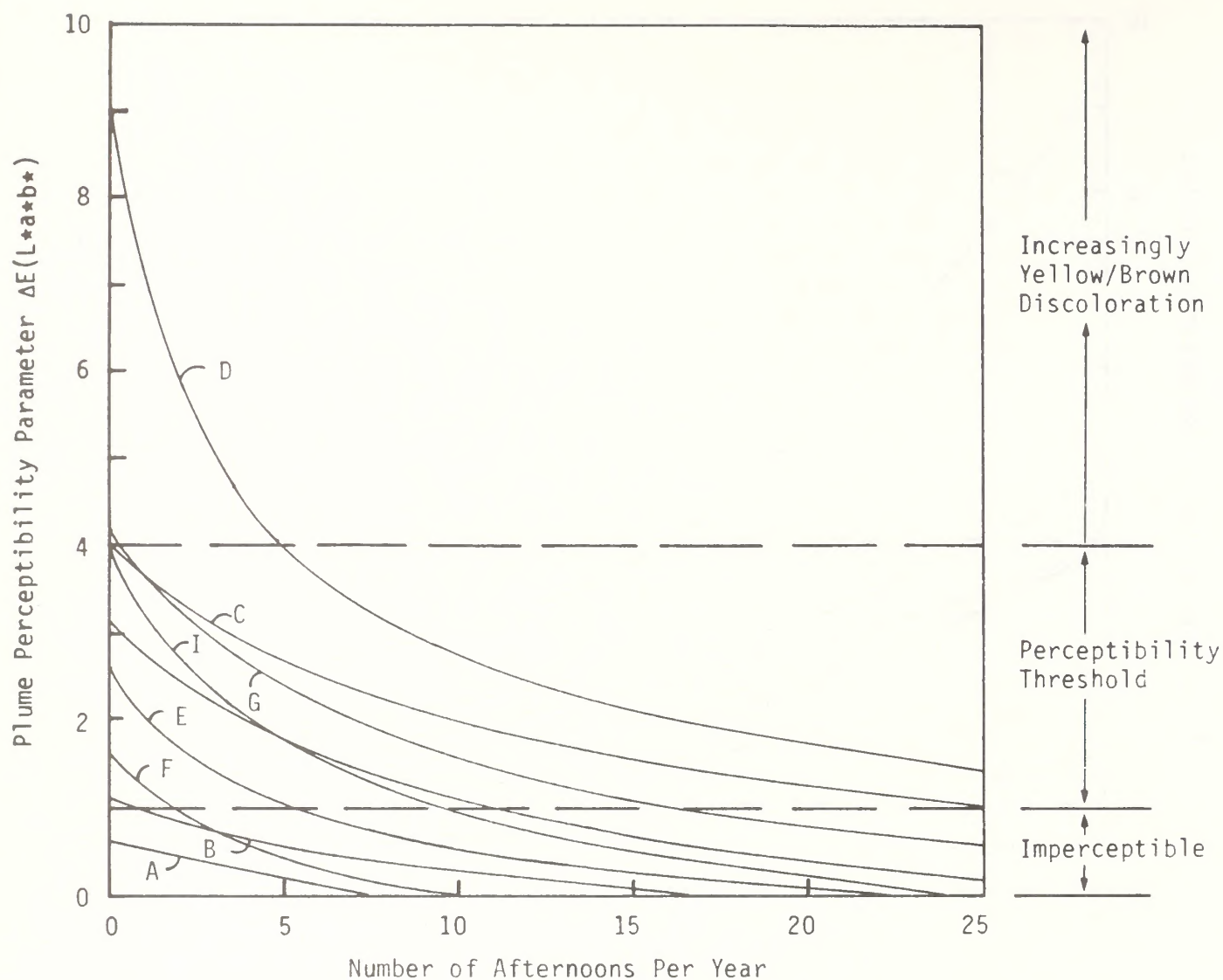


Key to Emission Sources:

- A - Enercor-Mono Power
- B - Geokinetics
- C - Magic Circle
- D - Moon Lake Power Plant Units 1 and 2
- E - Paraho
- F - Sohio
- G - Syntana
- H - Tosco
- I - White River

(a) Morning impacts

FIGURE 5-36. CUMULATIVE FREQUENCY OF PERCEPTIBLE PLUME DISCOLORATION RESULTING FROM EMISSIONS FROM VARIOUS UINTA BASIN SOURCES AT UINTAH AND OURAY INDIAN RESERVATION



Key to Emission Sources:

- A - Enercor-Mono Power
- B - Geokinetics
- C - Magic Circle
- D - Moon Lake Power Plant Units 1 and 2
- E - Paraho
- F - Sohio
- G - Syntana
- H - Tosco
- I - White River

(b) Afternoon impacts

FIGURE 5-36 (Concluded)

- > Lack of significant precipitation (which would wash out aerosols).

It is difficult to find periods in the study during which all these conditions occur simultaneously. For example, stagnation events, with low wind speeds, low mixing heights, and no significant precipitation are most common in winter when solar insolation and fugitive dust emissions are at their minimum annual values. Holzworth (1972) found that in Grand Junction, on average, there are six episodes of two days or more each (a total of 26 days) with no significant precipitation, mixing heights less than 1000 m, and wind speeds less than 4 m/s. These episodes occur primarily in winter. In summer, when insolation is at a maximum, mean afternoon mixed layers are 3900 meters thick, and wind speeds are about 6 m/s.

Although it must be noted that it is possible that significant regional visual range reduction would occur in the winter in populated areas due to fireplace and stove emissions trapped in stagnant layers, the magnitude of such impacts is difficult to quantify at this time.

We selected a summertime worst-case meteorological scenario for evaluation of regional visual range reduction. We choose a conservatively low summertime mixing height of 1000 meters and a low wind speed of 3 meters per second. We assumed that an air parcel was transported over the population centers and synfuel development areas of the Uinta and Piceance basins picking up emissions as it progressed eastward. Unlike plume discoloration effects, regional visual range reduction increases with transport time and the rate of plume mixing with reactive background species (primarily the hydroxyl radical). We therefore selected a C stability for plumes (trapped within the 1000-m mixed layer) and a long transport time of about 10 hours for Uinta Basin emissions. Impacts were evaluated for a line of sight northwest from Flat Tops. It is possible that somewhat larger reductions in visual range than those calculated here could occur further downwind in Mt. Zirkel and Rocky Mountain National Park because of longer transport and reaction times. However, we believe it is unlikely that impacts in these areas would be much larger, because at these more significant distances the mixed layer is likely to be deeper and much of the plume aerosol and its precursors would be deposited in a dry mode or in a wet mode during afternoon thunderstorms that are common at higher elevations.

Although regional visibility impacts deserve more detailed study than what is possible to present here, we believe we have identified a reasonable worst-case scenario.

PLUVUE model calculations were used to calculate percentage reductions in visual range. These percentage reductions are independent of the baseline visual range assumed. A background ozone concentration of 43 ppb was assumed. The model runs were not performed separately for each point source. All the oil shale source emissions for the Uinta Basin were summed and modeled using one plume, and the width of the initial plume was set at 10 km. (It should be noted that a sensitivity study of PLUVUE has shown that specification of horizontal plume dispersion is not critical to visibility predictions.) As noted above, the stability class within the 1000-m mixed layer was set to Pasquill-Gifford "C" stability. Separate model runs were performed for synfuel facilities in the Uinta Basin and in Colorado, for other point sources in the Uinta Basin and in Colorado, and for fugitive particulate emissions in the Uinta Basin, and Rio Blanco and Moffat counties in western Colorado.

Specification of the size distribution of the aerosol is very important in obtaining accurate estimates of visibility impacts due to scattering by particulate matter or secondary aerosol. We used size distributions specified by EPA (1981). Table 5-8 shows the size distributions and deposition velocities of the primary and secondary aerosols used in the various simulations. The only area source emissions considered were emissions of fugitive dust (TSP) from unpaved roads, which amount to more than 90 percent of the total area source TSP emissions.

A PLUVUE model simulation was performed for each source type, level of emissions, and location. For each simulation, the reduction in visual range from the background value was determined for an observer at the Flat Tops Wilderness Area looking toward the northwest horizon sky. The total visual-range reduction was obtained by adding the fractional visual-range reductions for all the different sources. The contributions of each source, and the total visual-range reduction for the three emission levels are shown in table 5-9. The visual-range reductions are 2.86 percent, 7.25 percent, and 9.48 percent for the 1980 baseline year, and for the low- and high-oil-shale-production scenarios, respectively.

Most of the visual-range reduction in the worst-case scenario results from sulfate aerosol formed from SO_2 emissions from oil shale facilities and other point sources. Little of the visual-range reduction is due to secondary emissions associated with population growth.

5.7 ACID DEPOSITION

The potential impact of air pollution on acid deposition in such forms as sulfurous, sulfuric, and nitric acid through both wet and dry processes is currently a growing concern. For the high-oil-production

TABLE 5-8. PARTICLE SIZE DISTRIBUTIONS AND DEPOSITION VELOCITIES
ASSUMED IN VISIBILITY MODEL SIMULATIONS

Type of Particle	Mass Median Diameter (μm)	Geometric Standard Deviation	Deposition Velocity (cm/sec)
Oil shale and other point source particulate emissions	6.0	2.0	0.19
Area source emissions (unpaved roads)	5.0 [*]	2.0	0.19
	10.0 [†]	2.0	0.75
Secondary aerosol	0.1	2.0	0.10

* 8 percent of TSP emissions.

† 24 percent of TSP emissions (the remaining 68 percent of TSP emissions are in an optically inactive size range, 30 to 100 μm , with large deposition rates).

TABLE 5-9. WORST-CASE REDUCTION OF VISUAL RANGE FOR A VIEW FROM
FLAT TOPS WILDERNESS AREA LOOKING TOWARD THE NORTHWEST

Source	Percentage Visual Range Reduction		
	Year 1980 Baseline	Low-Oil- Production Scenario	High-Oil- Production Scenario
Uinta Basin synfuel facilities			
site specifics	0.00%	0.31%	0.53%
conceptuals	0.00	0.64	1.75
Other Uinta Basin point sources	0.45	1.56	1.56
Piceance Basin oil shale	0.00	0.99	1.64
Other Piceance Basin point sources	1.96	2.95	2.97
Uintah County area sources*			
5 μm aerosol	0.04	0.08	0.12
10 μm aerosol	0.17	0.36	0.54
Rio Blanco County area sources*			
5 μm aerosol	0.03	0.03	0.03
10 μm aerosol	0.15	0.15	0.15
Moffat County area sources*			
5 μm aerosol	0.01	0.03	0.03
10 μm aerosol	<u>0.05</u>	<u>0.14</u>	<u>0.15</u>
Total visual range reduction	2.86%	7.25%	9.48%

* Only particulate emissions from unpaved roads, which are more than 90 percent of total particulate emissions, were considered in the visibility analysis.

scenario, we estimated dry deposition in the study region from annual-average concentration isopleth maps. The annual dry deposition is determined through multiplication of the annual-average concentration by the deposition velocity, which for SO_2 and NO_x is on the order of 1 cm/sec. Figures 5-37 and 5-38 summarize these calculations. Since these plots were derived from GPM calculations, they are expected to be conservative.

Wet deposition was estimated from precipitation statistics for Grand Junction and the surrounding region. Grand Junction has 69 days per year during which precipitation is greater than 0.01 inch, and has a total annual precipitation of 8.4 inches. However, higher elevations receive greater amounts of precipitation. For example, annual precipitation in the Flat Tops Wilderness Area is estimated to be as high as 40 to 50 inches. Assuming conservatively that virtually all SO_x and NO_x is scavenged in significant rainfall events, we estimated that annual wet deposition rates would be on the same order as dry deposition rates, though short-term wet deposition rates would be higher. These estimates are likely to be conservative--extremely conservative in the low-elevation areas that receive less precipitation than the high-elevation areas. Thus, these wet deposition estimates are upper-bound estimates. Wet deposition clearly deserves more detailed study than that possible in this study.

Wet deposition was estimated by calculating an annual effective deposition velocity by assuming that all emissions in the mixed layer throughout the region are deposited during one-hour precipitation events on the 69 days per year with measured precipitation in Grand Junction of 0.01 inch and greater. This is expected to be very conservative since it is unlikely that significant fractions of the atmospheric loading would be removed during light precipitation events.

Assuming an annual average mixing depth of 2600 m (Holzworth, 1972) and the complete atmospheric cleansing during the one-hour precipitation event on each of 69 days per year, we calculated the following effective, annual-average wet deposition velocity:

$$V_d = \frac{(2600 \text{ m})(100 \text{ cm/m})}{(69 \text{ hrs})(3600 \text{ s/hr})} = 1.05 \text{ cm/s} \quad .$$

This deposition rate is about equal to that for dry deposition. One would expect that over the course of a year the pattern of wet deposition would be similar to that for dry deposition. Of course it should be noted again that at lower elevations wet deposition is unlikely to be as great as that calculated here.

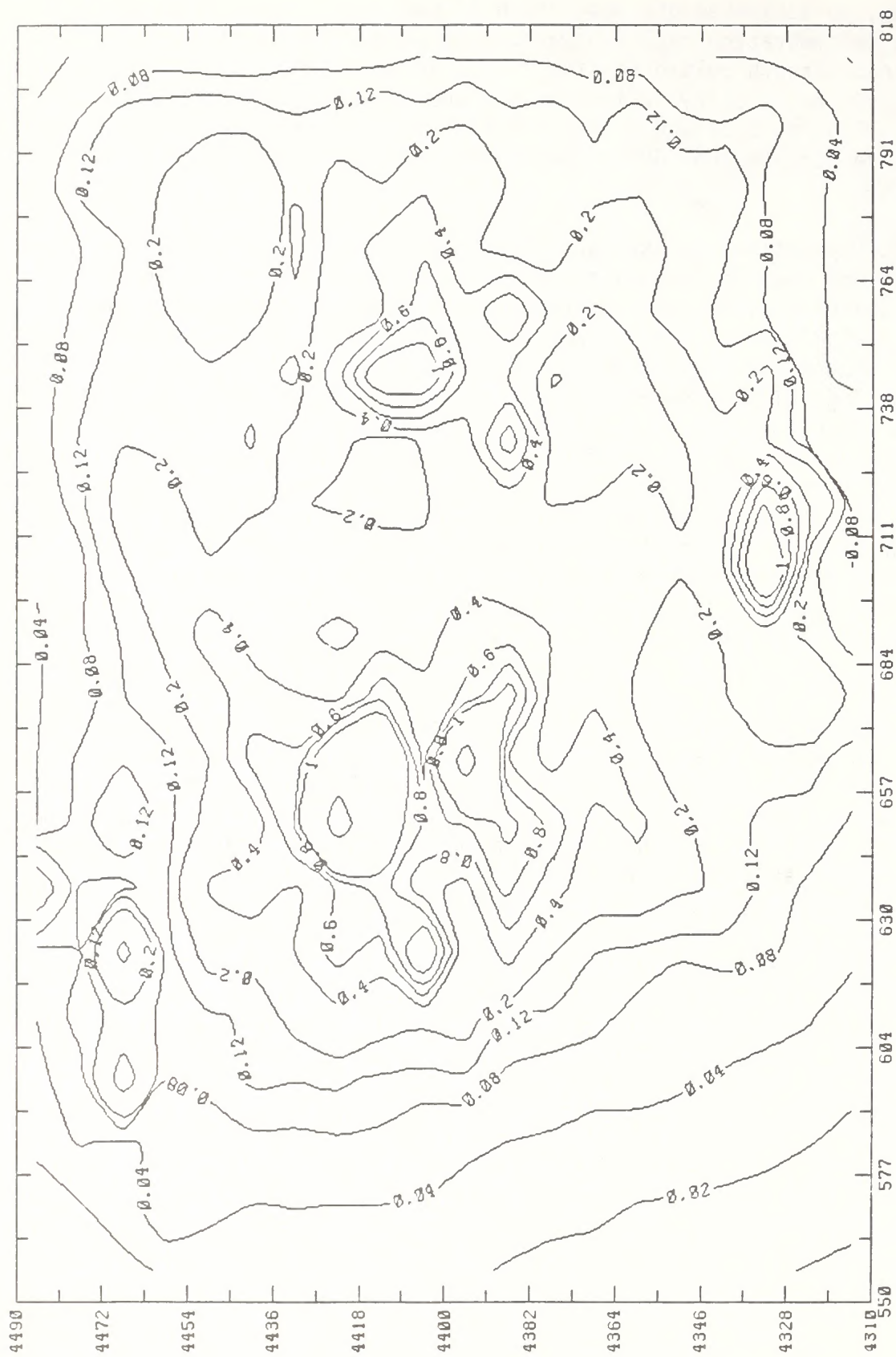
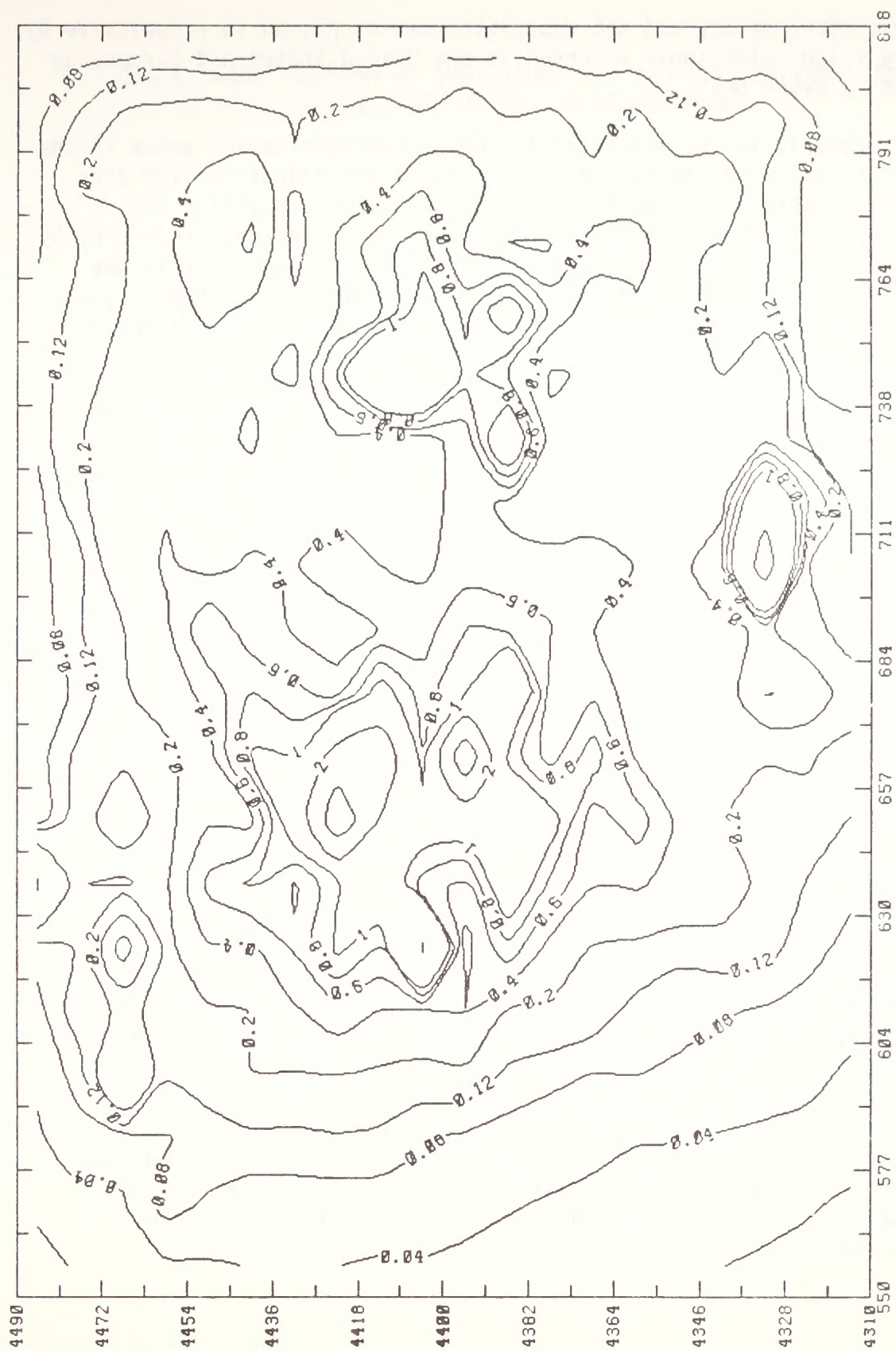


FIGURE 5-37. ANNUAL SULFUR ANION DRY DEPOSITION (G/M²/YR) FOR THE HIGH OIL PRODUCTION SCENARIO



These rates of dry and wet deposition can be placed in perspective by comparing values with those observed in the United States and Europe, as indicated in table 5-10.

For example, in the middle of the projected development areas in the Uinta and Piceance basins and in the populated and industrialized area near Grand Junction, both sulfur and nitrogen anion deposition are expected to be greater than 1 gram per square meter per year ($\text{g/m}^2/\text{yr}$) by dry deposition. This is greater than rates measured currently in Oak Ridge, Tennessee and northern California (see Table 5-10). However, dry deposition in wilderness areas such as Flat Tops and Mt. Zirkel and at Dinosaur National Monument is calculated to be about $0.1 \text{ g/m}^2/\text{yr}$, which is similar to rates measured at the above-mentioned locations. If wet deposition rates are comparable to dry rates, which is a conservative estimate, wet deposition values in the midst of the developed regions will be comparable to those measured currently in the eastern United States and in Europe, but wet deposition in wilderness areas will be at background values.

In Flat Tops Wilderness we have conservatively estimated that sulfur and nitrogen deposition will be as high as 0.2 and $0.4 \text{ g/m}^2/\text{yr}$, with approximately equal contributions due to wet and dry deposition. Turk and Adams (1982) have measured the buffering capacity of a number of lakes in Flat Tops. Using their titration curves for a well-buffered lake (Lower Marvine Lake) and a poorly buffered lake (Ned Wilson Lake), we calculated minimum lake pH values of 8.0 and 6.0, respectively. It is not currently known what effect, if any, these small shifts in lake pH will have on biota.

5.8 AIR QUALITY IMPACTS ASSOCIATED WITH CONSTRUCTION ACTIVITIES

Although it is difficult at this time to quantify construction impacts, they are expected to be small compared to impacts associated with the operation of synfuel facilities. The air quality impacts associated with construction activities will be temporary, lasting only a few years. Impacts will include fugitive dust emissions resulting from the use of large earth-moving equipment and small quantities of emissions from the exhaust of such equipment. Impacts resulting from population growth associated with construction activities will be proportional to such population growth and will be similar to those predicted for other secondary emissions, as discussed in Section 5.3.

TABLE 5-10. SUMMARY OF WORLD-WIDE WET AND DRY, SULFURIC AND NITRIC ACID DEPOSITION MEASUREMENTS

Location	Annual Deposition* (g/m ² /yr)
Background	0.2 N (wet) 0.2 S (wet)
Berkeley, California (1974-1975)	0.48 S (wet) 0.03 N (wet)
Central Europe (circa 1970)	0.6 N (wet)
Eastern United States (1977-1978)	1.2 S (wet)
Oak Ridge, Tennessee (1975-1976)	1.4 S (wet) 0.4 S (dry)
Sweden (1975)	2.5 S (wet)
Northern California (1978-1979)	0.1-0.3 S (wet) 0.1-0.4 N (wet) 0.0-0.1 S (dry) 0.0-0.2 N (dry)

* Stated in terms of mass of sulfur (S) or nitrogen (N).

6 AIR QUALITY IMPACTS OF SPECIFIC PROPOSED ACTIONS

In the previous section, the cumulative impacts of synthetic fuel development, other projects, and associated growth were discussed. In this section we discuss the impacts at maximum production rates of the following specific proposed actions:

- > Enercor-Mono Power
- > Magic Circle
- > Paraho
- > Syntana-Utah
- > Tosco.

Whereas we studied regional impacts within the large study region, we examine in this section individual site impacts on a smaller scale in the Uinta Basin, and impacts of ground-level releases of total suspended particulates (TSP) within 5 kilometers of each source. The Prevention of Significant Deterioration (PSD) increment consumption of each source is evaluated separately and together with other projects (primarily the White River oil shale project and the Moon Lake power plant). The impact of the emissions from facilities (together with the existing baseline, other project impacts, and secondary growth impacts) is evaluated with respect to applicable ambient air quality standards.

In this analysis, subregional Gaussian Puff Model (GPM) runs and COMPLEX-I model runs, as discussed in Section 4, were used to make best estimates of air quality impacts. These results are expected to be conservative, but not nearly as conservative as the regional results presented in Section 5. For this reason we provide the model results directly without any estimated error bounds. The TSP concentration calculations using GPM are overly conservative within 10 to 20 km of each source because multiple ground-level releases were aggregated into one point (see Section 4); we therefore supplemented the GPM calculations with COMPLEX-I calculations.

Clear plastic overlays showing the locations of the synthetic fuel facilities and terrain elevations in the small Uinta Basin modeling subregion are shown inside the back cover of this report.

6.1 ENERCOR-MONO POWER

Enercor-Mono Power proposes to operate tar sands synthetic fuel facilities at two locations to produce 55,000 barrels per day. The northern location, the Rainbow site, is just west of Three Mile Canyon at approximately 7000 feet MSL. At this site, local drainage winds to the north into Evacuation Creek are likely to compete with the prevailing westerly winds in causing worst-case impacts. The southern location, called the PR Springs, or Cedar Camp site, is located on Meadow Creek at about 8000 feet MSL right at the ridgeline above the Colorado River. This site should be quite well ventilated; drainage winds, if they exist at all, would carry emissions to the west and then to the north.

As indicated in tables 6-1 and 6-2 and figures 6-1 and 6-2, impacts are extremely small and well within air quality criteria. Visibility impairment resulting from this proposed project will be insignificant, with the facility passing EPA Level-1 screening tests at all mandatory and potential Class I areas (see table 6-3).

6.2 MAGIC CIRCLE

Magic Circle proposes to construct an oil shale facility to produce 31,500 barrels per day at a site in terrain gently sloping to the north and west toward the White and Green rivers, respectively. Drainage flows in the local area would carry emissions to the north and west.

Tables 6-4 and 6-5 and figures 6-3 and 6-4 summarize the impacts. Except for TSP impacts on-site, impacts are predicted to be well within criteria. Local TSP impacts are quite large on-site, but concentrations drop off rapidly with distance. On the basis of the more realistic COMPLEX model results, impacts beyond 5 km downwind are within PSD increments. Near-source (< 5 km downwind) impacts were calculated using EPA's COMPLEX model, taking into account the spatial distribution of TSP point sources. The facility passes the conservative EPA Level-1 visibility screening test for all mandatory and potential Class I areas (see table 6-6); thus, visibility impairment due to this source is not expected to be significant.

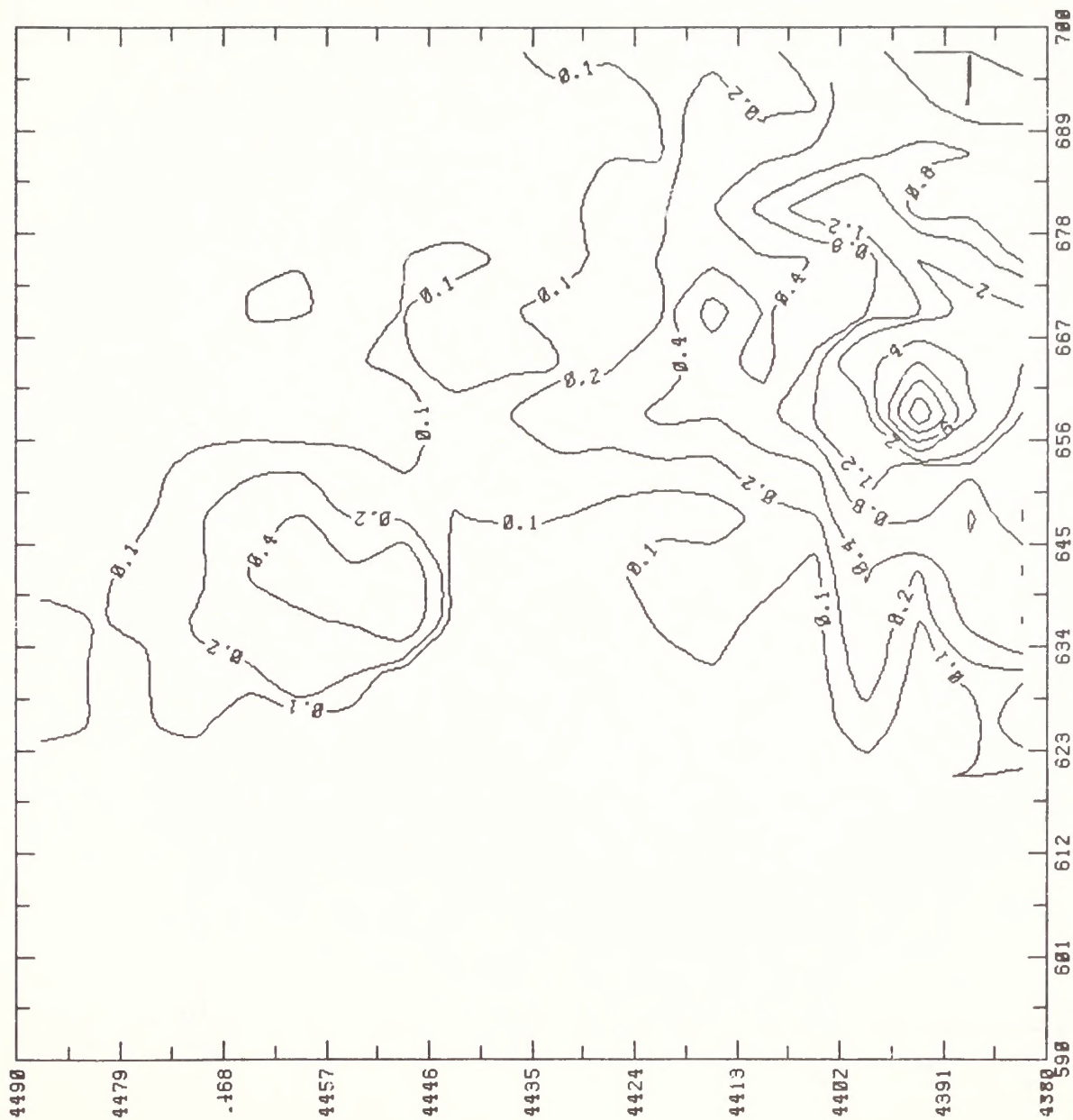
TABLE 6-1. SUMMARY OF PSD INCREMENT CONSUMPTION BY ENERCOR-MONO POWER

PSD Increments/Increment Consumption	SO ₂ Concentration ($\mu\text{g}/\text{m}^3$)			TSP Concentration ($\mu\text{g}/\text{m}^3$)	
	3-Hour Average	24-Hour Average	Annual Average	24-Hour Average	Annual Average
<u>Class II Areas</u>					
Allowable PSD Class II increment	512	91	20	37	19
Increment consumption at receptors of maximum impacts					
Impact alone	12	3	0	7	0
Impact with Moon Lake Unit 1	13	3	0	7	0
Impact with all interrelated (other) sources	14	3	0	8	0
Maximum increment consumption on Uintah/Ouray Indian Reservation					
Impact alone	0	0	0	0	0
Impact with Moon Lake Unit 1	6	1	0	1	0
Impact with all interrelated (other) sources	14	3	0	3	0
<u>Class I Areas</u>					
Allowable PSD Class I increment	25	5	2	10	5
Increment consumption at Flat Tops Wilderness Area (federal Class I)					
Impact alone	0	0	0	0	0
Impact with Moon Lake Unit 1	0	0	0	0	0
Impact with all interrelated (other) sources	1	0	0	0	0
Increment consumption at Maroon Bells- Snowmass Wilderness Area (federal Class I)					
Impact alone	0	0	0	0	0
Impact with Moon Lake Unit 1	0	0	0	0	0
Impact with all interrelated (other) sources	0	0	0	0	0
Increment consumption at Dinosaur National Monument (Colorado category I and potential federal Class I)					
Impact alone	0	0	0	0	0
Impact with Moon Lake Unit 1	2	0	0	0	0
Impact with all interrelated (other) sources	6	1	0	1	0

TABLE 6-2. SUMMARY OF MAXIMUM AMBIENT AIR QUALITY IMPACTS OF
ENERCOR-MONO POWER COMPARED WITH APPLICABLE STANDARDS

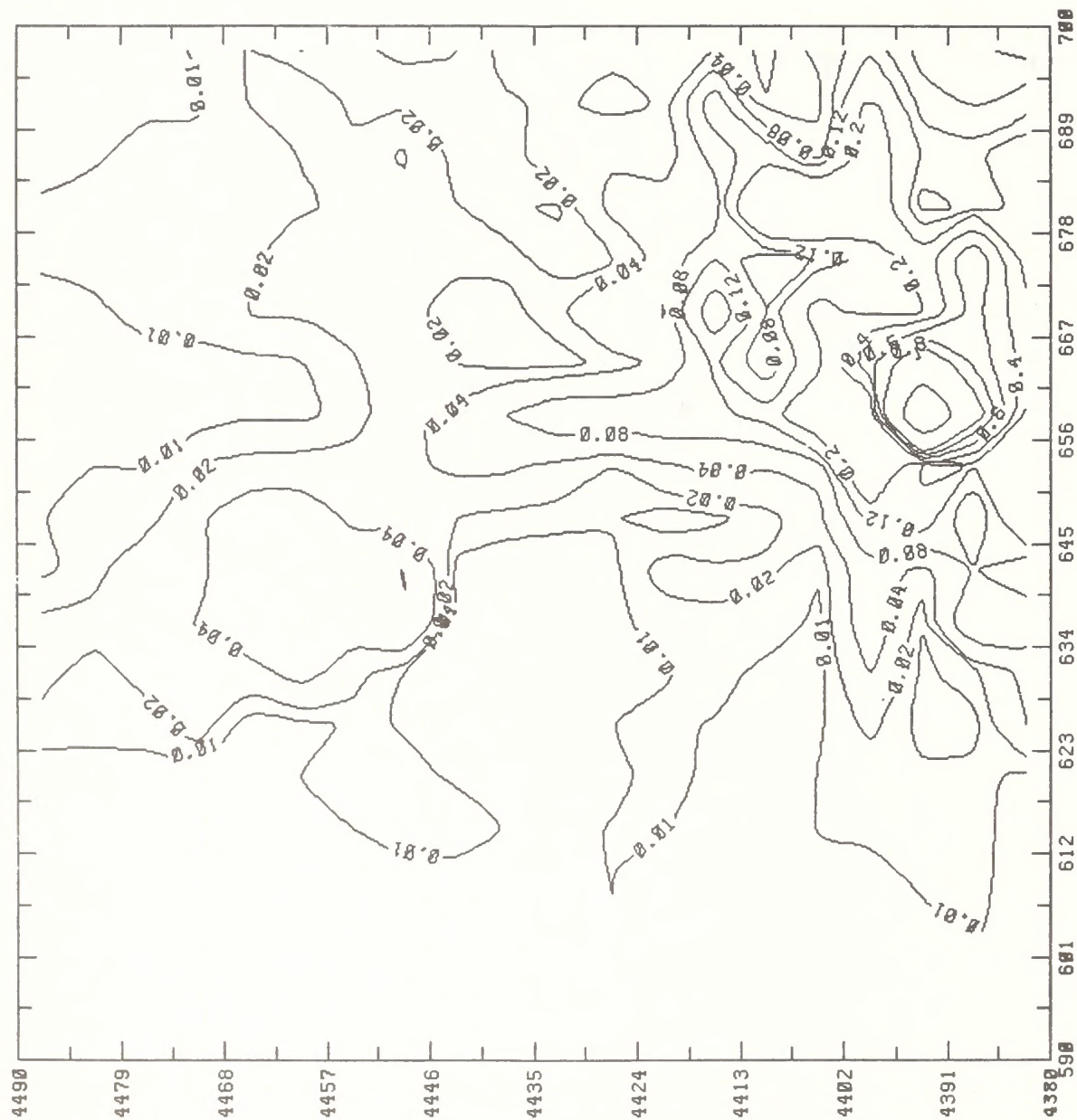
Pollutant/Averaging Time	Maximum Ground-Level Concentration ($\mu\text{g}/\text{m}^3$)					NAAQS* ($\mu\text{g}/\text{m}^3$)
	Baseline	Source Impact	Subtotal	Impact of Other Sources	Total	
Sulfur dioxide (SO_2)						
3-Hour	4	12	16	1	17	1300
24-hour	1	3	4	0	4	365
Annual	0	0	0	0	0	80
Total suspended particulate (TSP)						
24-Hour	140	7	147	1	148	150
Annual	35	0	35	0	35	60
Nitrogen dioxide (NO_2)						
Annual	1	0	1	0	1	100
Carbon monoxide (CO)						
1-Hour	200	1	201	0	201	40,000
8-Hour	200	1	201	0	201	10,000
Ozone (O_3)						
1-Hour	70	2	72	0	72	240
Hydrocarbons (HC)						
3-Hour	100	1	101	0	101	160

* National Ambient Air Quality Standards.



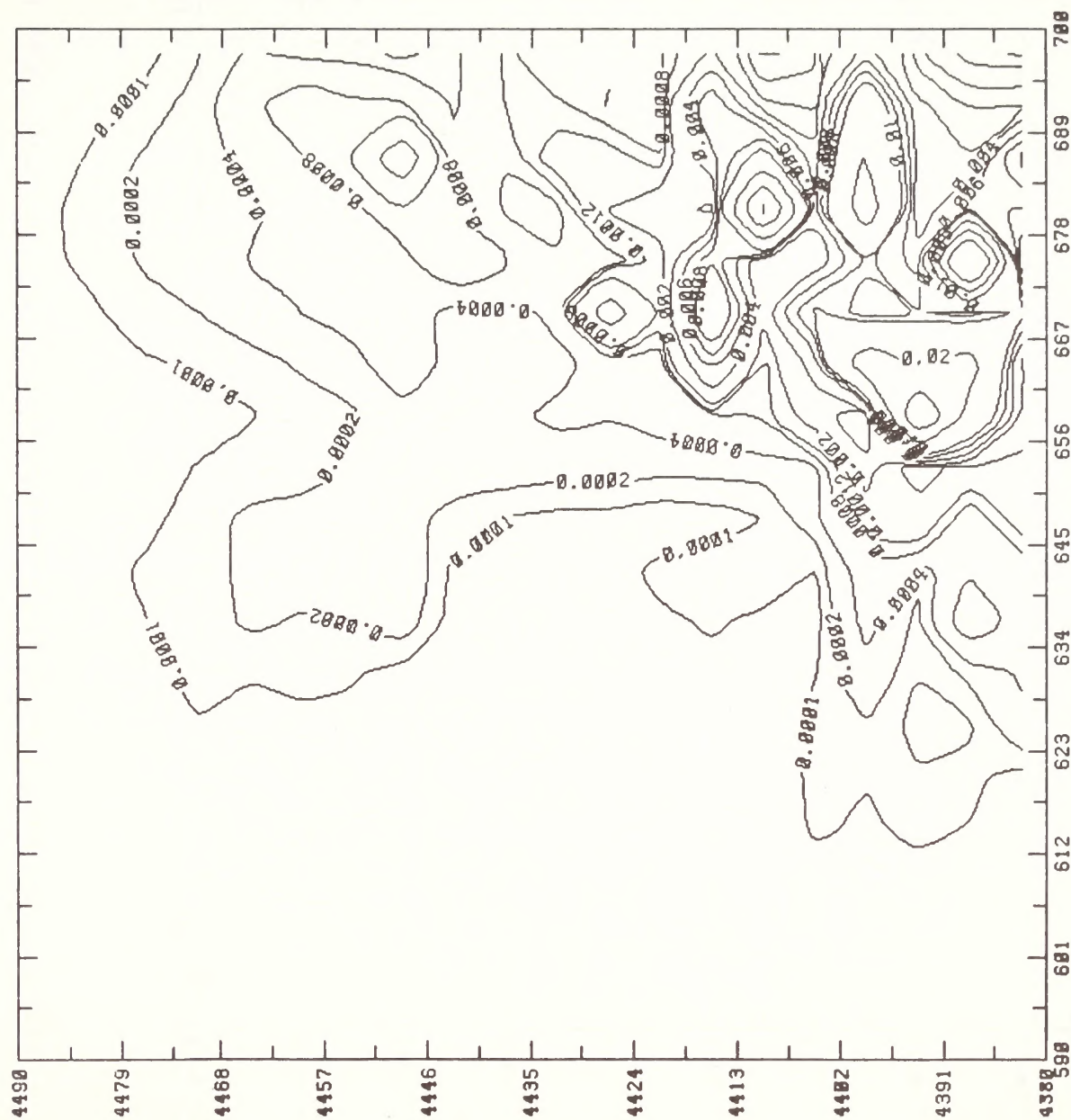
(a) Maximum 3-Hour Average

FIGURE 6-1. GROUND-LEVEL SO_2 CONCENTRATIONS ($\mu\text{g}/\text{m}^3$) DUE TO ENERCOR-MONO POWER EMISSIONS



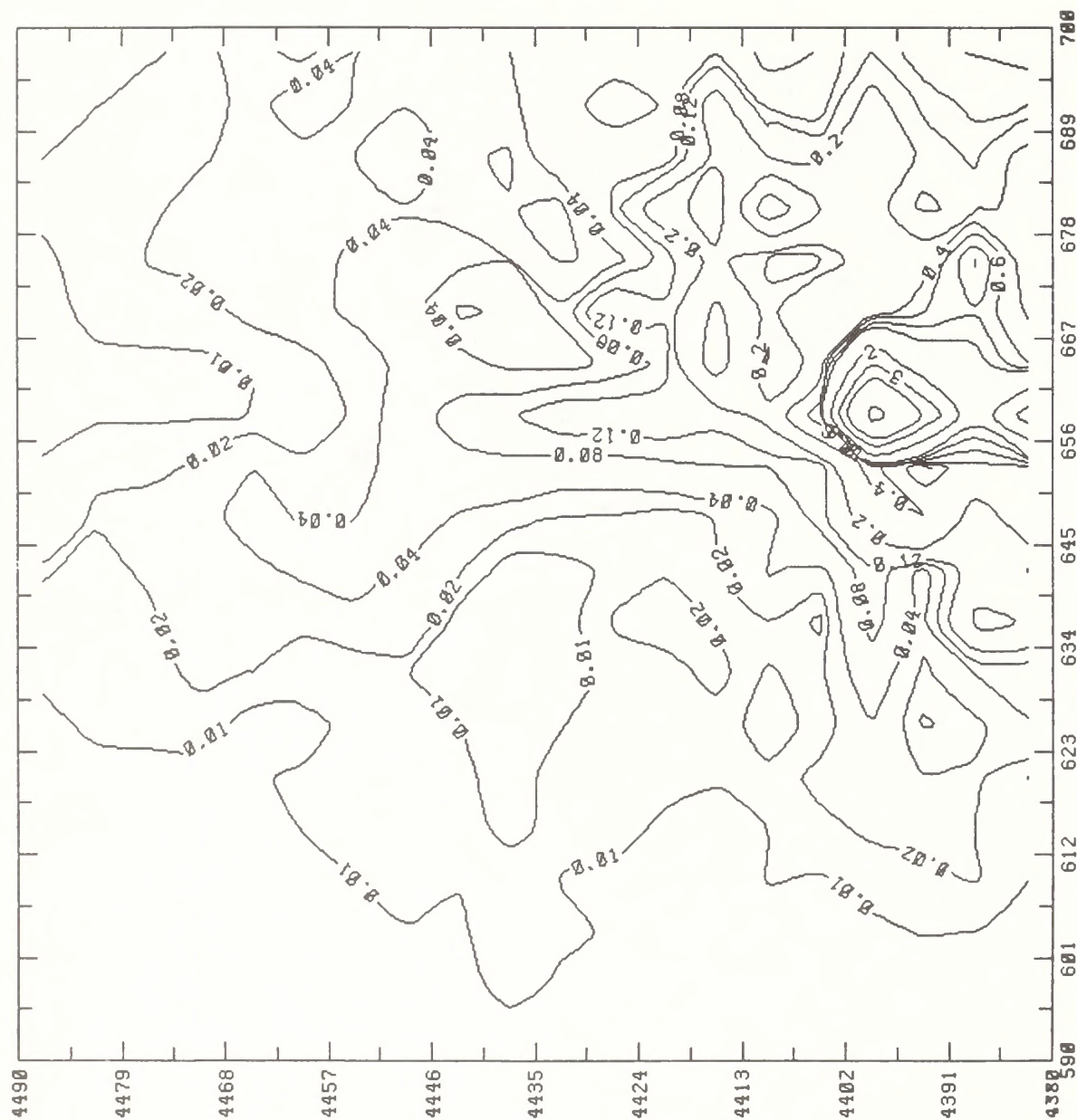
(b) Maximum 24-Hour Average

FIGURE 6-1 (Continued)



(c) Annual Average

FIGURE 6-1 (Concluded)



(a) Maximum 24-Hour Average

FIGURE 6-2. GROUND-LEVEL TSP CONCENTRATIONS ($\mu\text{g}/\text{m}^3$) DUE TO ENERCOR-MONO POWER EMISSIONS

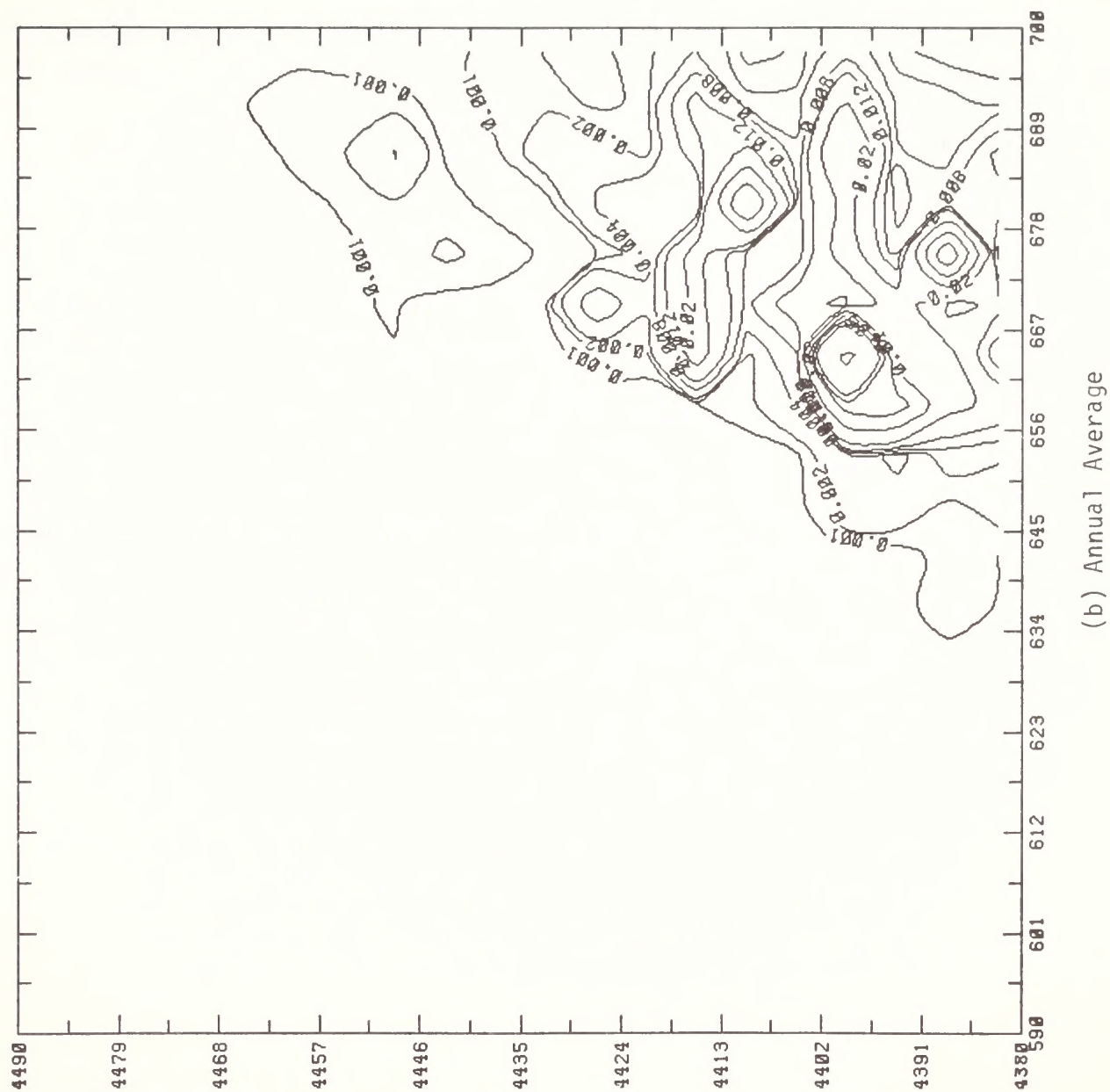


FIGURE 6-2 (Concluded)

TABLE 6-3. LEVEL-1 SCREENING ANALYSIS RESULTS FOR VISIBILITY
IMPACTS OF ENERCOR-MONO-POWER

Existing or Potential Class I Area or Area of Special Concern	Test for Dark Plume Against Sky C_1	Test for Light Plume Against Terrain C_2	Test for Regional Reduction Sky/Terrain Contrast C_3
Flat Tops Wilderness	-0.00	0.02	0.01
Dinosaur National Monument	-0.01	0.08	0.01
Colorado National Monument	-0.01	0.07	0.01
Uintah/Ouray Indian Reservation			
- North portion	-0.01	0.11 [*]	0.01
- South portion	-0.01	0.11 [*]	0.01
Uinta Primitive Area	-0.00	0.02	0.01

* Indicates that potential of adverse visibility impairment cannot be ruled out by Level-1 screening (i.e., $|C| > 0.1$).

TABLE 6-4. SUMMARY OF PSD INCREMENT CONSUMPTION BY MAGIC CIRCLE

<u>PSD Increments/Increment Consumption</u>	<u>SO₂ Concentration ($\mu\text{g}/\text{m}^3$)</u>			<u>TSP Concentration ($\mu\text{g}/\text{m}^3$)</u>	
	<u>3-Hour Average</u>	<u>24-Hour Average</u>	<u>Annual Average</u>	<u>24-Hour Average</u>	<u>Annual Average</u>
<u>Class II Areas</u>					
Allowable PSD Class II increment	512	91	20	37	19
Increment consumption at receptors of maximum impacts					
Impact alone	121	32	1	<32	<4
Impact with Moon Lake Unit 1	129	33	1	<34	<4
Impact with all interrelated (other) sources	137	34	1	<34	<4
Maximum increment consumption on Uintah/Ouray Indian Reservation					
Impact alone	10	1	0	<32	<4
Impact with Moon Lake Unit 1	16	2	0	<33	<4
Impact with all interrelated (other) sources	24	4	0	<35	<4
<u>Class I Areas</u>					
Allowable PSD Class I increment	25	5	2	10	5
Increment consumption at Flat Tops Wilderness Area (federal Class I)					
Impact alone	0	0	0	0	0
Impact with Moon Lake Unit 1	0	0	0	0	0
Impact with all interrelated (other) sources	1	0	0	0	0
Increment consumption at Maroon Bells- Snowmass Wilderness Area (federal Class I)					
Impact alone	0	0	0	0	0
Impact with Moon Lake Unit 1	0	0	0	0	0
Impact with all interrelated (other) sources	0	0	0	0	0
Increment consumption at Dinosaur National Monument (Colorado category I and potential federal Class I)					
Impact alone	1	0	0	0	0
Impact with Moon Lake Unit 1	3	0	0	0	0
Impact with all interrelated (other) sources	7	1	0	1	0

TABLE 6-4 (Concluded)

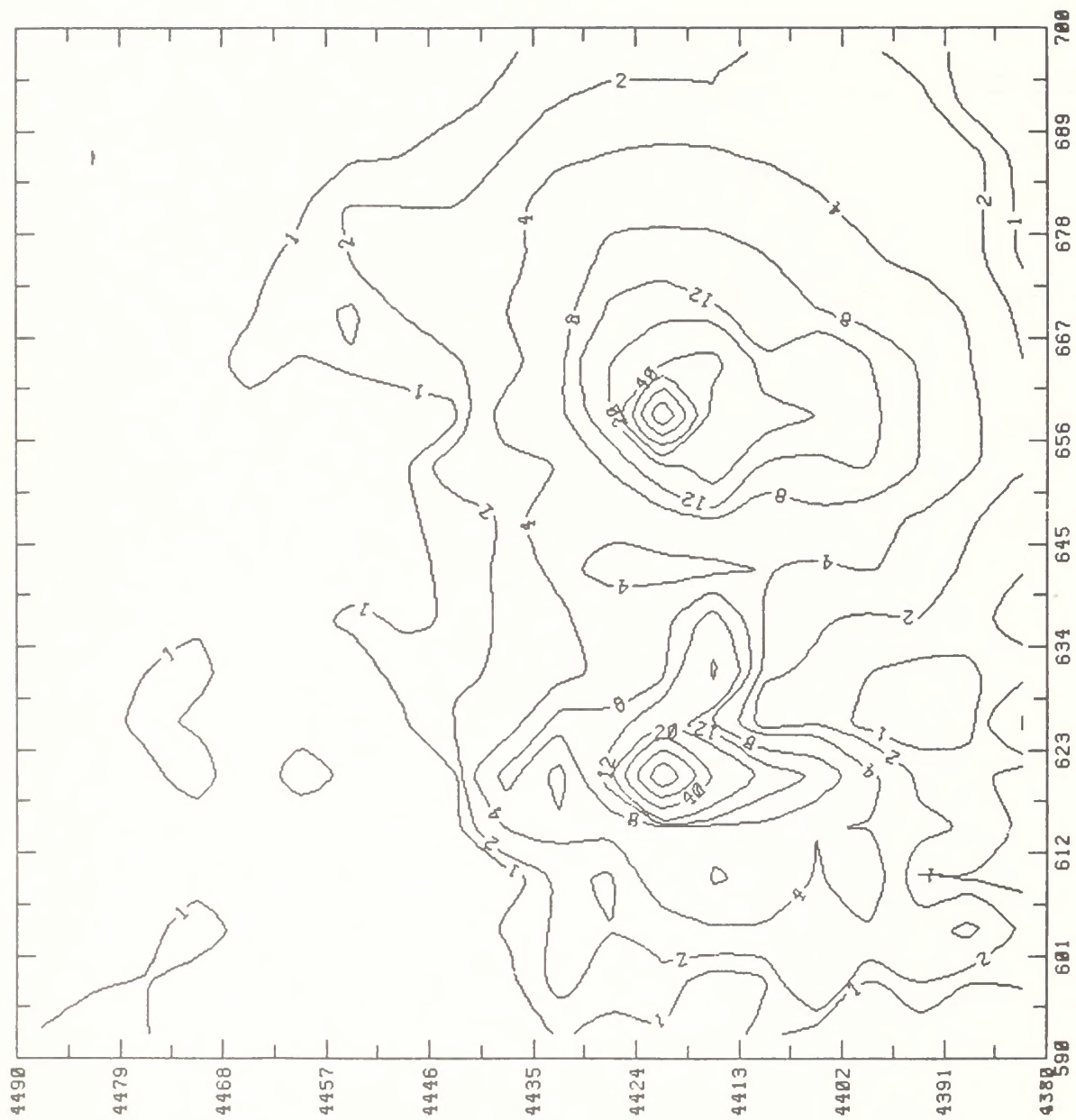
<u>PSD Increments/Increment Consumption</u>	<u>SO₂ Concentration</u> <u>($\mu\text{g}/\text{m}^3$)</u>			<u>TSP Concentration</u> <u>($\mu\text{g}/\text{m}^3$)</u>	
	<u>3-Hour</u> <u>Average</u>	<u>24-Hour</u> <u>Average</u>	<u>Annual</u> <u>Average</u>	<u>24-Hour</u> <u>Average</u>	<u>Annual</u> <u>Average</u>
Increment consumption at Colorado National Monument (Colorado category I and potential federal Class I)					
Impact alone	0	0	0	0	0
Impact with Moon Lake Unit 1	0	0	0	0	0
Impact with all interrelated (other) sources	0	0	0	0	0

TABLE 6-5. SUMMARY OF MAXIMUM AMBIENT AIR QUALITY IMPACTS OF MAGIC CIRCLE
COMPARED WITH APPLICABLE STANDARDS

Pollutant/Averaging Time	Maximum Ground-Level Concentration ($\mu\text{g}/\text{m}^3$)					NAAQS* ($\mu\text{g}/\text{m}^3$)
	Baseline	Source Impact	Subtotal	Impact of Other Sources	Total	
Sulfur dioxide (SO_2)						
3-Hour	185	121	306	8	314	1300
24-hour	23	32	55	1	56	365
Annual	0	1	1	0	1	80
Total suspended particulate (TSP)						
24-Hour	222 [†]	<32	<254 [†]	2	<256 [†]	150
Annual	55	<4	<59	0	<59	60
Nitrogen dioxide (NO_2)						
Annual	1	6	7	0	7	100
Carbon monoxide (CO)						
1-Hour	200	44	244	0	244	40,000
8-Hour	200	44	244	0	244	10,000
Ozone (O_3)						
1-Hour	70	2	72	0	72	240
Hydrocarbons (HC)						
3-Hour	100	3	103	0	103	160

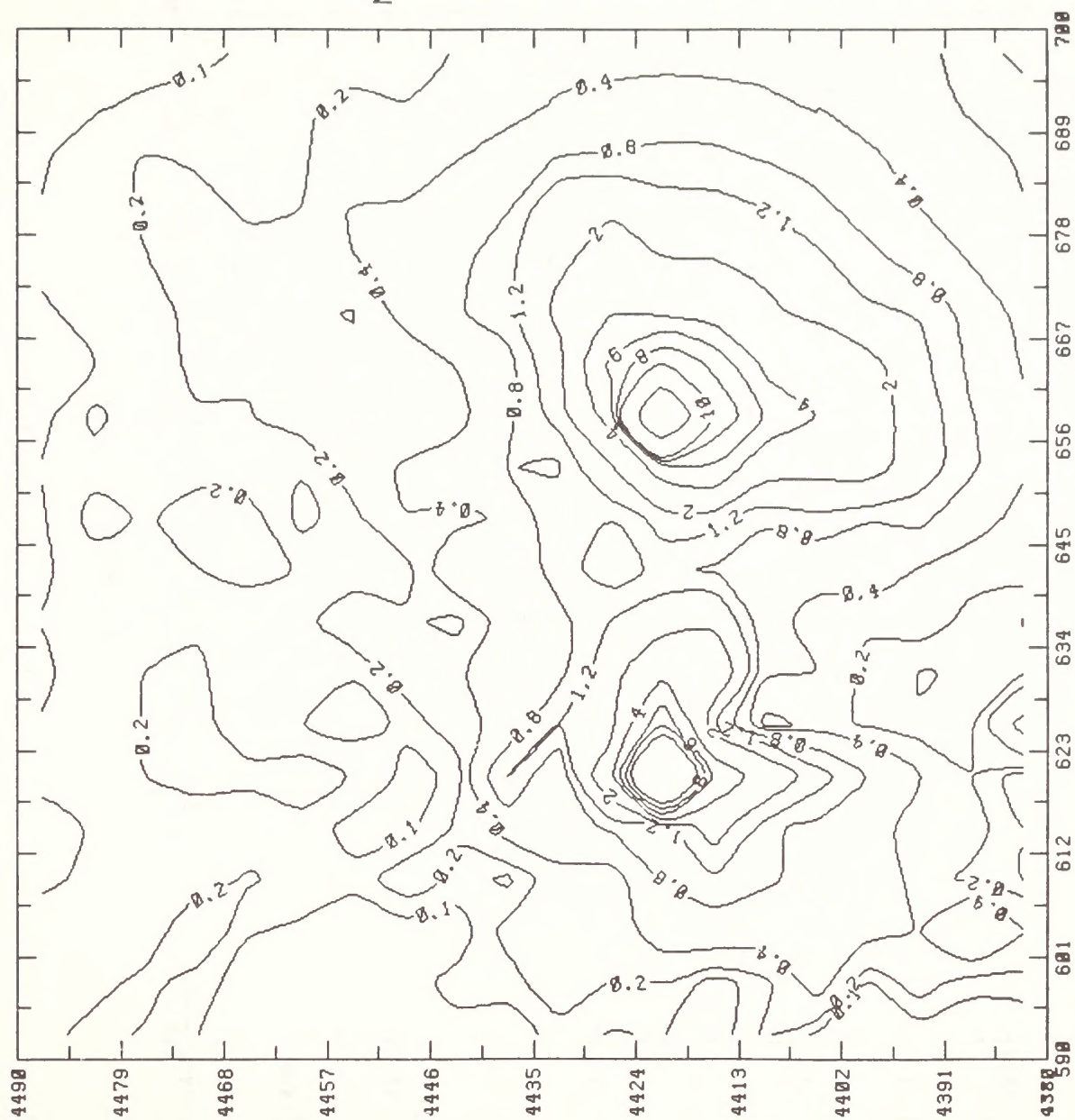
* National Ambient Air Quality Standards.

[†] Exceedance of NAAQS. It is assumed that baseline maximum coincides with source impact maximum.



(a) Maximum 3-Hour Average

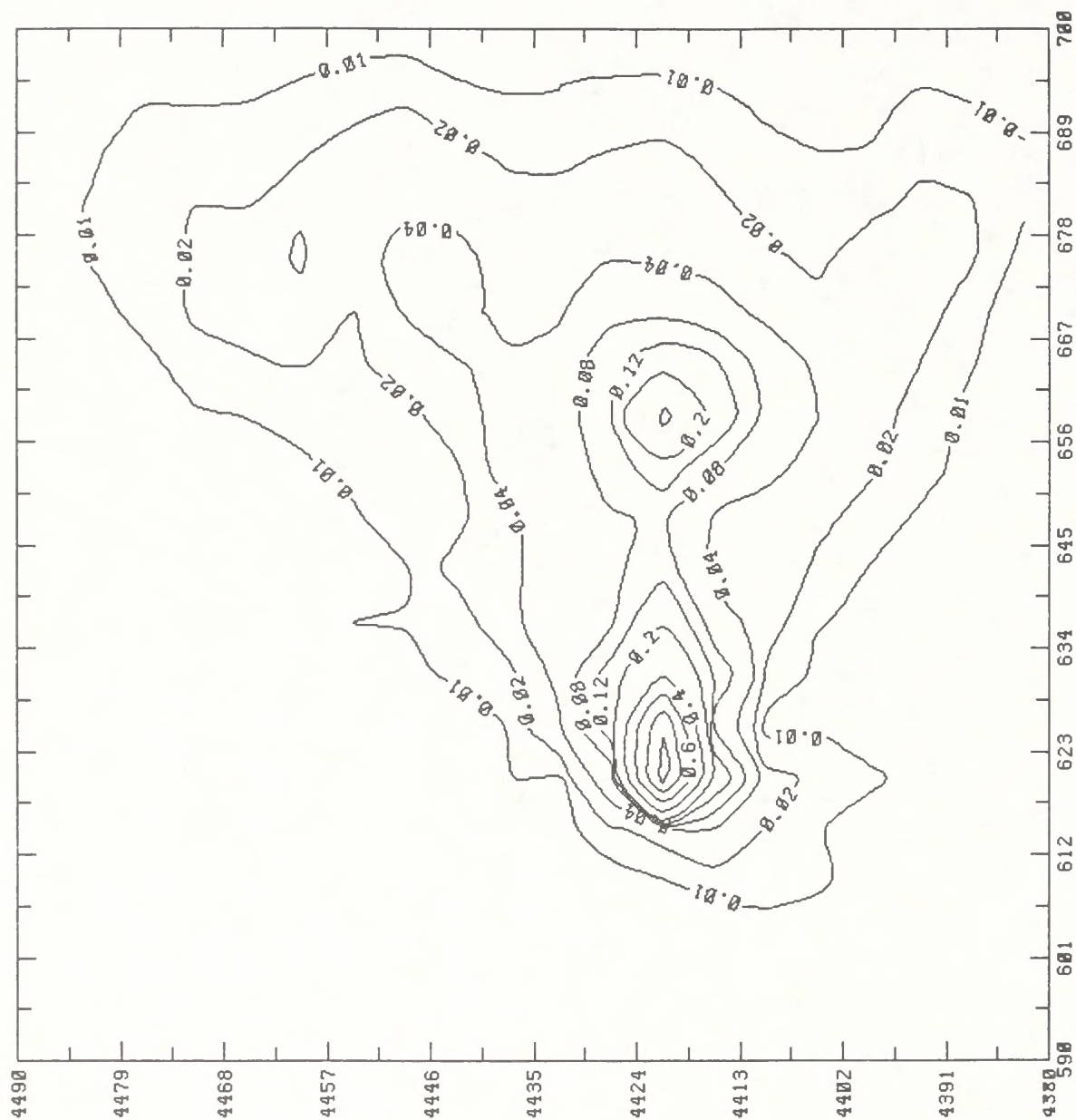
FIGURE 6-3. GROUND-LEVEL SO_2 CONCENTRATIONS ($\mu\text{g}/\text{m}^3$) DUE TO MAGIC CIRCLE EMISSIONS



(b) Maximum 24-Hour Average

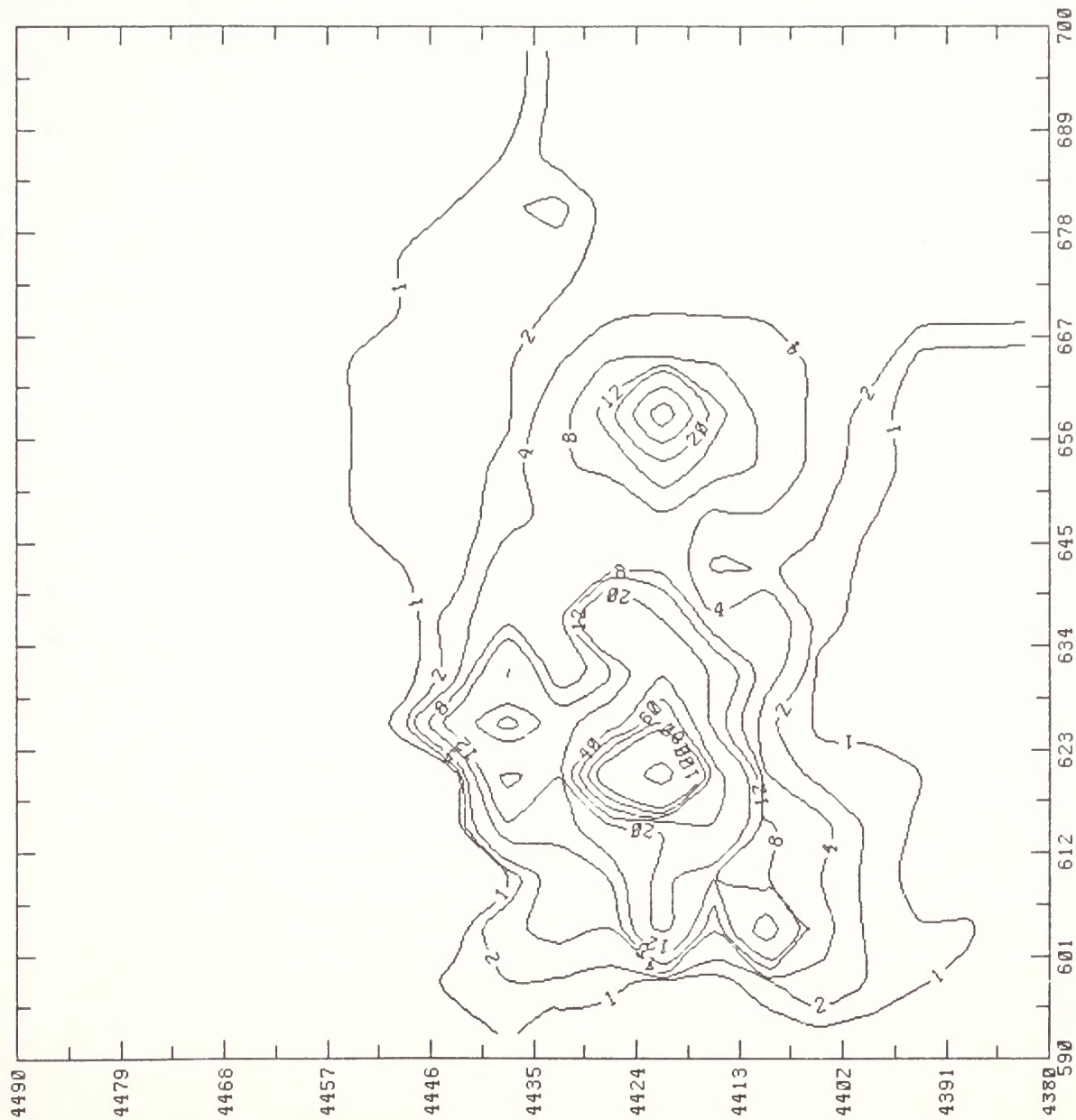
FIGURE 6-3 (Continued)

Maximum: 1.1 $\mu\text{g}/\text{m}^3$



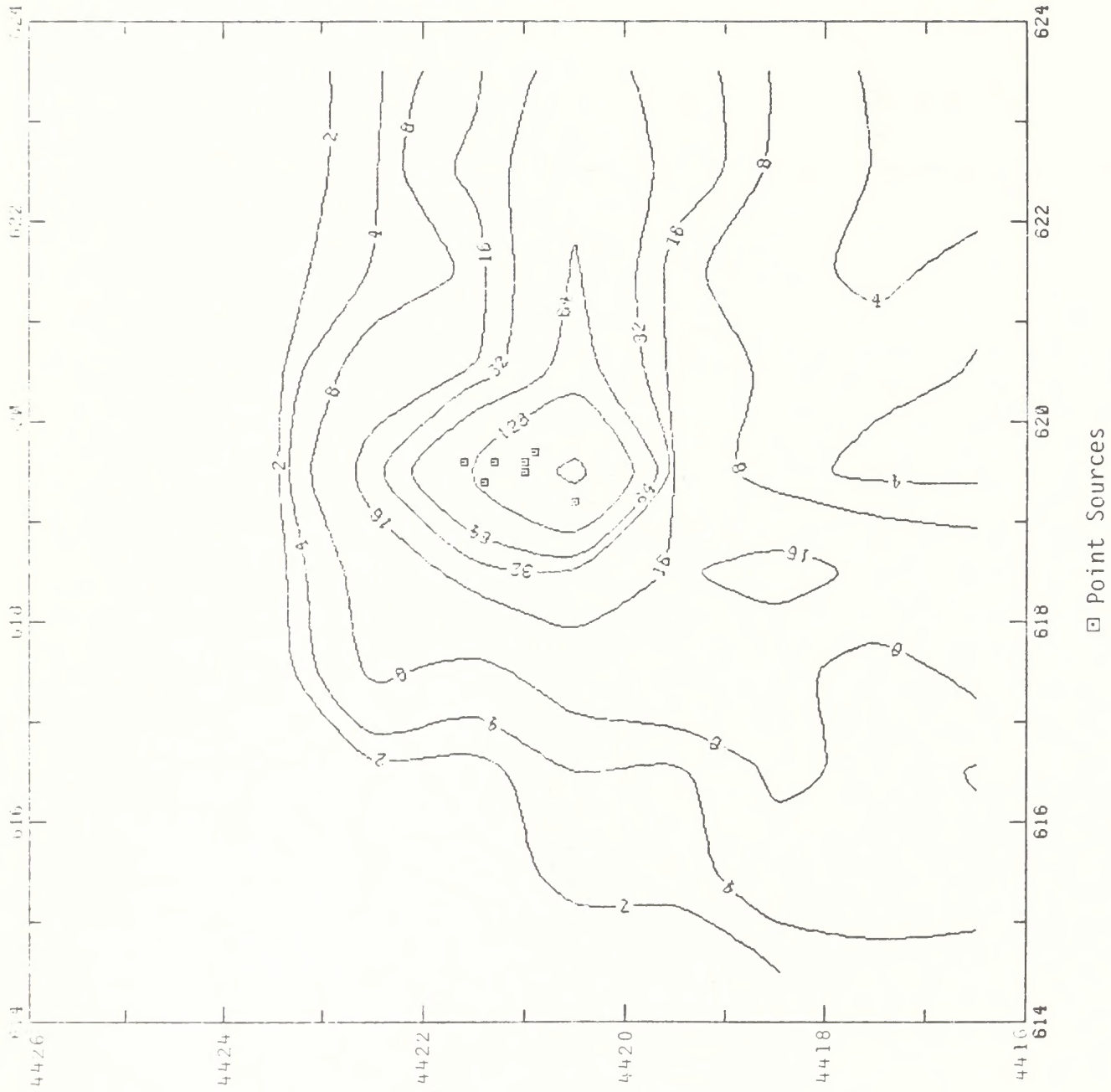
(c) Annual Average

FIGURE 6-3 (Concluded)



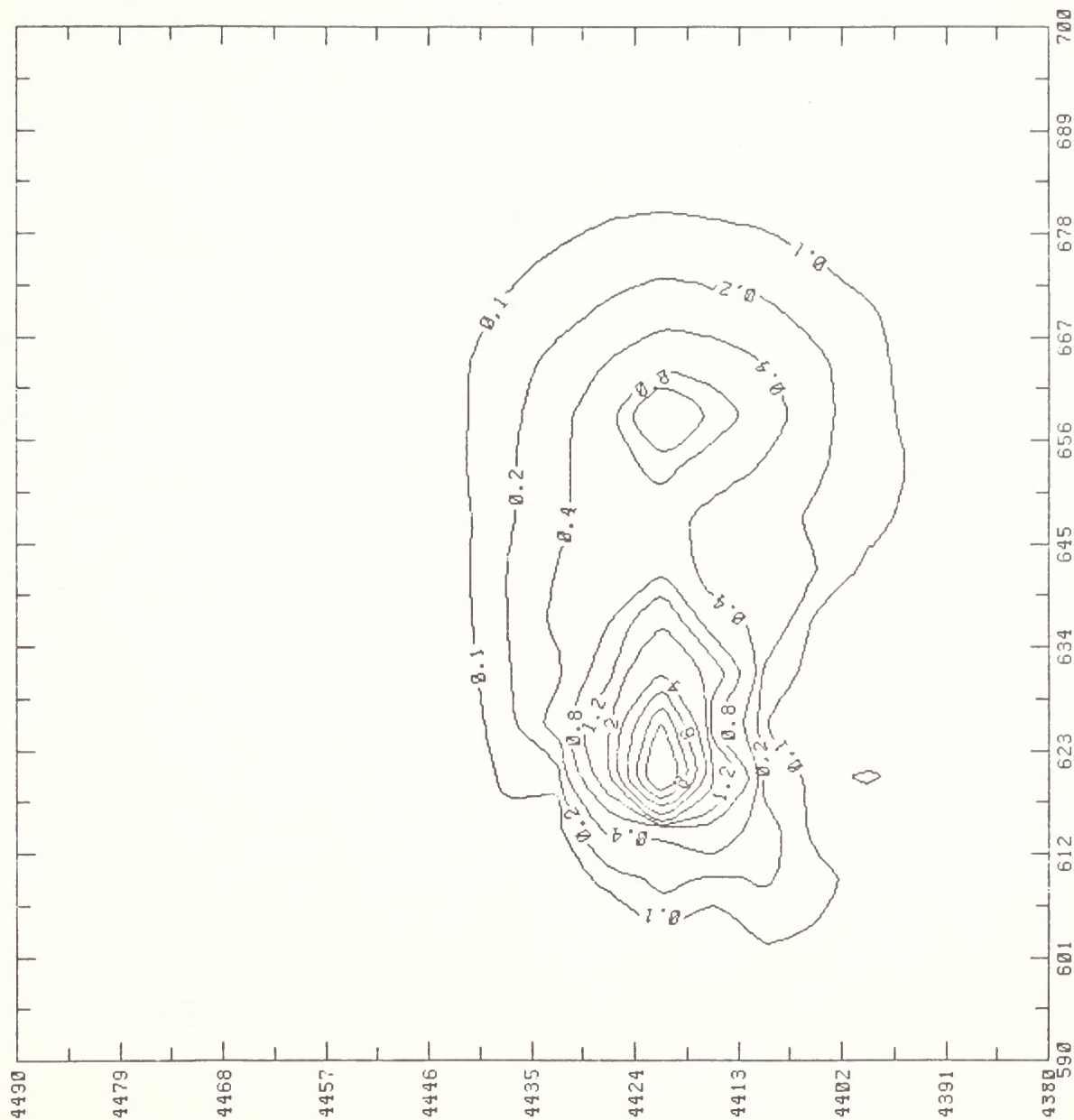
(a) Maximum 24-Hour Average

FIGURE 6-4. GROUND-LEVEL TSP CONCENTRATIONS ($\mu\text{g}/\text{m}^3$) DUE TO MAGIC CIRCLE EMISSIONS



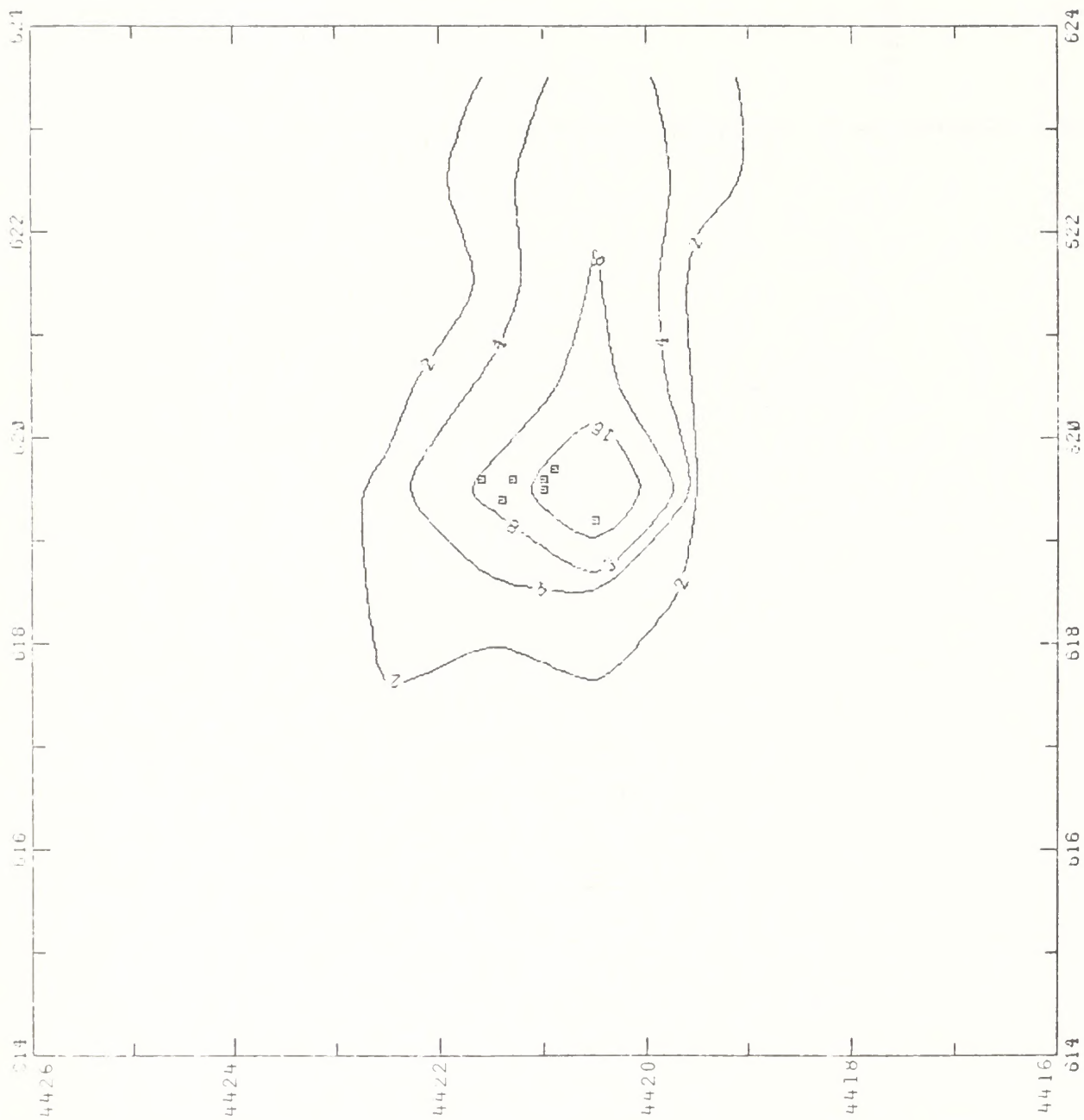
(b) Maximum 24-Hour Average (Near-Source)

FIGURE 6-4 (Continued)



(c) Annual Average

FIGURE 6-4 (Continued)



□ Point Sources
(d) Annual Average

FIGURE 6-4 (Concluded)

TABLE 6-6. LEVEL-1 SCREENING ANALYSIS RESULTS FOR VISIBILITY
IMPACTS OF MAGIC CIRCLE

Existing or Potential Class I Area or Area of Special Concern	Test for Dark Plume Against Sky C_1	Test for Light Plume Against Terrain C_2	Test for Regional Reduction Sky/Terrain Contrast C_3
Flat Tops Wilderness	-0.02	0.01	0.01
Dinosaur National Monument	-0.07	0.05	0.01
Colorado National Monument	-0.03	0.02	0.01
Uintah/Ouray Indian Reservation			
- North portion	-0.32*	0.37*	0.01
- South portion	-0.13*	0.12*	0.01
Uinta Primitive Area	-0.04	0.03	0.01

* Indicates that potential of adverse visibility impairment cannot be ruled out by Level-1 screening (i.e., $|C| > 0.1$).

6.3 PARAHO

The proposed Paraho oil shale facility would produce 42,000 barrels per day and would be located just north of the confluence of Evacuation Creek and the White River at 5400 feet MSL. Drainage flows in the area are easterly, while general prevailing flows are westerly. Maximum ground-level impacts are predicted to the east of the facility.

Tables 6-7 and 6-8 and figures 6-5 and 6-6 summarize the impacts, which are well within criteria. On-site TSP concentrations are above PSD increments, but off-site concentrations are well within the increments. Given the results of the EPA Level-1 visibility screening test, there is no possibility of adverse visibility impairment occurring as a result of Paraho emissions in any mandatory or potential Class I areas (see table 6-9).

6.4 SYNTANA-UTAH

Syntana-Utah is a proposed 57,000 barrel-per-day oil shale facility to be located just north of the White River at 5800 feet MSL.

Tables 6-10 and 6-11 and figures 6-7 and 6-8 summarize the projected air quality impacts, which are well within criteria. Although the Gaussian Puff Model (GPM) indicates that maximum 24-hour-average TSP concentrations near the source are greater than $60 \mu\text{g}/\text{m}^3$, the more realistic COMPLEX model, with distributed point source treatment, indicates a maximum of $13 \mu\text{g}/\text{m}^3$, a factor of 5 less than the GPM result. The EPA Level-1 visibility screening test indicates that the possibility of adverse visibility impairment due to Syntana emissions can be ruled out in all mandatory and potential Class I areas, except Dinosaur National Monument. In this area the screening test indicates that a particulate and NO_x plume might be visible from Dinosaur during stable, light-wind conditions a few times per year (see table 6-12). This was confirmed with the analysis presented in Section 5.6, which indicated that plume discoloration would be observed between 0 and 15 mornings per year in Dinosaur.

6.5 TOSCO

Tosco proposes to produce 45,000 barrels of shale oil per day at a facility located at 5000 feet MSL, south of the White River and east of the Green River.

TABLE 6-7. SUMMARY OF PSD INCREMENT CONSUMPTION BY PARAHO

PSD Increments/Increment Consumption	SO ₂ Concentration (µg/m ³)			TSP Concentration (µg/m ³)	
	3-Hour Average	24-Hour Average	Annual Average	24-Hour Average	Annual Average
<u>Class II Areas</u>					
Allowable PSD Class II increment	512	91	20	37	19
Increment consumption at receptors of maximum impacts					
Impact alone	317	40	1	<16	<4
Impact with Moon Lake Unit 1	319	40	1	<16	<4
Impact with all interrelated (other) sources	322	41	1	<25	<5
Maximum increment consumption on Uintah/Ouray Indian Reservation					
Impact alone	4	1	0	4	0
Impact with Moon Lake Unit 1	10	2	0	5	0
Impact with all interrelated (other) sources	18	4	0	7	0
<u>Class I Areas</u>					
Allowable PSD Class I increment	25	5	2	10	5
Increment consumption at Flat Tops Wilderness Area (federal Class I)					
Impact alone	0	0	0	0	0
Impact with Moon Lake Unit 1	0	0	0	0	0
Impact with all interrelated (other) sources	1	0	0	0	0
Increment consumption at Maroon Bells- Snowmass Wilderness Area (federal Class I)					
Impact alone	0	0	0	0	0
Impact with Moon Lake Unit 1	0	0	0	0	0
Impact with all interrelated (other) sources	0	0	0	0	0
Increment consumption at Dinosaur National Monument (Colorado category I and potential federal Class I)					
Impact alone	4	0	0	0	0
Impact with Moon Lake Unit 1	6	0	0	0	0
Impact with all interrelated (other) sources	10	1	0	1	0

TABLE 6-7 (Concluded)

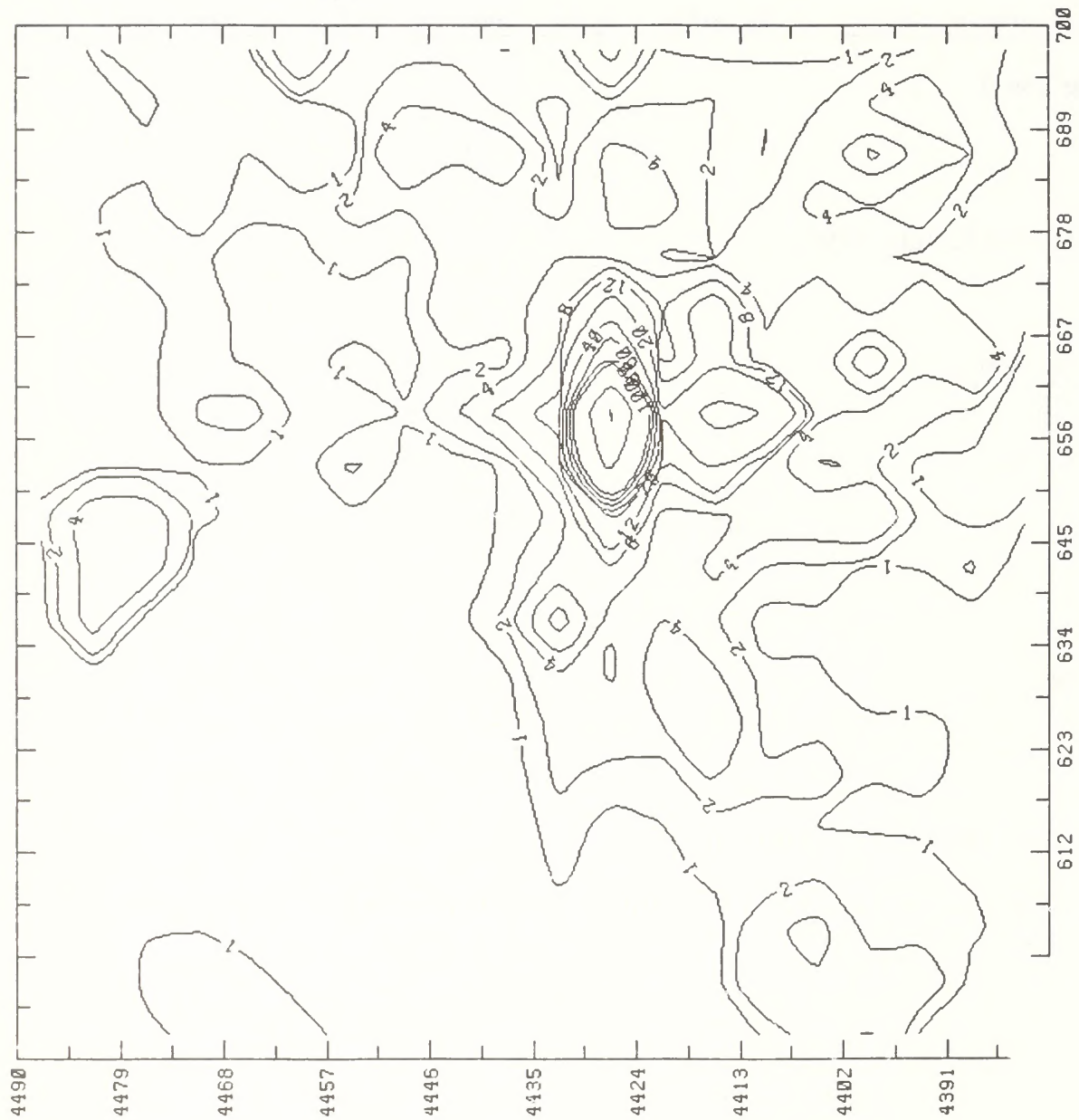
<u>PSD Increments/Increment Consumption</u>	<u>SO₂ Concentration ($\mu\text{g}/\text{m}^3$)</u>			<u>TSP Concentration ($\mu\text{g}/\text{m}^3$)</u>	
	<u>3-Hour Average</u>	<u>24-Hour Average</u>	<u>Annual Average</u>	<u>24-Hour Average</u>	<u>Annual Average</u>
Increment consumption at Colorado National Monument (Colorado category I and potential federal Class I)					
Impact alone	0	0	0	0	0
Impact with Moon Lake Unit 1	0	0	0	0	0
Impact with all interrelated (other) sources	0	0	0	0	0

TABLE 6-8. SUMMARY OF MAXIMUM AMBIENT AIR QUALITY IMPACTS OF
PARAHO COMPARED WITH APPLICABLE STANDARDS

Pollutant/Averaging Time	Maximum Ground-Level Concentration ($\mu\text{g}/\text{m}^3$)					NAAQS* ($\mu\text{g}/\text{m}^3$)
	Baseline	Source Impact	Subtotal	Impact of Other Sources	Total	
Sulfur dioxide (SO_2)						
3-Hour	10	317	327	5	333	1300
24-hour	1	40	41	1	42	365
Annual	0	1	1	0	1	80
Total suspended particulate (TSP)						
24-Hour	175 [†]	<16	<191 [†]	9	<200 [†]	150
Annual	44	<4	<48	1	<49	60
Nitrogen dioxide (NO_2)						
Annual	1	3	4	0	4	100
Carbon monoxide (CO)						
1-Hour	200	125	325	2	327	40,000
8-Hour	200	125	325	2	327	10,000
Ozone (O_3)						
1-Hour	70	2	72	0	72	240
Hydrocarbons (HC)						
3-Hour	100	24	124	0	124	160

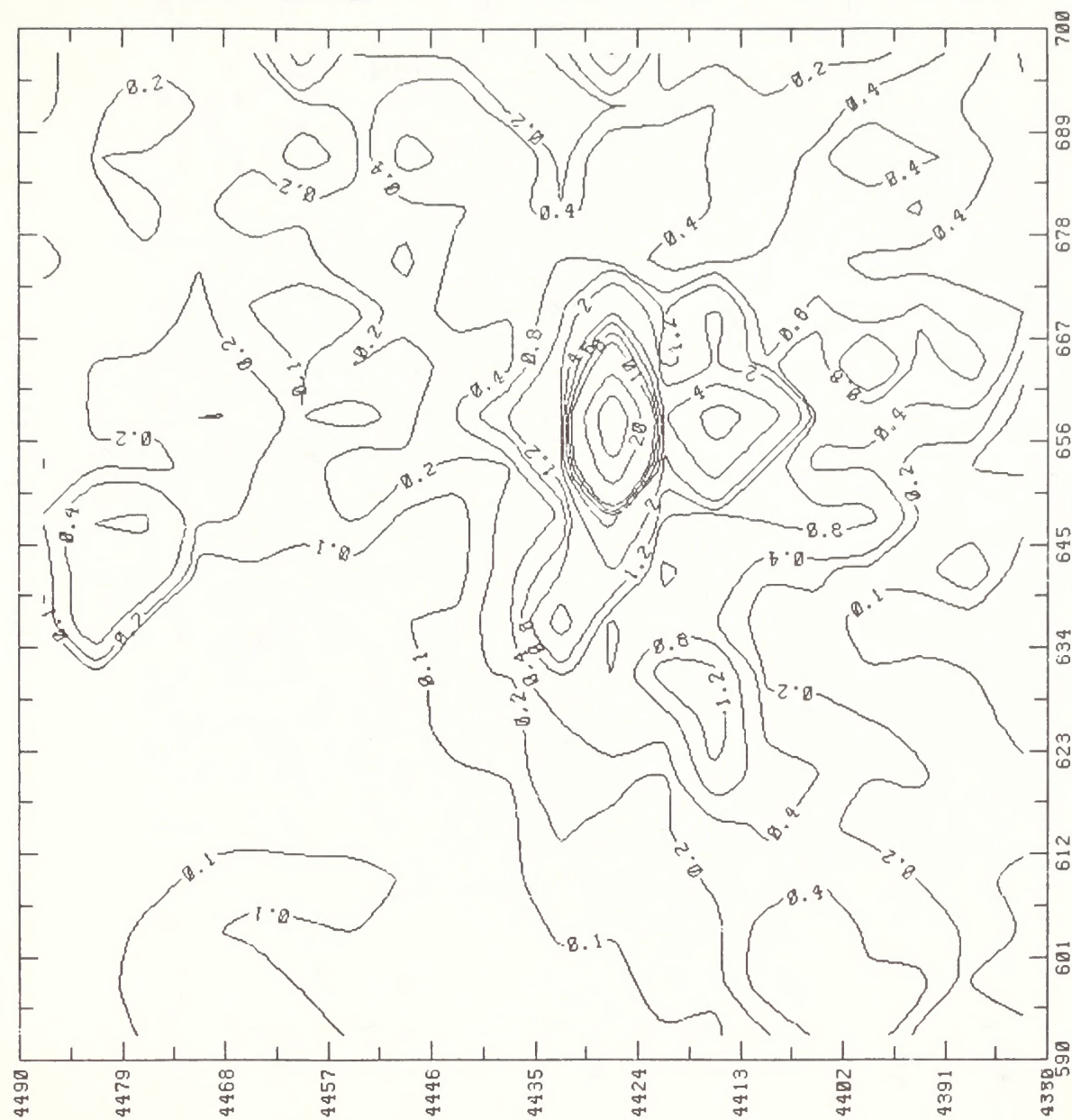
* National Ambient Air Quality Standards.

[†] Exceedance of NAAQS. It is assumed that baseline maximum coincides with source impact maximum.



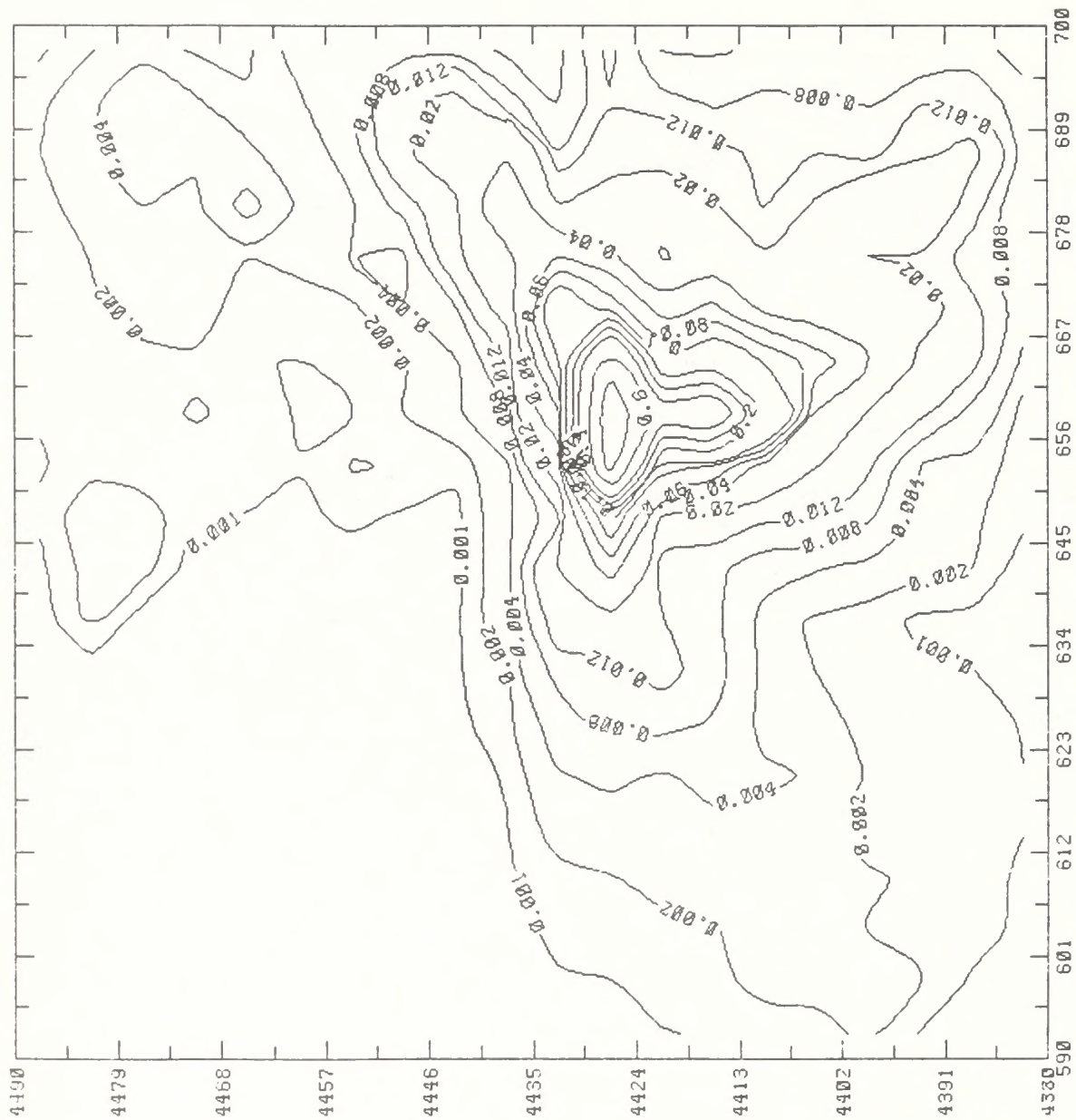
(a) Maximum 3-Hour Average

FIGURE 6-5. GROUND-LEVEL SO_2 CONCENTRATIONS ($\mu\text{g}/\text{m}^3$) DUE TO PARAHO EMISSIONS



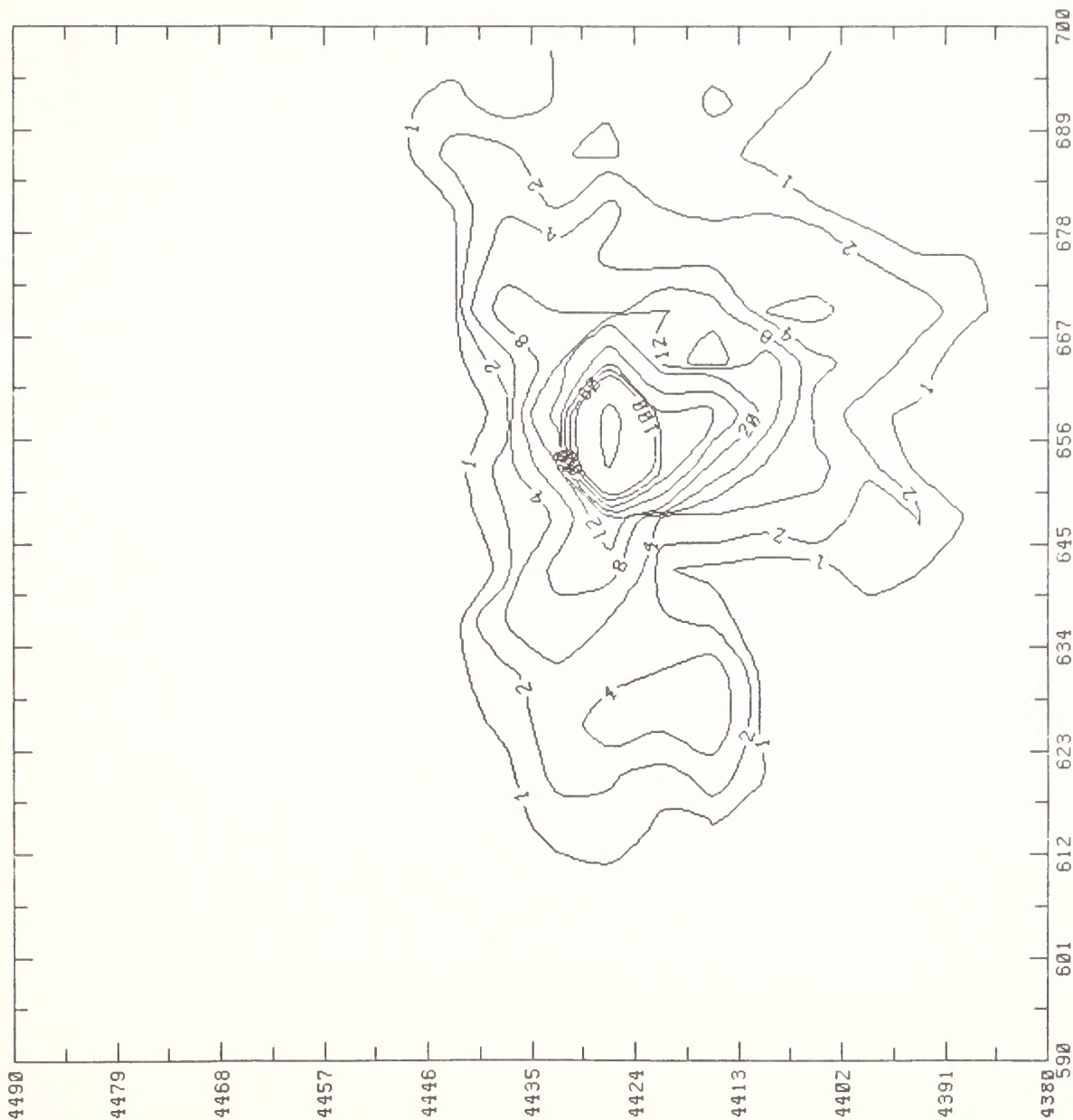
(b) Maximum 24-Hour Average

FIGURE 6-5 (Continued)



(c) Annual Averages

FIGURE 6-5 (Concluded)



Maximum: 69 $\mu\text{g}/\text{m}^3$ (on-site)
 <16 $\mu\text{g}/\text{m}^3$ (off-site)

Note: These GPM results are overly conservative near the source because of source emission aggregation; see COMPLEX-I results in Figure 6-6(b).

(a) Maximum 24-Hour Average

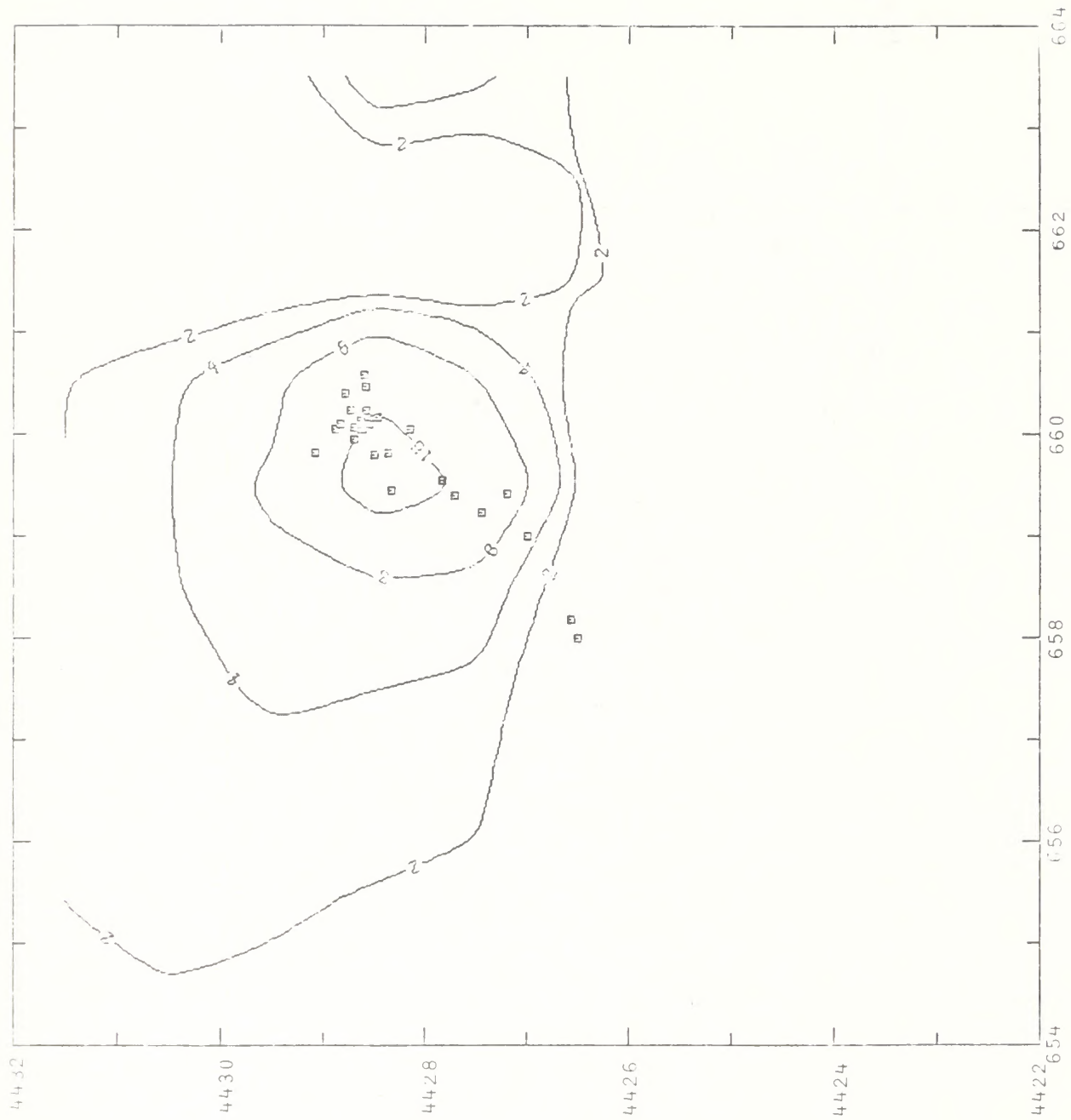
FIGURE 6-6. GROUND-LEVEL TSP CONCENTRATIONS ($\mu\text{g}/\text{m}^3$) DUE TO PARAHO EMISSIONS



□ Point Sources

(b) Maximum 24-Hour Average (Near-Source)

FIGURE 6-6 (Continued)



□ Point Sources

(d) Annual Average (Near-Source)

FIGURE 6-6 (Concluded)

TABLE 6-9. LEVEL-1 SCREENING ANALYSIS RESULTS FOR VISIBILITY
IMPACTS OF PARAHO

Existing or Potential Class I Area or Area of Special Concern	Test for Dark Plume Against Sky C_1	Test for Light Plume Against Terrain C_2	Test for Regional Reduction Sky/Terrain Contrast C_3
Flat Tops Wilderness	-0.02	0.01	0.01
Dinosaur National Monument	-0.07	0.09	0.01
Colorado National Monument	-0.02	0.02	0.01
Uintah/Ouray Indian Reservation			
- North portion	-0.06	0.06	0.01
- South portion	-0.04	0.04	0.01
Uinta Primitive Area	-0.02	0.02	0.01

TABLE 6-10. SUMMARY OF PSD INCREMENT CONSUMPTION BY SYNTANA

PSD Increments/Increment Consumption	SO ₂ Concentration ($\mu\text{g}/\text{m}^3$)			TSP Concentration ($\mu\text{g}/\text{m}^3$)	
	3-Hour Average	24-Hour Average	Annual Average	24-Hour Average	Annual Average
<u>Class II Areas</u>					
Allowable PSD Class II increment	512	91	20	37	19
Increment consumption at receptors of maximum impacts					
Impact alone	41	8	1	13	1
Impact with Moon Lake Unit 1	44	8	1	13	1
Impact with all interrelated (other) sources	47	9	1	18	1
Maximum increment consumption on Uintah/Ouray Indian Reservation					
Impact alone	8	1	0	<13	0
Impact with Moon Lake Unit 1	14	2	0	<14	0
Impact with all interrelated (other) sources	22	4	0	<16	0
<u>Class I Areas</u>					
Allowable PSD Class I increment	25	5	2	10	5
Increment consumption at Flat Tops Wilderness Area (federal Class I)					
Impact alone	0	0	0	0	0
Impact with Moon Lake Unit 1	0	0	0	0	0
Impact with all interrelated (other) sources	1	0	0	0	0
Increment consumption at Maroon Bells- Snowmass Wilderness Area (federal Class I)					
Impact alone	0	0	0	0	0
Impact with Moon Lake Unit 1	0	0	0	0	0
Impact with all interrelated (other) sources	0	0	0	0	0
Increment consumption at Dinosaur National Monument (Colorado category I and potential federal Class I)					
Impact alone	1	0	0	0	0
Impact with Moon Lake Unit 1	3	0	0	0	0
Impact with all interrelated (other) sources	7	1	0	1	0

TABLE 6-10 (Concluded)

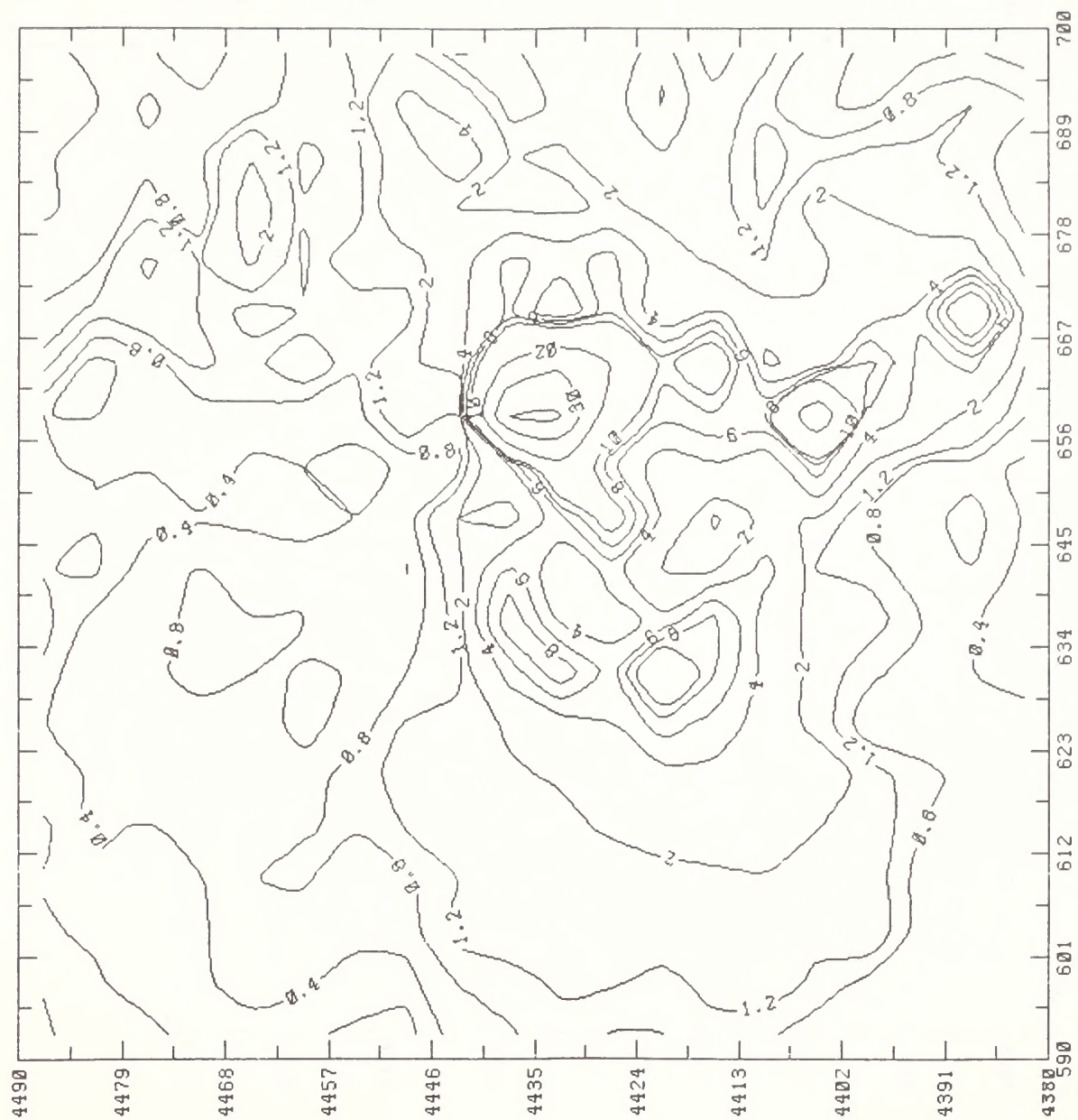
<u>PSD Increments/Increment Consumption</u>	<u>SO₂ Concentration ($\mu\text{g}/\text{m}^3$)</u>			<u>TSP Concentration ($\mu\text{g}/\text{m}^3$)</u>	
	<u>3-Hour Average</u>	<u>24-Hour Average</u>	<u>Annual Average</u>	<u>24-Hour Average</u>	<u>Annual Average</u>
Increment consumption at Colorado National Monument (Colorado category I and potential federal Class I)					
Impact alone	0	0	0	0	0
Impact with Moon Lake Unit 1	0	0	0	0	0
Impact with all interrelated (other) sources	0	0	0	0	0

TABLE 6-11. SUMMARY OF MAXIMUM AMBIENT AIR QUALITY IMPACTS OF SYNTANA COMPARED WITH APPLICABLE STANDARDS

Pollutant/Averaging Time	Maximum Ground-Level Concentration ($\mu\text{g}/\text{m}^3$)					NAAQS* ($\mu\text{g}/\text{m}^3$)
	Baseline	Source Impact	Subtotal	Impact of Other Sources	Total	
Sulfur dioxide (SO_2)						
3-Hour	2	41	43	6	49	1300
24-Hour	1	8	9	1	10	365
Annual	0	1	1	0	1	80
Total suspended particulate (TSP)						
24-Hour	153 [†]	13	166 [†]	5	171 [†]	150
Annual	39	1	40	0	40	60
Nitrogen dioxide (NO_2)						
Annual	1	6	7	0	7	100
Carbon monoxide (CO)						
1-Hour	200	20	220	0	220	40,000
8-Hour	200	20	220	0	220	10,000
Ozone (O_3)						
1-Hour	70	2	72	0	72	240
Hydrocarbons (HC)	100	20	126	0	126	160

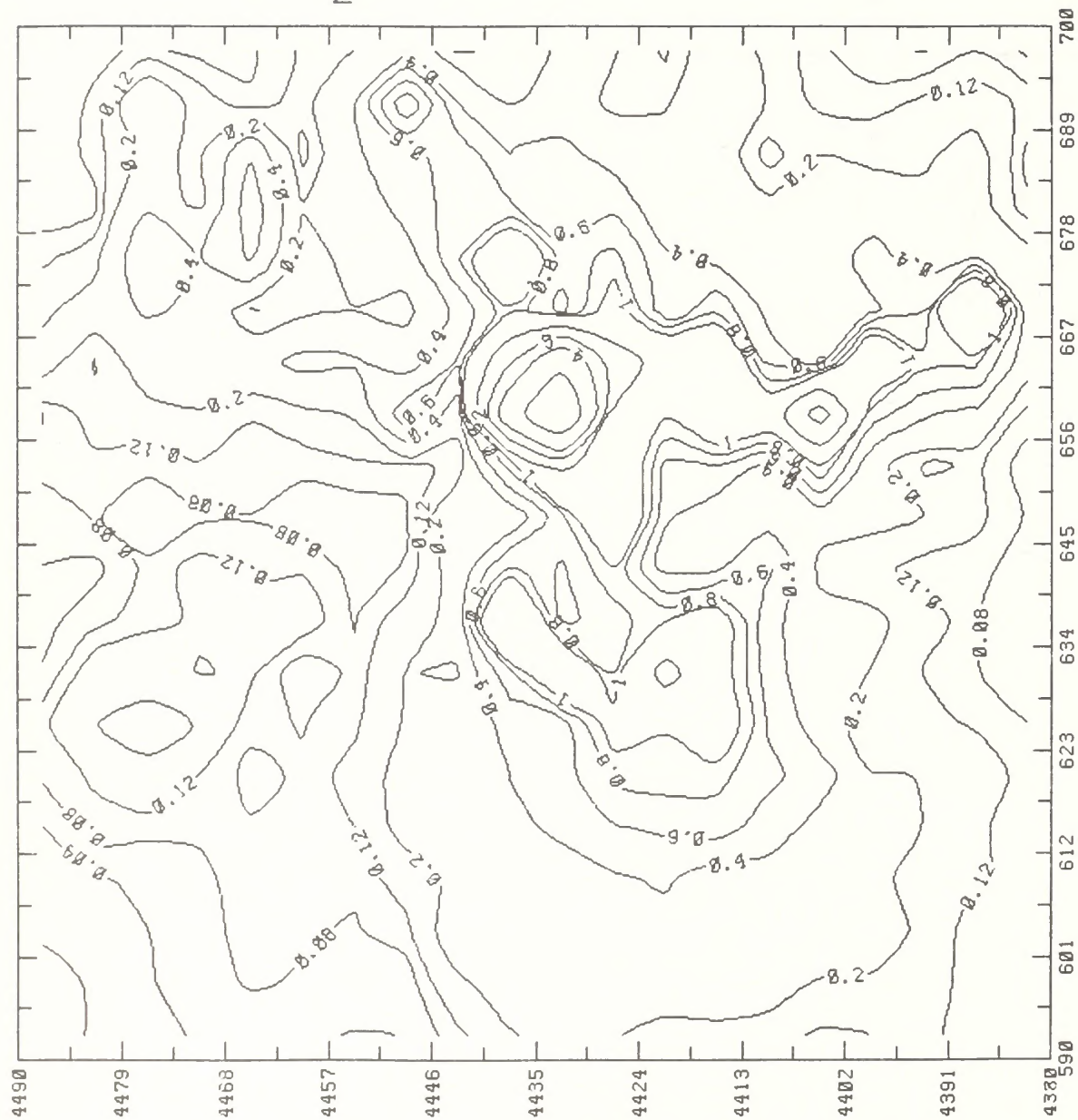
* National Ambient Air Quality Standards.

[†] Exceedance of NAAQS. It is assumed that baseline maximum coincides with source impact maximum.



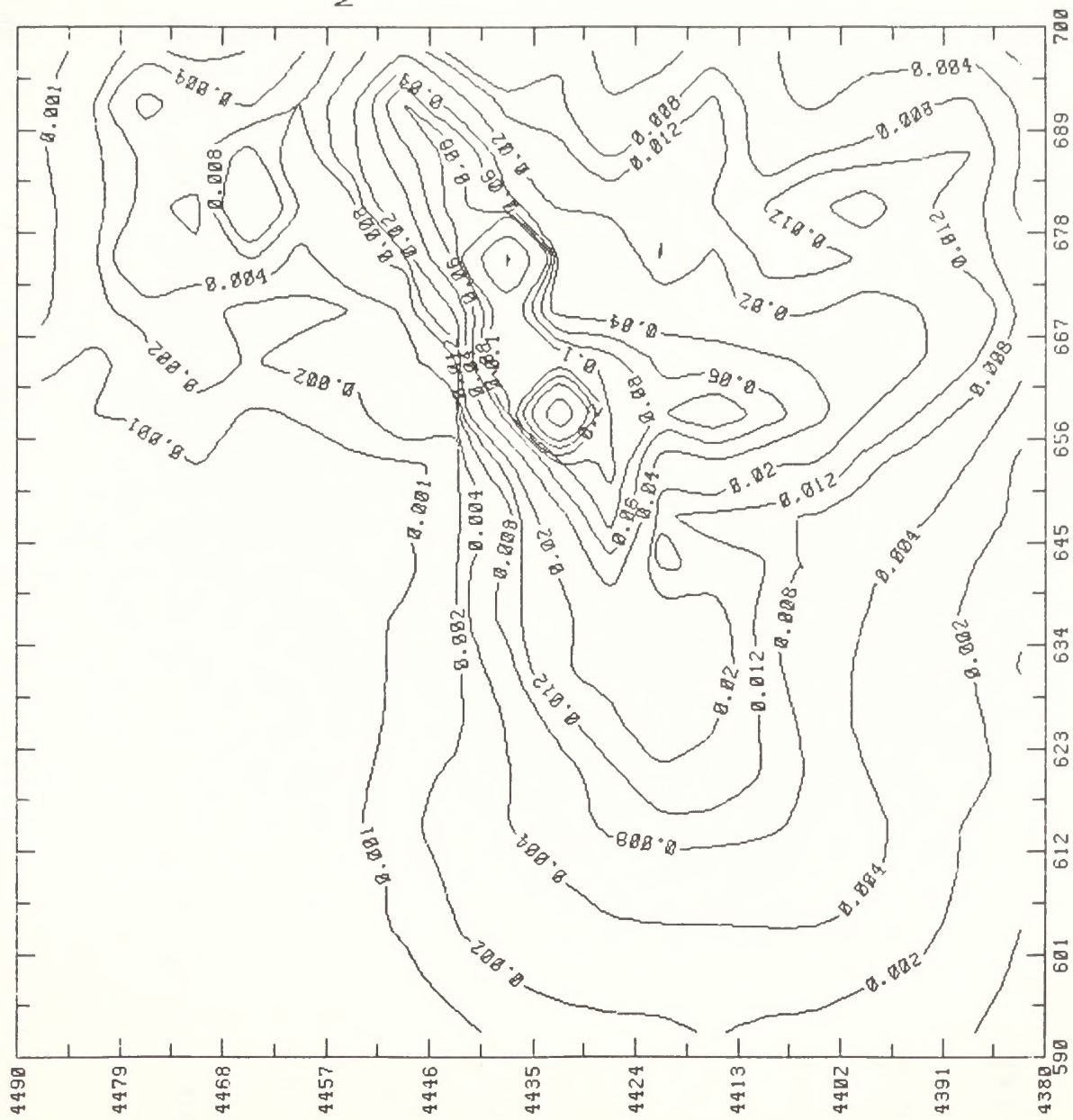
(a) Maximum 3-Hour Average

FIGURE 6-7. GROUND-LEVEL SO_2 CONCENTRATIONS ($\mu\text{g}/\text{m}^3$) DUE TO SYNTANA-UTAH EMISSIONS



(b) Maximum 24-Hour Average

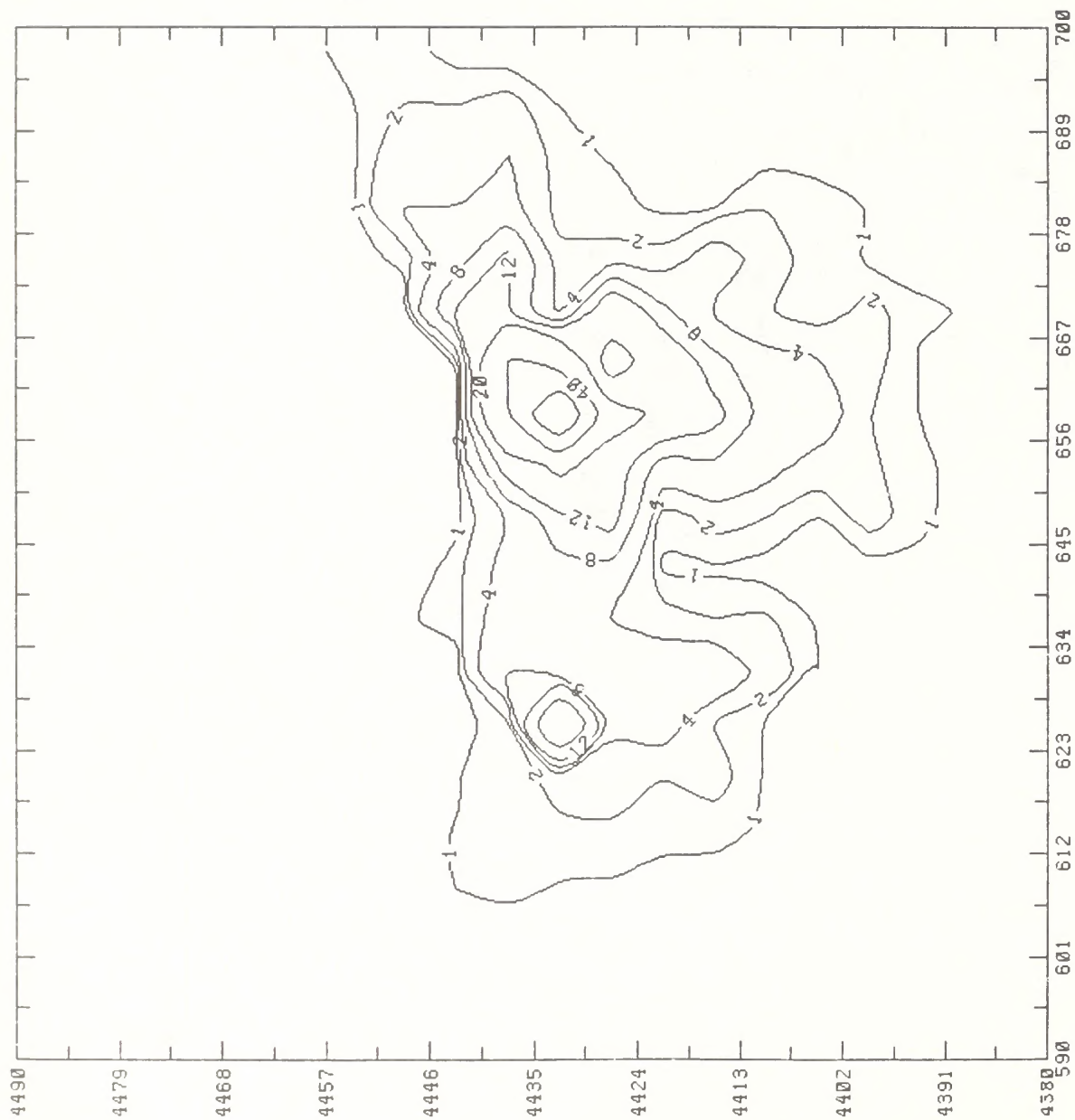
FIGURE 6-7 (Continued)



(c) Annual Average

FIGURE 6-7 (Concluded)

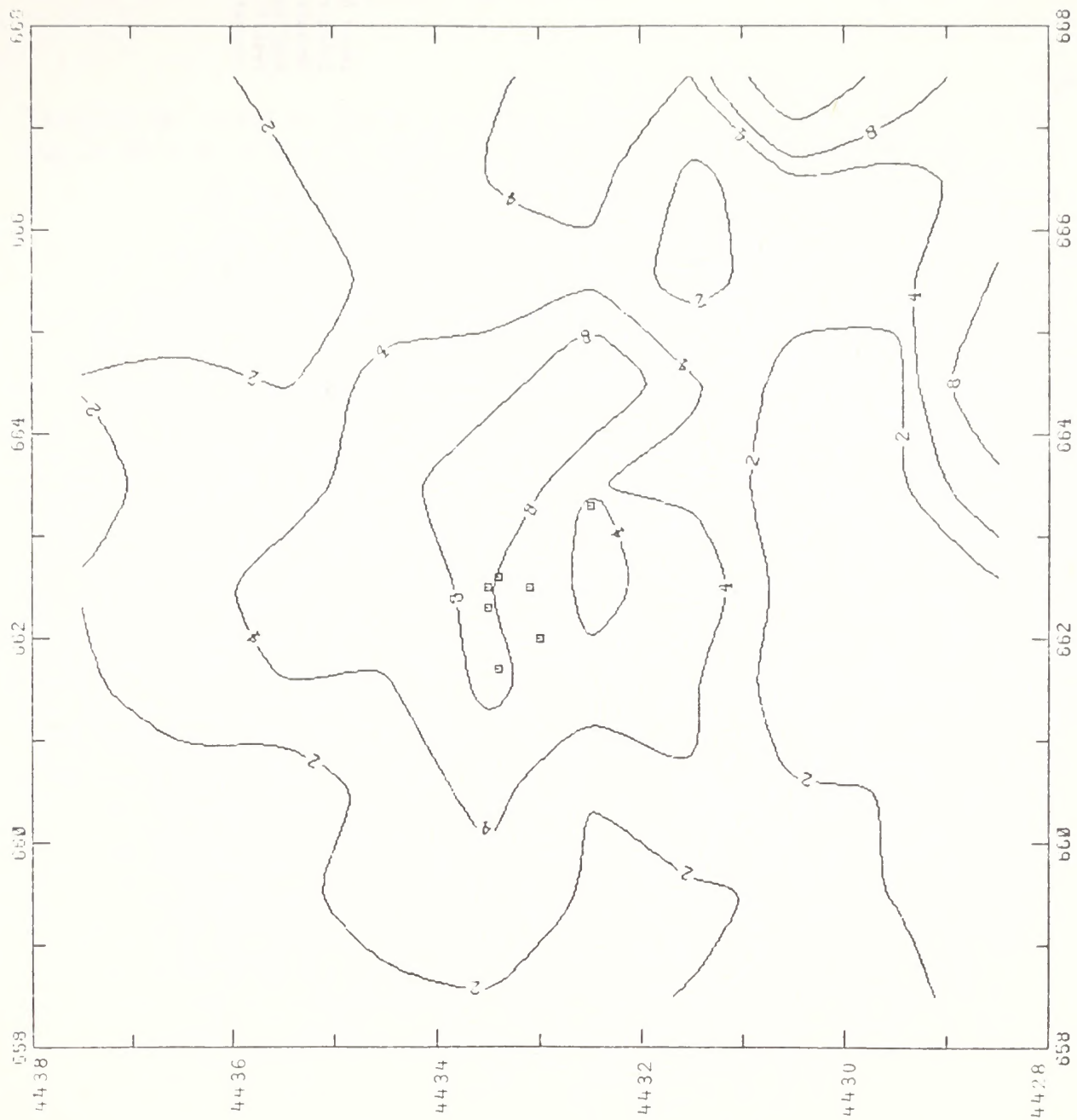
Maximum: 0.8 $\mu\text{g}/\text{m}^3$



Note: These GPM results are overly conservative near the source because of source emission aggregation; see COMPLEX-I results in Figure 6-8(b).

(a) Maximum 24-Hour Average

FIGURE 6-8. GROUND-LEVEL TSP CONCENTRATIONS ($\mu\text{g}/\text{m}^3$) DUE TO SYNTANA-UTAH EMISSIONS



□ Point Sources

(b) Maximum 24-Hour Average (Near-Source)

FIGURE 6-8 (Continued)

TABLE 6-12. LEVEL-1 SCREENING ANALYSIS RESULTS FOR VISIBILITY
IMPACTS OF SYNTANA

Existing or Potential Class I Area or Area of Special Concern	Test for Dark Plume Against Sky C_1	Test for Light Plume Against Terrain C_2	Test for Regional Reduction Sky/Terrain Contrast C_3
Flat Tops Wilderness	-0.02	0.02	0.01
Dinosaur National Monument	-0.13*	0.15*	0.01
Colorado National Monument	-0.03	0.03	0.01
Uintah/Ouray Indian Reservation			
- North portion	-0.08	0.08	0.01
- South portion	-0.05	0.05	0.01
Uinta Primitive Area	-0.03	0.02	0.01

* Indicates that potential of adverse visibility impairment cannot be ruled out by Level-1 screening (i.e., $|C| > 0.1$).

Tables 6-13 and 6-14 and figures 6-9 and 6-10 summarize the air quality impacts, which are well within criteria values. The on-site maximum 24-hour-average TSP concentration is predicted to be higher than the Class II increment of $37 \mu\text{g}/\text{m}^3$; however, off-site impacts are predicted to be less than $16 \mu\text{g}/\text{m}^3$. Tosco passes the EPA Level-1 visibility screening analysis at all mandatory and potential Class I areas (see table 6-15).

6.6 SUMMARY AND COMPARISON WITH OTHER ANALYSES

The air quality modeling studies performed by the applicants were reviewed. Only the following three provided model estimates of air quality impacts: Paraho, Syntana-Utah, and Tosco. Table 6-16 summarizes the air quality model approaches used by these applicants. Table 6-17 compares results of the current study, previous screening analyses performed by Systems Applications, Inc. for the EPA (Latimer and Doyle, 1981), and the applicant studies. This table compares maximum 24-hour-average SO_2 and TSP concentrations. This averaging time is of particular interest because the 24-hour-average SO_2 and TSP PSD Class II increments are most restrictive. Note that all the model estimates of impacts are reasonably close and that all impacts are within PSD increments.

TABLE 6-13. SUMMARY OF PSD INCREMENT CONSUMPTION BY TOSCO

PSD Increments/Increment Consumption	SO ₂ Concentration ($\mu\text{g}/\text{m}^3$)			TSP Concentration ($\mu\text{g}/\text{m}^3$)	
	3-Hour Average	24-Hour Average	Annual Average	24-Hour Average	Annual Average
<u>Class II Areas</u>					
Allowable PSD Class II increment	512	91	20	37	19
Increment consumption at receptors of maximum impacts					
Impact alone	54	13	1	<16	<1
Impact with Moon Lake Unit 1	57	14	1	<17	<1
Impact with all interrelated (other) sources	60	15	1	<18	<1
Maximum increment consumption on Uintah/Ouray Indian Reservation					
Impact alone	40	8	0	<16	<1
Impact with Moon Lake Unit 1	46	9	0	<17	<1
Impact with all interrelated (other) sources	54	11	0	<19	<1
<u>Class I Areas</u>					
Allowable PSD Class I increment	25	5	2	10	5
Increment consumption at Flat Tops Wilderness Area (federal Class I)					
Impact alone	0	0	0	0	0
Impact with Moon Lake Unit 1	0	0	0	0	0
Impact with all interrelated (other) sources	1	0	0	0	0
Increment consumption at Maroon Bells- Snowmass Wilderness Area (federal Class I)					
Impact alone	0	0	0	0	0
Impact with Moon Lake Unit 1	0	0	0	0	0
Impact with all interrelated (other) sources	0	0	0	0	0
Increment consumption at Dinosaur National Monument (Colorado category I and potential federal Class I)					
Impact alone	1	0	0	0	0
Impact with Moon Lake Unit 1	3	0	0	0	0
Impact with all interrelated (other) sources	7	1	0	1	0

TABLE 6-13 (Concluded)

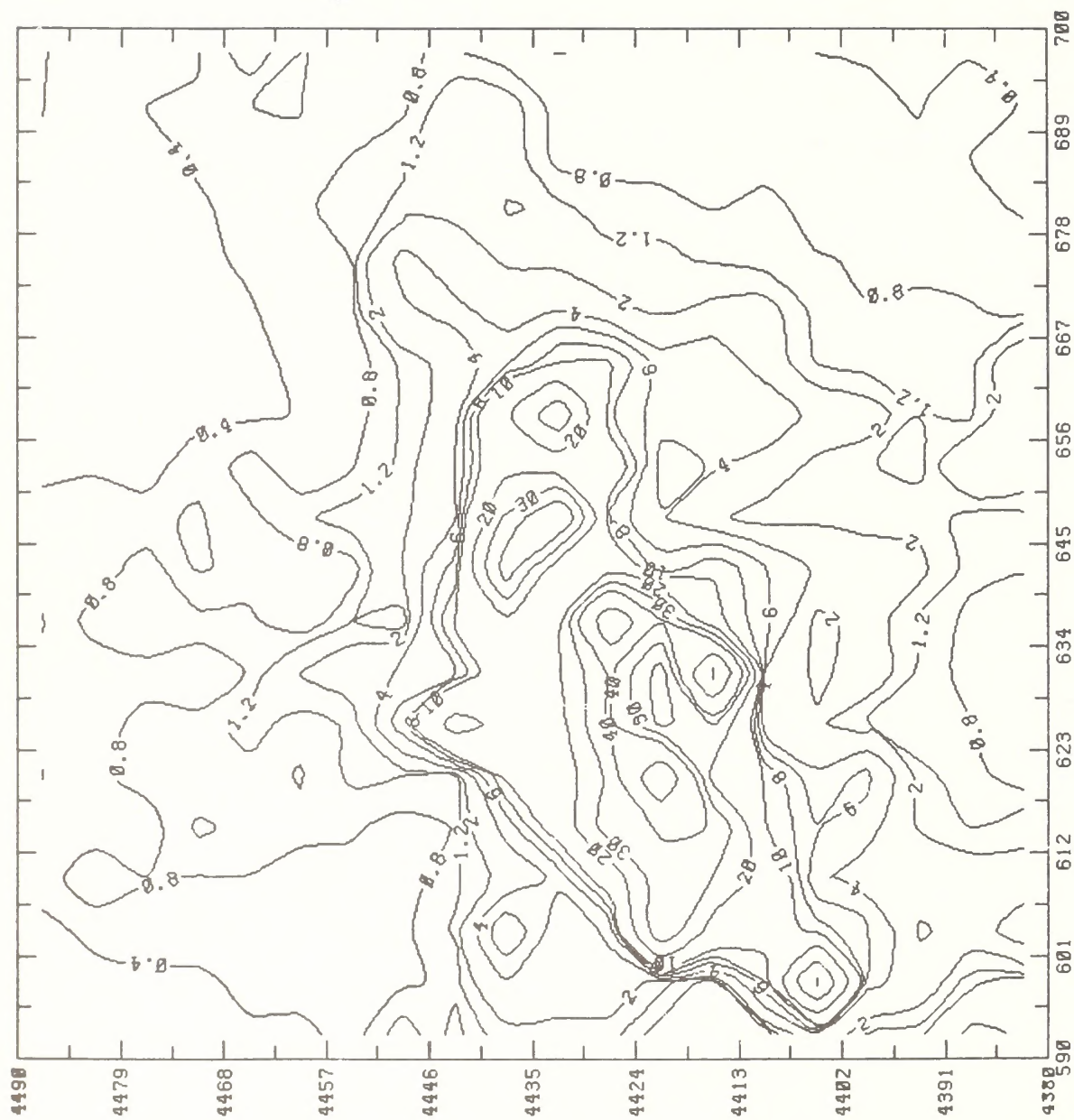
<u>PSD Increments/Increment Consumption</u>	<u>SO₂ Concentration</u> <u>($\mu\text{g}/\text{m}^3$)</u>			<u>TSP Concentration</u> <u>($\mu\text{g}/\text{m}^3$)</u>	
	<u>3-Hour</u> <u>Average</u>	<u>24-Hour</u> <u>Average</u>	<u>Annual</u> <u>Average</u>	<u>24-Hour</u> <u>Average</u>	<u>Annual</u> <u>Average</u>
Increment consumption at Colorado National Monument (Colorado category I and potential federal Class I)					
Impact alone	0	0	0	0	0
Impact with Moon Lake Unit 1	0	0	0	0	0
Impact with all interrelated (other) sources	0	0	0	0	0

TABLE 6-14. SUMMARY OF MAXIMUM AMBIENT AIR QUALITY IMPACTS OF
TOSCO COMPARED WITH APPLICABLE STANDARDS

Pollutant/Averaging Time	Maximum Ground-Level Concentration ($\mu\text{g}/\text{m}^3$)					NAAQS* ($\mu\text{g}/\text{m}^3$)
	Baseline	Source Impact	Subtotal	Impact of Other Sources	Total	
Sulfur dioxide (SO_2)						
3-Hour	185	54	239	3	242	1300
24-Hour	23	13	36	1	37	365
Annual	0	1	1	0	1	80
Total suspended particulate (TSP)						
24-Hour	222 [†]	<16	<236 [†]	1	<237 [†]	150
Annual	55	<1	<56	0	<56	60
Nitrogen dioxide (NO_2)						
Annual	1	8	9	0	9	100
Carbon monoxide (CO)						
1-Hour	200	5	205	0	205	40,000
8-Hour	200	5	205	0	205	10,000
Ozone (O_3)						
1-Hour	70	2	72	0	72	240
Hydrocarbons (HC)						
3-Hour	100	105	205	0	205	160

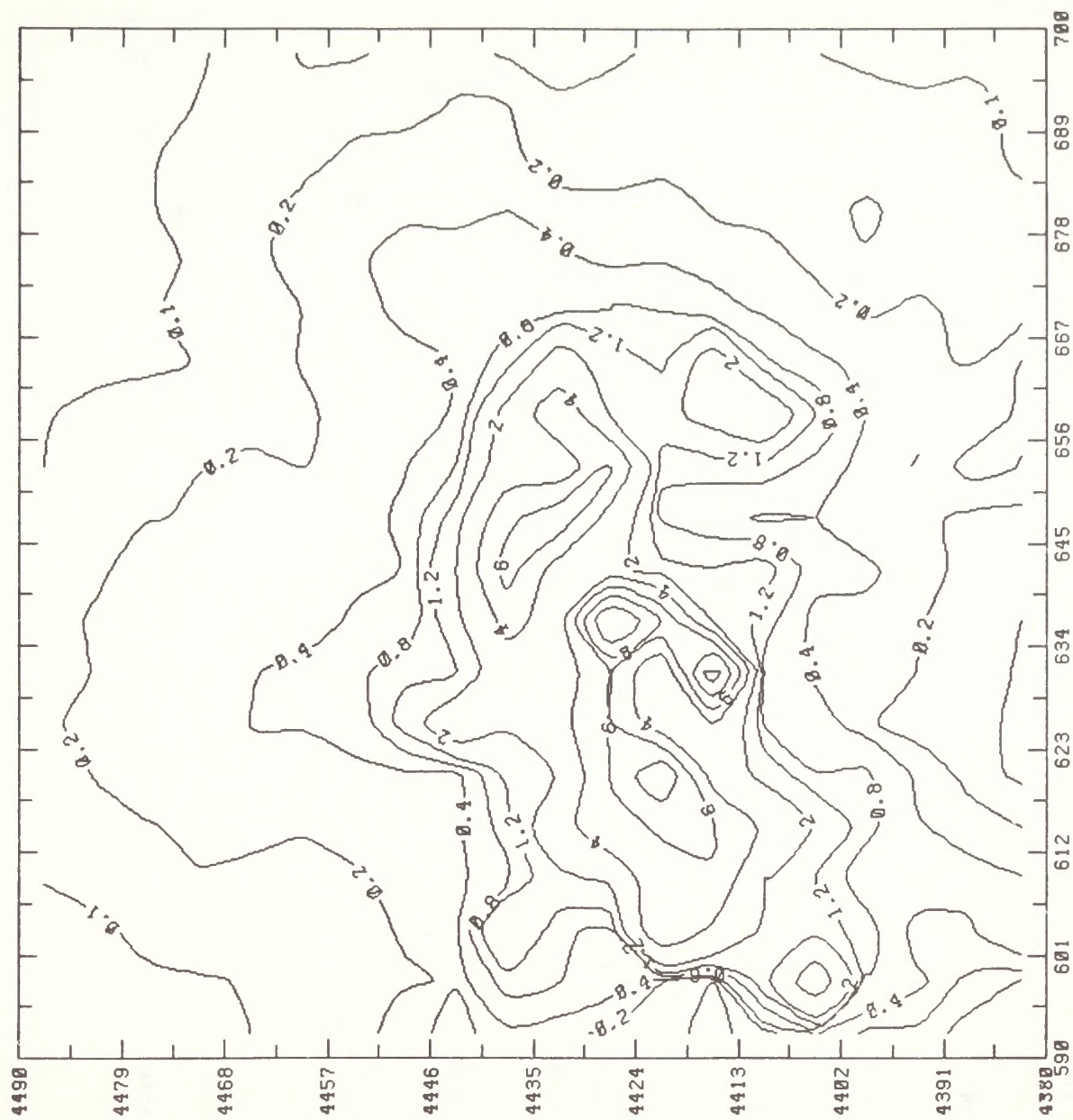
* National Ambient Air Quality Standards.

[†] Exceedance of NAAQS. It is assumed that baseline maximum coincides with source impact maximum.



(a) Maximum 3-Hour Average

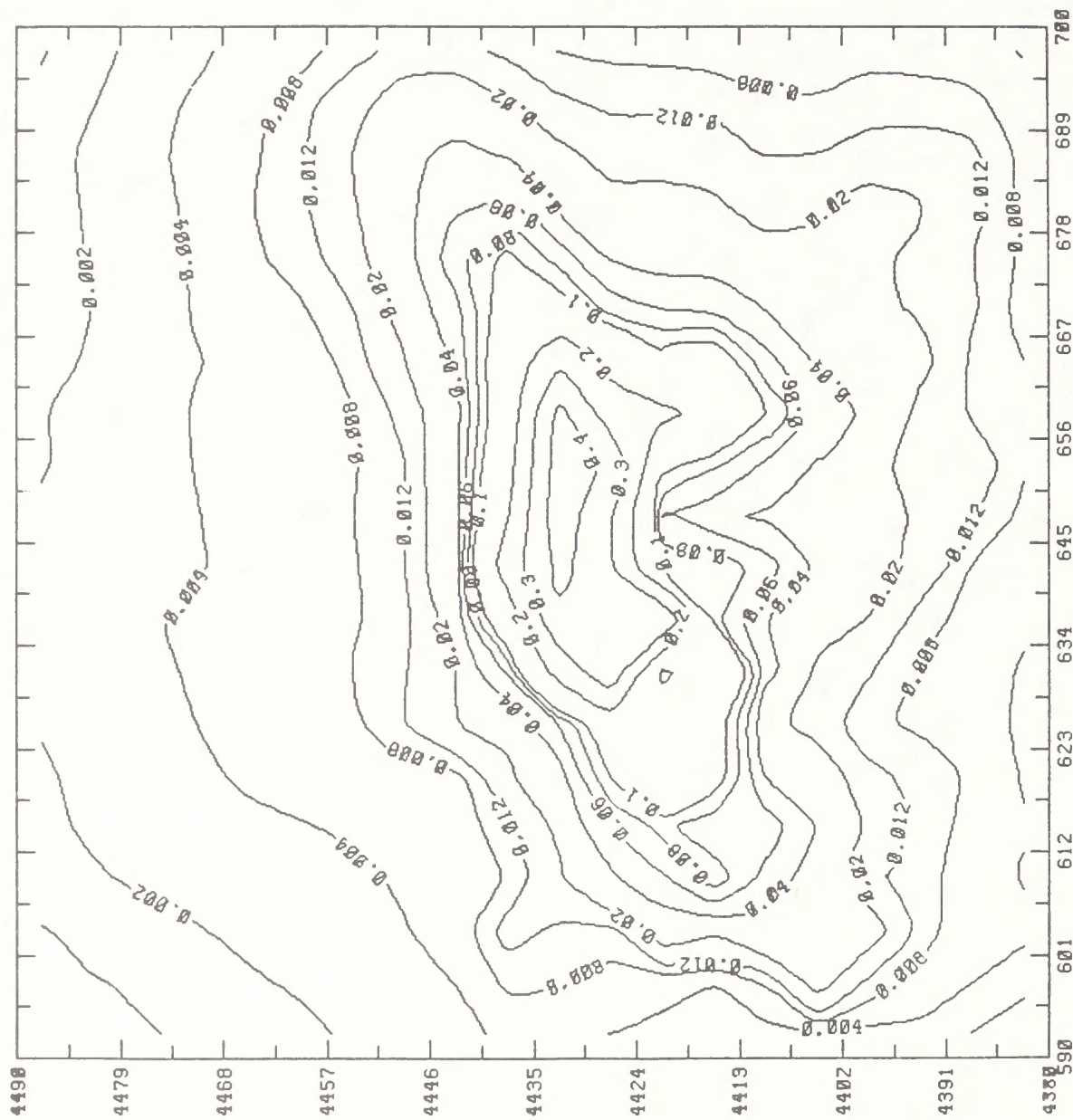
FIGURE 6-9. GROUND-LEVEL SO_2 CONCENTRATIONS ($\mu\text{g}/\text{m}^3$) DUE TO TOSCO EMISSIONS



Maximum: 13 $\mu\text{g}/\text{m}^3$

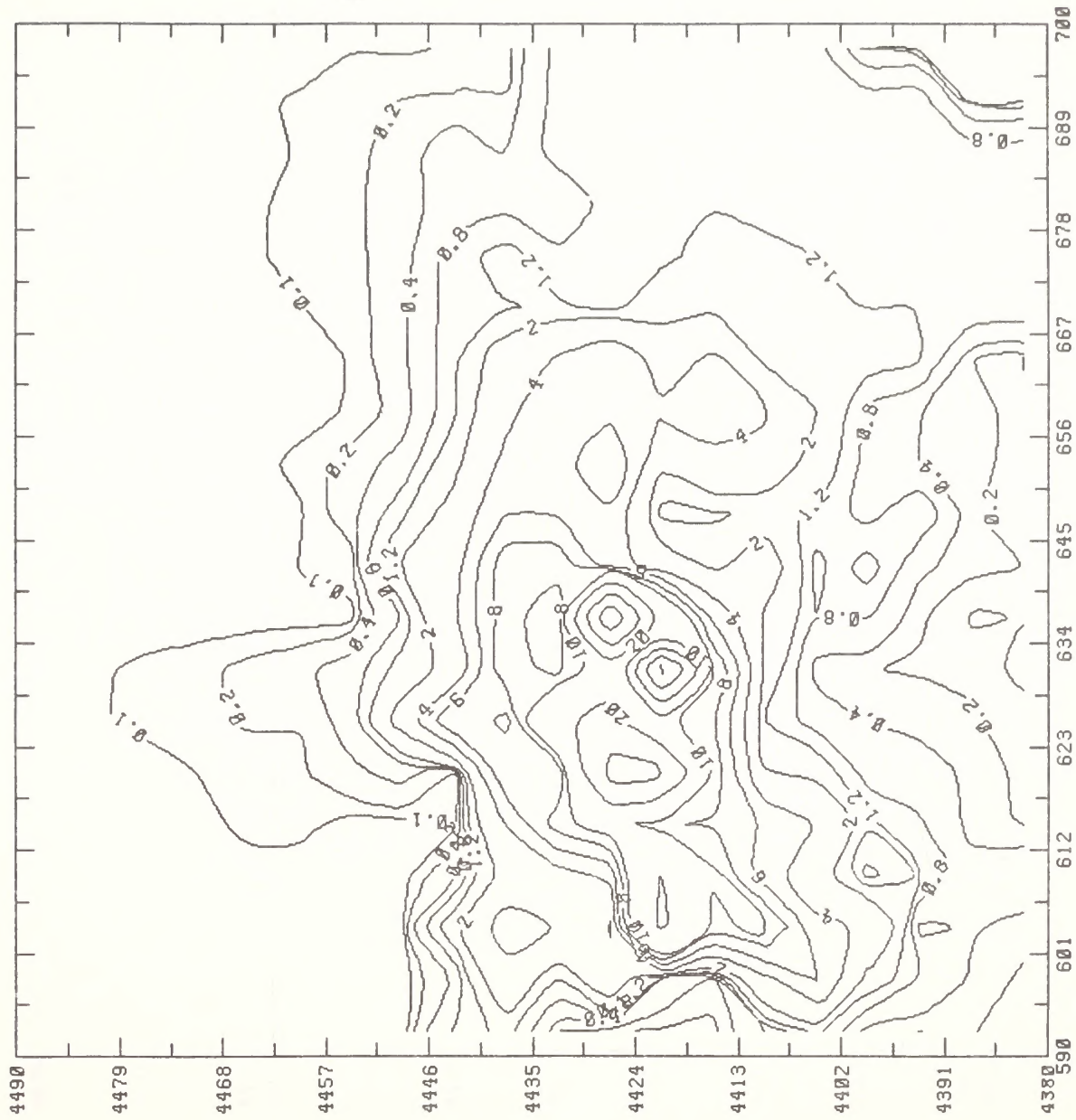
(b) Maximum 24-Hour Average

FIGURE 6-9 (Continued)



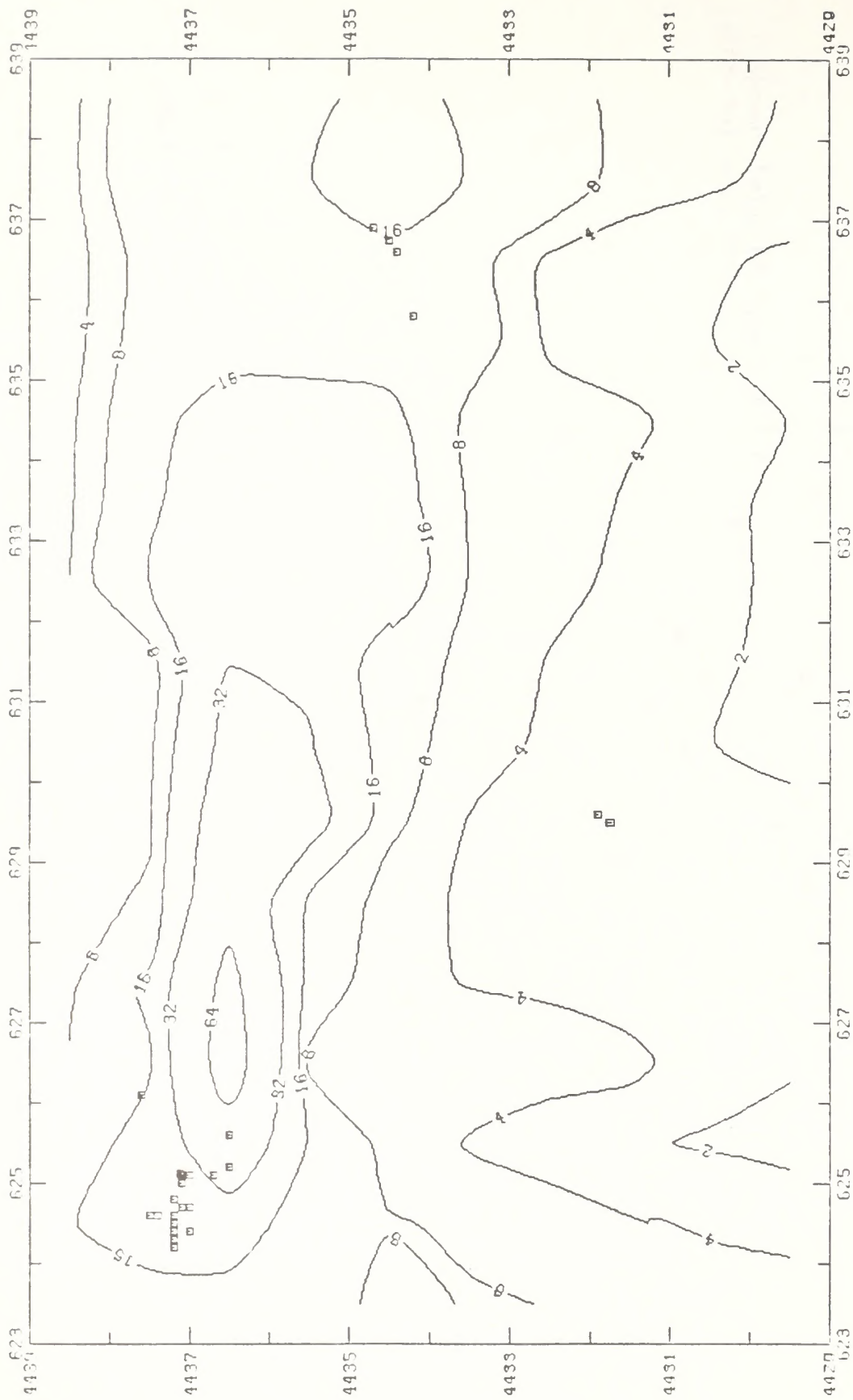
(c) Annual Average

FIGURE 6-9 (Concluded)



(a) Maximum 24-Hour Average

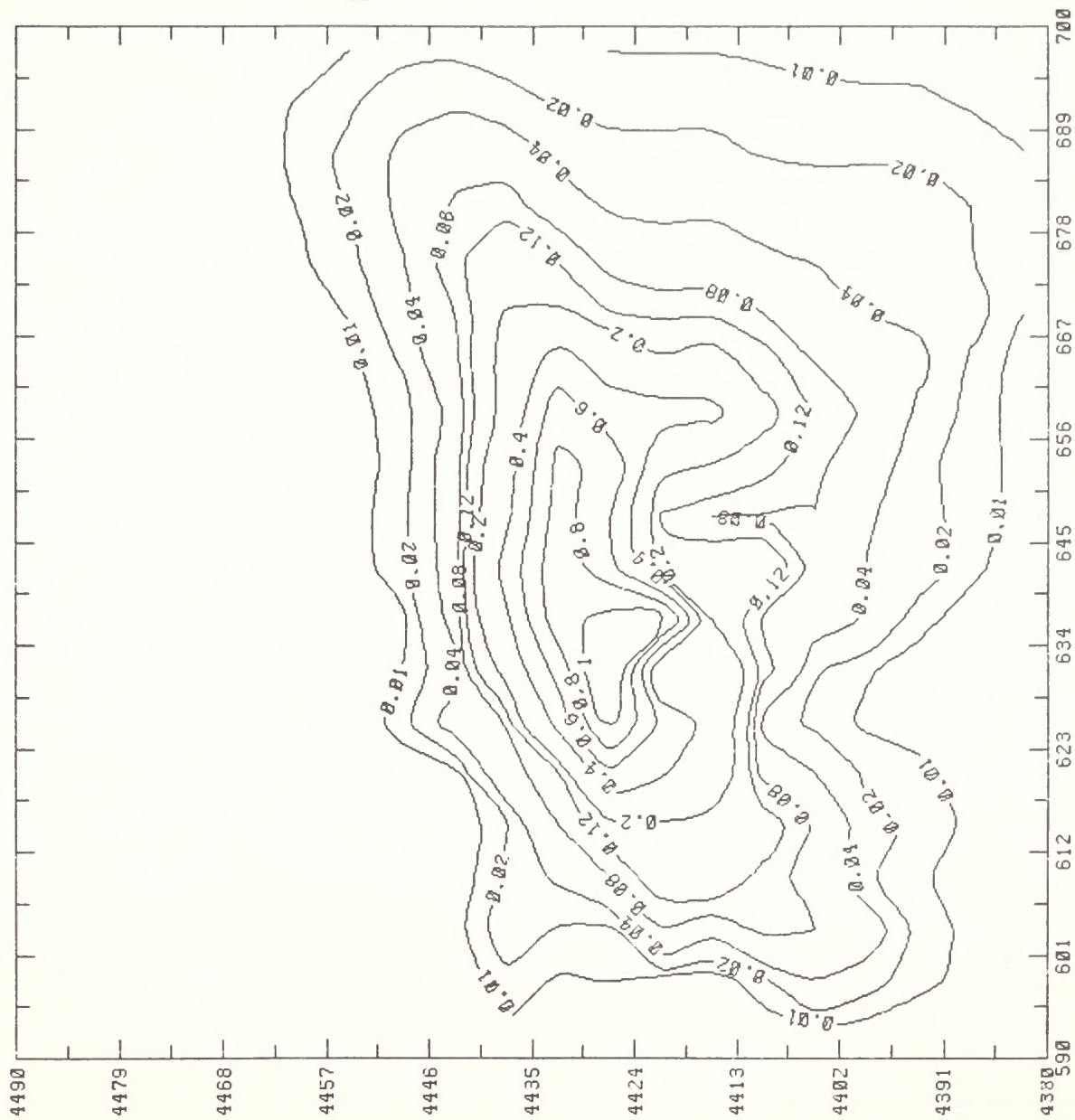
FIGURE 6-10. GROUND-LEVEL TSP CONCENTRATIONS ($\mu\text{g}/\text{m}^3$) DUE TO TOSCO EMISSIONS



□ Point Sources

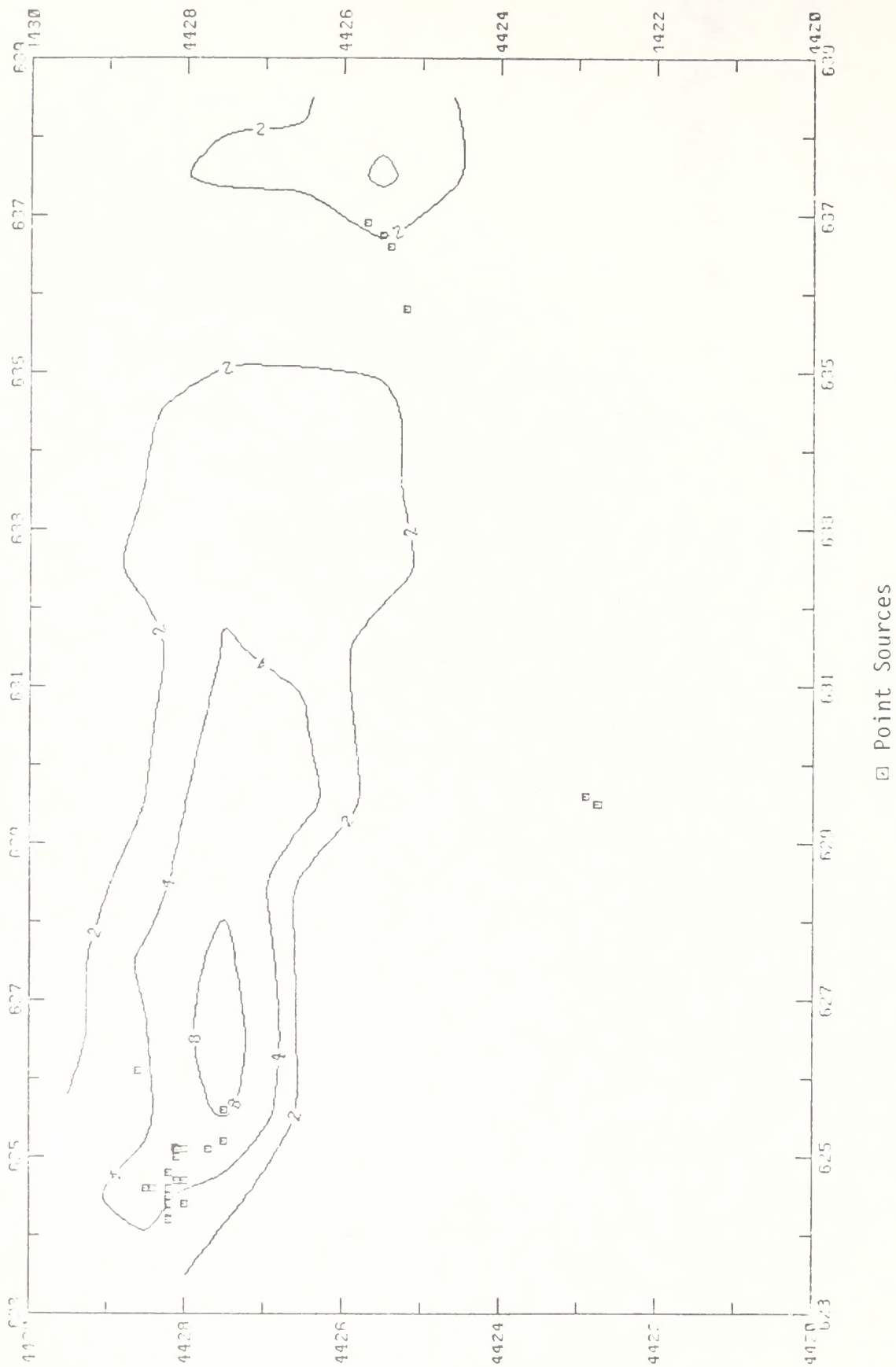
(b) Maximum 24-Hour Average (Near-Source)

FIGURE 6-10 (Continued)



(c) Annual Average

FIGURE 6-10 (Continued)



□ Point Sources
 (d) Annual Average (Near-Source)

FIGURE 6-10 (Concluded)

TABLE 6-15. LEVEL-1 SCREENING ANALYSIS RESULTS FOR VISIBILITY
IMPACTS OF TOSCO

Existing or Potential Class I Area or Area of Special Concern	Test for Dark Plume Against Sky C_1	Test for Light Plume Against Terrain C_2	Test for Regional Reduction Sky/Terrain Contrast C_3
Flat Tops Wilderness	-0.02	0.01	0.00
Dinosaur National Monument	-0.08	0.07	0.00
Colorado National Monument	-0.03	0.02	0.00
Uintah/Ouray Indian Reservation			
- North portion	-0.23*	0.27*	0.00
- South portion	-0.10*	0.10*	0.00
Uinta Primitive Area	-0.04	0.03	0.00

* Indicates that potential of adverse visibility impairment cannot be ruled out by Level-1 screening (i.e., $|C| > 0.1$).

TABLE 6-16. SUMMARY OF MODEL APPROACHES USED BY APPLICANTS

Site	Methods
Paraho	<ul style="list-style-type: none"> > WRSP baseline air quality data > VALLEY runs for annual means of SO₂, TSP, and NO₂; 24-hour averages of SO₂, TSP, and H₂SO₄; 3-hour SO₂ average; and 1-hour and 8-hour CO averages > REM2 was run to model O₃ hourly in a Lagrangian trajectory methodology > Visibility screening (EPA Level-1) for Dinosaur National Monument
Syntana-Utah	<ul style="list-style-type: none"> > White River Shale Project (WRSP) baseline air quality data > VALLEY used for 24-hour worst-case mode screening (with F stability, 2.5 m/s wind speed, and 6 hours of persistence in each sector); for annual mode, with STAR data from WRSP sites > Visibility screening (EPA Level-1) for Flat Tops Wilderness Area
Tosco	<ul style="list-style-type: none"> > VALLEY for complex terrain; standard assumptions for 24-hour worst-case mode screening > TSP and CO obtained via χ/Q scaling from SO₂ results > CDM for flat terrain for 24-hour SO₂, TSP, and annual average TSP > Sand Wash 1980 baseline air quality data > Visibility screening (EPA Level-1) for Dinosaur National Monument

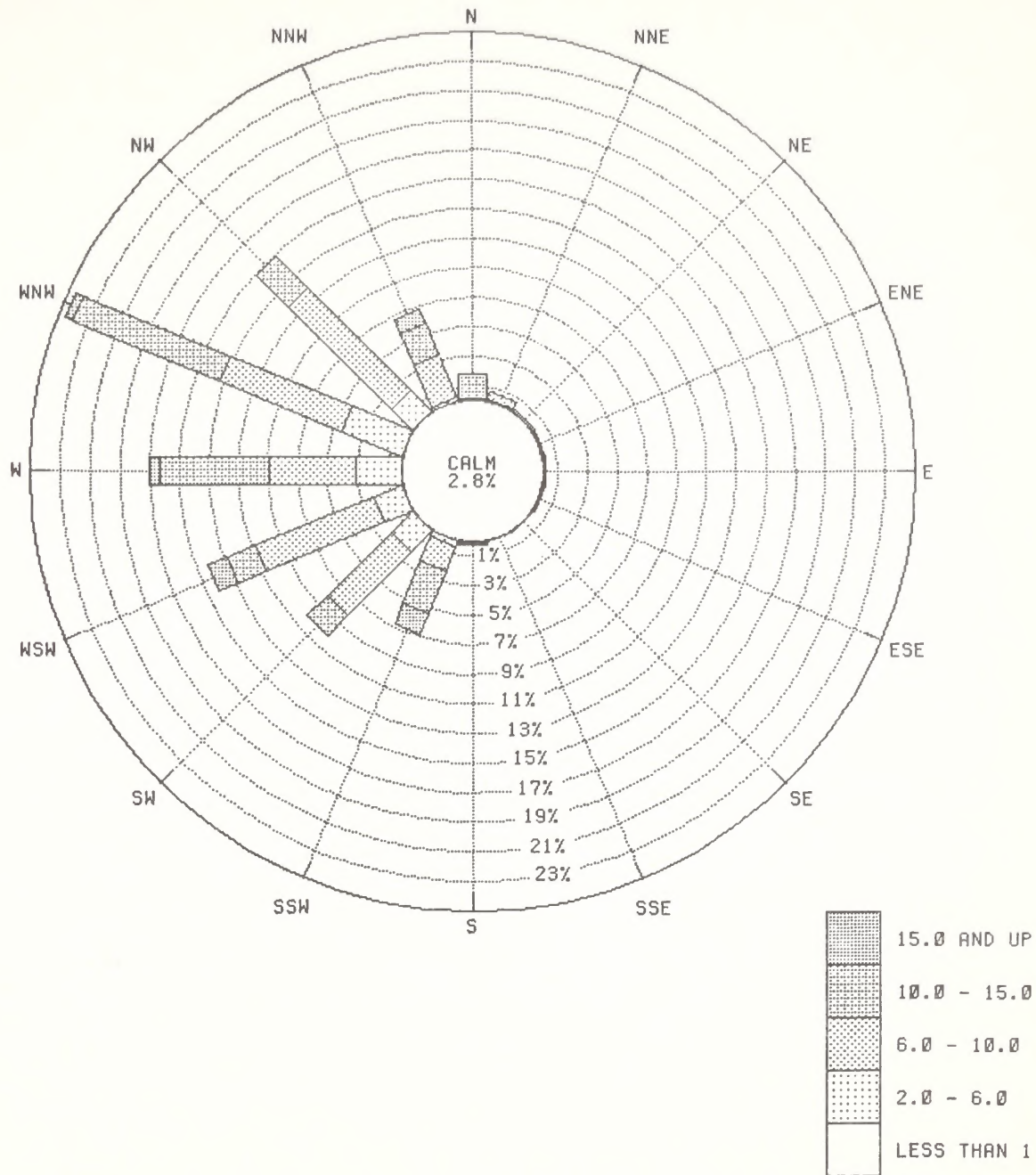
TABLE 6-17. COMPARISON OF WORST-CASE CALCULATIONS OF 24-HOUR CONCENTRATIONS NEAR SPECIFIC PROPOSED SYNTHETIC FUEL FACILITIES

Pollutant/Source	Ambient Air Quality Standard	PSD Class II Increment	EPA/Systems Applications			Applicant's Air Quality Modeling	Current BLM/ Systems Applications Study
			Original Estimate	Screening Study Corrected Estimate*	Study		
Sulfur dioxide (maximum 24-hour average)	365	91					
Enercor-Mono Power			--	--		--	3
Magic Circle			16	14		--	32
Paraho			16	18		44	40
Syntana-Utah			27	12		6	8
Tosco			14	9		32	13
Total suspended particulates (maximum 24-hour average)	150	37					
Enercor-Mono Power			--	--		--	7
Magic Circle			16	30		--	< 32
Paraho			16	27		25	< 16
Syntana-Utah			26	33		18	13
Tosco			71	35		33	< 16

* Original (Latimer and Doyle, 1981) concentration estimates, corrected for current production capacity and emission inventory.

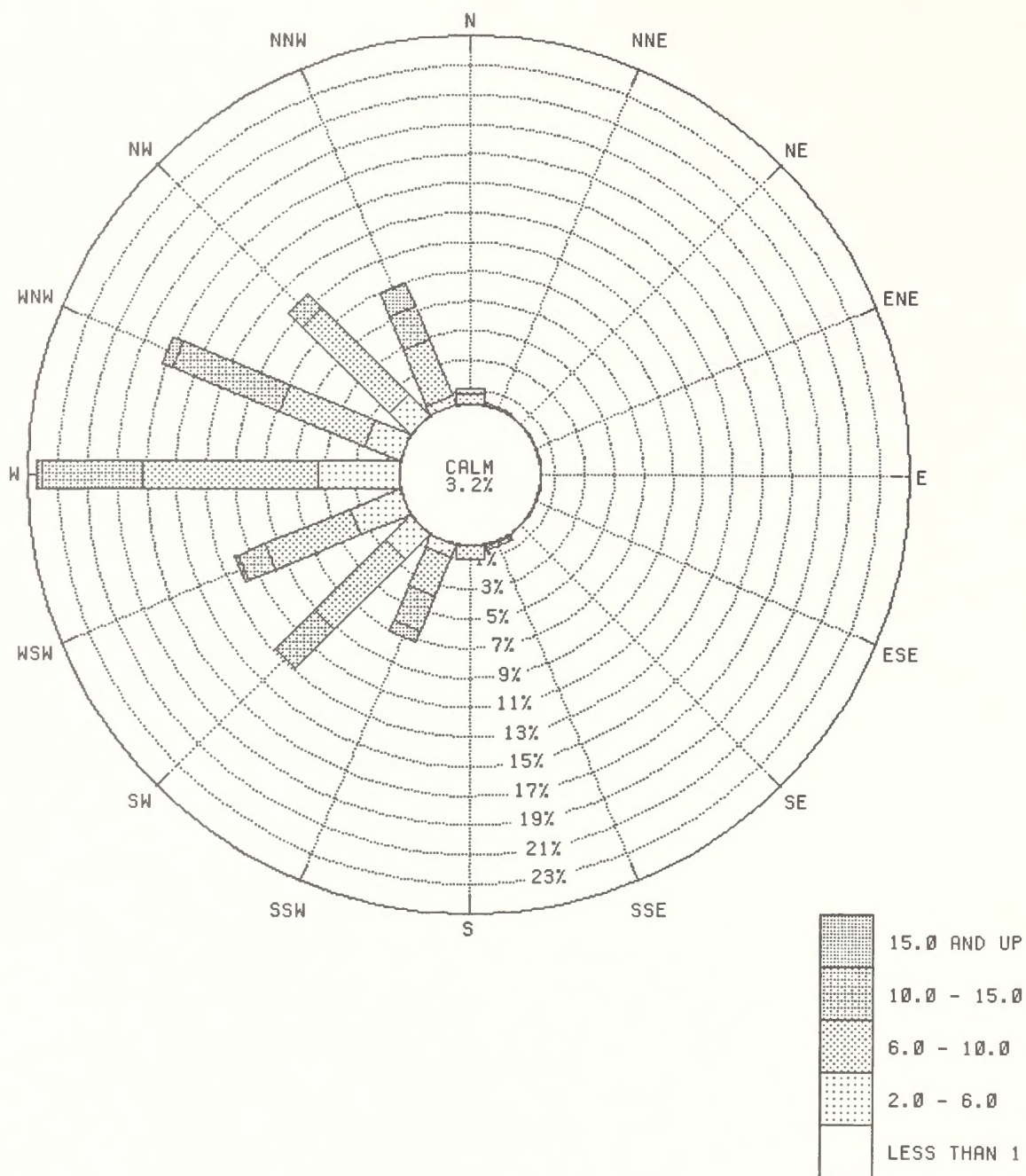
Appendix A

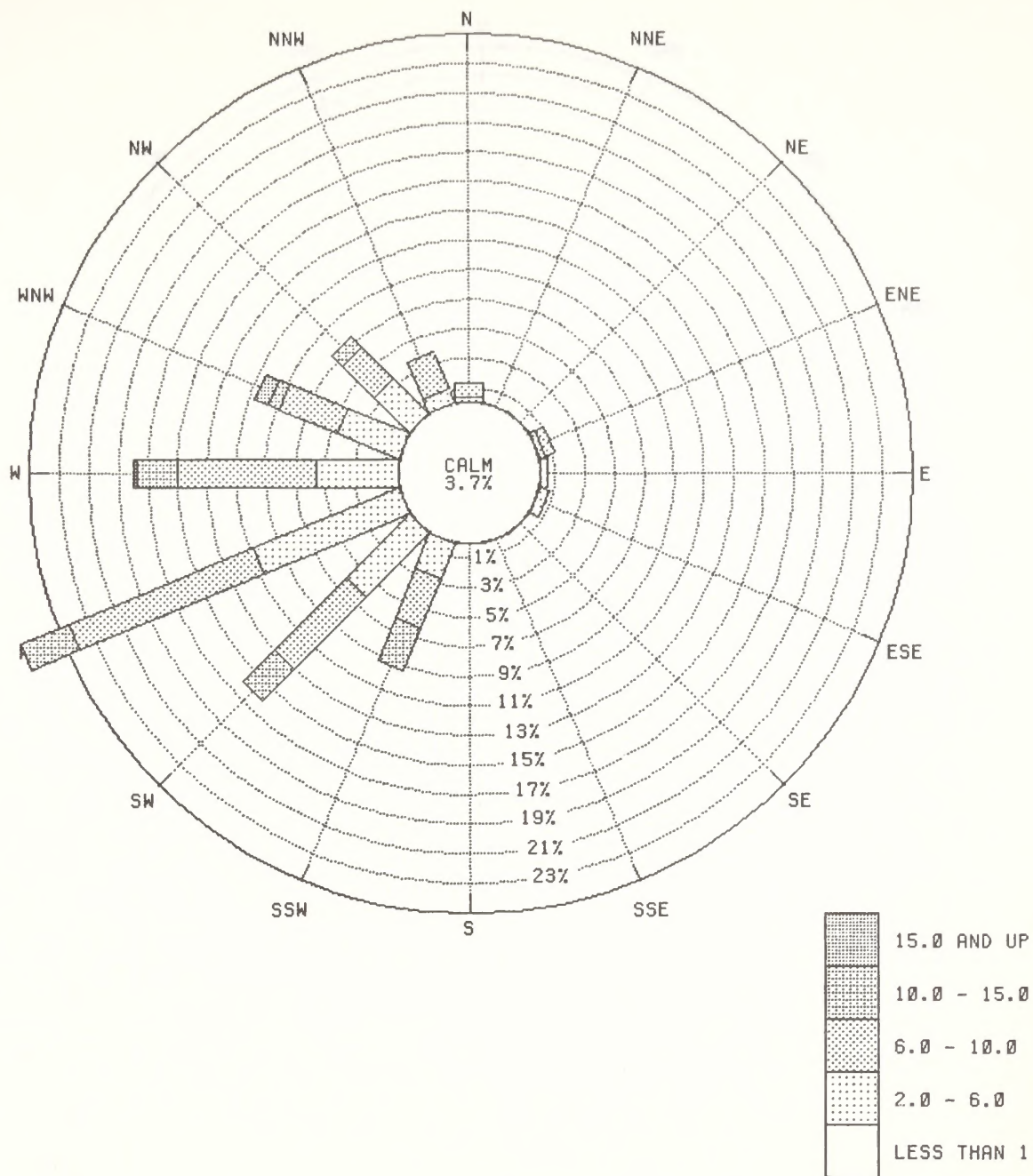
UPPER LEVEL WIND ROSE STRATIFIED BY SEASON AND
TIME OF DAY FOR STUDY REGION IN 1978

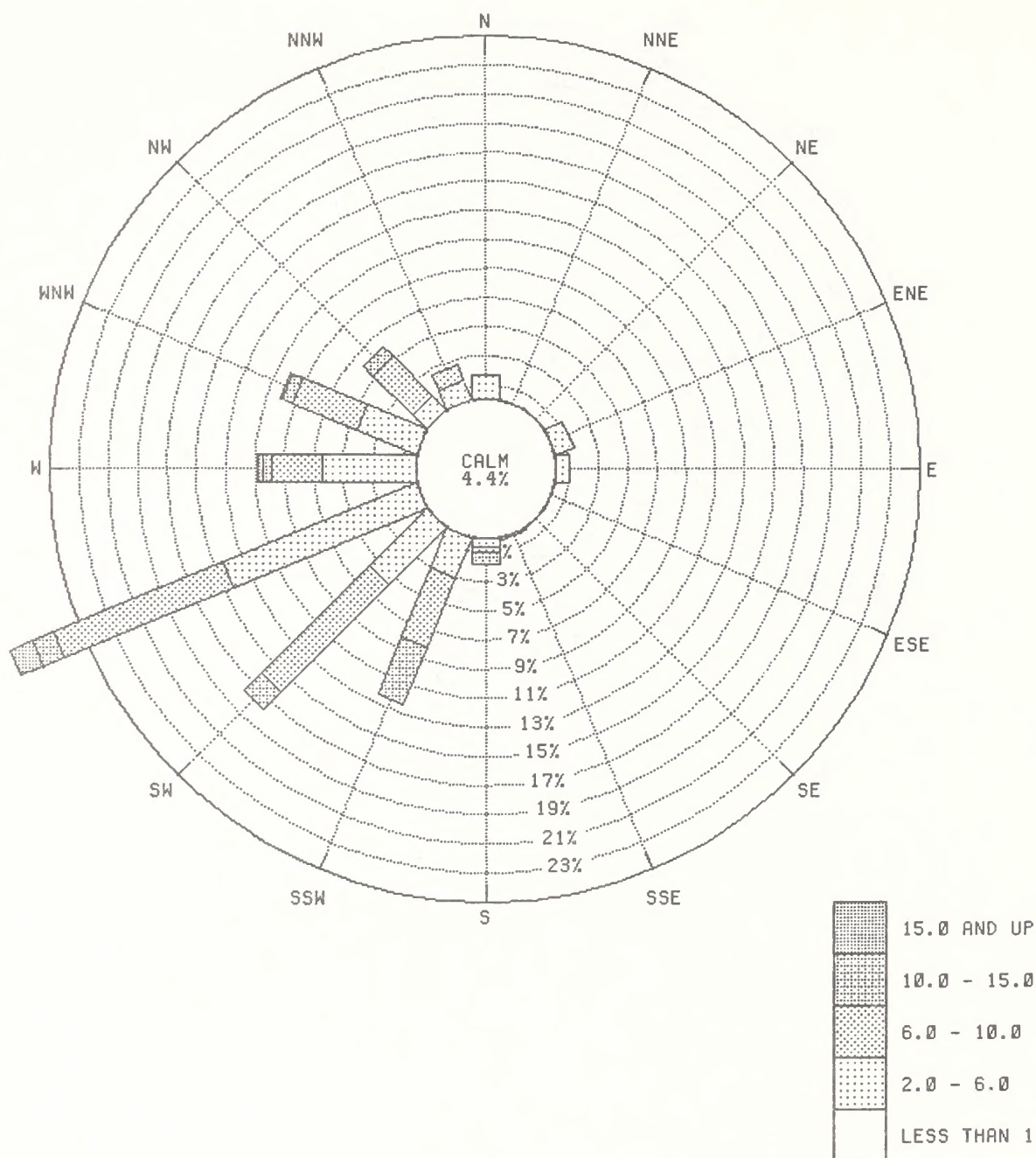


CLIMATOLOGICAL WIND ROSE
SPRING DAY
(MARCH - APRIL, 6 AM - 6 PM)

1104 VALID DATA POINTS

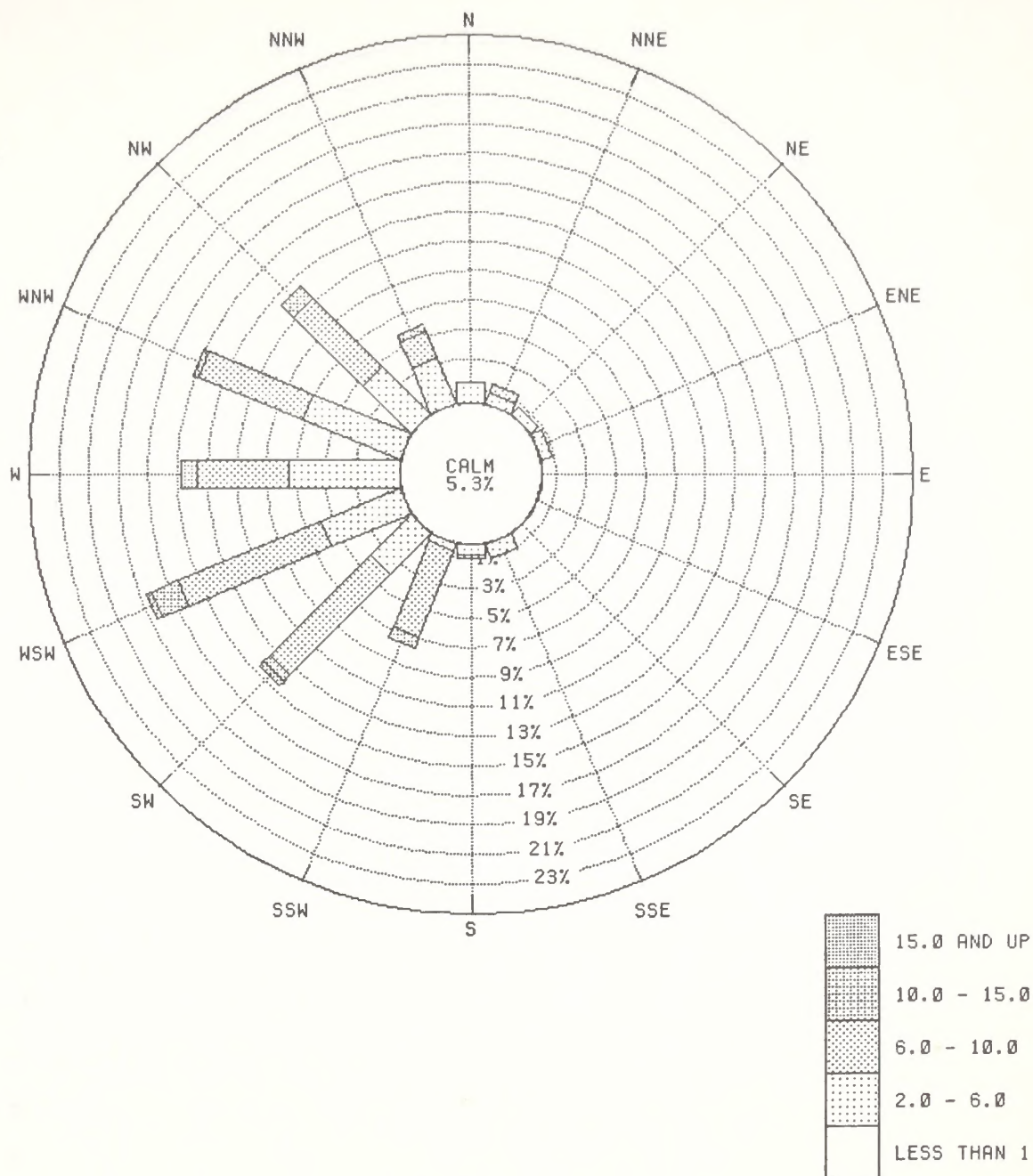


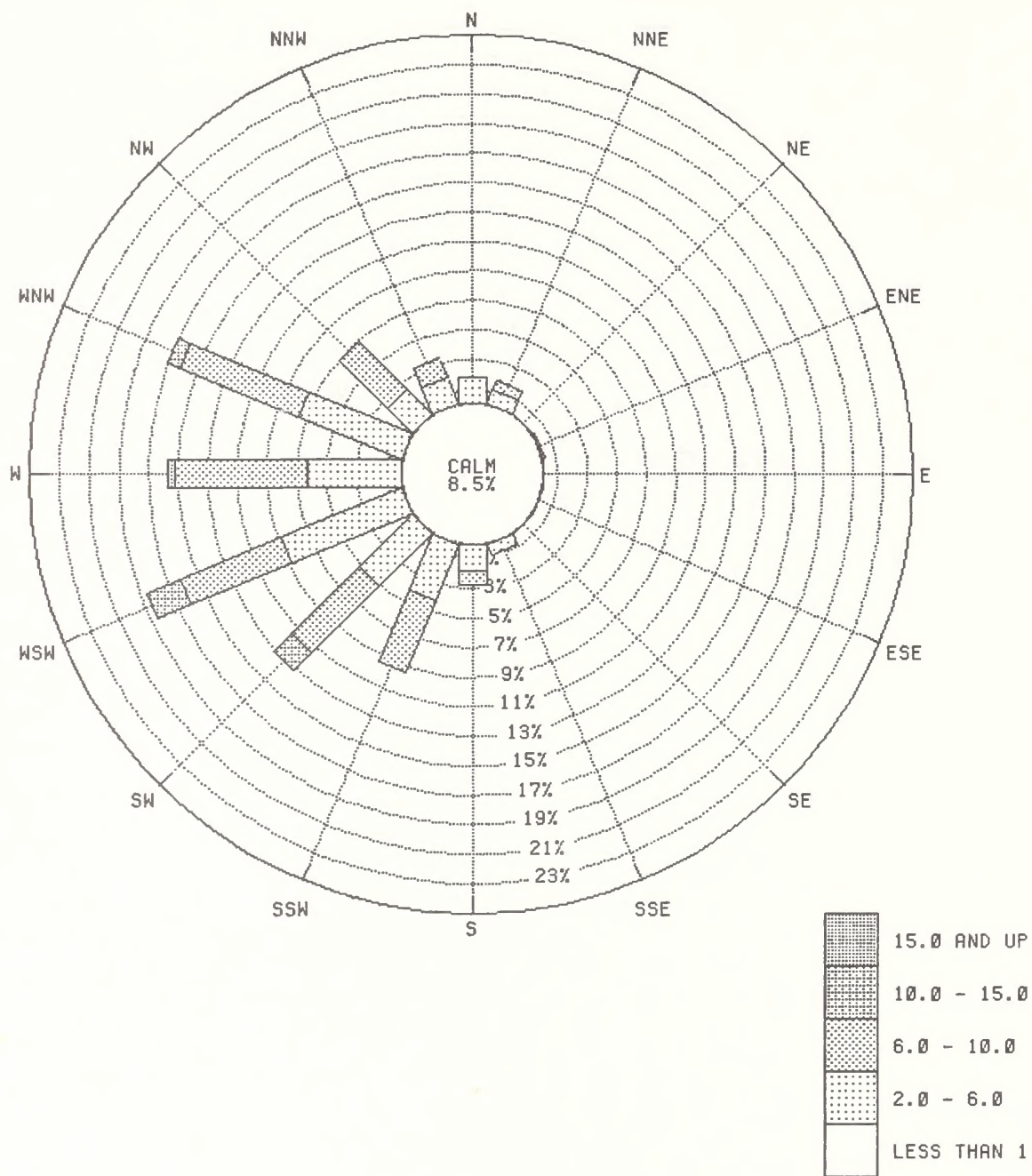


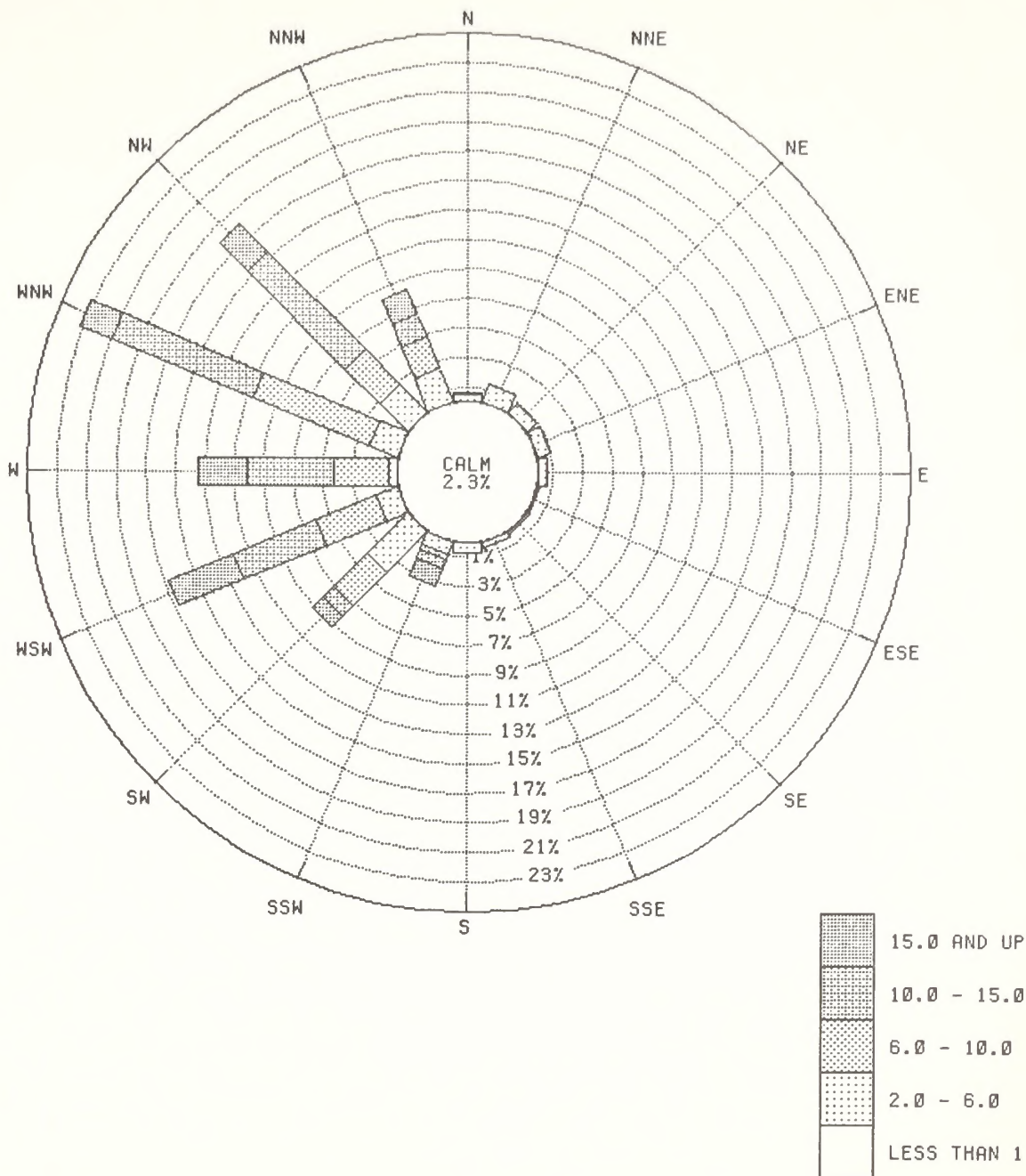


CLIMATOLOGICAL WIND ROSE
SUMMER NIGHT
(JUNE - AUGUST, 6 PM - 6 AM)

1104 VALID DATA POINTS

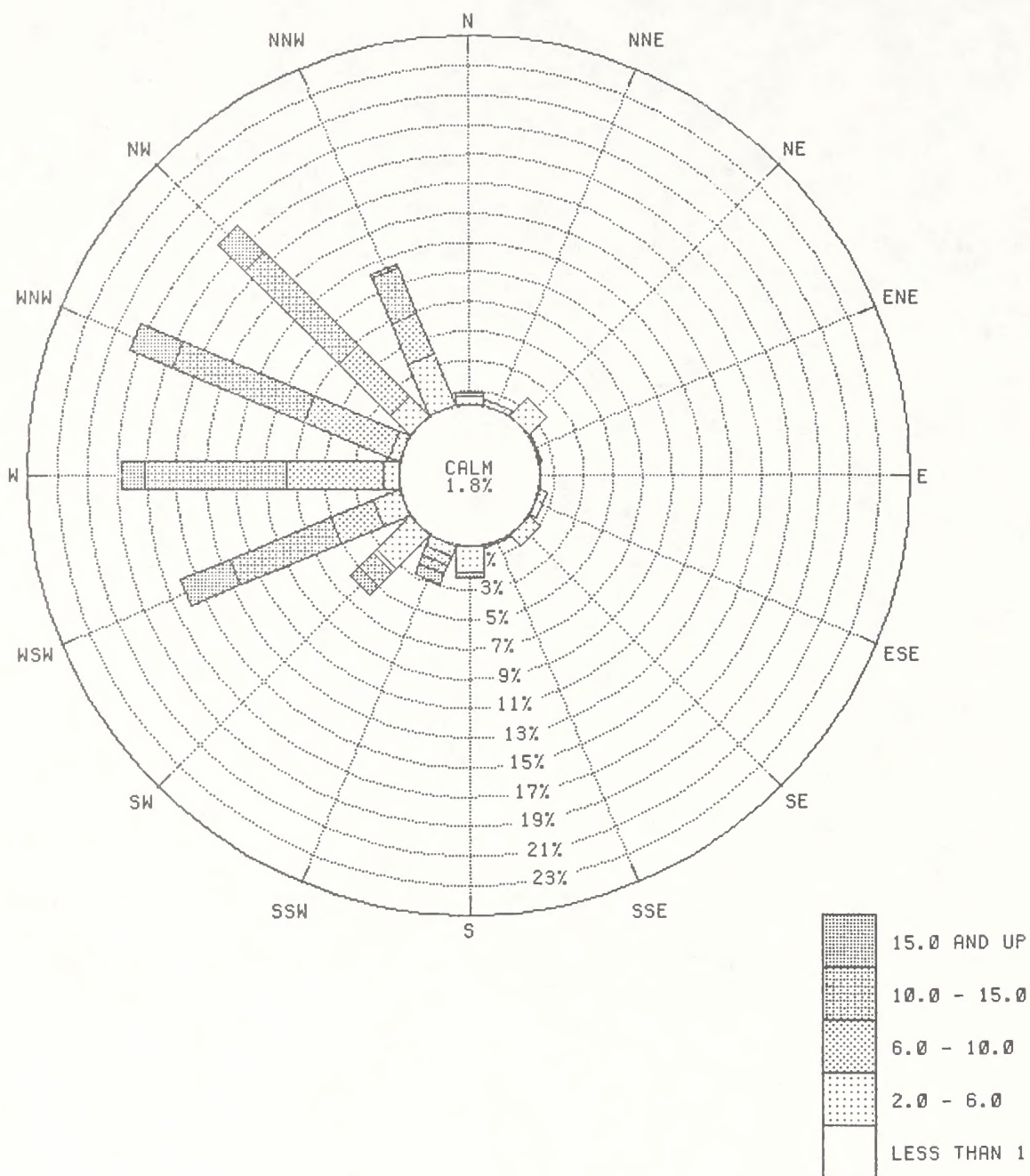






CLIMATOLOGICAL WIND ROSE
WINTER DAY
(DEC - FEB, 6 AM - 6 PM)

1080 VALID DATA POINTS

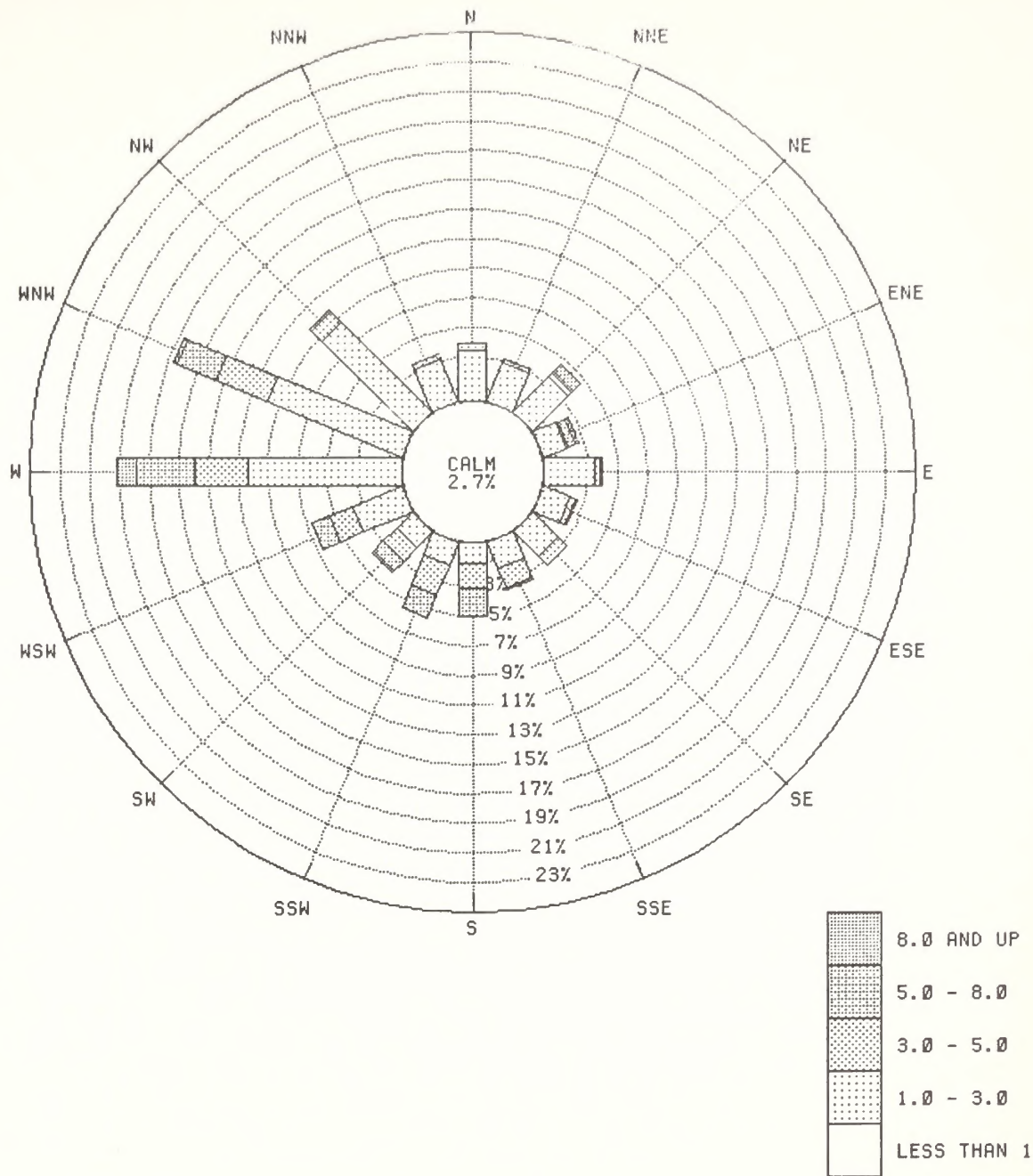


CLIMATOLOGICAL WIND ROSE
WINTER NIGHT
(DEC - FEB, 6 PM - 6 AM)

1080 VALID DATA POINTS

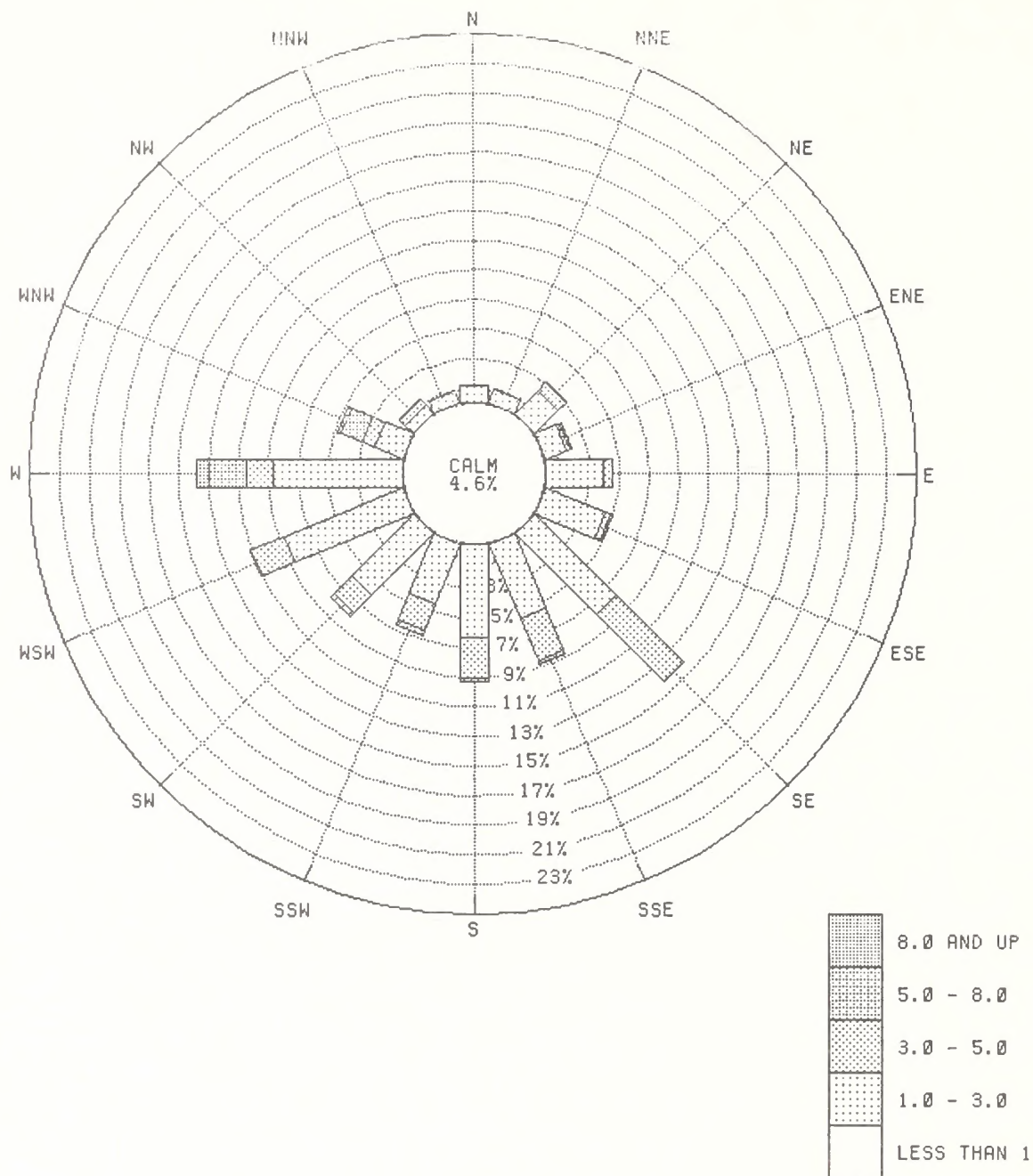
Appendix B

SURFACE (10-m) WIND ROSE STRATIFIED BY SEASON
AND TIME OF DAY AT U-A, U-B SITE IN 1978



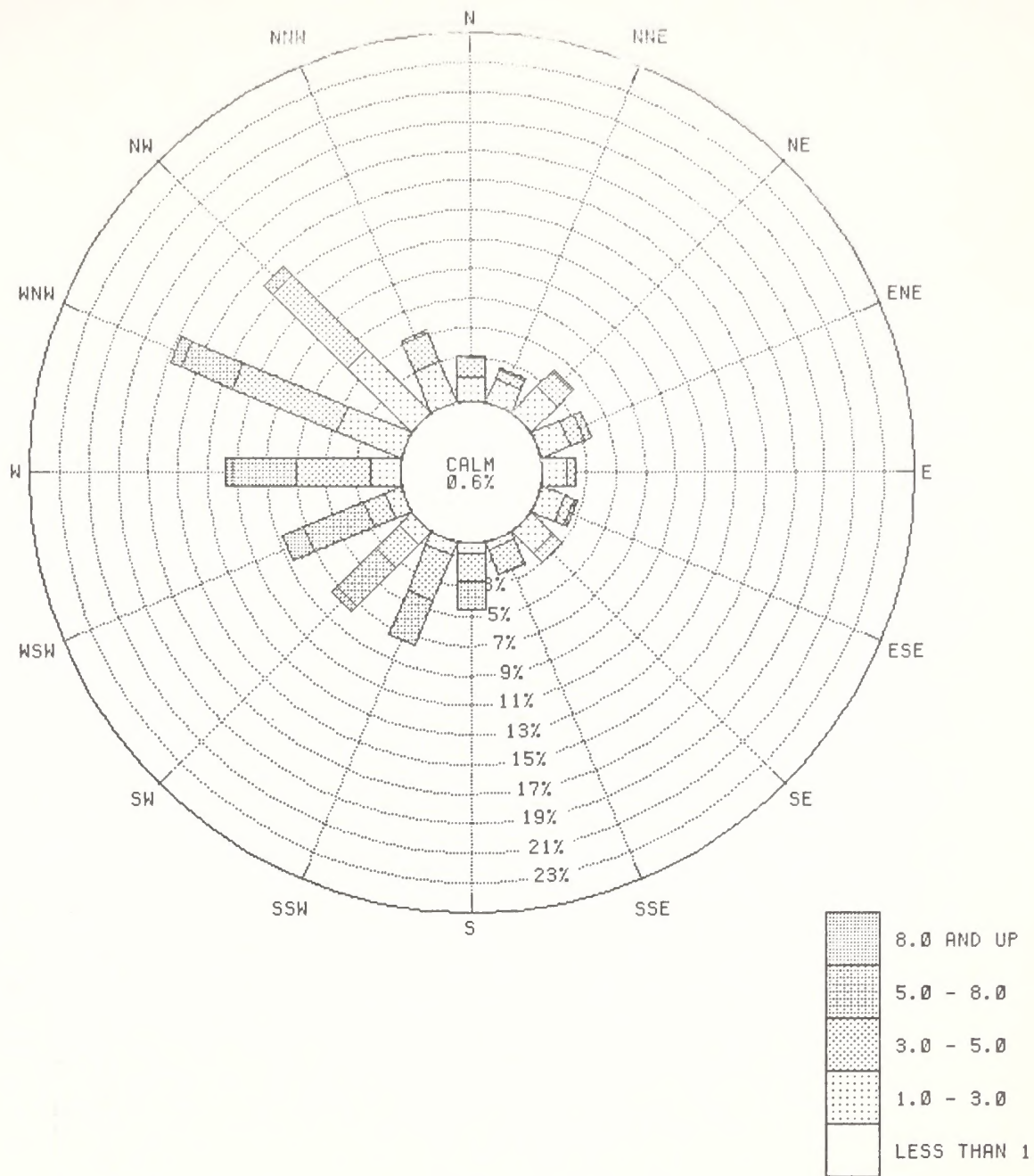
CLIMATOLOGICAL WIND ROSE
 SPRING DAY
 (MARCH - APRIL, 6 AM - 6 PM)

1031 VALID DATA POINTS



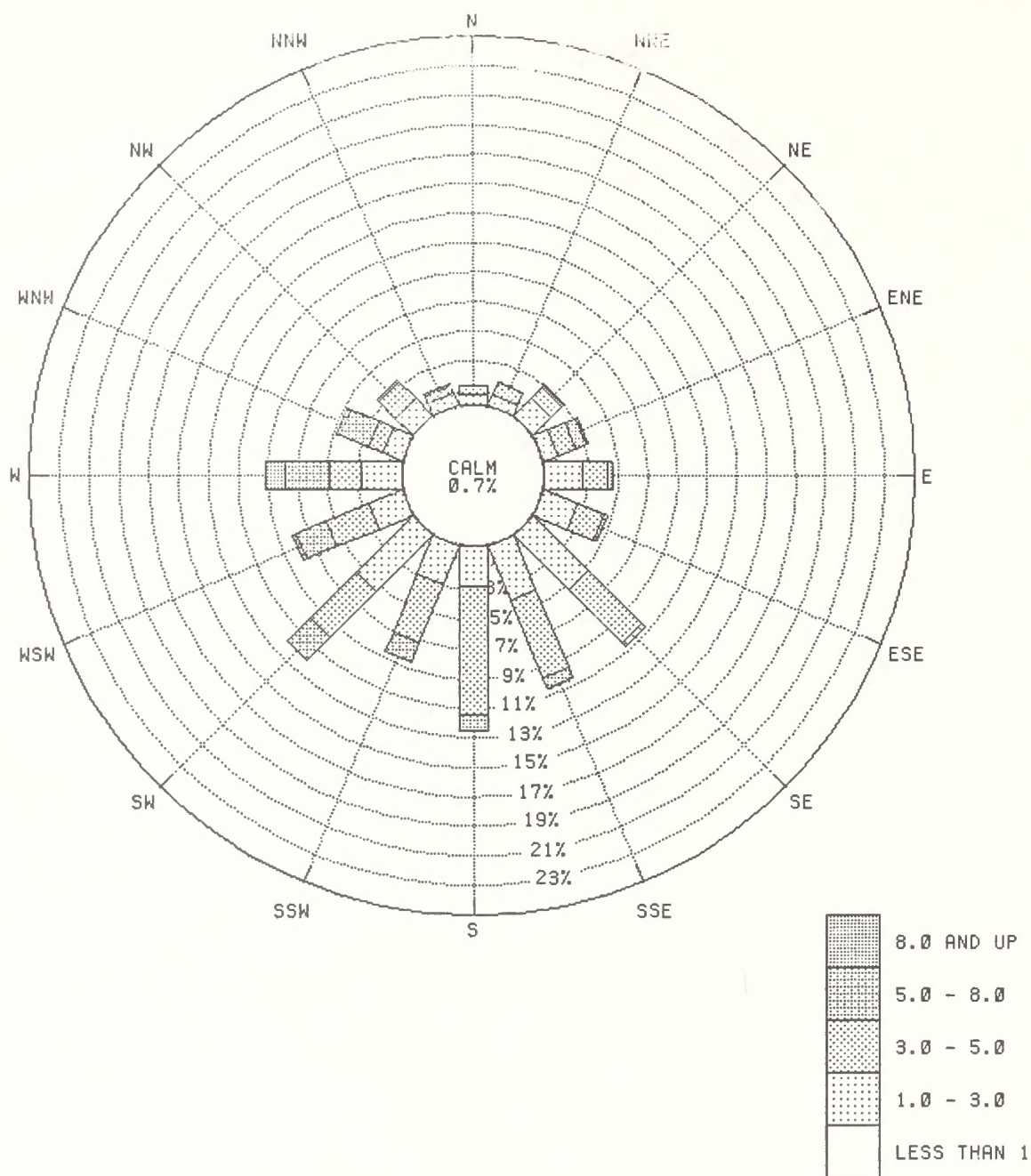
CLIMATOLOGICAL WIND ROSE
 SPRING NIGHT
 (MARCH - APRIL, 6 PM - 6 AM)

1007 VALID DATA POINTS



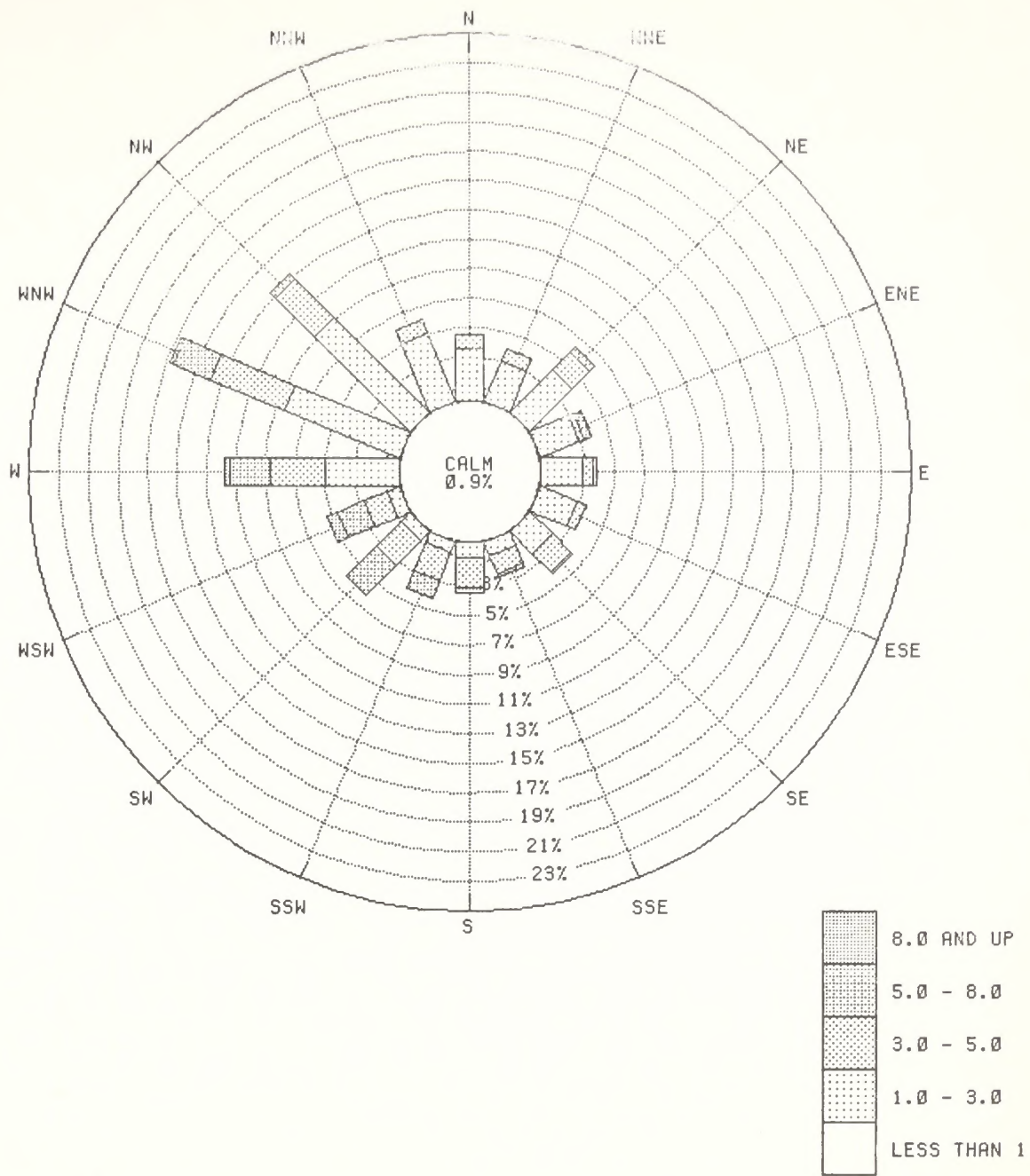
CLIMATOLOGICAL WIND ROSE
SUMMER DAY
(JUNE - AUGUST, 6 AM - 6 PM)

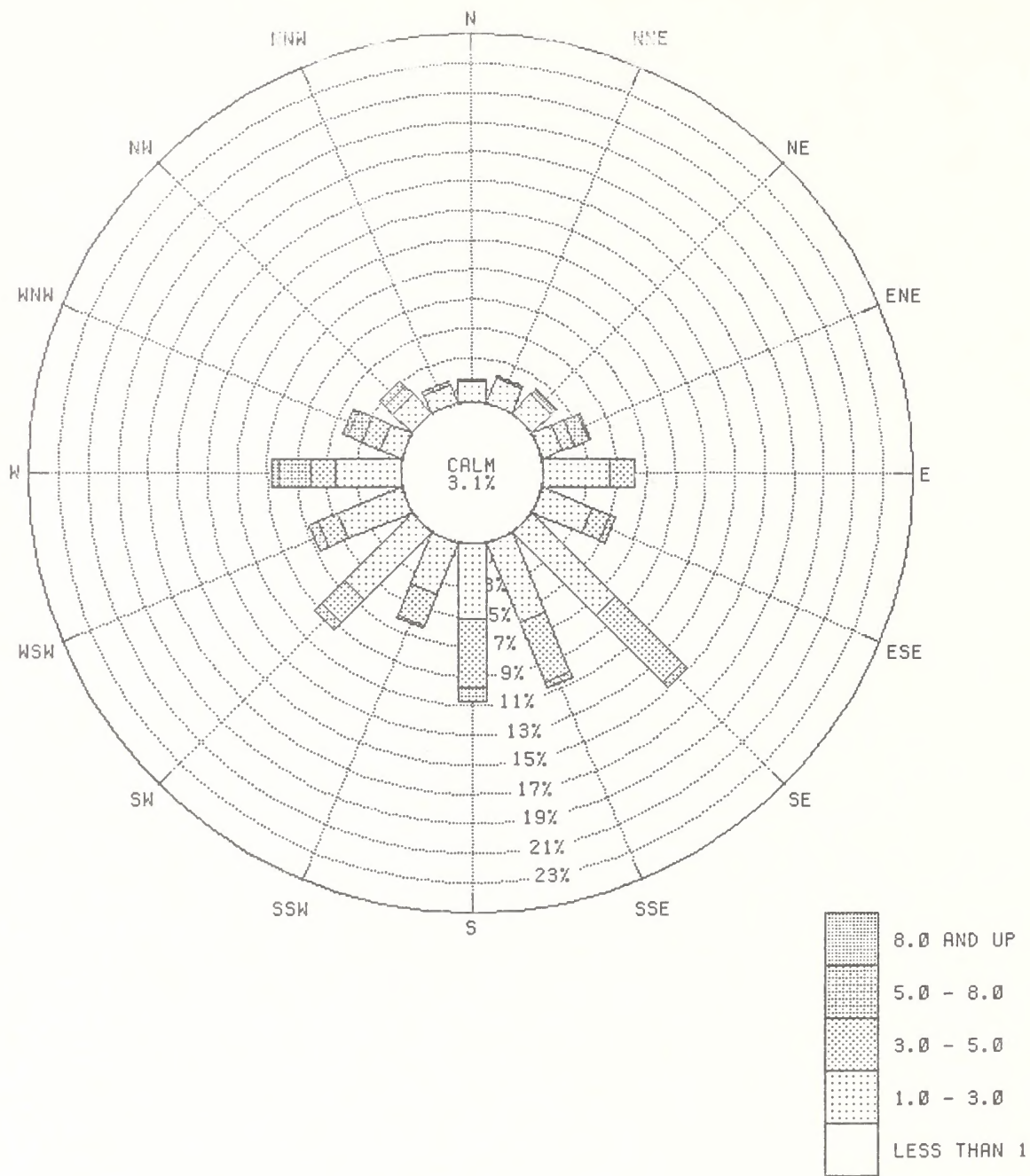
1048 VALID DATA POINTS



CLIMATOLOGICAL WIND ROSE
 SUMMER NIGHT
 (JUNE - AUGUST, 6 PM - 6 AM)

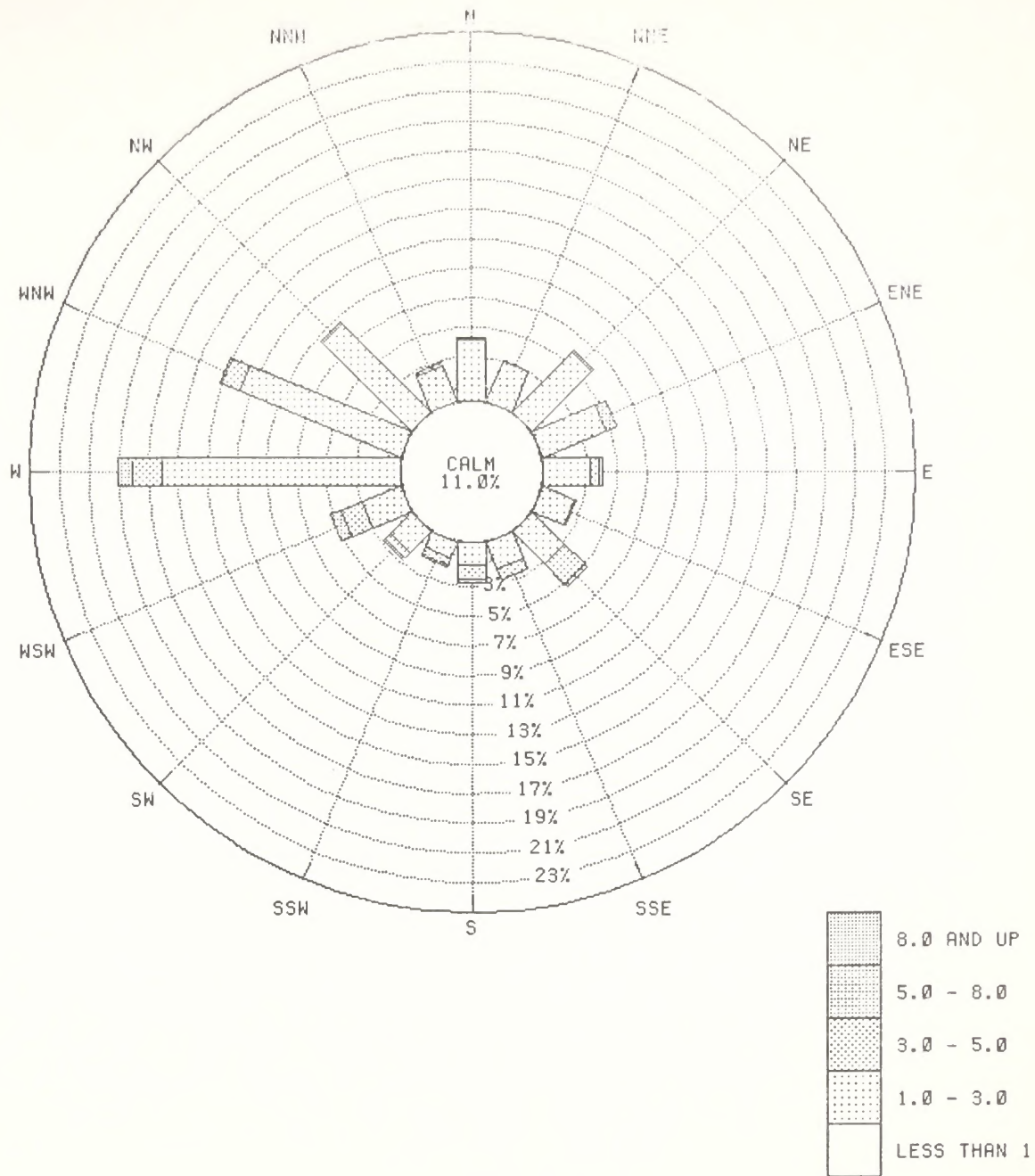
1037 VALID DATA POINTS





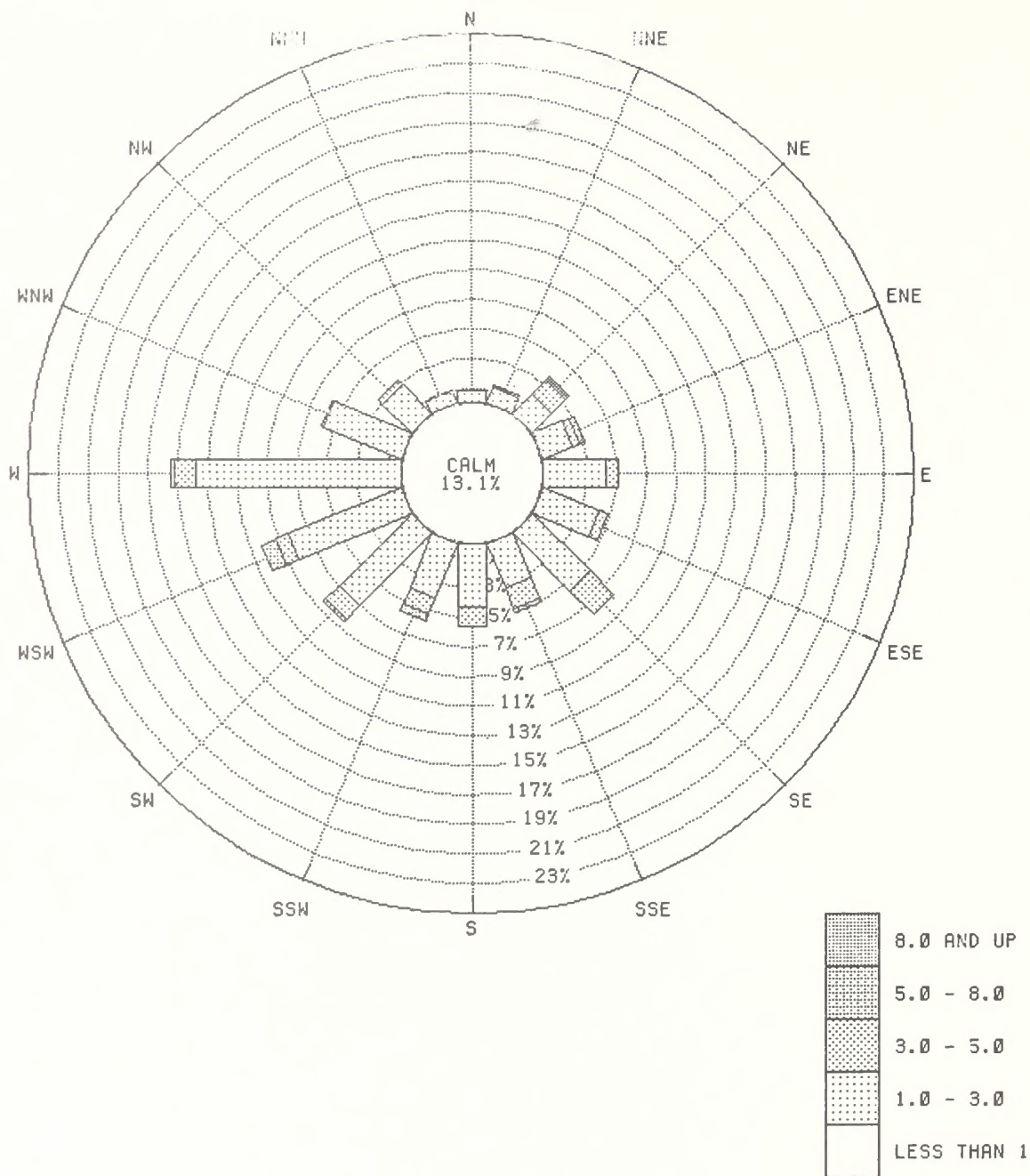
CLIMATOLOGICAL WIND ROSE
FALL NIGHT
(SEPT - NOV, 6 PM - 6 AM)

994 VALID DATA POINTS



CLIMATOLOGICAL WIND ROSE
WINTER DAY
(DEC - FEB, 6 AM - 6 PM)

900 VALID DATA POINTS



Appendix C

TECHNICAL DISCUSSION OF MODELS USED IN STUDY

Appendix C

TECHNICAL DISCUSSION OF MODELS USED IN STUDY

C.1 TECHNICAL DISCUSSION OF THE SYSTEMS APPLICATIONS THREE-DIMENSIONAL COMPLEX TERRAIN WIND MODEL

C.1.1 Model Equations

Modeling wind fields in the lower atmosphere is essentially tantamount to simulating the interactions between the free atmosphere and the surface boundary layer of the atmosphere. Depending on the characteristic spatial and temporal scales and other environmental parameters, such as the prevailing wind, the thermal stability, and the topography, these interactions take place at different levels of significance. For example, for a region having a characteristic horizontal dimension on the order of 10^3 km or larger and a characteristic time scale on the order of days, the surface layer can be viewed as a layer feeding energy to the free atmosphere. As a result, any successful model on this scale must include the dynamic changes in the large-scale motion that are due to the surface layer. In contrast, on the scale of interest to this study, with a horizontal dimension of about 200 km and a time scale of a few hours, the synoptic-scale air motion can be viewed as nearly steady-state. Consequently, the surface layer can be regarded as a passive system driven by the synoptic-scale flow and surface perturbations. This is the approach adopted in this model.

The model equation is based on the three-dimensional steady-state equation expressing the conservation of mass for an incompressible fluid:

$$\frac{\partial u}{\partial x} + \frac{\partial v}{\partial y} + \frac{\partial w}{\partial z} = 0 \quad , \quad (C-1)$$

where x , y , and z are the orthogonal Cartesian coordinates and u , v , and w are the corresponding wind components. As shown in figure C-1, the modeling region is first divided into vertical layers. Note that the terrain is allowed to intersect the modeling region; consequently,

portions of the modeling region (shaded in figure C-1) must be excluded in the calculations. Note also that it is not necessary to assume that the vertical layers are equally divided. By integrating Eq. (C-1) over each vertical slab, one can obtain the following set of equations:

$$\nabla \cdot \mathbf{v} = \frac{\partial \bar{u}_i}{\partial x} + \frac{\partial \bar{v}_i}{\partial y} = -\Omega_i(x,y) \quad , \quad i = 1, 2, \dots, N \quad , \quad (C-2)$$

where N is the total number of vertical layers and \bar{u}_i and \bar{v}_i are the vertically averaged wind in the i-th layer, defined as follows:

$$\bar{u}_i = \frac{1}{\Delta z_i} \int_{z_{i-1}}^{z_i} u \, dz \quad , \quad (C-3)$$

$$\bar{v}_i = \frac{1}{\Delta z_i} \int_{z_{i-1}}^{z_i} v \, dz \quad , \quad (C-4)$$

where

$$\Delta z_i = z_i - z_{i-1} \quad ,$$

and Ω_i is the wind divergence in the i-th layer:

$$\Omega_i(x,y) = \frac{w(z_i) - w(z_{i-1})}{\Delta z_i} \quad . \quad (C-5)$$

In its most general form, any velocity vector can be decomposed into two parts, one of which represents potential flow and the other rotational flow (Helmholtz's decomposition):

$$\bar{\mathbf{v}} = \bar{\mathbf{A}} + \bar{\mathbf{B}} = \nabla \phi + \bar{\mathbf{B}} \quad . \quad (C-6)$$

This decomposition is obviously not unique, because any potential flow can be used for $\bar{\mathbf{A}}$. By imposing the additional condition,

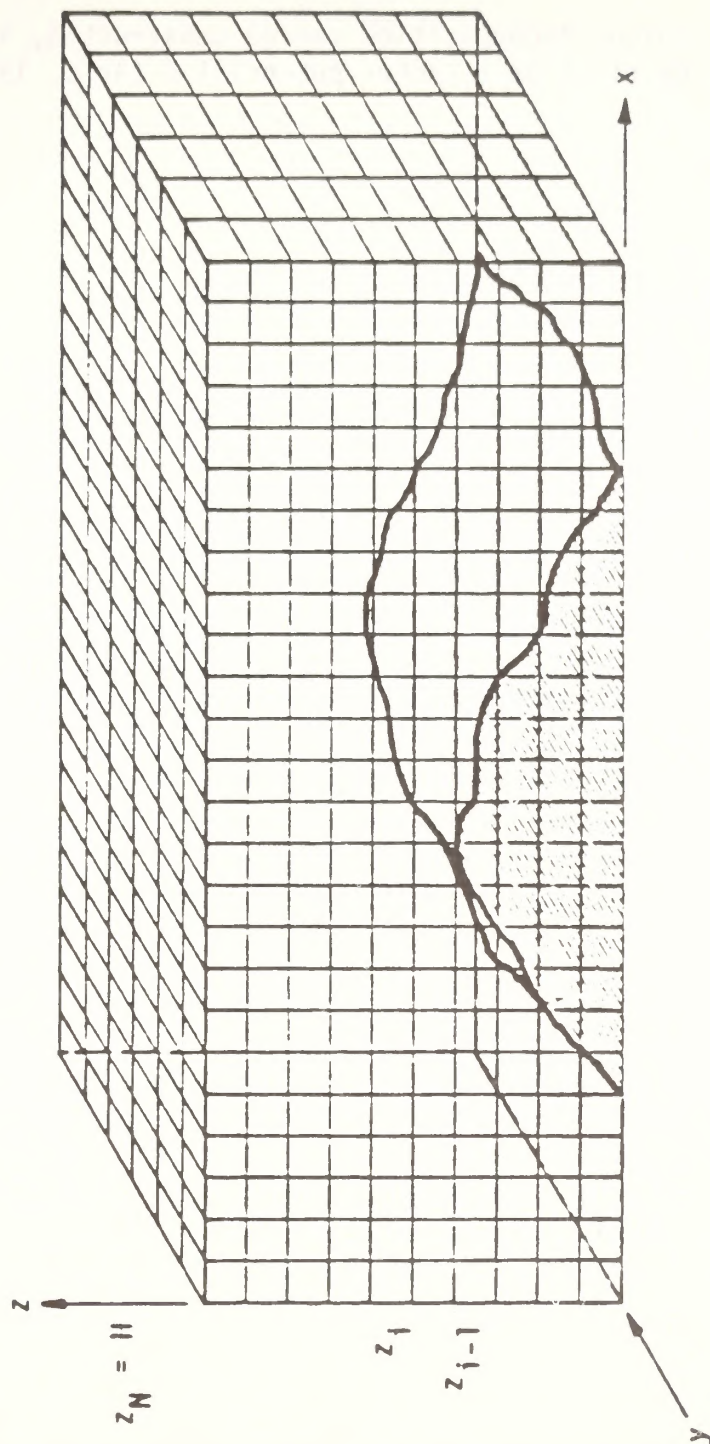


FIGURE C-1. CROSS-SECTIONAL VIEW OF THE INTERSECTION (SHOWN AS SHADED, DASHED GRID) OF A HYPOTHETICAL TERRAIN WITH A THREE-DIMENSIONAL MODELING GRID

$$\nabla \cdot \bar{B} = 0 \quad , \quad (C-7)$$

one can show that a unique decomposition can be constructed, and the second vector \bar{B} can be given by a vector potential $\bar{\beta}$ (Aris, 1962):

$$\bar{B} = \nabla \times \bar{\beta} \quad . \quad (C-8)$$

This vector potential will satisfy Poisson's equation,

$$\nabla^2 \bar{\beta} = -\bar{\omega} \quad , \quad (C-9)$$

where $\bar{\omega}$ is the vorticity of the flow. This is the well-known Helmholtz expression of decomposition for incompressible flow.

Although in prior analyses of surface winds it was conventional to assume that the flow field can be derived from a velocity potential, the validity of such an assumption is predicated on the irrotational nature of the flow field, namely,

$$\nabla \times \bar{v} \equiv i\Gamma_{yz} + j\Gamma_{zx} + k\Gamma_{xy} = 0 \quad ,$$

where

$$\Gamma_{yz} \equiv \frac{\partial w}{\partial y} - \frac{\partial v}{\partial z} \quad , \quad \Gamma_{zx} \equiv \frac{\partial u}{\partial z} - \frac{\partial w}{\partial x} \quad , \quad \Gamma_{xy} \equiv \frac{\partial v}{\partial x} - \frac{\partial u}{\partial y} \quad . \quad (C-10)$$

Since wind flows in the planetary boundary layer are not likely to be irrotational, particularly in the vertical plane, a slightly different approach is used in this model for the decomposition of the velocity vector. For each layer, a two-dimensional velocity potential ϕ is introduced such that

$$\bar{v} = iu + jv + kw = \nabla_2 \phi + k\bar{w} \quad , \quad (C-11)$$

where ∇_2 denotes the two-dimensional gradient vector,

$$\nabla_2 = \bar{i} \frac{\partial}{\partial x} + \bar{j} \frac{\partial}{\partial y} \quad .$$

As illustrated in figure C-2, the existence of the two-dimensional velocity potential would be contingent upon the condition that the wind flow is only weakly rotational in the horizontal plane, i.e.,

$$\Gamma_{xy} = \frac{\partial v}{\partial x} - \frac{\partial u}{\partial y} \approx 0 \quad . \quad (C-12)$$

With this approximation, it then follows from the incompressibility condition that

$$\nabla \cdot \bar{v} = \nabla_2^2 \phi + \frac{\partial w}{\partial z} = 0 \quad . \quad (C-13)$$

Therefore, by defining the following two-dimensional potential functions for each of the vertical layers, assuming that the flow is only weakly rotational in the horizontal plane,

$$\bar{u}_i = \frac{\partial \phi_i}{\partial x} \quad , \quad (C-14)$$

$$\bar{v}_i = \frac{\partial \phi_i}{\partial y} \quad , \quad (C-15)$$

Eq. (C-2) can be cast into the conventional Poisson form:

$$\nabla_2^2 \phi_i = \frac{\partial^2 \phi_i}{\partial x^2} + \frac{\partial^2 \phi_i}{\partial y^2} = -\Omega_i \quad . \quad (C-16)$$

Once the distribution of the wind convergence is specified, solutions to these equations with appropriate boundary conditions can be readily computed using numerical techniques discussed in section C.1.4.

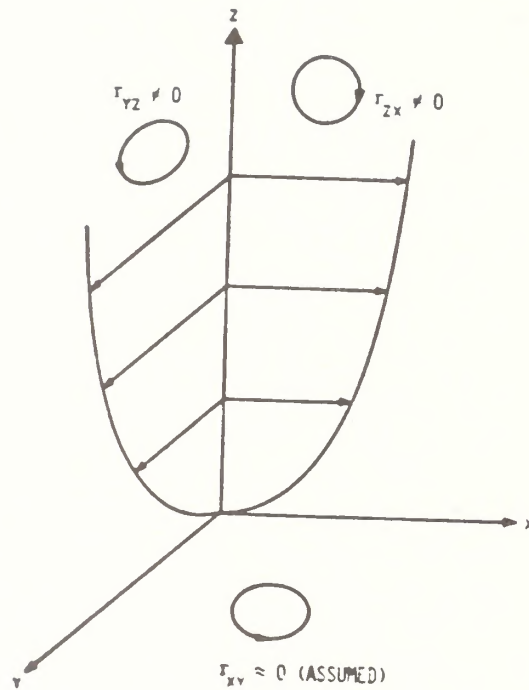


FIGURE C-2. DECOMPOSITION OF VELOCITY VECTORS
IN PLANETARY BOUNDARY LAYER

82062r3 24
82062r3 19

C-7

C.1.2 Parameterization of the Vertical Fluxes

The specification of wind convergence is the key feature of this model. It is proposed that the overall wind convergence is the sum of many components, Ω_{ij} , as weighted by coefficients, α_j ,

$$\Omega_i = \sum_{j=1}^n \alpha_j \omega_{ij} \quad . \quad (C-17)$$

The following perturbations to the wind field over rugged terrain are considered in the model:

- > Lifting and diversion of the flow due to topographic effects.
- > Wind profile modification due to frictional effects in the planetary boundary layer.
- > Convergence of the flow due to thermal effects.
 - Urban heat island
 - Mountain and valley winds.

These perturbations are treated through parameterization of the pertinent processes as follows.

C.1.2.1 Topographic Effects

Because the terrain is part of the modeling region in the present model formulation, certain aspects of the topographic effects are included indirectly as boundary conditions. For example, the no-slip condition is imposed whenever the flow encounters a solid surface. The often observed lifting and diversion of the flow is, however, handled by parameterizing the vertical fluxes.

For high wind speeds and neutral and unstable conditions, it is perhaps logical to view an airflow contacting the slope of a hill to be perfectly elastic. Based on kinematic considerations, the vertical velocity can be expressed as (see figure C-3)

$$w = U \cdot \sin [\arctan \nabla h(x,y)] \cdot e^{-k_1 z} \quad , \quad (C-18)$$

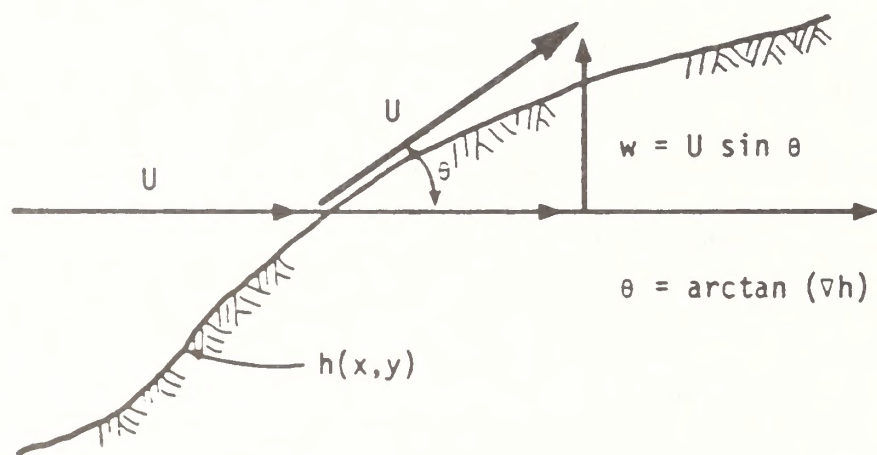


FIGURE C-3. SCHEMATIC DIAGRAM OF A FLOW CONTACTING THE SLOPE OF A HILL

where $h(x,y)$ is the terrain height as a function of location. The exponential term has been added to allow for the decay of the topographic influence away from the surface.

For low winds and stable conditions, the kinetic energy of the airstream approaching a hill may be too small to overcome the potential energy required to lift it over the obstacle. As a result, the flow is diverted around the hill. The physical processes governing the occurrence of these phenomena are rather complex, and they have only recently received the attention of researchers. To characterize this effect, Eq. (C-18) was further modified by a multiplicative factor (as shown in figure C-4),

$$B(F_r) = \begin{cases} 1, & \text{if } \gamma - \Gamma \leq c \\ F_r/F_{r_c}, & \text{if } \gamma - \Gamma > c \end{cases} \quad (C-19)$$

where

γ = environmental temperature lapse rate,

Γ = adiabatic lapse rate,

$$F_r = \frac{U}{\sqrt{\frac{g(\gamma - \Gamma)}{T_\infty} \Delta h}} \quad (\text{Froude number}),$$

$\Delta h = h_{\max} - h(x,y),$

T_∞ = free-stream temperature,

g = acceleration of gravity,

$$c = \frac{U^2}{\frac{g}{T_\infty} (F_{r_c} \Delta h)^2} \quad (\text{a cut-off constant}),$$

F_{r_c} = a critical Froude number where no flow diversion takes place.

Modification of the temperature lapse rate, γ , as air flows over a hill has been neglected as a first approximation herein. According to an analysis by Lilly (1973), the critical Froude number can be taken as 0.5 for an ellipsoidal mountain and 1.0 for a conical mountain.

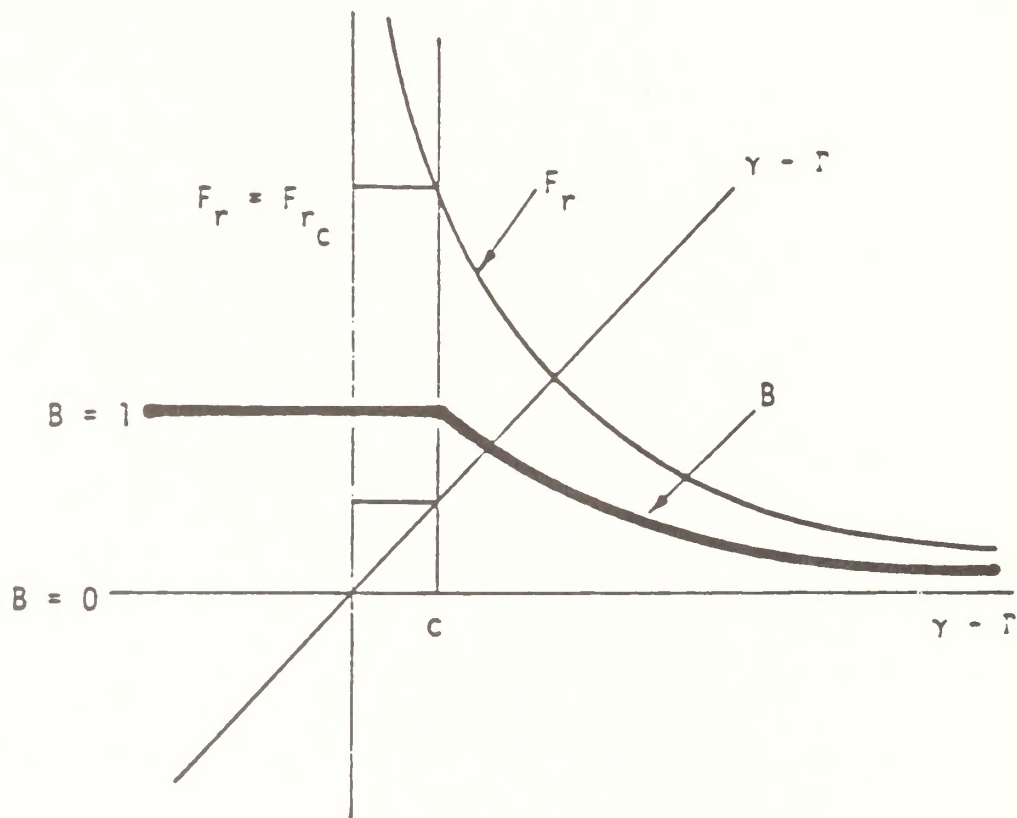
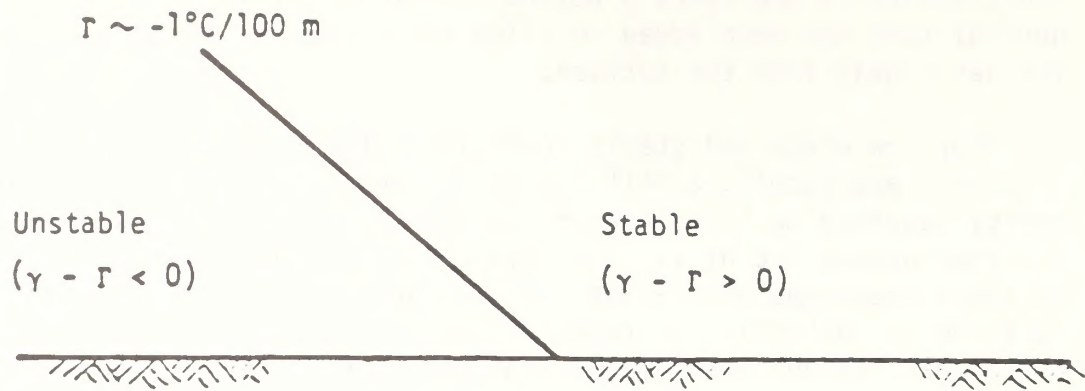


FIGURE C-4. PARAMETERS USED IN DEFINING THE DIVERSION EFFECT

C.1.2.2 Boundary Layer Effects

It is well known that surface friction plays an important role in determining the distribution of the horizontal wind, particularly the vertical wind profile in the atmospheric boundary layer. According to Blasius (1908), the vertical velocity in the boundary layer can be obtained as follows:

$$w = - \int_0^z \frac{\partial w}{\partial x} dz \quad . \quad (C-20)$$

So we can write

$$\frac{w_i - w_{j-1}}{\Delta z} = - \frac{u_j - u_{j-1}}{\Delta x} \quad , \quad (C-21)$$

or

$$w_i - w_{i-1} = - \frac{\Delta z}{\Delta x} (w_j - u_{j-1}) = - \alpha_2 \frac{\Delta z}{\Delta x} f(z, z_0)_j - f(z, z_0)_{j-1} \quad , \quad (C-22)$$

where

Δz = depth of layer i ,

Δx = dimension of horizontal grid j ,

z_0 = aerodynamic surface roughness,

α_2 = weighting coefficient (see Eq. C-17),

z = height above ground.

The dimensionless wind profiles $f(z, z_0)$ can be computed from relationships obtained empirically by Businger et al. (1973) as follows:

> for the stable case,

$$f(z, z_0) = \ln\left(\frac{z}{z_0}\right) + 4.7 \left(\frac{z - z_0}{L}\right) \quad ; \quad (C-23)$$

> for the unstable case,

$$f(z, z_0) = \ln \left[\frac{1 - g \left(\frac{z}{L} \right)}{1 + g \left(\frac{z}{L} \right)} \right] - \ln \left[\frac{1 - g \left(\frac{z_0}{L} \right)}{1 + g \left(\frac{z_0}{L} \right)} \right] \\ + 2 \tan^{-1} \left[\frac{1}{g \left(\frac{z}{L} \right)} \right] - 2 \tan^{-1} \left[\frac{1}{g \left(\frac{z_0}{L} \right)} \right] , \quad (C-24)$$

and

$$g \left(\frac{z}{L} \right) = 1 - 15 \left(\frac{z}{L} \right)^{-1/4} ,$$

where L is the Monin-Obukhov length.

C.1.2.3 Thermal Effects

It is also known that flow can be induced by the conditions of uneven surface heating. On the scale of interest to this study, over complex terrain in urban settings, two types of atmospheric circulation were deemed important:

- > Flows induced by an urban heat island
- > Mountain and valley winds (upslope and downslope flows).

C.1.2.3.1 Urban heat island

Air flow over a heated island has been shown to have an appearance similar to that over a mountain (Stern and Malkus, 1953). According to Stern and Malkus, an "equivalent mountain" function is defined as follows:

$$M(x, y) = \begin{cases} \frac{T(x, y) - \bar{T}}{\gamma - \Gamma} & \text{if } \gamma - \Gamma > 0 \\ 0 & \text{if } \gamma - \Gamma \leq 0 \end{cases} \quad (C-25)$$

where $T(x,y)$ is the spatial distribution of surface temperature. In parallel to the discussions that led to Eq. (C-18), it can be assumed that the vertical motion generated by heat island effects is

$$w = U \cdot \sin (\arctan \nabla M) \cdot e^{-k_2 z} \quad (C-26)$$

The reader should note that in the absence of a driving wind, U , vertical fluxes due to the urban heat island are zero. Furthermore, the equivalent mountain formulation was derived for flat terrain situations; therefore, this parameterization is used only for flat portions of the modeling grid. In sloping terrain, the treatment described in the following section is used.

C.1.2.3.2 Mountain-valley winds

Slope winds are micro/mesoscale breezes that blow normal to the topographic gradients due to temperature-dependent density differences. During the night, radiative cooling of the slope cools the air just above it. This process causes the air close to the ground to become denser than the air at the same altitude but farther above the sloping surface. As a result, the cold air slides down the slope. The reverse process occurs during the day when the sun's radiation warms the slope and the air just above the slope.

Defant (1933) proposed the following expression to describe the steady-state, average speed of a cold current gliding down a slope of average elevation angle α :

$$U_{\text{slope}} = \left[\frac{\bar{g}h(T_C - T_E)\sin \alpha}{C_D T_C} \right]^{1/2}, \quad (C-27)$$

where

C_D = a drag coefficient,

\bar{h} = the mean height of the cold current,

g = gravitational acceleration,

T_C, T_E = the temperatures of the current and environment, respectively.

The reader will note that a driving wind is not necessary to induce down-slope flow using Eq. (C-27).

Adapting Eq. (C-27) to our grid system, but retaining the important functional dependences, one can obtain the following expression for both up-slope and down-slope flow:

$$U_{\text{slope}} = \alpha_4 \left[\left(\frac{T_C - T_E}{T_C} \right) \left(\frac{H_{\text{max}} - H}{H_{\text{max}}} \right) \right]^{1/2}, \quad (\text{C-28})$$

where H is the average surface elevation in the grid cell and H_{max} is the highest terrain elevation affecting local flow. The term involving the terrain heights is substituted for the " $\sin \alpha$ " term in Eq. (C-27) because this is qualitatively correct only for estimating average slope velocity and only if the elevation angle is uniform along the entire slope. In the modeling grid, however, the velocity is computed at any point along a slope, not just the average slope velocity, and elevation angles are rarely uniform along a slope. The substitution allows qualitatively realistic, spatially resolved estimates of up-slope and down-slope flow behavior. With a proper selection of the constant in Eq. (C-28), quantitatively correct estimates should also be possible.

As in Defant's algorithm, Eq. (C-28) contains no dependence on driving wind. In this model, therefore, the vertical fluxes for the mountain-valley winds are self-generating. Since down-slope and up-slope flows have both horizontal and vertical components, to maintain consistency the model must account for the self-generating horizontal component as well as the vertical component. Therefore, the parameterization of mountain-valley winds is entered through the vertical flux term and through the horizontal boundary conditions. All previous parameterizations of vertical fluxes described are dependent on the horizontal wind and are intrinsically consistent with the horizontal flow component; thus, no adjustments to boundary conditions are necessary for them.

C.1.3 Specification of Parametric Coefficients

Equation (C-17) calls for the specification of a weighting coefficient for each of the four parameterized vertical fluxes discussed in the last section. A user may wish to vary these empirically to improve the model's performance for a given application. However, it is possible to determine values analytically for sample cases. In this section the specification of these coefficients is described.

C.1.3.1 Coefficient for Topographic Effects

As indicated earlier, on the basis of kinematic considerations, the empirical coefficient for topographic effect, α_1 , should be unity for a perfectly elastic wind flow. This will probably correspond to the neutrally stratified atmospheric conditions. For stable or unstable stratifications corresponding to the inelastic situations, this empirical coefficient is expected to be less or greater than 1, namely,

$$\alpha_1 \begin{cases} < 1 & \text{stable stratification} \\ = 1 & \text{neutral stratification} \\ > 1 & \text{unstable stratification} \end{cases} .$$

From model sensitivity tests, it was found that the resultant wind field is extremely sensitive to the specification of this coefficient.

C.1.3.2 Coefficient for Boundary Layer Effects

The parameterization scheme outlined earlier for the boundary layer effect essentially provides a correspondence between the horizontal and vertical wind velocities. The derivation of the expression given in Eq. (C-22) involves substitution of the dimensionless $f(z, z_0)$ term for u_j and u_{j-1} since

$$f(z, z_0) = \frac{ku(z)}{u_*} ,$$

where k is von Karman's constant and u_* is the friction velocity. Therefore, the frictional coefficient is given by

$$\alpha_2 = \alpha_f = \frac{u_*}{k} . \quad (C-29)$$

Typically, k is about 0.35 in the atmosphere (Businger et al., 1973) and an average u_* is about 0.316 m/sec (Tennekes, 1973). Substituting these values into Eq. (C-29) yields

$$\alpha_2 \approx 1.0 .$$

C.1.3.3 Coefficient for Urban Heat Island Effects

It can be seen from Eqs. (C-25) and (C-26) that the parameterization for the urban heat island effect is parallel to that for the topographic effects. For this reason, one would expect that the specification of the coefficients for the effects are the same. Therefore, the coefficient is given by

$$\alpha_3 \quad \left\{ \begin{array}{ll} < 1 & \text{stable} \\ \cong 1 & \text{neutral} \\ > 1 & \text{unstable} \end{array} \right. .$$

C.1.3.4 Coefficient for the Slope Wind Effect

To derive the range of values for this coefficient, we begin with the vertical momentum equation, assuming hydrostatic, steady-state conditions:

$$w \frac{\partial w}{\partial z} = - \frac{1}{\rho} \left(\frac{\partial p}{\partial z} \right) - g \quad . \quad (C-30)$$

Following Rao and Snodgrass (1981), Eq. (C-30) can be expressed in the following form:

$$w \frac{\partial w}{\partial z} = \left(\frac{g}{\theta_0} \right) \theta' \sin \alpha \quad , \quad (C-31)$$

where g is the gravitational constant, θ_0 is the reference-state temperature, θ' is the deviation of the mean potential temperature from the reference-state temperature, and α is the terrain slope angle. Integrating Eq. (C-32) from the surface to the top of the slope flow, h , one obtains

$$w = \sqrt{2g\theta' h \sin \alpha / \theta_0} \quad . \quad (C-32)$$

A comparison of Eqs. (C-27) and (C-32) yields the following expression:

$$\alpha_4 = \sqrt{gh/C_D} \quad . \quad (C-33)$$

Using a range of values between 10 and 50 meters for h (given by Defant [1951]) and between 0.001 and 0.005 for C_D (given by Munn [1966]), the following range is obtained for α_4 :

$$140 \leq \alpha_4 \leq 700 \quad .$$

C.1.4 Numerical Solution Procedure

To obtain a solution to Eq. (C-16) with complex boundary conditions, a numerical technique is required. Several direct Poisson solvers are available that are based on block-cyclic reduction of a set of finite difference equations (Buzbee, Golub, and Nielson, 1970; Swarztrauber and Sweet, 1975). Although these solvers are convenient and inexpensive to use, their application is restricted to simple rectangular modeling regions. This restriction presents a rather serious drawback for our formulation because, as described earlier, the terrain may intersect the modeling region.

Thus, an alternative solution technique was chosen that can accommodate the exclusion of portions of the modeling region having irregular shapes and yet incur only a modest increase in computation time over the direct solution techniques. The general form of the Poisson equation can be written as

$$\nabla^2 \phi = \frac{\partial^2 \phi}{\partial x^2} + \frac{\partial^2 \phi}{\partial y^2} = f(x,y) \quad , \quad (C-34)$$

and the five-point difference approximation to Eq. (C-34) is

$$\frac{\phi_{i-1,j} - 2\phi_{i,j} + \phi_{i+1,j}}{(\Delta x)^2} + \frac{\phi_{i,j-1} - 2\phi_{i,j} + \phi_{i,j+1}}{(\Delta y)^2} = f_{i,j} \quad , \quad (C-35)$$

$$i = 1, \dots, M \text{ and } j = 1, \dots, N \quad ,$$

where

ϕ = the potential function,

$f(x,y)$ = the forcing function,

x, y = orthogonal Cartesian coordinates,

i, j = the grid cell indices of a grid system that is superimposed on the modeling region and that has M grid cells in the x - (i -) direction and N grid cells in the y - (j -) direction.

Equation (C-35) is valid for all points within the modeling region, but for those along the modeling boundary some additional computations are required. Along the boundaries, the normal derivatives of ϕ (i.e., $d\phi/dx$ or $d\phi/dy$ --often referred to as Neumann-type boundary conditions) are specified, and these are used to compute values of ϕ at fictitious grid points outside the modeling region. For example, consider a grid cell (i,j) that forms part of the left boundary of the modeling region as shown in figure C-5. To solve Eq. (C-35) for this point, one must specify some value for $\phi_{i-1,j}$, which exists at a point outside the modeling region. One can simply compute $\phi_{i-1,j}$ using

$$\phi_{i-1,j} = \phi_{i,j} - \frac{d\phi}{dx}_{ij} \Delta x, \quad (C-36)$$

and substitute this expression in Eq. (C-35).

The commonly used modified Gauss-Seidel iterative solution method was selected because it is very well suited to the solution of the five-point operator [Eq. (C-35)] for the Poisson equation (Dahlquist and Björck, 1974). Like all iterative techniques, it starts from a first approximation, which is successively improved until a sufficiently accurate solution is obtained. To simplify the description of this method, consider the linear system of equations

$$Ax = b, \quad (C-37)$$

instead of the system described in Eq. (C-35). Equation (C-37) can be written as

$$x_i = \frac{- \sum_{\substack{j=1 \\ j \neq i}}^N (a_{ij}x_j + b_j)}{a_{ii}}, \quad i = 1, 2, \dots, n, \text{ and } a_{ii} \neq 0. \quad (C-38)$$

In Gauss-Seidel's method, a sequence of approximations $x^{(1)}, x^{(2)}, x^{(3)}, \dots$ is computed by

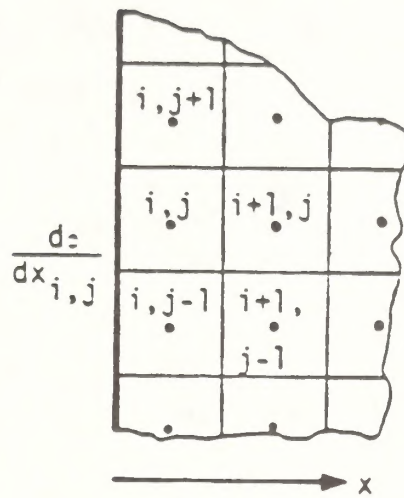


FIGURE C-5. SKETCH SHOWING A GRID CELL (i,j) ALONG THE LEFT BOUNDARY OF THE MODELING REGION

$$x_i^{(k+1)} = \frac{- \sum_{j=1}^{i-1} a_{ij} x_j^{(k+1)} - \sum_{j=i+1}^n a_{ij} x_j^{(k)} + b_i}{a_{ii}}, \quad (C-39)$$

Note that Eq. (C-39) can also be written as

$$x_i^{(k+1)} = x_i^{(k)} + r_i^{(k)}, \quad (C-40)$$

where $r_i^{(k)}$ is the current residual of the i -th equation and

$$r_i^{(k)} = \frac{- \sum_{j=1}^{i-1} a_{ij} x_j^{(k+1)} - \sum_{j=i+1}^n a_{ij} x_j^{(k)} + b_i}{a_{ii}}. \quad (C-41)$$

Now, to improve the rate of convergence, one can slightly modify Eq. (C-40) to give

$$x_i^{(k+1)} = x_i^{(k)} + \omega r_i^{(k)}, \quad (C-42)$$

where ω is called the relaxation parameter, which is chosen so that the rate of convergence is maximized. This improved iteration procedure is called the "successive overrelaxation method" (Dahlquist and Björck, 1974).

For this model, $\omega = 1.7$ is found to give the best rate of stable convergence in tests of the modified Gauss-Seidel solution to Eq. (C-35). The criterion for complete convergence is defined so that

$$\max_i r_i^{(k)} \leq 0.01 x_i^{(k)}. \quad (C-43)$$

C.2 TECHNICAL DISCUSSION OF THE SYSTEMS APPLICATIONS

GAUSSIAN PUFF MODEL

The Gaussian Puff Model (GPM) is a multiple-source Gaussian dispersion model utilizing temporally and spatially varying meteorological data that include temperature, exposure class, a three dimensional wind field, and height of the mixing layer.* As many as five species can be simulated. The GPM also treats time varying emissions. Complex advection and dispersion situations, such as plume backtracking or plume-terrain interactions, can also be accommodated with the GPM.

GPM contains two main sections. In the first, a plume rise model is used to predict the height of the plume. This model calculates either the height of a source from which the plume emanates, or the plume trajectory near the source. In the second section, the plume is treated as a series of segments or puffs, a puff being a part of the plume emitted during one time step.

The model keeps track of all of the puffs emitted from a source until they leave the modeling region. The model stores information about the location of the center of each puff (in three dimensions), the pollutant mass in the puff, and the standard deviation of the puff mass distribution in the vertical direction (σ_z), and in the horizontal direction perpendicular to the motion of the puff (σ_y). Each puff is advected according to the winds at the center of the puff, and the mass distribution of any cross-section of the plume is determined by the dispersion coefficients σ_z and σ_y and the Gaussian formulation. An area source is treated as a point source, but without plume rise, having an initial σ_y equal to one-half the diameter of the area source.

A display program plots ground-level concentration isopleths, plume paths, instantaneous concentrations, or average concentrations. Also, subgrid concentrations can be printed for any times within the interval of the simulation, and for any subregion of the modeling region.

GPM uses gridded two- or three-dimensional wind fields supplied by the user. In this study, three-dimensional wind fields were generated using the SAI Complex-Terrain Wind Model in a computer mode. In this mode, hourly gridded wind fields are generated by scaling one of sixteen cardinal wind direction flow patterns and then superimposing one of six slope wind flow patterns, if appropriate (see section 4.2.1.4). Since the

* The reader will note many similarities between GPM and the Gaussian puff submodel within RTM.

flow patterns were categorized within only 16 cardinal wind directions, the resolution of the wind fields was, at best, 22.5°. Therefore, each time a wind vector is selected by GPM for use in the advection algorithm, it is first randomized. The randomization occurs uniformly with a $\pm 12^\circ$ sector.

Another feature added to GPM for this study is a "trajectory look-ahead" option. "Trajectory look-ahead" is accomplished by subdividing the time step into sub-time steps sufficiently small that puffs are prevented from traveling more than 3/4 the length of a wind model grid cell during the sub-time step. The puffs' trajectories are then computed using the gridded winds at each sub-time step and are assembled to form an effective trajectory for the larger time step. This allows the model to use all the spatial resolution available in the gridded winds while permitting a large time step for greatest economy. The added economy of the option is most important for the year-long GPM runs required in this study.

The model accounts for several occurrences at each time step: all the old puffs are advected downwind; new values for puff location, mass, and dispersion coefficients are calculated. In addition, a new puff is created with a center a half-step downwind, at a height determined by the following plume rise equation (Briggs, 1971):

$$H_e = H_s + [1.6 F^{1/3} \cdot (10H_s)^{2/3} / U] \quad (C-44)$$

$$\text{where } F = 9.8 \frac{\Delta T}{T_s} \cdot V_s R_s^2 ,$$

where

$$\Delta T = T_s - T_a$$

$$H_e = \text{effective release height}$$

$$H_s = \text{stack height}$$

$$U = \text{wind velocity}$$

$$F = \text{buoyancy flux}$$

$$V_s = \text{exit velocity from stack}$$

$$R_s = \text{stack radius}$$

$$T_s = \text{temperature in stack}$$

$$T_a = \text{ambient temperature.}$$

Vertical winds are conservatively assumed to be zero; therefore, this height is used for the center of the puff downwind except in the vicinity of high terrain. Near high terrain, the height of the puff above local ground level is governed by the following expression (Queney, 1947), which is also used in the wind model (see section C.1.1):

$$H_P = H_T \exp [-K_S H_E] + H_E \quad (C-45)$$

where

H_P = local height of puff

H_E = effective stack height of puff at release

H_T = local height of terrain above terrain height at source

K_S = s/u

$$s = \left(\frac{g}{\theta} \frac{\partial \theta}{\partial z} \right)^{1/2} ; \quad \frac{\partial \theta}{\partial z} \geq 0$$

u = local wind speed

θ = potential temperature

g = gravitational constant.

The reader will note that the vertical displacement of a puff caused by the terrain is dependent on the stability in such a manner that displacement decreases with increasing stability and with increasing effective stack height. For neutral or unstable conditions, puff displacement is identical to the terrain height displacement. For added conservatism in the regional GPM applications (in which neutral stability is assumed), puffs are allowed to approach terrain to within one-half their effective stack height rather than maintaining their original terrain separation, as would be calculated using the expression above.

Two methods are implemented to calculate the dispersion coefficients within 40 km of the source: Pasquill-Gifford Turner (PGT) and TVA. For each point source, one of the methods is prescribed by the user. For this study, the PGT curves were used. These dispersion coefficients are functions of atmospheric stability class, downwind distance, and dispersion coefficient history. Although the stability class is a discrete

function of meteorological conditions and, therefore, can vary discontinuously in space or time, the dispersion coefficients are calculated to increase smoothly with time. The rate of change of the coefficients at the appropriate stability class and downwind distance is used to calculate increments that are added to the coefficients at each time step.

Fundamental diffusion theory (Taylor, 1921) indicates that plume growth becomes dependent on time after sufficient time. Therefore, beyond 40 km, GPM uses the following time-dependent algorithm (Heffter, 1965):

$$\begin{aligned}\Delta\sigma_y &= 1800 \, dt \\ \Delta\sigma_z &= 94.8 \, dt/VT \quad ,\end{aligned}$$

where

dt = time step (hours)

T = age of puff (hours)

Time-dependent stability class information is supplied by the user. In the regional-scale applications of GPM, stability class was assumed to be neutral (Pasquill-Gifford Class D) at all times, because it is more appropriate for long-range transport than are the time-varying stabilities derived from micrometeorological (small-scale) measurements. In the near-source GPM applications, stability class is time-dependent and derived from sigma-theta measurements made at Tracts U-a and U-b.

Changes in each puff's mass, caused by deposition and oxidation, are also calculated during each time step. To calculate the percentage of plume mass near the ground, deposition is calculated using the vertical dispersion coefficient and the Gaussian distribution in the vertical direction. Deposition is then calculated using a first-order decay model. Oxidation is also calculated using a simple first-order decay approximation and user-specified decay rate.

The first-order decay or loss of mass in a puff due to chemical transformation and surface deposition is given by

$$\text{Mass Loss} = \text{Current Puff Mass} \times \left\{ 1 - \exp \left[-(K1 + K2)\Delta t \right] \right\}$$

where

$K1$ = chemical conversion rate in (sec^{-1})

$K2$ = deposition rate (sec^{-1}) deposition velocity/puff depth

Δt = time step

The usual Gaussian equation is

$$x(P) = \frac{Q}{U} F(Y, \sigma_y) G(Z, S, \sigma_z, L) \quad (C-46)$$

where

x = the concentration at P due to the plume (g/m^3),

X = the downwind distance of point P from the source,

Y = the crosswind distance from P to the plume centerline (m),

Z = the vertical coordinate of the point P (m),

S = the vertical coordinate of the point (X_C, Y_C, Z_C) on the plume centerline that is closest to P (m),

Q = the rate of emission (g/sec),

U = the wind speed (m/sec),

σ_y = the horizontal (transverse) dispersion coefficient (m),

σ_z = the vertical dispersion coefficient (m),

L = the mixing height (m).

σ_y and σ_z are calculated at (X_C, Y_C, Z_C) .

$$F(Y, \sigma_y) = \frac{1}{\sqrt{2\pi} \sigma_y} \exp \left[\frac{-Y^2}{2\sigma_y^2} \right] \quad (C-47)$$

$$G(Z, S, \sigma, L) = \frac{1}{\sqrt{2\pi} \sigma} \left\{ \exp \left[-\frac{(S - Z)^2}{2\sigma^2} \right] \right.$$

$$+ \exp \left[-\frac{(ZL - S - Z)^2}{2\sigma^2} \right] + \exp \left[-\frac{(2L - S - Z)^2}{2\sigma^2} \right]$$

$$\sum_{\substack{n \text{ even} \\ n > 0}} \left(\exp \left[-\frac{(nL - S - Z)^2}{2\sigma^2} \right] + \exp \left[-\frac{[n + 2]L - na - S - Z)^2}{2\sigma^2} \right] \right)$$

$$+ \exp \left[\frac{(nL - na + S - Z)^2}{2 \sigma^2} \right] + \exp \left[- \frac{[n + 2] a - nL - S - Z)^2}{2 \sigma^2} \right] \Bigg\} \quad (C-48)$$

where a is the height of the ground (or lower barrier). If $a = Z = 0$, this reduces to

$$G(0, S, \sigma, L) = \frac{2}{\sqrt{2\pi} \sigma} \sum_{n=-\infty}^{\infty} \exp \left[- \frac{(S + 2nL)^2}{2 \sigma^2} \right] \quad (C-49)$$

When σ_z/L is large enough, the pollutant is considered to be uniformly distributed in the mixing layer, and then $G = 1/L$.

Equations (C-47) and (C-48) are implemented as shown in Eq. (C-46). The concentration due to a puff is calculated in ppm:

$$C(P) = \frac{A \cdot 10^6}{\phi \cdot dx} F(y, \sigma_y) G(Z, Z_c, \sigma_z, L) \quad (C-50a)$$

$$C(P) = \frac{A \cdot 10^6}{(\phi \cdot dx \cdot 4\sigma_y, \text{mixing depth})} \quad (C-50b)$$

where

C = the concentration at the point P (ppm),

A = the number of moles of pollutant in the puff,

dx = the distance the puff traveled during the current time step (m),

ϕ = the number of moles per cubic meter (air) = 40.82,

F, G = the same as above (except we use a finite sum).

Beyond 50 km, concentrations are calculated by Eq. (C-50b) assuming uniform mixing. The concentration at P due to the plume is then the result of summing Eq. (C-50b) over all puffs, with the following two exceptions:

- > If the point P is at P_1 , then the contribution at P due to puff B is ignored (see figure C-6).
- > If P is at P_2 , then Eq. (C-50b) gives zero contribution at P from both puffs A and B. In this case, Eq. (C-50b) is used with y equal to the horizontal distance from X to P, and (X_c, Y_c, Z_c) equal to X.

C.3 OVERVIEW OF THE EPA/SYSTEMS APPLICATIONS PLUME VISIBILITY MODEL

The design objective of the plume visibility model (PLUVUE) used in this analysis is to calculate visual range reduction and atmospheric discoloration caused by plumes consisting of primary particulates, nitrogen oxides, and sulfur dioxides emitted by a single emissions source. Primary emissions of sulfur dioxide (SO_2) and nitric oxide (NO) do not scatter or absorb light and therefore do not cause visibility impairment. However, these emissions are converted in the atmosphere to secondary species that do scatter or absorb light and have the potential to cause visibility impairment. SO_2 emissions are converted to sulfate ($SO_4^{=}$) aerosol, such as sulfuric acid and acid ammonium sulfates. These aerosols are generally formed or grow to a size (0.1 to 1.0 μm) that is effective in scattering light. Nitric oxide (NO) emissions are converted to nitrogen dioxide (NO_2) gas, which is effective in absorbing light. In turn, NO_2 is converted to nitric acid vapor (HNO_3), which neither absorbs nor scatters light. In some situations, nitric acid may form ammonium nitrate or organic nitrate aerosol, which scatters light. However, in many nonurban plumes nitrate probably remains as HNO_3 vapor without visual effects. Eventually, all primary particulates, secondary aerosol, and gases in a plume are removed from the atmosphere as a result of surface deposition and precipitation scavenging. PLUVUE is designed to predict the transport, atmospheric diffusion, chemical conversion, optical effects, and surface deposition of point-source emissions. Figure C-7 shows schematically the logic flow of PLUVUE.

The model uses a Gaussian formulation for transport and dispersion. The spectral radiance $I(\lambda)$ (i.e., the intensity of light) at 39 visible wavelengths ($0.36 < \lambda < 0.75 \mu m$) is calculated for views with and without the plume; the changes in the spectrum are used to calculate various parameters that predict the perceptibility of the plume and contrast reduction caused by the plume (see Latimer et al., 1978). The four key perception parameters for predicting visual impact are

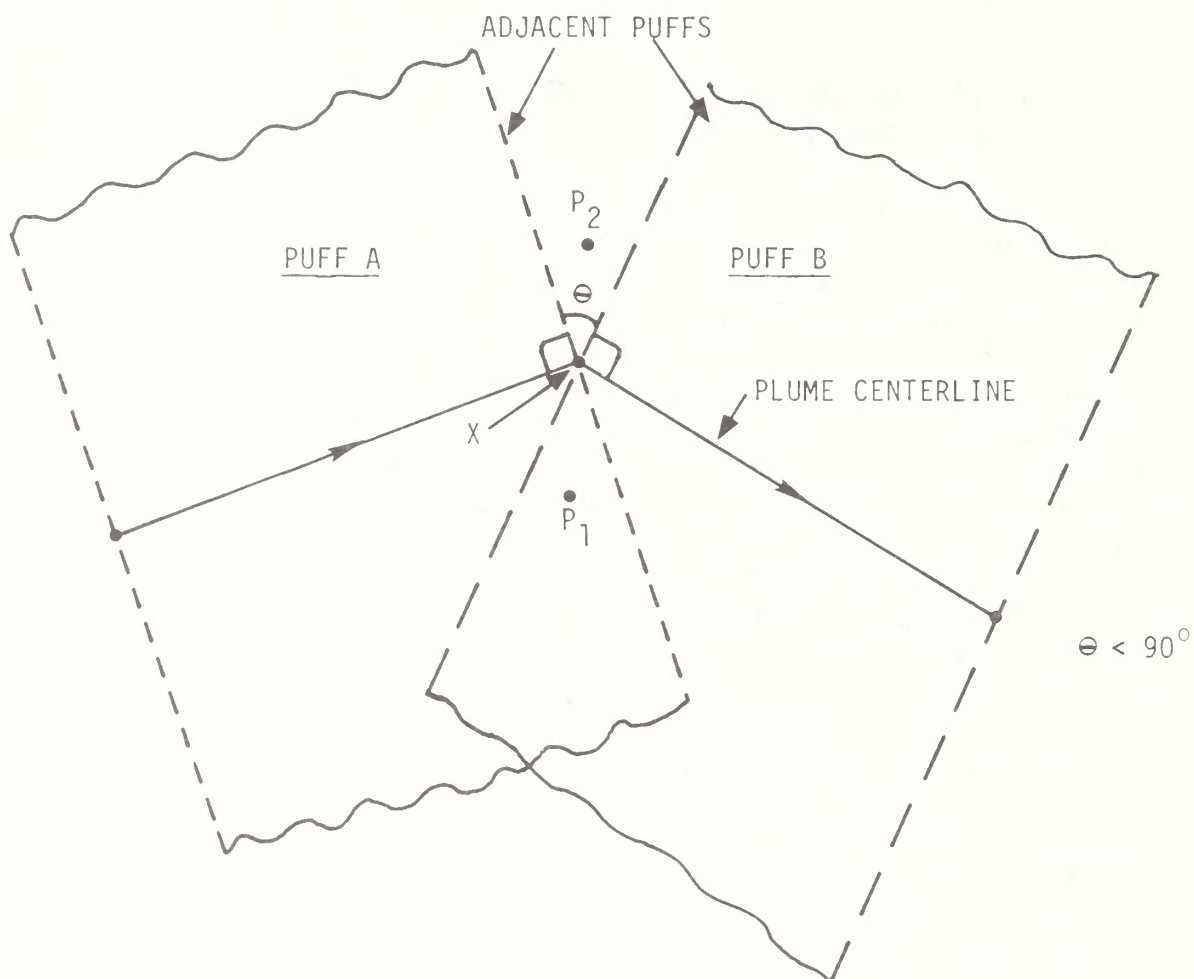


FIGURE C-6. DIAGRAM OF GPM TREATMENT OF PUFF INTERSECTIONS

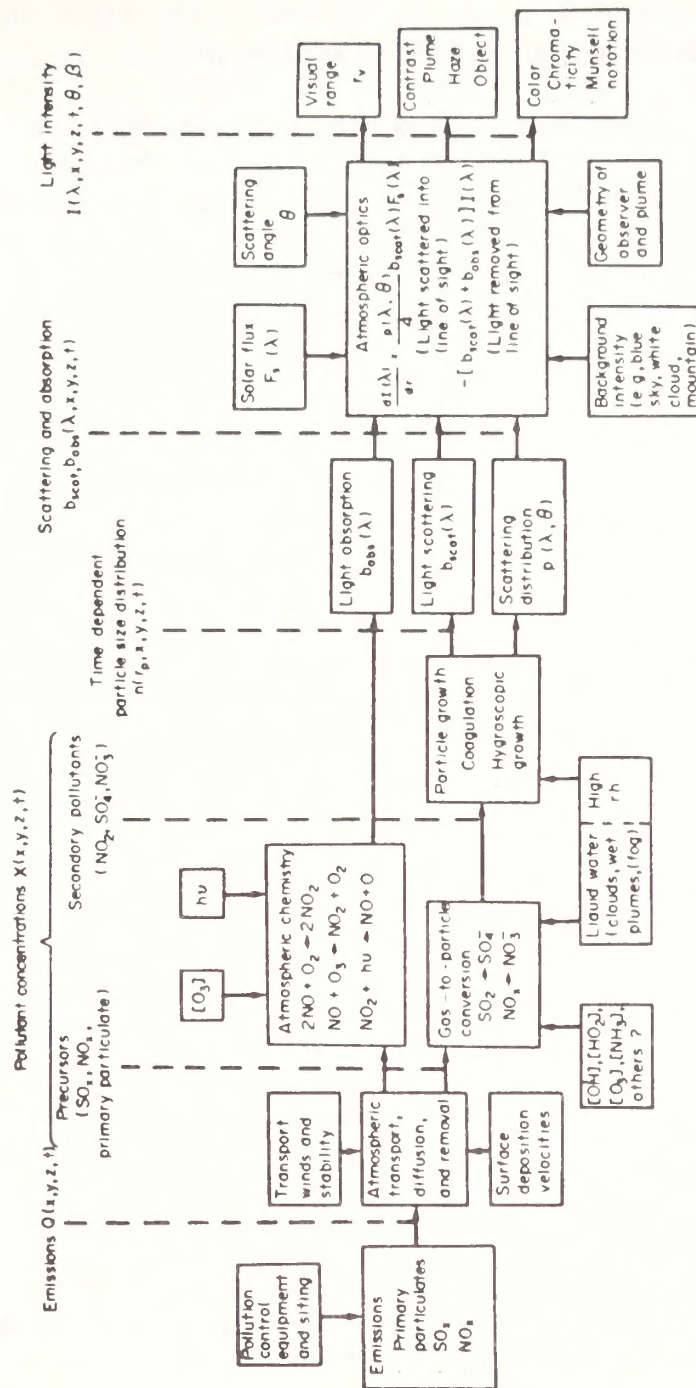


FIGURE C-7. SCHEMATIC LOGIC FLOW DIAGRAM OF THE PLUME VISIBILITY MODEL

- > Reduction in visual range.
- > Contrast of the plume against a viewing background at the 0.55 μm wavelength.
- > The blue-red ratio (color shift) of the plume.
- > The color change perception parameter $\Delta E(L^*a^*b^*)$.

PLUVUE is designed to perform plume optics calculations in two modes. In the plume-based mode, the visual effects are calculated for a variety of lines of sight and observer locations relative to the plume parcel; in the observer-based mode, the observer position is fixed and visual effects are calculated for the specific geometry defined by the positions of the observer, plume, and sun. For either mode, the model requires the user to select up to 16 different distances downwind of the emissions source. These distances determine the locations of the optics calculations along the plume trajectory. In this analysis, the observer-based calculation mode was used.

For the observer-based calculations, both the observer position and the direction of the plume trajectory are fixed by user-supplied specifications appropriate to the given application:

- > Wind direction
- > Location of the source
- > Location of the observer
- > Date and time.

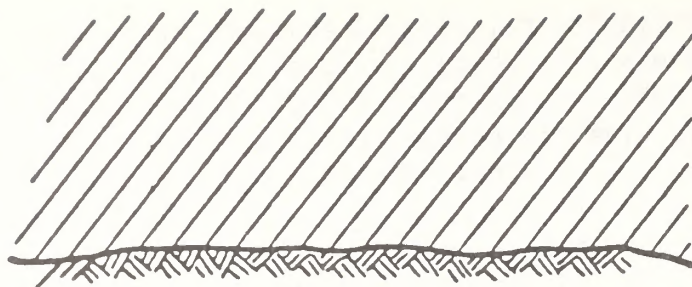
These specifications allow the specific plume observer geometry (θ , α , β , r_p) to be calculated for each downwind distance on the plume trajectory.^p Calculations are performed for lines of sight emanating from the observer's location and through the plume center at various downwind distances. Each line of sight is matched with its particular set of these specifications.

Several types of calculations can be performed at each downwind distance. One calculates the effects for horizontal lines of sight with a clear sky background. Plume-based calculations include a range of scattering angles (θ), azimuthal angles between the line of sight and the plume centerline (α), and observer-to-plume distances (r_p). The observer-based computation uses the specific values of these variables for each downwind point appropriate for the given plume-observer geometry.

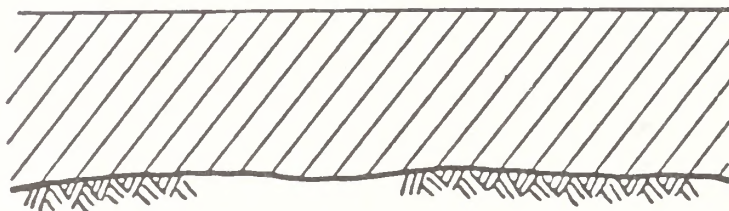
Another type of calculation evaluates the effect of the plume on horizontal views with white, gray, and black viewing object (terrain) backgrounds with uniform spectral reflectances of 1.0, 0.3, and 0.0, respectively. The plume-based calculations are done for the range of scattering angles (θ), observer-to-plume distances (r_p), and observer-to-background object distances (r_o) assuming the line of sight is perpendicular to the plume centerline ($\alpha = 90^\circ$). However, in the observer-based calculations, the values of the angles and distances for the specific geometry are used. In this analysis, appropriate viewing object colors and distances were used to characterize terrain-viewing backgrounds.

Figure C-8 illustrates five situations in which air pollution is visually perceptible. There are two basic kinds of visibility impacts. In one case, of which figures C-8(b), (c), and (e) are examples, air pollution is perceptible as a result of the comparison of two objects viewed simultaneously by an observer. The haze layer and plume in figures C-8(b) and (c), for example, are perceptible because they contrast with the background atmosphere. The plume in figure C-8(e) is perceptible because it contrasts with the viewed objects; in other words, it is brighter or darker or colored differently from the viewed object. In the other case, of which figures C-8(a) and (d) are examples, perception of pollution results from the difference between the currently observed scene and the scene remembered under clear conditions. For example, the haze in figure C-8(c) may be perceptible because it is colored differently from what is considered to be normal sky color; it appears white, gray, yellow, or brown instead of blue. The situation shown in figure C-8(d) is similar. The scene may appear hazy because the contrast of viewed objects is decreased from that observed on a clear day.

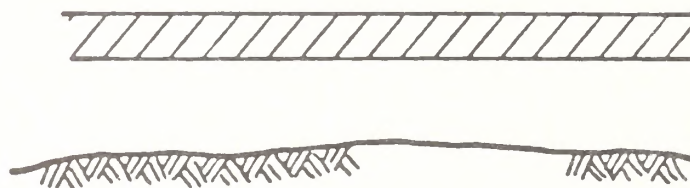
Visual impacts associated with oil shale development are best characterized by the situations shown in figure C-8(a), (b), and (d), where well-mixed emissions within a surface-based layer affect the coloration of the horizon sky or the contrast of distant landscape features. Since TSP and NO_x emissions from individual oil shale facilities are relatively low, plume visual impacts as shown in figure C-8(c) and (e), will be localized near the individual oil shale facilities and will occur rarely on stable, stagnant mornings. The visual impacts of greatest regulatory concern are those that occur in mandatory Class I areas. Flat Tops, which is 60 km from the Piceance Basin and 140 km from the Uinta Basin, is the nearest Class I area to the projected oil shale developments. At this distance, plumes from oil shale facilities will be relatively well mixed and, if perceptible at all, will be perceived as haze (see figure C-8(a), (b), and (d)).



(a) General, uniformly discolored haze

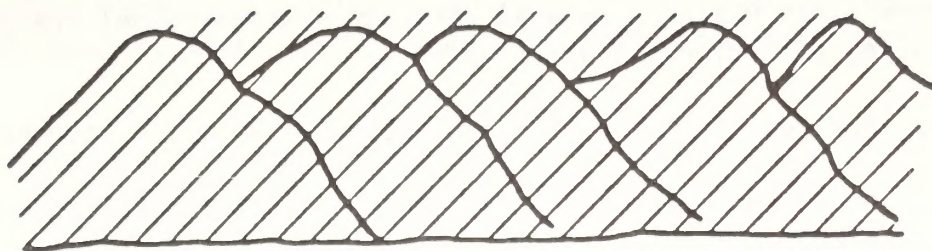


(b) Surface-based haze layer contrasting with background atmosphere above

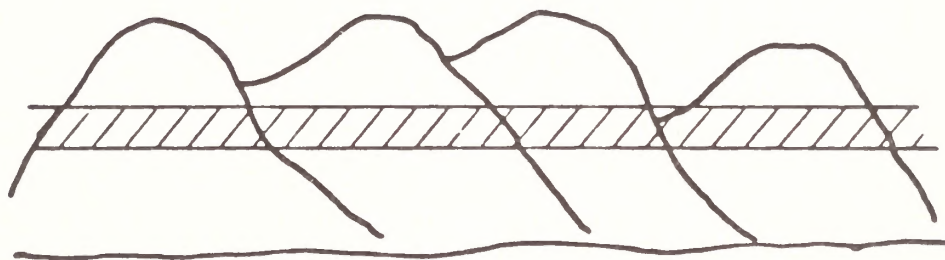


(c) Elevated plume or haze layer contrasting with background atmosphere above and below

FIGURE C-8. FIVE BASIC SITUATIONS IN WHICH AIR POLLUTION IS VISUALLY PERCEPTIBLE



(d) General haze reducing contrast of viewed objects



(e) Elevated plume or ground-based or elevated haze layer reducing contrast of a portion of a viewed object

FIGURE C-8. (Concluded)

C.4 TECHNICAL DISCUSSION OF THE SYSTEMS APPLICATIONS REGIONAL TRANSPORT MODEL

The Regional Transport Model (RTM), developed by Liu and Durran (1977), was first applied to regional SO_2 and sulfate transport in the northern Great Plains. Several attributes of the model are essential to simulation of regional-scale transport:

- > The ability to handle a multitude of emission sources.
- > Adequate treatment of pollutant transport over large distances.
- > Adequate treatment of pollutant surface depletion processes.
- > Provision for treatment of SO_2 -to-sulfate transformations.
- > Moderate computation requirements.
- > Reasonable input data requirements.

The model is composed of a mixing layer and an upper layer, and has a nested surface layer treatment contained in the mixing layer.

The mixing-layer model is designed to treat transport and diffusion above the surface and below the mixing height. A second (upper) layer above the mixing height is intended to treat transport and diffusion of pollutants released above the mixing height. It also tracks mass that is vented out of the mixing layer when the mixing height decreases. A grid approach was adopted for this model to facilitate the handling of multiple sources and complex chemistry. The major feature of this model is its assumption that, for each layer, pollutant distribution is nearly uniform in the vertical direction. With this assumption, a simplified form of the general atmospheric diffusion equation can be invoked.

The surface-layer model is designed to calculate the pollutant flux deposited on the ground. The surface layer, a shallow layer immediately above the terrain, is embedded within the mixing layer. For pollutants originating from either elevated sources or distant ground-level sources, most of the pollutant mass is contained in the mixing layer. The removal processes consist of the diffusion of the pollutants through the surface layer to the ground, followed by absorption or adsorption at the atmosphere-ground interface. A unique feature of the surface layer is its diurnal variation in surface temperature, which is a result of daytime heating and nighttime cooling. This variation affects the vertical

pollutant distribution through atmospheric stabilities and, consequently, affects the rate of surface uptake of pollutants.

The three layers--surface layer, mixing layer, and upper layer--are discussed in the following sections. It should be emphasized that RTM contains most of the basic and most desirable elements of an ideal regional air quality model, but it does not address several important issues:

- > Predictions from the regional grid model in its basic form are not likely to be applicable within, say, a few kilometers downwind of a major emission source. Sub-grid-scale concentration distributions must be dealt with by portions of the computer code intended to deal with sub-grid-scale concentration distributions are described in section C.4.1.3.
- > The only pollutant removal process treated by this version of the model is dry deposition at the surface. Other important removal processes such as rainout and washout are not considered. Unless these processes are included, the present model is, strictly speaking, applicable only during periods of no precipitation.
- > The treatment of chemical reactions is limited to a first-order overall reaction between SO_2 and sulfate. Although computational time is the only constraint that imposes a problem, the inclusion of complex chemistry awaits the development of a kinetic model capable of simulating both chemical transformations during nighttime and the effects of natural emissions of hydrocarbons.

C.4.1 The Mixing Layer and Upper Layer

The mixing layer and upper layer are designed to treat the transport and diffusion of air pollutants over long distances. The model formulation is discussed in section C.4.1.1. As stated earlier, the grid approach was adopted in the present study. There are a number of significant advantages to the grid approach--it is quite versatile and can easily handle time- and space-varying emissions and meteorological variables, complex chemistry, and surface sinks. There is one major disadvantage associated with this approach: pseudo-diffusion involved in the numerical solution of the governing equation can be overwhelming if not properly treated (the numerical solution method is discussed in section C.4.1.2). Furthermore, an accurate scheme is required for the simulation of the advection term.

There is no vertical diffusion between the mixing layer and the upper layer. The only pollutant transfer between the mixing layer and the upper layer is associated with either temporal or spatial variations in the mixing height.

C.4.1.1 The Model Equations

Within the framework of the so-called gradient-transport theory,* the concentration distributions of N reactive species can be described by the atmospheric diffusion equation of the following form (Monin and Yaglom, 1971):

$$\begin{aligned} \frac{\partial c_i}{\partial t} + u \frac{\partial c_i}{\partial x} + v \frac{\partial c_i}{\partial y} + w \frac{\partial c_i}{\partial z} = \frac{\partial}{\partial x} K_x \frac{\partial c_i}{\partial x} + \frac{\partial}{\partial y} K_y \frac{\partial c_i}{\partial y} \\ + \frac{\partial}{\partial z} K_z \frac{\partial c_i}{\partial z} + R_i(c_1, c_2, \dots, c_N) \\ + S_i(c_i) \quad i = 1, 2, \dots, N, \end{aligned} \quad (C-51)$$

where c_i denotes concentration for pollutant species i , u , v , w , and K_x , K_y , K_z represent wind speeds and turbulent eddy diffusivities in the x , y , and z directions, respectively, and R and S are the chemical reaction and source (and/or sink) terms.

One of the major simplifications in this model is the assumption of vertical homogeneity in the concentration distribution. One of the reasons for choosing this simplification is that the vertical diffusion term, based on the dimensional analysis shown above, is about 100 times greater than the transport term, and the horizontal diffusion term is only a fraction of the transport term. Thus, retaining the vertical variation

* The gradient-transport theory, analogous to molecular diffusion theory, states that a pollutant flux in the direction of decreasing concentration is established as a result of turbulent fluctuations. The magnitude of this flux is assumed to be proportional to the gradient of the average concentration. The limitations of models based on the gradient-transport theory, also known as K-theory, were examined by Corrsin (1974).

terms in the diffusion equation will compound difficulties in the numerical solution of the governing equation, without necessarily improving the accuracy of the model's prediction. As shown in figure C-9 measurements of the vertical distributions of sulfur compounds over central Germany (Georgii, 1970) show that in these remote areas the profiles are fairly uniform beneath the temperature inversion. Similar observations were also reported by Rodhe (1971) in southern Sweden.

Assuming that the concentration distribution in the vertical is nearly uniform below the base of the temperature inversion, a vertically averaged concentration can be defined as

$$\bar{c}_i = \frac{1}{H} \int_0^H c_i dz, \quad (C-52)$$

where H is the height of the layer. Performing the same operation on Eq. (C-51) and imposing the appropriate vertical boundary conditions, one obtains

$$\begin{aligned} \frac{\partial \bar{c}_i}{\partial t} + \bar{u} \frac{\partial \bar{c}_i}{\partial x} + \bar{v} \frac{\partial \bar{c}_i}{\partial y} = \frac{\partial}{\partial x} K_x \frac{\partial \bar{c}_i}{\partial x} + \frac{\partial}{\partial y} K_y \frac{\partial \bar{c}_i}{\partial y} + R_i(\bar{c}_1, \bar{c}_2, \dots, \bar{c}_N) + S_i(\bar{c}_i) \\ + D \cdot \zeta(D) \quad i = 1, 2, \dots, N, \quad (C-53) \end{aligned}$$

where

c_{0i} = the upper-layer concentration for species i for the mixing layer and the background concentration of species i for the upper layer.

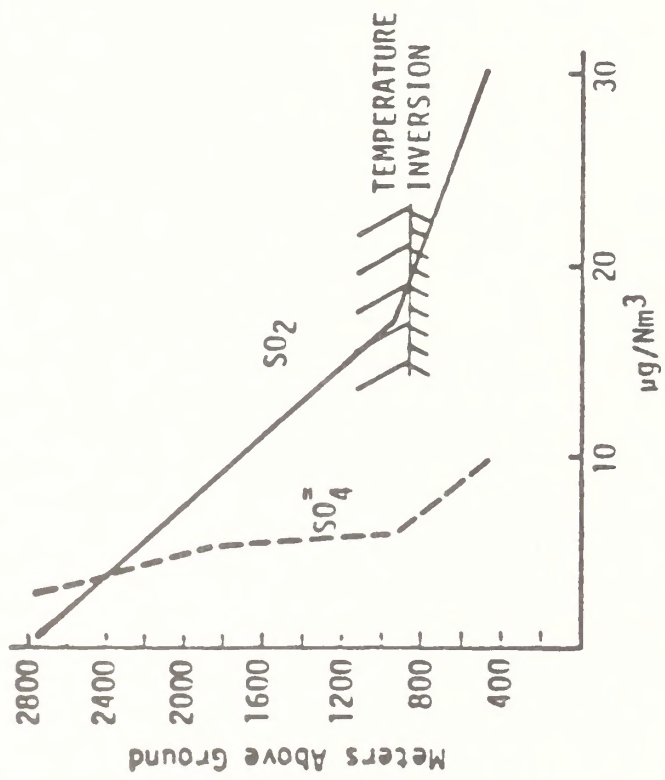
\bar{u} and \bar{v} = the vertically averaged horizontal wind components

$$(\bar{u} = \frac{H}{0} u dz/H, \bar{v} = \frac{H}{0} v dz/H),$$

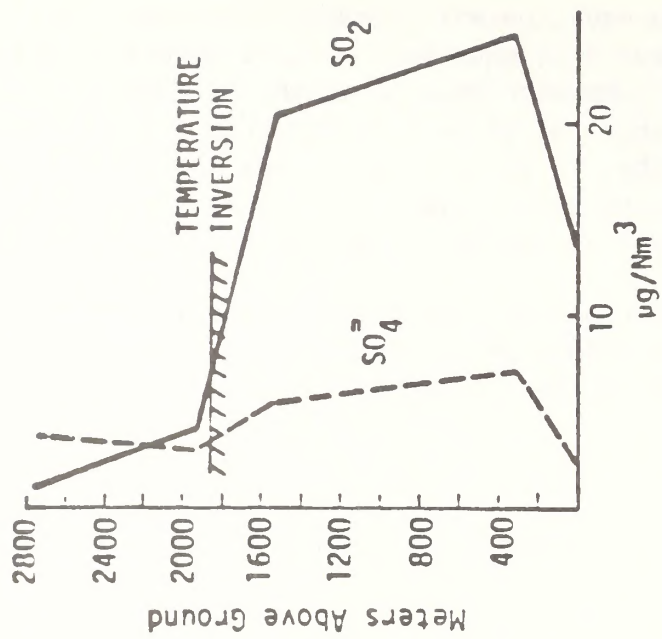
D = the two-dimensional divergence

$$D = [(\partial \bar{u}/\partial x) + (\partial \bar{v}/\partial y)], \text{ and}$$

$\zeta(D)$ = a step function defined by



(a) 25 February 1967



(b) 26 April 1967

Source: Georgii (1970).

FIGURE C-9. VERTICAL DISTRIBUTION OF SO₂ AND SO₄ OVER CENTRAL GERMANY

$$\zeta(D) = \begin{cases} \bar{C}_{0_i} & \text{for } D > 0 \text{ or, } \omega < 0 \\ \bar{C}_i & \text{for } D \leq 0 \text{ or, } \omega \geq 0 \end{cases} \quad (C-54)$$

In the derivation of Eq. (C-53), the following assumptions were made:

- > Deviations from the average concentration, \bar{C}_i , in the vertical direction are small.
- > The vertical velocity at the top boundary is given approximately by

$$w = - \int_0^H \left(\frac{\partial u}{\partial x} + \frac{\partial v}{\partial y} \right) dz \approx - H \left(\frac{\partial \bar{u}}{\partial x} + \frac{\partial \bar{v}}{\partial y} \right) \quad (C-55)$$

- > The diffusive flux of pollutants at the top boundary is negligible.
- > The following relationships hold for the reaction and source/sink terms:

$$R_i(c_1, c_2, \dots, c_N) = R_i(\bar{C}_1, \bar{C}_2, \dots, \bar{C}_N) \quad (C-56)$$

$$\bar{S}_i(c_i) = S_i(\bar{C}_i) \quad (C-57)$$

One of the problems encountered in the original model formulation was the disparity of scales in the treatment of emission sources. Since most of the sulfur dioxide emissions of interest come from point sources, the spatial scales associated with these sources and the grid spacings adopted in the mixing-layer model are certainly not commensurate. To resolve this sub-grid-scale problem, we developed a special algorithm that first treats emissions as puffs. These puffs are emitted from each major point source at regular time intervals and tracked downwind along their separate trajectories. The horizontal spread of each puff is calculated according to the Gaussian formula (Turner, 1969). When the width of a puff reaches that of one grid cell, the emissions contained in that puff are released into that cell. Table C-1 lists typical downwind distances at which the width of the puff* equals 10 km. It is apparent that the puff can travel a few grid cells before it is picked up in the mixing layer or the upper

* The width has been chosen to be 4σ , within which the puff contains more than 95 percent of the pollutant mass.

layer, particularly under stable conditions. The treatment of puffs used in the model code is described in section C.4.1.3.

TABLE C-1. DOWNWIND DISTANCE TRAVELED BY A PUFF AS A FUNCTION OF ATMOSPHERIC STABILITY

<u>Stability Category</u>	<u>Downwind Distance Where $4\sigma = 10 \text{ km}^*$</u>
A	13.3 km
B	17.7 km
C	25.8 km
D	42.8 km
E	59.0 km
F	88.5 km

* From Turner (1969); σ adjusted for a one-hour sampling time.

C.4.1.2 The Numerical Method

The solution of Eq. (C-53) with appropriate initial conditions and boundary conditions surrounding the modeling region requires a numerical method. Since the transport of pollutants on this scale is dominated, as demonstrated above, by horizontal advection, the problem of numerical solution arises in the discretization processes. That is, the numerical solution tends to smooth any sharp concentration profiles as the pollutants are advected downwind, even when the horizontal diffusivity is zero. We investigated and compared the accuracy and computing time requirements of three finite difference methods for solving simplified forms of Eq. (C-53):

- > The upstream difference method
- > The SHASTA method
- > The Egan-Mahoney method.

The upstream difference method is the simplest of the three. It is also well known and widely used (Forsythe and Wasow, 1960). The SHASTA method (Sharp and Smooth Transport Algorithm) was developed by Boris and Book (1973). The method proposed by Egan and Mahoney (1972a, 1972b) has the

distinctive feature that the first and second moments of the mass distribution in each cell are also calculated. The performance of each method was examined by means of hypothetical situations. Considering accuracy and computing speed, the SHASTA method appeared to be most suitable to the needs of regional modeling; it was thus selected for treating the horizontal advection terms. In the following paragraphs we present a brief description of the numerical method used in the mixing layer and upper layer.

Let the continuous variables be represented on a grid with mesh widths Δx and Δy so that $x_{ij} = x(i\Delta x, j\Delta y)$. Define the operators

$$D_{\pm}^{(1)} c_{ij} = \pm (c_{i\pm 1, j} - c_{ij}) \quad D_{\pm}^{(2)} c_{ij} = \pm (c_{i, j\pm 1} - c_{ij}) \quad (C-58)$$

$$D_0^{(1)} c_{ij} = c_{i+1, j} - c_{i-1, j} \quad D_0^{(2)} c_{ij} = c_{i, j+1} - c_{i, j-1}$$

$$Q_{\pm}^{(1)} u_{ij} = \frac{\frac{1}{2} \pm u_{ij} \frac{\Delta t}{\Delta x}}{1 \pm (u_{i\pm 1, j} - u_{ij}) \frac{\Delta t}{\Delta x}} \quad Q_{\pm}^{(2)} v_{ij} = \frac{\frac{1}{2} \pm v_{ij} \frac{\Delta t}{\Delta x}}{1 \pm (v_{i, j\pm 1} - v_{ij}) \frac{\Delta t}{\Delta x}} \quad (C-59)$$

Then our numerical method is given by the following three fractional steps (Yanenko, 1971):

Step 1--x-direction

$$c^* = \alpha_1 + \frac{1}{2} (Q_+^{(1)} u)^2 D_+^{(1)} c^n - \alpha_1 + \frac{1}{2} (Q_-^{(1)} u)^2 D_-^{(1)} c^n$$

$$+ Q_+^{(1)} u + Q_-^{(1)} u + (r - d) \Delta t c^n$$

$$\tilde{c} = \frac{1}{2} Q_+^{(1)} u^2 D_+^{(1)} c^n - \frac{1}{2} Q_-^{(1)} u^2 D_-^{(1)} c^n + Q_+^{(1)} u + Q_-^{(1)} u c^n$$

$$c^{**} = c^* - \frac{1}{8} D_+^{(1)} D_-^{(1)} \tilde{c} \quad , \quad (C-60)$$

Step 2--y-direction

$$c^{***} = \alpha_2 + \frac{1}{2} (Q_+^{(2)} v)^2 D_+^{(2)} c^{**} - \alpha_2 + \frac{1}{2} (Q_-^{(2)} v)^2 D_-^{(2)} c^{**} \\ + Q_+^{(2)} v + Q_-^{(2)} v - \frac{w \Delta t}{\Delta H} c^{**}$$

$$\tilde{c} = \frac{1}{2} (Q_+^{(2)} v)^2 D_+^{(2)} c^{**} - \frac{1}{2} (Q_-^{(2)} v)^2 D_-^{(2)} c^{**} + (Q_+^{(2)} v + Q_-^{(2)} v) c^{**}$$

$$c^+ = c^{***} - \frac{1}{8} D_+^{(2)} D_-^{(2)} \tilde{c}, \quad (C-61)$$




Step 3--point sources

$$c^{n+1} = c^+ + S,$$

$$\text{where } \alpha_1 = \frac{K_x \Delta t}{\Delta x^2}, \quad \alpha_2 = \frac{K_y \Delta t}{\Delta y^2}. \quad (C-62)$$

The chemical reaction rate is r , and d is the surface deposition rate. The advection terms are treated with at least second-order accuracy, while the fractionalized scheme as a whole is accurate to the second order in space and to the first order in time.

An estimate of the accuracy of the numerical method adopted is useful. Table C-2 gives the effective pseudo-diffusivities produced by the model on a 10-km grid with an optimum step size. The pseudo-diffusion generated appears to be small when compared with the physical diffusivity in the horizontal plane, which is estimated to be on the order of $10^4 \text{ m}^2/\text{sec}$ (Randerson, 1972). With a 10-km-square grid cell, the most restrictive stability constraint derives from the advection terms [Eq. (C-63)] if K_x and K_y are less than $10^5 \text{ m}^2/\text{sec}$. For higher horizontal diffusivities, Eq. (C-64) becomes more stringent. The time step used in the model is chosen so that these conditions are always satisfied. Thus, accurate and stable solutions are obtained. A more thorough analysis of the problem of pseudo-diffusion is presented in Liu and Durran (1977).

Wave Type	Wave Number (m ⁻¹)	Pseudo-Diffusivity (m ² /sec)
	60π/10 ⁶	2.5 × 10 ³
	30π/10 ⁶	1.6 × 10 ²
	15π/10 ⁶	40

Computational stability is guaranteed when

$$\max \left(\frac{u \Delta t}{\Delta x}, \frac{v \Delta t}{\Delta y} \right) < 0.6 \quad (C-63)$$

$$\max \left(\frac{K_x \Delta t}{\Delta x^2}, \frac{K_y \Delta t}{\Delta y^2} \right) < 0.15 \quad (C-64)$$

TABLE C-2. PSEUDO-DIFFUSIVITY IN ADVECTIVE TRANSPORT
FOR A 10 KILOMETER GRID AND $v \Delta t / \Delta x = 1/2$

C.4.1.3 The Gaussian Puff Sub-Model

Although not used in this study a Gaussian Puff Model (GPM) was used for the near-source plume simulation within the mixing layer. In this model, the plume is considered to be composed of a series of puffs. A puff, illustrated in figure C-10, is that part of the plume emitted during one time step.

The model keeps track of all of the puffs emitted from a source until they are released into the larger grid. The model stores information about the location of the center of each puff (in 3 dimensions), the mass of SO_2 and SO_4 in the puff, and the standard deviation of the puff mass distribution in the vertical direction (σ_z) and in the horizontal direction perpendicular to the motion of the puff (σ_y). Each puff is advected according to the winds at the center of the puff, and the mass distribution of any cross section of the plume is determined by the dispersion coefficients σ_z and σ_y and the Gaussian formulation.

The model accounts for several occurrences at each time step: all the old puffs are advected downwind; new values for puff location, SO_2 and SO_4 mass, and dispersion coefficients are calculated; and a puff, if it is sufficiently dispersed, is released into the regular grid model. In addition, a new puff is created with a center a half-step downwind, at a height determined by the following plume rise equation (Briggs, 1971):

$$H_e = H_s + [1.6 F^{1/3} \cdot (10H_s)^{2/3} / U] \quad (\text{C-65})$$

$$\text{where } F = 9.8 \frac{\Delta T}{T_s} \cdot V_s R_s^2 ,$$

where

$$\Delta T = T_s - T_a$$

H_e = effective release height

H_s = stack height

U = wind velocity

F = buoyancy flux

V_s = exit velocity from stack

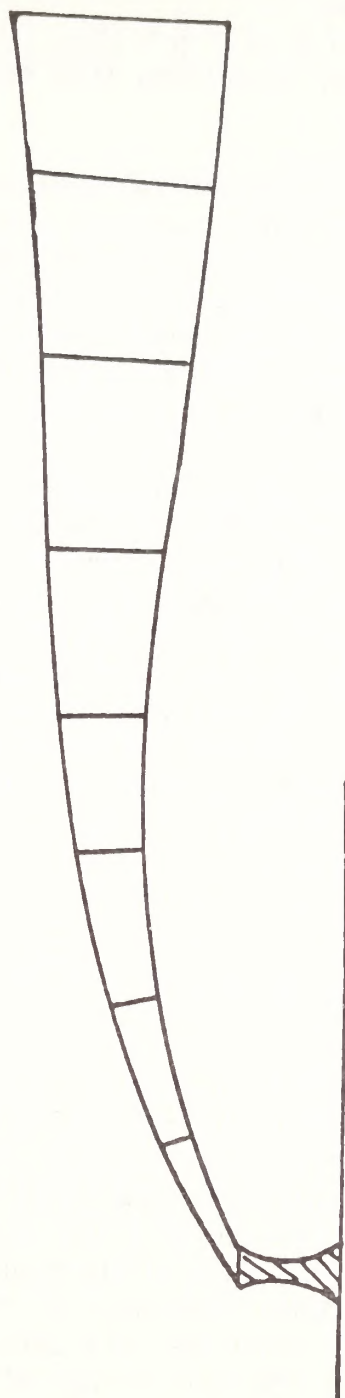


FIGURE C-10. ILLUSTRATION OF A PLUME COMPOSED OF PUFFS

R_s = stack radius

T_s = temperature in stack

T_a = ambient temperature.

Vertical winds are assumed to be zero; therefore, this height is used for the center of the puff downwind.

Dispersion coefficients for the puffs are calculated using the Pasquill-Turner-Gifford (Turner, 1969) method. The dispersion coefficients are functions of atmospheric stability class, downwind distance of the puff, and dispersion coefficient history. The coefficients are calculated to increase smoothly with time. The rate of change of coefficients at the appropriate stability class and downwind distance is used to calculate increments that are added to the coefficient with each time step.

Changes in each puff's SO_2 and SO_4 mass, caused by deposition and SO_2 and SO_4 oxidation, are also calculated for each time step. To calculate the percentage of plume mass near the ground, deposition is calculated using the vertical dispersion coefficient and the Gaussian normal distribution in the vertical direction. Then deposition is calculated from the surface-layer model equations. Oxidation is calculated as it is throughout the grid model. This process is described in section C.4.1.4.

When a puff is dispersed sufficiently so that its dimensions reach those of a grid cell, the mass of the puff is released into the grid cell containing the puff's center. This condition is met when

$$4 \sigma_y \geq \text{MAX} (\Delta X, \Delta Y),$$

or when

$$4 \sigma_z \geq \text{mixing height in that cell or depth of the upper layer} \\ \text{if the puff's height is above the mixing layer.}$$

The RTM plume model stores information about the history of the puffs from each source and determines when and where to release these puffs into the grid model and how much to deposit and oxidize from each puff. The near-source concentrations can be calculated in two ways at the option of the user: by adding the mass of the puff into the grid cell in which the puff was centered; the mass is then divided by the full volume of that cell, or, as explained in the following section, by the Gaussian equation method for calculating puff concentrations at a point.

C.4.1.3.1 Gaussian plume equation

The usual Gaussian equation is

$$\chi(P) = \frac{Q}{U} F(Y, \sigma_y) G(Z, S_c, \sigma_z, L) \quad , \quad (C-66)$$

where

χ = the concentration at P due to the plume (g/m^3),

X = the downwind distance of point P from the source,

Y = the crosswind distance from P to the plume centerline (m),

Z = the vertical coordinate of the point P (m),

S = The vertical coordinate of the point (X_c, Y_c, Z_c) on the plume centerline that is closest to P (m).

Q = the rate of emission (g/sec),

U = the wind speed (m/sec),

σ_y = the horizontal (transverse) dispersion coefficient (m),

σ_z = the vertical dispersion coefficient (m),

L = the mixing height (m).

σ_y and σ_z are calculated at (X_c, Y_c, Z_c) .

$$F(Y, \sigma_y) = \frac{1}{\sqrt{2\pi} \sigma_y} \exp \left(-\frac{Y^2}{2\sigma_y^2} \right)$$

$$G(Z, S, \sigma, L) = \frac{1}{\sqrt{2\pi} \sigma} \left\{ \exp \left(-\frac{(S - Z)^2}{2\sigma^2} \right) \right.$$

$$+ \exp \left(-\frac{(ZL - S - Z)^2}{2\sigma^2} \right) + \exp \left(-\frac{(2a - S - Z)^2}{2\sigma^2} \right) \left. \right\}$$

$$+ \sum_{\substack{n \text{ even} \\ n > 0}} \left(\exp \left[-\frac{(na - nL + S - Z)^2}{2 \sigma^2} \right] + \exp \left[-\frac{[n + 2] L - na - S - Z)^2}{2 \sigma^2} \right] \right. \\ \left. + \exp \left[-\frac{(nL - na + S - Z)^2}{2 \sigma^2} \right] + \exp \left[-\frac{[n + 2] a - nL - S - Z)^2}{2 \sigma^2} \right] \right) \Bigg\}$$

where a is the height of the ground (or lower barrier). If $a = Z = 0$, this reduces to

$$G(0, S, \sigma, L) = \frac{2}{\sqrt{2\pi} \sigma} \sum_{\substack{n=Z \\ n=-\infty}}^{\infty} \exp \left[-\frac{(S + 2nL)^2}{2 \sigma^2} \right] .$$

When σ/L is large enough, the pollutant is considered to be uniformly distributed in the mixing layer, and then $G = 1/L$.

Equation (C-86) is implemented as shown in Eq. (C-87). The concentration due to a puff is calculated in ppm:

$$C(P) = \frac{A \cdot 10^6}{\phi \cdot dx} F(y, \sigma_y) G(Z, Z_c, \sigma_z, L) \quad , \quad (C-67)$$

where

C = the concentration at the point P (ppm),

A = the number of moles of pollutant in the puff,

dx = the distance the puff traveled during the current time step (m),

ϕ = the number of moles per cubic meter (air) = 40.82,

F, G = the same as above (except we use a finite sum).

The concentration at P resulting from the plume is then the result of summing Eq. (C-87) over all puffs.

C.4.1.4 Oxidation of SO_2 to SO_4

Another feature of the RTM is its capability to vary the rate of oxidation of SO_2 to SO_4 diurnally, according to changes in the intensity of solar radiation. Altshuller (1979) presented clean-air homogeneous oxidation rates of SO_2 by latitude and by the month of the year. The maximum noontime values calculated are shown in table C-3.

The oxidation rate $r(t)$ at time t used in the model is calculated by

$$r(t) = r_{\text{night}} + \frac{\sin[\theta_z(t)]}{\sin[\theta_z(\text{noon})]} \cdot (r_{\text{noon}} - r_{\text{night}}) \quad , \quad (\text{C-68})$$

where $\theta_z(t)$ is the solar zenith angle at time t , and $\sin[\theta_z(t)]$ is thus proportional to the solar radiation intensity. $\theta_z(t)$ is calculated in the model from inputs of latitude and longitude of the modeling region and of the time zone, and $\theta_z(\text{noon})$ is calculated as the maximum daily solar zenith angle that can occur in that particular standard time. r_{noon} is the peak oxidation rate at 1200 local time for a given latitude (Altshuller, 1979), and r_{night} accounts for the slow oxidation that continues after sunset.

It should be noted that this oxidation rate calculation assumes relatively clear skies. With substantial cloud cover or high humidities, and as heterogeneous reactions take on more importance, SO_2 oxidation to SO_4 becomes more complex. Accounting for cloud cover in the calculation would involve a considerable increase in the levels of model complexity and input preparation. Since the method chosen uses maximum and minimum rates of oxidation, the user can adjust these inputs to allow the use of reasonable values in the model.

C.4.2 The Surface-Layer Model

Pollutants are removed from the atmosphere via both dry and wet deposition. Only dry deposition at the earth's surface is considered by this model. The importance of the effects of surface deposition on pollutant concentrations at large distances has been well established (e.g., Bolin and Granat, 1973, 1974; Scriven and Fisher, 1975). Thus, an indispensable element in the regional air pollution model is the treatment of pollutant depletion processes near the surface. In this section, we describe the surface-layer model. We begin with a discussion of previous studies concerning surface deposition and conclude with a description of the approach adopted.

TABLE C-3. HOMOGENEOUS OXIDATION OF SULFUR DIOXIDE*

(Percent reaction per hour at noontime of sulfur dioxide of
HO, HO₂, and CH₃O₂, at 0.1 km)

Month	Latitude (°N)						
	5	15	25	35	45	55	65
January	1.81	1.10	0.61	0.26	0.08	0.01	<0.01
February	1.81	1.21	0.74	0.32	0.13	0.04	0.01
March	2.06	1.55	1.01	0.48	0.21	0.09	0.03
April	2.01	1.79	1.36	0.73	0.35	0.17	0.07
May	1.82	1.68	1.48	1.01	0.58	0.30	0.16
June	1.81	1.72	1.56	1.22	0.74	0.42	0.25
July	1.78	1.80	1.58	1.30	0.88	0.52	0.31
August	1.86	1.78	1.61	1.31	0.82	0.45	0.26
September	1.91	1.68	1.50	1.15	0.65	0.34	0.17
October	1.79	1.54	1.29	0.84	0.39	0.17	0.06
November	1.56	1.33	0.98	0.48	0.19	0.06	0.02
December	1.58	1.16	0.74	0.33	0.11	0.02	<0.01

* Taken from Altshuller (1979).

C.4.2.1 Dry Deposition on Surfaces

In most studies, removal of pollutants by the ground surface is generally characterized by

$$F = V_d c \quad , \quad (C-69)$$

where F is the mass flux to the surface, c is the concentration measured at an unspecified reference height, and V_d , having the units of velocity, is commonly referred to as the deposition velocity. In this expression, the deposition velocity is viewed as a proportionality constant whose magnitude is empirically established. The surface deposition is governed by many complex physical processes that depend primarily on

- > The state of the atmosphere near the ground
- > The types and configurations of the surface.

For example, Bolin, Aspling, and Persson (1974) noted that for a perfect sink of a particular gas, in which all molecules of that gas that reach the surface are absorbed, the ground-level concentration is zero and the deposition velocity is theoretically infinite. In this case the flux is diffusion-limited. Consequently, the simple concept of the deposition velocity is generalized.

In analogy with electrical circuits, surface deposition is treated in terms of resistance to mass transfer (Owen and Thompson, 1963; Chamberlain, 1966). The transfer of gases from the atmosphere to a surface is described by three resistances in parallel:

- > The resistance to momentum transfer, r_m
- > The excess resistance to mass or heat transfer, r_h
- > The resistance at the ground surface, r_s .

The total resistance, R , which is defined as the reciprocal of the deposition velocity, is then given by

$$v_d = \frac{1}{R} = \frac{1}{r_m} + \frac{1}{r_h} + \frac{1}{r_s} \quad . \quad (C-70)$$

Within the framework of the surface boundary layer (Owen and Thompson, 1963)

$$r_m = \frac{u(z)}{u^* 14} , \quad (C-71)$$

where $u(z)$ is the vertical wind profile and u^* is the friction velocity. The deviation between momentum and mass/heat transfer is characterized by

$$r_h = \frac{1}{\beta u^*} , \quad (C-72)$$

where β is dependent on the surface roughness, a Reynolds number appropriate to the flow in the roughness layer, and the ratio of the kinematic viscosity of air to the molecular diffusion coefficient of the pollutant gas. This correction is necessary because the process of mass transfer is generally less efficient than that of momentum transfer, resulting in a nonzero concentration of the gas at the surface. On the basis of a study of heat transfer to roughened glass plates, Owen and Thompson (1963) suggested

$$\beta^{-1} = \alpha (u^* z_0 / \nu)^{0.45} \frac{\nu}{D}^{0.8} , \quad (C-73)$$

where u^* , z_0 , ν , and D are the friction velocity, surface roughness, kinematic viscosity, and molecular diffusivity, respectively, and α is an empirical constant determined by the shape of the roughness elements. In further investigations by Chamberlain (1966) and Thom (1972), little functional relation was found between β and z_0 . Thus, Thom proposed

$$\beta^{-1} = \alpha_1 u^{*1-3} \alpha_2 \frac{\nu}{D}^{2/3} - 1 , \quad (C-74)$$

where α_1 and α_2 are empirical constants determined primarily by the surface roughness elements.

C.4.2.2 The Formulation of a Surface Deposition Model

For pollutants originating from either elevated sources or distant ground-level sources, most of the pollutant mass is contained in the mixing layer. The removal processes, as discussed above, consist of diffusion of the pollutants through the surface layer to the ground and absorption or adsorption at the atmosphere-ground interface. As illustrated in figure C-11, the diurnal variation of temperature in the surface

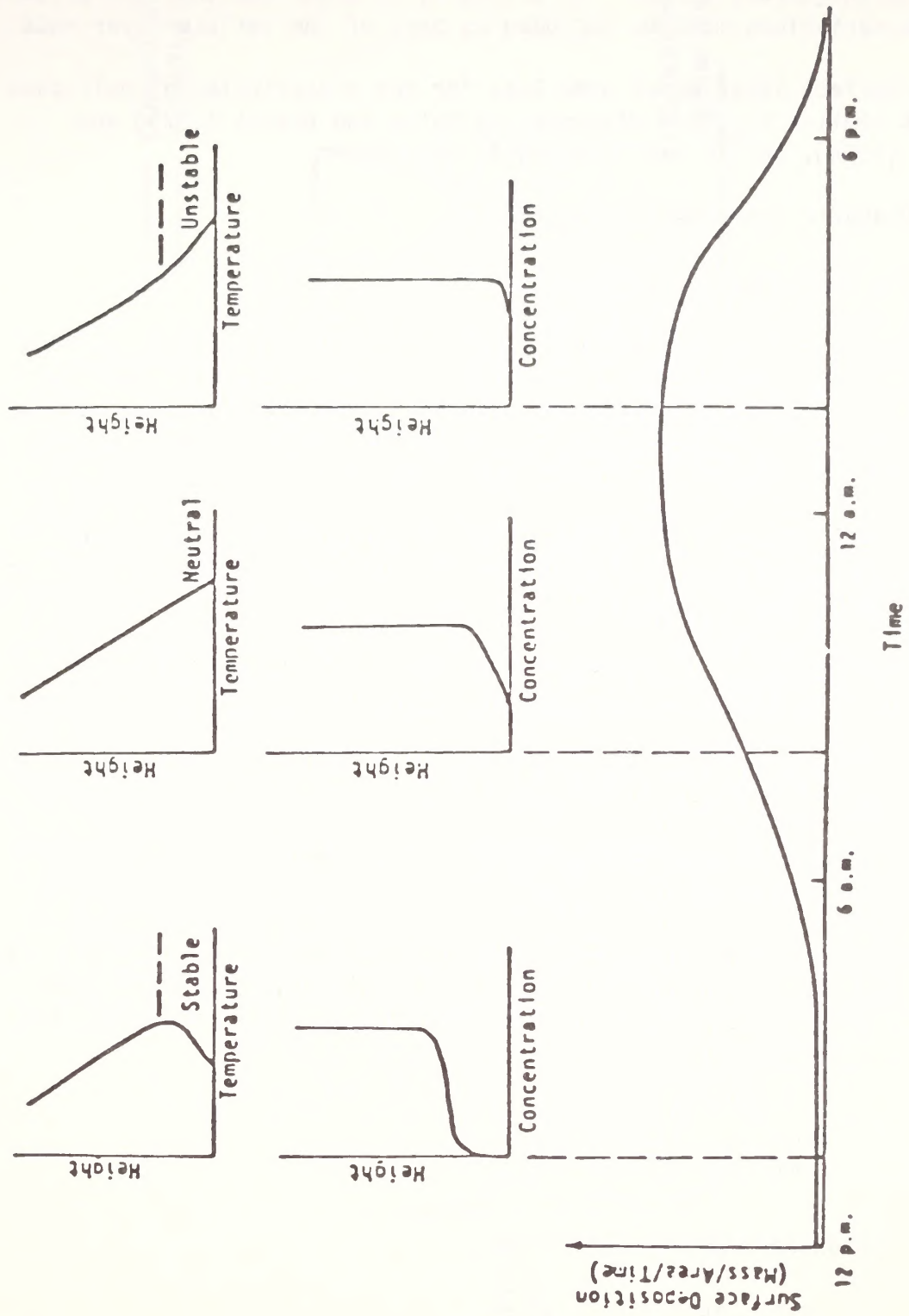


FIGURE C-11. SCHEMATIC ILLUSTRATION OF DIURNAL VARIATIONS IN SURFACE DEPOSITION

layer affects the vertical pollutant distribution through atmospheric stabilities and, consequently, affects the rate of surface uptake of pollutants (Högström, 1975). As a result, an algorithm that can account for these variations must be included as part of the surface-layer model.

The surface-layer model used here for the prescription of pollutant fluxes is similar to those discussed by Bolin and Granat (1973) and Galbally (1974), but it was extended to include

- > Diabatic atmospheric conditions
- > Nonlinear surface reactions.

This approach is favored over the relatively simple resistance approach primarily because the latter is restricted to linear surface reactions, which may not fit all situations of interest. For example, Hill (1971) observed that the adsorption of ozone by leaves does not vary linearly with concentration at high concentration levels.

The model assumes that the transfer of pollutant gases from the atmosphere to a surface is accomplished via three stages (Sehmel, Sutter, and Dana, 1973; Galbally, 1974):

- > The gases are transported, primarily by turbulent diffusion, to a laminar sublayer just above the surface.
- > The gases are transported, primarily by molecular diffusion, through this laminar sublayer.
- > The gases interact by adsorption or chemical reaction with the surface.

Thus, as shown in figure C-12, the surface layer is divided into two parts: the turbulent layer and the laminar sublayer. In the turbulent layer, after the atmosphere reaches an equilibrium state, the atmospheric diffusion equation becomes

$$\frac{\partial}{\partial z} K_V \frac{\partial c}{\partial z} = 0 \quad , \quad (C-75)$$

with the following boundary conditions,

$$c = \bar{c} \text{ at } z = h \quad ,$$

$$K_V \frac{\partial c}{\partial z} = F \text{ at } z = z_0 \quad ,$$

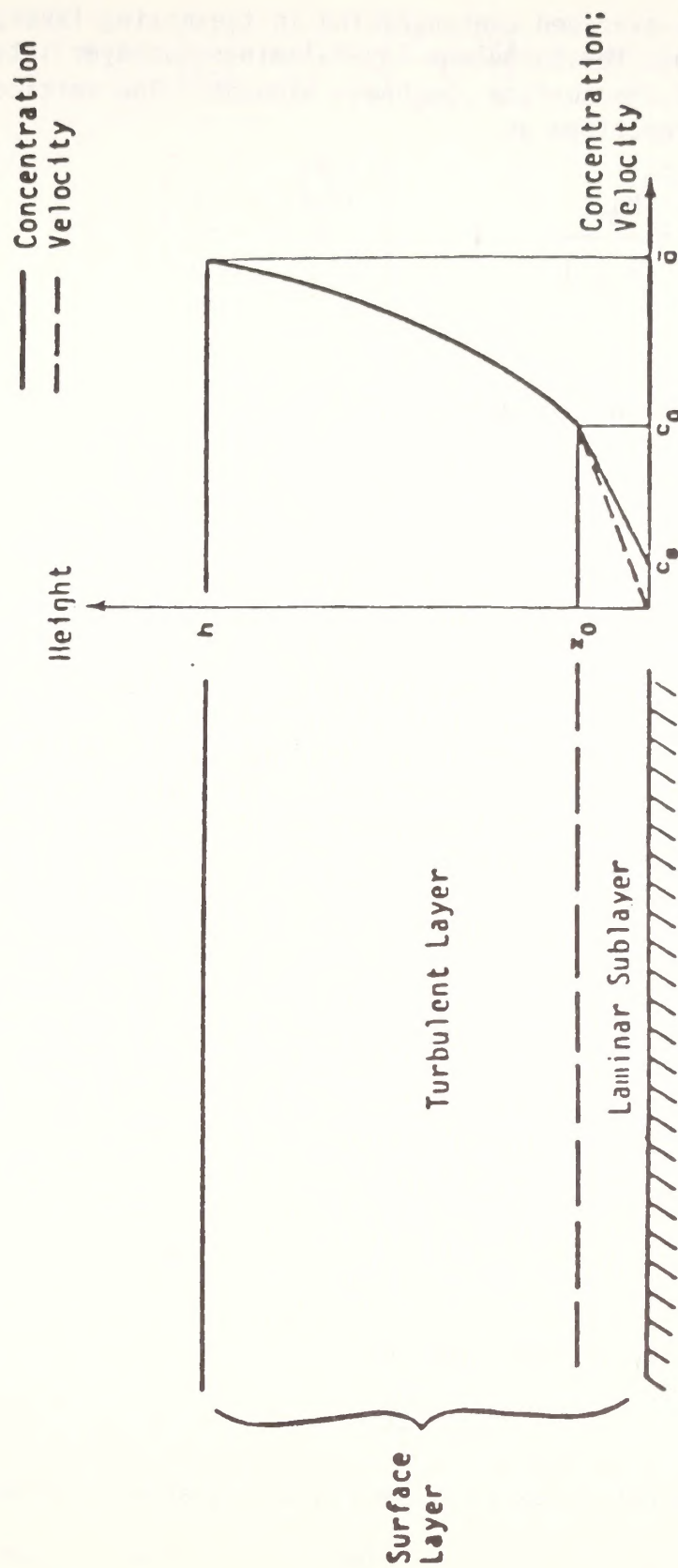


FIGURE C-12. SCHEMATIC ILLUSTRATION OF THE SURFACE LAYER

where \bar{c} is the cell-averaged concentration in the mixing layer, F is the pollutant flux across the turbulent layer-laminar sublayer interface, and z_0 is the height of the surface roughness element. The vertical diffusivity K_V can be prescribed as

$$K_V = \frac{ku_* z}{\phi \left(\frac{z}{L} \right)} \quad , \quad (C-76)$$

where

k = von Karman constant (= 0.35)

u_* = friction velocity

z = height

L = Monin-Obukhov length.

This formula is the result of the similarity theory for the constant-flux surface layer (Businger et al., 1971). For the neutral case, the ϕ -function equals unity. For the stable and unstable cases, the ϕ -function is greater and less than one, respectively. The following empirical expressions for the ϕ -function were proposed by Businger et al. (1971) on the basis of observational data:

For the stable case ($L > 0$)

$$\phi_s \left(\frac{z}{L} \right) = 1 + 4.7 \left(\frac{z}{L} \right) \quad . \quad (C-77)$$

For the unstable case ($L < 0$)

$$\phi_u \left(\frac{z}{L} \right) = \left[1 - 15 \left(\frac{z}{L} \right) \right]^{-1/4} \quad . \quad (C-78)$$

The friction velocity is determined by

$$u_* = \frac{ku_r}{f} \quad , \quad (C-79)$$

where u_r denotes a reference wind speed measured at a reference height, z_r , and

$$f = \ln \left(\frac{z_r}{z_0} \right) + 4.7 \left(\frac{z_r - z_0}{L} \right) \quad (\text{stable}) \quad , \quad (\text{C-80})$$

$$f = \ln \left[\frac{1 - \phi_u \left(\frac{z_r}{L} \right)}{1 + \phi_u \left(\frac{z_r}{L} \right)} \right] - \ln \left[\frac{1 - \phi_u \left(\frac{z_0}{L} \right)}{1 + \phi_u \left(\frac{z_0}{L} \right)} \right] \\ + 2 \tan^{-1} \left[\frac{1}{\phi \left(\frac{z_r}{L} \right)} \right] - 1 \tan^{-1} \left[\frac{1}{\phi_u \left(\frac{z_0}{L} \right)} \right] \quad (\text{unstable}). \quad (\text{C-81})$$

For either the stable or unstable case, the solution of Eq. (C-81) is simply

$$c = \bar{c} - F \cdot \int_z^h \frac{\phi(z)}{ku_* z} dz \quad . \quad (\text{C-82})$$

Across the laminar sublayer, it is assumed that the pollutant flux can be written as

$$F = \beta u_* (c_0 - c_s) \quad , \quad (\text{C-83})$$

where c_0 and c_s denote the concentrations at the interface and the surface, respectively, and β , analogous to the Stanton number in heat transfer, is the inverse of a dimensionless resistance for the laminar sublayer. If it is further assumed that mass and momentum are transferred in an identical manner in the turbulent layer, but differently through the laminar sublayer, then the relationships established by Owen and Thompson (1963) and Thom (1972) discussed above can be used:

$$\beta^{-1} = \alpha \left(u_* \frac{z_0}{\nu} \right)^{0.45} \left(\frac{\nu}{d} \right)^{0.8} \quad (\text{Owen-Thompson}) \quad , \quad (\text{C-84})$$

$$\beta^{-1} = \alpha_1 u_*^{1/3} \left[\alpha_2 \left(\frac{\nu}{D} \right)^{2/3} - 1 \right] \quad (\text{Thom}) \quad . \quad (\text{C-85})$$

Equation (C-81) is used in the model. To complete the description of the surface-layer model, a boundary condition is required at the surface.

Uptake of air pollutants occurs by chemical reaction with, or catalytic decomposition within, either the soil or vegetation, or it can occur by these processes at soil or vegetation surfaces. These processes are generally dependent on the gas concentration at the surface. A general equation for the gas loss per unit area per unit time can be written as (Benson, 1968),

$$F = \gamma c_s^a, \quad (C-86)$$

where F is the pollutant flux, γ is a reaction rate constant, and c_s is the concentration of the gas at the soil or vegetation surface. The exponent, a , denotes the reaction order. Eliminating c_0 and c_s from Eq. (C-82), (C-83), and (C-86), the following transcendental equation is obtained for F ,

$$I \cdot F + \gamma^{-1/a} \cdot F^{1/a} - \bar{c} = 0, \quad (C-87)$$

where

$$I \equiv \frac{1}{\beta u_*} + \int_{z_0}^h \frac{\phi(z)}{k u_* z} dz.$$

Although the reaction order is most likely to be 1, closed-form solutions can be found for the cases of $a = 1, 2$, and 3 ,

$$F = \begin{cases} \frac{\bar{c}}{I + \frac{1}{\gamma}} & a = 1 \\ \frac{-\frac{1}{\sqrt{\gamma}} + \frac{1}{\gamma} + 4I\bar{c}^{1/2}}{2I} & a = 2 \\ A_+ + A_-^3 & a = 3 \end{cases}, \quad (C-88)$$

where

$$A_{\pm} = 3 \left[\frac{\bar{c}}{I} \pm \left(\frac{\bar{c}^2}{2I} + \frac{1}{27\gamma I^3} \right)^{1/2} \right]^{1/2}.$$

It is interesting to note that these formulas reduce to that of Chamberlain (1966) or Galbally (1974) for the special case of (1) a first-order surface reaction, and (2) a neutrally stratified atmosphere.

C.5 TECHNICAL DESCRIPTION OF EKMA

The Empirical Kinetic Modeling Approach (EKMA) has been developed as a procedure for relating photochemical oxidants (expressed as ozone) to organic compounds and oxides of nitrogen (EPA, 1977). The EKMA calculates maximum afternoon concentrations of ozone as a function of the following parameters:

- > Morning concentrations of nonmethane hydrocarbons (NMHC) and oxides of nitrogen (NO_x).
- > Emissions of NMHC and NO_x occurring during the day.
- > Meteorological conditions.
- > Reactivity of the NMHC mix.

Detailed documentation of the EKMA and its associated computer programs is given by EPA (1977); Whitten and Hogo (1978a, 1978b); and EPA (1981).

C.5.1 Kinetic Mechanism

The EKMA uses a two-hydrocarbon/ NO_x mechanism to describe the photochemical formation of ozone (Dodge, 1977). This mechanism contains two hydrocarbons (propylene and butane) to represent typical urban emissions. Studies by Whitten and Hogo (1981), Hogo, Whitten, and Reynolds (1981), and Whitten, Hogo, and Johnson (1981) have shown that different chemical mechanisms can behave differently with changing hydrocarbon reactivity. For this study the Carbon-Bond Mechanism is used instead of the propylene/butane mechanism for the following reasons:

- > The Carbon-Bond Mechanism is more responsive to a wider range of reactivity than is the propylene/butane mechanism.
- > It is harder to define reactivity as a function of propylene and butane.
- > The Carbon-Bond Mechanism is based on more recent measurements of rate constants.

Table C-4 shows the Carbon-Bond Mechanism used in this study. Further discussions of the Carbon-Bond Mechanism are reported by Whitten, Hogo, and Killus (1980) and Killus and Whitten (1981).

C.5.2 Concepts

The physical model underlying the EKMA is similar in concept to a trajectory-type photochemical model. A column of air consisting of initial concentrations of ozone and precursors is transported along an assumed trajectory. As the column moves, it can encounter fresh precursor emissions, which are assumed to be mixed uniformly within the column. The column is assumed to act like a large smog chamber in which the precursors react according to the kinetic mechanism in table C-4 to form ozone and other products. The column extends from the earth's surface to the base of an elevated inversion. Because the diameter of the column is such that concentrations inside and just outside the column are similar, the horizontal exchange of air in and out of the column can be ignored. The volume of the column increases only as the inversion rises. Thus, the pollutants within the column are diluted as they are mixed with the air aloft. If the air aloft is polluted, the inversion rise also introduces ozone and precursors. The EKMA mathematically simulates these physical and chemical processes.

The "trajectory" mode of the EKMA computer code can be used to consider impacts due to specific sources in rural areas of the horizontal area (or size) of the parcel is small in relation to the size of the source. In this situation the horizontal exchange of reactants is not important.

C.5.3 Summary of Input Data

Values of the parameters that can be input to EKMA include the following:

- > Latitude.
- > Longitude.
- > Time zone.
- > Date.
- > Morning and afternoon inversion heights (also called mixing depths) or hourly mixing depths.
- > Times at which the inversion starts and stops rising.

- > Concentrations of NMHC, NO_x , and ozone in the air above the inversion layer due to transport aloft.
- > Concentrations of NMHC, NO_x and ozone initially in the surface layer.
- > NMHC and NO_x emissions.
- > NMHC reactivity.
- > Initial ratio of aldehydes to NMHC.
- > NO_x reactivity (initial fraction of NO_x that is NO_2).

C.5.4 Output

As previously described, the major function of EKMA is to calculate ozone concentrations. The output includes a table summarizing the simulation conditions, a table summarizing the results of each simulation performed. The user also has the option to obtain detailed information for the simulation (e.g., concentrations of all species, rates of reactions, etc.).

C.5.5 Conceptual Basis for the EKMA Kinetics Model

As previously described, the physical model underlying the kinetics model in OZIPM is similar in concept to a trajectory-type photochemical model. In the kinetics model, a column of air transported along an assumed trajectory is modeled. The column is assumed to extend from the earth's surface to the base of a temperature inversion. The horizontal dimensions of this column are such that the concentration gradients are small. This makes it unnecessary to consider horizontal exchange of air between the column and its surroundings. The air within the column is assumed to be uniformly mixed at all times.

At the beginning of a simulation, the column is assumed to contain some specified initial concentrations of NMHC and NO_x . These pollutants, sometimes called background, are in this report termed pollutants "transported in the surface layer." As the column moves along the assumed trajectory, the height of the column can change because of temporal and spatial variations in mixing height. The height of the column is assumed to change with time during a user-selected period, and to be constant before and after that period. As the height of the column increases, its

volume increases, and air above the inversion layer is mixed in. Pollutants in the inversion layer are described as "transported above the surface layer" or "transported aloft" in this report. Any ozone or ozone precursors from the inversion layer that are mixed into the column as it expands are assumed to be immediately mixed uniformly throughout the column.

The kinetics model in EKMA can also consider emissions of NMHC and NO_x into the column as it moves along its trajectory. The concentrations of the species within the column are physically decreased by dilution due to the inversion rise, and physically increased by entrainment of pollutants transported aloft and by fresh emissions. All species react chemically according to the kinetic mechanism shown in table C-4. Certain photolysis rates within that mechanism are functions of the intensity and spectral distribution of sunlight, and they vary diurnally according to time of year and location.

The assumptions and specifications that describe the kinetics model are

- > The air mass of interest is an imaginary air parcel (column) of fixed horizontal area at a constant temperature, within which pollutants are well mixed.
- > There is sufficient homogeneity that horizontal diffusion does not affect pollutant concentrations within the column.
- > The height of the column varies with time during a specified period and is constant at other times.
- > The column contains specified initial concentrations of NMHC and NO_x prior to the simulation starting time.
- > Pollutants transported within the surface layer from outside the area of interest (sometimes called background) may be present in the column at the start of each simulation. The pollutant concentrations due to transport in the surface layer are normally assumed to be zero, but the user may specify other values for the NMHC, NO_x , and ozone concentrations transported within this layer.
- > The changes in pollutant concentrations within the column are calculated, by computer simulation, from a user-specified period. The chemical reactions involving these pollutants are listed in table C-4.

- > Entrainment of pollutants transported aloft is possible during the rise of the inversion layer. EKMA only permits entrainment of constant concentrations of NMHC, NO_x , and ozone.
- > Pollutants emitted into the column after the starting time can be represented by specifying additions of NMHC and NO_x each hour.
- > The rate constants of all chemical reactions in the kinetic mechanism are as shown in table C-4, except for the photolysis reactions. Photolytic rate constants vary according to the time of day, date, and location being simulated. (Default photolysis rate constants are intended to represent the period from 0800 to 1800 PDT on the summer solstice in Los Angeles.)
- > Zero cloud cover is assumed.

Other assumptions relating to the use of EKMA to predict control requirements or changes in urban ozone concentrations as a result of changes in precursor emissions are discussed by EPA (1981).

C.5.6 Mathematical Formulation of Kinetics Model

The kinetics model in EKMA mathematically simulates physical and chemical processes taking place in the atmosphere. This simulation is accomplished by numerically solving a system of ordinary, nonlinear differential equations that describe the effects of these processes on pollutant concentrations. The solution gives the concentration of pollutants as a function of time. The mathematical formulation of the system of differential equations is described in this section.

In EKMA, there are four processes that are assumed to affect pollutant concentrations:

- (1) Chemical reactions
- (2) Dilution
- (3) Entrainment of pollutants transported aloft
- (4) Emissions.

Differential equations have been formulated to describe the time rate of change of pollutant concentrations due to each process, and these are presented below. The total time rate of change of each pollutant's concentration is then simply equal to the sum of all these effects. Thus, the system of equations consists of one equation for each species in the kinetic mechanism shown in table C-4.

C.5.6.1 Chemical Reaction Effects

The change in pollutant concentration due to chemical reaction is a function of the rates of the chemical reactions in table C-4. The rate of each reaction is the product of a rate constant and a concentration term. The rate constants for the nonphotolytic reactions are shown in table C-4. The photolytic rate constants are calculated by the procedures described above. The concentration term for unimolecular or pseudo-first-order reactions (such as photolytic reactions) is simply the concentration of the reactant. Bimolecular reaction rates are calculated similarly, except that the concentration term is the product of the two reactant concentrations. For example, the reaction rate (RT) for the first reaction in table C-4 would be expressed as follows:

$$(RT)_1 = k_1 C_{NO_2} \quad , \quad (C-89)$$

where

$$(RT)_1 = \text{rate of reaction, ppm min}^{-1}$$

$$k_1 = \text{photolytic rate constant for reaction}$$

$$C_{NO_2} = \text{concentration of } NO_2, \text{ ppm}$$

The time rate of change of a species due to chemical reaction is simply equal to the sum of all rates for those reactions in which the species is a product minus the sum of the rates for those reactions in which the species is a reactant. Thus,

$$\frac{\Delta C_i}{\Delta t} R = \sum (RT)_{PROD} - \sum (RT)_{REAC} \quad (C-90)$$

where

$$\frac{\Delta C_i}{\Delta t} R = \text{reaction rate contribution to the time rate of change of species } i$$

$\Sigma (RT)_{\text{PROD}}$ = the sum of all reaction rates in which species i appears as a product

$\Sigma (RT)_{\text{REAC}}$ = the sum of all reaction rates in which species i appears as a reactant

C.5.6.2 Dilution Effects

The mathematical representation for simple dilution due to inversion rise is a first-order decay process. The rate of change due to this effect can be represented as follows:

$$\frac{\Delta C_i}{\Delta t} D = -DC_i \quad (C-91)$$

where

$$\frac{\Delta C_i}{\Delta t} D = \text{dilution effect contribution to the time rate of change of pollutant species i, ppm min}^{-1}$$

$$D = \text{dilution factor, min}^{-1}$$

$$C_i = \text{concentration of species i, ppm}$$

The dilution factor is calculated from the following equation:

$$D = \frac{\ln(Z_2/Z_1)}{\Delta t} \quad (C-92)$$

where

$$D = \text{dilution factor, min}^{-1}$$

$$Z_2 = \text{afternoon mixing height}$$

$$Z_1 = \text{morning mixing height}$$

$$\Delta t = \text{total time during which the inversion rise takes place, minutes}$$

Note that, before and after the inversion rise period, the dilution factor is zero since there are no dilution effects for those periods.

When hourly mixing depths are specified, the dilution factor is calculated as follows:

$$D_t = \dot{HT}/HT_t$$

where

D_t = dilution factor at time t , min^{-1}

\dot{HT} = the change in mixing depth from the previous time to the current time

HT_t = current mixing depth

The dilution factor is not constant when hourly mixing depths are specified.

C.5.6.3 Entrainment Effects

Only hydrocarbons, NO_x , and O_3 are subject to being entrained from pollutants transported aloft. The mathematical treatment of entrainment assumes that the concentrations aloft do not change with time and extend uniformly to at least the height of the afternoon mixed layer. The pollutants entrained are assumed to be instantaneously mixed within the enlarged surface layer. The mathematical expressions for the rates of change for the pollutants are shown below:

$$\frac{\Delta C_{\text{O}_3}}{\Delta t} \text{ AL} = D(C_{\text{O}_3})_{\text{AL}} \quad (\text{C-93})$$

$$\frac{\Delta C_{\text{NO}_2}}{\Delta t} \text{ AL} = D(C_{\text{NO}_2})_{\text{AL}} \quad (\text{C-94})$$

$$\frac{\Delta C_{\text{HC}_i}}{\Delta t} \text{ AL} = D(C_{\text{NMHC}})_{\text{AL}} R_{\text{HC}_i} C_{\text{HC}_i} \quad (\text{C-95})$$

where

$$\frac{\Delta C_{\text{O}_3}}{\Delta t} \text{ AL}, \frac{\Delta C_{\text{NO}_2}}{\Delta t} \text{ AL}, \frac{\Delta C_{\text{HC}_i}}{\Delta t} \text{ AL}, = \text{entrainment effect contribution to the time rates of change of ozone, nitrogen dioxide, and hydrocarbons, respectively, ppm min}^{-1}$$

D = dilution factor (i.e., the rate constant for the mixing height rise), min^{-1}

$C_{O_3 \text{ AL}}$ = concentration of ozone trapped aloft, ppm

$C_{NO_2 \text{ AL}}$ = concentration of NO_2 trapped aloft, ppm

$(C_{\text{NMHC}})_{\text{AL}}$ = concentration of total nonmethane hydrocarbon trapped aloft, ppmC

It should be noted that the effect of the change in mixing height is the sum of the dilution and the entrainment effects.

C.5.6.4 Emissions Effects

The fourth factor affecting the rate of change of pollutant concentration is emissions. The rates of change due to emissions are equal to the additional concentrations produced by the emissions.

Because equivalent emissions into different volumes will produce different concentrations, it is necessary to adjust the relative emissions to reflect the change in the column volumes due to the inversion rise. This is done internally by EKMA by first calculating the ratio of the starting inversion height to the current inversion height. (This is equivalent to the ratio of initial volume to the current volume.) Before the inversion rise begins, this ratio is simply one. After the inversion rise has ceased, the ratio is the starting mixing height divided by the final mixing height. For the period during which the inversion rises, the ratio (f_t) is calculated as follows:

$$f_t = \exp[-(D)(\Delta t)] \quad , \quad (\text{C-96})$$

where

f_t = ratio of the starting mixing height to the mixing height at time t

D = dilution factor (i.e., the rate constant for the mixing height rise, min^{-1})

Δt = elapsed time between the start of the mixing height rise and the current time, minutes.

The rates of change due to the emissions are calculated from the values of the emission rates (calculated using the polynomial spline functions described earlier), the f_t ratio described above, and the reactivity assumptions. The equations for the rates of change due to emissions for each of the affected species are shown below:

$$\frac{\Delta C_i}{\Delta t} E = f_t (E_i)_t [C_i] \quad . \quad (C-97)$$

$$\frac{\Delta C_i}{\Delta t} E = \text{emissions contribution to the rates of change of species } i, \text{ ppm min}^{-1}$$

f_t = defined above (Eq. C-97)

$(E_i)_t$ = value of emission rate, ppm per minute

Note that, in the above formulations, a conversion from ppmC to ppm is performed for hydrocarbon species, and the reactivity of the hydrocarbons is taken into account.

Under the EPA guidelines for the use of EKMA, trajectories are assumed to be straight-line to the maximum observed ozone. The column of air is assumed to be moving at uniform speed throughout the day. Thus, although it seems that the wind speed is an important factor in determining emission rates, a simple calculation shows otherwise. As an example, we define an air parcel moving through an area of length L meters as illustrated in figure C-13.

The fractional emissions contained in the air parcel after moving through the area of length L are:

$$\text{fractional emissions} = \frac{qs L}{\rho a HV}$$

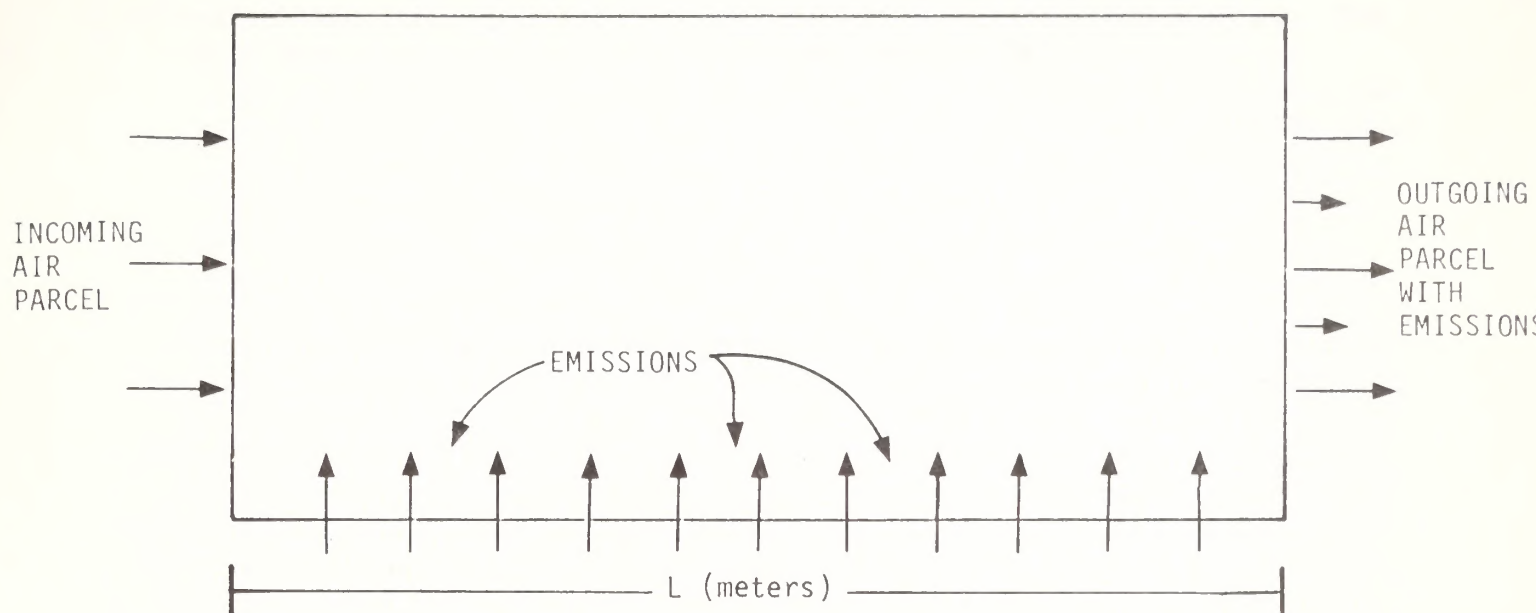


FIGURE C-13. SCHEMATIC OF AN AIR COLUMN MOVING THROUGH AN AREA CONTAINING EMISSIONS

where

q_s = the emission rate in $\text{mol/m}^2 \text{ sec}$

L = length of the area

ρ_a = density of air (mol/m^3)

H = the vertical height in meters

V = wind speed (m/sec)

The emissions in ppm would be

$$\begin{aligned} & (\text{fractional emissions}) \times 10^6 / L/V \\ & \text{or} \\ & [q_s / \rho_a H] \times 10^6, \end{aligned}$$

which is the emissions in units of ppm/sec. Thus, we see that the emission rate required for the OZIPM is independent of wind speed.

To determine an emission rate for EKMA in units of ppm/hr, the emissions in mols per unit time is assumed to be evenly distributed spatially within a certain area (usually the county area since emissions are most often reported as county totals). The emissions density is divided by the initial mixing height and multiplied by $24450 \text{ m}^3/\text{mol}$ to convert to ppm units. As described above, the factor f_t readjusts the emissions for the increase in mixing depth.

C.5.7 Description of Numerical Integration

The kinetics model in EKMA employs a Gear-type integration scheme to numerically solve the set of differential equations described in the previous section. A detailed description is not given here because the method is not unique to EKMA, and the procedure has been described elsewhere (Gear, 1971; Spellman and Hindmarsh, 1975; and Sherman, 1975). The integration scheme initially uses a time step of 1×10^{-10} minutes (i.e., pollutant concentrations are to be calculated 1×10^{-10} minutes after the start time). Subsequent time steps are computed by the Gear-type integration scheme according to the estimated error at each step. However, since the onset and cessation of dilution represent changing conditions, it is necessary for maximal numerical accuracy to begin or end a time step at precisely these points (i.e., the times at which onset and cessation of dilution take place). The pollutant concentrations are calculated at each time step throughout the simulation period. (Once the

time reaches the final hour, there is no restriction on precisely matching the final time step, since the concentrations can be interpolated back to exactly the last hour.) A typical simulation in EKMA takes from 150 to 200 times steps for a ten-hour simulation period; about one-half of these time steps are used in simulating the first minute.

The total rate of change of any species is the sum of the rates of change due to dilution, entrainment, emission, and chemical reaction described above. At each time step, the concentrations of all species are calculated along with the current rates of change for each species. The Gear method utilizes a Taylor series polynomial for each species to predict the species concentration at the end of the time step. The order of the polynomial is varied internally for optimum efficiency and is based on the values at the beginning of the time step. A corrective scheme then "corrects" the new concentration values, updates the Taylor polynomials, and estimates the average error. The corrector is a set of linear equations based on a matrix whose elements are the set of partial derivatives of the rate of change of concentrations of each species with respect to all other species. EKMA utilizes a linear system solving package for sparse matrices (i.e., those matrices in which most elements are equal to zero). The integration method used in EKMA has been modified somewhat from the version published by Spellman and Hindmarsh (1975). In particular, the error estimation is performed relative to the current concentration of a species rather than to its maximum concentration. The method utilizes the error estimate to determine the optimum step size and order, so that the allowable error specified by the user is met with the minimum number of integration steps.

The final task performed by the differential equations integrator is the calculation of the maximum one-hour average ozone concentration. Ozone concentrations are calculated for precisely every minute of the simulation. This calculation is performed by interpolation between the time step solutions to the differential equations. Running one-hour average concentrations are calculated using Simpson's rule. The largest one-hour average concentration is then selected as the maximum.

C.5.8 Description of a Sample Simulation

This section describes in considerable detail the mathematical procedures used in EKMA to calculate the maximum one-hour average ozone concentration that results from given initial concentrations of NMHC and NO_x . The procedures are based on the physical and chemical processes described in the last section. Before the beginning of a simulation, data-preparation steps are performed. A simulation is conducted by first determining concentrations at the starting time and then numerically

integrating the equations that form the basis of the model. The numerical solution yields species concentration as a function of time for each hour of the simulation period. The following discussion describes the data-preparation steps, the calculation of initial concentrations, model formulation, and the numerical integration technique.

C.5.8.1 Data-Preparation Steps

Because all simulations performed by EKMA in generating an ozone isopleth diagram have identical conditions except for the initial NMHC and NO_x concentrations, a data-preparation step is performed before any simulation is commenced. The purpose of this step is to eliminate abrupt changes in photolytic rate constants and emission rates. Elimination of these abrupt changes (i.e., discontinuities) is desirable for three reasons:

- > The integration scheme requires less computer time (discontinuities require the use of small time steps).
- > The results are more accurate numerically (stepping past discontinuities can lead to error).
- > The atmosphere does not normally have discontinuities. (The simulation of intermittent cloud cover or sudden changes in emissions is outside the scope of EKMA.)

The photolytic rate constants are evaluated every hour using an algorithm developed by Schere and Demerjian (1977). The algorithm uses input data of latitude, longitude, time zone, and date to calculate photolytic constants. A set of third-order polynomial spline functions is then generated so that photolytic constants can be easily calculated from a smooth curve for any time of the day. A set of four coefficients for each of the eight photolytic rate constants in the kinetic mechanism shown in table 3-7 is prepared for each hour of the ten-hour simulation period. Thus, at any time during the simulation period, the photolytic rate constants can be calculated from a simple third-order polynomial equation.

If emissions are to be considered, it is necessary to specify the emission rate(s) of NMHC and/or NO_x injected into the column each hour after the simulation start time. These emission rates are expressed as concentrations in ppm per hour. A set of cubic spline coefficients is determined each hour so that the instantaneous emission rate(s) can be evaluated for any time during the simulation period. For the first hour, a straight line is used, and for each subsequent hour a simple cubic (or lower order) polynomial is used subject to the following limitations:

- > The total, or integrated, emissions for each hour must equal the input value.
- > The spline functions at each hour must match in value, slope, and curvature unless lower-order functions are used.
- > At the end of the last hour of emissions, the emissions must be zero with zero curvature.
- > If cubic splines lead to any minima (points of zero slope) that are less than zero, then a lower-order spline function is used for that hour.

C.5.8.2 Determination of Initial Concentrations

Before a simulation can begin, the concentrations of all pollutant species at the starting time must be determined. These initial concentrations are based on assumed initial concentrations of NMHC and NO_x and on the concentrations of pollutants transported in the surface layer. The concentrations of transported pollutants are assumed to be zero unless otherwise specified.

The concentrations of the nonzero species are calculated as described below.

- (1) NO_2 is set to the initial NO_x concentration multiplied by the NO_2/NO_x fraction (default is 0.25).
- (2) NO is set to the initial NO_x concentration multiplied by the quantity one minus the NO_2/NO_x fraction.
- (3) O_3 is set to the concentration transported in the surface layer (default is zero).
- (4) The concentrations of the hydrocarbon species are determined from the assumed initial NMHC concentration and the assumed reactivity fraction. Mathematically,

$$[\text{HC}]_i = [\text{NMHC}] (R_i)/C_i \quad (\text{C-98})$$

where

$[HC]_i$ = i-th hydrocarbon species in ppm

$[NMHC]$ = initial NMHC concentration, ppmC

R_i = fraction of initial NMHC that is species i

C_i = number of carbon atoms in species i.

- (5) Species other than hydrocarbon, NO_x , and O_3 are specified explicitly in the inputs in units of ppm as described by Whitten and Hogo (1978b).

C.6 TECHNICAL DESCRIPTION OF COMPLEX-I

COMPLEX-I is a multiple point source model developed by the U.S. Environmental Protection Agency for application to situations in rural complex terrain settings. The model is based upon the EPA MPTEP model (Pierce and Turner, 1980) but has several optional treatments of plume-terrain interactions not included in MPTEP.

As applied in this study, COMPLEX-I was developed by EPA but is not an EPA approved model. This version used here has three plume-terrain interaction options. We have used option 3 because it has been shown to perform better than options 1 and 2 (New Mexico EID, 1981). The version of COMPLEX-I that is currently being evaluated by the EPA for approval uses a different treatment of the terrain effect (optional) than that used here. COMPLEX-I can estimate concentrations from sources for one simulated hour for one or more receptors, either at ground-level or varying heights above the ground, or it can simulate concentrations hour-by-hour for a year that result from up to 250 point sources at as many as 180 receptors.

COMPLEX-I is most applicable within 10 km of the source (EPA, 1980). Its use beyond this distance will be less accurate due to meso-scale influences, such as wind change with height, and to meteorological conditions that may vary during the time of transport. COMPLEX-I is suited to the same types of multiple-source applications for which MPTEP and CRSTER are.

C.6.1 Model Formulation

The following assumptions are made in COMPLEX-I's formulation: (1) continuous plumes are diluted upon release by the wind speed at stack top;

(2) dispersion from continuous plumes results in time averaged Gaussian distributions in both the horizontal and vertical directions through the dispersing plume; (3) concentration estimates may be made for each hourly period using the mean meteorological conditions appropriate for each hour; (4) the total concentration at a receptor is the sum of the concentrations estimated at the receptor from each source, i.e., concentrations are additive; and (5) concentrations at a receptor for periods longer than an hour can be determined by averaging the hourly concentrations over the period.

The downwind distance x and the crosswind distance y of the source from the receptor is determined as a function of the mean hourly wind direction. Dispersion parameter values are determined as functions of stability class and upwind distance. Equations to estimate concentrations are selected dependent upon stability class, and, for neutral or unstable conditions, upon the relation of dispersion parameter value to mixing height.

The contribution to the concentration, x_p , from a single point source to a receptor is given by one of the three following equations where the expressions g_2 and g_3 , are defined below

Component:

$$x_p = Q \cdot \frac{1}{u \sqrt{2\pi} w} \cdot \frac{g_2}{\sqrt{2\pi} \sigma_z} \quad (C-99)$$

$$x_p = Q \cdot \frac{1}{u \sqrt{2\pi} w} \cdot \frac{1}{L} \quad (C-100)$$

$$x_p = Q \cdot \frac{1}{u \sqrt{2\pi} w} \cdot \frac{g_3}{\sqrt{2\pi} \sigma_z} \quad (C-101)$$

where:

- x_p , concentration, $g \cdot m^{-3}$
- Q , emission rate, $g \cdot s^{-1}$
- u , wind speed, $m \cdot s^{-1}$
- w , horizontal plume distribution width = $392.7 \cdot x$ (evaluated at the distance x assuming 22.5° sector spread).
- σ_z , standard deviation of plume concentration vertical distribution (evaluated at the distance x and for appropriate stability), m
- L , mixing height, m
- H , effective height of emission, m
- z , receptor height above ground, m
- y , crosswind distance, m

For stable conditions or unlimited mixing equation (C-99) is used. For unstable or neutral conditions, where σ_z is equal to or greater than 1.6 L, equation (C-100) is used. For unstable or neutral conditions where σ_z is less than 1.6 L, equation (C-102) is selected, provided that both H and z are less than L.

Definitions for expressions g_2 and g_3 follow:

$$g_2 = \exp [-0.5(z-H)^2/\sigma_z^2] + \exp [-0.5(z+H)^2/\sigma_z^2] \quad (C-102)$$

$$g_3 = \sum_{N=-\infty}^{\infty} \{ \exp [-0.5(zH+2NL)^2/\sigma_z^2] + \exp [-0.5(z+H+2NL)^2/\sigma_z^2] \} \quad (C-103)$$

Sensitivity tests using equation (C-101) have indicated that for all H and all z between the ground and the mixing height, the vertical distribution of concentration with height is uniform when σ_z has increased to 1.6 L. Therefore, when σ_z is equal to or greater than 1.6 L for neutral or unstable conditions, use equation (C-100). For special cases such as $z = 0$, equation (C-100) may give appropriate concentrations for σ_z much less than 1.6 L. However, the above recommendation covers the more general case. (Note that this recommendation differs from that of Pasquill (1976) which indicates that σ_z should not be allowed to increase beyond 0.8 L.) For ground level receptors, $z = 0$, the use of $\sigma_z = 0.8L$ in equation (C-99) reduces to equation (C-101). However, the above recommendation allows σ_z to increase beyond the value of L, specifically as large as 1.6 L; it also allows for a smooth transition to a uniform vertical profile for receptors above the ground, $z \neq 0$, and for effective heights of emission approaching the mixing height.

C.6.1.1 Dispersion Parameter Values

The vertical dispersion parameter values used in COMPLEX-I are the Pasquill-Gifford (P-G) parameters (Pasquill, 1961; Gifford, 1960) representative for open country (a roughness of approximately 0.03 m). The subroutines used to determine the parameter values are the same as in the UNAMAP programs PTDIS, PTMTP, and RAMR. A 22.5° sector spread is assumed in the horizontal, as in VALLEY.

Except for stable layers aloft, which inhibit vertical dispersion, the atmosphere is treated as a single layer in the vertical that has the same rate of vertical dispersion throughout. Complete eddy reflection is assumed both from the ground and from the stable layer aloft (except in option 3 and some option 2 cases), given by the mixing height for neutral and unstable stabilities.

C.6.1.2 Plume Rise

Plume rise is calculated using the methods of Briggs (1969, 1971, 1972, and 1975). Although the plume rise from point sources is usually dominated by buoyancy, plume rise due to momentum is also considered. (merging of nearby buoyant plumes is not considered).

C.6.1.3 Input Data

All input data are assumed to be representative for the area being modeled. Since concentration estimates are proportional to emissions, consideration of variations may be necessary, such as diurnal or weekday vs. weekend. COMPLEX-I can utilize hourly emissions as an option. The meteorological data consisting of wind direction, wind speed, temperature, stability class, and mixing height for each hour should be representative of region being modeled. Wind speed is measured at the anemometer height and then extrapolated to the stack top, using power law wind speed profiles with the exponent dependent upon stability.

C.6.1.4 Mixing Height

Except in option 3 and option 2 cases, the entire plume is completely eddy-reflected if the effective plume height is below the mixing height. The entire plume is assumed to be within the stable layer aloft if the effective plume height is above the mixing height.

COMPLEX-I does not include calculations for the transitional phenomenon of fumigation, which is the elimination of an inversion layer containing a stable plume from below (which causes mixing of pollutants downward, resulting in uniform concentrations with height beneath the original plume centerline).

C.6.1.5 Removal or Depletion

Transformations of a pollutant resulting in loss of that pollutant throughout the entire depth of each plume can be approximated by COMPLEX-I. If the loss to be simulated is realistic and occurs through the whole plume without dependence upon concentration, then this exponential loss may provide a reasonable simulation. If, however, the loss mechanism is selective, the loss mechanism built into the model will not approximate

the atmospheric chemistry very well. Examples of selective loss mechanisms include impaction with features on the ground surface, reactions with materials on the ground, or dependence on a given small parcel of air for concentration (requiring consideration of contributions from all sources to this parcel).

C.6.2 Special Features

COMPLEX-I has the following special plume terrain interaction options. Option 1 entails the following adjustments:

- > In stable conditions, plume centerline height is set to 10 m whenever the effective stack height is less than or equal to 10 m above a ground-level receptor height.
- > In neutral or unstable conditions, the plume centerline is not allowed to approach the terrain closer than one-half the effective-stack height.

Option 2 includes all the provisions of option 1 but in addition:

- > Calculated ground-level concentrations are not allowed to exceed the corresponding centerline plume concentrations (without ground or inversion reflections). This ensures that the second law of thermodynamics is not violated.

Features associated with option 3 are:

- > Ground reflection is regarded to be an inappropriate assumption under stable impaction conditions (as is also the treatment in option 2 in some cases).
- > Final plume elevation is assumed to be unmodified by terrain.

Verification studies have shown that all three options yield conservative concentration estimates in complex terrain settings (New Mexico EID, 1981). However, option 1 and option 2 consistently over-predict concentrations by wider margins than option 3.

TABLE C-4. CARBON-BOND MECHANISM III USED IN THIS STUDY

	Reaction	Rate Constant at 298K (ppm ⁻¹ min ⁻¹)	Activation Energy (K)
1	$\text{NO}_2 \rightarrow \text{NO} + \text{O}$	*	0
2	$\text{O} + (\text{O}_2) + (\text{M}) \rightarrow \text{O}_3$	$4.40 \times 10^{6\dagger}$	0
3	$\text{NO} + \text{O}_3 \rightarrow \text{NO}_2 + \text{O}_2$	26.6	1450
4	$\text{NO}_2 + \text{O}_3 \rightarrow \text{NO}_3 + \text{O}_2$	0.048	2450
5	$\text{NO}_2 + \text{O} \rightarrow \text{NO} + \text{O}_2$	1.3×10^4	0
6	$\text{OH} + \text{O}_3 \rightarrow \text{HO}_2 + \text{O}_2$	100	1000
7	$\text{HO}_2 + \text{O}_3 \rightarrow \text{OH} + 2\text{O}_2$	2.40	1525
8	$\text{OH} + \text{NO}_2 \rightarrow \text{HNO}_3$	1.60×10^4	0
9	$\text{OH} + \text{CO} \xrightarrow{\text{O}_2} \text{HO}_2 + \text{CO}_2$	440	0
10	$\text{NO} + \text{NO} + (\text{O}_2) \rightarrow \text{NO}_2 + \text{NO}_2$	$1.50 \times 10^{-4\dagger}$	0
11	$\text{NO} + \text{NO}_3 \rightarrow \text{NO}_2 + \text{NO}_2$	2.80×10^4	0
12	$\text{NO}_2 + \text{NO}_3 + \text{H}_2\text{O} \rightarrow 2\text{HNO}_3$	§	-1.06×10^4
13	$\text{NO} + \text{HO}_2 \rightarrow \text{NO}_2 + \text{OH}$	1.20×10^4	0
14	$\text{HO}_2 + \text{HO}_2 \rightarrow \text{H}_2\text{O}_2 + \text{O}_2$	1.50×10^4	0
15	$\text{X} + \text{PAR} \rightarrow$	10^5	0
16	$\text{OH} + \text{PAR} \xrightarrow{\text{O}_2} \text{MEO}_2 + \text{H}_2\text{O}$	1300	0
17	$\text{O} + \text{OLE} \xrightarrow{\text{O}_2} \text{MEO}_2 + \text{ACO}_3 + \text{X}$	2700	0
18	$\text{O} + \text{OLE} \rightarrow \text{CARB} + \text{PAR}$	2700	0
19	$\text{OH} + \text{OLE} \xrightarrow{\text{O}_2} \text{RAO}_2$	3.70×10^4	0
20	$\text{O}_3 + \text{OLE} \rightarrow \text{CARB} + \text{CRIG}$	0.008	1900
21	$\text{O}_3 + \text{OLE} \rightarrow \text{CARB} + \text{MCRG} + \text{X}$	0.008	1900
22	$\text{O} + \text{ETH} \xrightarrow{\text{O}_2} \text{MEO}_2 + \text{HO}_2 + \text{CO}$	600	800
23	$\text{O} + \text{ETH} \rightarrow \text{CARB} + \text{PAR}$	600	800

TABLE C-4 (Continued)

Reaction		Rate Constant at 298K (ppm ⁻¹ min ⁻¹)	Activation Energy (K)
24	OH + ETH $\xrightarrow{O_2}$ RBO ₂	1.20 x 10 ⁴	0
25	O ₃ + ETH → CARB + CRIG	0.0024	0
26	NO + ACO ₃ $\xrightarrow{O_2}$ NO ₂ + MEO ₂	1.04 x 10 ⁴	0
27	NO + RBO ₂ $\xrightarrow{O_2}$ NO ₂ + CARB + HO ₂ + CARB	1.20 x 10 ⁴	0
28	NO + RAO ₂ $\xrightarrow{O_2}$ NO ₂ + CARB + HO ₂ + CARB	1.20 x 10 ⁴	0
29	NO + MEO ₂ $\xrightarrow{O_2}$ NO ₂ + CARB + MEO ₂ + X	3800	0
30	NO + MEO ₂ $\xrightarrow{O_2}$ NO ₂ + CARB + HO ₂	7700	0
31	NO + MEO ₂ → NRAT	500	0
32	O ₃ + RBO ₂ → CARB + CARB + HO ₂ + O ₂	500	0
33	O ₃ + RAO ₂ → CARB + CARB + HO ₂ + O ₂	200	0
34	OH + CARB → CRO ₂ + X	1000	0
35	OH + CARB $\xrightarrow{O_2}$ HO ₂ + CO	7000	0
36	OH + CARB $\xrightarrow{O_2}$ ACO ₃ + X	6000	0
37	CARB → CO + H ₂	(≈0.001 K ₁) [*]	0
38	CARB + (O ₂) $\xrightarrow{O_2}$ 2/3 (2HO ₂ + CO) 1/3 (2MEO ₂ + CO + 2X)	(≈0.002 K ₁) [*]	0
39	NO ₂ + ACO ₃ → PAN	7000	0
40	PAN → ACO ₃ + NO ₂	0.022	1.35 x 10 ⁴
41	HO ₂ + ACO ₃ → Stable products	1.50 x 10 ⁴	0
42	HO ₂ + MEO ₂ → Stable products	9000	0

TABLE C-4 (Continued)

	Reaction	Rate Constant at 298K (ppm ⁻¹ min ⁻¹)	Activation Energy (K)
43	NO + CRIG → NO ₂ + CARB	1.20 × 10 ⁴	0
44	NO ₂ + CRIG → NO ₃ + CARB	8000	0
45	CARB + CRIG → Ozonide	2000	0
46	NO + MCRG → NO ₂ + CARB + PAR	1.20 × 10 ⁴	0
47	NO ₂ + MCRG → NO ₃ + CARB + PAR	8000	0
48	CARB + MCRG → Ozonide	2000	0
49	CRIG → CO + H ₂ O	670 ^{**}	0
50	CRIG → Stable products	240 ^{**}	0
51	CRIG $\xrightarrow{O_2}$ HO ₂ + HO ₂ + CO	90 ^{**}	0
52	MCRG → Stable products	150 ^{**}	0
53	MCRG $\xrightarrow{O_2}$ MEO ₂ + OH + CO	340 ^{**}	0
54	MCRG $\xrightarrow{O_2}$ MEO ₂ + HO ₂	425 ^{**}	0
55	MCRG $\xrightarrow{O_2}$ CARB + HO ₂ + CO + HO ₂	85 ^{**}	0
56	OH + ARO $\xrightarrow{O_2}$ RARO + H ₂ O	8000	600
57	OH + ARO $\xrightarrow{O_2}$ HO ₂ + OPEN	1.45 × 10 ⁴	400
58	NO + RARO $\xrightarrow{O_2}$ NO ₂ + PHEN + HO ₂	4000	0
59	OPEN + NO $\xrightarrow{O_2}$ NO ₂ + DCRB + X + APRC	6000	0
60	APRC $\xrightarrow{O_2}$ DCRB + CARB + CO	10 ^{4**}	0
61	APRC $\xrightarrow{O_2}$ CARB + CARB + CO + CO	10 ^{4**}	0
62	PHEN + NO ₃ → PHO + HNO ₃	5000	0
63	PHO + NO ₂ → NPHN	4000	0

TABLE C-4 (Concluded)

	Reaction	Rate Constant at 298K (ppm ⁻¹ min ⁻¹)	Activation Energy (K)
64	PHO + HO ₂ → PHEN	5.00 × 10 ⁴	0
65	OPEN + O ₃ → DCRB + X + APRC	40	0
66	OH + PHEN $\xrightarrow{O_2}$ HO ₂ + APRC + PAR + CARB	3.00 × 10 ⁴	0
67	DCRB $\xrightarrow{O_2}$ 1/2 (HO ₂ + ACO ₃ + CO) 1/2 (MEO ₂ + HO ₂ + 2CO)	(≈0.04 K ₁) [*]	0
68	PHEN + OH → PHO	10 ⁴	0
69	CRO ₂ + NO $\xrightarrow{O_2}$ NO ₂ + HO ₂ + DCRB	1.20 × 10 ⁴	0
70	DCRB + OH → ACO ₃	7000	0
71	HONO → OH + NO	(≈0.06 K ₁) [*]	0
72	OH + NO → HONO	9770	0
73	O ₃ → O ¹ D	(≈10 ⁻³ K ₁) [*]	0
74	O ¹ D $\xrightarrow{+ (M)}$ O	4.44 × 10 ¹⁰	0
75	OH + SO ₂ → HSO ₅	2.00 × 10 ³	0
76	NO + HSO ₅ → NO ₂ + HSO ₄	8.00 × 10 ²	0
77	NO ₂ + HSO ₄ → SULF + HNO ₃	1.00 × 10 ⁴	0

* Sunlight-dependent; units of min⁻¹.

† Units of ppm⁻²min⁻¹.

§ Heterogeneous; pseudo third order. Equal to 591 × N₂O₅ + H₂O.

** Units of min⁻¹.

Appendix D

LEVEL-1 VISIBILITY SCREENING RESULTS FOR EMISSIONS FROM
ALL SYNTHETIC FUEL FACILITIES IN THE REGION
AT THE HIGH OIL PRODUCTION RATES

LEVEL I VISIBILITY SCREENING ANALYSIS

FOR FLAT TOPS WILDERNESS

UTAH SYNFOEL PROJECTS - HIGH LEVEL SCENARIO

<u>EMISSION SOURCE</u>	<u>SKY/PLUME</u>	<u>PLUME/TERRAIN</u>	<u>SKY/TERRAIN</u>
ENERCOR-MONO POWER	-0.004	0.024	0.001
GEOKINETICS	-0.019	0.016	0.038
MAGIC CIRCLE	-0.017	0.010	0.005
PARAHQ	-0.015	0.014	0.003
SDHIO	-0.006	0.035	0.010
SYNTANA-UTAH	-0.024	0.019	0.005
TOSCO	-0.017	0.012	0.004

LEVEL I VISIBILITY SCREENING ANALYSIS

FOR DINOSAUR NATIONAL MONUMENT

UTAH SYN FUEL PROJECTS - HIGH LEVEL SCENARIO

<u>EMISSION SOURCE</u>	<u>SKY/PLUME</u>	<u>PLUME/TERRAIN</u>	<u>SKY/TERRAIN</u>
ENERCOR-MONO POWER	-0.010	0.078	0.006
GEOKINETICS	-0.057	0.066	0.030
MAGIC CIRCLE	-0.066	0.052	0.005
PARAHO	-0.072	0.086	0.005
SOHIO	-0.039	0.381	0.018
SYNTANA-UTAH	-0.129	0.145	0.00
TOSCO	-0.075	0.072	0.00

LEVEL I VISIBILITY SCREENING ANALYSIS

FOR COLORADO NATIONAL MONUMENT

UTAH SYNFUEL PROJECTS - HIGH LEVEL SCENARIO

<u>EMISSION SOURCE</u>	<u>SKY/PLUME</u>	<u>PLUME/TERRAIN</u>	<u>SKY/TERRAIN</u>
ENERCOR-MONO POWER	-0.009	0.073	0.001
GEOKINETICS	-0.042	0.045	0.030
MAGIC CIRCLE	-0.031	0.022	0.005
PARAHO	-0.022	0.022	0.005
SOHIO	-0.008	0.048	0.010
SYNTANA-UTAH	-0.032	0.028	0.005
TOSCO	-0.029	0.023	0.004

LEVEL I VISIBILITY SCREENING ANALYSIS

FOR UINTAH & OURAY RES - NORTH

UTAH SYNFOEL PROJECTS - HIGH LEVEL SCENARIO

<u>EMISSION SOURCE</u>	<u>SKY/PLUME</u>	<u>PLUME/TERRAIN</u>	<u>SKY/TERRAIN</u>
ENERCOR-MONS POWER	-0 013	0 111	0 008
GEOKINETICS	-0 126	0 169	0 033
MAGIC CIRCLE	-0 323	0 371	0 005
PARAHO	-0 056	0 064	0 005
SOHIO	-0 034	0 325	0 012
SYNTANA-UTAH	-0 076	0 078	0 005
TOSCO	-0 226	0 274	0 005

LEVEL I VISIBILITY SCREENING ANALYSIS
FOR UINTAH & OURAY RES - SOUTH

UTAH SYNFOEL PROJECTS - HIGH LEVEL SCENARIO

<u>EMISSION SOURCE</u>	<u>SKY/PLUME</u>	<u>PLUME/TERRAIN</u>	<u>SKY/TERRAIN</u>
ENERCOR-MONO POWER	-0.013	0.112	0.004
GEOKINETICS	-0.111	0.146	0.038
MAGIC CIRCLE	-0.131	0.117	0.009
PARAHO	-0.040	0.043	0.005
SOHIO	-0.018	0.144	0.010
SYNTANA-UTAH	-0.053	0.051	0.005
TOSCO	-0.098	0.099	0.004

LEVEL I VISIBILITY SCREENING ANALYSIS
FOR UINTA PRIMITIVE AREA

UTAH SYNFUEL PROJECTS - HIGH LEVEL SCENARIO

<u>EMISSION SOURCE</u>	<u>SKY/PLUME</u>	<u>PLUME/TERRAIN</u>	<u>SKY/TERRAIN</u>
ENERCOR--MOND POWER	-0.003	0.021	0.006
GEOKINETICS	-0.024	0.024	0.038
MAGIC CIRCLE	-0.036	0.027	0.005
PARAHIO	-0.018	0.017	0.005
SOHIO	-0.023	0.203	0.010
SYNTANA-UTAH	-0.028	0.021	0.005
TOSCO	-0.037	0.031	0.004

LEVEL I VISIBILITY SCREENING ANALYSIS
FOR FLAT TOPS WILDERNESS

UTAH OTHER PLANNED PROJECTS

<u>EMISSION SOURCE</u>	<u>SKY/PLUME</u>	<u>PLUME/TERRAIN</u>	<u>SKY/TERRAIN</u>
MOON LAKE	-0.052	0.022	0.006
WHITE RIVER	-0.025	0.024	0.006

LEVEL I VISIBILITY SCREENING ANALYSIS
FOR DINOSAUR NATIONAL MONUMENT

UTAH OTHER PLANNED PROJECTS

<u>EMISSION SOURCE</u>	<u>SKY/PLUME</u>	<u>PLUME/TERRAIN</u>	<u>SKY/TERRAIN</u>
MOON LAKE	-0.284	0.163	0.006
WHITE RIVER	-0.097	0.130	0.006

LEVEL I VISIBILITY SCREENING ANALYSIS
FOR COLORADO NATIONAL MONUMENT

UTAH OTHER PLANNED PROJECTS

<u>EMISSION SOURCE</u>	<u>SKY/PLUME</u>	<u>PLUME/TERRAIN</u>	<u>SKY/TERRAIN</u>
MOON LAKE	-0.073	0.034	0.006
WHITE RIVER	-0.040	0.045	0.006

LEVEL I VISIBILITY SCREENING ANALYSIS
FOR UINTAH & DURAY RES - NORTH

UTAH OTHER PLANNED PROJECTS

<u>EMISSION SOURCE</u>	<u>SKY/PLUME</u>	<u>PLUME/TERRAIN</u>	<u>SKY/TERRAIN</u>
MOON LAKE	-0.259	0.145	0.006
WHITE RIVER	-0.103	0.140	0.006

LEVEL I VISIBILITY SCREENING ANALYSIS
FOR UINTAH & DURAY RES - SOUTH

UTAH OTHER PLANNED PROJECTS

<u>EMISSION SOURCE</u>	<u>SKY/PLUME</u>	<u>PLUME/TERRAIN</u>	<u>SKY/TERRAIN</u>
MOON LAKE	-0.155	0.079	0.006
WHITE RIVER	-0.076	0.097	0.006

LEVEL I VISIBILITY SCREENING ANALYSIS
FOR UINTA PRIMITIVE AREA

UTAH OTHER PLANNED PROJECTS

<u>EMISSION SOURCE</u>	<u>SKY/PLUME</u>	<u>PLUME/TERRAIN</u>	<u>SKY/TERRAIN</u>
MOON LAKE	-0.087	0.042	0.006
WHITE RIVER	-0.030	0.031	0.006

LEVEL I VISIBILITY SCREENING ANALYSIS
FOR FLAT TOPS WILDERNESS

COLORADO OIL SHALE PROJECTS - 2000 SCENARIO

<u>EMISSION SOURCE</u>	<u>SKY/PLUME</u>	<u>PLUME/TERRAIN</u>	<u>SKY/TERRAIN</u>
COLONY	-0.105	0.169	0.006
UNION/LONG RIDGE	-0.017	0.023	0.002
CATHEDRAL BLUFFS	-0.313	0.296	0.022
CHEVRON	-0.018	0.023	0.004
RIO BLANCO	-0.051	0.085	0.005
MOBIL	-0.016	0.021	0.002
EXXON	-0.085	0.129	0.006
SUPERIOR	-0.009	0.021	0.004
GETTY	-0.011	0.014	0.002
MULTIMINERAL	-0.011	0.014	0.002
NAVAL OIL SHALE	-0.076	0.172	0.004

LEVEL I VISIBILITY SCREENING ANALYSIS
FOR DINOSAUR NATIONAL MONUMENT

COLORADO OIL SHALE PROJECTS - 2000 SCENARIO

<u>EMISSION SOURCE</u>	<u>SKY/PLUME</u>	<u>PLUME/TERRAIN</u>	<u>SKY/TERRAIN</u>
COLONY	-0.035	0.043	0.006
UNION/LONG RIDGE	-0.004	0.005	0.002
CATHEDRAL BLUFFS	-0.165	0.124	0.022
CHEVRON	-0.013	0.015	0.004
RIO BLANCO	-0.066	0.117	0.005
MOBIL	-0.004	0.004	0.002
EXXON	-0.043	0.056	0.006
SUPERIOR	-0.007	0.014	0.004
GETTY	-0.005	0.006	0.002
MULTIMINERAL	-0.010	0.013	0.002
NAVAL OIL SHALE	-0.017	0.028	0.004

LEVEL I VISIBILITY SCREENING ANALYSIS
FOR COLORADO NATIONAL MONUMENT

COLORADO OIL SHALE PROJECTS - 2000 SCENARIO

<u>EMISSION SOURCE</u>	<u>SKY/PLUME</u>	<u>PLUME/TERRAIN</u>	<u>SKY/TERRAIN</u>
COLONY	-0.062	0.087	0.006
UNION/LONG RIDGE	-0.009	0.012	0.002
CATHEDRAL BLUFFS	-0.170	0.128	0.022
CHEVRON	-0.023	0.030	0.004
RIO BLANCO	-0.038	0.059	0.005
MOBIL	-0.010	0.012	0.002
EXXON	-0.066	0.095	0.006
SUPERIOR	-0.003	0.005	0.004
GETTY	-0.012	0.016	0.002
MULTIMINERAL	-0.006	0.006	0.002
NAVAL OIL SHALE	-0.035	0.067	0.004

LEVEL I VISIBILITY SCREENING ANALYSIS
FOR UINTAH & DURAY RES - NORTH

COLORADO OIL SHALE PROJECTS - 2000 SCENARIO

<u>EMISSION SOURCE</u>	<u>SKY/PLUME</u>	<u>PLUME/TERRAIN</u>	<u>SKY/TERRAIN</u>
COLONY	-0.022	0.024	0.006
UNION/LONG RIDGE	-0.003	0.003	0.002
CATHEDRAL BLUFFS	-0.087	0.054	0.022
CHEVRON	-0.008	0.009	0.004
RIO BLANCO	-0.027	0.039	0.005
MOBIL	-0.003	0.003	0.002
EXXON	-0.025	0.028	0.006
SUPERIOR	-0.002	0.004	0.004
GETTY	-0.003	0.004	0.002
MULTIMINERAL	-0.004	0.004	0.002
NAVAL OIL SHALE	-0.011	0.015	0.004

LEVEL I VISIBILITY SCREENING ANALYSIS
FOR UINTAH & DURAY RES - SOUTH

COLORADO OIL SHALE PROJECTS - 2000 SCENARIO

<u>EMISSION SOURCE</u>	<u>SKY/PLUME</u>	<u>PLUME/TERRAIN</u>	<u>SKY/TERRAIN</u>
COLONY	-0.022	0.024	0.006
UNION/LONG RIDGE	-0.003	0.003	0.002
CATHEDRAL BLUFFS	-0.085	0.052	0.022
CHEVRON	-0.008	0.009	0.004
RIO BLANCO	-0.024	0.034	0.005
MOBIL	-0.003	0.003	0.002
EXXON	-0.026	0.029	0.006
SUPERIOR	-0.002	0.003	0.004
GETTY	-0.004	0.004	0.002
MULTIMINERAL	-0.004	0.004	0.002
NAVAL OIL SHALE	-0.012	0.016	0.004

LEVEL I VISIBILITY SCREENING ANALYSIS

FOR UINTA PRIMITIVE AREA

COLORADO OIL SHALE PROJECTS - 2000 SCENARIO

<u>EMISSION SOURCE</u>	<u>SKY/PLUME</u>	<u>PLUME/TERRAIN</u>	<u>SKY/TERRAIN</u>
COLONY	-0.012	0.010	0.006
UNION/LONG RIDGE	-0.001	0.001	0.002
CATHEDRAL BLUFFS	-0.052	0.027	0.023
CHEVRON	-0.004	0.003	0.004
RIO BLANCO	-0.015	0.018	0.005
MOBIL	-0.001	0.001	0.002
EXXON	-0.013	0.012	0.006
SUPERIOR	-0.001	0.002	0.004
GETTY	-0.002	0.001	0.002
MULTIMINERAL	-0.002	0.002	0.002
NAVAL OIL SHALE	-0.006	0.007	0.004

REFERENCES

- Altshuller, A. P. (1979), "Model Predictions of the Rates of Homogeneous Oxidation of Sulfur Dioxide to Sulfate in the Troposphere," Atmos. Environ., Vol. 13, pp. 1653-1661.
- Anderson, G. E., et al. (1981), "Air Quality Impacts of Anticipated Development in Oil Shale Operations in Western Colorado and Eastern Utah," Systems Applications, Inc., San Rafael, California.
- Anderson, G. E., et al. (1980), "Air Quality Interrelationships in the Piceance Basin with Massive Oil Shale Development," SAI No. ES80-152, Systems Applications, Inc., San Rafael, California.
- Aris, R. (1962), Vectors, Tensors, and the Basic Equations of Fluid Mechanics (Prentice-Hall, Incorporated, Englewood Cliffs, New Jersey).
- Baur, E. (1973), "Dispersion of Tracers in the Atmosphere: Survey of Meteorological Data," Institute of Defense Analysis, Paper P-925, Arlington, Virginia.
- Bergstrom, R. W., et al. (1981), "Comparison of the Observed and Predicted Visual Effects Caused by Power Plant Plumes," Atmos. Environ., Vol. 15, pp. 2135-2150.
- Blasius, H. (1908), Z. Angew. Math. Phys., Vol. 56, pp. 1-37 (English translation, NACA Tech. Mem., 1256).
- Bolin, B., G. Aspling, and C. Persson (1974), "Residence Time of Atmospheric Pollutants as Dependent on Source Characteristics, Atmospheric Diffusion Processes, and Sink Mechanisms," Tellus, Vol. 26, pp. 185-194.
- Bolin, B., and L. Granat (1973), "Local Fallout and Long Distance Transport of Sulfur," Ambio, Vol. 2, pp. 87-90.

- Boris, J. P., and D. L. Book (1973), "Flux Corrected Transport--I. SHASTA, A Fluid Transport Algorithm That Works," J. Comput. Phys., Vol. 11, pp. 38-69.
- Briggs, G. A. (1975), "Plume Rise Predictions," in Lectures on Air Pollution and Environmental Impact Analysis, Duane A. Haugen, ed., pp. 59-111 (American Meteorological Society, Boston, Massachusetts).
- Briggs, G. A. (1973), "Diffusion Estimation for Small Emissions," Atmospheric Turbulence and Diffusion Laboratory, Contribution File No. (Draft) 79. Oak Ridge, Tennessee, p. 59.
- Briggs, G. A. (1972), "Discussion on Chimney Plumes in Neutral and Stable Surroundings," Atmos. Environ., Vol. 6, pp. 507-510.
- Briggs, G. A. (1971), "Some Recent Analyses of Plume Rise Observation," Proc. Second International Clean Air Congress, H. H. Englund and W. T. Beery, eds., pp. 1029-1032 (Academic Press, New York, New York).
- Briggs, G. A. (1969), "Plume Rise," USAEC Critical Review Series, TID-25075, National Technical Information Service, Springfield, Virginia.
- Burns & McDonnell (1980), "Assessment of Visibility Impairment for the Deseret Generation and Transmission Cooperative, Inc. Moon Lake Power Plant Units 1 and 2," Burns & McDonnell Engineers, Kansas City, Missouri.
- Chamberlain, A. C. (1966), "Transport of Gases to and from Grass and Grass-Like Surfaces," Proc. Roy. Soc., Vol. 3, pp. 63-88.
- Dahlquist, G., and A. Björck (1974), Numerical Methods (Prentice-Hall, Englewood Cliffs, New Jersey).
- Defant, A. (1951), "Local Winds," in Compendium of Meteorology, pp. 655-672 (American Meteorological Society, Boston, Massachusetts).
- Defant, A. (1933), "Der Abfluss Schwerer Luftmassen auf geneigtem Boden, nebst einigen Bemerkungen zu der Theorie stationärer Luftströme," Sitzungsberichte der Preuss. Akad. Wiss. Phys.-Math. Klasse, Vol. 18, No. 3, pp. 624-635.
- DOC (1981), "1978 Census of Agriculture, Volume 1, State and County Data," U.S. Department of Commerce, Washington, D.C.

DOC (1980), "County Business Patterns--1979," U.S. Department of Commerce, Washington, D.C.

Dodge, M. C. (1977), "Effect of Selected Parameters on Predictions of a Photochemical Model," EPA-600/3-77-048, U.S. Environmental Protection Agency, Research Triangle Park, North Carolina.

DOE (1981), "Energy Data Reports--1979," U.S. Department of Energy, Washington, D.C.

Egan, B. A., and J. R. Mahoney (1972), "Numerical Modeling of Advection and Diffusion of Urban Area Source Pollutants," J. Appl. Meteorol., Vol. 11, pp. 312-322.

EPA (1981a), "Guideline for Use of City-Specific EKMA in Preparing Ozone SIPs," EPA-450/4-80-027, U.S. Environmental Protection Agency, Research Triangle Park, North Carolina.

EPA (1981b), "Compilation of Air Pollution Emission Factors (Including Supplements 1-12)," AP-42, U.S. Environmental Protection Agency, Research Triangle Park, North Carolina.

EPA (1981c), "Control Strategy Demonstration: New Mexico Air Quality Control Regulation 602, Coal Burning Equipment--Sulfur Dioxide," Air Quality Bureau, Health and Environment Department, New Mexico Environmental Improvement Division, Santa Fe, New Mexico.

EPA (1980), "Procedures for the Preparation of Emission Inventories for Volatile Organic Compounds," Volume I, EPA-450/2-77-028, U.S. Environmental Protection Agency, Research Triangle Park, North Carolina.

EPA (1977), "Uses, Limitations and Technical Basis of Procedures for Quantifying Relationships between Photochemical Oxidants and Precursors," EPA-450/2-77-021a, U.S. Environmental Protection Agency, Research Triangle Park, North Carolina.

Forsythe, G. E., and W. R. Wasow (1960), Finite-Difference Methods for Partial Differential Equations (John Wiley & Sons, New York, New York).

Galbally, I. E. (1974), "Gas Transfer near the Earth's Surface," Adv. in Geophysics, Vol. 18B, pp. 329-340.

Garratt, J. R. (1977), "Review of Dry Coefficients over Oceans and Continents," Monthly Weather Review, Vol. 105, pp. 915-929.

- Gear, C. W. (1971), "The Automatic Integration of Ordinary Differential Equations," in Communication of the Association for Computing Machinery, Vol. 14, No. 3, pp. 176-179.
- Geiger, R. (1971), The Climate near the Ground, Third Printing (Harvard University Press, Cambridge, Massachusetts).
- Georgii, H. W. (1970), "Contributions to the Atmospheric Sulfur Budget," J. Geophys. Res., Vol. 75, pp. 2365-2371.
- Gifford, F. A., Jr. (1960), "Atmospheric Dispersion Calculations Using the Generalized Gaussian Plume Model," Nucl. Saf., Vol. 2, No. 2, pp. 56-59.
- Heffter, J. (1965), "The Variations of Horizontal Diffusion Parameters with Time for Travel Periods of One Hour or Longer," J. Appl. Meteorol., Vol. 4.
- Hill, A. C. (1971), "A Sink for Atmospheric Pollutants," J. Air Pollut. Control Assoc., Vol. 21, pp. 946-947.
- Hogo, H., G. Z. Whitten, and S. D. Reynolds (1981), "Application of the Empirical Kinetic Modeling Approach to Urban Areas, Volume II: Tulsa," EPA-450/4-81-005b, Systems Applications, Inc., San Rafael, California.
- Höglström, U. (1975), "Further Comments on the Long Range Transport of Airborne Material and Its Removal by Deposition and Washout," Atmos. Environ., Vol. 9, pp. 946-947.
- Holzworth, G. C. (1972), "Mixing Heights, Wind Speeds, and Potential for Urban Air Pollution throughout the Contiguous United States," AP-101, Office of Air Programs, Environmental Protection Agency, Research Triangle Park, North Carolina.
- Johnson, C. D., et al. (1980), "User's Manual for the Plume Visibility Model (PLUVUE)," EPA-450/4-80-032, Systems Applications, Inc., San Rafael, California.
- Killus, J. P., and G. Z. Whitten (1981), "User's Guide to the Carbon-Bond Mechanism," SAI No. 75-81-EF81-90, Systems Applications, Inc., San Rafael, California.

- Latimer, D. A., and J. R. Doyle (1981), "Prevention of Significant Deterioration Policy Implications for Projected Oil Shale Development," report for U.S. Environmental Protection Agency, Systems Applications, Inc., San Rafael, California.
- Latimer, D. A., and R. G. Ireson (1980), "Workbook for Estimating Visibility Impairment," EPA-450/4-80-031, Systems Applications, Inc., San Rafael, California.
- Latimer, D. A., et al. (1980), "An Assessment of Visibility Impairment in Capitol Reef National Park Caused by Emissions from the Hunter Power Plant," EF80-43, Systems Applications, Inc., San Rafael, California.
- Latimer, D. A., et al. (1978), "The Development of Mathematical Models for the Prediction of Anthropogenic Visibility Impairment," EPA-450/3-78-110 a, b, c, Systems Applications, Inc., San Rafael, California.
- Lilly, D. K. (1973), "Calculation of Stably Stratified Flow around Complex Terrain," Research Note No. 40, Flow Research, Incorporated, Kent, Washington.
- Liu, M. K., and D. R. Durran (1977), "The Development of a Regional Air Pollution Model and Its Application to the Northern Great Plains," EPA-908/1-77-001, Systems Applications, Inc., San Rafael, California.
- McMahon, T. A., and P. J. Denison (1979), "Empirical Atmospheric Deposition Parameters--A Survey," Atmos. Environ., Vol. 13, pp. 571-585.
- Monin, A. S., and A. M. Yaglom (1971), Statistical Fluid Mechanics: Mechanics of Turbulence, Vol. 1 (MIT Press, Cambridge, Massachusetts).
- Munn, R. E. (1966), Descriptive Micrometeorology (Academic Press, New York, New York).
- NPS (1982), Socioeconomic data for Uintah and Grand counties, private communication, National Park Service, Denver, Colorado.
- ORNL (1982), "Agricultural Production in the United States by County," Oak Ridge National Laboratory, Oak Ridge, Tennessee.
- Owen, P. R., and W. R. Thompson (1963), "Heat Transfer across Rough Surfaces," J. Fluid Mech., Vol. 15, pp. 321-324.

- Pasquill, F. (1976), "Atmospheric Dispersion Parameters in Gaussian Plume Modeling. Part II. Possible Requirements for Change in the Turner Workbook Values," EPA-600/4-76-030b, U.S. Environmental Protection Agency, Research Triangle Park, North Carolina.
- Pasquill, F. (1961), "The Estimation of the Dispersion of Windborne Material," Meteorol. Mag., Vol. 90, No. 1063, pp. 33-49.
- PEDCo (1981), "Emission Inventory: Secondary Impacts (Draft)," PEDCo Environmental, Inc., Kansas City, Missouri.
- Pierce, T. E., and D. B. Turner (1980), "User's Guide for MPTEP, A Multiple Point Gaussian Dispersion Algorithm with Optional Terrain Adjustment," EPA-600/8-80-016, Environmental Sciences Research Laboratory, Office of Research and Development, U.S. Environmental Protection Agency, Research Triangle Park, North Carolina.
- Queney, P. (1947), "The Problem of Air Flow over Mountains: A Summary of Theoretical Studies," Bull. Am. Meteorol. Soc., Vol. 29, pp. 16-27.
- Randerson, D. (1972), "Temporal Changes in Horizontal Diffusion Parameters of a Single Nuclear Debris Cloud," J. Appl. Meteorol., Vol. 11, pp. 670-673.
- Rao, K. S., and H. F. Snodgrass (1981), "A Nonstationary Nocturnal Drainage Flow Model," Boundary-Layer Meteorol., Vol. 20, pp. 309-320.
- Schere, K. L., and K. L. Demerjian (1977), "Calculation of Selected Photolytic Rate Constants over a Diurnal Range," EPA-600/4-77-015, U.S. Environmental Protection Agency, Research Triangle Park, North Carolina.
- Schock, M. R. (1981), "The Selection of a Computer Modeling Procedure for the Simulation of Mesoscale Ground Level Air Quality Concentrations," Division of Environmental Waste Management and Research, North Dakota State Department of Health, Bismarck, North Dakota.
- Scriven, R. A., and B.E.A. Fisher (1975), "The Long Range Transport of Airborne Material and Its Removal by Deposition and Washout--I. General Considerations," Atmos. Environ., Vol. 9, pp. 49-58.
- Sehmel, G. A., S. L. Sutter, and M. T. Dana (1973), "Dry Deposition Processes," in Pacific Northwest Laboratory Annual Report for 1971, to the USAEC, Division of Biomedical and Environmental Research, Vol. II: Physical Sciences, Part 1, Atmospheric Science, BNWL-1751, pp. 150-153 (Battelle Northwest Laboratories, Richland, Washington).

- Sherman, A. H. (1975), "Yale Sparse Matrix Package User's Guide," UCID-30114, University of California, Livermore, California.
- Smagorinsky, J. (1963), "General Circulation Experiments with the Primitive Equations. I. The Basic Experiments," Monthly Weather Review, Vol. 91, pp. 99-164.
- Spellman, J. W., and A. C. Hindmarsh (1975), "GEARS: Solution of Ordinary Differential Equations Having a Sparse Jacobian Matrix," UCID-30116, University of California, Livermore, California.
- Stern, M. E., and J. S. Malkus (1953), "The Flow of a Stable Atmosphere over a Heated Island, Part II," J. Meteorol., Vol. 10, pp. 105-120.
- Taylor, G. I. (1921), "Diffusion by Continuous Movements," Proc. London Math. Soc., Vol. 2, No. 20, pp. 196-202.
- Tennekes, H. (1973), "A Model for the Dynamics of the Inversion above a Convective Layer," J. Atmos. Sci., Vol. 30, p. 558.
- Thom, A. S. (1972), "Momentum, Mass and Heat Exchange of Vegetation," Q. J. Roy. Meteorol. Soc., Vol. 98, pp. 124-134.
- Turk, J. T., and D. B. Adams (1982), "Sensitivity to Acidification of Lakes in the Flat Tops Wilderness Area, Colorado," unpublished manuscript prepared for submission to Water Resources Research.
- Turner, D. B. (1969), "Workbook of Atmospheric Dispersion Estimates," 999-AP-26, U.S. Public Health Service, Cincinnati, Ohio.
- UDOT (1982), Estimates of traffic counts on county and class "D" roads, private communication, Utah Department of Transportation, Salt Lake City, Utah.
- UDOT (1979), "Traffic on Utah Highways--1979," Utah Department of Transportation, Salt Lake City, Utah.
- Utah State Planning Coordinator's Office (1982), "Economic and Demographic Projections," State Planning Coordinator's Office, Salt Lake City, Utah.
- VanWagoner (1980), "Uinta Basin Transportation Study," Wayne T. VanWagoner and Associates, Inc., Salt Lake City, Utah.

- Walther, E. G., and R. M. Newburn (1980), "Standard Visual Range Measured in the NPS/EPA Regional Visibility Network from December 1978 through August 1979," Visibility Research Center, Las Vegas, Nevada.
- Whitten, G. Z., and H. Hogo (1981), "Comparative Applications of the EKMA in the Los Angeles Area," SAI No. 10R2-EF80-73, Systems Applications, Inc., San Rafael, California.
- Whitten, G. Z., and H. Hogo, (1978a), "User's Manual for Kinetics Model and Ozone Isopleth Plotting Package," EPA-600/8-78-014a, Systems Applications, Inc., San Rafael, California.
- Whitten, G. Z., and H. Hogo (1978b), "User's Manual for Ozone Isopleth Plotting with Optional Mechanism (OZIPM)," SAI No. EF78-30, Systems Applications, Inc., San Rafael, California.
- Whitten, G. Z., H. Hogo, and R. G. Johnson (1981), "Application of the Empirical Kinetic Modeling Approach (EKMA) to Urban Areas, Volume 1: San Francisco/Sacramento," EPA-450/4-81-005a, Systems Applications, Inc., San Rafael, California.
- Whitten, G. Z., H. Hogo, and J. P. Killus (1980), "The Carbon-Bond Mechanism: A Condensed Kinetic Mechanism for Photochemical Smog," Environ. Sci. Technol., Vol. 14, pp. 690-700.
- Williams, M. D., et al. (1981), "NCAQ Report 2, Air Quality in the Four Corners Region, Vol. I: Local Analysis," Report No. LA-UR-81-1145 to National Commission on Air Quality, Los Alamos National Laboratory, Los Alamos, New Mexico.

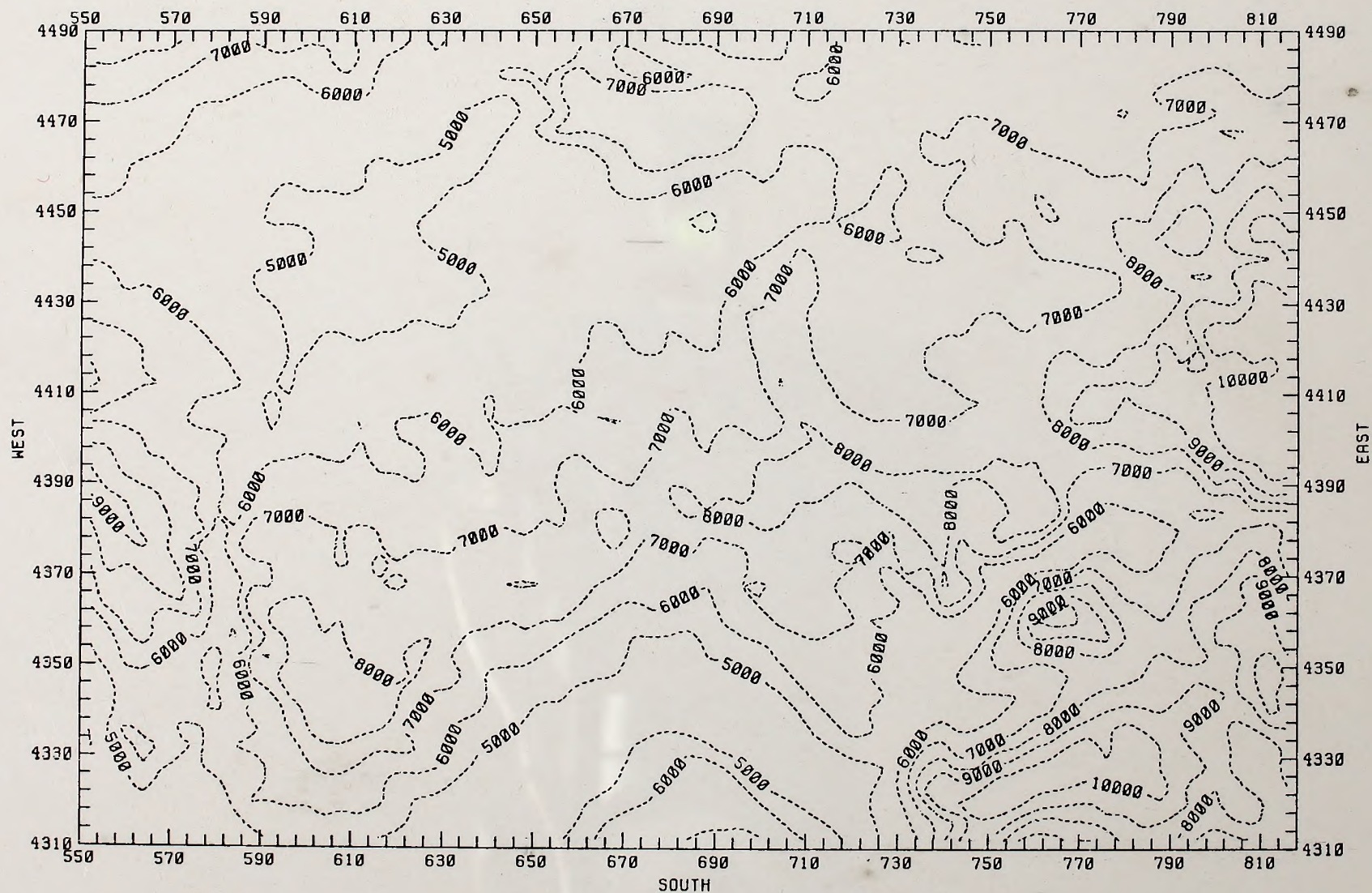
Form 1279-3
(June 1984)

BORROWER'S

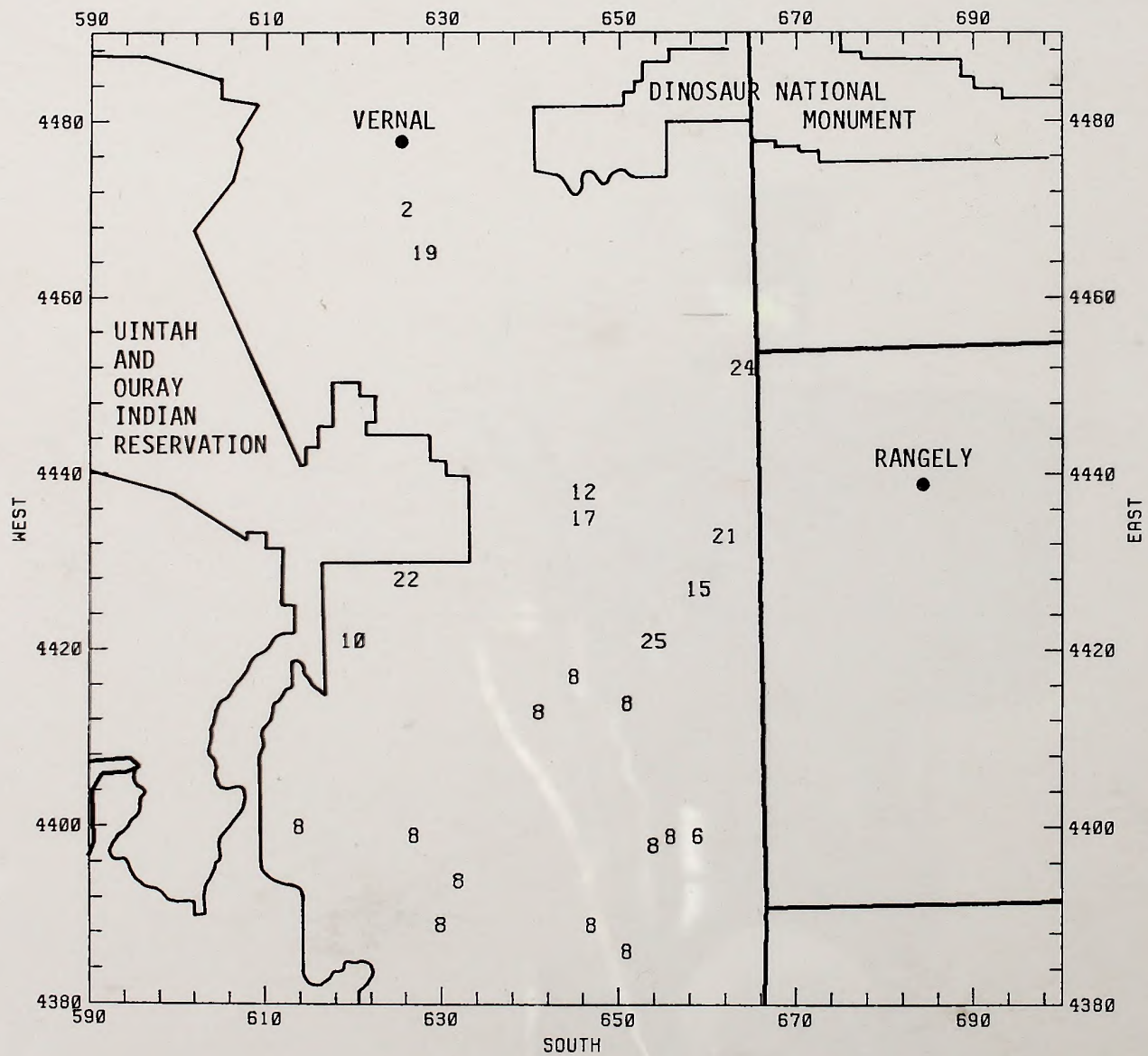
TD 195 .595 U35
Draft air qual
report for he

DATE LOANED	BORROWER

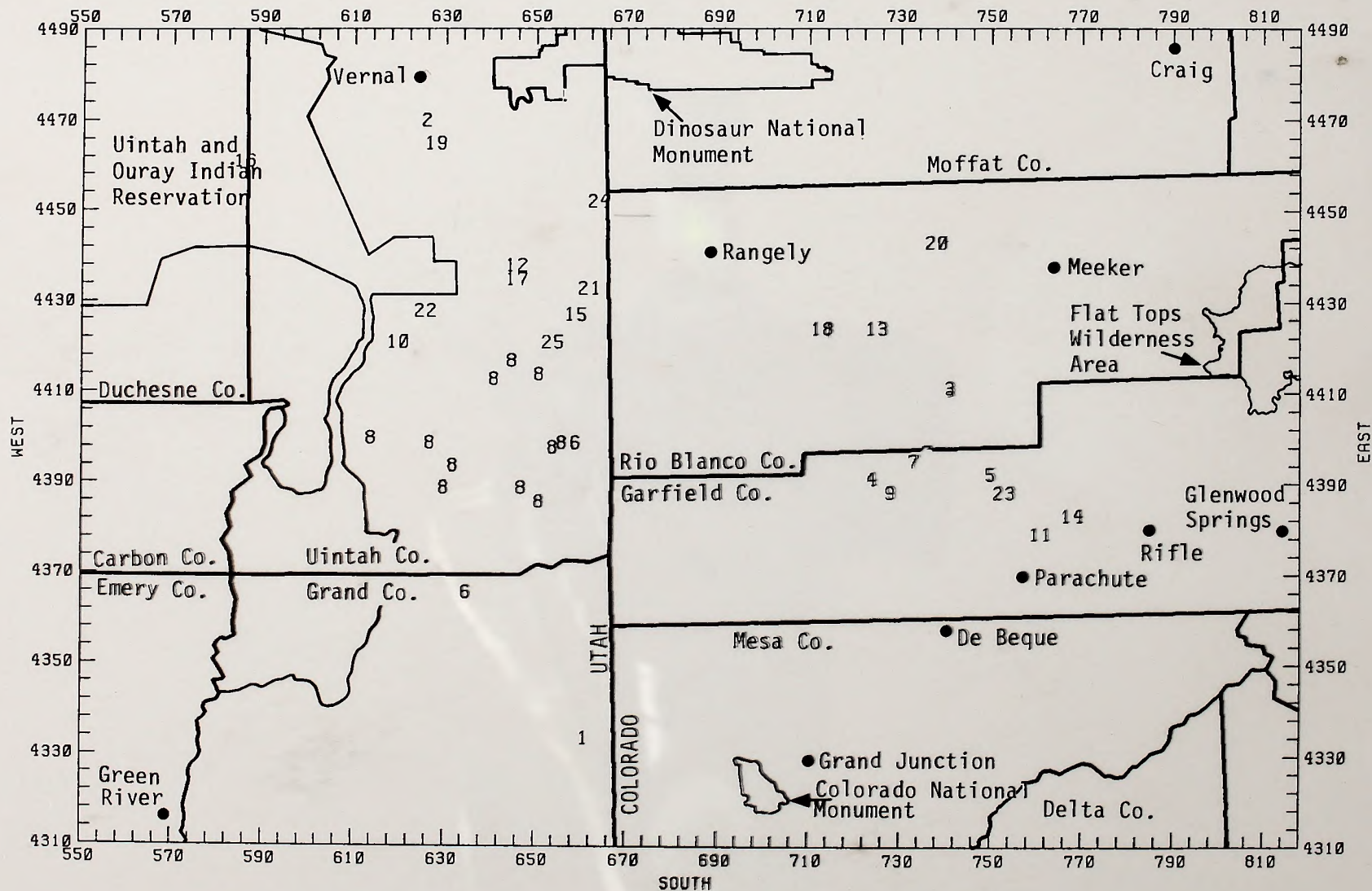
USDI - BLM

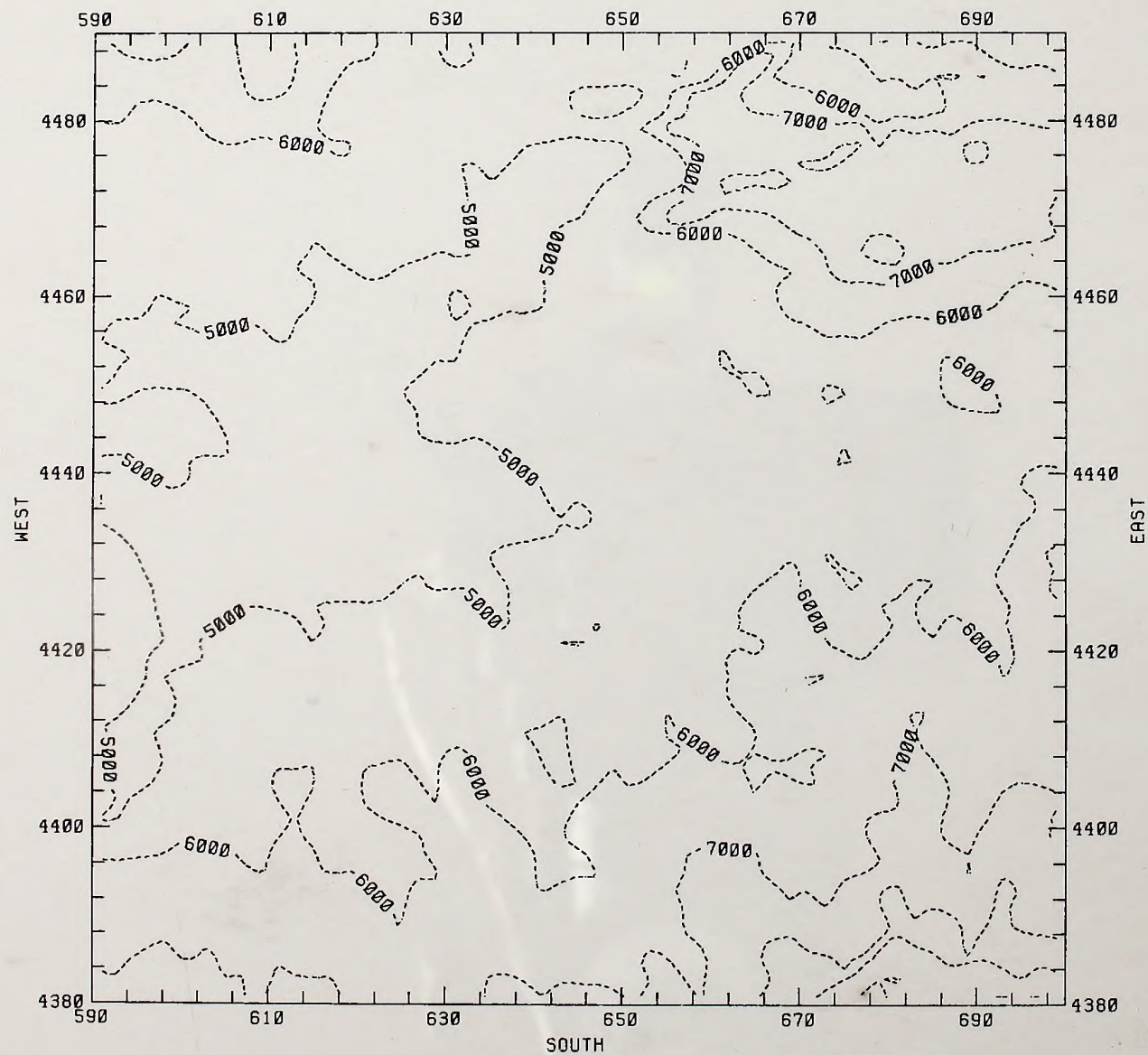


TERRAIN HEIGHTS IN FEET ABOVE SEA LEVEL



82062 4
82062 3 19





LEGEND FOR POINT SOURCES IN STUDY REGION

1. Baker (O)
2. C&A Tar Sands (O)
3. Cathedral Bluffs, C-b site (P)
4. Chevron (P)
5. Colony (P)
6. Enercor-Mono Power (U)
7. Exxon (P)
8. Geokinetics (U)
9. Getty (P)
10. Magic Circle (U)
11. Mobil (P)
12. Moon Lake Power Plant (E, O)
13. Multimineral (P)
14. Naval Oil Shale (P)
15. Paraho (U)
16. Plateau refinery (E, O)
17. Ramex (O)
18. Rio Blanco, C-a site (P)
19. Sohio (U)
20. Superior (P)
21. Syntana (U)
22. Tosco (U)
23. Union (P)
24. Western Tar Sands (O)
25. White River, U-a, U-b site (O)

Legend:

- (E) Existing source in 1980
- (O) Other planned sources (Uinta Basin)
- (U) Uinta Basin synfuel facilities
- (P) Piceance Basin oil shale facilities

